Surveyor Spacecraft System

SURVEYOR VII FLIGHT PERFORMANCE FINAL REPORT

JPL Contract 950056/March 1968

SSD 68189-7

This work was performed for the Jet Propulsion Laboratory, California Institute of Technology, sponsored by the National Aeronautics and Space Administration under Contract NAS7-100.

J. D. CLOUD
Manager
System Engineering and Analysis Laboratory

T. B. VAN HORNE
Manager
Analysis Department

W. B. MC INTYRE
Project Engineer
Analysis Department

HUGHES
HUGHES AIRCRAFT COMPANY
SPACE SYSTEMS DIVISION

CONTENTS

		Page
1.0	INTRODUCTION AND SCOPE	1-1
2.0	DESCRIPTION OF SURVEYOR SYSTEM	
2.1	Surveyor VII Mission Objectives	2-1
2.2	Surveyor VII Flight Configuration	2-1
2.3	References	2-9
3.0	SYSTEM SUMMARY	
3.1	Summary of Significant Anomalies	3-1
3.2	Conclusions	3-1
4.0	SYSTEM PERFORMANCE ANALYSIS	
4.1	General Mission Summary	4-1
4.1.1	Spacecraft Transit Phase Command Log	4-1
4.1.2	Prelaunch Countdown	4-15
4.1.3	Launch, Injection, and Separation	4-15
4.1.4	DSIF Acquisition	4-15
4.1.5	Coast Phase I Including Canopus Acquisition	4-15
4.1.6	Midcourse Correction and Coast Phase II	4-18
4.1.7	Terminal Descent Phase	4-18
4.1.8	Initial Lunar Operation	4-19
4.2	Reliability Analysis	4-19
4.2.1	Surveyor VII Reliability Estimates	4-19
4.2.1.1	System and Subsystem Reliability	4-19
4.2.1.2	Summary of Data Base for Surveyor VII Reliability Estimates	4-19
4.2.1.3	Time/Cycle/Reliability History for Surveyors I Through VI	4-21
4.2.2	Surveyor Spacecraft Reliability Growth	4-21
4.2.3	Reliability Estimate Base	4-21
4.3	References and Acknowledgments	4-29
5.0	PERFORMANCE ANALYSIS	
5.1	THERMAL CONTROL SUBSYSTEM	5.1-1
5.1.1	Introduction: Surveyor Thermal Control Techniques	5.1-1
5.1.2	Thermal Anomalies	5.1-2
5.1.2.1	Thermal Sensor Failure	5.1-2
5.1.2.2	Propulsion System Thermal Anomalies	5.1-2

5.1.3	Thermal Subsystem Summary		5.1-2
	5.1.3.1	Transit	5.1-2
	5.1.3.2	Lunar	5.1-3
5.1.4	Thermal Performance in Transit		5.1-3
	5.1.4.1	Prelaunch	5.1-11
	5.1.4.2	Postlaunch	5.1-11
	5.1.4.3	Midcourse	5.1-11
	5.1.4.4	Coast Phases	5.1-13
	5.1.4.5	Terminal Descent Phase	5.1-15
5.1.5	Thermal Performance – First Lunar Day		5.1-17
	5.1.5.1	Touchdown and Orientation	5.1-17
	5.1.5.2	Heater Performance	5.1-21
	5.1.5.3	Television Camera Operation	5.1-23
	5.1.5.4	Alpha Scattering System	5.1-23
	5.1.5.5	Soil Mechanics/Surface Sampler Subsystem	5.1-24
	5.1.5.6	Liftoff and Translation Window	5.1-24
5.1.6	First Lunar Night Thermal Performance		5.1-25
	5.1.6.1	Compartments A and B	5.1-25
	5.1.6.2	Compartment C	5.1-29
5.1.7	References		5.1-31
5.1.8	Acknowledgments		5.1-31
APPENDICES TO SECTION 5.1			
	A.	Transit Temperature Plots	5.1-A1
	B.	First Lunar Day Temperature Plots	5.1-B1
	C.	First Lunar Night Temperature Plots	5.1-C1
5.2	ELECTRICAL POWER SUBSYSTEM		
5.2.1	Introduction		5.2-1
5.2.2	Anomaly Description		5.2-1
5.2.3	Summary		5.2-5
	5.2.3.1	Transit	5.2-5
	5.2.3.2	Lunar	5.2-5
5.2.4	Analysis		5.2-5
	5.2.4.1	Mission Telemetry Plots	5.2-5
	5.2.4.2	Power Loads and Sources Budget	5.2-5
	5.2.4.3	Comparison of Flight Loads and Flight Acceptance Test Loads	5.2-23
	5.2.4.4	Cyclic Loads	5.2-23
5.2.5	References		5.2-25
5.3	RF DATA LINK SUBSYSTEM		
5.3.1	Introduction		5.3-1
5.3.2	Anomaly Discussion		5.3-16
	5.3.2.1	Receiver/Decoder Indexing During Transit	5.3-16
	5.3.2.2	Signal Level Variations During Lunar Operation	5.3-16

	5.3.2.3	Transmitter A Wide-Band Voltage-Controlled Crystal Oscillator Frequency Drift	5.3-17
5.3.3	Summary and Conclusions		5.3-19
5.3.4	Subsystem Performance Analysis		5.3-24
	5.3.4.1	General Discussion	5.3-24
	5.3.4.2	Mission Phase 1: Prelaunch to Spacecraft Acquisition	5.3-31
	5.3.4.3	Mission Phase 2: Coast	5.3-39
	5.3.4.4	Mission Phase 3: Canopus Acquisition Maneuver	5.3-41
	5.3.4.5	Mission Phase 4: Midcourse Maneuvers	5.3-43
	5.3.4.6	Mission Phase 5: Terminal Maneuver	5.3-47
	5.3.4.7	Mission Phase 6: Descent and Touchdown	5.3-49
	5.3.4.8	Mission Phase 7: Lunar	5.3-49
5.3.5	References and Documentation		5.3-50
5.3.6	Acknowledgments		5.3-51
5.4	SIGNAL PROCESSING		
5.4.1	Introduction		5.4-1
5.4.2	Anomalies		5.4-1
5.4.3	Summary		5.4-1
5.4.4	Signal Processing Analysis		5.4-3
	5.4.4.1	Unbalance Current Corrections	5.4-3
	5.4.4.2	Potentiometer Reference Voltage Corrections	5.4-3
	5.4.4.3	Current Calibration Signals	5.4-3
	5.4.4.4	Touchdown Strain Gage Data	5.4-5
5.4.5	Documentation		5.4-9
5.4.6	Acknowledgments		5.4-9
5.5	FLIGHT CONTROL		
5.5.1	Introduction		5.5-1
	5.5.1.1	Attitude Control	5.5-1
	5.5.1.2	Angular Maneuvers	5.5-1
	5.5.1.3	Velocity Correction	5.5-1
	5.5.1.4	Soft Landing	5.5-2
	5.5.1.5	Mission Performance	5.5-2
	5.5.1.6	Analysis	5.5-2
5.5.2	Anomaly Description		5.5-2
5.5.3	Summary		5.5-2
5.5.4	Subsystem Performance Analysis		5.5-9
	5.5.4.1	Prelaunch	5.5-9
	5.5.4.2	Launch Through Separation From Centaur	5.5-9
	5.5.4.3	Sun Acquisition	5.5-10
	5.5.4.4	Canopus (Star Acquisition)	5.5-10
	5.5.4.5	Coast Phase Attitude Control	5.5-23

	5.5.4.6	Premidcourse Attitude Maneuvers	5.5-24
	5.5.4.7	Postmidcourse Attitude Maneuvers	5.5-29
	5.5.4.8	Midcourse Velocity Correction	5.5-32
	5.5.4.9	Preretro Maneuvers	5.5-40
	5.5.4.10	Main Retro Phase	5.5-45
	5.5.4.11	Terminal Descent Phase	5.5-51
5.5.5	References		5.5-54
5.5.6	Acknowledgments		5.5-55
5.6	VERNIER PROPULSION		
5.6.1	Introduction		5.6-1
	5.6.1.1	Description	5.6-1
	5.6.1.2	Purpose	5.6-1
5.6.2	Anomalies		5.6-3
5.6.3	Summary		5.6-3
5.6.4	Subsystem Performance Analysis		5.6-4
	5.6.4.1	Prelaunch	5.6-4
	5.6.4.2	Launch	5.6-4
	5.6.4.3	Coast Phase I	5.6-4
	5.6.4.4	Midcourse	5.6-5
	5.6.4.5	Coast Phase II	5.6-7
	5.6.4.6	Terminal Descent	5.6-12
	5.6.4.7	First Lunar Day	5.6-12
5.6.5	References		5.6-15
5.6.6	Acknowledgments		5.6-15
	APPENDICES TO SECTION 5.6		
	A.	Surveyor VII First Lunar Day Vernier System Pressure Loss Study	5.6-A1
	B.	Surveyors I Through VII Vernier Propulsion System Performance Summary	5.6-B1
5.7	PROPULSION – MAIN RETRO		
5.7.1	Introduction		5.7-1
5.7.2	Anomaly Description		5.7-2
5.7.3	Summary		5.7-2
5.7.4	Subsystem Performance Analysis		5.7-3
	5.7.4.1	Thrust Versus Time	5.7-3
	5.7.4.2	Specific Impulse	5.7-5
	5.7.4.3	Retro Disturbance Torques	5.7-5
	5.7.4.4	T_{3500}	5.7-5
5.7.5	References		5.7-6
5.7.6	Acknowledgments		5.7-6

5.8 ALTITUDE MARKING RADAR
5.8.1 Introduction 5.8-1
5.8.2 Anomalies 5.8-2
5.8.3 Summary 5.8-2
5.8.4 Subsystem Performance Analysis 5.8-3
5.8.4.1 Event Times 5.8-3
5.8.4.2 Load Current Signals 5.8-4
5.8.4.3 Late Gate Signal 5.8-4
5.8.4.4 DB Budget 5.8-4
5.8.4.5 Expected Marking Range 5.8-5
5.8.4.6 Marking Range Dispersion 5.8-6
5.8.4.7 AMR Parameter Reconstruction 5.8-10
5.8.4.8 AMR AGC Evaluation 5.8-11
5.8.5 References and Documentation 5.8-14
5.8.6 Acknowledgments 5.8-15

5.9 RADVS PERFORMANCE
5.9.1 Introduction 5.9-1
5.9.2 Anomalies 5.9-4
5.9.3 Summary 5.9-4
5.9.4 Subsystem Performance Analysis 5.9-4
5.9.4.1 RADVS Turn-on 5.9-4
5.9.4.2 Velocity Acquisition Conditions 5.9-4
5.9.4.3 Range Acquisition Conditions 5.9-5
5.9.4.4 Revised Nominal db Budget 5.9-7
5.9.4.5 Surveyor VII Event Times 5.9-8
5.9.4.6 Descent Reconstruction 5.9-10
5.9.4.7 Radar Reflectivity Analysis 5.9-10
5.9.4.8 Reflectivity Model 5.9-11
5.9.5 RADVS Documentation 5.9-18
5.9.6 Acknowledgments 5.9-19

5.10 STRUCTURES PERFORMANCE
5.10.1 Introduction 5.10-1
5.10.2 Anomaly Description 5.10-1
5.10.3 Summary 5.10-1
5.10.4 Performance Analysis 5.10-3
5.10.4.1 Launch Phase 5.10-3
5.10.4.2 Touchdown 5.10-3
5.10.4.3 First Lunar Day 5.10-6
5.10.4.4 Second Lunar Day 5.10-6
5.10.5 References 5.10-7
5.10.6 Acknowledgment 5.10-7

5.11 MECHANISMS SUBSYSTEM
5.11.1 Introduction 5.11-1
5.11.2 Anomaly Description 5.11-3
5.11.3 Summary 5.11-3
5.11.4 Subsystem Performance Analysis 5.11-3
5.11.4.1 Landing Gear Deployment 5.11-3
5.11.4.2 Omnidirectional Antenna Deployment 5.11-3
5.11.4.3 A/SPP Performance 5.11-3
5.11.5 References 5.11-14
5.11.6 Acknowledgments 5.11-14

5.12 TERMINAL DESCENT TRAJECTORY PERFORMANCE
5.12.1 Introduction 5.12-1
5.12.2 Anomaly Description 5.12-3
5.12.3 Summary 5.12-3
5.12.4 Performance Analysis 5.12-3
5.12.4.1 Introduction 5.12-3
5.12.4.2 Postflight Analysis Computer Program 5.12-7
5.12.4.3 Velocity Change Due to Thrusting During Retro Phase 5.12-8
5.12.4.4 Main Retro Thrust Versus Time Curve 5.12-13
5.12.4.5 6DOF Simulation of Doppler Data 5.12-17
5.12.4.6 Vernier Propellant Consumption 5.12-19
5.12.4.7 Spacecraft Landing Location and Touchdown Attitude 5.12-21
5.12.4.8 Trajectory Reconstruction 5.12-21
5.12.4.9 Radar Beam Incidence Traces on Lunar Surface 5.12-33
5.12.5 References 5.12-35
5.12.6 Acknowledgments 5.12-35

5.13 TELEVISION
5.13.1 Introduction 5.13-1
5.13.2 Anomalies 5.13-1
5.13.3 Summary 5.13-2
5.13.4 Subsystem Performance Analysis 5.13-3
5.13.4.1 Television Subsystem 5.13-3
5.13.4.2 Television Camera 5.13-9
5.13.5 Acknowledgments 5.13-10

5.14 ALPHA SCATTERING EXPERIMENT
5.14.1 Introduction 5.14-1
5.14.1.1 Purpose 5.14-1
5.14.1.2 Description 5.14-1
5.14.2 Anomalies 5.14-4
5.14.3 Summary 5.14-4
5.14.4 Subsystem Performance Analysis 5.14-4
5.14.5 References 5.12-16

5.15 SOIL MECHANICS/SURFACE SAMPLER
5.15.1 Introduction 5.15-1
5.15.2 Anomalies 5.15-3
5.15.3 Summary 5.15-3
5.15.4 Acknowledgments 5.15-6

1.0 INTRODUCTION AND SCOPE

On day 7, 1968 at 06:30:00.545 GMT, the seventh Surveyor spacecraft was launched from pad 36A at AFETR at a launch azimuth of 102.914 degrees. The launch into parking orbit was near perfect, with the spacecraft being injected into its translunar trajectory after the second Centaur burn at 07:05:16.055 GMT. Subsequent transit operations were nominal, and terminal descent to a soft landing on the moon was accomplished at 10:01:05:37.620 GMT 1968. During lunar operations, over 21,000 high quality television pictures were taken, approximately 84 hours were accumulated by the alpha scattering device, and 36 hours and 21 minutes of operation were logged by the soil mechanics/surface sampler. Noteworthy was the successful revival of Surveyor VII during the second lunar day during which 45 television pictures were received and 20 additional hours of alpha scattering data accumulated.

2.0 DESCRIPTION OF SURVEYOR SYSTEM

The Surveyor spacecraft is designed and built by Hughes Aircraft Company for the National Aeronautics and Space Administration under the direction of the California Institute of Technology Jet Propulsion Laboratory. It has been conceived and designed to effect a transit from earth to the moon, perform a soft landing, and transmit to earth basic scientific and engineering data relative to the moon's environment and characteristics.

2.1 SURVEYOR VII MISSION OBJECTIVES

The primary objectives of the Surveyor VII spacecraft system were as follows:

1) Accomplish a soft landing north of the crater Tycho at 40.87° S and 11.37° W

2) Demonstrate spacecraft capability to soft land on the moon with an oblique approach angle of 36 degrees

3) Obtain postlanding television pictures

4) Obtain data on radar reflectivity, thermal characteristics, touchdown dynamics, and other measurements of the lunar surface through use of various payload equipment, including the alpha scattering device and the soil surface sampler.

Surveyor VII achieved these objectives. A soft landing occurred on the Tycho ejecta blanket at an approach angle of 35.9 degrees. Television pic-pictures were transmitted from the lunar surface. Extensive use was made of the alpha scattering device and the soil mechanics/surface sampler (SM/SS).

2.2 SURVEYOR VII FLIGHT CONFIGURATION

For a summary description of the major Surveyor functions and design mechanization, consult the "Surveyor I Flight Performance Final Report" or Section 2.3 of the "Surveyor Spacecraft Equipment Specification" (References 1

TABLE 2-1. MAJOR SURVEYOR V DESIGN CHANGES

Subsystem	Change
RF	Elimination of power dropoff with temperature Elimination of microswitches in transfer and SPDT switches
Signal Processing	Data channel reassignment
Solar Panel	Use of flat cell mounting Lower voltage output
Power	Elimination of auxiliary battery Elimination of OCR in battery charge regulator Higher efficiency and current limiting in boost regulator
Flight Control	Separation latch Increased midcourse timing capability Terminal descent staging Nitrogen tank thermal characteristics
Radars	Improved AMR noise figure RADVS 3-beam crosscoupled sidelobe logic RADVS crosscoupled sidelobe logic at low altitudes RADVS on/off relay
Propulsion	Helium check and relief valve assembly Pressure and temperature transducers on fuel lines
A/SPP	High torque motors Strengthened axes locks Strengthened sector gear Solar axis support tube
Television	Removable mirror assembly – Strengthened drive ring gear and drive shaft Potentiometers – New dry lube and thicker wiper Vidicons – Survival heater and optical front porch Spherical viewing mirrors
Alpha Scattering System	Instrument sensor Deployment mechanism Compartment C – Instrument electronics, instrument auxiliary, and thermal control

and 2). Surveyor VII is a reconfigured spacecraft (as compared to Surveyors I through 4). Major design changes were first made on Surveyor V, and Table 2-1 provides a summary of these (from Reference 3). In Table 2-2, changes to the reconfigured design, which occurred on Surveyor VI, are given (summarized from Reference 4), and in Table 2-3 additional changes to the reconfigured design, which occurred first on Surveyor VII, are given (summarized from Reference 5). To define the spacecraft configuration at launch, a list of Surveyor VII control items, separated by subsystem or function, is given in Table 2-4 (Reference 6).

TABLE 2-2. SIGNIFICANT DESIGN CHANGES FROM SURVEYOR V TO VI

Change flight compartment B thermal blankets, permitting their installation and use for STV. Test access installed in compartment.
A third auxiliary TV viewing mirror was added to permit viewing of the lunar surface where the alpha scattering experiment is deployed.
A/SPP position potentiometer drive was changed to eliminate slippage.
Survey camera incorporates survivable vidicon and gain change.
Change in manufacturer source of subcarrier oscillators.

TABLE 2-3. SIGNIFICANT DESIGN CHANGES FROM SURVEYOR VI TO VII

Installation of SM/SS in conjunction with the alpha scattering device.
Change in thermostat point of thermal control and heater A.
Installation of auxiliary mirrors.

TABLE 2-4. SPACECRAFT UNIT CONFIGURATION AT LAUNCH

Subsystem	Part Name, Number, S/N
Electrical Power	Main battery, 237900, S/N 156
	Thermal control and heater A, 283724-3, S/N 11
	Thermal control and heater B, 283724-2, S/N 14
	Boost regulator, 3024240-1, S/N 12
	Battery charge regulator, 3024260-1, S/N 14
	Solar panel, 251167, S/N 4
	Main power switch, 254112, S/N 16
	Engineering mechanisms auxiliary, 263500-10, S/N 17
Flight Control	Flight control sensor group, 3023450-2, S/N 2
	Roll actuator, 235900-3, S/N 11
	Gas supply, attitude jet, 235600-3, S/N 3
	Attitude jets, 235700-2, S/N 21 and 20
	Attitude jet, 235700-3, S/N 11
	Canopus sensor, 235300-2, S/N 6
	Secondary solar sensor, 235450-1, S/N 9
Radar	Altitude marking radar, 283810, S/N 11
	KPSM (RADVS), 232909, S/N 13
	SDC (RADVS), 232908-6, S/N 7
	Altitude velocity sensor antenna (RADVS), 232910, S/N 11
	Velocity sensor antenna (RADVS), 232911, S/N 12
	Waveguide assembly (RADVS), 232912, S/N 11
	RADVS on/off switch, 274153, S/N 14

Table 2-4 (continued)

Subsystem	Part Name, Number, S/N
Telecommunications	Transmitter A, 3024400-1, S/N 11
	Transmitter B, 3024400-1, S/N 15
	Command receiver A, 231900-3, S/N 21
	Command receiver B, 231900-3, S/N 24
	Omnidirectional antennas A and B, 232400, S/N 18 and 28
	Telemetry buffer amplifiers A and B, 290780-1, S/N 27 and 18
	Planar array antenna, 232300, S/N 20
	Low pass filters A and B, 233466, S/N 29 and 30
	RF switch, SPDT, 284344, S/N 16
	RF transfer switch, 284345, S/N 16
Signal Processing	Signal processing auxiliary, 232540-1, S/N 9
	Central command decoder, 232000-5, S/N 9
	Low data rate auxiliary, 264875-2, S/N 9
	Engineering signal processor, 233350-10, S/N 4
	Auxiliary engineering signal processor, 264900-7, S/N 4
	Central signal processor, 232200-7, S/N 4
	TV auxiliary, 232106-7, S/N 15
Television	Survey camera, 290512-2, S/N 13
	Photo chart, antenna A, 231051, S/N 13
	Photo chart, antenna B, 231051, S/N 19
	Photo chart, leg 2, 230992, S/N 13
	Viewing mirror, 3035010, S/N 4

Table 2-4 (continued)

Subsystem	Part Name, Number, S/N
Television (continued)	Viewing mirror, 3035000, S/N 4
	Viewing mirror, 3035080, S/N 4
	Small mirror, 3023929, S/N 3
	Mirror assembly, 3024180-4, S/N 13
Propulsion	Oxidizer tank, 287119-1, S/N 2
	Oxidizer tank, 287121-1, S/N 1
	Oxidizer tank, 3026126, S/N 1
	Fuel tank, 3026123, S/N 1
	Fuel tank, 287118-1, S/N 1
	Fuel tank, 287117-1, S/N 11
	Check and relief valve assembly 1, 287290-30, S/N 5
	Check and relief valve assembly 2, 287290-50, S/N 22
	Helium tank and valve assembly, 3026042, S/N 5
	Thrust chamber assembly, 285063-4 (Hughes), S/N 558
	Thrust chamber assembly, 285063-7 (Hughes), S/N 559
	Thrust chamber assembly, 285063-6 (Hughes), S/N 536
	Main retro, 238612-1, S/N A22-14
Mechanisms	Spaceframe, 3025093-2, S/N 1
	Omnidirectional antenna A mechanism, 3028000-1, S/N 7
	Omnidirectional antenna B mechanism, 273880-2, S/N 3

Table 2-4 (continued)

Subsystem	Part Name, Number, S/N
Mechanisms (continued)	Antenna/solar panel positioner, 3035092-1, S/N 2
	Leg position pots, 988684-1, S/N 345, 430, and 347
	Retro-rocket release mechanisms, 230069-1, S/N 22, 41, and 42
	Separation sensing and arming devices, 293400, S/N 12, 26, and 28
	Shock absorbers, legs 1 through 3, 238927, S/N 14, 19, and 20
	Magnet leg 2 and leg 3, 3050886, S/N 3 and 5
	Footpad leg 1, 263947, S/N 570
	Footpads legs 2 and 3, 263947-1, S/N 465 and 569
	Landing gear, 261278, S/N 10
	Landing gear, 261279, S/N 9
	Landing gear, 3025100, S/N 3
	Crushable block, 261281-2
	Crushable block, 3050736
	Crushable block, 3050697
	Strain gauge amplifier, 238930, S/N 8
Alpha Scattering	Auxiliary, 274350-1, S/N 2
	Electronics, 239305, S/N FU-2
	Deployment mechanism, 3024801, S/N 4
	Sensor head, 239304, S/N FU-2
	Standard sample, 239397, S/N 4
	Heater, compartment C, 290900, S/N 4
	Passive simulator, 3024506, S/N 3

Table 2-4 (continued)

Subsystem	Part Name, Number, S/N
SM/SS	Auxiliary, 3024536, S/N 3
	Mechanism, 3024700, S/N 3
Thermal Control	Thermal switch A, 3028200-2, S/N 8
	Thermal switch A, 3028200-1, S/N 10, 24, 26, 30, 31, 33, 34, and 35
	Thermal switch B, 3028200-4, S/N 7
	Thermal switch B, 3028200-3, S/N 19, 20, 21, 23, and 25
	Thermal tray, compartment A, 3025094, S/N 4
	Thermal tray, compartment B, 3025096, S/N 4
Harness	Wiring harness compartment B, 3025792, S/N 1
	Wiring harness compartment A, 3050850, S/N 1
	Wiring harness basic bus 1, 3050852, S/N 1
	Wiring harness TV camera, 285833, S/N 3
	Wiring harness basic bus 2, 3050799, S/N 2
	Wiring harness TV auxiliary, 3050868, S/N 1
	Wiring harness retro motor, 285832, S/N 1
	Wiring harness battery cell volt, 3025155, S/N 9
	Wiring harness separation squibs, 285831, S/N 4
	Wiring harness A/SPP, 3025420, S/N 1
	Wiring harness ASI, 3025641, S/N 5
Cable	RF, omni A, 285838-1, S/N 4
	RF, omni B, 285838, S/N 4
	RF, planar array, 285838, S/N 4

Table 2-4 (continued)

Subsystem	Part Name, Number, S/N
Cable (continued)	RF, transmitter switch A, 285841, S/N 7
	RF, transmitter switch B, 285842, S/N 2
	RF, transmitter switch SPDT, 285842-1, S/N 6
	RF, transmitter B, receiver B, 285843, S/N 4
	RF, planar array, 261714, S/N 8
	RF, planar array, 276828-1, S/N 13
	RF, transmitter A, receiver A, 285843-1, S/N 7
	RF, transmitter B SPDT, 285844, S/N 7
	RF, transmitter A SPDT, 285844-1, S/N 1
	RF, omni A, 261720, S/N 9
	RF, omni B, 261720-1, S/N 13
	RF, omni B, 261721-1, S/N 15
	Retro igniter, 285834, S/N 4
	SM/SS, 3025707, S/N 3
	SM/SS squib, 3025706, S/N 4

2.3 REFERENCES

1) "Surveyor I Flight Performance Final Report," Hughes Aircraft Company, SSD 68189R, October 1966.

2) "Surveyor Spacecraft Equipment Specification," Hughes Aircraft Company 224832, Revision A.

3) "Surveyor V Flight Performance Final Report," Hughes Aircraft Company, SSD 68189-5, November 1967.

4) "Minutes of SC-6 Consent to Ship Meeting," Hughes Aircraft Company, SSD 74092, 5 September 1967.

5) "Minutes of SC-7 Consent to Ship Meeting," Hughes Aircraft Company, SSD 74124, 3 November 1967.

6) "Spacecraft Configuration Index, Spacecraft SC-7," Hughes Aircraft Company, Engineering Order 239607, Revision E, 3 January 1968.

3.0 SYSTEM SUMMARY

3.1 SUMMARY OF SIGNIFICANT ANOMALIES

One anomaly occurred during the transit portion of Mission G. Table 3-1 summarizes the problems that occurred on the lunar surface. For this report an anomaly is defined as an unexpected occurrence that might be indicative of a spacecraft trouble or failure.

3.2 CONCLUSIONS

Performance of the Surveyor VII spacecraft was excellent during transit flight and on the moon. A selected group of performance parameters which could be directly determined through analysis of spacecraft telemetry for the seven Surveyor flights are summarized in Table 3-2. Required or predicted values of these parameters for Surveyor VII are included in this summary. The success of this, the last of the Surveyor missions, is highlighted by the overall performance of the spacecraft, by the accuracy of the midcourse correction making a second correction unnecessary, and by successful operation of all scientific instrumentation. Of further significance was the revival of the spacecraft for a second lunar days operation, including operation of the television camera and accumulation of alpha scattering science and engineering data.

TABLE 3-1. SPACECRAFT ANOMALIES

GMT, day:hr:min	Anomaly	Effect on Mission
007:14:24	During Canopus star map, star lock signal was not obtained when the star Canopus was in the Canopus sensor field of view (see subsection 5.5.2)	None. Acquired Canopus by manual lockon as in Missions A and B.
010:22:01	The alpha scattering head did not deploy to the surface upon command. Indications are that the squib fired and pulled the pin, but that the escapement mechanism for the nylon cable either failed to work or the cable jammed in the mechanism (TFR 87255). The alpha scattering head was successfully deployed to the surface by using the soil mechanics/surface sampler to exert force on the alpha scattering instrument head. (See subsections 5.14.2 and 5.15.)	None. Science data were successfully accumulated by the alpha scattering device on the first and second lunar days. Three different locations were monitored.
014:23:08	Transmitter A wideband voltage-controlled crystal oscillator frequency drifted in and out of the DSS 11 receiver tuning range. This was a known expected drift for this transmitter wideband oscillator (TFR 87206). (See subsection 5.3.2.3.)	Transmitter B was used for television operation during part of the remainder of the first lunar day.
Day 14	Vernier fuel line 3 temperature telemetry signal failed. Suspected open sensor.	None

Table 3-1 (continued)

GMT, day:hr:min	Anomaly	Effect on Mission
Days 14 and 15	During some television surveys when spacecraft receiver automatic gain control was not available, commands were missed due to one of the receiver signal levels drifting below the command threshold. Probably due to multipath reflections. (See subsection 5.3.2.2.)	None
Day 20 and after	Vernier engine 2 temperature (P-10) had a sudden unpredictable drop (88° to 0°F), and the oxidizer pressure (P-2) unexpectedly decreased from 699 to 601 psi. A fuel and gas leak occurred through engine 2 shutoff valve poppet, and a gas leak occurred in the oxidizer subsystem. (See Appendix A, Section 5.6.)	None on normal operations.
Day 23	As vehicle entered lunar night, a deflection of 2.39 degrees was observed on leg 2, indicating this leg had failed to lock. Upon revival on day 43, leg 1 had deflected 23.5 degrees, indicating leg 1 had failed to lock (TFR 18274). (See subsection 5.10.2.)	None on normal operations. Spacecraft survived first lunar night. All mission objectives were met. Additional television and alpha scattering data were received during second lunar day from different spacecraft orientation.
Day 23 and after	Several switches in compartments A and B did not actuate at proper temperature, and two switches were stuck closed in compartment A at time of spacecraft shutdown for first lunar night. (See subsection 5.1.6.1.)	The extent of spacecraft operations into lunar night was shortened, and the probability of lunar night survival would have been reduced. Surveyor VII was recovered for a second lunar day.

Table 3-2

TABLE 3-2. SUMMARY PERFORMANCE PARAMETERS

Spacecraft		Actual							Subsection or Reference	Predicted or Specified for Surveyor VII	Reference	Comments
		1	2	3	4	5	6	7				
Parameters	Units											
LAUNCH TO ACQUISITION SUMMARY												
Ignition-liftoff	GMT	0 second is 1966 150:14:41:00.99	0 second is 1966 263:12:31:59.824	0 second is 1967 107:07:05:01.059	0 second is 1967 195:11:53:29.215	0 second is 1967 251:07:57:01.257	0 second is 1967 311:07:39:01.075	0 second is 1968 007:06:30:00.545				
Booster engine cutoff	seconds from liftoff	142.2	142.29	142.5	141.88	153.4	153.4	152.5	FPAC	153.5	Preflight nominal trajectory	
Booster jettison		145.6	145.75	145.5	145.38	156.8	156.7	155.5		156.6		
Insulation panel jettison		176.2	176.06	176.2	176.18	198.4	198.3	197.5		198.5		
Nose fairing jettison		203.0	202.90	203.5	203.38	228.6	228.6	226.5		228.5		
Sustainer engine cutoff		239.3	235.17	237.7	237.98	246.4	245.6	248.5		248.2		
Atlas/Centaur separation		241.8	237.03	239.6	241.58	248.7	248.2	250.5		250.2		
Centaur main engine cutoff 1		689.3	686.3	569	687.98	587.0	581.0	592.5		589.2		
Centaur main engine cutoff 2		None	None	2028.8	None	1103.9	1468.7	2054.5		2049.		
Surveyor:												
Extend landing gear		715.5	710.7	2051.8	715.78	1124.2	1487.9	2075.5		2069.3		
Extend omnidirectional antenna		725.7	720.7	2061.8	725.28	1134.4	1498.4	2083.5		2079.8		
Transmitter to high power		745.4	741.4	2072.5	745.98	1154.7	1518.9	2099.5		2100.3		
Electrical disconnect from Centaur		752.3	742.08	2087.8	751.28	1160.9	1524	2110		2105.8		
Centaur separation		757.1	752.58	2093.4	756.88	1165.5	1528.9	2115.5		2111.3		
Time to null rates to 0.1 deg/sec	seconds	≤15	<4	<11	<13	<20	<17	<26		Within 50 seconds		
Pitch	degrees	≈0	–	–	+0.35							
Yaw	degrees	≈2.3	–	–	-2.0		≈0	Small				
Roll	degrees	≈0	–	–	~0							
Centaur retro maneuver time	seconds	L+996.0	L+992.8	L+2355.5	L+996.88	L+1405.5	L+1768.9	L+2355.5	FPAC	L+2351.3		
Solar axis deployment time	seconds	617	360	358	348	298	337	323	5.11.4	331		
Spacecraft separated weight	pounds	~2192.8	2203	2281.3	2294.9	2216.8	2220.	2289.2				Spacecraft weight, cg and moments of inertia at separation
Spacecraft cg location												
X	inch	-0.116	-0.101	+0.058	+0.044	-0.070	-0.063	+0.342				
Y	inch	-0.092	+0.010	+0.179	-0.188	+0.779	+0.732	+0.110				
Z	inch	~59.185	59.16	58.95	58.88	59.69	59.7	59.7				
Spacecraft moment of inertia												
I_{xx}	slug-ft^2	195.4	200	202	204	210	210	215				
I_{yy}	slug-ft^2	191.7	196	198	200	211	211	213				
I_{zz}	slug-ft^2	213.3	215	223	225	211	211	216				
COAST SUMMARY												
Sun acquisition												
Roll angle	degrees	-87	-71.5	-181	-59.4	-342	-264	-224	5.5.4.3		224832A (7.3.3.3.4)	Roll maneuver until activation of acquisition sun sensor and then a yaw maneuver until primary sun sensor illumination
Yaw angle	degrees	+99	+15	+38	+42.1	+18.0	+22	+37		18 minutes maximum		
Total time	seconds	372	174.8	438.2	203	722	572	523				
Star acquisition												
Proper acquisition and Canopus verification		Manual	Manual	Automatic	Automatic	Automatic	Automatic	Manual	5.5.4.4		224832A (7.3.3.3.5)	
Roll angle from beginning of maneuver to Canopus	degrees	580.6	240	+205	+210.5	+179	+298	+269				
Objects identified		Alpha Doradus Phi Eridani Markab Pi Cygni Alderamin Regulus Alpha Hydrae Naos Canopus	Zeta Draconis Beta Draconis Ras Alhague Shaula Theta Scorpii Gamma Arae Alpha Tr. Australis Alpha Arae Zeta C Majoris Canopus	Canopus Moon Jupiter Earth Procyon Altair Adhara	Eta U Majoris Delta Velorum Gamma Casiopeiae Canopus Moon Earth	Zeta Ophiuchi (Antares, Tau Scorpii) Gamma Tr. Australis Canopus (Alnitak, Alnilam, Mintaka) Alpha Leporis Earth Bellatrix Polaris	Deneb Canopus Earth	Canopus Earth Moon Alpha C. Venaticorn Mizar Gamma U. Minoris Kochab Caph/Shedar/Zeta Cassiopeiae				
Mean roll rate during star map phase	deg/sec	+0.5004	+0.4998	0.5011	0.5003	0.5007	0.5009	0.5018		0.5		
Effective gain of Canopus sensor	X Canopus	1.5	>1.5	1.03 - 1.22	1.16	1.32	1.10	> 1.5			Design	Normally the gain setting is 1 X Canopus
Attitude orientation												
Average error from sunline												Sensor group roll axis shall be held within 0.2 degree of sun-spacecraft line
Pitch	degree	-0.058	-0.07	0	+0.009	Very small	Very small	Very small		Within 0.2 degree	224832A (7.3.3.3.6)	
Yaw	degree	-0.053	-0.1	+0.02	+0.08							
Roll	degree	-0.055	-0.08	-0.06	~0							

Table 3-2 (continued)

Spacecraft		Actual							Subsection or Reference	Predicted or Specified for Surveyor VII	Reference	Comments
Parameters	Units	1	2	3	4	5	6	7				
TERMINAL DESCENT SUMMARY (continued)												
Command of first maneuver	GMT		NA	109:23:23:30	198:01:24:44.2	254:00:12:15.1	314:00:25:20	010:00:27:14.2				
First maneuver	degrees	+89.3 roll		-158 yaw	+80.8 roll	+73.8 roll	+82.0 roll	+80.5 roll				
Command of second maneuver	GMT			109:23:30:17	198:01:29:34.2	254:00:16:20.5	314:00:29:38	010:00:35:49.8				
Second maneuver	degrees	+60.0 yaw		-76.8 pitch	+92.7 yaw	+119.6 yaw	+111.8 yaw	+96.1 yaw				
Command of third maneuver	GMT			109:23:34:35	198:01:35:04.6	None	314:00:34:56	010:00:41:06.9				
Third maneuver	degrees	+94.4 roll		-64 roll	-25.4 roll	None	+120.5 roll	-16.5 roll				
AMR enabled (station time)	GMT	153:06:12:57.684		109:23:59:35.252	198:02:00:16.99	254:00:43:00.9	314:00:56:19.6	010:01:00:36.3				AMR times received at DSS
AMR mark (station time)	GMT	153:06:14:39.708		110:00:01:12.829	198:02:01:56.08	254:00:44:39.081	314:00:57:57.038	010:01:02:11.892				
AMR backup mark (station time)	GMT			110:00:01:13.439	198:02:01:56.35	254:00:44:46.38	314:00:57:58.99	010:01:02:13.2				
Ignition delay time	seconds	7.85		5.09	2.73	12.33	5.900	2.775				
Retro delay time	seconds	1.1		1.1	1.12	1.07	1.100	1.100			224832A (7.3.3.3.9)	
Retro action time (T3500)	seconds	38.9		41.02	≈42	38.56	39.37	42.86	5.7.3			SC-4 loss of signal at 198:02:02:41.018
Maximum retro thrust	pounds	9900		9550	9250	9950	9700	9200	5.7.3			
Thrust to velocity vector	degree	0.26		0.34	0.17°	0.30	0.8	0.27	5.5.3			
Retro thrust to cg offset	inch	<0.02		0.024	–	-0.048	0.04	0.04	5.5.3			
Start RADVS – controlled descent												
Slant range	feet	27820		36158	NA	6300	40574	51259	5.12.3		5.12.3	Burnout data for SC-4 is at signal loss
Altitude	feet	27800		32900	49420	4139	36625	41510		38,736		
V_z	fps	425		462	NA	+46	463	428		444		
V_x	fps	71.3		171	NA	-41	225	-56		-42		
V_y	fps	-4.1			NA	+50	0	-132		-171		
V-Total	fps	430		483	1092	79	515	452		477		
Flight-path angle	degrees			26.8	26.8	-35.67	8.1	18.1		14.62		
Peak attitude transient at retro ignition												
Roll	degree	–		-0.22	~0	-0.16	-0.77	-0.23	5.5.3		224832A (7.3.3.3.10)	
Pitch	degree	-0.41		-0.10	-0.09	+0.5	-0.17	-0.08				
Yaw	degree	-1.03		~0	-0.35	-0.5	-0.08	-0.44				
RODVS acquire condition												
Slant range	feet	55000		63900	78000		68022	80639				
Velocity	fps	3280		3230	3414		3202	3267				
RORA acquire condition												
Slant range	feet	36000		43700	NA		35924	41673				
Velocity	fps	690		640	NA		515	452				
Beam loss of locks												
Retro case	NA	No. 3 once		No. 4 once	None	Nos. 4, 3 once	None	No. 1 once				
Other	NA	None		Nos. 3, 4 once	None	None		None				
Segment acquisition					NA							
Slant range	feet	18000		22300		806	24730	20246	5.12.3	22,000		
Velocity	fps	442		495		97	522	464	5.12.3	490		
1000 foot mark conditions												
Time	GMT	153:06:17:10.494		110:00:03:53.023		254:00:46:19.697	314:01:00:40.534	010:01:05:13.285				
Velocity	fps	103.1		103.27		96.03	106	102.5	5.12.3	106		
Attitude	degree(s)	1.11		0.51		-7.5	1.04	1.62	5.12.3	1.5		
10-fps mark conditions												
Slant range	feet	43		46		46	50	46	5.12.3	46		
Time	GMT	153:06:17:28.719		110:00:04:10.623		254:00:46:37.097	314:01:00:57.634	010:01:05:30.784				
Attitude	degree	0.7		0.025		-0.53	0.03	0.03	5.12.3	0.03		
Δ Time 1000 foot mark to 10-fps mark	seconds	18.22		17.6		17.4	17.1	16.9				
Δ Time 10 fps mark to 14-foot mark	seconds	6.45		NA		5.6	6.5	6.1				
Vernier engine shutoff												
14 foot mark	GMT	153:06:17:34.169		NA		254:00:46:42.697	314:01:01:04.133	010:01:05:36.284				
Altitude (from foot pads)	feet	13		NA		14.5	14	13.02	5.12.3	13.0		
Vertical velocity	fps	5		NA		5.2	5	5.02	5.12.3	5 01		
Lateral velocity	fps	≈0		NA		~0	~0	~0		~0		
Angle to local vertical	degree	≈0.3		NA		-0.11	0.03	0.03	5.12.3	0.02		
Time to touchdown	seconds	1.53		NA		1.7	1.33	1.336				
Touchdown condition trajectory												
Vertical velocity	fps	12.2		6-8		13.5	12.5	12.5				
Lateral velocity	fps	≈0.6		≈0		0.5	0	0	5.12.3	12.5		
Attitude	degree	≈0		≈0		≈0	≈0	≈0	5.12.3	0		
									5.12.3	–		
Touchdown conditions (strain gages)												
Vertical velocity	fps	10		6		12 to 13	11.5	12	5.10.4.2			
Lateral velocity	fps	2		0.5		<1	<1	1	5.10.4.2			
Attitude	degree	1		≈0		≈0	≈2	≈0				
Spacecraft attitude after landing												
Roll orientation (+ x-axis to north)	degrees	179 clockwise		134.2 clockwise		114.5 clockwise	148.99 clockwise	290.23 clockwise				
Tilt magnitude	degrees			12		19.5	-0.86	3.17				
Tilt direction	degrees			277 clockwise		7.6 clockwise	335.04 clockwise	279 clockwise				
Vernier fuel used	pounds	139.0		140.1		136.62	146.33	152.89	5.12.3	149.41		

4.0 SYSTEM PERFORMANCE ANALYSIS

4.1 GENERAL MISSION SUMMARY

Surveyor VII was launched from pad 36A at Cape Kennedy on a parking orbit lunar intercept trajectory at a launch azimuth of 102.914 degrees. Sixty-six hours, 35 minutes, and 37 seconds later the transit flight culminated in a soft landing on the moon. The flight began on 6 January 1968 PST (007:06:30:00.545 GMT) and soft landed on 9 January (010:01:05:37.620 GMT). Approximately 21,091 television pictures were taken (45 during the second lunar day), 84 hours of lunar science data were accumulated by the alpha scattering experiment (64 hours on the first lunar day and 20 on the second), and 36 hours and 21 minutes were logged by the soil mechanics/surface sampler. Performance of the Atlas and Centaur (AC-15) launch vehicles appeared normal throughout the launch and the injection flight period, as mark events, occurred close to the predicted times. One anomaly was noted during transit. The only significant problem encountered during lunar operations was the failure of the alpha scattering instrument head to deploy to the lunar surface upon command. The soil mechanics/surface sampler was used to exert force on the head and successfully deploy it after tests at Hughes Aircraft Company demonstrated the feasibility of this method.

A summary of the mission event history is contained in Table 4-1. Injection of the spacecraft occurred at 07:07:05:16.055 GMT on a trajectory that, with one midcourse correction, provided a total miss of 1.69 km from the desired landing site of 11.37°W longitude and 40.87°S latitude for a landing site estimated, from Lunar Orbiter evaluation, to be 11.44°W longitude and 40.89°S latitude. During transit, the sun acquisition, solar panel deployment, Deep Space Station acquisition, initial commanding and interrogations, star acquisition and verification, and midcourse and terminal descent maneuvers were successfully executed.

The earth track traced by Surveyor VII is shown in Figure 4-1, and predicted view periods for the tracking stations are given in Table 4-2.

4.1.1 Spacecraft Transit Phase Command Log

A detailed list of spacecraft commands sent during transit flight is presented in Table 4-3. This table includes the time the command was sent, bit rate, telemetry mode, and tracking station originating the command.

TABLE 4-1. SURVEYOR VII MISSION MILESTONES

Event	GMT, 1968, day:hr:min:sec
Launch	07:06:30:00.545
Separation – electrical disconnect*	07:07:05:10.541
Separation – mechanical (Centaur)*	07:07:05:16.055
A/SPP solar panel unlocked*	07:07:05:15 ± 2.0
A/SPP solar panel locked in transit position*	07:07:10:37.254 ± 1.2
A/SPP roll axis locked in transit position*	07:07:14:27.657 ± 1.2
Automatic sun acquisition complete*	07:07:14:30
Initial DSS acquisition (one-way) confirmed*	07:07:20
Initial DSS acquisition (two-way lock) confirmed*	07:07:28
First ground command sent to spacecraft	07:07:31:46.6
Canopus verification begins	07:14:18:28
Canopus lockon (manual)*	07:14:47:32
First premidcourse (roll) maneuver executed	07:23:18:28.0
Second premidcourse (yaw) maneuver executed	07:23:21:13.3
Midcourse correction executed	07:23:30:09.4
Sun reacquired	07:23:37:43
Canopus reacquired	07:23:41:08
Transmitter high power on	10:00:12:21.5
1100 bps	10:00:08:03.0
Mode 5 on	10:00:12:32.5
Transponder off	10:00:21:14.9
Start roll maneuver	10:00:27:14.2
Start yaw maneuver	10:00:35:49.8
Start roll maneuver	10:00:41:06.9
Reset nominal thrust	10:00:43:39.4
Retro sequence delay	10:00:45:09.9
Mode 6 on	10:00:50:09.7
Retro sequence mode on	10:00:56:11.1
AMR power on	10:00:57:33.7
AMR on (R-1)*	10:00:57:36.351 ± 0.19
FC thrust phase power on	10:00:58:33.9
Enable AMR	10:01:00:33.7
AMR enabled (R-11)*	10:01:00:36.345 ± 0.19
AMR mark (FC-64)*	10:01:02:11.892 ± 0.05
Emergency AMR signal (first command sent)	10:01:02:13.2
Vernier ignition (FC-28)*	10:01:02:14.692 ± 0.05
Retro ignition (FC-29)*	10:01:02:15.792 ± 0.05
Backup command received*	10:01:02:15.942 ± 0.19
RADVS pyro switch (EP-33)*	10:01:02:16.752 ± 0.6
RADVS on (R-28)*	10:01:02:15.752 ± 0.6
RODVS (FC-34)*	10:01:02:48.850 ± 0.6
Inertial switch signal*	10:01:02:58.975 ± 0.025
Retro burnout (FC-30)*	10:01:02:58.990 ± 0.05

Table 4-1 (continued)

Event		GMT, 1968, day:hr:min:sec
Start maximum thrust (FC-78)*		10:01:03:09.250 ± 0.6
Retro eject signal (FC-31)*		10:01:03:10.990 ± 0.05
Retro ejected (V-4)*		10:01:03:11.550 ± 0.6
Vernier high thrust off (FC-78)*		10:01:03:12.850 ± 0.6
Start RADVS-controlled descent (FC-42)*		10:01:03:13.090 ± 0.05
RORA (FC-33)*		10:01:03:17.649 ± 0.6
Segment acquisition*		10:01:04:03.018 ± 0.15
1000-foot mark (FC-37)*		10:01:05:13.285 ± 0.05
10-fps mark (FC-36)*		10:01:05:30.184 ± 0.05
14-foot mark (FC-38)*		10:01:05:36.284 ± 0.05
Touchdown (leg 1)*		10:01:05:37.620 ± 0.003
Selected Lunar Events		
First 200-line picture		010:01:47
Initial sun and earth acquisition		010:03:21
First 600-line picture		010:03:41
Alpha scattering turned on		010:09:27
A/SPP fine positioning completed		010:12:38
ASI deployed to background position		010:15:48
Failure of ASI to deploy to surface (command)		010:21:01
ASI successfully deployed to surface using SM/SS		012:09:00
Multipath telecommunication test	From	016:15:49
	To	016:18:31
	From	017:14:03
	To	017:15:03
Laser experiment	From	019
	Through	021
Sunset (spacecraft television camera)		023:06:06
SM/SS operation concluded		023:08:41
ASI data accumulation terminated		023:15:36
Television operations terminated		023:21:10
Spacecraft revived (second lunar day)		043:
Television operation		
Alpha scattering operation		
Last signal received (second lunar day)		052:00:24

*Telemetry time at ground station.

TABLE 4-2. PREDICTED VIEW PERIOD SUMMARY

Station	Event		GMT		
			January 1968	Hour	Minute
DSS 51 Johannesburg	5° elevation	Rise	7	11	28
DSS 61 Madrid	5° elevation	Rise	7	13	08
DSS 42 Tidbinbilla	5° elevation	Set	7	13	26
DSS 11 Goldstone	270° hour angle	Rise	7	20	58
DSS 51 Johannesburg	5° elevation	Set	7	22	14
DSS 61 Madrid	5° elevation	Set	8	01	40
DSS 42 Tidbinbilla	5° elevation	Rise	8	04	38
DSS 11 Goldstone	90° hour angle	Set	8	09	01
DSS 51 Johannesburg	5° elevation	Rise	8	12	34
DSS 61 Madrid	5° elevation	Rise	8	13	19
DSS 42 Tidbinbilla	5° elevation	Set	8	14	06
DSS 11 Goldstone	270° hour angle	Rise	8	21	20
DSS 51 Johannesburg	5° elevation	Set	8	22	35
DSS 61 Madrid	5° elevation	Set	9	02	13
DSS 42 Tidbinbilla	5° elevation	Rise	9	04	58
DSS 11 Goldstone	90° hour angle	Set	9	09	16
DSS 51 Johannesburg	5° elevation	Rise	9	12	47
DSS 61 Madrid	5° elevation	Rise	9	13	22
DSS 42 Tidbinbilla	5° elevation	Set	9	14	14
DSS 11 Goldstone	270° hour angle	Rise	9	21	26
DSS 51 Johannesburg	5° elevation	Set	9	22	40

TABLE 4-3. SURVEYOR VII COMMAND SEQUENCE

Command Number	Description	GMT, hr:min:sec	Telemetry Mode	Bit Rate
	Day 007 – DSS 42			
0107	Xmtr Hi Volt Off	07:31:46.6	5	550
0110	Xmtr Fil Pwr Off	31:55.1		
0130	Xfer Sw B Lo Pwr	31:55.6		
0236	A/D Iso Amp Off	34:45.9		
0316	SP Deploy Logic Off	34:46.4		
0126	Xfer Sw A Lo Pwr	34:46.9		
0402	Step SP Minus (x10)	36:13.6		
0401	Step SP Plus (x5)	36:19.6		
0405	Step Roll Axis Plus (x10)	37:49.1		
0406	Step Roll Axis Minus (x5)	37:54.6		
0510	AESP Off	38:44.6		
0226	Mode 1	38:52.6	1	
0237	Low Mod SCOs Off	40:05.1		
0216	7.35 kc SCO On	40:05.6		
0205	1100 bps	40:06.1		1100
0231	Mode 4	42:26.7	4	
0227	Mode 2	45:13.1	2	
0232	ESP Off	47:48.1		
0507	Mode 6	47:54.6	6	
0506	Mode 5	49:56.1	5	
0510	AESP Off	10:36:15.2		
0226	Mode 1	36:21.7	1	
0227	Mode 2	38:19.7	2	
0231	Mode 4	40:11.7	4	
0232	ESP Off	41:59.8		
0506	Mode 5	42:04.8	5	
	Day 007 – DSS 51			
0306	SP Sw On, Bypass Off	12:27:48.4		
0306	SP Sw On, Bypass Off	46:02.0		
	Day 007 – DSS 61			
0510	AESP Off	14:06:32.0		
0231	Mode 4	06:36.5	4	
0227	Mode 2	10:31.1	2	
0226	Mode 1	12:04.0	1	
0105	Xmtr B Fil Pwr On	16:16.6		
0306	SP Sw On, Bypass Off	17:55.1		
0127	Xfer Sw B Hi Pwr	18:27.1		1100

Table 4-3 (continued)

Command Number	Description	GMT, hr:min:sec	Telemetry Mode	Bit Rate
0106	Xmtr Hi Volt On	14:18:27.6	1	1100
0220	7.35 kc SCO Off	19:09.1		
0217	33 kc SCO On	19:09.6		
0206	4400 bps	19:10.1		4400
0124	Xpdr Pwr Off	21:19.9		
0715	Man Delay Mode	22:16.9		
0710	Pos Angle Maneuver	22:46.0		
0714	Sun and Roll	24:05.4		
0702	Sun Acq. Mode	44:59.4		
0716	Man Lock-On	47:31.9		
0232	ESP Off	49:58.9		
0506	Mode 5	52:00.4	5	
0123	Xponder B Pwr On	51:04.0		
0205	1100 bps	56:45.4		1100
0220	Hi Data Rate SCOs Off	56:45.9		
0216	7.35 kc SCO On	56:46.3		
0107	Xmtr Hi Volt Off	57:55.8		
0110	Xmtr Fil Pwr Off	58:13.2		
0130	Xfer Sw B Lo Pwr	58:13.7		
0700	Inertial Mode	15:36:01.7		
0510	AESP Off	16:30:31.7		
0231	Mode 4	30:35.7	4	
0227	Mode 2	35:42.8	2	
0226	Mode 1	39:05.0	1	
0232	ESP Off	42:57.5		
0506	Mode 5	43:02.0	5	
0704	Cruise Mode	17:31:27.8		
0716	Man Lock-On	31:33.8		
0700	Inertial Mode	36:32.5		
0306	SP Sw On, Bypass Off	37:09.6		
	Day 007 – DSS 51			
0510	AESP Off	18:23:13.3		
0231	Mode 4	23:19.8	4	
0227	Mode 2	31:26:3	2	
0226	Mode 1	35:54.3	1	
0232	ESP Off	38:39.8		
0506	Mode 5	38:46.8	5	
0704	Cruise Mode	19:09:42.7		
0716	Man Lock-On	09:53.2		
	Day 007 – DSS 11			
0510	AESP Off	21:27:19.3		
0231	Mode 4	27:25.8	4	1100

Table 4-3 (continued)

Command Number	Description	GMT, hr:min:sec	Telemetry Mode	Bit Rate
0227	Mode 2	21:35:51.1	2	1100
0226	Mode 1	39:37.4	1	
0232	ESP Off	43:07.4		
0506	Mode 5	43:13.9	5	
0220	33, 7.35, 3.9 kc SCOs Off	45:02.2		
0221	Gyro Spd Sig Pro On	45:07.2		
0222	Next Gyro	46:11.4		
0222	Next Gyro	47:14.4		
0222	Next Gyro	48:24.9		
0223	Gyro Spd Sig Pro Off	49:07.4		
0216	7.35 kc SCO On	49:12.9		
0510	AESP Off	22:46:40.1		
0231	Mode 4	46:45.6	4	
0227	Mode 2	48:57.1	2	
0226	Mode 1	51:08.1	1	
0105	Xmtr B Fil Pwr On	57:33.4		
0127	Xfer Sw B Hi Pwr	23:02:02.4		
0106	Xmtr Hi Volt On	02:02.9		
0220	37, 7.35, 3.9 kc SCOs Off	02:39.9		
0217	33 kc SCO On	02:40.4		
0206	4400 bps	02:40.9		4400
3617	Interlock	08:04.4		
M0020	Magnitude (16 BCD) (-3.1 degrees)	08:04.9		
0714	Sun and Roll	18:28.0		
0710	Pos Angle Maneuver	19:00.9		
3617	Interlock	19:01.4		
M2212	Magnitude (586 BCD) (+117.1 degrees)	19:01.9		
0713	Yaw	21:13.3		
0521	Prop S-Gage Pwr On	26:49.6		
0700	Inertial Mode	26:50.1		
0720	Reset – Set VI Outputs	27:34.9		
0604	AMR Htr Off	27:45.2		
0613	VL2 FT2 Ther Pwr Off	27:45.7		
0616	VL1 OT2 Ther Pwr Off	27:46.2		
0621	VL3 OT3 Ther Pwr Off	27:46.7		
3617	Interlock	27:47.2		
0605	Unlk Roll Act, Press VPS	27:47.7		
0727	FC T-φ Pwr On	28:39.2		
3617	Interlock	29:20.9		
M0322	Magnitude (114 BCD) (11.35 sec.)	29:21.4		
3617	Interlock	30:08.9		
0721	Vernier Ignition	30:09.4		4400

Table 4-3 (continued)

Command Number	Description	GMT, hr:min:sec	Telemetry Mode	Bit Rate
0735	Emer Vernier Eng Off	23:30:22.9	1	4400
0735	Emer Vernier Eng Off	30:25.4		
0737	FC T-φ Pwr Off	30:42.9		
0737	FC T-φ Pwr Off	30:45.4		
0522	Prop S-Gage Pwr Off	31:03.2		
0516	TD S-Gage Pwr Off	31:03.7		
0232	ESP Off	31:34.2		
0506	Mode 5	31:39.2	5	
0611	VL2 Ther Pwr On	32:33.9		
0614	VL1 Ther Pwr On	32:34.4		
0617	VL3 Ther Pwr On	32:34.9		
0624	AMR Htr On	32:35.4		
3617	Interlock	33:29.7		
M2212	Magnitude (586 BCD) (-117.1 degrees)	33:30.2		
0713	Yaw	34:10.7		
0704	Cruise Mode	40:39.2		
0716	Man Lock-On	41:07.7		
0510	AESP Off	43:31.6		
0227	Mode 2	43:37.6	2	
0231	Mode 4	45:40.2	4	
0232	ESP Off	48:08.2		
0506	Mode 5	48:13.2	5	
0205	1100 bps	48:58.6		1100
0220	Hi Data Rate SCOs Off	48:59.1		
0216	7.35 kc SCO On	48:59.6		
0107	Xmtr Hi Volt Off	51:18.9		
0110	Xmtr Fil Pwr Off	51:25.4		
0130	Xfer Sw B Lo Pwr	51:26.1		
	Day 008 – DSS 11			
0700	Inertial Mode	00:04:12.0	5	
0510	AESP Off	01:31:55.5		
0231	Mode 4	32:01.0	4	
0227	Mode 2	37:26.6	2	
0226	Mode 1	38:24.6	1	
0232	ESP Off	40:59.9		
0506	Mode 5	41:05.9	5	
0704	Cruise Mode	02:42:58.2		
0716	Man Lock-On	43:08.5		
0702	Sun Acq Mode On	48:54.6		1100

Table 4-3 (continued)

Command Number	Description	GMT, hr:min:sec	Telemetry Mode	Bit Rate
		Day 008 – DSS 42		
0716	Man Lock-On	06:02:42.2	5	1100
0700	Inertial Mode	06:23.2		
0510	AESP Off	48:45.7		
0231	Mode 4	49:00.3	4	
0227	Mode 2	51:03.3	2	
0226	Mode 1	54:26.0	1	
0232	ESP Off	56:10.3		
0506	Mode 5	56:16.3	5	
0704	Cruise Mode	08:36:49.6		
0716	Man Lock-On	37:05.1		
0510	AESP Off	11:52:04.3		
0231	Mode 4	52:11.7	4	
0227	Mode 2	55:49.2	2	
0226	Mode 1	12:00:23.7	1	
0232	ESP Off	03:44.7		
0506	Mode 5	03:51.2	5	
		Day 008 – DSS 51		
0700	Inertial Mode	14:02:22.2		
0510	AESP Off	16:00:37.3	5	
0231	Mode 4	00:45.3	4	
0227	Mode 2	05:59.3	2	
0226	Mode 1	09:09.2	1	
0232	ESP Off	13:16.5		
0506	Mode 5	13:24.7	5	
		Day 008 – DSS 61		
0704	Cruise Mode	17:14:33.0		
0716	Man Lock-On	14:41.0		
		Day 008 – DSS 51		
0510	AESP Off	19:09:41.7		
0231	Mode 4	09:50.2	4	
0227	Mode 2	13:24.7	2	
0226	Mode 1	17:47.7	1	
0232	ESP Off	23:50.1		
0506	Mode 5	23:58.8	5	
0615	OT2 Ther Pwr On	20:04:58.1		1100

Table 4-3 (continued)

Command Number	Description	GMT, hr:min:sec	Telemetry Mode	Bit Rate
		Day 008 – DSS 61		
0510	AESP Off	21:55:27.8	5	1100
0231	Mode 4	55:34.3	4	
0227	Mode 2	58:03.0	2	
0226	Mode 1	59:55.5	1	
0232	ESP Off	22:01:37.3		
0506	Mode 5	01:44.3	5	
		Day 009 – DSS 11		
0510	AESP Off	01:19:29.0	5	
0231	Mode 4	19:36.0	4	
0227	Mode 2	21:50.5	2	
0226	Mode 1	24:00.5	1	
0232	ESP Off	26:11.6		
0506	Mode 5	26:19.0	5	
0700	Inertial Mode	03:05:44.9		
0704	Cruise Mode	05:34:24.3		
0716	Man Lock-On	34:33.8		
		Day 009 – DSS 42		
0510	AESP Off	06:11:36.1		
0231	Mode 4	11:44.5	4	
0227	Mode 2	14:11.0	2	
0226	Mode 1	16:45.2	1	
0232	ESP Off	19:09.0		
0506	Mode 5	19:15.5	5	
0700	Inertial Mode	07:16:24.4		
0704	Cruise Mode	09:48:32.5		
0716	Man Lock-On	48:39.0		
0510	AESP Off	10:59:41.0		
0231	Mode 4	59:48.9	4	
0227	Mode 2	11:06:18.4	2	
0226	Mode 1	09:15.4	1	
0232	ESP Off	12:24.1		
0506	Mode 5	12:30.9	5	
		Day 009 – DSS 51		
3737	Interrupt	13:49:43.4	5	
3737	Interrupt	59:48.6		
0700	Inertial Mode	14:00:05.8		
0411	Comp A Htr Pwr On	00:20.6		1100

Table 4-3 (continued)

Command Number	Description	GMT, hr:min:sec	Telemetry Mode	Bit Rate
0510	AESP Off	14:14:01.1	5	1100
0231	Mode 4	14:10.6	4	
0227	Mode 2	18:23.6	2	
0226	Mode 1	21:55.6	1	
0232	ESP Off	24:41.1		
0506	Mode 5	24:50.1	5	
	Day 009 – DSS 61			
0704	Cruise Mode	17:04:12.9		
0716	Man Lock-On	04:25.3		
	Day 009 – DSS 51			
0510	AESP Off	18:06:51.4		
0231	Mode 4	07:00.4	4	
0227	Mode 2	11:10.4	2	
0226	Mode 1	14:37.9	1	
0232	ESP Off	19:11.9		
0506	Mode 5	19:20.9	5	
1136	Sur Camera ETC On	19:46.4		
0503	550 bps	19:55:16.1		550
0204	Coast Phase Clock Rates	55:30.6		
0220	33, 7.35 3.9 kc SCOs Off	55:41.1		
0215	3.9 kc SCO On	55:49.6		
0510	AESP Off	20:58:08.9		
0231	Mode 4	58:17.9	4	
0227	Mode 2	21:03:38.9	2	
0226	Mode 1	05:22.9	1	
0232	ESP Off	07:44.8		
0506	Mode 5	07:54.3	5	
	Day 009 – DSS 11			
0136	Comp C Temp Cont On	22:27:23.7		
3503	Alpha Scat Htr Pwr On	31:59.6		
0413	Comp A Htr Pwr Off	44:03.7		
0510	AESP Off	47:50.0		
0231	Mode 4	47:57.5	4	
0227	Mode 2	49:48.0	2	
0226	Mode 1	53:04.0	1	
0232	ESP Off	58:00.4		
0506	Mode 5	58:08.4	5	
0220	33, 7.35, 3.9 kc SCOs Off	59:16.9		
0221	Gyro Spd Sig Pro On	22:59:22.4		550

Table 4-3 (continued)

Command Number	Description	GMT, hr:min:sec	Telemetry Mode	Bit Rate
0222	Next Gyro	23:00:07.9	5	550
0222	Next Gyro	00:30.9		
0222	Next Gyro	01:02.4		
0223	Gyro Spd Sig Pro Off	01:51.9		
0215	3.9 kc SCO On	02:00.9		
0124	Xpdr Pwr Off	04:26.4		
0123	Xpdr B Pwr On	06:08.4		
1133	Sur Camera VTC On	54:48.1		
0507	Mode 6	59:11.0	6	
	Day 010 – DSS 11			
0510	AESP Off	00:01:18.5		
0231	Mode 4	01:26.5	4	
0105	Xmtr B Fil Pwr On	03:12.5		
0127	Xfer Sw B Hi Pwr	05:55.0		
0106	Xmtr Hi Volt On	05:55.5		
0127	Xfer Sw B Hi Pwr	07:18.5		
0106	Xmtr Hi Volt On	07:23.0		
0220	33, 7.35, 3.9 kc SCOs Off	08:02.0		
0216	7.35 kc SCO On	08:02.5		
0205	1100 bps	08:03.0		1100
0214	Sum Amps Off	08:41.5		
0211	Phase Sum Amp B On	08:42.0		
0227	Mode 2	09:13.0	2	
0232	ESP Off	11:32.5		
0232	ESP Off	12:21.5		
0506	Mode 5	12:32.5	5	
0521	Prop S-Gage Pwr On	18:28.7		
0515	TD S-Gage Pwr On	19:03.4		
0517	TD S-Gage D-Ch On	19:03.9		
0124	Xpdr Pwr Off	21:14.9		
3737	Interrupt	21:45.4		
0124	Xpdr Pwr Off	21:51.4		
0710	Pos Angle Maneuver	22:56.2		
3617	Interlock	23:23.4		
M1423	Magnitude (403 BCD) (+80.5 degrees)	23:23.9		
0714	Sun and Roll	27:14.2		
3617	Interlock	30:28.8		
M1701	Magnitude (481 BCD) (+96.1 degrees)	30:29.3		
0713	Yaw	35:49.8		
0700	Inertial Mode	39:45.7		
3617	Interlock	39:45.9		1100

Table 4-3 (continued)

Command Number	Description	GMT, hr:min:sec	Telemetry Mode	Bit Rate
M0223	Magnitude (83 BCD) (-16.5 degrees)	00:39:46.4	5	1100
0711	Roll	41:06.9		
0207	Pre Sum Amp On	42:32.8		
0723	Reset Nom Thr Bias	43:39.4		
3617	Interlock	45:09.4		
M0130	Magnitude (56 BCD) (2.775 seconds)	45:09.9		
0507	Mode 6	50:09.7	6	
0720	Reset Set IV Outputs	50:55.2		
3617	Interlock	56:10.6		
0724	Retro Seq Mode On	56:11.1		
0613	VL2 FT2 Ther Pwr Off	56:25.7		
0616	VL1 OT2 Ther Pwr Off	56:27.7		
0621	VL3 OT3 Ther Pwr Off	56:28.7		
1134	Sur Camera VTC Off	56:29.7		
1137	Sur Camera ETC Off	56:30.2		
0604	AMR Htr Off	56:30.7		
0135	Comp C Temp Cont Off	56:31.2		
3504	Alpha Scat Htr Off	56:31.7		
0625	AMR Pwr On	57:33.7		
0727	FC T-φ Pwr On	58:33.7		
0626	Enable AMR	01:00:33.7		
0730	Emer AMR Signal	02:13.2		
0730	Emer AMR Signal	02:14.2		
0737	FC T-φ Pwr Off	06:12.1		
0737	FC T-φ Pwr Off	06:14.1		
3617	Interlock	06:35.8		
0630	RADVS Pwr Off	06:36.3		
3617	Interlock	06:37.3		
0630	RADVS Pwr Off	06:37.8		
3617	Interlock	06:38.3		
0311	All FC Pwr Off	06:38.8		
3617	Interlock	06:39.3		
0311	All FC Pwr Off	06:39.8		
0506	Mode 5	07:44.2	5	
0510	AESP Off	08:56.2		
0227	Mode 2	09:03.6	2	
0516	TD S-Gage Pwr Off	10:49.8		
0520	TD S-Gage D-Ch Off	11:00.1		
0522	Prop S-Gage Pwr Off	11:05.6		1100

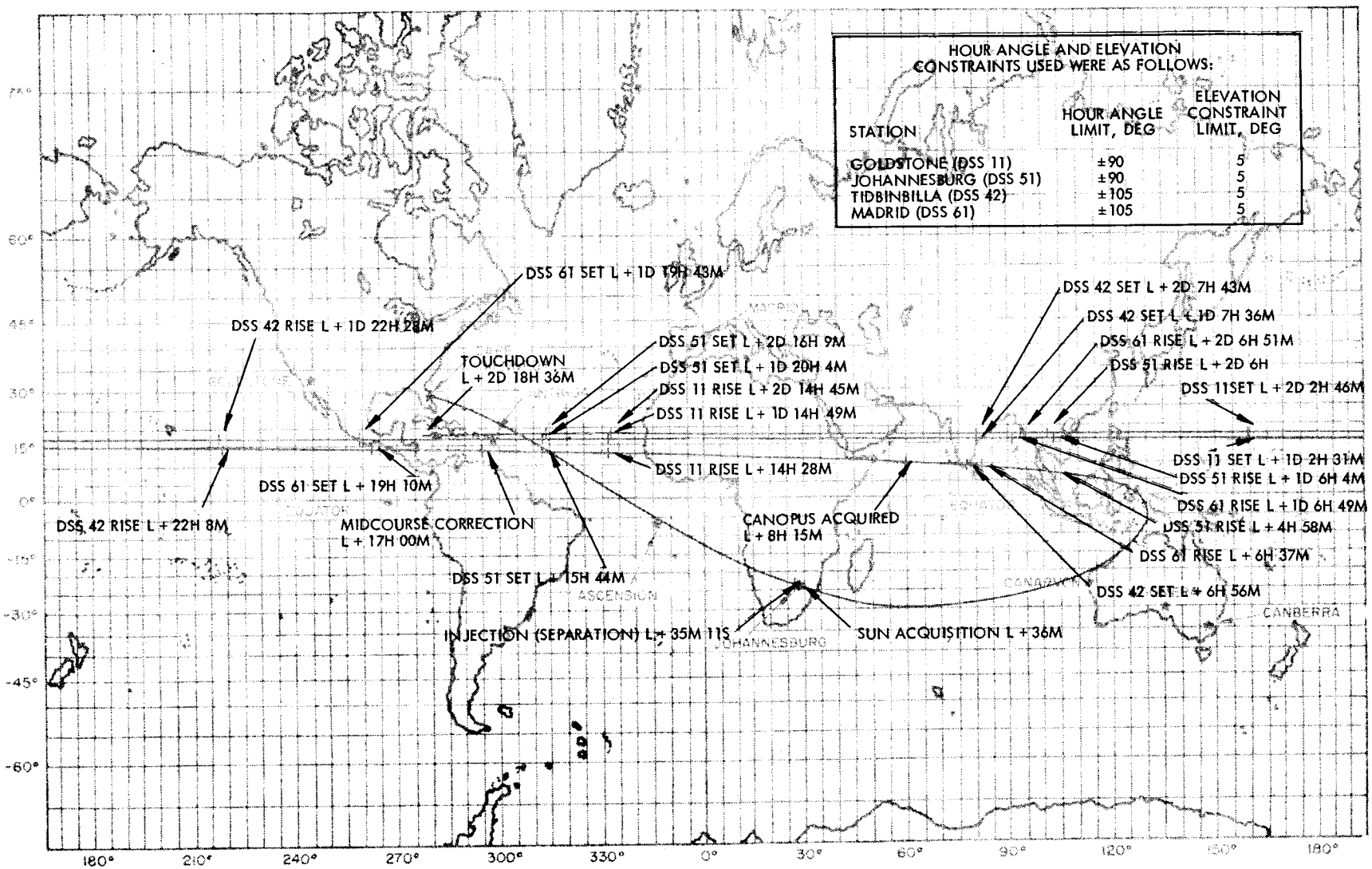

Figure 4-1. Surveyor VII Earth Track

88014-20(U)

4.1.2 Prelaunch Countdown

No anomalies were noted during countdown. The launch was rescheduled 35 minutes later to provide more optimum ship tracking.

4.1.3 Launch, Injection, and Separation

The parking orbit boost phase was normal, with the Atlas roll and pitch programs and the normal opening and closing of the spacecraft inertia switch being confirmed by spacecraft telemetry. Figure 4-2 shows the major events of the trajectory through separation as seen in profile. Table 4-4 contains Atlas/Centaur mark events. Subsequent to injection and just prior to its separation from the spacecraft, the Centaur issued the preprogrammed commands "extend landing gears," "extend omni antennas," and "transmitter high power on" all of which are verified by spacecraft telemetry. Separation of Centaur and Surveyor occurred immediately thereafter. The poor quality of telemetry at separation prevented effective monitoring of separation transients.

Following separation, solar panel stepping was initiated, the cold gas jets were enabled, and the roll-yaw sequence to acquire the sun was initiated. Verification of solar panel axis stepping to the transit position, A/SPP roll axis stepping to the transit position, and achievement of sun lockon were finally accomplished.

4.1.4 DSIF Acquisition

At 007:07:20 GMT, the spacecraft became visible to DSS 42 (Tidbinbilla), which achieved one-way lock at this time. At 007:07:28 GMT, the acquisition was completed when two-way lock was established between DSS 42 and the spacecraft.

The first ground-controlled sequence (initial spacecraft operations) was initiated at L+61M46S by commanding off the transmitter high voltage and filament power. In addition, commands were sent to the spacecraft to turn off other equipment required only for the launch-to-DSIF-acquisition phase (e.g., solar panel deployment logic off and analog-to-digital isolation amplifier off); to seat the solar panel and roll axis locking pins securely (i.e., by rocking the axes back and forth); to switch from the 550-bps, low modulation index mode to the 1100-bps, normal modulation index mode; and to interrogate telemetry commutator modes so that the overall condition of the spacecraft could be assessed. All spacecraft responses to commands were normal.

4.1.5 Coast Phase I Including Canopus Acquisition

The star verification acquisition sequence was initiated at approximately 007:14:18:28 with the spacecraft being commanded to high power and 4400 bps, followed by transponders off, manual delay mode on, and positive angle maneuver. Sun and roll were executed at 007:14:24:05 GMT, Canopus, earth, moon, Alpha C. Venaticoru, Mizar, Gamma U. Minoris, Kochab, and

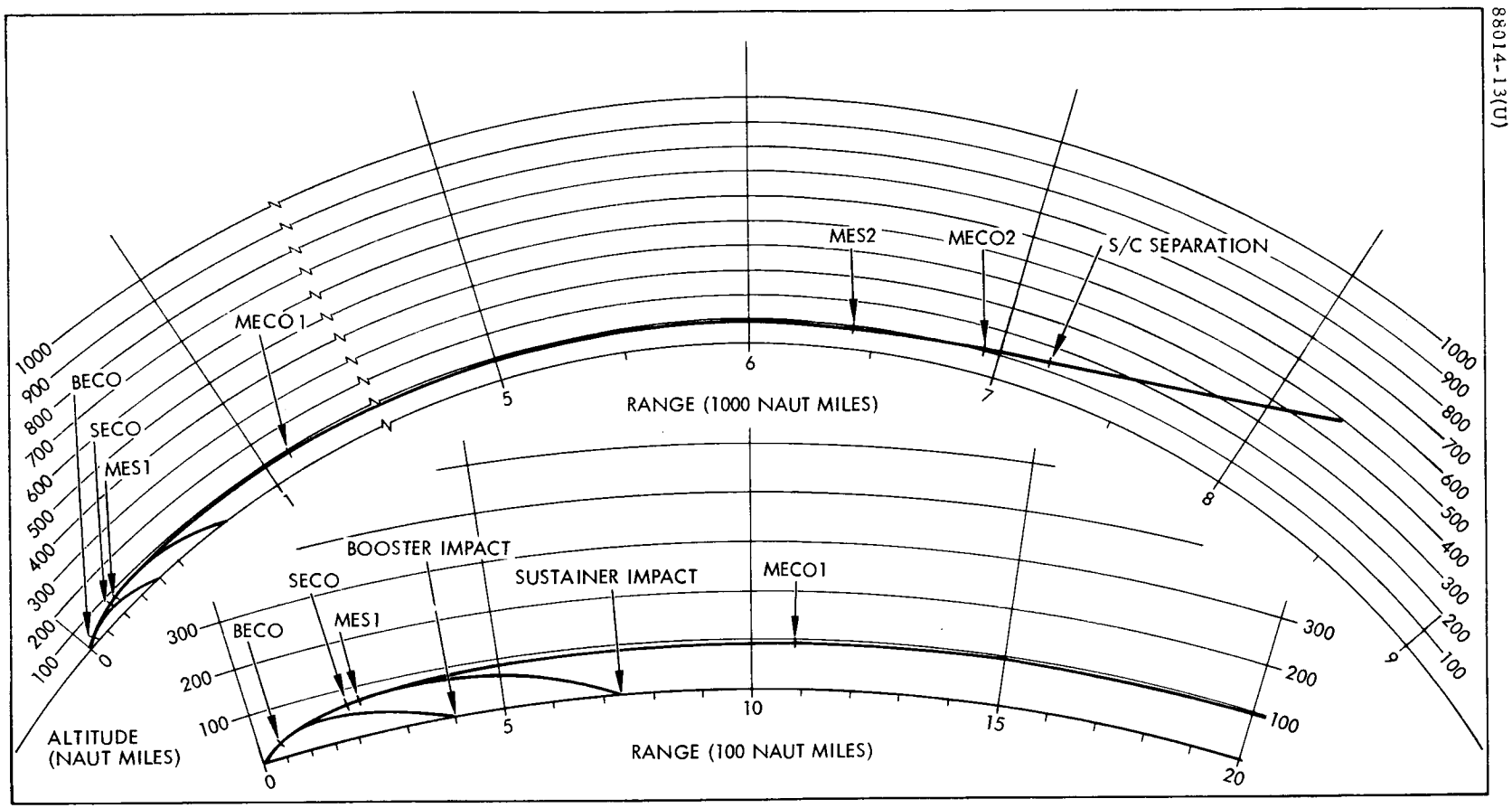

Figure 4-2. AC-15 Launch Phase Trajectory Profile

TABLE 4-4. MARK EVENTS

Mark Number	Event	Actual Time, GMT, hr:min:sec	Actual Time, seconds	Nominal Time, seconds
	Liftoff (2-inch motion)	06:30:00.545	L + 0.0	L + 0.0
1	Atlas BECO	06:32:33.995	152.47	153.5
2	Atlas booster engine jettison	06:32:37.095	155.54	156.6
3	Centaur insulation panel jettison	06:33:18.055	197.51	198.5
4	Centaur nose fairing jettison	06:33:47.055	226.51	228.5
5	Atlas SECO and VECO	06:34:09.015	248.47	248.2
6	Atlas/Centaur separation	06:34:11.045	250.50	250.2
7	Centaur MES1	06:34:22.055	261.57	259.7
8	Centaur MECO1	06:39:53.075	592.53	579.2
9	100-pound thrust on	06:39:54.055	593.51	579.2
10	100-pound thrust off	Not available	–	655.6
11	6-pound thrust on	06:41:10.995	670.45	655.6
12	100-pound thrust on	Not available	–	1895.32 S - 216.0
13	Centaur MES2 engine C2	07:02:21.015	1940.47	1935.32 176.0
14	Centaur MES2 engine C1	07:02:21.015	1940.47	1935.32 176.0
15	Centaur MECO2	07:04:15.055	2054.51	2049.02 63.1
16	Extend landing gear	07:04:36.075	2075.53	2069.32 42.0
17	Unlock omnidirectional antenna	07:04:44.075	2083.53	2079.82 31.5
18	Surveyor high power transmitter on	07:05:00:005	2099.46	2100.32 11.0
19	Centaur/Surveyor electrical discount	Not available	–	2105.82 5.5
20	Spacecraft separate (injection)	07:05:16.055	2115.51	2111.32 S + 0.0
21	Begin Centaur turn around maneuver	07:05:20.005	2119.46	2116.32 5.0
22	Start Centaur lateral thrust	07:06:30.005	2189.55	2156.32 45.0
23	End Centaur lateral thrust	Not available	–	2176.32 65.0
24	Start Centaur tank blowdown	07:09:16.005	2355.46	2351.32 240.0
25	End Centaur tank blowdown	07:13:26.085	2605.54	2601.32 490.0
26	Power changeover switch	07:15:06.055	2705.51	2701.32 590.0

Caph/Shedar/Zeta Cassiopeiae were identified from the start of the roll. The Canopus lockon signal did not stay on while Canopus passed through the field of view. Lockon on was achieved by stopping the spacecraft roll (sun mode on commanded at 007:14:44:59) followed by manual lockon at 007:14:47:32 GMT. Thereafter, the transponder was commanded on, 1100-bps established, and the spacecraft returned to low power mode. The spacecraft systems continued to operate normally. Manual lockon was the only transit anomaly.

4.1.6 Midcourse Correction and Coast Phase II

The midcourse velocity correction was executed at 007:23:30:09.4 for 11.3 seconds after successful premidcourse roll (-3.1 degrees) and yaw (+117.1 degrees) maneuvers. The attitude rotations were initiated at limit cycle nulls to further minimize pointing errors. Following successful execution of the midcourse correction, the postmidcourse maneuver (yaw only) was performed in a nominal manner. Cruise mode on was commanded at 007:23:40:39 and manual lockon at 007:23:41:07.

In addition to normal spacecraft operations in the second coast phase, nine gyro drift checks were performed during transit to provide accurate gyro rates for terminal operations planning. The gyro drift rates provided prior to terminal descent were: roll (+0.65 deg/hr), pitch (+0.2 deg/hr), and yaw (0.0 deg/hr).

The retro engine temperature at retro ignition was predicted (54°F), and a resulting engine burn time of 42.78 seconds (from ignition to the 3500-pound thrust level) was provided.

4.1.7 Terminal Descent Phase

Terminal descent closely followed design and predicted performance. An initial roll of +80.5 degrees, followed by a yaw of +96.1 degrees, and then a final roll of -16.5 degrees, aligned the retro engine thrust axis to the desired direction. The three attitude maneuvers, as well as other preretro ignition spacecraft operations (e.g., loading the proper altitude mark to vernier ignition delay quantity – -2.775 seconds, establishing the retro sequence mode for ensuring that the desired automatic flight control sequences would occur in response to the altitude radar mark, establishing the proper vernier engine thrust level for the retro burning phase, turning on flight control thrust phase power, etc.), were executed on schedule. Retro separation was smooth, vernier descent contour acquisition was obtained, and vernier descent control was normal. Event times occurred at the proper time (Table 4-1). The engines were turned off automatically by the 14-foot mark, and a soft landing was verified from the retention of the communication link and continued nominal spacecraft performance, and later by the touchdown strain gage data.

Strain gage data indicated that touchdown occurred at approximately 010:01:05:37.620 GMT, with leg 1 touching the surface first, followed by legs 2 and 3, in that order. The peak loads experienced by legs 1, 2, and 3 were approximately 1650, 1840, and 1360 pounds, respectively. These levels

are indicative of a landing velocity of approximately 12.0 fps on a surface with a 5-psi static bearing strength and a slope of approximately 3.0 degrees.

4.1.8 Initial Lunar Operation

After the initial engineering assessment, a 200-line television survey was conducted. The first 200-line picture was obtained at 010:01:47. The initial sun and earth acquisition was completed at 010:03:21. The spacrcraft was then configured for 600-line television, the first such picture being received at 010:03:41.

The primary method of Surveyor VII attitude determination on lunar day 1 was based on a combination of television, A/SPP, and FPAC data. Attitude determination is presented in Figure 4-3 for the first and second lunar days. Change in attitude is due to landing gear lock failures as the spacecraft entered the first lunar night (subsection 5.10.2). The roll orientation computed (20.65 degrees) in the terminal descent reconstruction (subsection 5.12.4.7) compares very favorably with that presented in Figure 4-3a (20.23 degrees between spacecraft +X axis and selenographic east).

4.2 RELIABILITY ANALYSIS

4.2.1 Surveyor VII Reliability Estimates

4.2.1.1 System and Subsystem Reliability

The final reliability point estimate for Surveyor VII is 0.67. This estimate is based upon Surveyor VII flight and systems test data and applicable Surveyor I through VI system test and flight experience. Final reliability point estimates for each subsystem are given in Table 4-5.

4.2.1.2 Summary of Data Base for Surveyor VII Reliability Estimates

The primary source of data for reliability estimates is the operating time and cycles experienced by Surveyor VII units during systems tests and flight and the accumulated reliability relevant failure data provided by Trouble and Failure Reports. Data from Surveyor I through VI test and flight experience are included where there are no significant design differences between the units. A failure is considered relevant if it affects equipment reliability and could occur during a mission. Relevance of failures is based upon a joint Reliability-Systems Engineering decision. In addition, relevant failures are weighted as follows:

1.0 Critical – Would normally cause a safety hazard, mission abort, or failure of mission objective.

0.6 Major – Would significantly degrade system performance but not cause mission abort or failure.

0.1 – Would not significantly affect ability of system to function as designed.

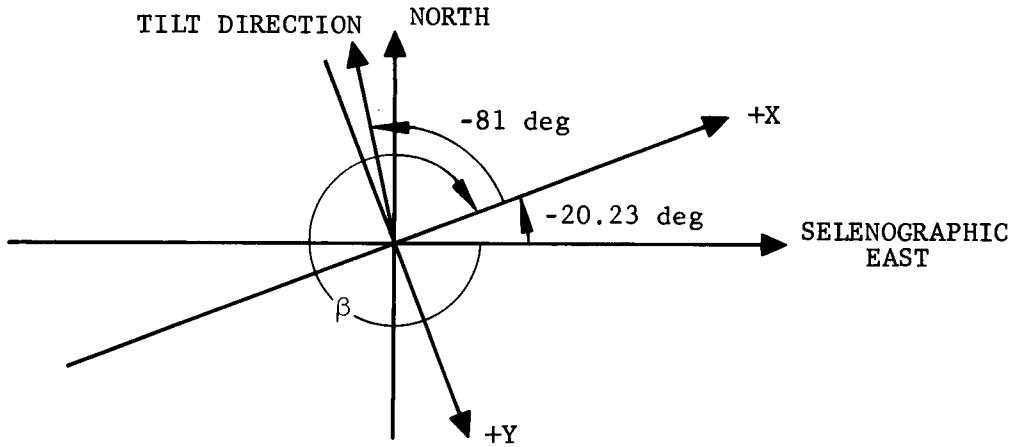

Magnitude of tilt = 3.17 degrees, direction = 279 degrees
X_{tilt} = 0.50 degree
Y_{tilt} = -3.13 degrees

Roll orientation (X axis clockwise from selenographic east)
β = 339.77 degrees

a) Touchdown on First Lunar Day

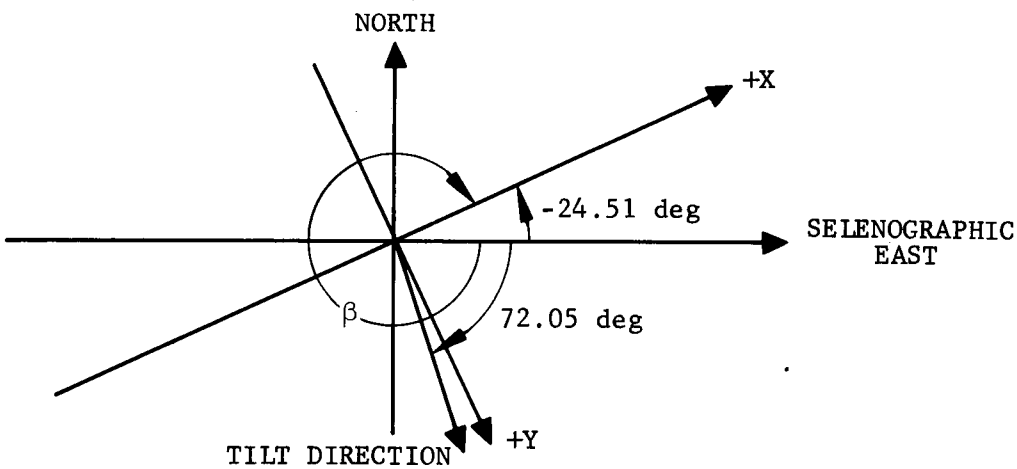

Magnitude of tilt = 5.73 degrees, direction = 72.05 degrees
X_{tilt} = 1.86 degrees
Y_{tilt} = 5.42 degrees

Roll orientation (X axis clockwise from selenographic east)
β = 335.49 degrees

b) Revival on Second Lunar Day

Figure 4-3. Spacecraft Attitude

TABLE 4-6. SUMMARY OF DATA BASE FOR SURVEYOR VII RELIABILITY ESTIMATES

Units	Total Weighted Relevant Failures	Test Time, hours or cycles	Reliability
Receiver-decoder select	0	11,169.9	1.0
Central decoder	0.6	11,169.9	0.995
Subsystem decoder	0	55,849.5	1.0
Engineering signal processor	1.2	3,365.7	0.991
Auxiliary engineering signal processor	2.5	4,880.1	0.968
Signal processing auxiliary	0	1,086.0	1.0
Central signal processor	0.7	10,229.5	0.994
Low data rate auxiliary	1.0	2,950.1	0.998
Omnidirectional antenna	0	7,260.9	1.0
Omnidirectional mechanisms	0	922 cycles	1.0
Diplexer	0.6	20,084.5	0.997
Transmitter	2.8	8,527.5	0.972
Low pass filter	0	21,015.8	1.0
Telemetry buffer amplifier	0	19,296.3	1.0
Receiver	1.2	21,490.9	0.995
Transponder	0	3,134.4	1.0
RF transfer switch	0	8,527.5	1.0
SPDT switch	0	8,527.5	1.0
Thermal sensors	0.4	277,177.6	0.993
Passive controls	0	4,949.6	1.0
Thermal control and heater assembly	0.6	5,739.6	0.982
Thermal switch	0.1	33,861.0	0.996
Thermal shell	0	9,899.2	1.0
Space frame	0	25 mission cycles	1.0
Landing gear structure	0	184 mission cycles	1.0

Table 4-6 (continued)

Units	Total Weighted Relevant Failures	Test Time, hours or cycles	Reliability
Compartment A thermal tray	0	25 mission cycles	1.0
Compartment B thermal tray	0	25 mission cycles	1.0
Wiring harness			
Wiring harness separation squibs	0	1,955.7	1.0
Wiring harness compartment A	1.0	5,233.8	0.984
Wiring harness compartment B	0	8,900.7	1.0
Wiring harness basic bus 1	1.0	11,437.9	0.993
Wiring harness basic bus 2	1.0	11,437.9	0.993
Wiring harness A/SPP	1.4	2,680.8	0.957
Wiring harness RF cabling	0	11,168.8	1.0
Wiring harness retro motor	0	1,072.4	1.0
Retro-rocket release	0	590 cycles	1.0
Engineering mechanism auxiliary	0.2	10,455.1	0.998
Antenna/solar panel positioner*			
Roll	0	320,127 cycles	1.0
Solar	0.2	260,736 cycles	0.999
SS and A device*	0	317 actuations	1.0
Retro-rocket system	0	19 mission cycles	1.0
Solar panel	0	1,017.4	1.0
Battery charge regulator	0.6	4,059.4	0.987
Boost regulator	1.4	11,572.6	0.990
Main power switch	0	10,451.1	1.0
Main battery	0	6,157.7	1.0
Flight control sensor group	3.2	5,276.9	0.950
Altitude marking radar	1.2	171.4	0.993

Table 4-6 (continued)

Units	Total Weighted Relevant Failures	Test Time, hours or cycles	Reliability
RADVS			
Signal data converter	3.4	616.8	0.994
Klystron power supply modulator	3.6	614.6	0.993
Altimeter/velocity sensor antenna	2.6	614.6	0.995
Velocity sensor antenna	2.2	616.6	0.996
Waveguide	0	595.2	1.0
Roll actuator	0	254.5	1.0
Attitude jet system	0.2	670,125 cycles	0.998
Pin puller*	0	16,148 cycles	1.0
Pin puller cartridge*	0	16,148 equivalent firings	1.0
Helium tank and valves assembly*	1.2	39 mission cycles	0.969
Propellant tank assembly*			
Fuel tank	0	76 mission cycles	1.0
Oxidizer tank	0.6	88 mission cycles	0.994
Lines and fittings	0.1	114 mission cycles	0.999
Thrust chamber assembly (JPL-supplied)			
Propellant shutoff valve	0	7,980 cycles	1.0
Throttle valve	2.0	704 mission cycles	0.997
Thrust chamber and injector assembly	1.0	269 cycles	0.996
Helium release valves*	0	19 firings	1.0
Valve cartridge*	0	16,067 equivalent firings	1.0
Shock absorber*	0	409 cycles	1.0
Crushable structure*	0	79 cycles	1.0
System**	1.1	935.8	0.905

*Includes unit flight acceptance and type approval test data.
**Based on main power switch operating time in system test.

TABLE 4-7. TIME/CYCLE/RELIABILITY FOR SURVEYORS I THROUGH VI

Unit	Time, hours, or Cycles						Failures						Reliability					
	I	2	III	4	V	VI	I	2	III	4	V	VI	I	2	III	4	V	VI
Receiver decoder select	2,137.3	4,073.4	5,602.1	6,776.5	8,015.9	9,849.0	0	0	0	0	0	0	1.0	1.0	1.0	1.0	1.0	1.0
Central decoder	2,137.3	4,073.4	5,602.1	6,776.5	8,015.9	9,848.0	0.6	0.6	0.6	0.6	0.6	0.6	0.972	0.987	0.990	0.992	0.994	0.995
Subsystem decoder	10,686.5	20,367.0	28,010.5	33,882.5	40,079.5	49,245.0	0	0	0	0	0	0	1.0	1.0	1.0	1.0	1.0	1.0
Engineering signal processor	691.3	1,300.5	1,711.8	1,954.2	2,360.0	2,980.0	2.2	2.3	0.8	1.1	0.3	0.3	0.752	0.861	0.960	0.953	0.997	0.998
Auxiliary engineering signal processor	838.0	1,478.2	2,290.4	2,862.4	3,472.1	4,268.6	1.0	2.4	2.8	4.8	4.1	2.5	0.893	0.870	0.901	0.866	0.928	0.964
Signal processing auxiliary	292.7	461.8	530.4	620.7	762.0	945.0	0	0	0	0	0	0	1.0	1.0	1.0	1.0	1.0	1.0
Central signal processor	1,828.3	3,133.0	4.661.7	5,836.1	7,075.5	8,908.6	0.7	1.4	0.7	0.7	0.7	0.7	0.960	0.963	0.990	0.994	0.992	0.993
Low data rate auxiliary	449.9	847.1	1,484.3	1,637.9	1,938.3	2,629.1	0	0	0.1	1.1	1.0	1.0	1.0	1.0	0.994	0.944	0.997	0.998
Omnidirectional antenna	716.7	1,068.4	2,075.4	2,310.6	2,632.8	5,707.2	0	0	0	0	0	0	1.0	1.0	1.0	1.0	1.0	1.0
Omnidirectional mechanism	42 cycles	510 cycles	663 cycles	784 cycles	824 cycles	872 cycles	0	0.2	0	0	0	0	1.0	0.999	1.0	1.0	1.0	1.0
Diplexer	2,173.8	5,891.5	8,948.9	11,297.7	13,776.5	17,442.7	0	0	0	0	0	0	1.0	1.0	1.0	1.0	1.0	1.0
Transmitter	1,019.1	2,373.0	3,685.9	4,527.1	5,699.3	7,309.3	2.3	1.0	2.4	1.4	2.5	2.7	0.874	0.961	0.942	0.971	0.964	0.969
Low pass filter	3,176.6	6,822.8	9,880.2	12,229.0	14,707.8	18,374.0	0	0	0	0	0	0	1.0	1.0	1.0	1.0	1.0	1.0
Telemetry buffer amplifier	1,874.4	5,103.3	8,160.7	10,509.5	12,988.3	16,654.5	0	0	0	0	0	0	1.0	1.0	1.0	1.0	1.0	1.0
Receiver	3,580.2	7,297.9	10,355.3	12,704.1	15,182.9	18,849.1	0.2	0.2	0.1	0.1	0.2	0.2	0.995	0.998	0.999	0.999	0.999	0.999
Transponder	529.1	1,153.4	1,663.2	2,054.8	2,467.9	2,822.5	0	0	0	0	0	0	1.0	1.0	1.0	1.0	1.0	1.0
RF Transfer switch	1,019.1	2,373.0	3,685.9	4,527.1	5,699.3	7,309.3	0	0	0	0	0	0	1.0	1.0	1.0	1.0	1.0	1.0
SPDT switch	1,019.1	2,373.0	3,685.9	4,527.1	5,699.3	7,309.3	0	0	0	0	0	0	1.0	1.0	1.0	1.0	1.0	1.0
Thermal sensors	40,953.8	76,038.0	104,180.8	118,431.6	165,065.6	230,232.8	0	0	0	0.1	0.3	0.3	1.0	1.0	1.0	0.997	0.991	0.994
Thermal control and heater assembly	1,455.9	1,591.7	2,359.7	2,664.4	3,011.9	4,813.5	0	0	0	0	0.6	0.6	1.0	1.0	1.0	1.0	0.967	0.979
Thermal switch	14,755.5	26,196.0	35,373.0	4,647.0	10,242.0	22,687.5	0	1.2	1.2	1.2	0.1	0.1	1.0	0.943	0.958	0.973	0.988	0.994
Thermal shell	1,967.4	3,492.8	4,716.4	5,336.0	6,082.0	8,409.4	0	0	0	0	0	0	1.0	1.0	1.0	1.0	1.0	1.0
Spaceframe	8 cycles	11 cycles	16 cycles	18 cycles	22 cycles	24 cycles	0	0	0	0	0	0	1.0	1.0	1.0	1.0	1.0	1.0
Landing gear	21 cycles	139 cycles	160 cycles	166 cycles	178 cycles	181 cycles	0	0	0	0	0	0	1.0	1.0	1.0	1.0	1.0	1.0
Compartment A thermal tray	8 cycles	11 cycles	17 cycles	18 cycles	22 cycles	24 cycles	0	0	0	0	0	0	1.0	1.0	1.0	1.0	1.0	1.0
Compartment B thermal tray	8 cycles	11 cycles	17 cycles	18 cycles	22 cycles	24 cycles	0	0	0	0	0	0	1.0	1.0	1.0	1.0	1.0	1.0
Aux. battery compartment	8 cycles	11 cycles	17 cycles	18 cycles	DNA	DNA	0	0	0	0	-	-	1.0	1.0	1.0	1.0	-	-
Wire harness compartment A	2,587.2	1,868.5	3,332.9	1,174.4	2,413.8	3,912.9	1.0	0	0	1.0	1.0	1.0	0.963	1.0	1.0	0.930	0.965	0.978
Wire harness compartment B	2,587.2	1,868.5	3,332.9	4,507.3	5,746.7	7,579.8	0.1	0	0	0	0	0	0.997	1.0	1.0	1.0	1.0	1.0
Wire harness basic bus 1	2,537.2	4,405.7	5,870.1	7,044.5	8,283.9	10,117.0	0.1	2.1	2.1	3.0	1.0	1.0	0.996	0.960	0.970	0.963	0.990	0.992
Wiring harness basic bus 2	2,537.2	4,405.7	5,870.1	7,044.5	8,283.9	10,117.0	1.0	2.0	1.0	1.0	1.0	1.0	0.962	0.962	0.986	0.988	0.990	0.992
Wiring harness ASPP	1,063.9	1,111.7	1,121.2	1,128.4	1,135.9	2,220.8	0	0	0	0	0.6	1.4	1.0	1.0	1.0	1.0	0.956	0.948
Wiring harness aux. battery	1,129.1	1,333.8	1,440.2	1,482.4	DNA	DNA	0	0	0	0	-	-	1.0	1.0	1.0	1.0	-	-
Wiring harness RF cable	2,601.3	4,227.5	5,601.0	6,775.4	8,014.8	9,847.9	0.1	0	0	0	0	0	0.996	1.0	1.0	1.0	1.0	1.0
Wiring harness retro rocket	1,053.2	1,059.5	1,070.8	1,070.8	1,072.8	1,072.4	0	0	0	0	0	0	1.0	1.0	1.0	1.0	1.0	1.0
Nitrogen lines	1,147.0	1,963.0	2,814.7	3,395.9			0	0	0	0	-	-	1.0	1.0	1.0	1.0	-	-

Table 4-7 (continued)

Unit	Time, hours, or Cycles						Failures						Reliability					
	I	2	III	4	V	VI	I	2	III	4	V	VI	I	2	III	4	V	VI
Retro Rocket release	540 cycles	575 cycles	578 cycles	581 cycles	584 cycles	587 cycles	0	0	0	0	0	0	1.0	1.0	1.0	1.0	1.0	1.0
Engineering Mechanical Aux.	1,576.3	3,358.6	4,887.3	6,061.7	7,301.1	9,134.2	0	0	0	0.2	0.2	0.2	1.0	1.0	1.0	0.998	0.998	0.998
Antenna/solar panel posit.	240,504 cycles	511,506 cycles	482,446 cycles	581,620 cycles	165,831 cycles	427,804 cycles	22.7	1.4	1.4	0.1	0.1	0.2	0.891	0.995	0.995	0.997	0.999	0.999
Separation sensing and arming device	75 cycles	72 cycles	178 cycles	212 cycles	230 cycles	269 cycles	0	0	0	0	0	0	1.0	1.0	1.0	1.0	1.0	1.0
Retro rocket system	13 cycles	14 cycles	15 cycles	16 cycles	17 cycles	18 cycles	0	0	0	0	0	0	1.0	1.0	1.0	1.0	1.0	1.0
Solar panel	375.1	402.7	467.7	529.3	64.0	565.7	0	0	0	0	0	0	1.0	1.0	1.0	1.0	1.0	1.0
Battery charge regulator	1,128.4	3,072.0	4,600.7	5,775.1	1,230.4	2,738.5	0.1	0.7	0.7	0	0	0	0.989	0.980	0.987	1.0	1.0	1.0
Boost regulator	2,457.8	4,476.1	6,004.8	7,179.2	8,418.6	10,251.7	0.8	1.4	1.4	1.4	1.4	1.4	0.968	0.974	0.982	0.984	0.986	0.988
Auxiliary battery control	1,929.3	3,998.0	5,526.7	6,701.1	DNA	-	0	0.6	0.7	0.7	-	-	1.0	0.998	0.998	0.998	-	-
Main power switch	1,475.4	3,354.6	4,883.3	6,057.7	7,297.1	9,130.2	0	0	0	0	0	0	1.0	1.0	1.0	1.0	1.0	1.0
Main battery	1,037.4	1,553.8	2,685.5	3,220.2	3,673.4	5,080.1	1.0	1.0	0	0	0	0	0.882	0.994	1.0	1.0	1.0	1.0
Auxiliary battery	90.7	113,6	248.5	291.3	DNA	-	0.6	0.6	0.6	0.6	-	-	0.880	0.924	0.962	0.967	-	-
Boost regulator input choke	937.2	2,623.9	4,152.6	5,327.0	DNA	-	0	0	0	0	-	-	1.0	1.0	1.0	1.0	-	-
Boost regulator unregulated filter	937.2	2,627.9	4,152.6	5,331.0	DNA	-	0	0	0	0	-	-	1.0	1.0	1.0	1.0	-	-
Flight control sensor group	1,147.2	1,963.2	2,815.1	3,396.5	4,065.5	4,737.3	0	2.0	0	1.8	1.4	2.1	1.0	0.917	1.0	0.956	0.971	0.963
Altitude marking radar	62.9	92.9	106.3	131.9	162.1	166.2	0	0	0	0.1	0.1	0.2	1.0	1.0	1.0	0.999	0.999	0.999
RADVS-signal data converter	595.1	987.1	1,131.7	1,504.4	1,790.0	577.0	6.5	10.3	11.1	13.1	17.9	3.3	0.982	0.989	0.989	0.990	0.989	0.994
Klystron pwr. supply modulator	311.5	725.7	921.0	1,090.5	1,246.3	554.8	5.4	5.9	5.9	6.9	6.9	2.8	0.981	0.991	0.993	0.993	0.994	0.995
Attitude velocity sens. ant.	295.9	522.7	823.9	987.8	1,182.0	554.8	2.2	2.2	4.4	4.4	5.0	2.6	0.992	0.996	0.994	0.995	0.995	0.995
Velocity sensing antenna	266.6	424.1	652.5	955.2	1,142.0	556.8	0	1.6	2.2	2.8	2.8	2.2	1.0	0.996	0.996	0.996	0.997	0.996
RADVS waveguide	194.1	278.0	424.2	530.1	633.7	535.4	0	0	0	0	0	0	1.0	1.0	1.0	1.0	1.0	1.0
Roll actuator	56.6	98.1	148.6	190.5	195.4	222.4	0	0	0	0	0	0	1.0	1.0	1.0	1.0	1.0	1.0
Attitude jet system	147,381 cycles	269,576 cycles	370,756 cycles	444,675 cycles	559,208 cycles	611,556 cycles	0.1	0.1	0.1	0.1	0.2	0.2	0.995	0.998	0.998	0.999	0.998	0.998
Pin pullers	16,071 cycles	16,080 cycles	16,092 cycles	16,101 cycles	16,110 cycles	16,131 cycles	0	0	0	0	0	0	1.0	1.0	1.0	1.0	1.0	1.0
Pin puller cartridge	16,071 cycles	16,429 cycles	16,441 cycles	16,101 cycles	16,110 cycles	16,131 cycles	0	0	0	0	0	0	1.0	1.0	1.0	1.0	1.0	1.0
Helium tank and valve assy.	30 cyc.	33 cyc.	34 cyc.	36 cyc.	37 cyc.	38 cyc.	0	0.1	0.1	0.1	0.7	1.1	1.0	0.997	0.977	0.977	0.981	0.971
Fuel tanks	46 cyc.	49 cyc.	52 cyc.	58 cyc.	64 cycl	70 cyc.	0	0	0	0	0	0	1.0	1.0	1.0	1.0	1.0	1.0
Oxidizer tanks	64 cyc.	67 cyc.	70 cyc.	76 cyc.	82 cyc.	88 cyc.	0	0	0	0.6	0.6	0.6	1.0	1.0	1.0	0.977	0.993	0.993
Lines and fittings	54 cyc.	60 cyc.	66 cyc.	78 cyc.	90 cycl	102 cyc.	0	0	0.1	0.1	0.1	0.1	1.0	1.0	0.998	0.999	0.999	0.999
Propellant shut off valve	7,944 cycles	7,947 cycles	7,953 cycles	7,956 cycles	7,965 cycles	7,971 cycles	0	0	0	0	0	0	1.0	1.0	1.0	1.0	1.0	1.0

Table 4-7 (continued)

Unit	Time, hours, or Cycles						Failures						Reliability					
	I	2	III	4	V	VI	I	2	III	4	V	VI	I	2	III	4	V	VI
Throttle valve	693 cyc.	694 cyc.	697 cyc.	698 cyc.	701 cyc.	704 cyc.	2.0	2.0	2.0	2.0	2.0	2.0	0.997	0.997	0.997	0.997	0.997	0.997
Thrust chamber and injection assembly	255 cyc.	256 cyc.	259 cyc.	260 cyc.	263 cyc.	266 cyc.	0	1.0	1.0	1.0	1.0	1.0	1.0	0.995	0.996	0.996	0.996	0.996
Helium release valve	13 cyc.	14 cyc.	15 cyc.	16 cyc.	17 cyc.	18 cyc.	0	0	0	0	0	0	1.0	1.0	1.0	1.0	1.0	1.0
Valve cartridges	16,061 cycles	16,062 cycles	16,063 cycles	16,064 cycles	16,065 cycles	16,066 cycles	0	0	0	0	0	0	0	1.0	1.0	1.0	1.0	1.0
Shock absorber	391 cyc.	391 cyc.	400 cyc.	400 cyc.	403 cyc.	406 cyc.	0.2	0	0	0	0	0	0.999	1.0	1.0	1.0	1.0	1.0
Crushable structures	61 cyc.	61 cyc.	70 cyc.	70 cyc.	73 cyc.	76 cyc.	0	0	0	0	0	0	1.0	1.0	1.0	1.0	1.0	1.0
System interaction	1,717.1	1,013.2	1,528.7	1,174.4	1,239.4	1,063.5	5.0	0.6	0.6	0.3	0.2	0	0.736	0.949	0.967	0.978	0.986	1.0

TABLE 4-8. SURVEYOR SPACECRAFT RELIABILITY GROWTH

Subsystem	I	2	III	4	V	VI	VII
Telecommunications	0.925	0.944	0.965	0.929	0.987	0.991	0.992
Vehicle and mechanism	0.816	0.868	0.907	0..854	0..853	0.880	0.899
Propulsion	0.991	0.991	0.968	0.947	0.934	0.927	0.927
Electrical power	0.869	0.958	0.935	0.953	0.985	0.988	0.977
Flight control	0.952	0.889	0.971	0.931	0.945	0.940	0.922
Systems interaction factor	0.736	0.949	0.967	0.978	0.986	1.0	0.904
Spacecraft	0.456	0.658	0.745	0.653	0.723	0.751	0.674

interaction of all spacecraft units. For convenience, the spacecraft is referred to at three basic levels: systems, set, and control item or unit. Reliability is defined as follows:

> Reliability of the A-21 Surveyor spacecraft for the flight and landing phase is the probability that the spacecraft equipment will operate successfully as required from launch through soft landing. Successful soft landing is assumed if two-way communications is established and there is no apparent damage to spacecraft equipment required to support intended lunar operations.

In the derivation of the model, the following general assumptions were made:

1) No human error will occur during the mission which will cause failure.

2) All equipment inspection and test procedures are perfect and comprehensive, and all equipment will be used only in applications within the boundaries of its design parameters.

3) Every performance characteristic is verified up to the instant of no return in launch operations, and the launch will be aborted if fault exists.

4) All parts and designs are used in applications proven by test.

5) All scheduled changes to improve reliability of performance have been physically incorporated and tested prior to launch.

6) Natural hazards, such as meteorites and deep lunar dust, are nonexistent.

4.3 REFERENCES AND ACKNOWLEDGMENTS

The material in Sections 1, 2, 3, and 4 was coordinated (and originated or compiled) by W. McIntyre from the following sources:

1) "Surveyor VII Flight Path Analysis and Command Operations Report," Hughes Aircraft Company, SSD 88014, 25 January 1968.

2) "Surveyor Mission G Space Flight Operations Report," Hughes Aircraft Company, SSD 88016, February 1968.

Mention is also due to the following people:

W. R. Heathcote for information concerning postlanding attitude determination for Surveyor VII.

L. K. Cooley for the reliability analysis in subsection 4.2.

G. A. Young and C. A. Wasynczuk for systems analyses review.

S. A. Volansky for on-call system programming support, and J. M. Berger for the tedious data handling throughout the seven Surveyor missions.

R. H. Leuschner for inspiration and general systems analyses throughout the postmission analyses of the Surveyor missions.

5.0 PERFORMANCE ANALYSIS

5.1 THERMAL CONTROL SUBSYSTEM

5.1.1 INTRODUCTION: SURVEYOR THERMAL CONTROL TECHNIQUES

The Surveyor thermal design utilizes a variety of temperature control techniques. Active, passive, and semiactive mechanisms are employed to provide the required temperature control (storage, operational, and/or survival) throughout the transit and lunar phases of the mission. Each spacecraft subsystem is individually controlled, and the thermal coupling between subsystems is minimized by using conduction and radiation isolation wherever advantageous. Subsystem analyses are accomplished by evaluating in detail the thermal environment for each subsystem, with consideration being given to all significant thermal interactions between the subsystems whenever a high degree of isolation is not possible.

The following temperature control techniques are used on the Surveyor spacecraft:

1) Passive thermal control utilizing combinations of paints and metal processes to provide surfaces with solar absorptance and infrared emittance characteristics to produce the required subsystem temperatures. Solar energy reflections are used to provide energy in cases where insufficient direct solar illumination exists.

2) Active thermal control systems utilizing heaters and radiation shields provide energy in cases where:

   a) Sufficient solar illumination is not available

   b) The unit's storage temperature is significantly different from its optimum operational temperature

3) Subsystems having large heat capacities are thermally decoupled from the transit and lunar environments by utilizing superinsulation blankets to minimize radiative heat transfer and thermal isolators to minimize conductive heat transfer. Such systems never reach equilibrium conditions and therefore depend on heat capacity and a controlled rate of heat rejection to provide optimum operational temperatures.

4) Bimetallically activated thermal switches control the temperature of the electronics compartments during transit and lunar operations.

Combinations of the above techniques are used on many of the subsystems to optimize the temperature control system.

5.1.2 THERMAL ANOMALIES

5.1.2.1 Thermal Sensor Failure

A post-touchdown anomaly occurred in temperature readings of the vernier fuel line 3 flight sensor (P-25). The transit data and the first 101 hours of first lunar day data (010:01:00 GMT to 014:06:00 GMT) appeared to be very good. Between 014:06:00 and approximately 023:05:00, the sensor exhibited an open reading of 592°F. However, the sensor readings appeared to be normal again at 023:06:00. It is conceivable that, as the line temperatures cooled down as lunar night approached, the sensor wire contracted, closing the circuit that was previously opened by expansion resulting from high temperatures.

5.1.2.2 Propulsion System Thermal Anomaly

Following touchdown the thermal flight sensor attached to vernier engine 2 exhibited the maximum temperature observed on any thrust chamber assembly during lunar operations. Thrust chamber assembly 2 reached a temperature of 288°F during the lunar morning. At lunar noon the assembly temperature sensor registered 244°F; hence, the sensor displayed engine temperatures in excess of 240°F for most of the lunar morning.

Thermal sensor P-10 installed on thrust chamber assembly 2 exhibited an 88°F decrease on day 20 (20 January 1968) between 21:00 and 24:00 GMT. The thrust chamber assembly temperature was 88°F prior to the temperature drop. Thermal investigations indicate that the temperature drop was probably due to a propellant leak. An examination of the thermal data indicates that the leak occurred over approximately a 50-hour period.

5.1.3 THERMAL SUBSYSTEM SUMMARY

5.1.3.1 Transit

Spacecraft thermal response during transit was excellent. All steady-state temperatures were close to the preflight predictions except for the soil mechanics/surface sampler (SM/SS) mechanism. The SM/SS retraction and elevation motor temperatures (SS-14 and SS-15) equilibriated approximately 32°F higher than predicted; however, this was within prediction tolerances. Of the 75 temperature sensors, 92 percent were within 10°F of their predicted steady-state values.

The survey TV camera electronics and hood and mirror assembly heaters were activated at R-6H53M instead of R-5H, the nominal turn-on time during previous missions. These heaters were activated early to ensure that the camera electronics temperature reached operational limits prior to the scheduled time of camera vidicon heater activation. The camera electronics reached operational limits at R-2H52M, well in advance of the scheduled vidicon heater activation at R-1H5M.

At touchdown compartment C and alpha scattering head temperatures were within operational limits. Surveyor VII was the first spacecraft to be equipped with both the SM/SS and alpha scattering device. Also, Surveyor VII carried seven particle mirrors and four television viewing mirrors (of which one was a stereo mirror located on the A/SPP mast). The effects of the mirrors on the thermal balance of the spacecraft during transit was negligible as predicted. Several commutator changes had to be incorporated to accommodate the SM/SS equipment. Signals P-22 (retro nozzle) and V-29 (thermal tunnel) were deleted, and signals SS-12 (SM/SS electronics), SS-14 (SM/SS retraction motor), and SS-15 (SM/SS elevation motor) were added. In addition, signals V-28 (lower spaceframe) and V-33 (shock absorber 3) were removed from commutator 4, but retained on commutator 5.

5.1.3.2 Lunar

Spacecraft temperatures during the first lunar day were as expected. The scientific payload was hotter during the midmorning, noon, and midafternoon periods than during those of previous missions since the planar array and solar panel could not cast shadows over the equipment because of the sun angles involved. In addition, operation of the television camera was limited during the midmorning to midafternoon interval because of high temperatures. Upper operational temperatures for the alpha scattering system, television system, and SM/SS were exceeded.

During the onset of lunar night, the switches in compartments A and B behaved well as compared with previous spacecraft. Two switches were stuck in compartment A, with none stuck in compartment B at spacecraft shutdown. Survival on a second lunar day was consequently more probable.

5.1.4 THERMAL PERFORMANCE IN TRANSIT

A summary of equilibrium temperatures for Missions A through G and Mission G predictions are presented in Table 5.1-1. All temperature signals were plotted in real time during the mission (see Appendix A). A table of events for Mission G is presented in Table 5.1-2. This table includes events that may affect the thermal response of the spacecraft.

Only thermal responses which were unique or of special interest are discussed in this subsection. For those units with temperature histories consistent with previous missions, the equilibrium temperature summary and transit plots are supplied in lieu of further discussion.

TABLE 5.1-1. SURVEYOR TRANSIT STEADY-STATE TEMPERATURE DATA, FLIGHT PREDICTIONS, AND LIMITS

Flight Sensor Location by Subsystem		Transit Steady-State Temperature, °F								Temperature Limits, °F	
		Mission A Actual	Mission B Actual	Mission C Actual	Mission D Actual	Mission E Actual	Mission F Actual	Mission G			
								Predicted	Actual	Operational	Survival
Vehicle and mechanisms											
Compartment A											
Upper tray	V-15	70	74	49	58	46	41	47	46	125/0	135/-10
Lower tray	V-16	93	94	70	76	56	51	57	56	125/0	135/-10
Transmitter A	D-13	68	71	49	55	42	39	42	43	185/5	210/0
Transmitter B	D-14	68	73	48	57	44	41	45	44	185/5	210/0
Main battery	EP-8	97	99	69	75	58	52	58	58	125/40	125/0
Battery charge regulator	EP-34	123	118	94	98	64	60	65	62	170/5	190/0
Radiators											
No. 5	V-20	42	31	30	25	-3	21	15	24	145/-300	150/-320
No. 8	V-25	44	28	36	42	29	31	26	36	145/-300	150/-320
No. 2	V-47	35	34	19	22	-31	15	8	-33	145/-300	150/-320
No. 3	V-49	*	*	*	*	4	9	5	-10	145/-300	150/-320
Thermal shell inside	V-17	92	92	68	74	*	*	*	*	125/0	130/-10
Thermal shell outside	V-18	-85	-82	-84	-87	-93	-82	-90	-86	160/-210	DNA
Thermal switch No. 5 inside	V-19	66	69	47	56	43	39	44	43	130/-5	150/-15
Compartment B											
Upper tray	V-21	93	99	76	77	74	78	77	81	140/0	150/-10
Lower tray	V-22	98	103	81	81	77	81	81	83	140/0	150/-10
Boost regulator	EP-13	115	128	94	97	82	83	84	87	175/5	190/0
Radiators											
No. 4	V-24	67	70	55	54	52	53	52	60	145/-300	150/-320
No. 1	V-45	73	84	61	62	58	61	60	63	145/-300	150/-320
No. 5	V-46	66	70	56	53	51	55	55	53	145/-300	150/-320
Thermal shell outside	V-23	-70	-72	-64	-72	-78	-76	-82	-72	160/-210	DNA
Thermal switch No. 4 inside	V-26	88	93	74	72	68	73	70	71	130/-5	150/-15
Thermal tunnel	V-29	89	91	72	74	67	68	*	*	125/0	135/-10
Auxiliary battery	EP-26	35	64**	54	60	*	*	*	*	130/40	145/15
Auxiliary battery outer compartment canister	V-48	2	9**	12	*	*	*	*	*	160/140	DNA

*Not on spacecraft.

**Steady state not obtained.

Table 5.1-1 (continued)

Flight Sensor Location by Subsystem		Transit Steady-State Temperature, °F								Temperature Limits, °F	
		Mission A	Mission B	Mission C	Mission D	Mission E	Mission F	Mission G			
		Actual	Actual	Actual	Actual	Actual	Actual	Predicted	Actual	Operational	Survival
Landing gear assembly											
Leg 2	V-31	83	74	77	65	*	*	*	*	160/-140	DNA
Crushable block	V-44	-62	-48	-63	-55	-68	-76	-61	-57	160/-140	DNA
Shock absorber											
No. 1	V-30	84	76	74	77	80	79	80	79	125/20	125/-25
No. 2	V-32	72	73	76	76	76	84	80	80	125/20	125/-25
No. 3	V-33	82	82	79	74	70	76	80	76	125/20	125/-25
Planar antenna/solar panel/positioner mechanism											
Solar panel drive	M-10	60	45	51	46	45	63	64	60	260/-225	265/-235
Elevation axis drive	M-12	1	-17	-11	-20	-23	-8	-6	-6	260/-225	265/-235
Solar panel	EP-12	109	111	112	110	126	128	128	126	150/-150	235/-200
Planar array	M-8	-50	-50	-50	-52	-50	-43	-45	-40	275/-225	280/-225
A/SPP mast	V-34	-84	-88	-88	-90	*	*	*	*	264/-225	DNA
Spaceframe and substructure											
Upper spaceframe											
Near leg 1	V-27	60	53	57	52	56	59	59	63	160/-140	DNA
Near leg 2	V-35	-79	-81	-82	-84	-82	-80	-80	-78	160/-140	DNA
Lower spaceframe											
Under compartment B	V-28	48	42	43	38	39	40	40	46	160/-140	DNA
Under compartment A	V-36	-27	-24	-32	-34	-31	-25	-25	-26	160/-140	DNA
Retro attach points											
Leg 1	V-37	39	44	42	37	38	42	42	43	120/-95	140/-100
Leg 2	V-38	-36	-32	-52	-53	-41	-37	-52	-47	120/-95	140/-100
Leg 3	V-39	44	44	46	37	41	42	40	46	120/-95	140/-100
Flight control											
Flight control electronics											
Chassis board 1	FC-44	90	90	71	66	67	69	65	74	150/0	165/-20
Chassis board 6	FC-45	124	137	60	59	61	62	60	63	127/30	132/0
Canopus sensor	FC-47	78	85	74	76	70	73	68	74	130/-20	145/-20

*Not on spacecraft.

TABLE 5. 1-2. SURVEYOR VII TRANSIT THERMAL EVENT LOG

Day	Time		Event
	GMT, hr:min:sec	Mission Time, hr:min:sec	
07	06:30:01	0	Launch
	06:33:47	00:03:46	Shroud jettison
	06:34:22	00:04:21	MEIG 1
	06:39:54	00:09:53	MECO 1
	06:50:19	00:20:18	Out of earth's shadow
	07:02:15	00:32:14	MEIG 2
	07:04:15	00:34:14	MECO 2
	07:05:00	00:35:00	Transmitter B high power on
	07:05:16	00:35:15	Surveyor – Centaur separation
	07:14:30	00:44:30	Sun acquisition (solar panel)
	07:32	01:02	High power off
	07:40	01:10	1100 bps
	09:00	02:30	Vernier line 2 heater started cycling
	09:11	02:41	SM/SS heater cycling
	12:08	05:38	Solar panel switch off
	12:46	06:16	Solar panel switch on
	13:43	07:13	AMR heater started cycling
	14:00	07:30	Solar panel switch off
	14:18	07:48	Transmitter B high power on
	14:18	07:48	Solar panel switch on
	14:24	07:54	Start of roll (627 degrees)
	14:44	08:14	End of roll
	14:57	08:27	1100 bps
	14:58	08:28	Transmitter B high power off
	15:36	09:06	Gyro drift check 1 (three-axis)
	17:28	10:58	Solar panel switch off
	17:31	11:01	End gyro drift check 1
	17:36	11:06	Start gyro drift check 2
	17:37	11:07	Solar panel switch on

Table 5. 1-2 (continued)

Day	Time		Event
	GMT, hr:min:sec	Mission Time, hr:min:sec	
	23:02	16:32	Transmitter B high power on
	23:02	16:32	4400 bps
	23:18:26	16:48:26	Start roll (+3 degrees)
	23:18	16:48	End roll
	23:21:10	16:51	Start yaw (+117 degrees)
	23:25	16:55	End yaw
	23:27	16:57	Turn off heaters: AMR, vernier lines, and SM/SS.
	23:30	17:00	Thrusting (11.3 seconds)
	23:32	17:02	Heaters back on
	23:34	17:04	Initiate reverse yaw
	23:38	17:08	Terminate reverse yaw (-117 degrees)
	23:40	17:10	Start of roll
	23:49	17:19	1100 bps
	23:51	17:21	High power off
8	00:04	17:36	Initiate gyro drift check 3 (three-axis)
	02:43	20:15	Terminate gyro drift check 3
	02:49	20:21	Initiate gyro drift check 4 (roll only)
	06:02	23:34	Terminate gyro drift check 4
	06:06	23:38	Initiate gyro drift check 5 (three-axis)
	08:30	26:02	Terminate gyro drift check 5
	14:02	31:32	Initiate gyro drift check 6 (three-axis)
	17:14	34:44	Terminate gyro drift check 6
	20:05	37:35	Oxidizer tank 2 heater enabled
9	03:05	44:35	Initiate gyro drift check 7 (three-axis)
	05:34	47:04	Terminate gyro drift check 7
	07:16	48:46	Initiate gyro drift check (three-axis)
	09:48	51:18	Terminate gyro drift check 18

TABLE 5.1-3. SURVEYOR VII MIDCOURSE THERMAL RESPONSE (° F)

Sensor	Preignition Temperature	Peak Temperature Observed	Temperature Increase
Engine 1 (P-7)	70	367	297
Engine 2 (P-10)	77	349	272
Engine 3 (P-11)	78	277	199
Oxidizer line 1 (P-8)	45	69	24
Oxidizer line 2 (P-4)	28	67	39
Oxidizer line 3 (P-9)	50	80	30
Oxidizer tank 1 (P-15)	63	70	7
Oxidizer tank 2 (P-16)	41	56	15
Oxidizer tank 3 (P-6)	50	66	16
Fuel tank 1 (P-13)	59	68	9
Fuel tank 2 (P-5)	44	58	14
Fuel tank 3 (P-14)	59	68	9

The spacecraft was oriented off-sun for approximately 17 minutes, during which time the midcourse correction was applied. During this period, all spacecraft temperature signals remained within appropriate limits.

During the midcourse maneuver, all cyclic heater loads (except the gyro heaters) were commanded off for approximately 5 minutes to observe vernier propulsion system electrical loads prior to and subsequent to thrusting. Propellant tank temperature stratification was observed during midcourse on this flight as in all previous flights. Temperature changes induced at the temperature sensor locations due to propellant motion within the tanks are presented in Table 5.1-3.

Transmitter B was in high power operation for 49 minutes and 16 seconds during midcourse operations. Transmitter B temperature reached 106°F at termination of high power operation.

5.1.4.4 Coast Phases

Heater Performance

The thermal performance of subsystems with active temperature control systems was normal as all thermal control heaters cycled to maintain all units above their lower operational temperature limits as required. The duty cycles exhibited by thermal control heaters are presented in Table 5.1-4.

As anticipated, the vernier line 1 heater did not cycle and the line 2 heater cycled as expected; however, the vernier line 3 heater failed to cycle during the transit mission phase. The AMR heater cycled between 11° and 12°F.

TABLE 5.1-4. HEATER DUTY CYCLES, PERCENT ON TIME

Heater	Mission Time, hours		
	30:00	49:00	55:00
Vernier line 2	32	37	38
SM/SS	100	100	100
AMR	56	57	57
Pitch gyro	40	41	43
Yaw gyro	31	30	18

Compartment Thermal Performance

There were no anomalies in the compartment A and B thermal performances. All thermal tray and electronics steady-state temperatures were within about 5°F of the preflight predicted values. Prior to flight, it was predicted that thermal switch 3 on compartment A might open during transit since it started to open during solar thermal vacuum testing when the compartment reached steady state.

Thermal switch 2 (sensor V-47) opened partially during flight. The switch 2 radiator was about 90 percent shaded, and switch 3 radiator was 100 percent shaded. Since none of the switches were removed between the solar thermal vacuum test and flight, there is no logical explanation for switch 2 to open. The flight data for these sensors is presented in Appendix A.

Alpha Scattering Electronics (Compartment C)

The alpha scattering electronics compartment, compartment C, was predicted to have a nominal transit temperature of -10°F; however, the

temperature exhibited by the compartment thermal sensor during transit was -3°F. The lower operational temperature limit for the compartment is -4°F; hence, the compartment active thermal control system was not required to provide compartment operational temperatures at touchdown.

During solar thermal vacuum testing of Surveyor VII, the compartment thermal sensor (AS-4) exhibited temperatures of -24° and -45°F during high and low simulated solar intensities, respectively. The compartment C temperature was substantially higher during transit than in test because the thermal effect of the solar panel and planar array on the compartment subsystem is not properly simulated during solar thermal vacuum and flight acceptance testing for the following reasons:

1) A finite geometric view factor exists between the compartment C radiator and the solar panel and planar array. The absence of these units does not provide compartment C with its two most vital infrared energy sources; hence, the compartment radiator has a larger view factor to the cold solar thermal vacuum chamber walls in test than to space in flight.

2) While steps were taken to provide the correct shadow pattern over the compartment C radiator, the simulated shadow pattern across the compartment top face, sloping inboard, is still in error. This surface is polished and exhibits a lower temperature in test than in flight; hence, the radiator is conductively coupled to a surface that is cooler in test than in flight.

Television System

The survey television camera thermal control electronics and mirror heaters were enabled at R-6H53M, 113 minutes earlier than in previous missions, to compensate for the thermal lag observed in solar thermal vacuum testing and during Mission F. However, the warmup characteristics exhibited by the Surveyor VII survey camera in flight were similar to those exhibited during Missions A through E; hence, the additional time (113 minutes) was not required to ensure proper operational temperatures at touchdown.

Soil Mechanics/Surface Sampler Subsystem

The SM/SS compartment differed from that of previous spacecraft in that: 1) the vernier propulsion system line 1 heater on command and the SM/SS electronics compartment on command were coupled, and 2) the SM/SS compartment (SS-12) heater capacity was increased from 5 watts nominally (on Surveyors III and 4) to 7-1/2 watts nominally for Surveyor VII. The Surveyor VII heater duty cycle was 50 percent for a 26-volt battery, and the temperature cycled between 0° and 16°F. However, at 22 watts the temperature was 6°F and full on.

The temperature of the SM/SS motors equilibrated at approximately -60°F, 30°F warmer than the predicted -90°F. A reevaluation of the analysis indicates that the SM/SS structure attach locations for the motors should have

been 30°F warmer than the -125°F used. The nominal prediction should have been -75°F instead of -90°F. The additional 15°F difference between -75°F and the equilibrium temperature of -60°F can be accounted for in the uncertainty of conduction coupling between the motors and SM/SS structure-motor interface.

5.1.4.5 Terminal Descent Phase

The thermal response during terminal descent was nominal. Engine 1 exhibited the peak engine temperature of 438°F. Propellant tank temperature statificiation was evident again as during midcourse. A summary of the propulsion temperature excursions due to terminal descent operations is presented in Table 5.1-5.

TABLE 5.1-5. SURVEYOR VII TERMINAL DESCENT THERMAL RESPONSE (° F)*

Sensor	Preignition Temperature	Peak Temperature Observed	Temperature Increase
Engine 1 (P-7)	75	438	363
Engine 2 (P-10)	91	333	242
Engine 3 (P-11)	66	325	259
Oxidizer line 1 (P-8)	39	84	45
Oxidizer line 2 (P-4)	24	58	34
Oxidizer line 3 (P-9)	23	72	49
Oxidizer tank 1 (P-15)	47*	66	19
Oxidizer tank 2 (P-16)	16	39	23
Oxidizer tank 3 (P-6)	43	62	19
Fuel tank 1 (P-13)	55	72	17
Fuel tank 2 (P-5)	30	52	22
Fuel tank 3 (P-14)	55	70	15

*P-15 increased from 42° to 47° F due to the yaw maneuver.

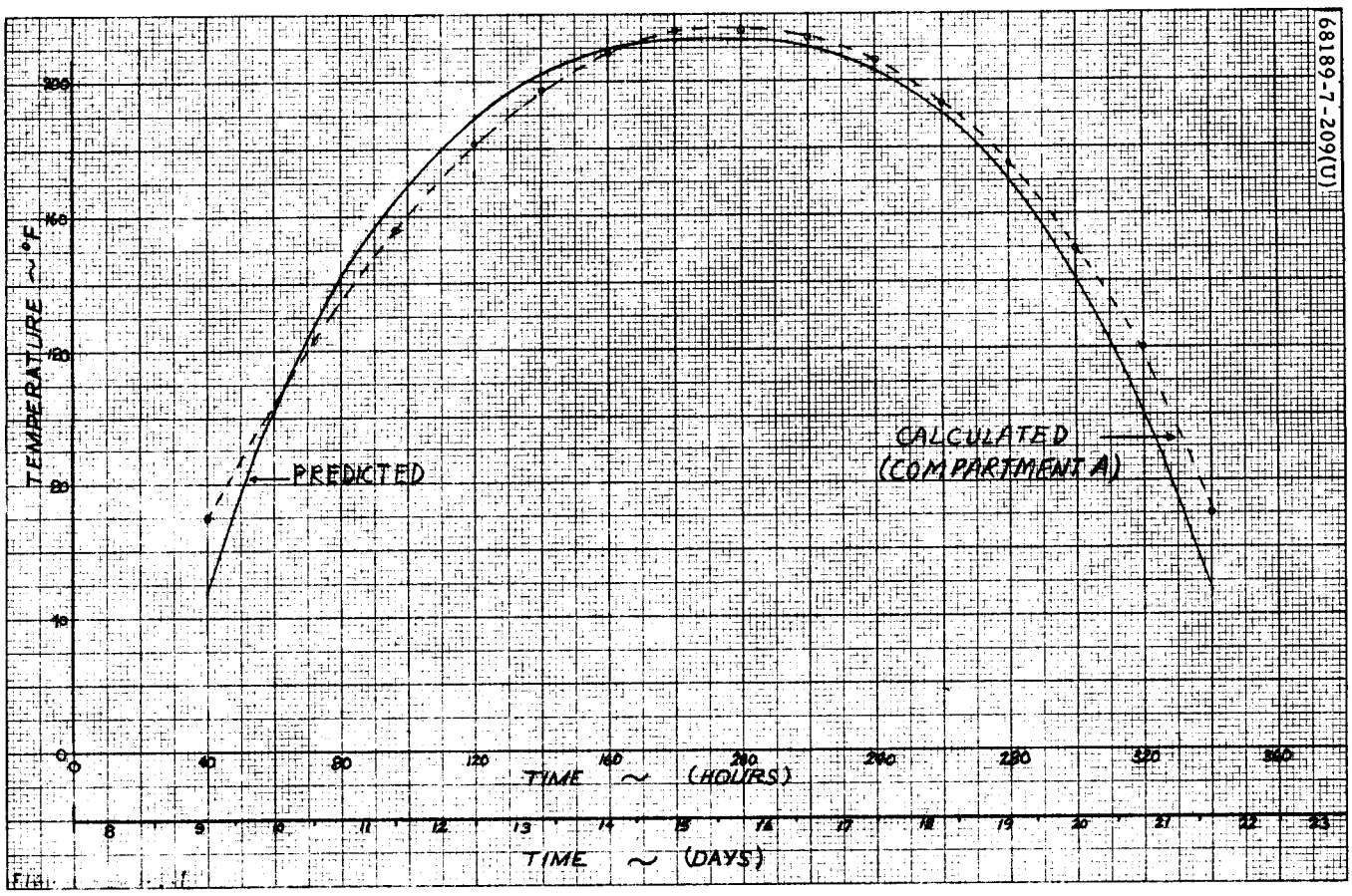

Figure 5.1-1. Lunar Surface Temperature Profile

At retro ignition, the retro bulk temperature was 54.5 °F. Incorporation of the battery warmup procedure resulted in a battery temperature of 92.2°F at the time of RADVS turn-on. Thus, the battery was at a desirable temperature to support the loads associated with terminal descent. The battery temperature reached 93.1°F at touchdown.

The spacecraft was in an off-sun attitude for approximately 29 minutes and 52 seconds prior to touchdown. All thermal signals remained within proper temperature limits during this period (see Appendix A). All cyclic heater loads (except the gyro heaters) were commanded off 9 minutes and 16 seconds prior to touchdown.

Transmitter B high power operation was initiated at T-58M19S and terminated at T+17M49S, providing approximately 1.27 hours of continuous high power. During this period, the transmitter B temperature increased to 119.5°F. The klystron power supply modulator temperature (R-8) increased from 35° to 100°F during RADVS operation.

5.1.5 THERMAL PERFORMANCE – FIRST LUNAR DAY

Prior to the launch of Surveyor VII, thermal studies indicated that spacecraft subsystems would exhibit cooler temperatures at or near Tycho than at equatorial landing sites. Calculations indicated that the lunar surface temperature in the vicinity of Tycho would be approximately 211°F at noon, whereas it is approximately 261°F at noon on the equator. Thermal calculations were based on an infrared emittance of 0.88, a solar absorptance of 0.93, and a smooth lunar surface and did not account for local surface variations, i.e., surface slopes, boulders, craters, etc. Solar heat loads for the southern latitude were obtained using Lambert's cosine law. A nominal lunar surface temperature profile is shown in Figure 5.1-1 for a 40-degree southerly latitude. Perturbation analyses have shown that the local surface temperature is a strong function of the localized environment; however, for the purpose of preflight thermal performance evaluation, the ideal or "smooth moon" concept was used to estimate local surface temperatures.

A summary of Surveyor maximum lunar day temperatures is presented in Table 5.1-6 for Surveyors I, III, V, VI, and VII. Operational temperature requirements are presented in the last two columns of the table. First lunar day thermal parameters are presented in Appendix B (Figures 5.1-B1 through 5.1-B71).

5.1.5.1 Touchdown and Orientation

Surveyor VII, unlike its predecessors whose primary objective was to explore possible equatorial landing sites for Project Apollo, had as its targeted landing site a small area some 40°S of the equator near the crater Tycho. Surveyor VII touchdown on the lunar surface occurred at 010:01:05:37 GMT. The spacecraft touchdown attitude is shown in Figure 4-3a.

TABLE 5.1-6. MAXIMUM QUASI-STEADY STATE TEMPERATURES AND MINIMUM TEMPERATURES OF SPACECRAFT ON LUNAR SURFACE

	Sensor and Location	Maximum Temperature, °F					Operational Temperature Limits, °F	
		Surveyor I	Surveyor III	Surveyor V	Surveyor VI	Surveyor VII	Minimum	Maximum
AS-3	Alpha scattering sensor head	–	–	143/146*	163	163	–	–
AS-4	Compartment C electronics	–	–	132/138	147	157	–	–
D-13	Transmitter A	185	118	120/112	110	106	5	185
D-14	Transmitter B	106	110	109/111	110	104	5	185
EP-8	Main battery	118	116	114/118	115	110	40	125
EP-12	Solar panel	217	220	248/250	241	230	-150	150*
EP-13	Boost regulator	132	132	124/127	115	107	5	175
EP-26	Auxiliary battery	155	166	–	–	–	40	130
EP-34	Battery charge regulator	142	125	124/125	136	115	5	170
FC-44	Flight control electronics	192	202	180/184	196	177	0	150
FC-45	Flight control electronics	200	201	185/190	197	178	30	127
FC-46	Roll gyro	167	198	157/290**	160	162	165	185
FC-47	Canopus	180	194	170/177	200	192	-20	130
FC-48	Nitrogen tank	173	165	195/187	225	238	0	130
FC-54	Pitch gyro	188	–	157/289**	159	162	165	185
FC-55	Yaw gyro	170	–	157/291**	161	162	165	185
FC-70	Attitude jet 2	205	210	219/226	214	198	-40	150
FC-71	Roll actuator	224	239	230/238	244	140	10	190
M-8	Planar array	228	230	296/296	290	216	-225	275
M-10	Solar motor	218	230	242/245	222	198	-225	260
M-12	Elevation motor	190	201	210/208	223	180	-225	260
P-4	Oxidizer line 2	203	203	210/207	182	230	0	100
P-5	Fuel tank 2	164	197	206/201	194	225	0	100
P-6	Oxidizer tank 3	154	179	173/181	179	189	0	100
P-7	Vernier engine 1	244	256	250/250	246	132	5	145
P-8	Oxidizer line 1	221	202	220/226	213	137	0	110
P-9	Oxidizer line 3	184	200	182/186	195	210	0	110
P-10	Vernier engine 2	229	256	272/252	256	288	5	145
P-11	Vernier engine 3	227	232	210/219	271	277	5	145
P-13	Fuel tank 1	190	208	209/204	200	129	0	100
P-14	Fuel tank 3	171	188	166/160	195	208	0	100
P-15	Oxidizer tank 1	173	183	192/187	180	143	0	100
P-16	Oxidizer tank 2	166	185	182/183	166	204	0	100
P-17	Helium tank	145	178	197/213	186	190	0	110
P-23	Fuel line 1	–	–	213/210	214	126	0	110
P-24	Fuel line 2	–	–	219/208	208	246	0	110
P-25	Fuel line 3	–	–	210/210	245	Bad	0	110
R-8	Klystron power supply modulator	225	214	222/227	247	200	–	–
R-9	Signal data converter	149	168	174/180	161	133	15	105

*First day/second day values.
**IRU radiator damaged during lunar night.

Table 5.1-6 (continued)

Sensor and Location		Maximum Temperature, °F					Operational Temperature Limits, °F	
		Surveyor I	Surveyor III	Surveyor V	Surveyor VI	Surveyor VII	Minimum	Maximum
R-10	Doppler preamplifier	235	260	260/260	215	193	-58	122
R-13	Altitude preamplifier	214	232	243/226	243	251	-58	122
SS-12	Surface sampler electronics	–	144	–	–	180	-4	158
TV-16	TV electronics	127	140	150/157	143	141	-20	160
TV-17	TV hood	124	148	152/155	136	158	-50	180
V-15	Compartment A tray top	110	109	109/117	110	105	0	125
V-16	Compartment A tray bottom	118	117	119/124	124	111	0	125
V-17	Compartment A shell, retainer	–	120	–	–	–	0	125
V-18	Compartment A shell, canister	97	108	100/110	119	93	-210	160
V-19	Compartment A switch 5, base	–	112	108/115	110	104	-5	130
V-20	Compartment A switch 5, radiator	78	101	100/104	97	91	-300	145
V-21	Compartment B tray top	118	117	117/122	112	101	0	140
V-22	Compartment B tray bottom	124	122	124/127	115	106	0	140
V-23	Compartment B shell, canister	111	152	105/114	100	59	-210	160
V-24	Compartment B switch 4, radiator	99	100	100/106	96	83	-300	145
V-25	Compartment A switch 8, radiator	88	100	100/110	98	90	-300	145
V-26	Compartment B switch 4, base	–	114	114/118	109	96	-5	130
V-27	Upper spaceframe	138	156	160/168	159	129	-140	160
V-28	Lower spaceframe	190	186	196/201	182	185	-140	160
V-29	Thermal tunnel	–	115	130/134	126	–	0	125
V-30	Shock absorber 1	193	190	178/187	184	143	20	125
V-31	Leg 2 upper web	148	158	–	–	–	-140	160
V-32	Shock absorber 2	171	183	195/201	183	180	20	125
V-33	Shock absorber 3	175	186	189/195	184	177	20	125
V-34	Antenna/solar panel positioner mast	130	142	–	–	–	-225	264
V-35	Upper spaceframe	125	154	168/172	154	148	-140	160
V-36	Lower spaceframe	166	179	187/188	192	200	-140	160
V-37	Retro bolt 1	122	202	219/222	234	168	-95	120
V-38	Retro bolt 2	175	227	222/206	206	242	-95	120
V-39	Retro bolt 3	185	200	185/188	214	221	-95	120
V-44	Crushable block 3 heat shield	189	193	210/211	236	238	-140	160
V-45	Compartment B switch 1, radiator	104	105	108/112	102	90	-300	145
V-46	Compartment B switch 5, radiator	96	100	100/105	95	80	-300	145
V-47	Compartment A switch 2, radiator	–	104	105/110	100	97	-300	145
V-49	Compartment A switch 3, radiator	–	–	105/110	102	98	-300	145
SS-14	Mechanism	–	–	–	–	196	-40	257
SS-15	Elevation motor	–	–	–	–	186	-40	257

The sun vector azimuthal angle at touchdown was 194 degrees measured from the -X axis (the corresponding elevation angle was 13.3 degrees). A comparison of landed orientations for Surveyors I, III, V, VI, and VII is presented in Table 5.1-7.

TABLE 5.1-7. COMPARISON OF LANDING ORIENTATIONS FOR SURVEYOR SPACECRAFT

Spacecraft	Sun Elevation Angle to Spacecraft X-Y Plane, degrees	Sun Direction at Touchdown
I	29	1 degree from -Y toward +X
III	12	44 degrees from +X toward -Y
V	20.5	24 degrees from +X toward -Y
VI	4.5	59 degrees from -X toward -Y
VII*	13.3	

*Surveyor VII touchdown site was 40°S of the equator.

Surveyors I through VI were aimed at equatorial landing sites. At the equator the sun vector is characterized only by its elevation angle. Thermally, the Tycho touchdown site differs from previous equatorial sites in the orientation of the surface normals to direct solar energy and in the physical surface environment, i.e., craters, boulders, rocks, local surface slopes, etc. A comparison of the preflight lunar surface temperature profile and the profile computed by using Surveyor compartment thermal sensor data is shown in Figure 5.1-1. The lunar surface thermal profiles are in good agreement and certainly are within the predictability of the thermal analyses except as low solar elevation angles. An examination of the data indicates that the lunar surface temperature in the proximity of Tycho can be approximated by using Lambertian concepts to determine the solar intensity, i.e., a cosine law distribution, for much of the lunar day.

The Surveyor VII orientation resulted in the scientific payload being illuminated for most of the lunar day. Data obtained from Surveyors III, V, and VI, together with the projected cooler environment, predicted that the scientific payload units would not exceed their survival limits during the lunar day. However, the SM/SS electronics auxiliary, the alpha scattering sensor head, and compartment C were expected to exceed their upper operational temperature limits of 158°, 122°, and 131°F, respectively.

Following touchdown, the scientific payload subsystems were above their maximum operational temperature limits longer than payloads from

previous spacecraft; hence, the available time for scientific exploration was less for the Surveyor VII mission. During previous missions, the solar panel and planar array were often used to shield units and subsystems from direct solar illumination, thereby increasing the units' operational time. However, because of the touchdown site and spacecraft orientation, it was not possible to use the planar array and solar panel to cast shadows over the scientific payload during the midmorning to midafternoon interval.

5.1.5.2 Heater Performance

Subsequent to touchdown (GMT day 10), several thermal control heaters were enabled. However, because most subsystems with active thermal control systems equilibrated above the lower temperature cyclic or control point, most heaters were not activated. A summary of heater enable and disable commands is presented in Table 5.1-8. In less than 8 hours after touchdown, all heaters were turned off either through disabling commands or through temperature control logic.

All Surveyor active thermal control heaters remained in the off condition until the compartment A heater was commanded on on day 21. The compartment thermal control heater assembly was activated to increase the thermal energy level in the compartment, thereby maximizing the opportunity for lunar night survival. The SM/SS electronics auxiliary heater was enabled on day 22, and the survey television heaters were enabled on day 23 to permit operation of the television and soil mechanics experiments into the lunar night. The television camera terminator occurred at 06:30 on day 23.

TABLE 5.1-8. SURVEYOR VII HEATER ACTIVITY

GMT, day:hr:min:sec	Number	Command Title	Remarks
010:01:15:02	0136	Comp C Htr On	Temperature was below cycling range
15:10	3503	Alpha Scat Htr Pwr On	Temperature was below cycling range
16:21	1133	Sur Camera VTC On	
16:29	1136	Sur Camera ETC On	Temperature was below cycling range
17:43	0611	VL2 Ther Pwr On	Temperature above cycling range
17:48	0614	VL1 SM/SS Ther Pwr On	Temperature above cycling range of R-8 and within cycling range of SS-12
17:52	0615	OT2 Ther Pwr On	Temperature above cycling range
17:53	0617	VL 3 Ther Pwr On	Temperature above cycling range

Table 5. 1-8 (continued)

GMT, day:hr:min:sec	Number	Command Title	Remarks
010:03:30:21	1137	Sur Camera ETC Off	Temperature above cycling range
31:03	0616	VL1, OT2, SM/SS Ther Pwr Off	
31:54	0614	VL1 SM/SS Ther Pwr On	
32:42	0613	VL2 FT2 Ther Pwr Off	
05:33:40	1134	Sur Camera VTC Off	
07:43:43	3504	Alpha Scat Htr Pwr Off	Temperature within cycling range
19:06:29	0616	VL1, OT2, SM/SS Ther Pwr Off	All above cycling range
07:24	0621	VL3, OT3 Ther Pwr Off	All above cycling range
021:00:05:56	0411	Comp A Htr On	To warm battery
08:43	0613	VL2, FT2, SM/SS Ther Pwr Off	
09:42	0616	VL1, OT2, SM/SS Ther Pwr Off	
11:17	0621	VL3, OT3 Ther Pwr Off	
11:48	0604	AMR Htr Off	
12:44	3504	Alpha Scat Htr Pwr Off	
14:35	1134	Sur Camera VTC Off	
15:05	1137	Sur Camera ETC Off	
022:18:23:24	0614	VL1, SM/SS Ther Pwr On	
023:05:11:24	1136	Sur Camera ETC On	DAY
21:14:11	1134	Sur Camera VTC Off	NIGHT
21:15:02	1137	Sur Camera ETC Off	
024:11:41:20	0412	Comp A Temp Cont Auto	
46:09	0413	Comp A Htr Off	
46:15	0411	Comp A Htr On	
47:28	0412	Comp A Temp Cont Auto	
025:17:13:36	0413	Comp A Htr Off	
21:48:34	0624	AMR Htr On	
50:28	0604	AMR Htr Off	
51:19	0624	AMR Htr On	
026:14:12:04	0314	Non-Ess Loads Off	

5.1.5.3 Television Camera Operation

Operation of the survey television camera was limited during the midmorning to midafternoon interval because of high temperatures. Preflight thermal analyses indicated that survey television camera operation would be limited at the southerly latitude. Thermal predictions indicated that the electronics conversion unit could exhibit temperature rise rates of 1.1°F/min. The actual electronics conversion unit temperature rise rate is a function of the camera duty cycle and actual internal power dissipation (which is dependent on available battery voltage). The Surveyor VII electronics conversion unit exhibited an average temperature rise of 1.0°F/min during one operational interval of approximately 7 minutes. The upper operational temperature limit for the survey camera electronics conversion unit is 165°F.

5.1.5.4 Alpha Scattering Subsystem

Alpha Scattering Sensor Head

Preflight predictions indicated that the alpha scattering sensor head would exceed its upper operational temperature limit of 122°F at a solar azimuthal angle of 95 degrees (or 45 degrees from the solar azimuth corresponding to a 0-degree elevation). The alpha scattering sensor head exceeded its upper temperature limit at a solar azimuthal angle of approximately 93 degrees. However, contrary to predictions, the alpha scattering sensor head also exceeded its survival temperature limit of 158°F by reaching a peak temperature of 163°F. Preliminary thermal analyses indicated that the higher than expected temperatures are probably attributable to the following:

1) Uncertainties in the optical properties, especially the solar absorptance, associated with the alpha scattering sensor head vycor mirror and in the thermal contribution of the sides of the container to radiator and electronic temperatures.

2) Uncertainties in the thermal contribution due to infrared energy exchange with the lunar surface and the reflected component of insolation from the spacecraft. Alpha scattering sensor head radiator (vycor mirror) optical properties are measured prior to subjecting the spacecraft to systems level solar thermal vacuum tests. Property measurement data indicate that the optical properties are nominal, i.e., $\alpha \sim 0.11 \pm 0.02$ and $\epsilon \sim 0.80 \pm 0.02$. In general, if contamination prior to launch is eliminated, then it becomes plausible to argue that the thermal coupling between the alpha scattering sensor head electronics/radiator assembly and the shielding compartment is probably an order of magnitude greater than predicted.

Alpha Scattering Electronics Compartment

The alpha scattering electronics compartment, like the alpha scattering sensor head, exceeded its upper operational temperature limit

of 131°F. The compartment reached a peak temperature of 157°F during the first lunar day. The orientation of the alpha scattering electronics compartment thermal radiator results in peak solar heating at sun elevation angles of 45 ± 5 degrees for equatorial landings (approximately 20 hours). However, the thermal radiator is subjected to peak or near-peak solar loads for several days at the Tycho latitude. The increased period of near-peak solar heating, combined with the infrared energy exchange with the lunar surface, resulted in the alpha scattering electronics compartment being above its upper operational temperature limit longer than on previous missions.

5.1.5.5 Soil Mechanics/Surface Sampler Subsystem

The soil mechanics/surface sampler subsystem has two major units: a mechanism and an auxiliary electronics compartment. The lunar day thermal performance of the Surveyor VII auxiliary compartment indicates that the compartment experienced either/or both a "hotter" thermal environment and a higher solar energy heating load than previous Surveyor spacecraft.

The spacecraft touchdown orientation and Tycho location resulted in the maximum period of direct illumination in the landing leg 2 region. The SM/SS auxiliary electronics compartment and the mechanism which are located in this region were insolated throughout most of the lunar day.

The maximum SM/SS compartment temperature of 180°F was 40°F higher than that experienced on Surveyor III (the previous successful spacecraft with an SM/SS subsystem). The maximum operating temperature of 158°F was exceeded for 95 hours. An extrapolation of Surveyor III thermal data for the period when the compartment was shaded indicates that a maximum temperature of 155°F could have been attained. Therefore, the maximum temperature of the Surveyor VII auxiliary electronics compartment was 25°F warmer than the extrapolated peak for Surveyor III.

There were no flight sensors on the Surveyor III SM/SS motors; therefore, no comparison may be made with the Surveyor III and VII thermal performances. However, the bulk temperature of the mechanism had been analytically predicted as a function of percentage illumination. A maximum bulk temperature of 196°F was predicted for 50 percent illumination. This compares closely with actual maximum temperature of 186° and 196°F, respectively, for the Surveyor VII elevation and retraction motors.

5.1.5.6 Liftoff and Translation Window

Preflight predictions indicated that liftoff and translation windows occurred between a solar elevation angle of 23 and 31 degrees during the lunar morning and 23 and 16 degrees during the lunar afternoon. However, the liftoff windows did not occur during the lunar day as predicted. Subsystems required to perform the liftoff and translation were above their upper temperature limits during most of the day.

Subsequent to touchdown, the temperature of shock absorber 3 decreased to -63°F. The lower operational limit for shock absorbers is 0°F. Prior to shock absorber 3 warming up to its lower operational limit, thrust chamber assembly 2 exceeded its upper operation temperature limit of 220°F. Shadowing of thrust chamber assembly 2 and/or 3 with the solar panel or planar array was not possible because of the southerly landing site and touchdown orientation. Subsequent to touchdown, thrust chamber assembly 2 exceeded its upper temperature limit of 220°F and reached a peak temperature of 288°F during the morning. Thrust chamber assembly 3 exceeded its maximum temperature prior to thrust chamber assembly 2 decreasing below its maximum allowable operational temperature. Thrust chamber assembly 1, being on the south side of the spacecraft, did not exceed its upper temperature limit. Thrust chamber assembly 3 reached a peak temperature of 277°F during the lunar afternoon. The temperature of thrust chamber assembly 3 was above its upper operational limit until sunset minus approximately 9 hours. However, at this time (sunset minus 9 hours), thrust chamber assembly 2 was below its lower operational temperature limit. Hence, no liftoff and translation window was available during the Surveyor VII mission.

5.1.6 FIRST LUNAR NIGHT THERMAL PERFORMANCE

5.1.6.1 Compartments A and B

An analysis was made to determine Surveyor VII compartment A and B thermal switch behavior during first lunar night operations. Figure 5.1-2 shows the power and temperature history of both compartments. Analysis indicated that two switches were stuck in compartment A, with none stuck in compartment B at spacecraft shutdown. First lunar night temperatures are contained in Appendix C.

The analysis (Reference 1) indicates that two compartment A switches remained closed until spacecraft shutdown, but all compartment B switches opened. Of the 15 switches, 7 opened during the period when their temperatures were within the specified limits of 35° ± 10°F for switch activation. Five others opened at a time when they were outside the specified temperature range. One additional uninstrumented switch opened, but the exact time cannot be determined. The number of closed switches was determined by performing heat balances on each compartment during specific time periods. Table 5.1-9 summarizes this switch condition.

Based on a review of the data, it is felt that the additional switch in compartment B opened within the specified activation range of temperatures. The remaining two switches in compartment A, as previously indicated, were stuck closed as of spacecraft shutdown.

The data given in Figure 5.1-2 represent all spacecraft power configurations during the time period shown, based on information found in the detailed command log and/or real-time records.

TABLE 5.1-9. STATUS OF SURVEYOR VII THERMAL SWITCHES AT FIRST LUNAR NIGHT SHUTDOWN

Category	Compartment A		Compartment B		Totals
	Telemetered	Untelemetered	Telemetered	Untelemetered	
Opened within specified temperature range of 35 ± 10°F	3	2	2	–	7
Opened outside specified temperature range	0	2	1	2	5
Opened – time not known	–	–	–	1*	1*
Stuck closed	1	1	0	0	2
Totals	4	5	3	3	15

NOTE: Based on observations of compartment B temperature data and switch opening times, it is considered likely that this switch also opened in the specified temperature range.

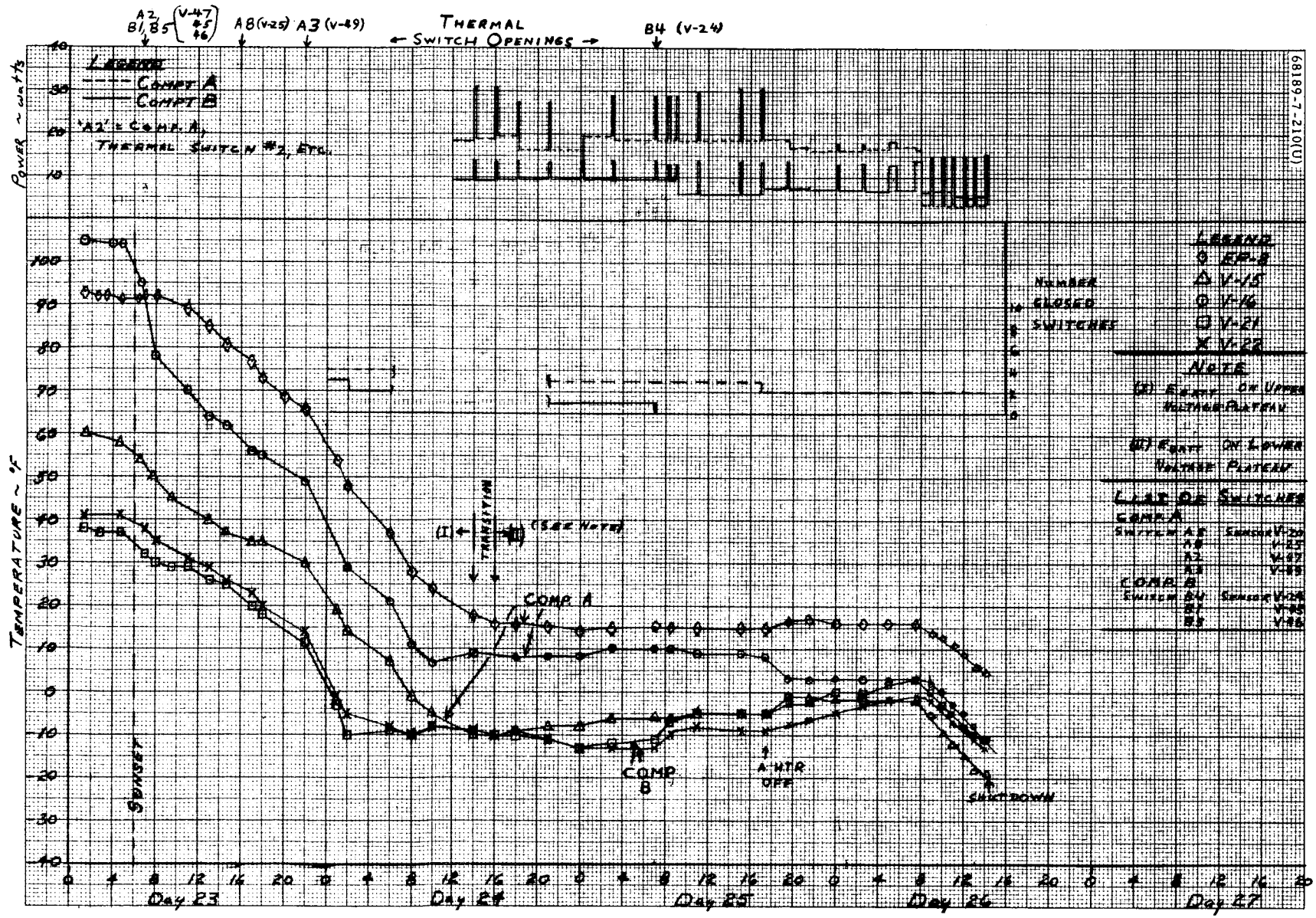

Figure 5.1-2. First Lunar Night Compartment Study Data

TABLE 5.1-10. METHOD OF CALCULATING STUCK THERMAL SWITCHES

$$P = \frac{\Sigma P_i \, \Delta \theta_i}{\Sigma \Delta \theta_i}$$

$$Q_r = \sigma \epsilon \left(T_r^4 - T_b^4\right), \text{ watts/ft}^2$$

$$Q_1 = \Delta Q \Big|_{\text{steady state}}^{\text{actual}} = P - Q_s - G \frac{\Delta T}{\Delta \theta}$$

$$A_r = \frac{Q_1}{Q_r}$$

$$N_s = \frac{A_r}{A_s} = \frac{Q_1}{Q_r A_s}$$

where:

$\Delta\theta$ = time interval

P = average power level during $\Delta\theta$

T_r = average closed switch radiator temperature during $\Delta\theta$

T_b = radiator background temperature (assumed equal to average open switch radiator temperature)

Q_r = heat flux from closed switch radiators, $\epsilon = 0.79$ for Vycor mirrors

Q_s = heat loss from compartment at steady state at T_c with all switches open

G = compartment "heat rate" — watts/°F/hr (6.2 for compartment A, 2.2 for compartment B)

Q_1 = heat loss in excess of steady-state conditions (watts)

A_r = area required to radiate excess heat (ft^2)

A_s = radiating area per switch (0.313 ft^2 for compartment A, 0.33 ft^2 for compartment B)

N_s = number of closed switches

The general method of analysis used (Reference 1) postulates that any heat input above that required to maintain the compartment at steady state when all switches are open (based on Surveyor V experience) is lost through closed switches. During the Surveyor VII first lunar night, true steady-state temperature conditions were obtained. Since the analysis is based on the bulk temperature of the compartment, the necessity of using the rate of temperature change introduces considerable uncertainty in the calculations when the compartment internal temperature gradients are significant as in Surveyor VI. For temperature gradients in the compartment A and B trays, the bulk temperatures were assumed to be given by

$$T_c(A) = 0.75\ T_{EP-8} + 0.25\ T_{V-15}$$

$$T_c(B) = 0.5\ T_{V-21} + 0.5\ T_{V-22}$$

The method of calculating the number of stuck switches is outlined in Table 5.1-10.

A comparison of compartment heat losses for Surveyors V and VII is presented in Table 5.1-11. Heat loss data for Surveyor VII compares well with heat loss data for Surveyor V (Reference 5) and the preflight predictions (Reference 6) which are based on the lunar night tests of the S-10 thermal control model.

5.1.6.2 Compartment C

During the first lunar night operations, the compartment C temperature dropped much more rapidly than anticipated (Reference 2). Examination of postsunset compartment C temperatures and their effect on postsunset operation of the alpha scattering devices on Surveyors VI and VII indicated that heat losses through the compartment walls were not insignificant in predicting cooldown behavior (Reference 3). The alpha scattering sensor heat temperature (AS-3) for the Surveyor VI lunar night (Figure B-70 of Reference 4) shows a cooldown similar to that of Figure 5.1-C1.

TABLE 5.1-11. STEADY-STATE COMPARTMENT HEAT LOSSES FOR SURVEYORS V AND VII

	Compartment A				Compartment B			
	Mean Temperature, °F	Heat Loss, watts	Stuck Switch Loss, watts	Net Loss, watts	Mean Temperature, °F	Heat Loss, watts	Stuck Switch Loss, watts	Net Loss, watts
Surveyor V First lunar night	20	9.23	0	9.23	-15	10.86	3.4**	7.46
Second lunar night	18	10.1 ± 1	0	10.1 ± 1	-30	8,15	3.0***	5.15
Surveyor VII First lunar night	11	17.05	2 x 3.96*	9.13	- 8	6.63	0	6.63
Predicted (Reference 5)	20	–	–	9.7	-15	–	–	6.3
	18	–	–	9.6	-30	–	–	5.9
	11	–	–	9.2	- 8	–	–	6.5

*Stuck switch loss for T_r = -30°F

**Stuck switch loss for T_r = -55°F

***Stuck switch loss for T_r = -60°F

5.1.7 REFERENCES

1) J. B. Goodblatt, "Thermal Switch Performance During Surveyor VII First Lunar Night Operations," Hughes Aircraft Company, IDC 2221.19/262, February 1968.

2) M. E. Goble, "SC-7 First Lunar Night Performance Data," Jet Propulsion Laboratory, Interoffice Memo 317-23, 6 February 1968.

3) W. J. Bruecks, "Post Sunset Compartment C Temperatures," Hughes Aircraft Company, IDC 2292/453, 22 February 1968.

4) "Addendum to Surveyor Mission F Space Flight Operations Report," Hughes Aircraft Company, SSD 88017R, January 1968.

5) D. J. Ritchie, "Surveyor V Compartments A and B Heat Losses During the Second Lunar Night," IDC 2221.19/246, 26 December 1967.

6) H. E. Knudson, "Lunar Night Survival Improvement Studies," IDC 2221.19/209, 14 July 1967.

7) L. L. Gamer, "SC-VII Spacecraft Shadow Plots for First Lunar Day Using Actual ASPP Stepping History," Hughes Aircraft Company IDC 2292/450, 7 February 1968.

5.1.8 ACKNOWLEDGMENTS

Data in subsections 5.1.4 and 5.1.5 was compiled by J. Lewis.

First lunar night analysis for compartments A and B (subsection 5.1.6.1) was provided by J. B. Goodblatt.

Cooldown analyses for compartment C (subsection 5.1.6.2) was provided by W. J. Bruecks of Systems Analysis.

APPENDIX A TO SECTION 5.1

TRANSIT TEMPERATURE PLOTS

Appendix A contains Figures 5.1-A1 through 5.1-A6, transit thermal plots. These plots were recorded in real time by Spacecraft Performance Analysis and Command.

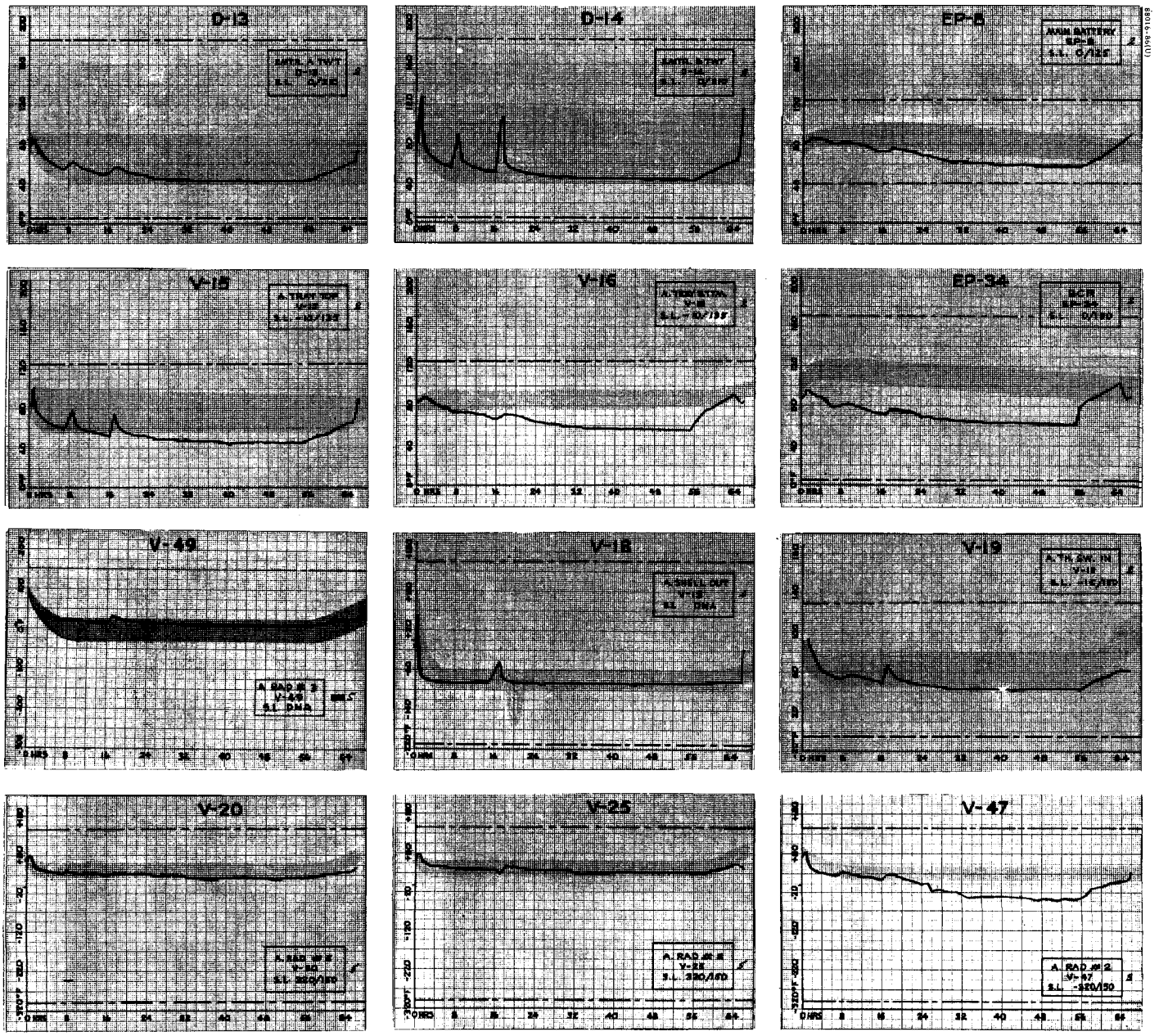

Figure 5.1-A1. Compartment A

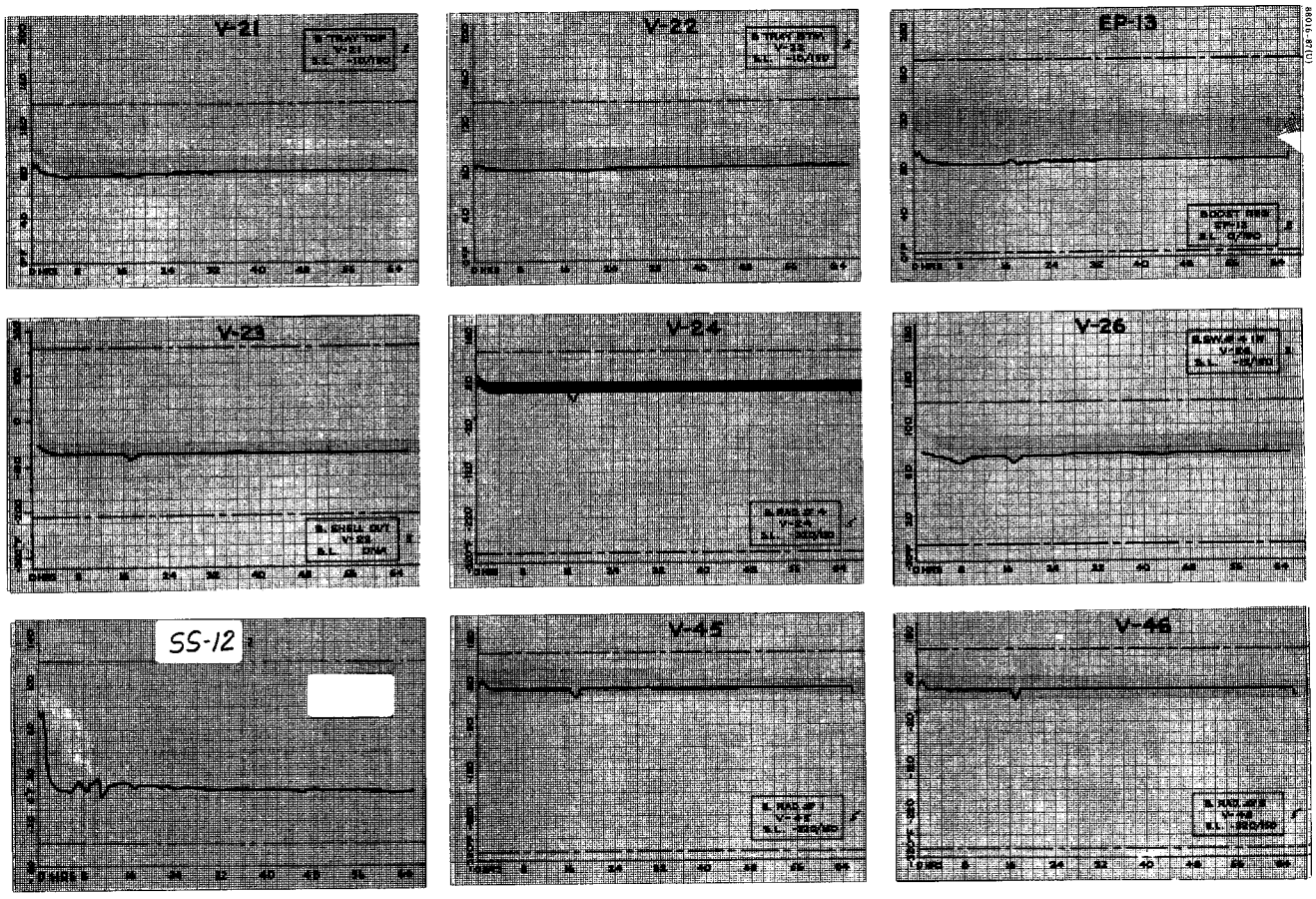

Figure 5.1-A2. Compartment B

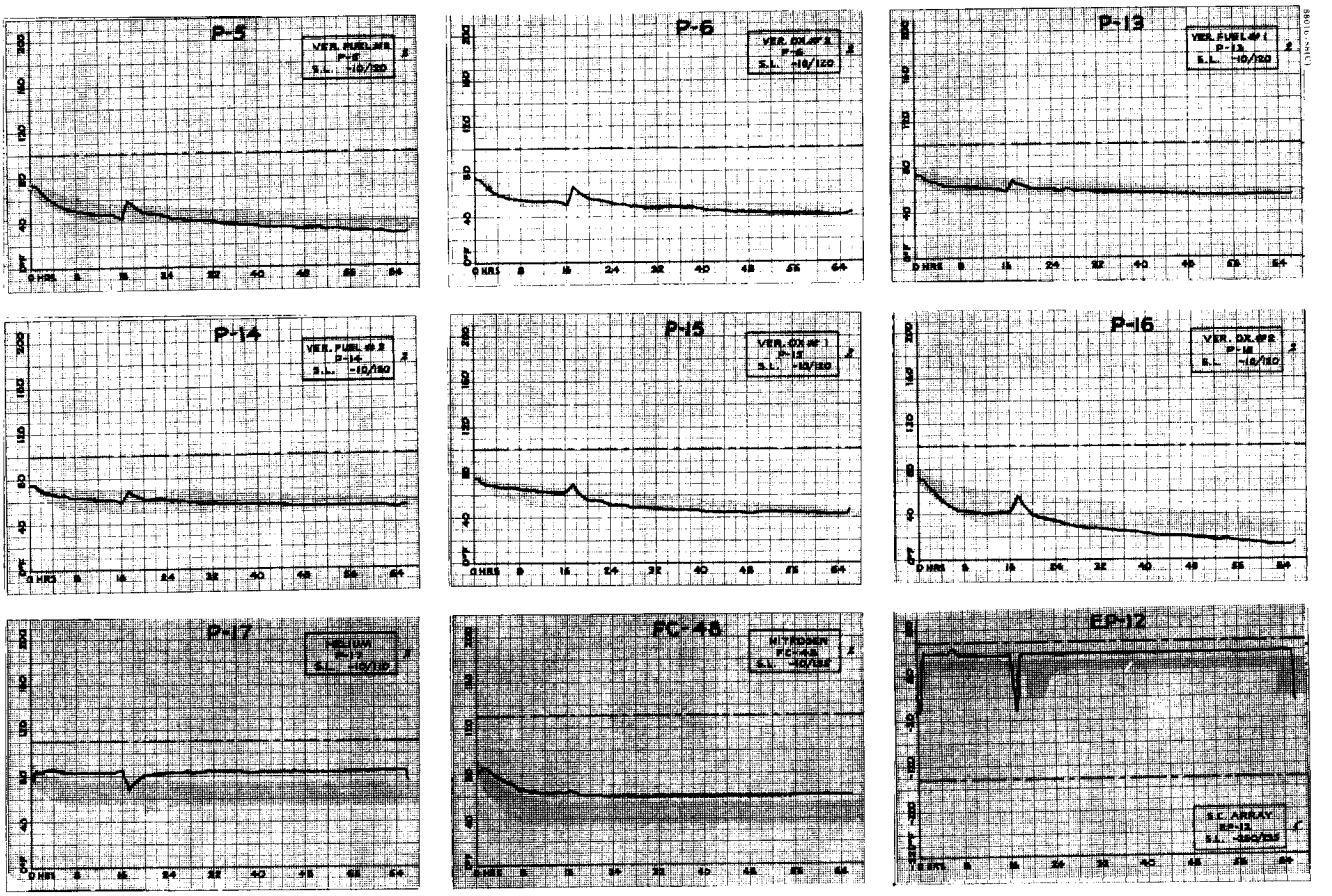

Figure 5.1-A3. Tanks

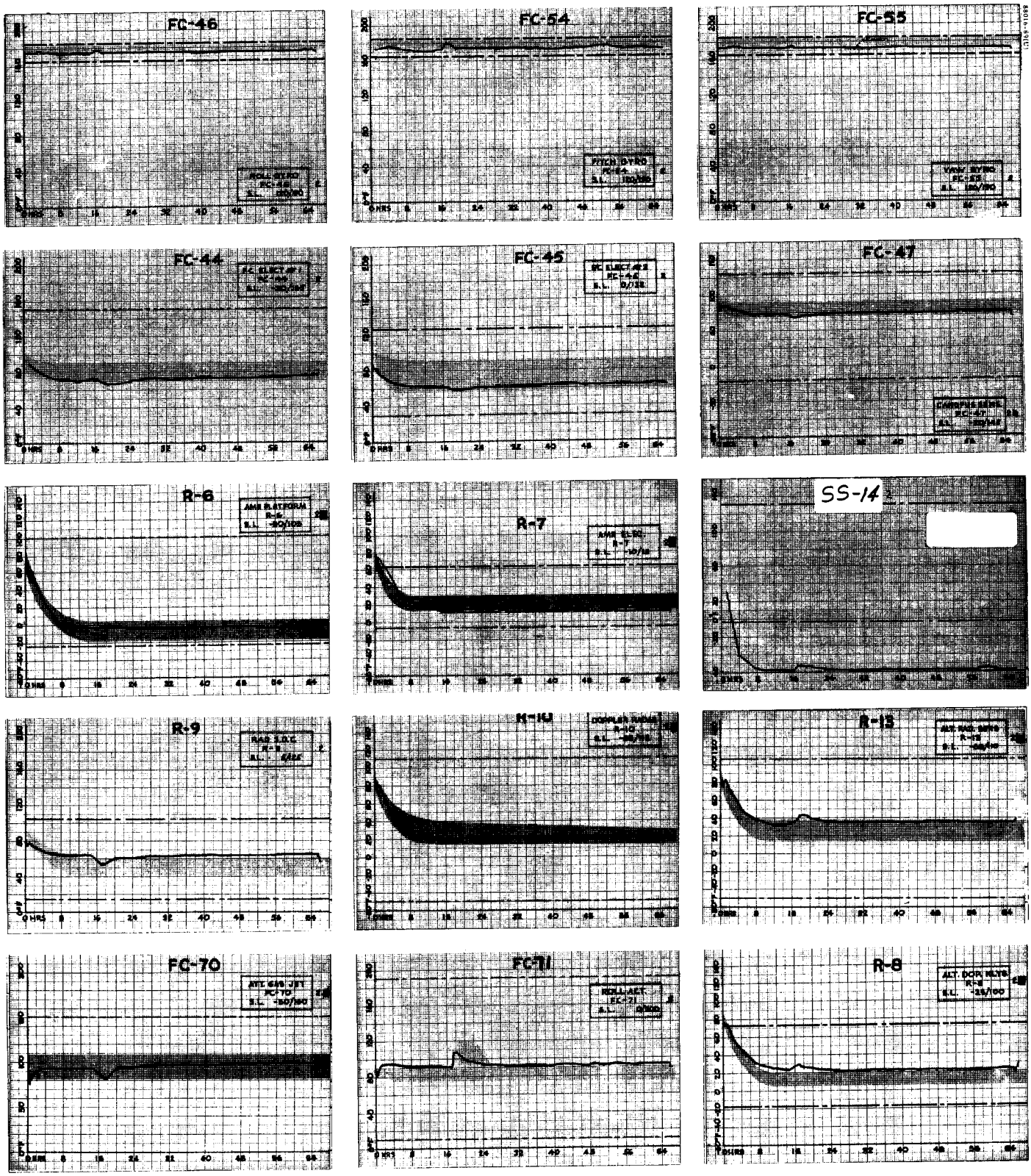

Figure 5.1-A4. Flight Control

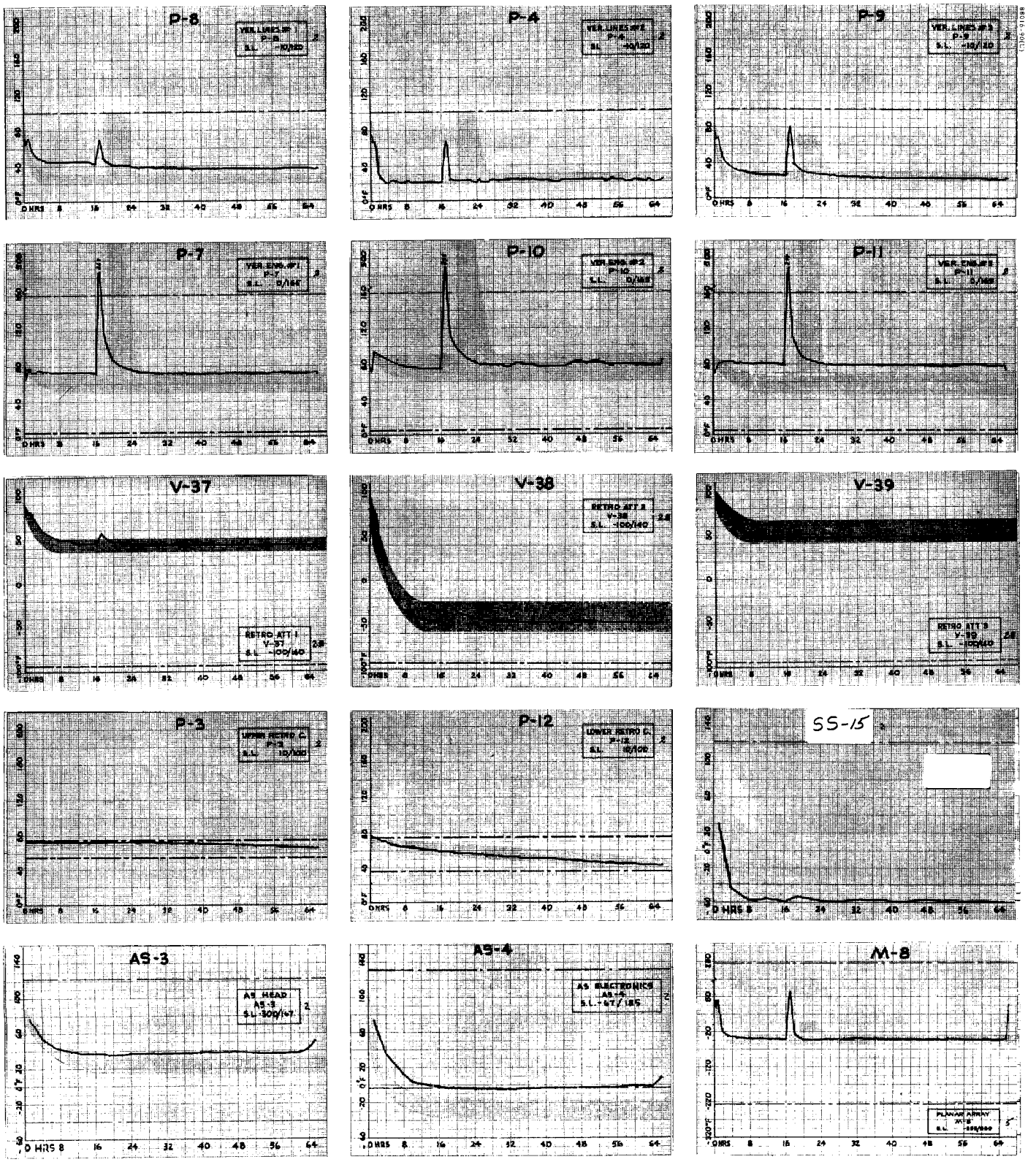

Figure 5.1-A5. Propulsion

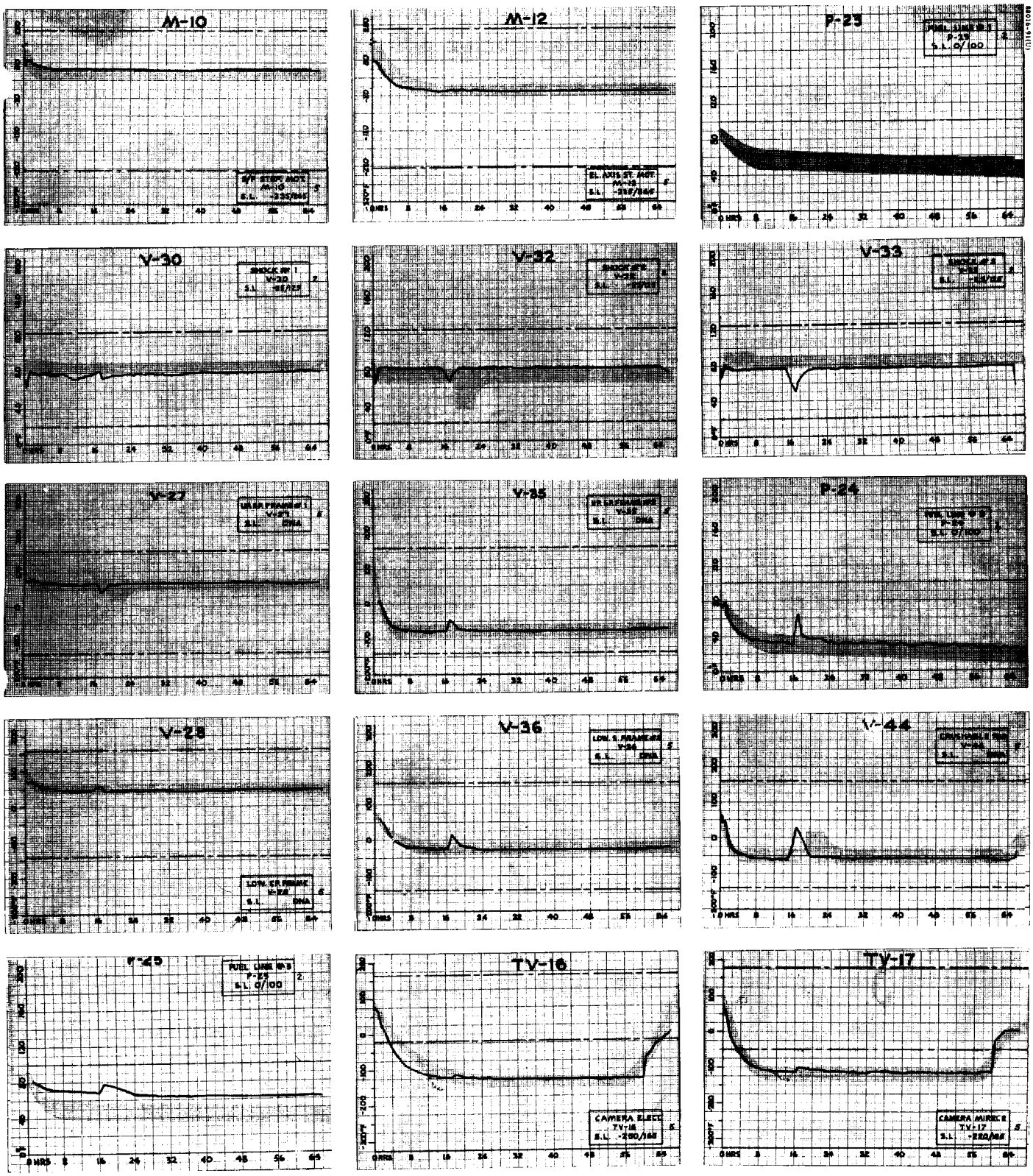

Figure 5.1-A6. Space Frame

APPENDIX B TO SECTION 5.1

FIRST LUNAR DAY TEMPERATURE PLOTS

Appendix B contains Figures 5.1-B1 through 5.1-B71, first lunar day temperature plots. The sun elevation angle is noted on these plots. Reference 7 to Section 5.1 contains shadow plots for the first lunar day using the actual A/SPP stepping history. These plots were recorded in real time by Spacecraft Performance Analysis and Command.

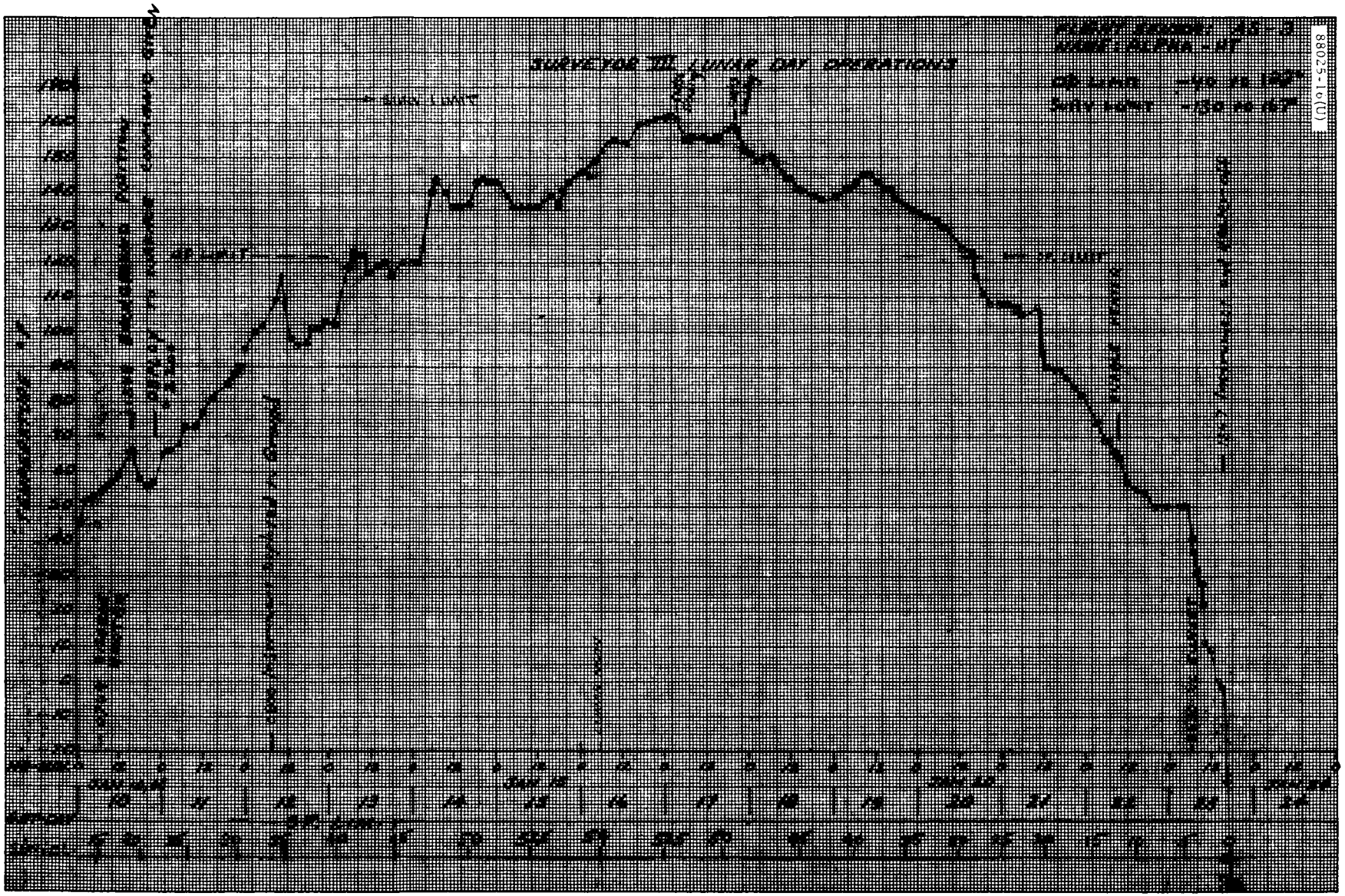

Figure 5.1-B1. Sensor AS-3: Alpha Scattering Head

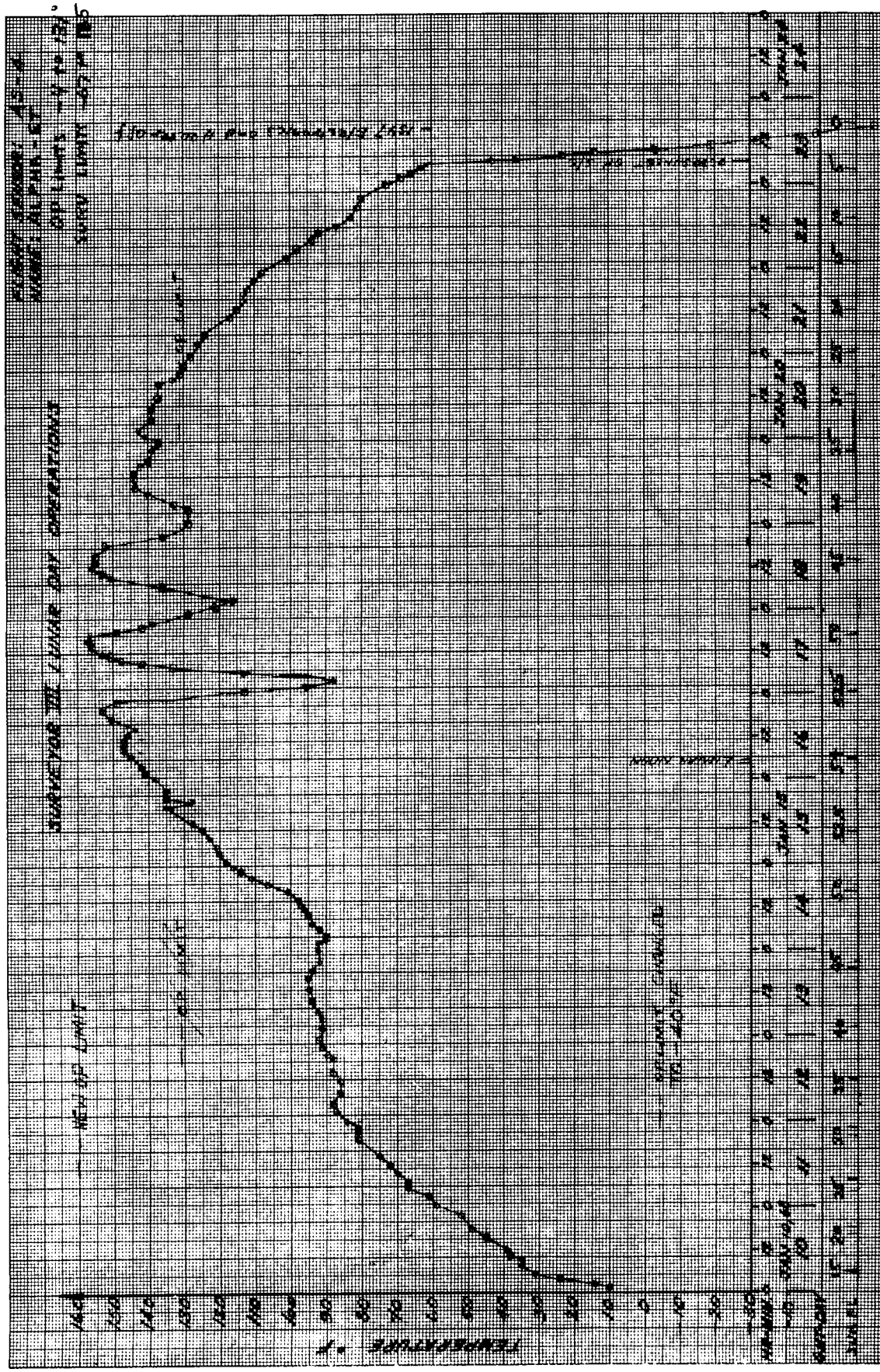

Figure 5.1-B2. Sensor AS-4: Compartment C

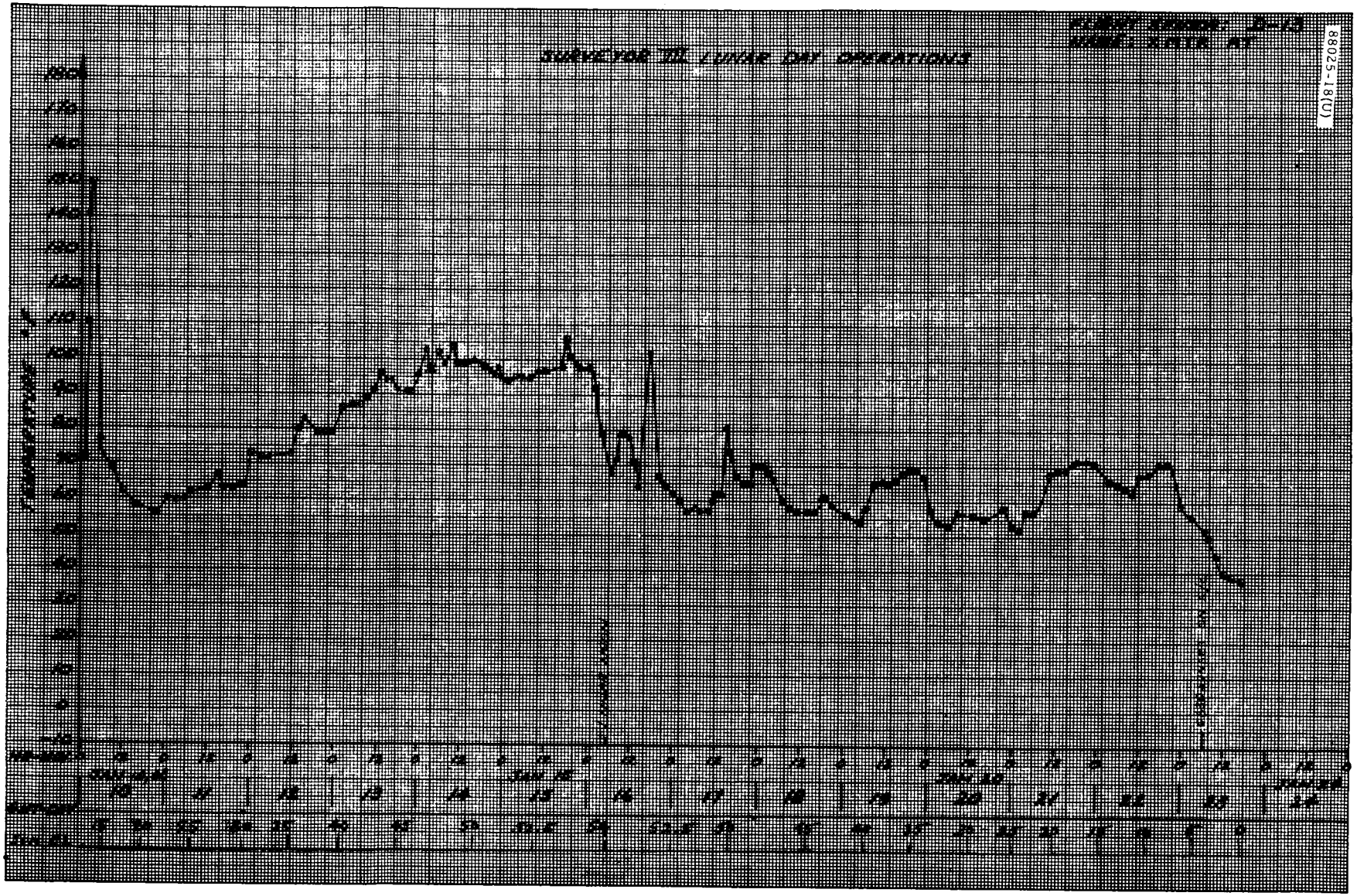

Figure 5.1-B3. Sensor D-13: Transmitter A

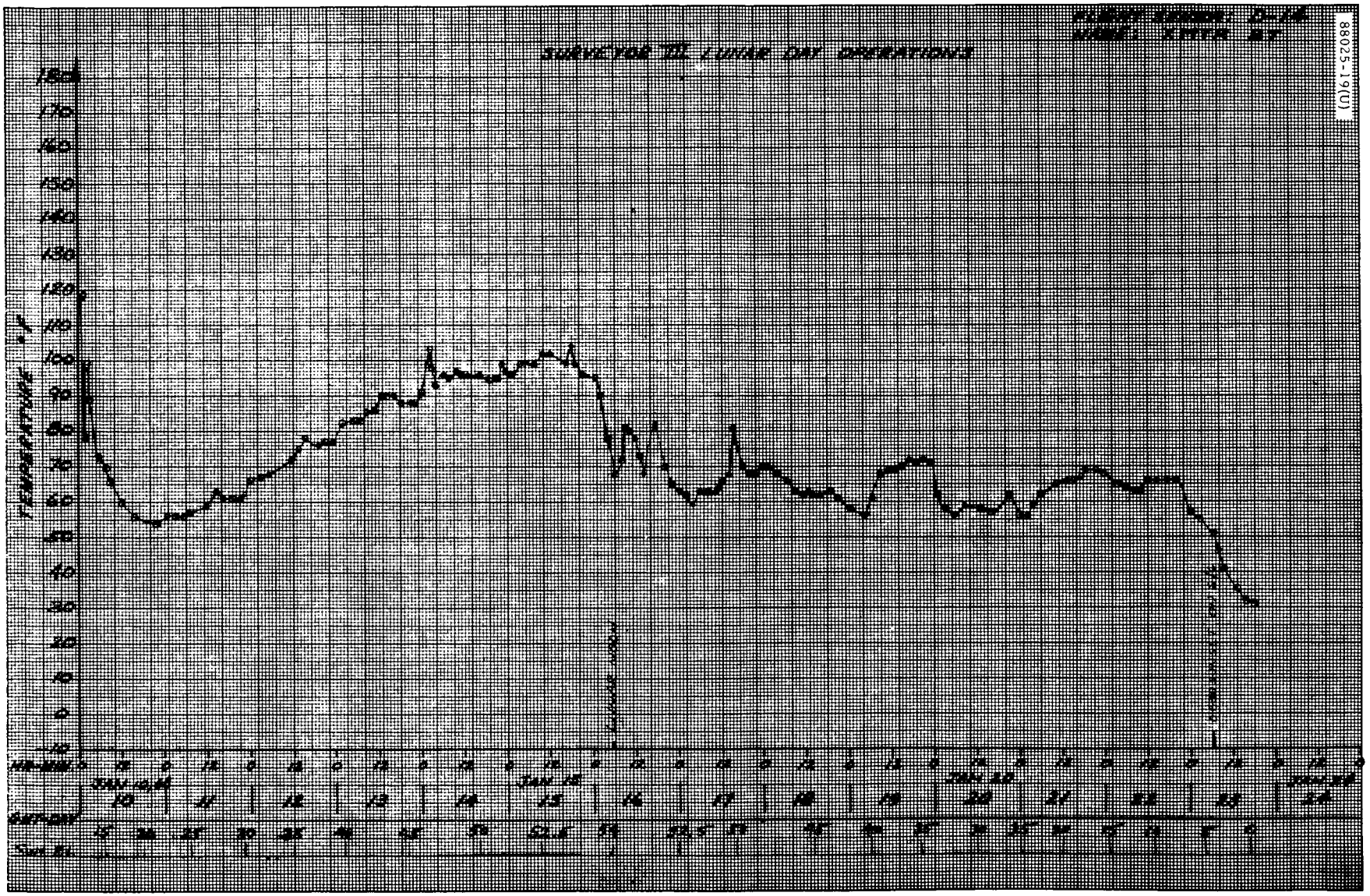

Figure 5.1-B4. Sensor D-14: Transmitter B

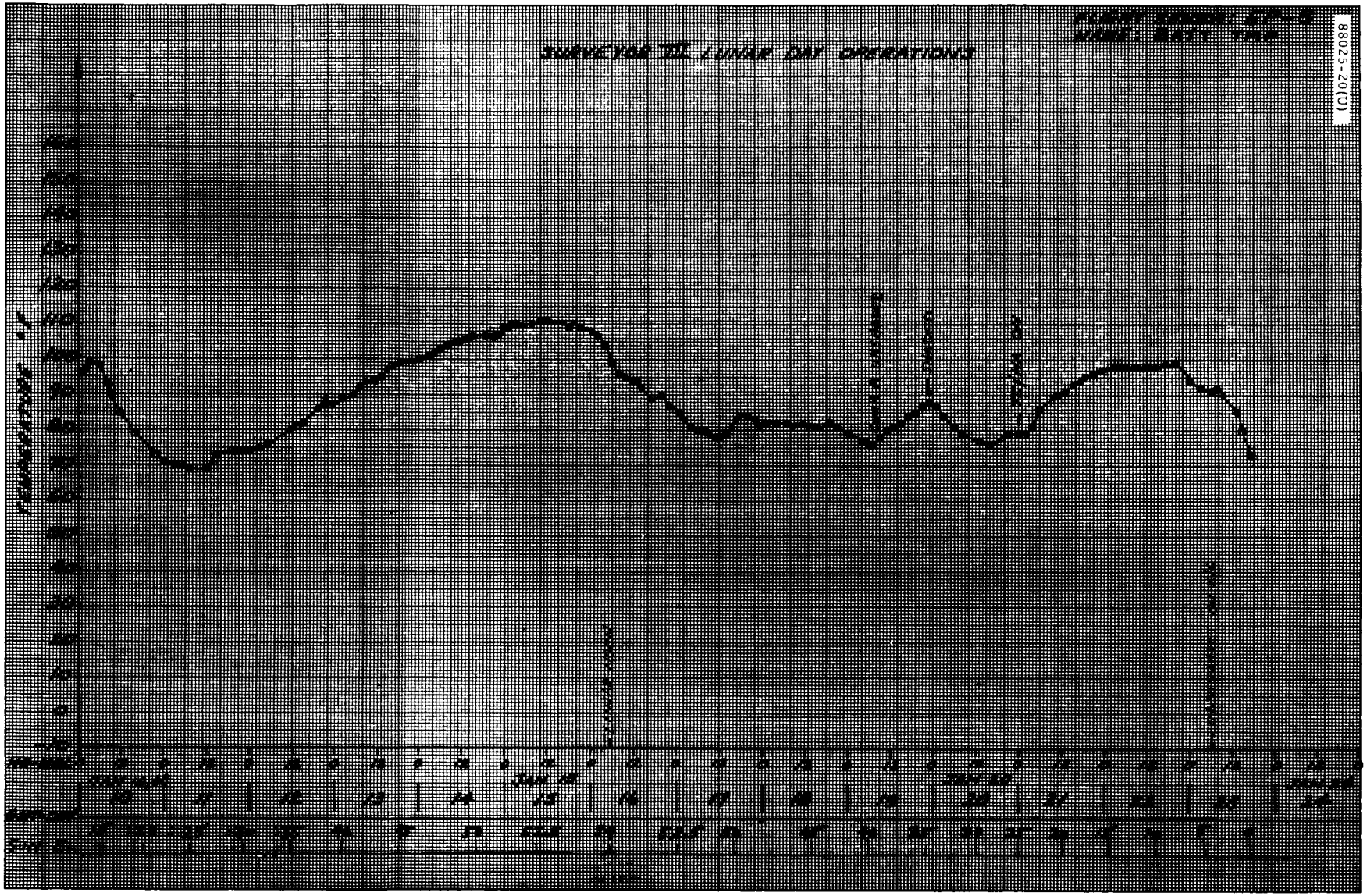

Figure 5.1-B5. Sensor EP-8: Main Battery

88025-21(U)

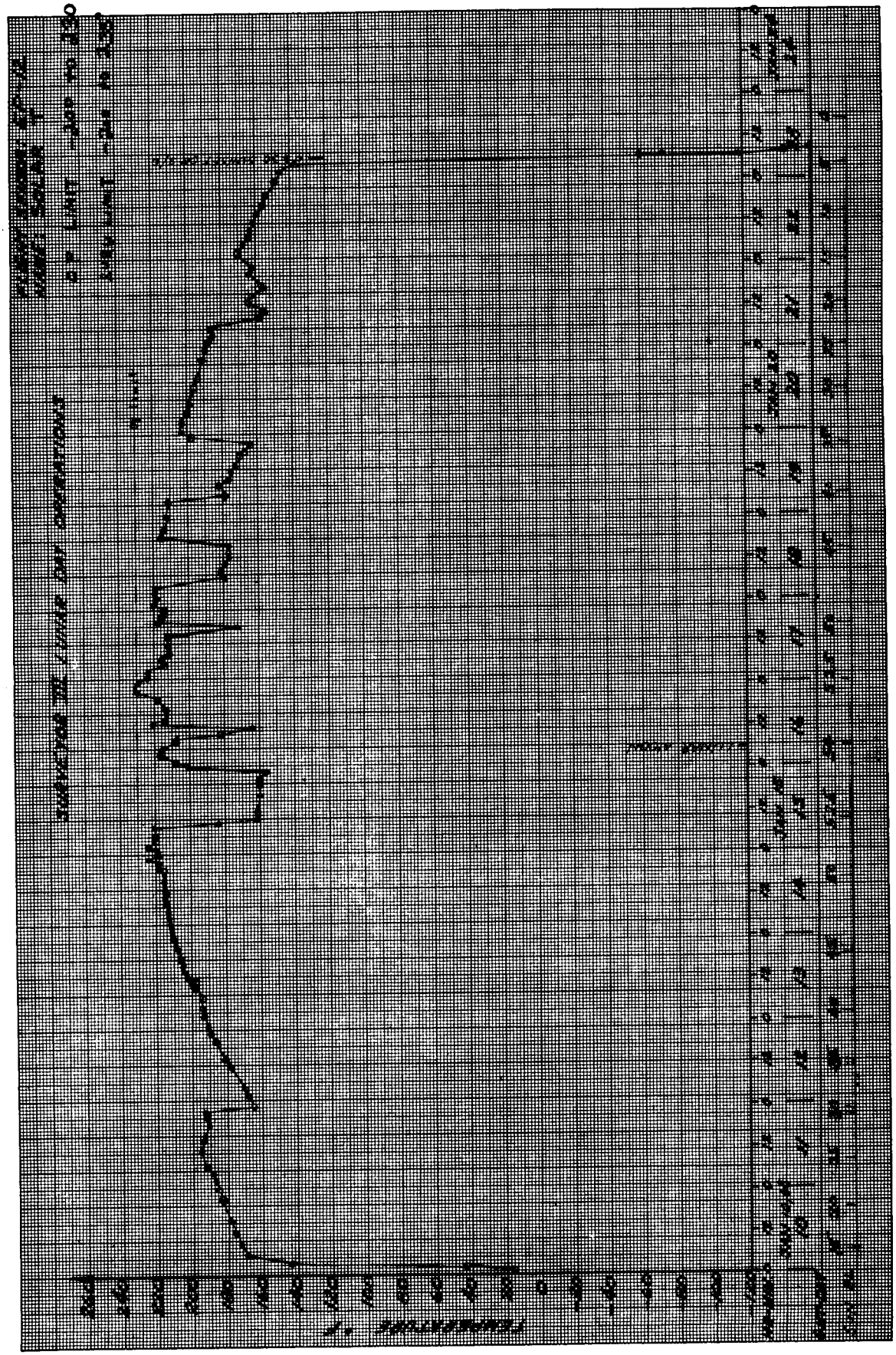

Figure 5.1-B6. Sensor EP-12: Solar Array

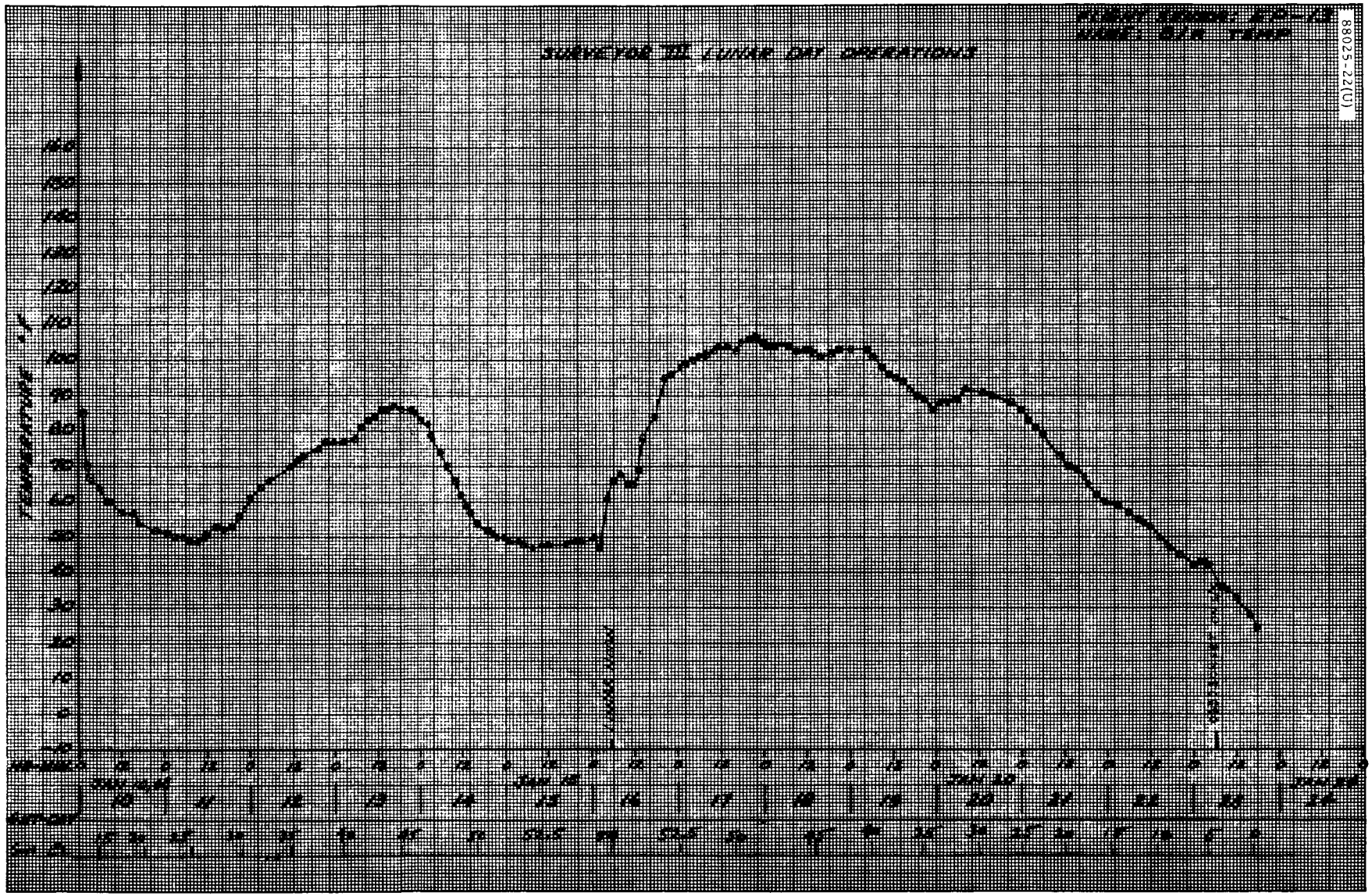

Figure 5.1-B7. Sensor EP-13: Boost Regulator

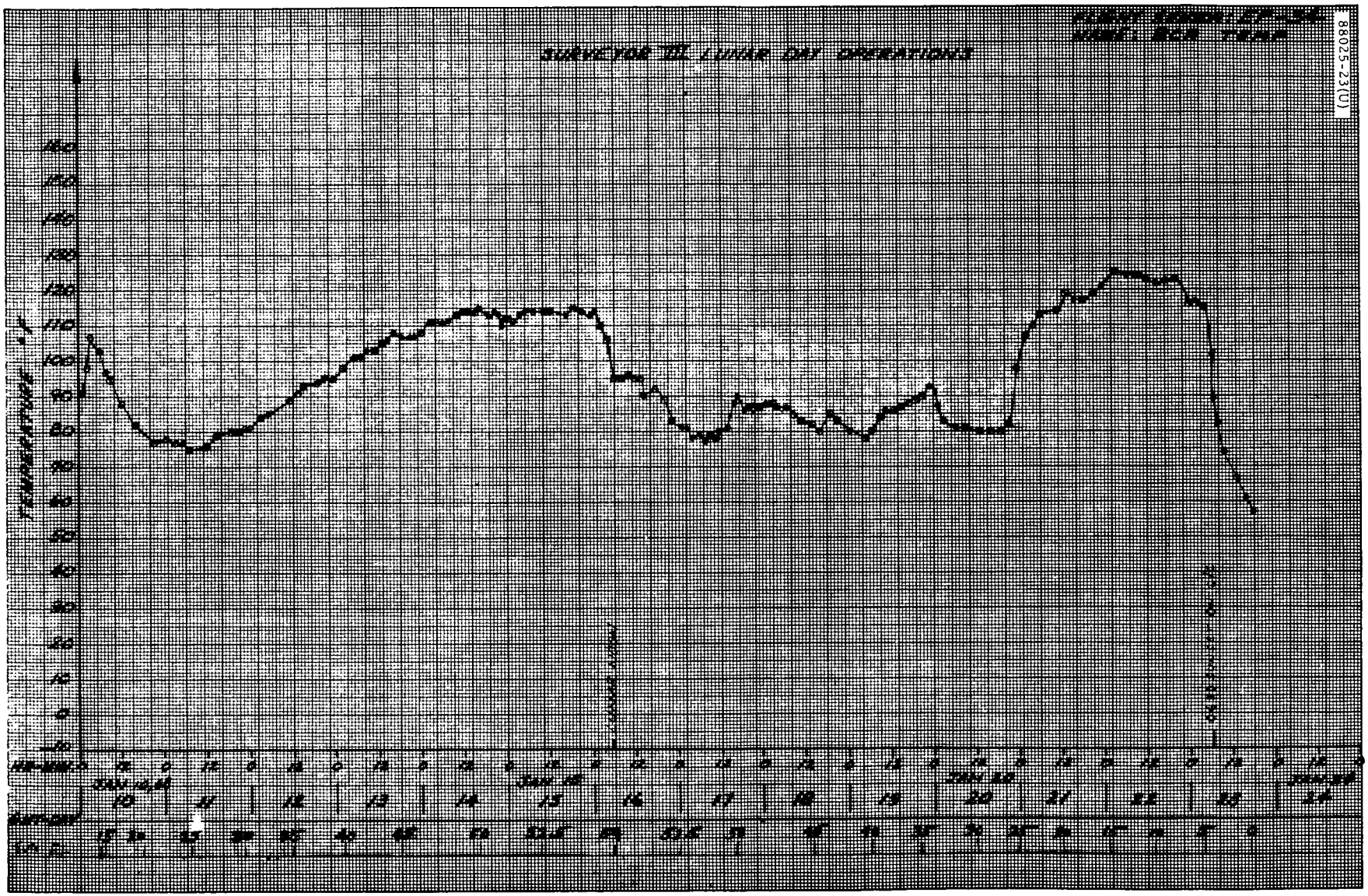

Figure 5.1-B8. Sensor EP-34: Battery Charge Regulator

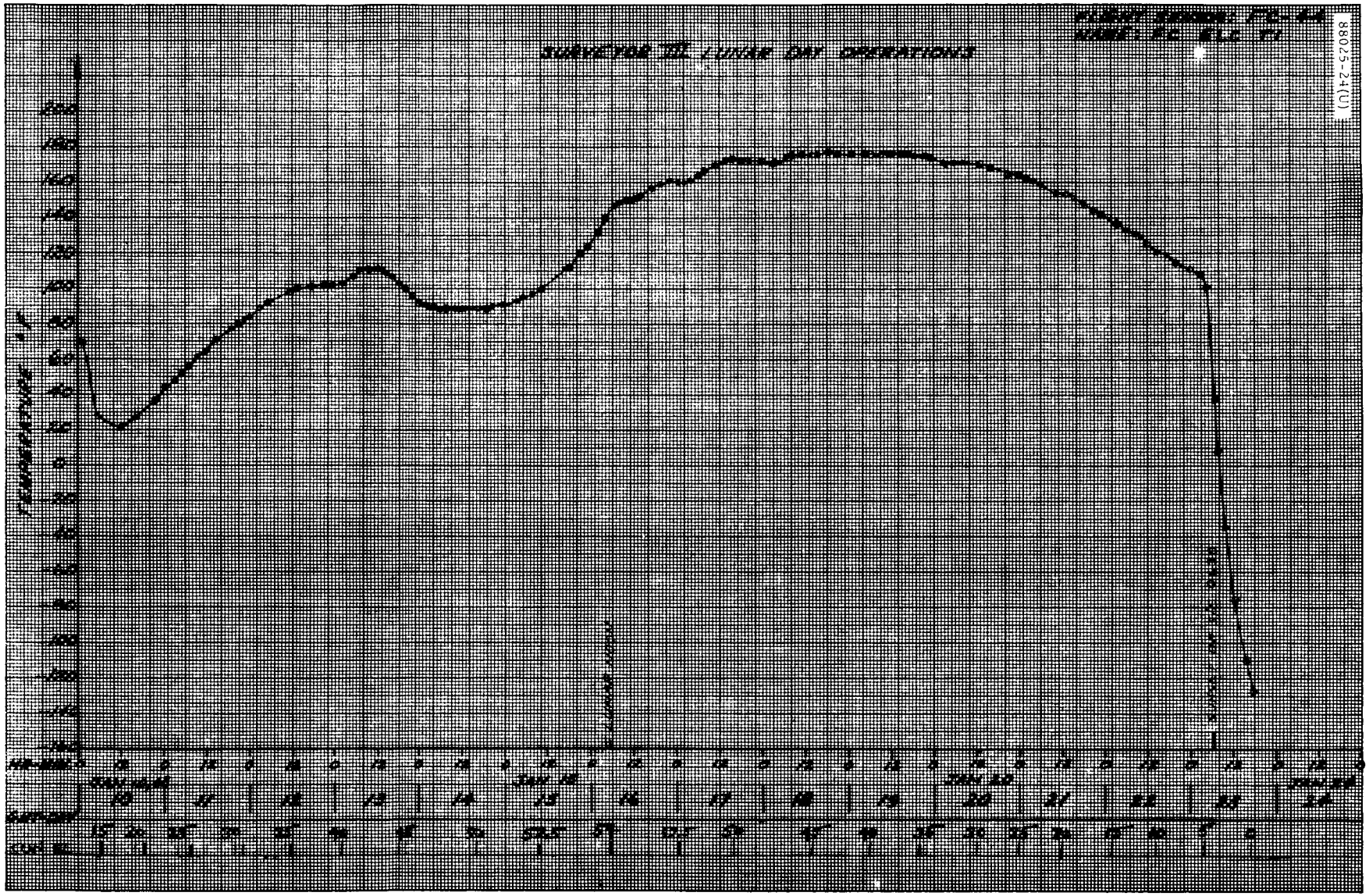

Figure 5.1-B9. Sensor FC-44: Flight Control Electronics 1

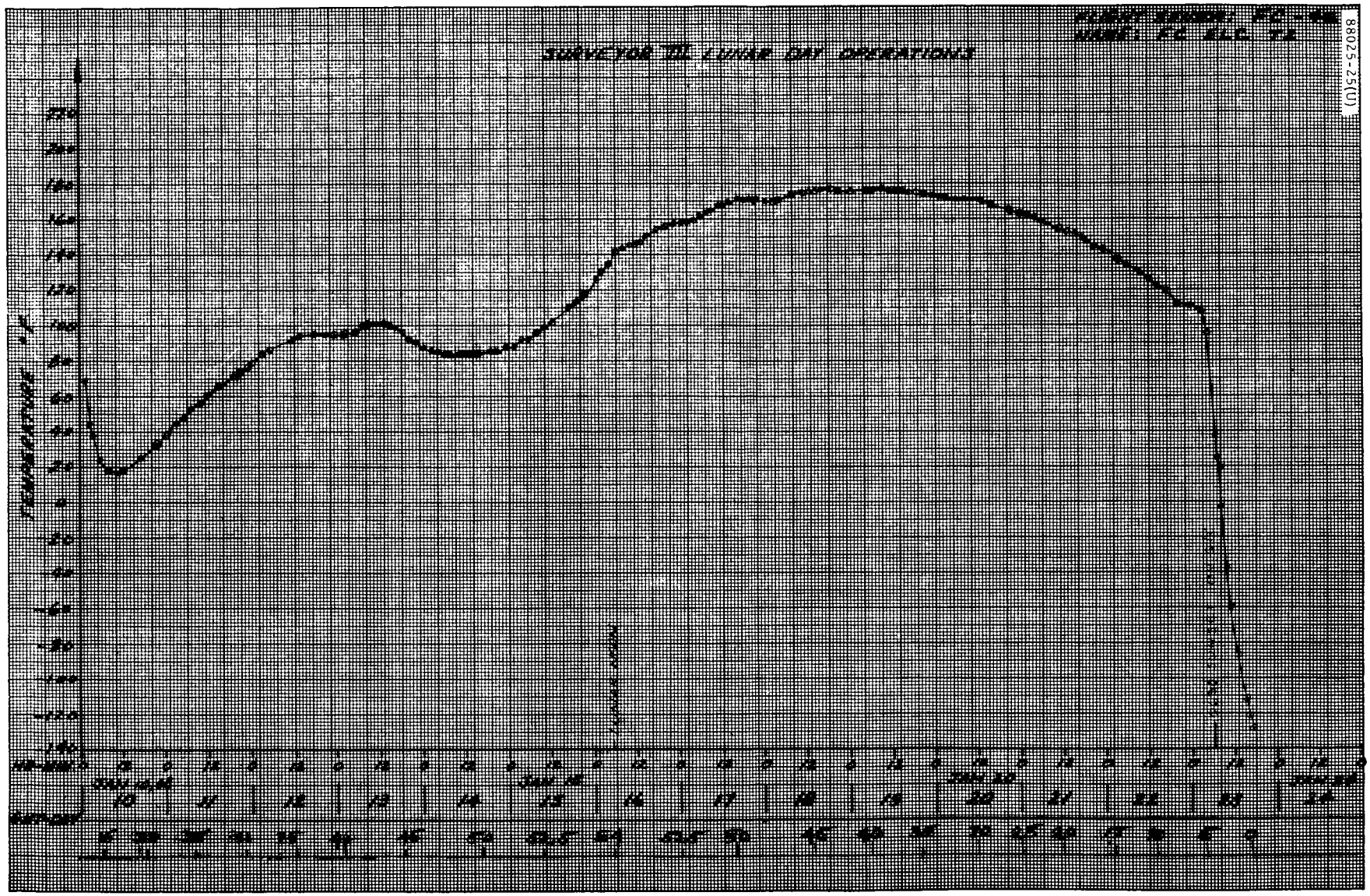

Figure 5. 1-B10. Sensor FC-45: Flight Control Electronics 2

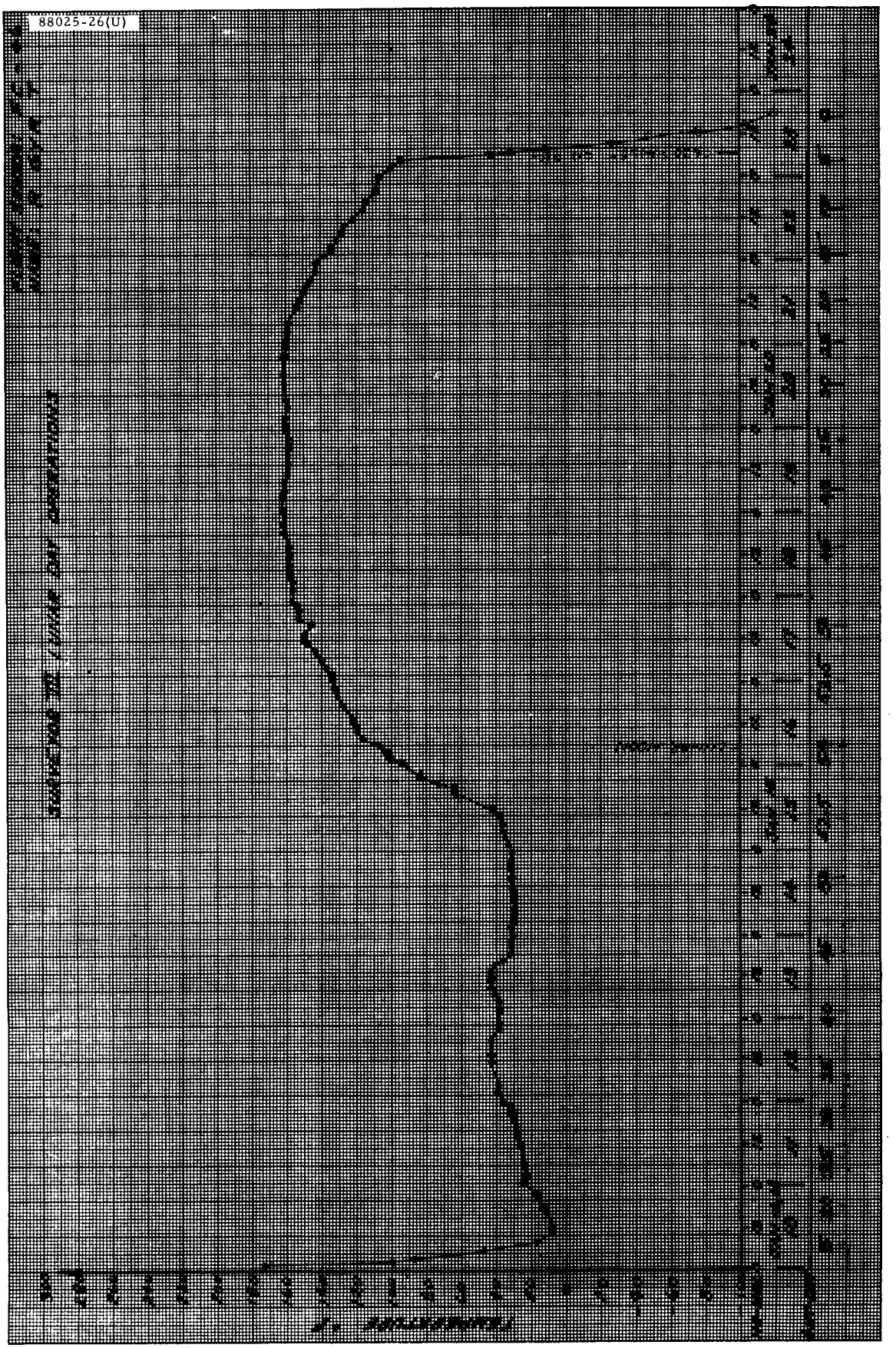

Figure 5.1-B11. Sensor FC-46: Roll Gyro

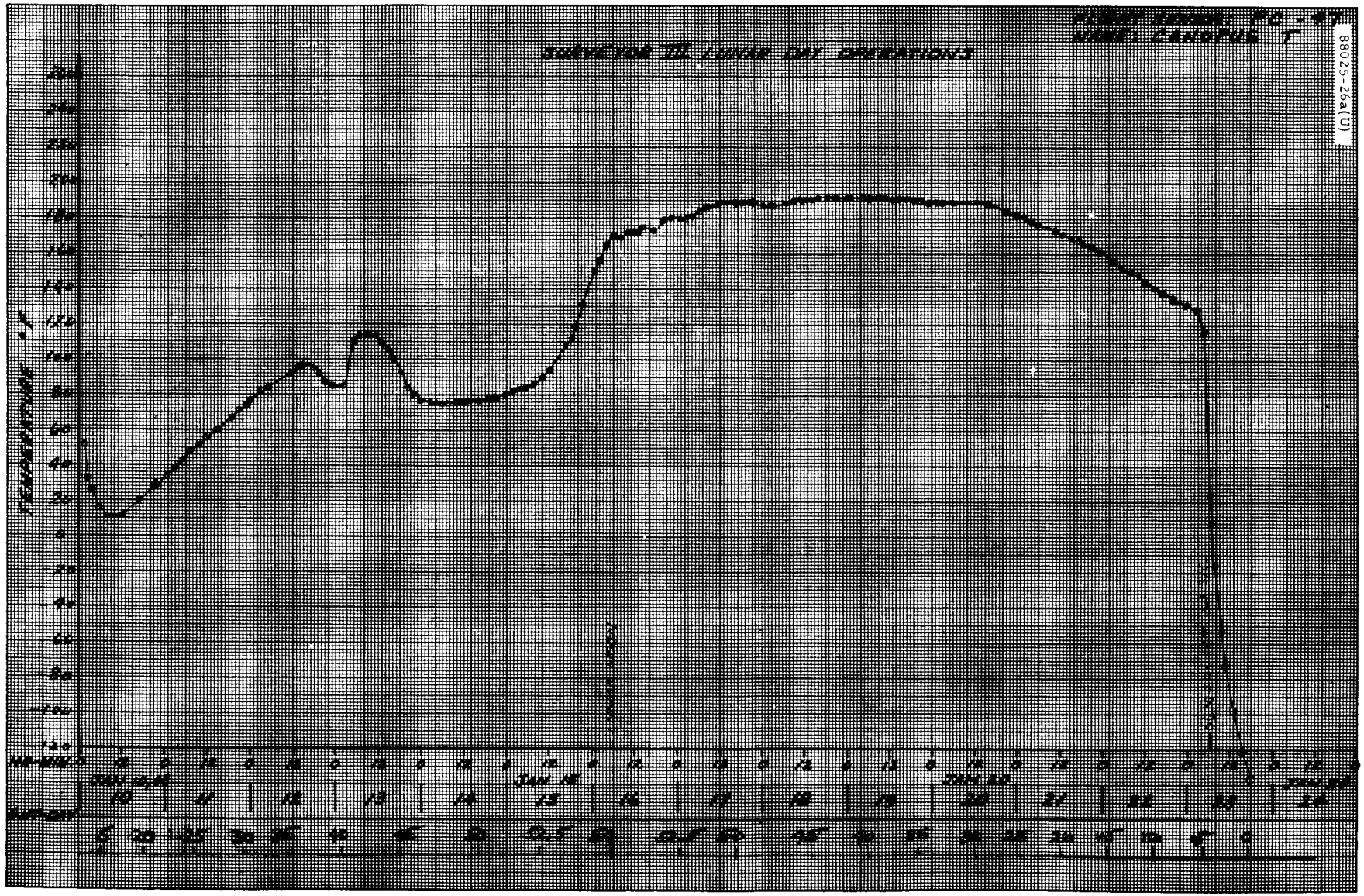

Figure 5.1-B12. Sensor FC-47: Canopus Sensor

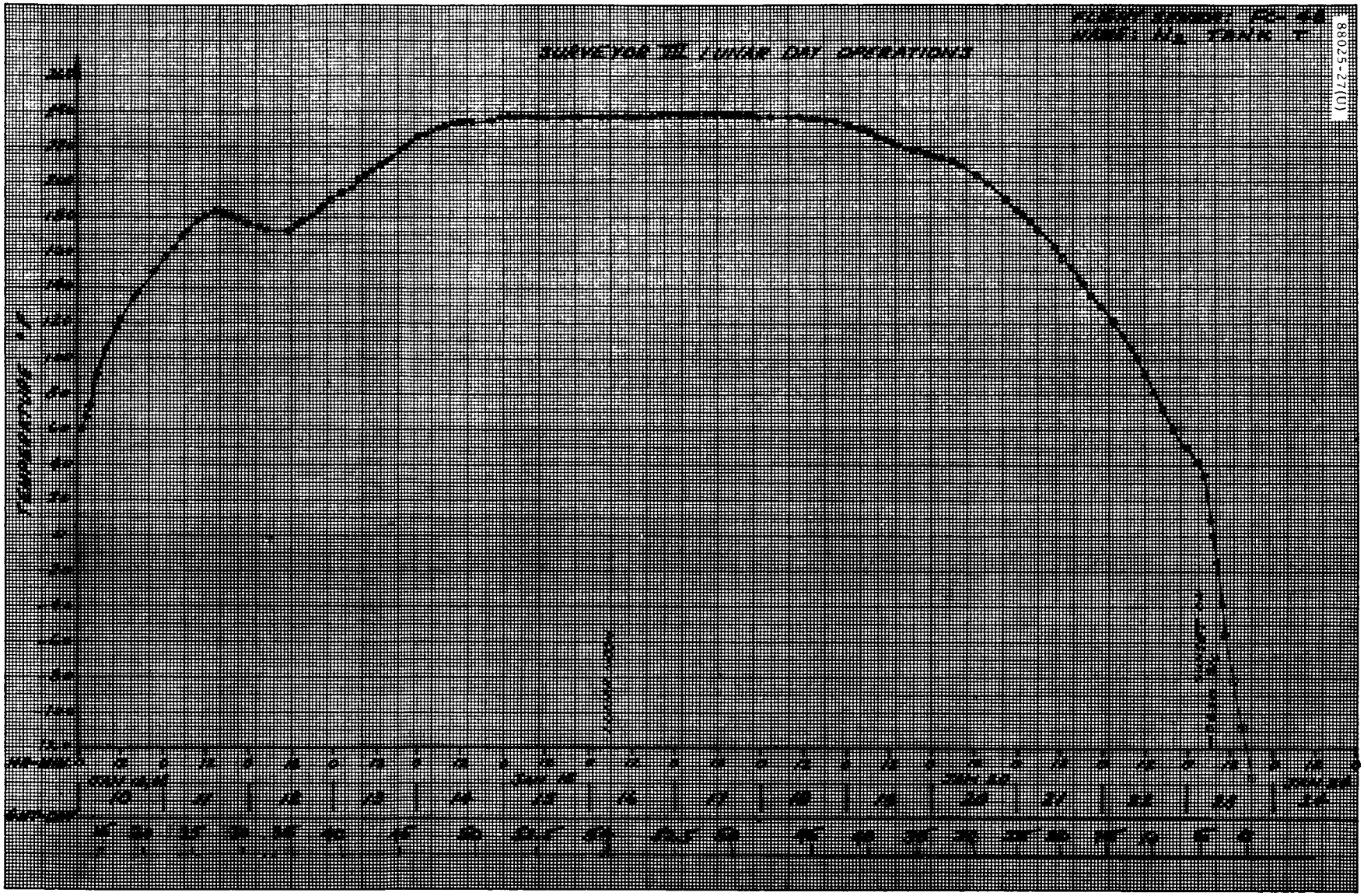

Figure 5. 1-B13. Sensor FC-48: Nitrogen Gas Tank

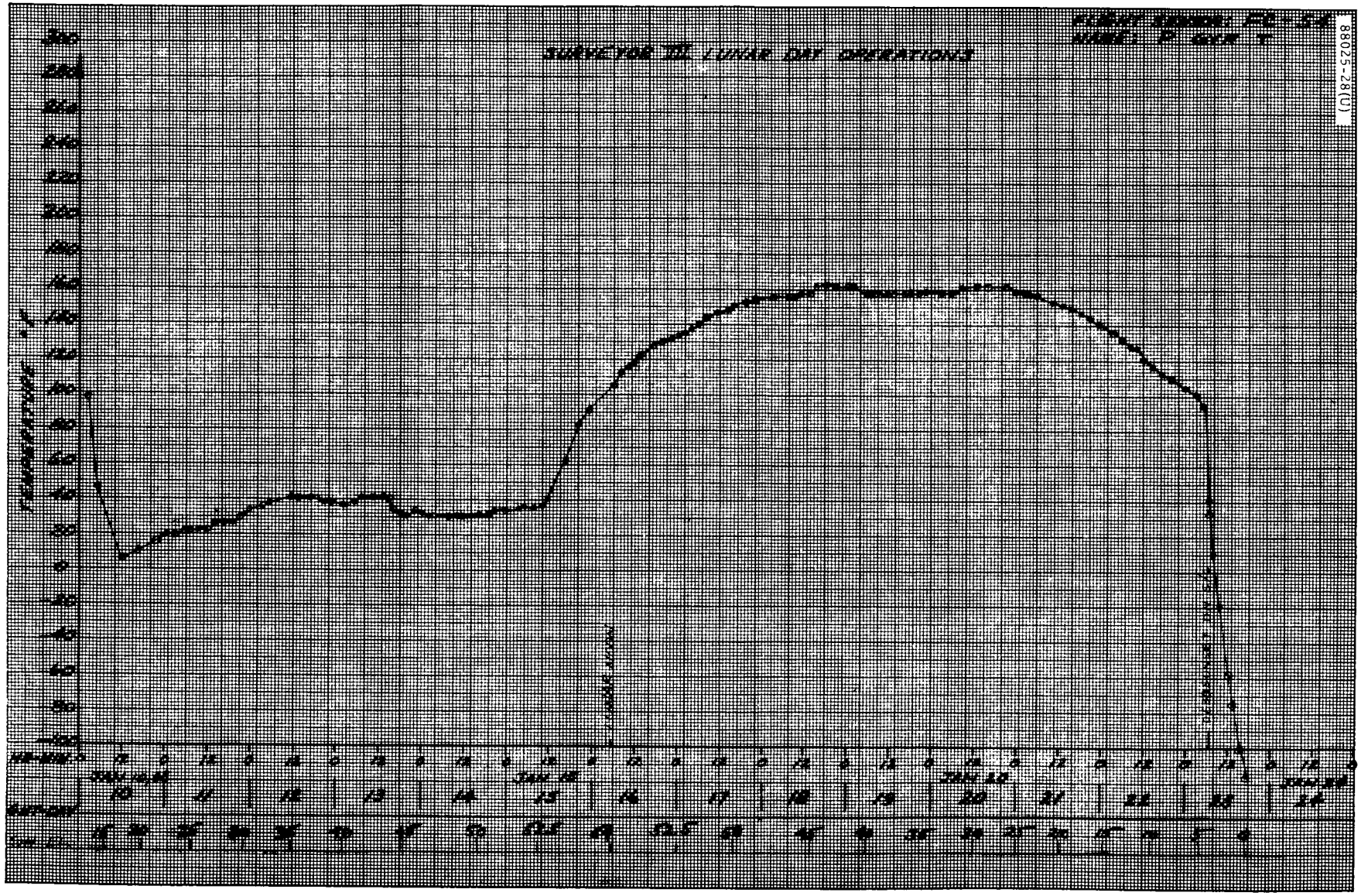

Figure 5. 1-B14. Sensor FC-54: Pitch Gyro

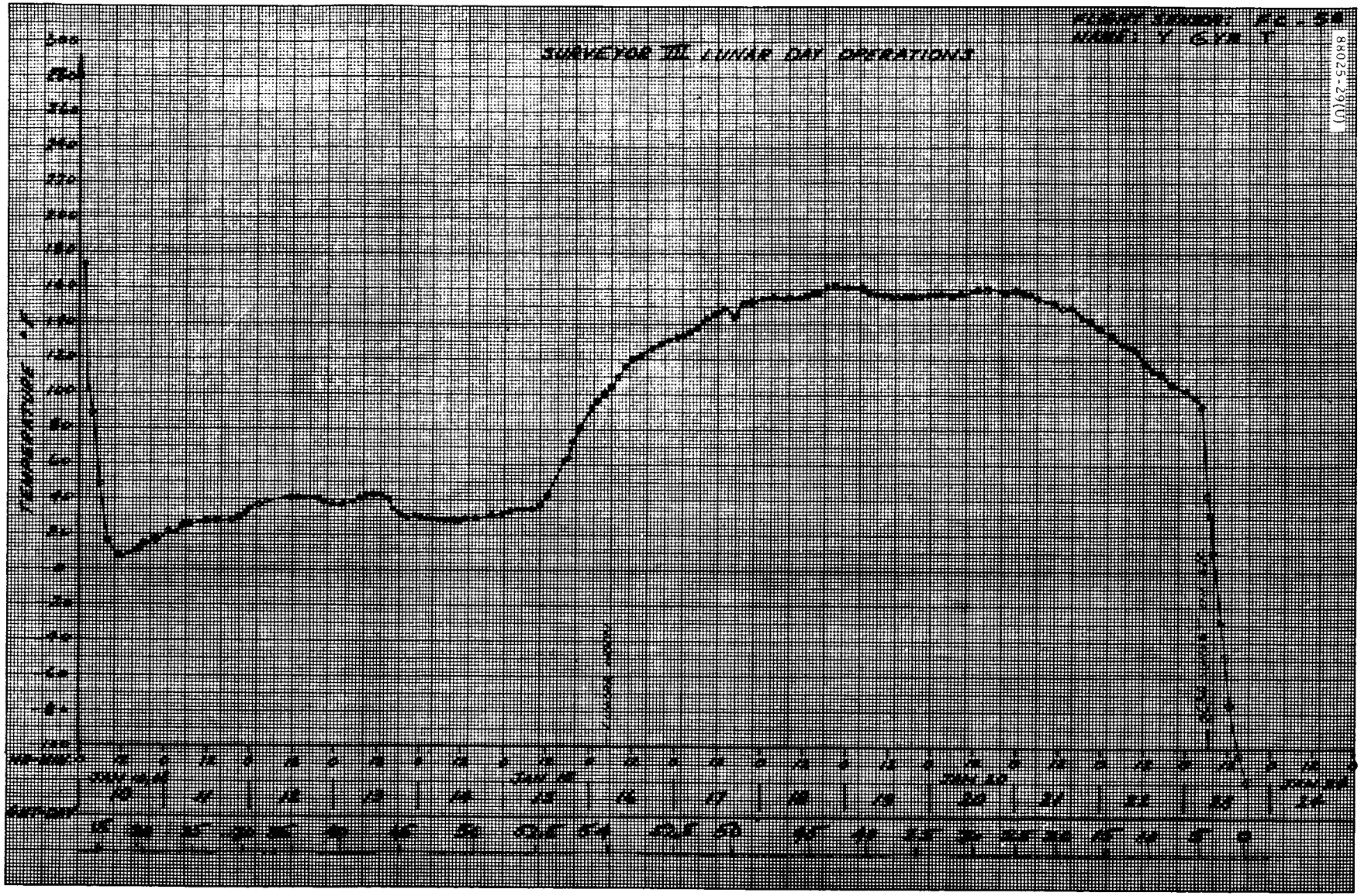

Figure 5.1-B15. Sensor FC-55: Yaw Gyro

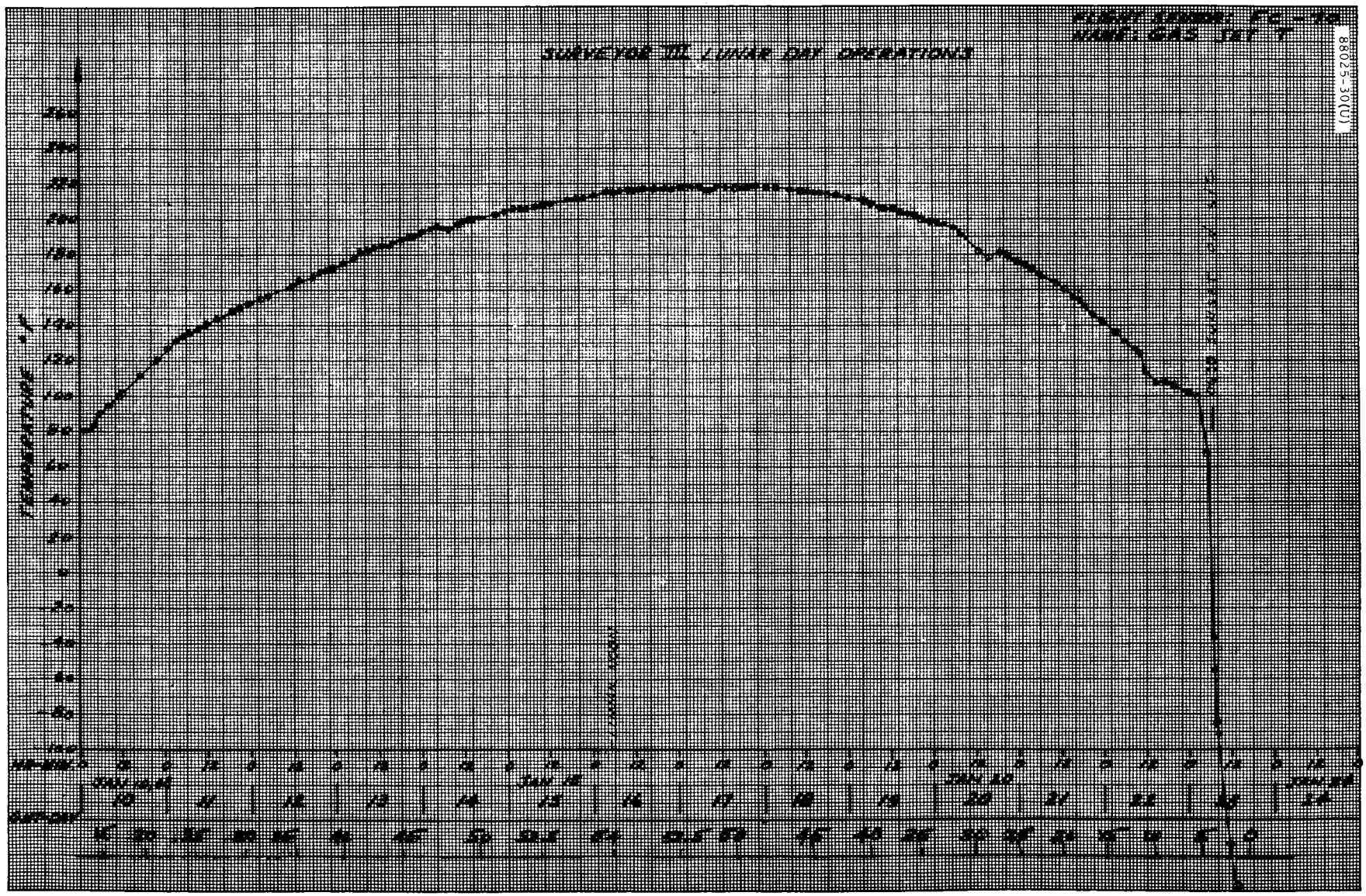

Figure 5.1-B16. Sensor FC-70: Attitude Gas Jet 2

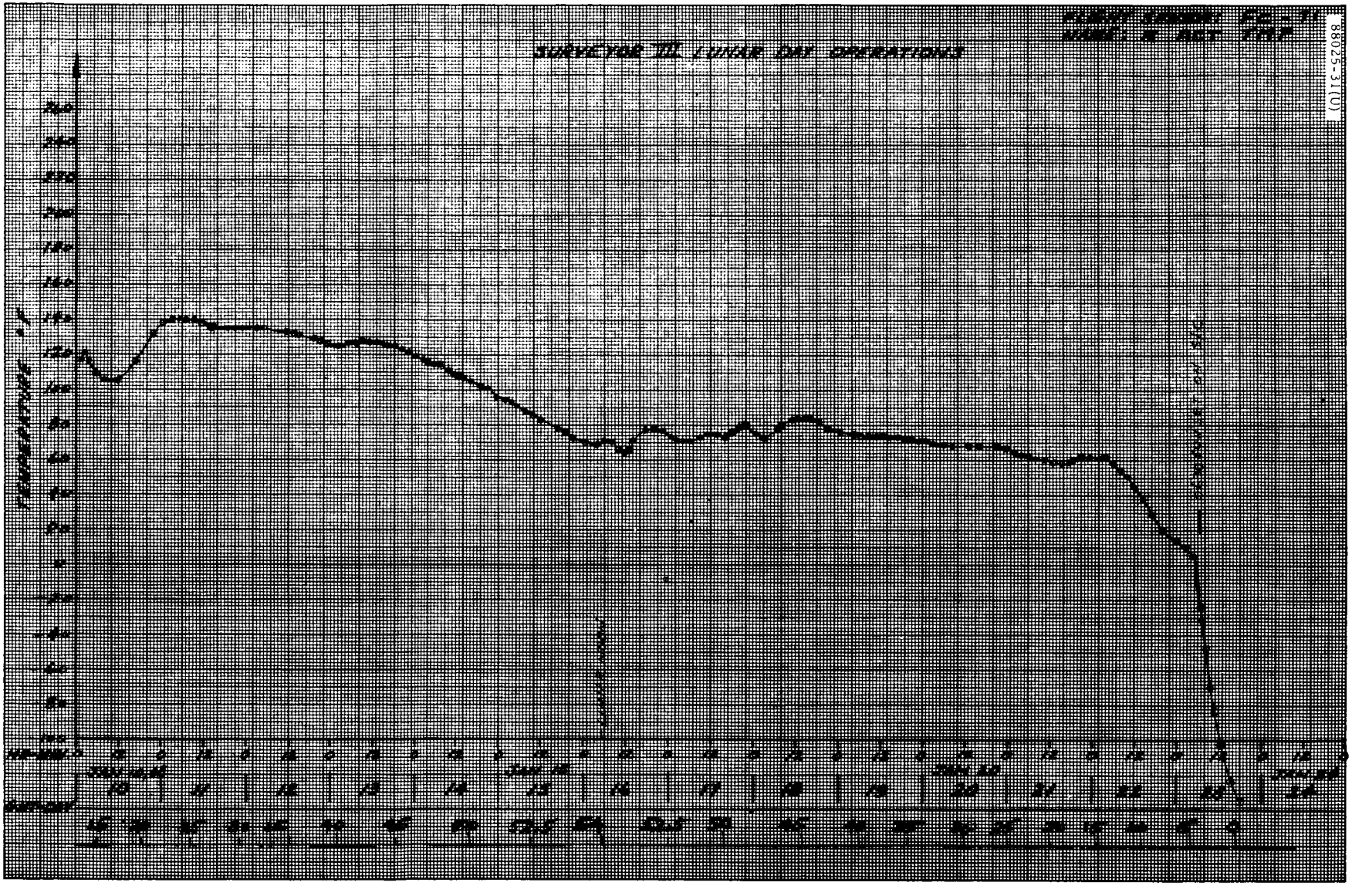

Figure 5.1-B17. Sensor FC-71: Roll Actuator

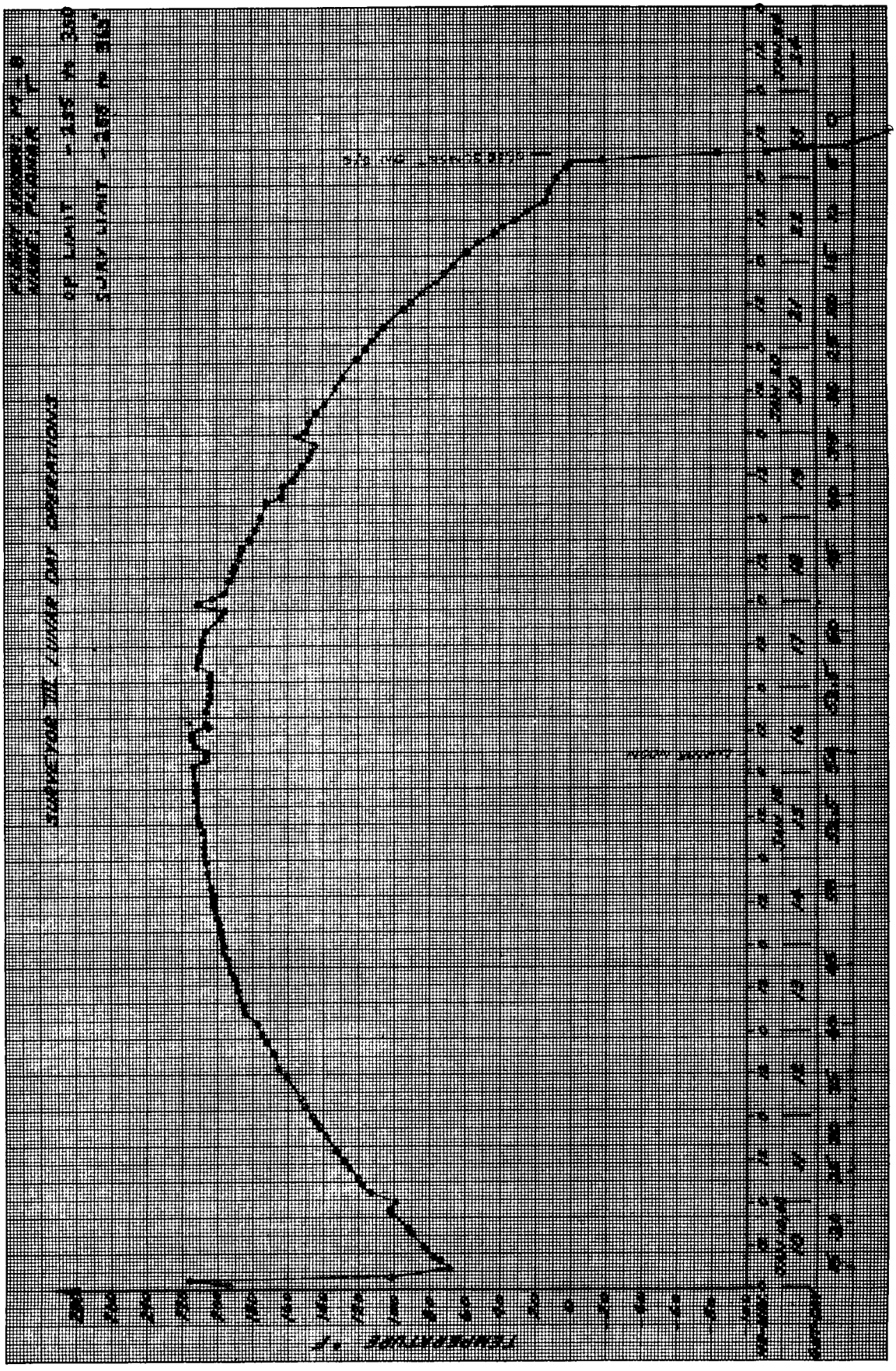

Figure 5.1-B18. Sensor M-8: Planar Array

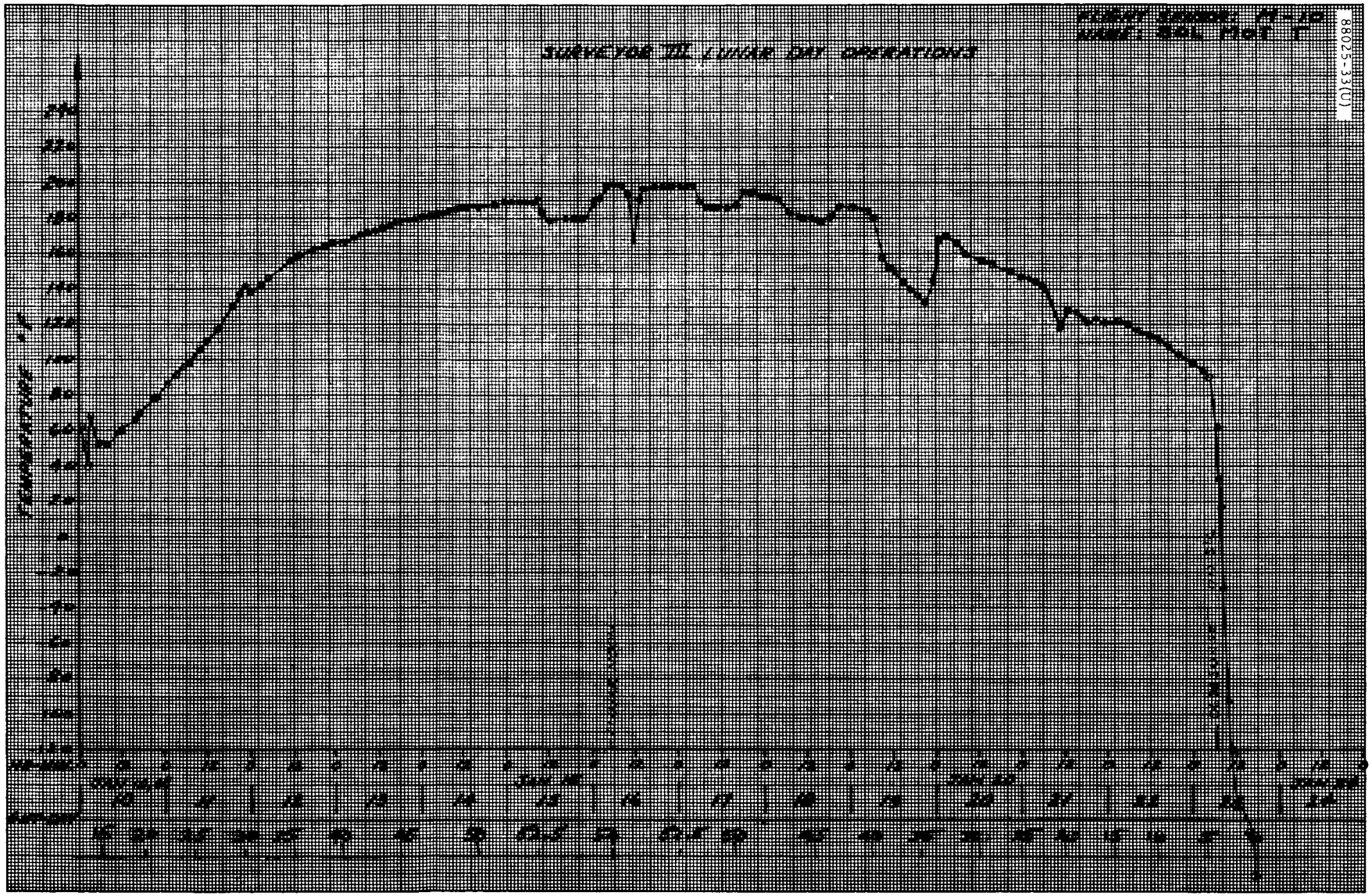

Figure 5.1-B19. Sensor M-10: Solar Panel Stepping Motor

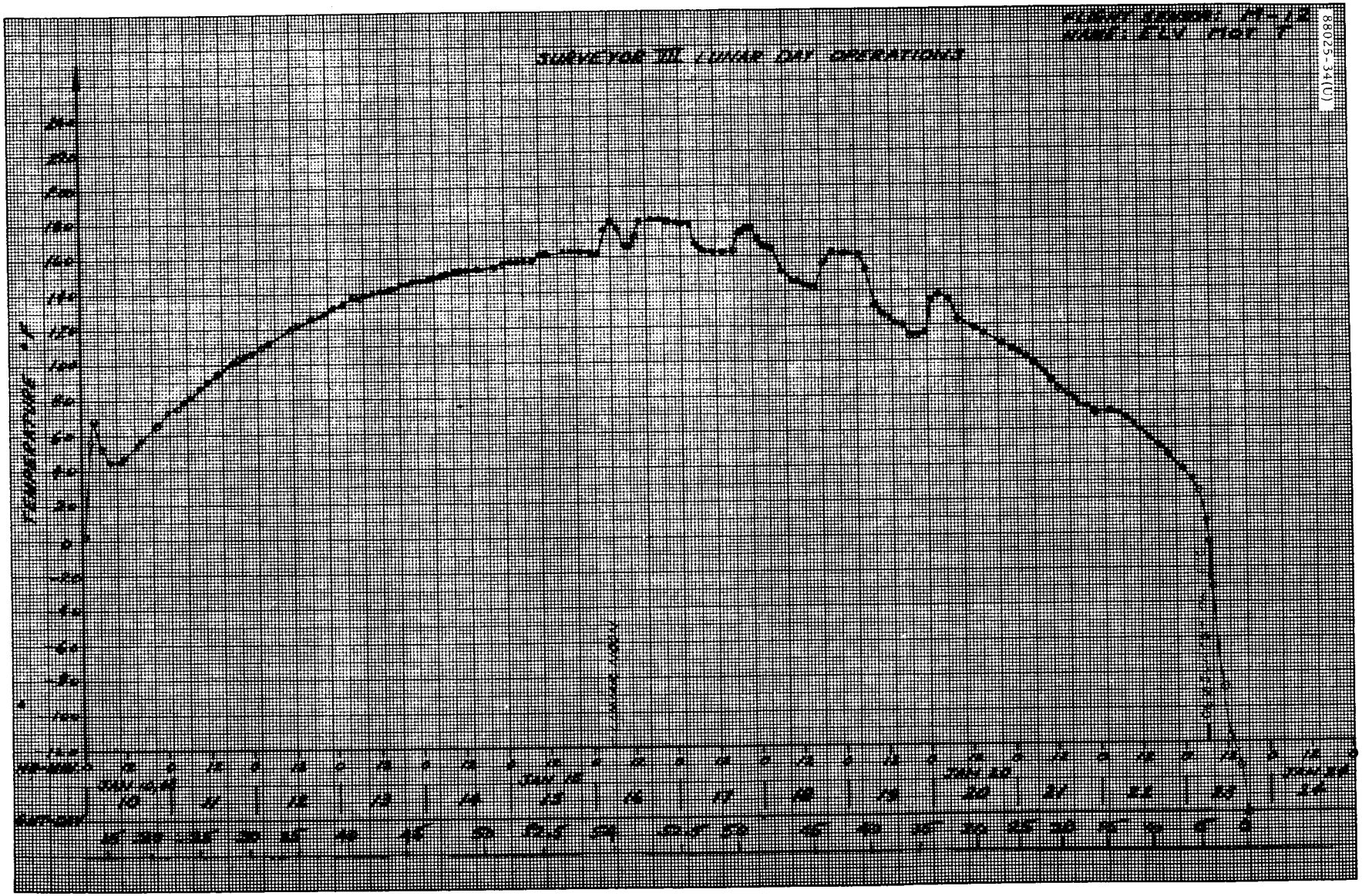

Figure 5. 1-B20. Sensor M-12: Elevation Axis Stepping Motor

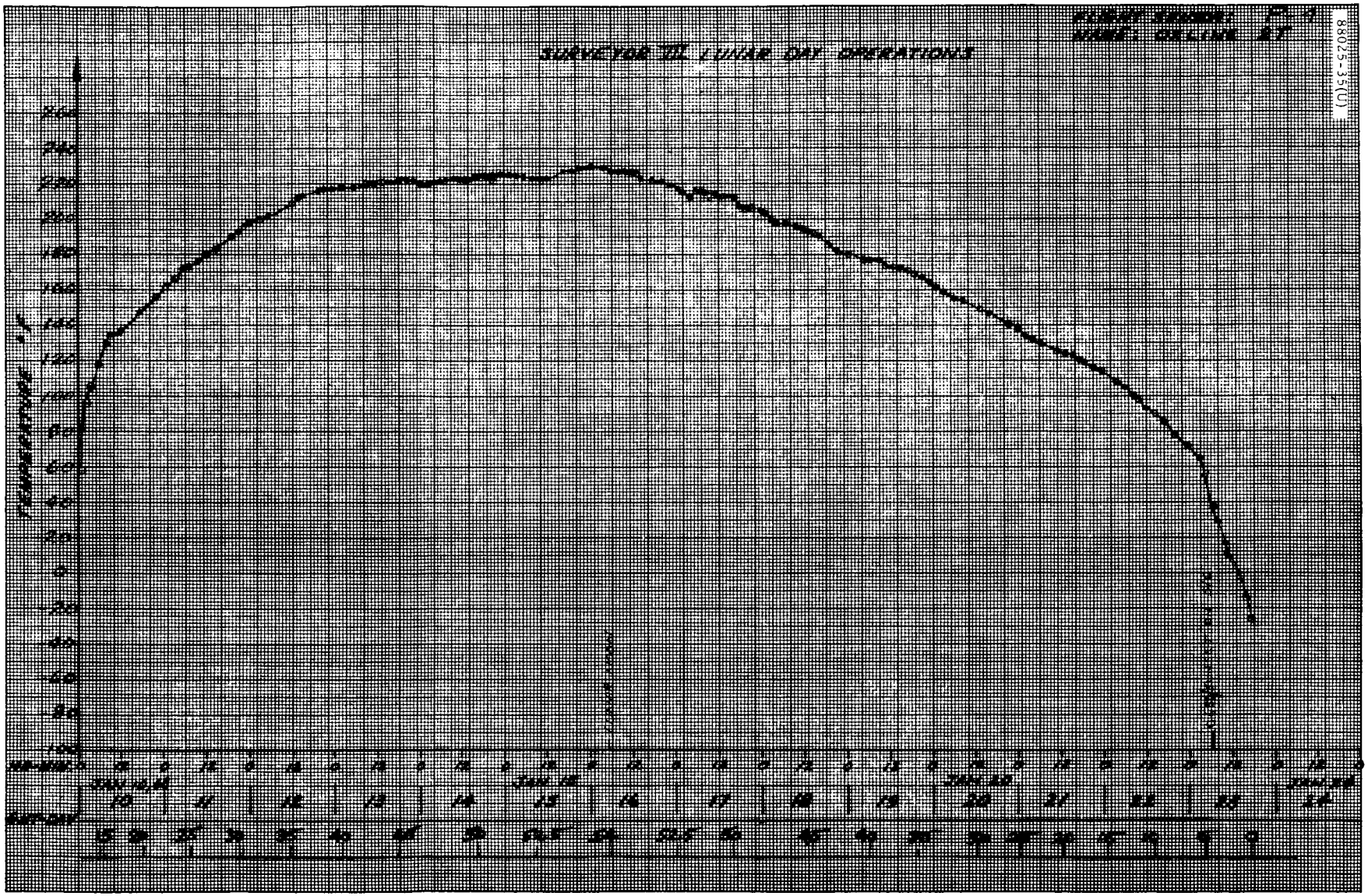
SURVEYOR III LUNAR DAY OPERATIONS
88025-35(U)
TEMPERATURE, °F
280
240
200
160
120
80
40
0
-40
-80
-120
-160
-200
-240
-280
-320
-360
-400
-440
-480
-520
-560
-600
-640
-680
-720
-760
-800
-840
-880
-920
-960
-1000
-1040
-1080
-1120
-1160
-1200
-1240
-1280
-1320
-1360
-1400
-1440
-1480
-1520
-1560
-1600

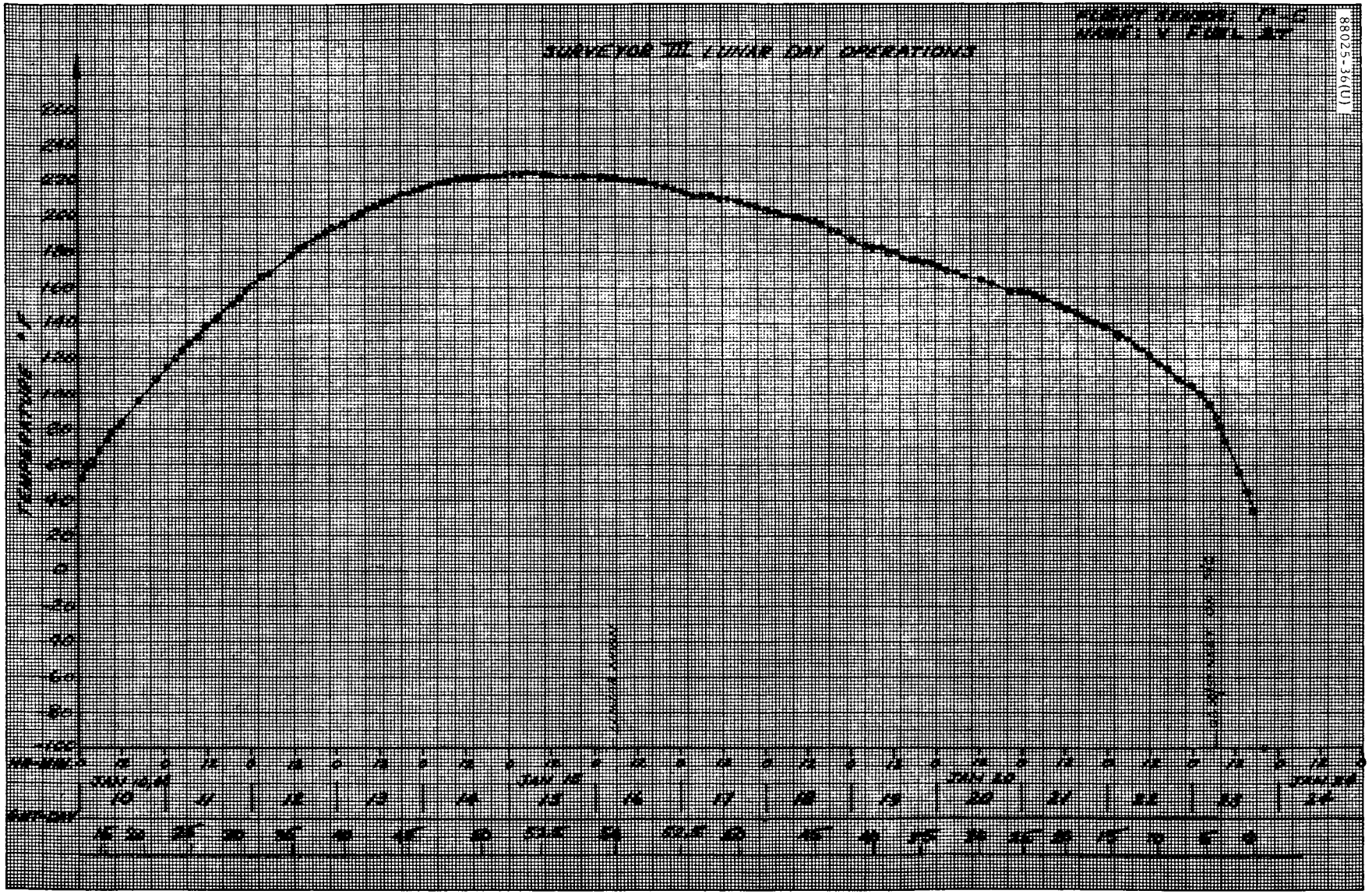

Figure 5.1-B22. Sensor P-5: Vernier Fuel Tank 2

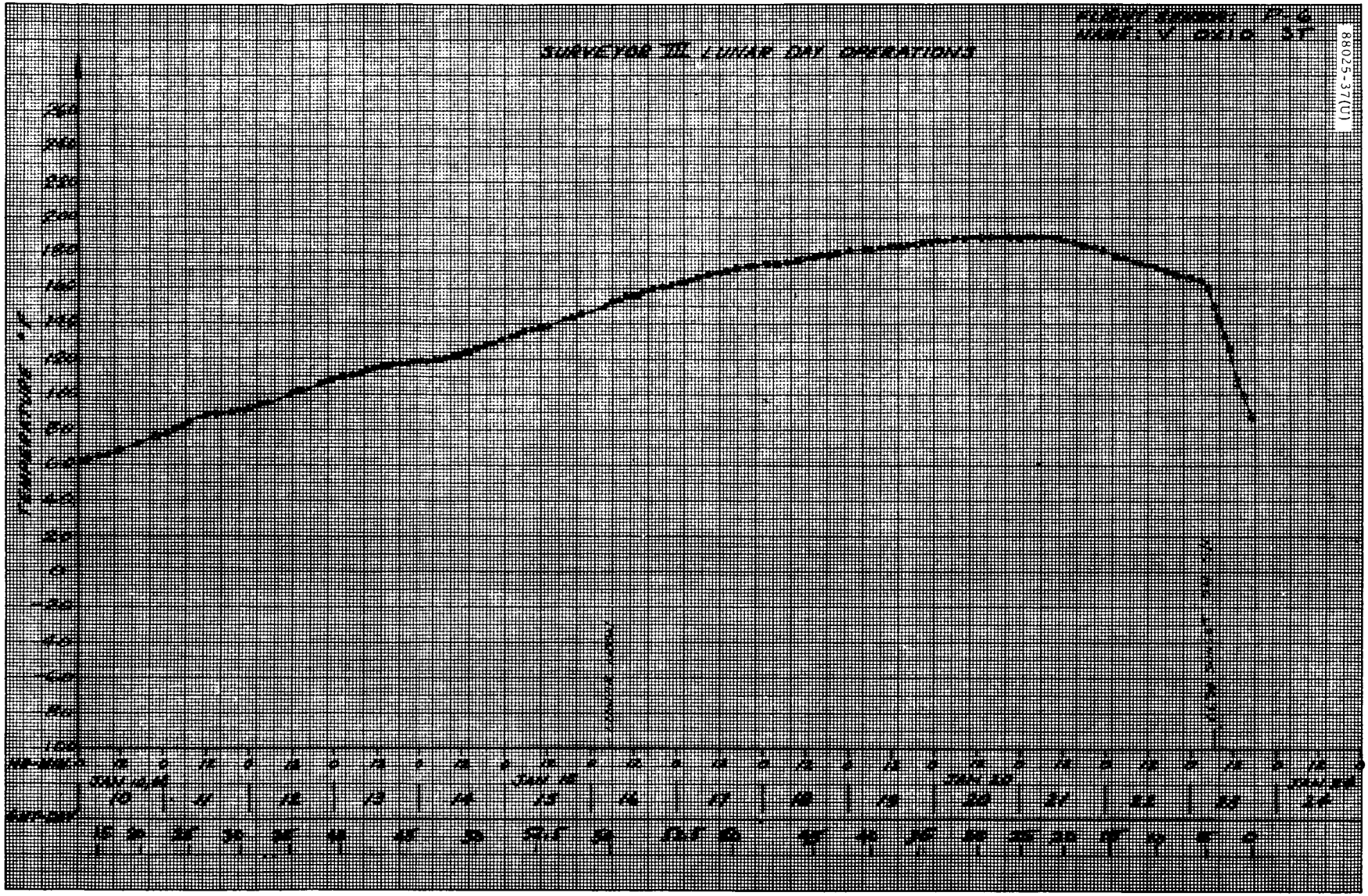

Figure 5. 1-B23. Sensor P-6: Vernier Oxidizer Tank 3

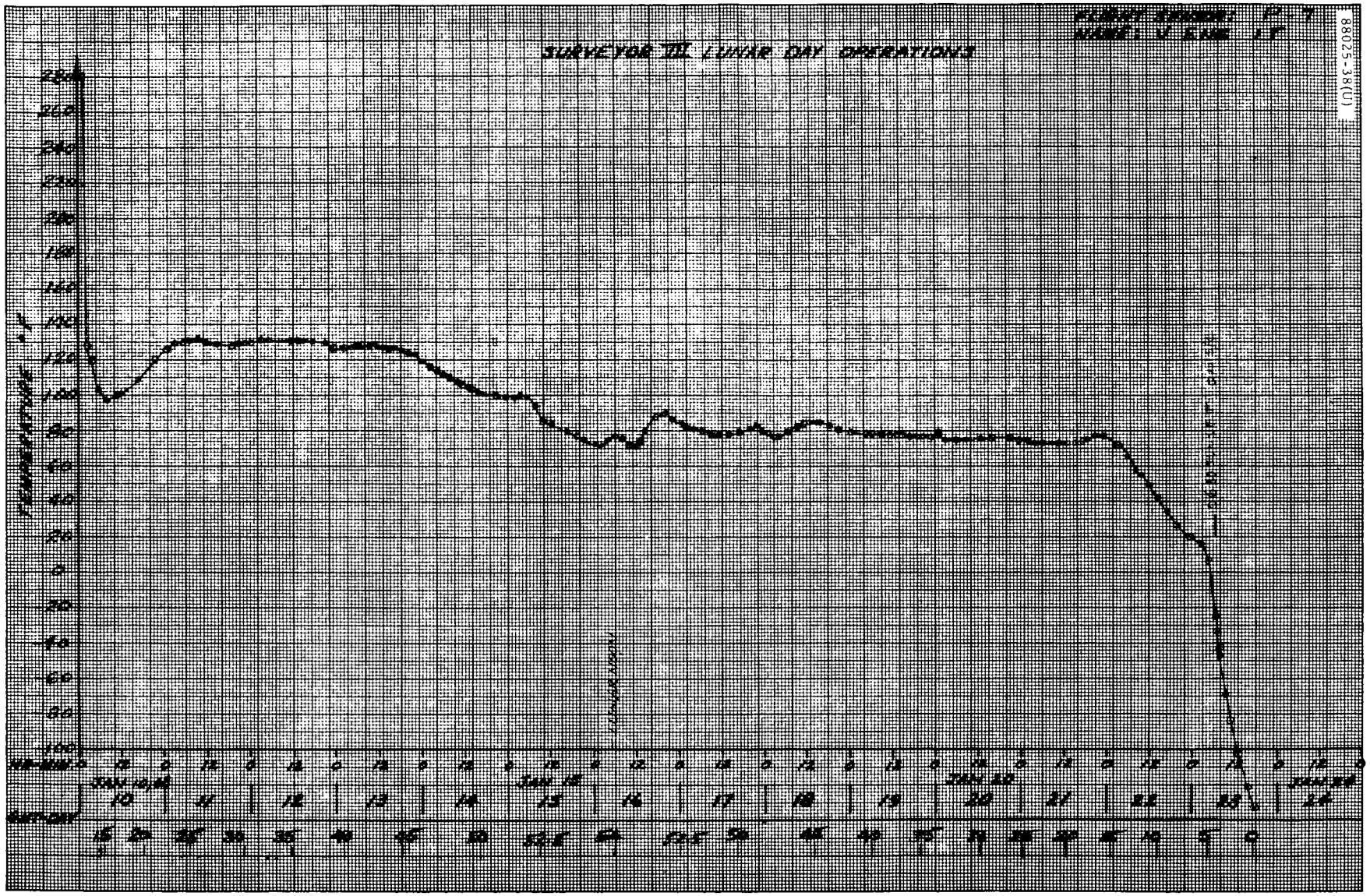

Figure 5.1-B24. Sensor P-7: Vernier Engine 1

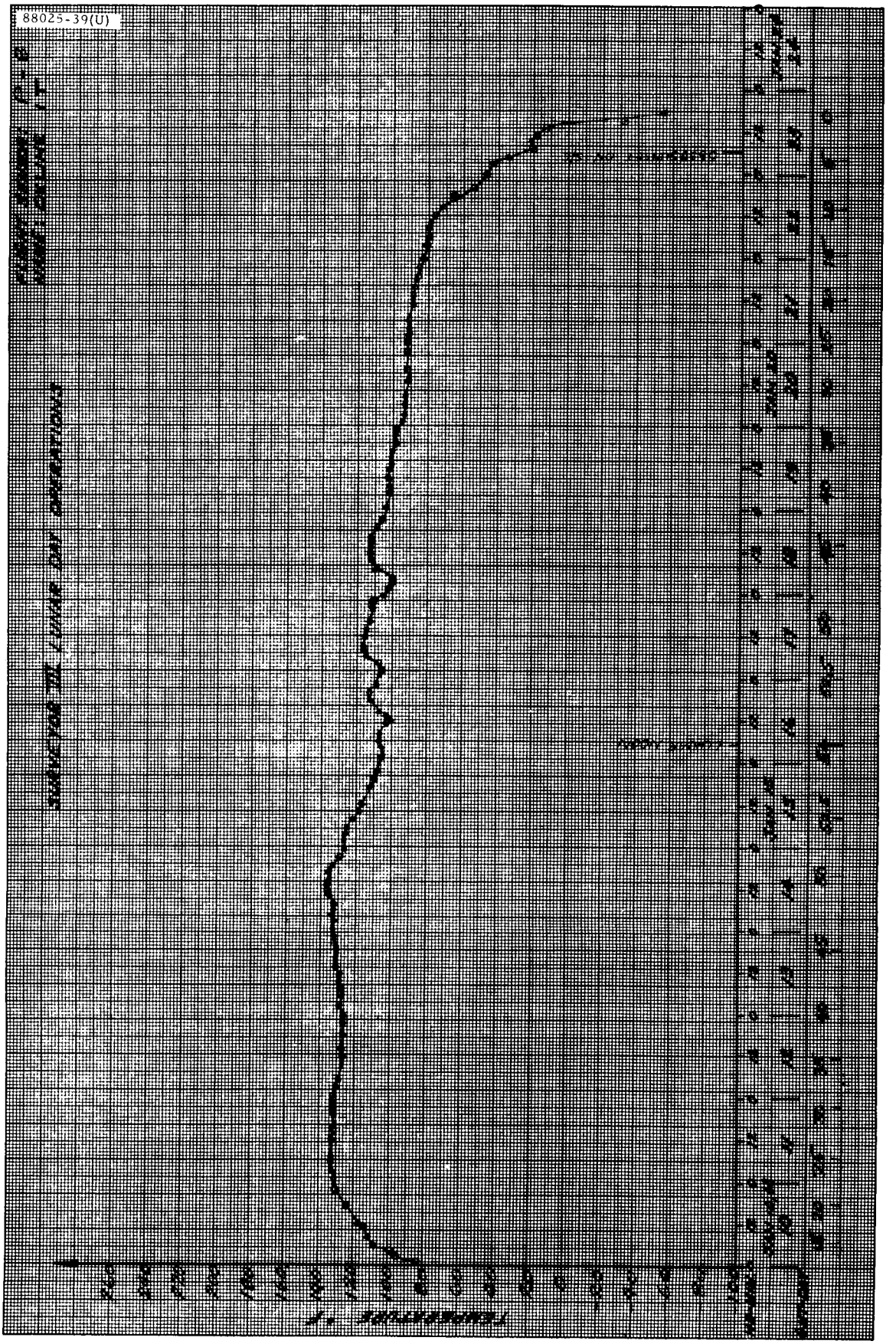

Figure 5.1-B25. Sensor P-8: Vernier Lines 1

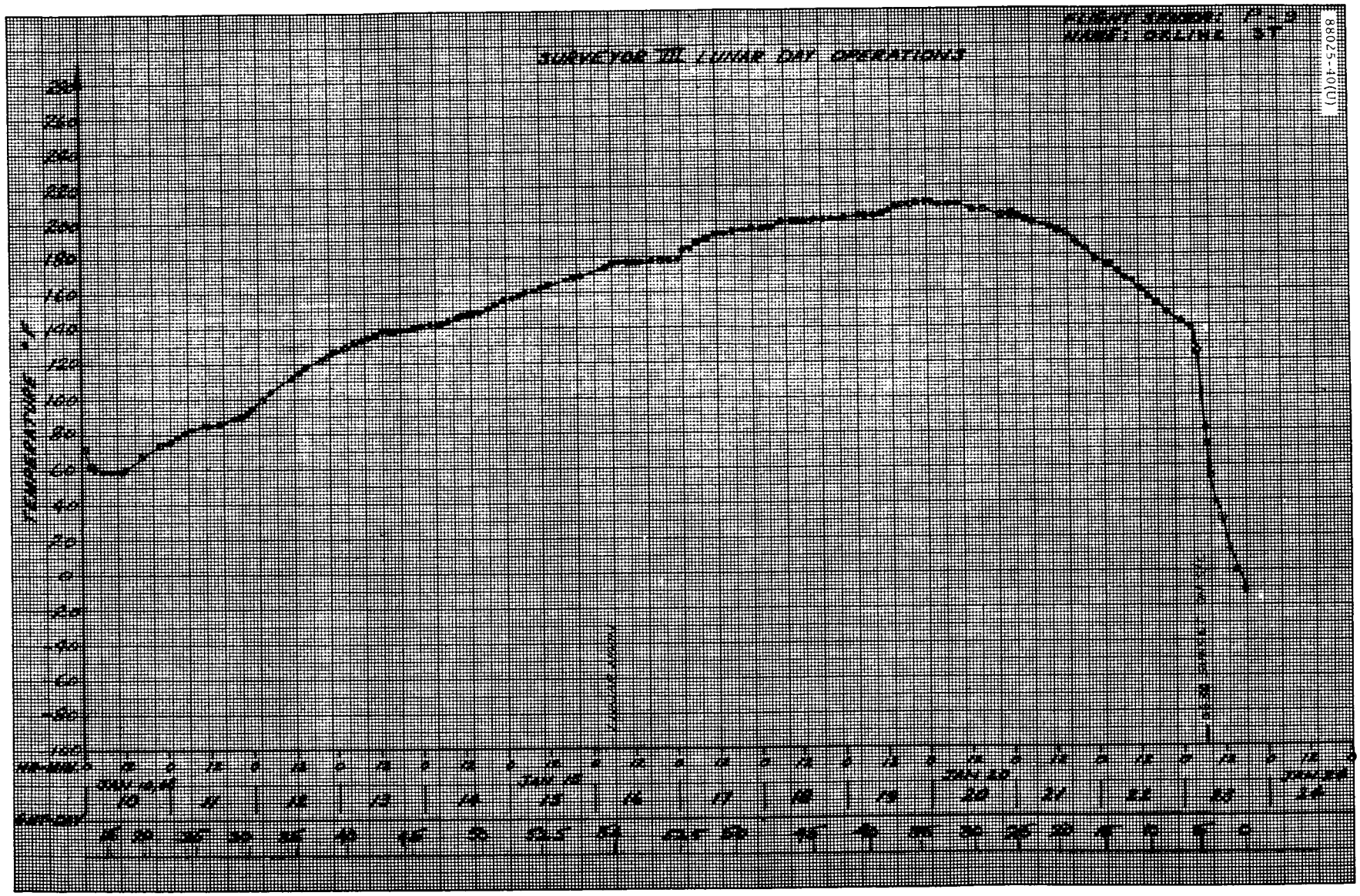

Figure 5.1-B26. Sensor P-9: Vernier Lines 3

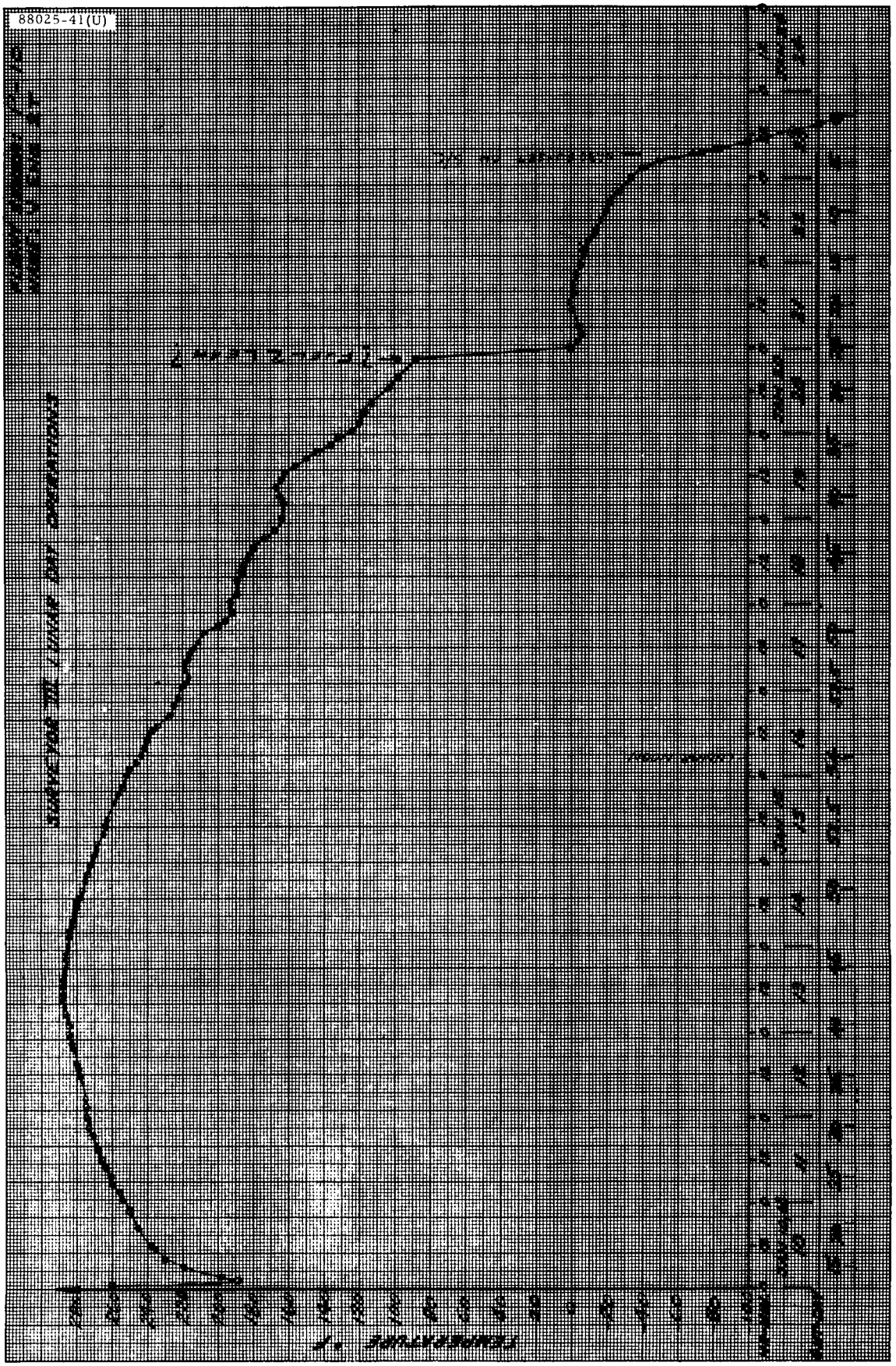

Figure 5.1-B27. Sensor P-10: Vernier Engine 2

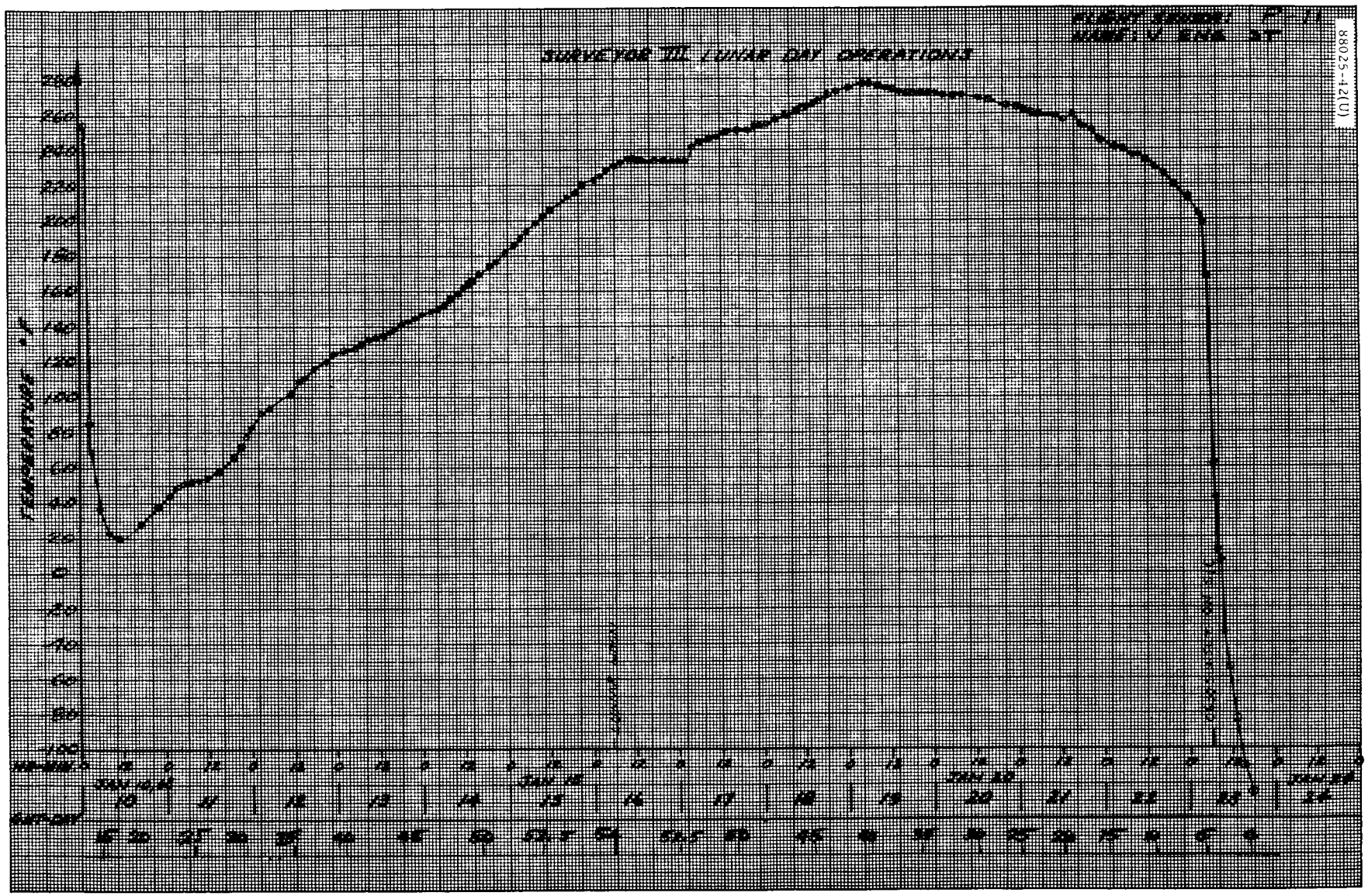

Figure 5.1-B28. Sensor P-11: Vernier Engine 3

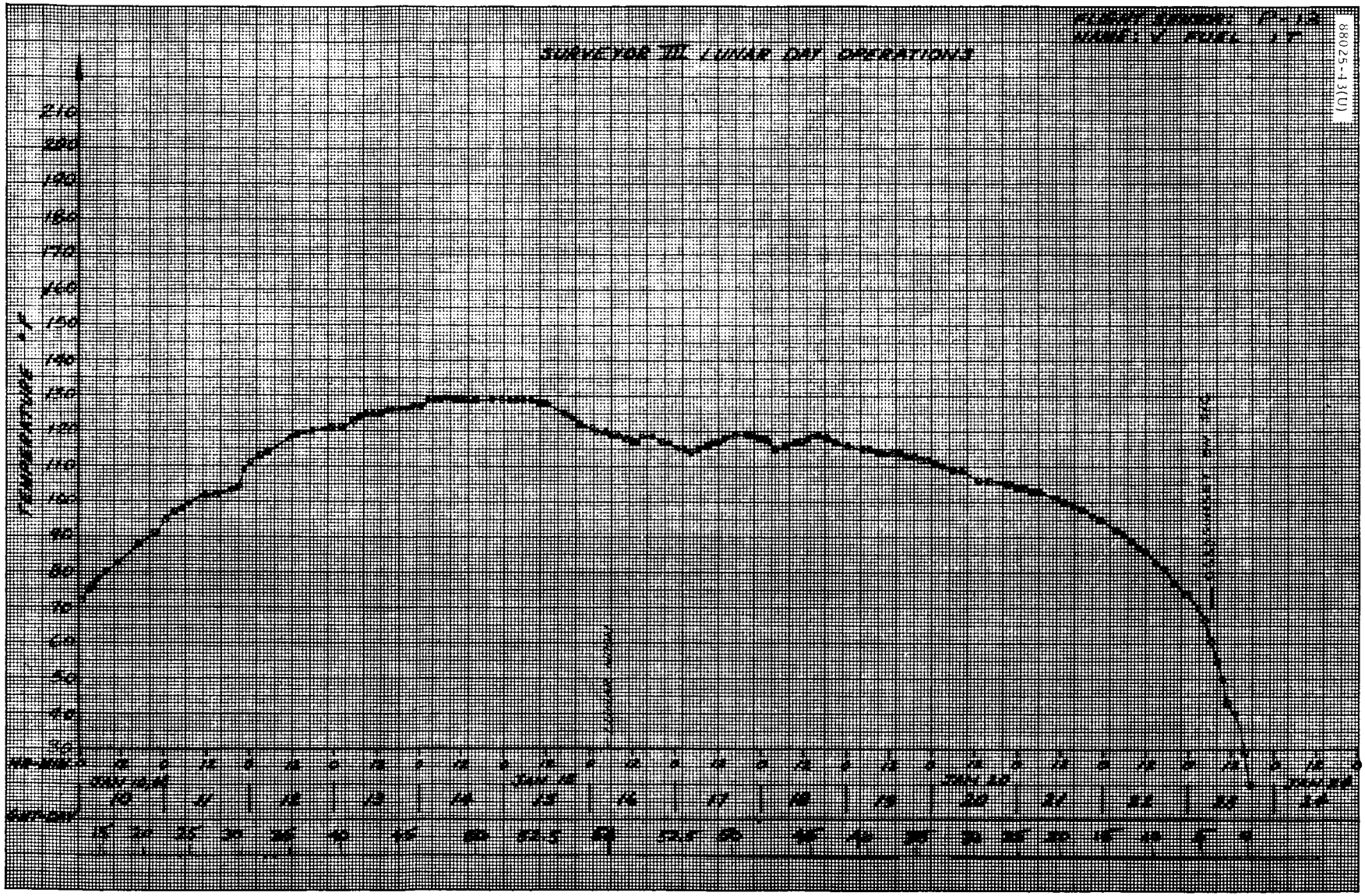

Figure 5. 1-B29. Sensor P-13: Vernier Fuel Tank 1

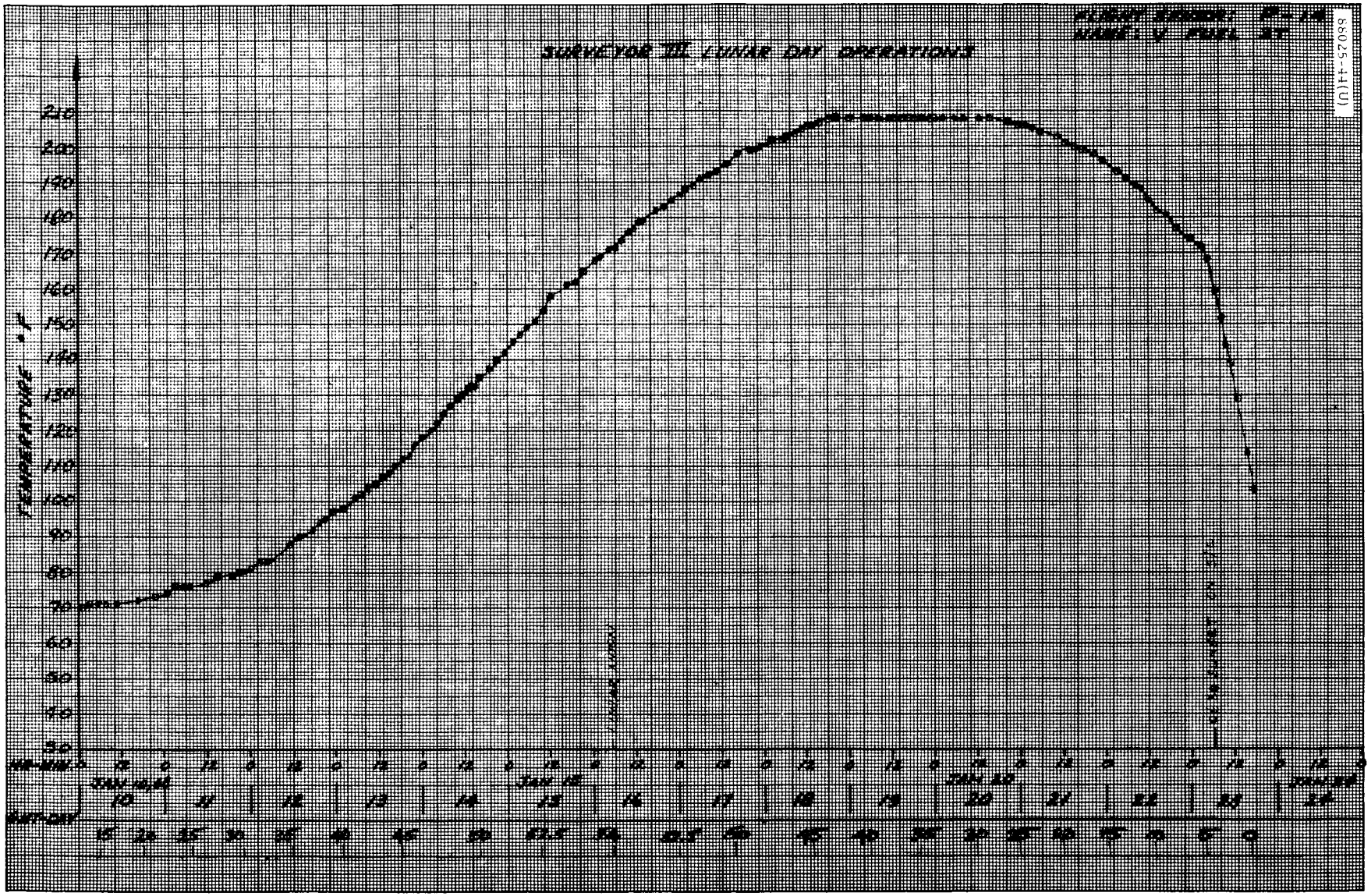

Figure 5.1-B30. Sensor P-14: Vernier Fuel Tank 3

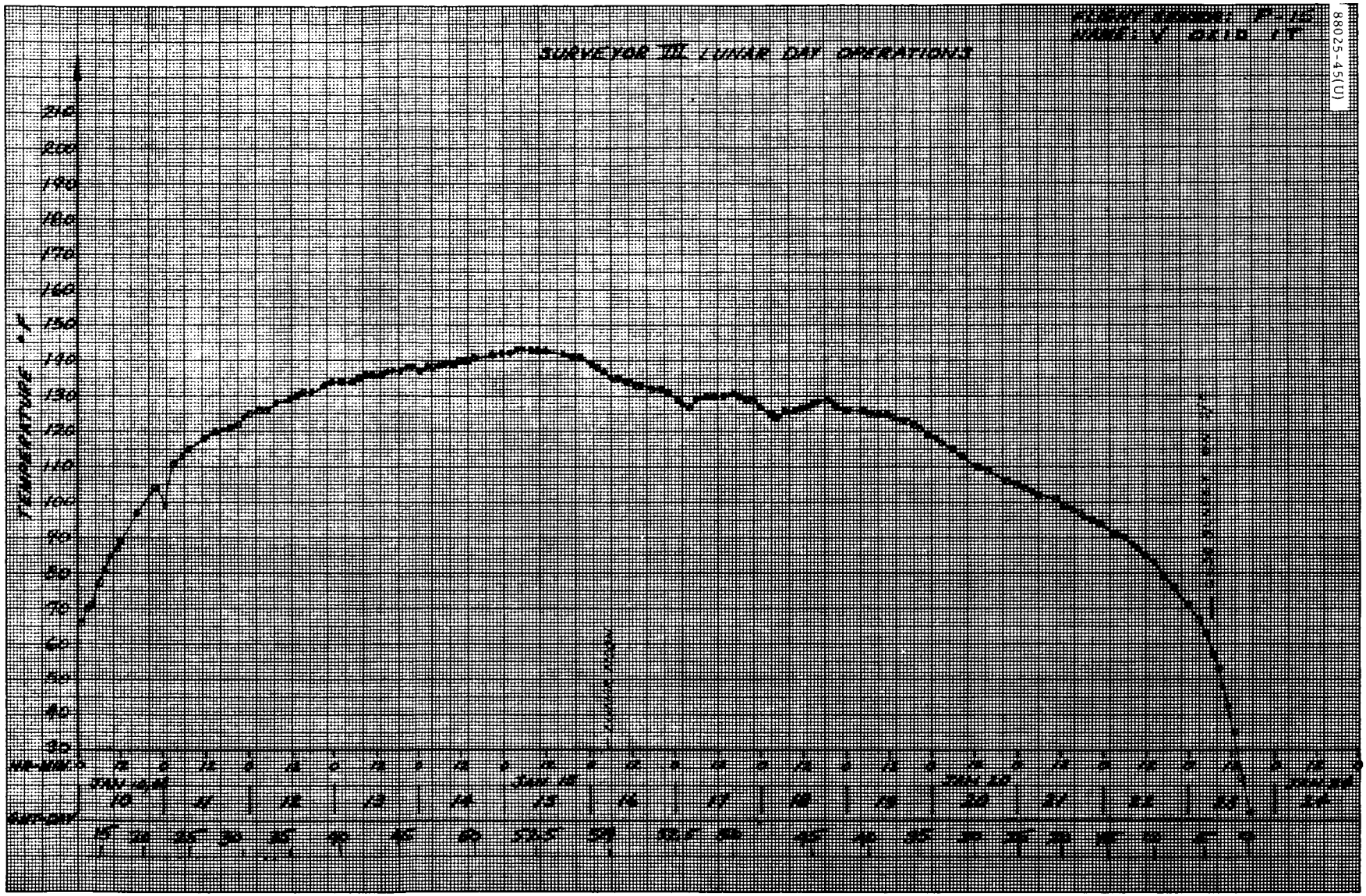

Figure 5.1-B31. Sensor P-15: Vernier Oxidizer Tank 1

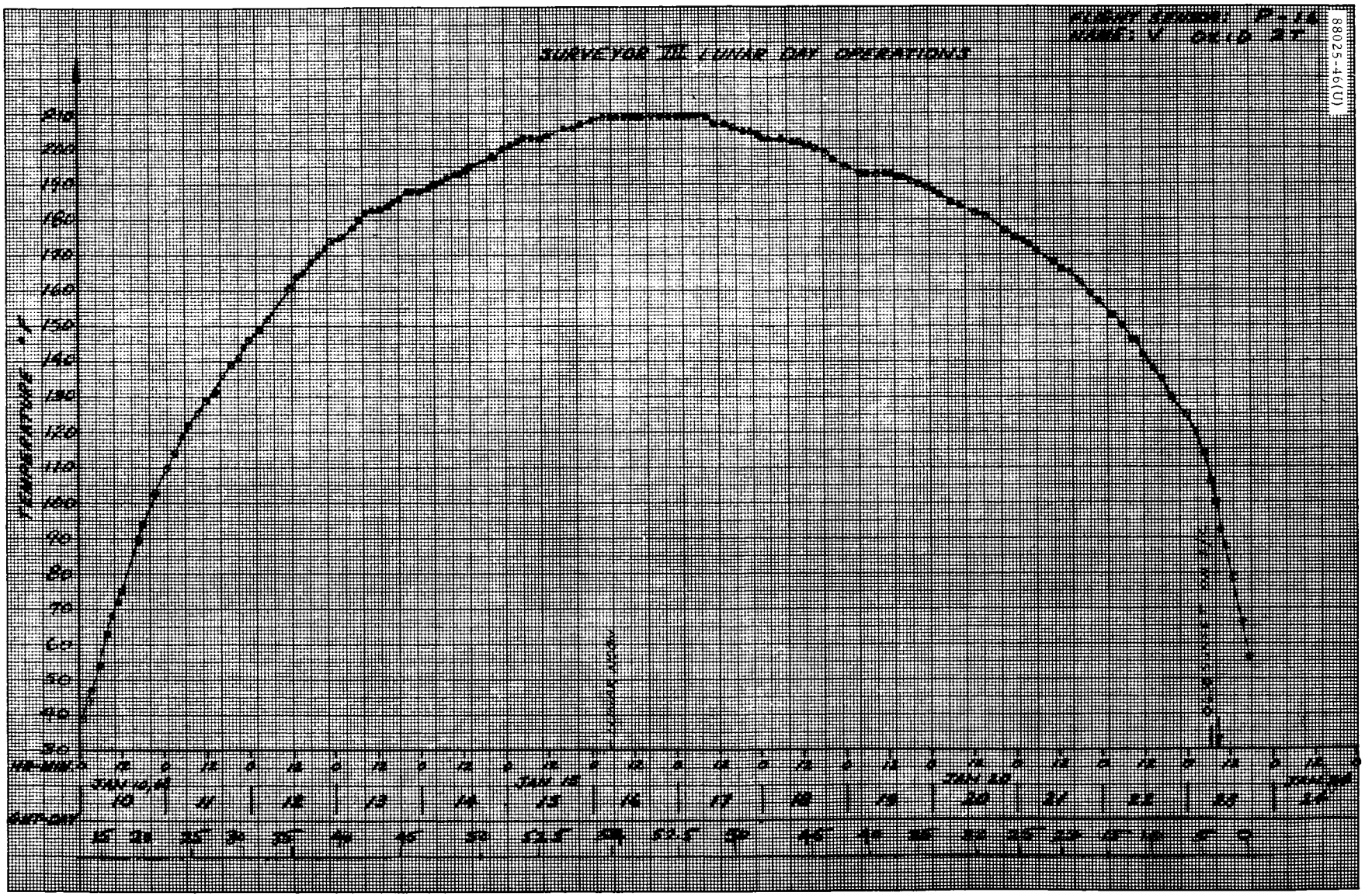

Figure 5.1-B32. Sensor P-16: Vernier Oxidizer Tank 2

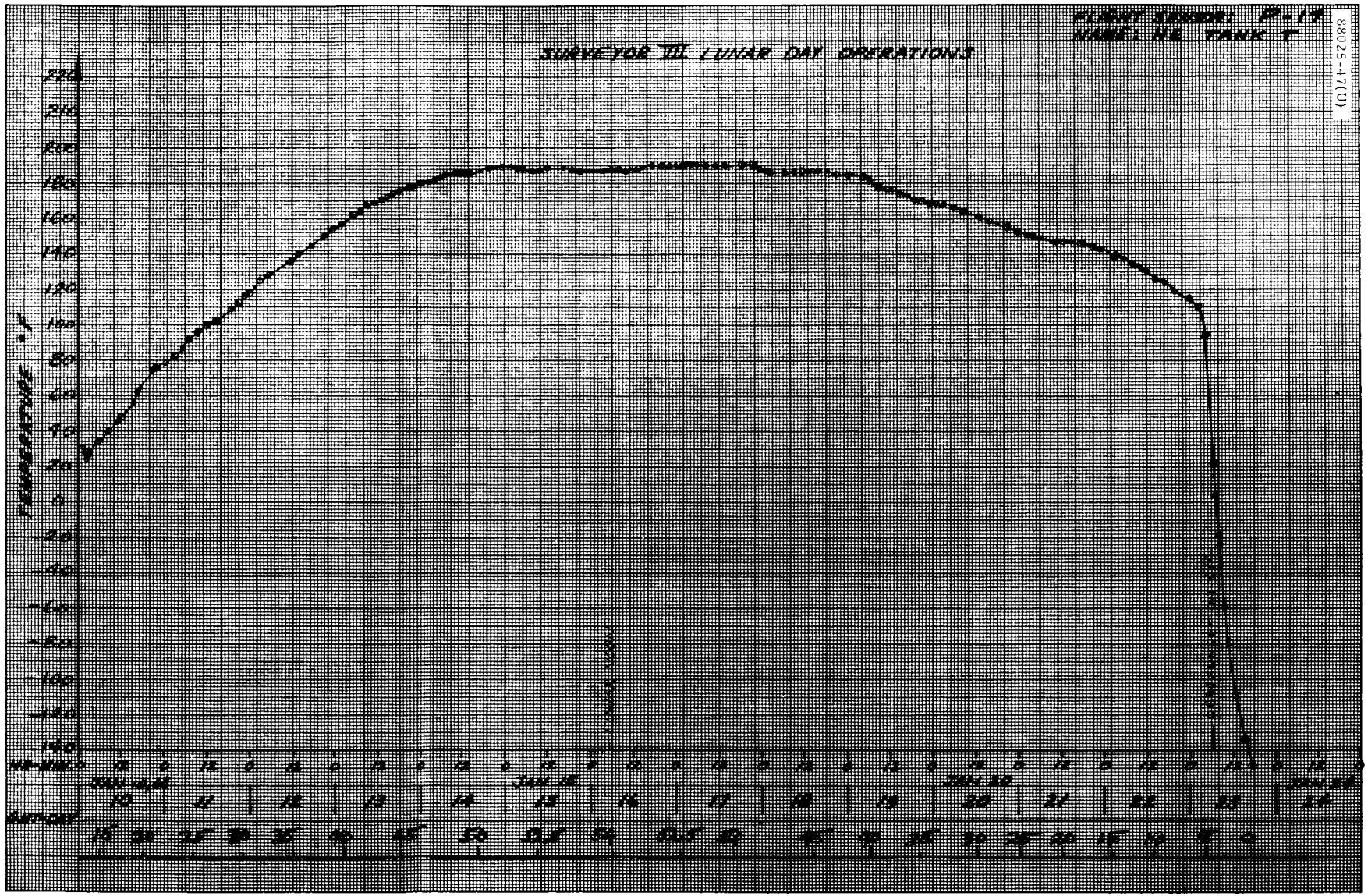

Figure 5. 1-B33. Sensor P-17: Helium Tank

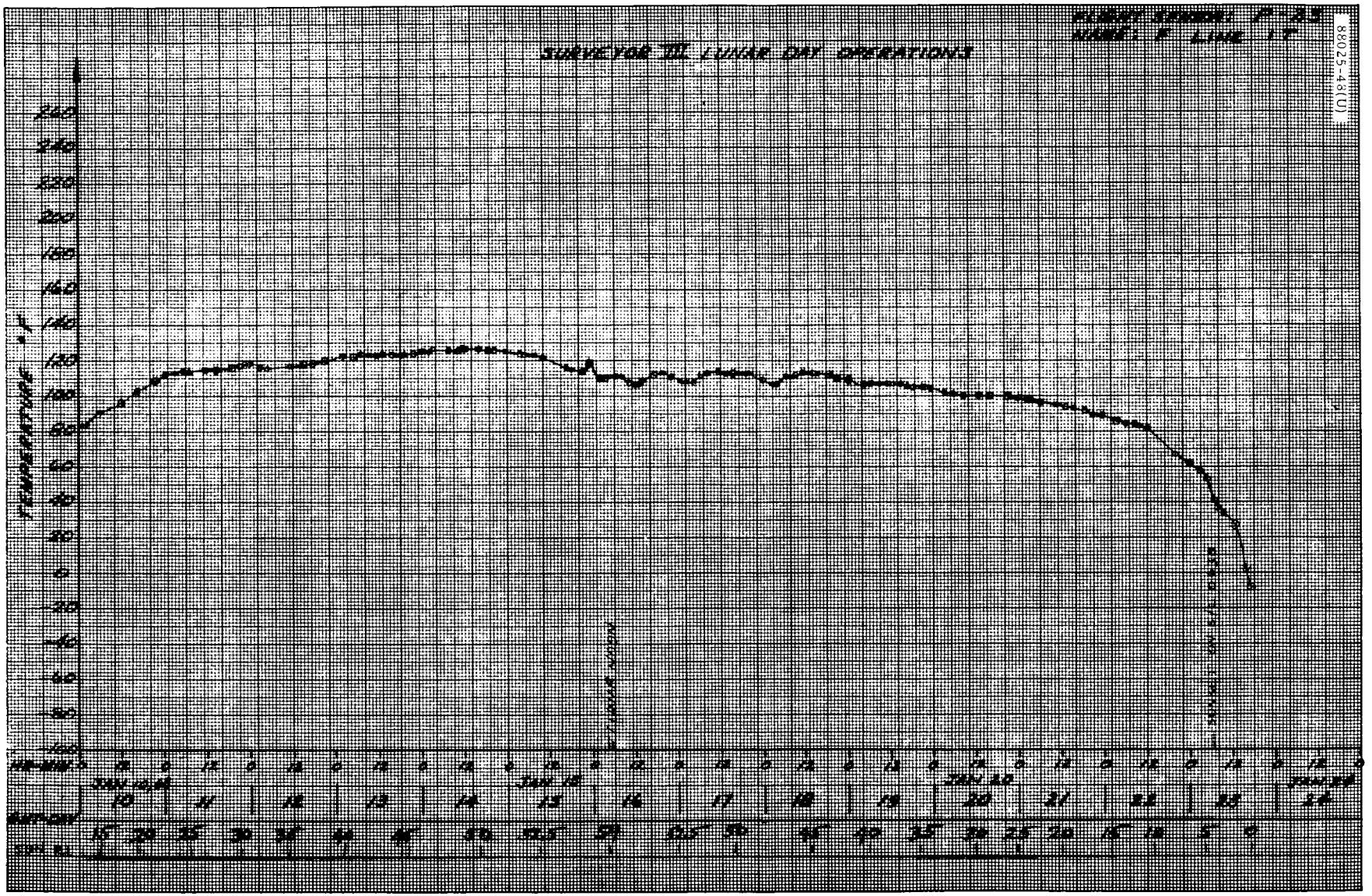

Figure 5.1-B34. Sensor P-23: Vernier Fuel Line 1

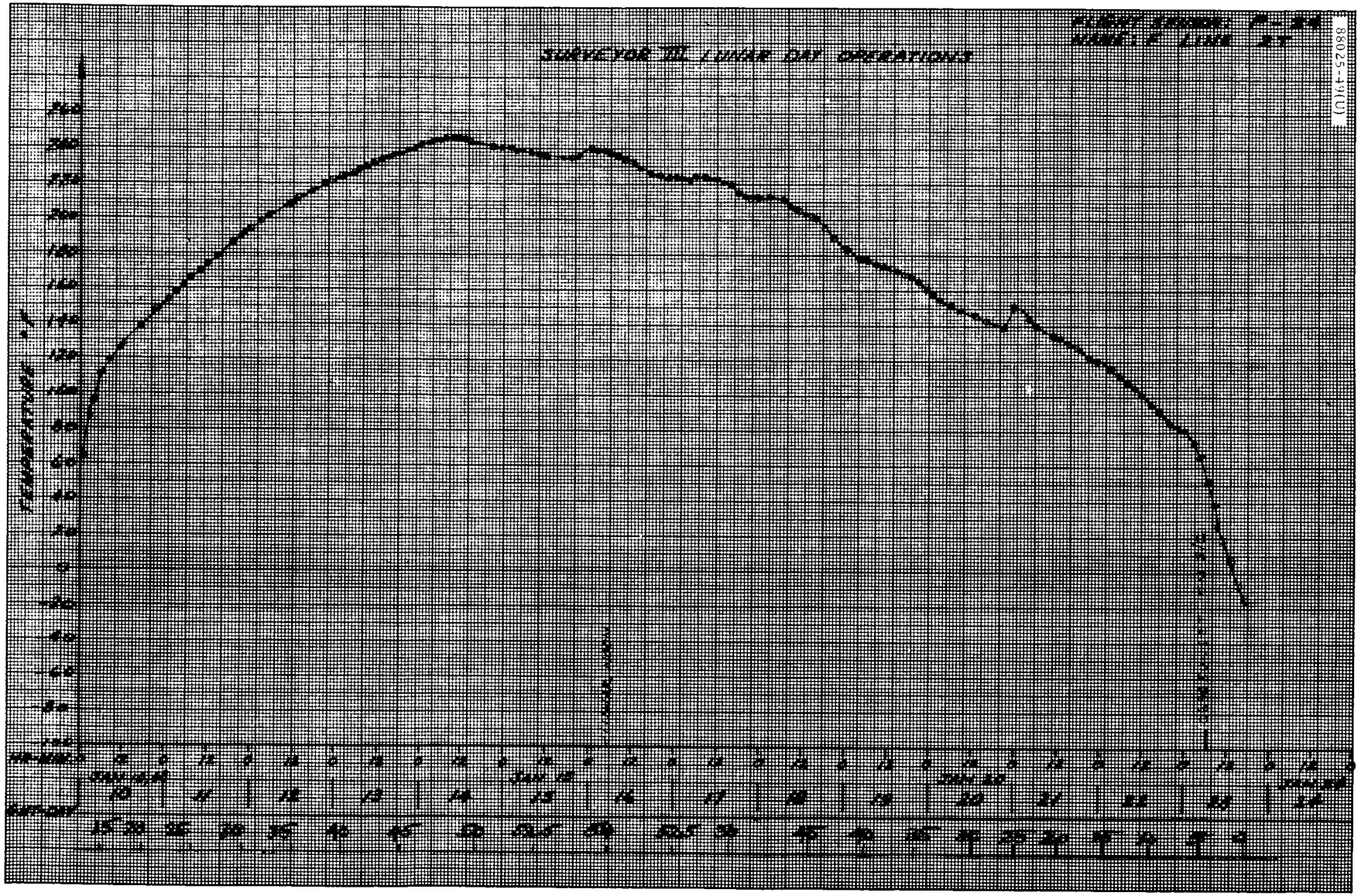

Figure 5.1-B35. Sensor P-24: Vernier Fuel Line 2

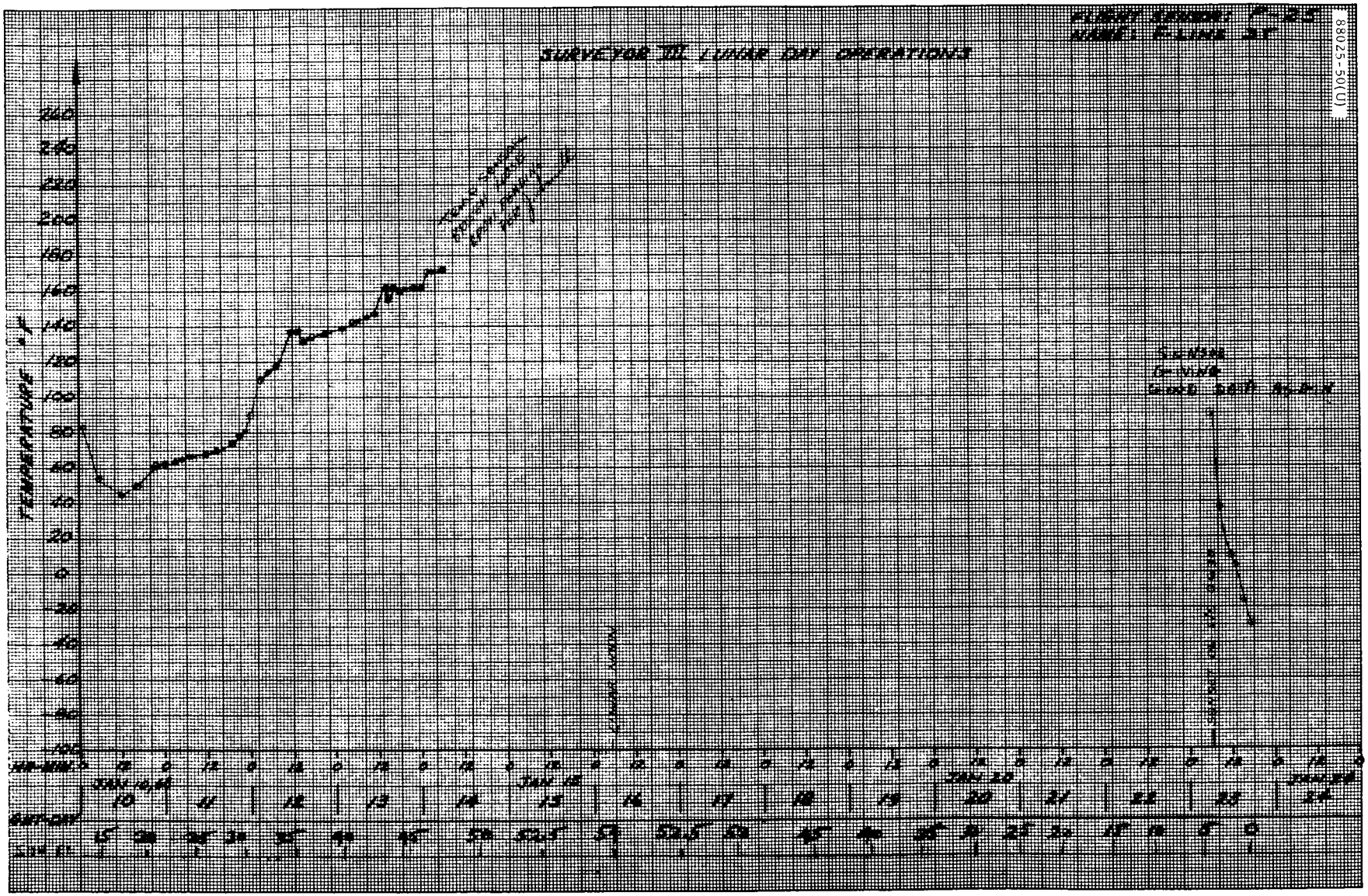

Figure 5.1-B36. Sensor P-25: Vernier Fuel Line 3

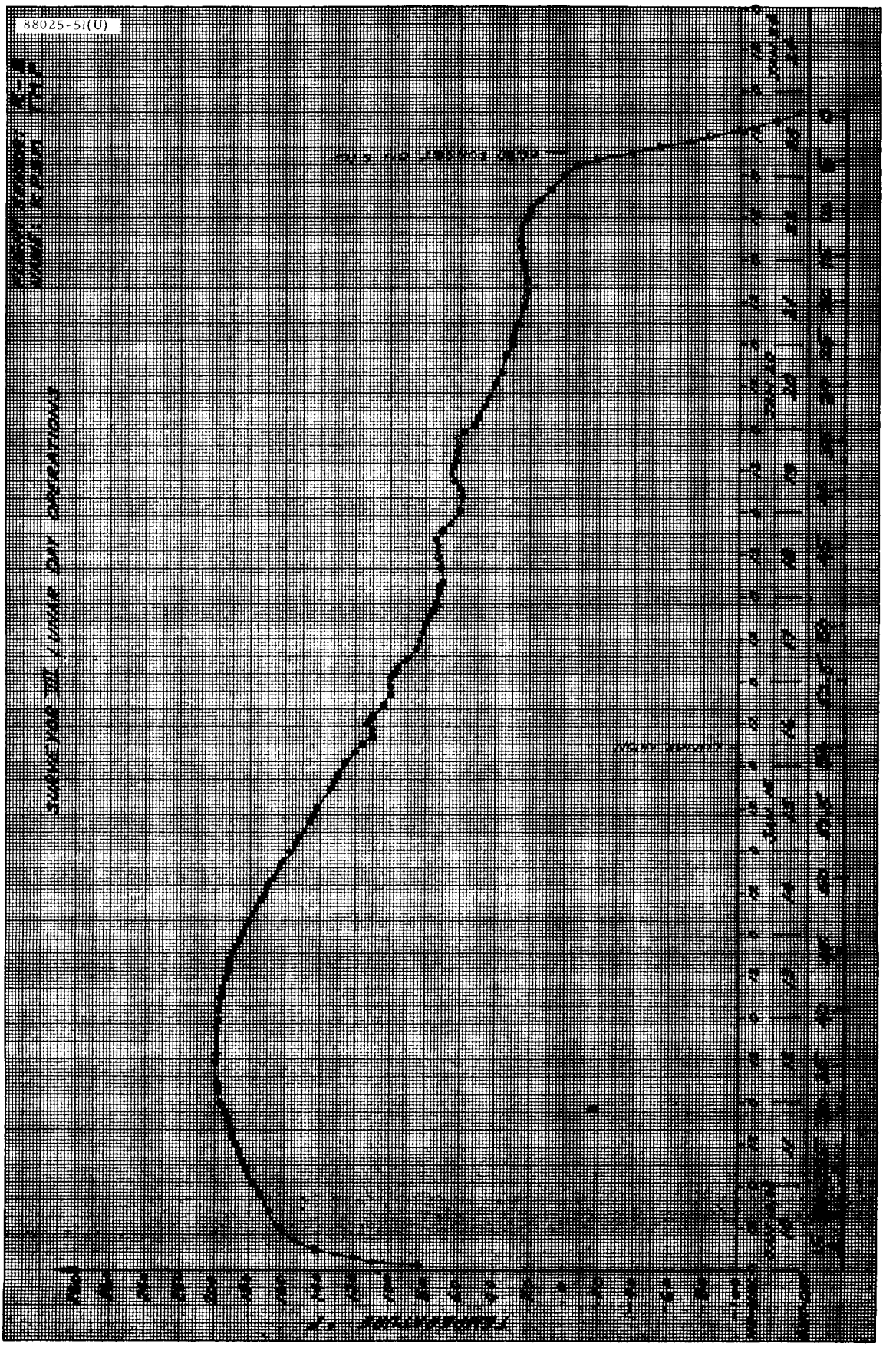

Figure 5.1-B37. Sensor R-8: RADVS (Klystron) Unit

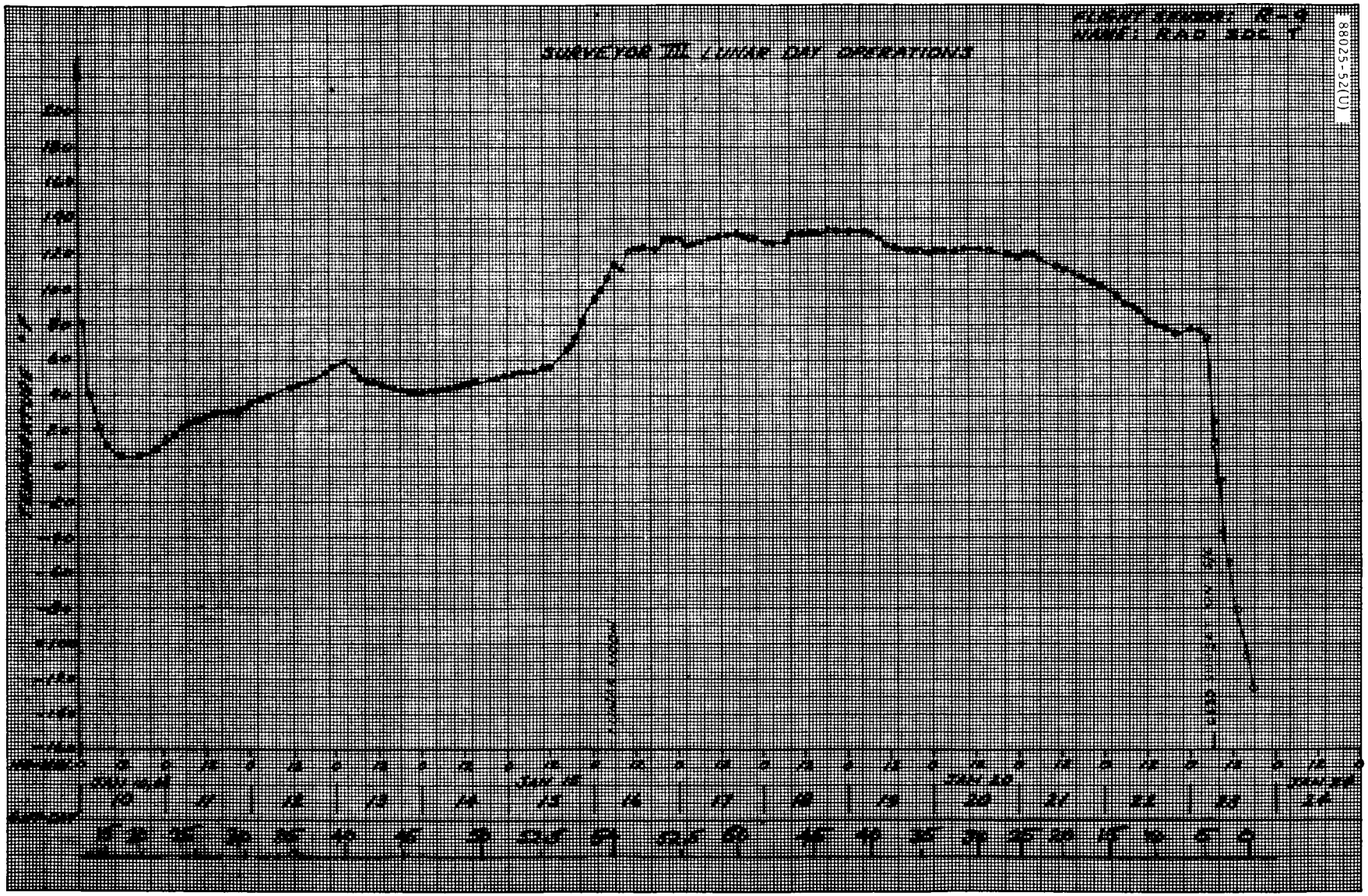

Figure 5.1-B38. Sensor R-9: RADVS Signal Data Converter

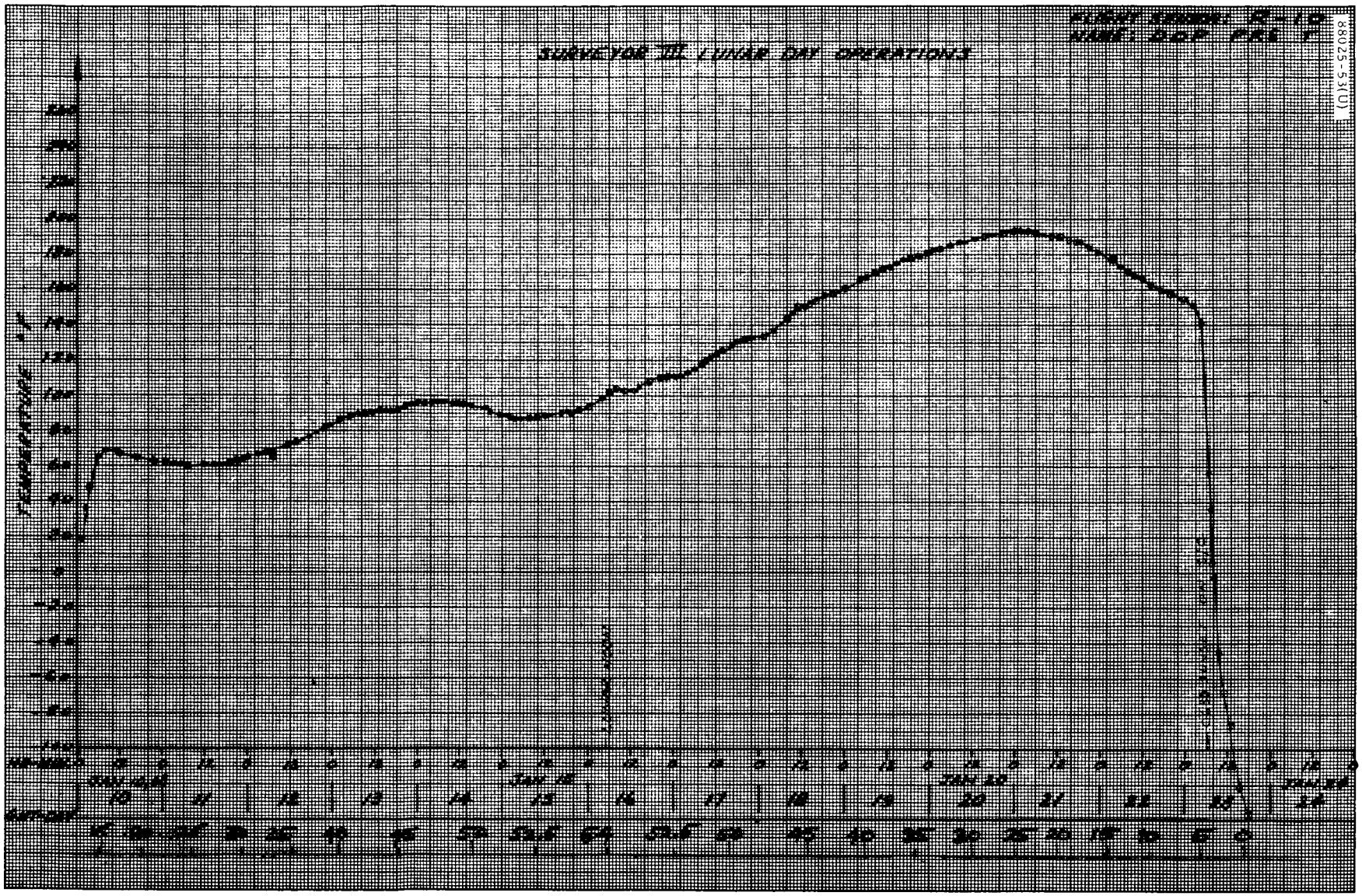

Figure 5.1-B39. Sensor R-10: Doppler Radar Sensor

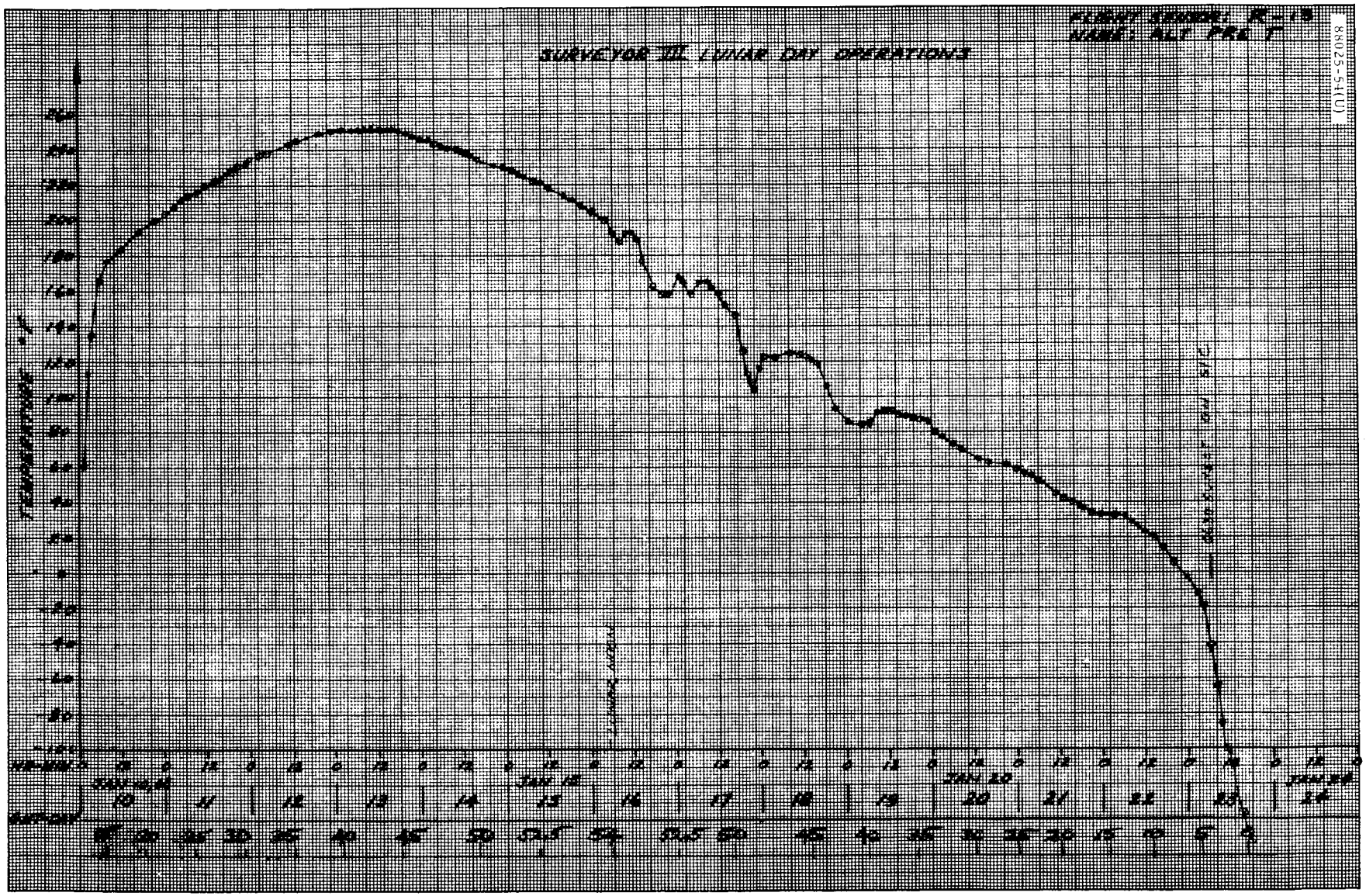

Figure 5.1-B40. Sensor R-13: Altimeter Radar Sensor

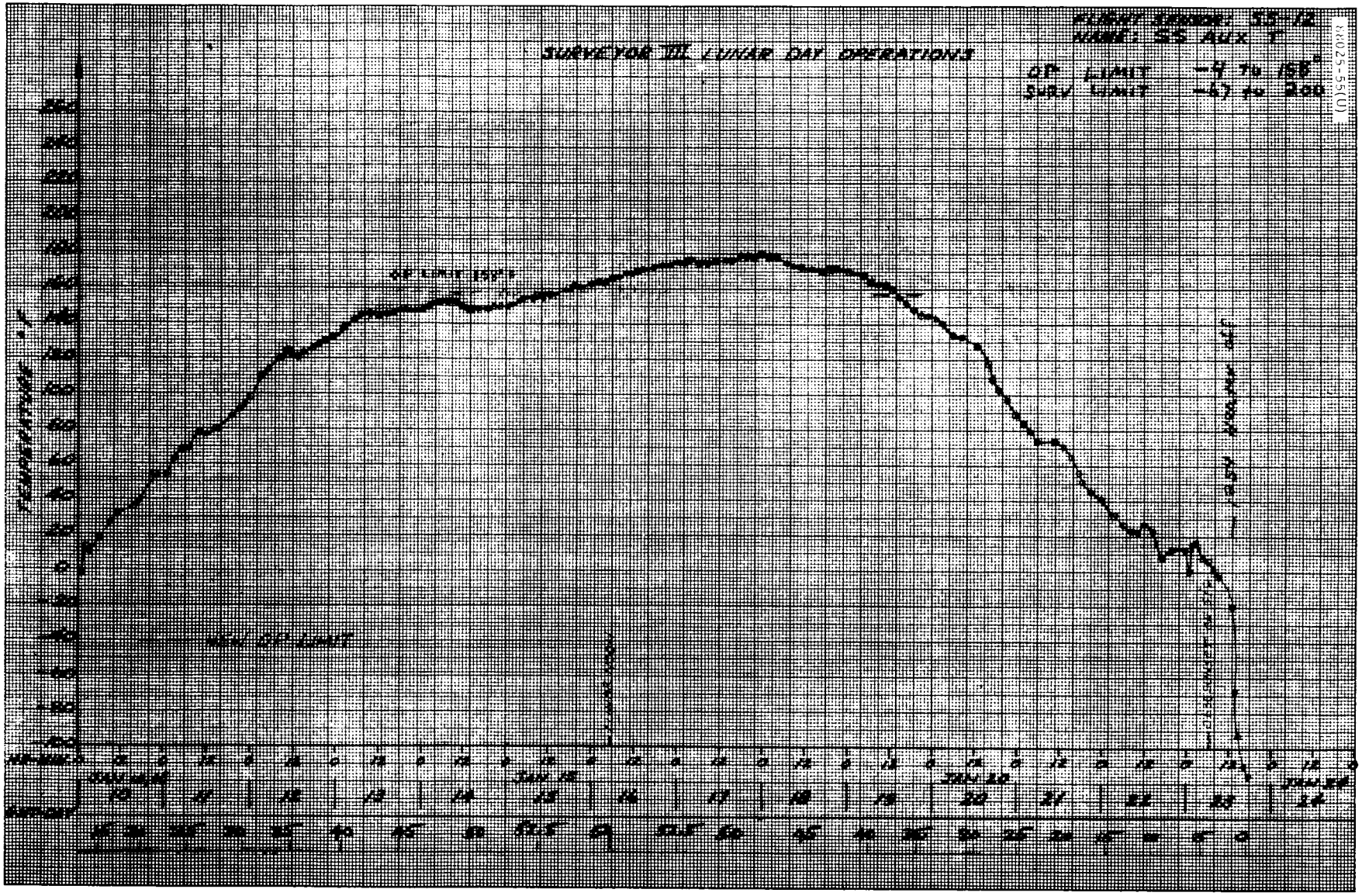

Figure 5.1-B41. SM/SS Auxiliary Electronics

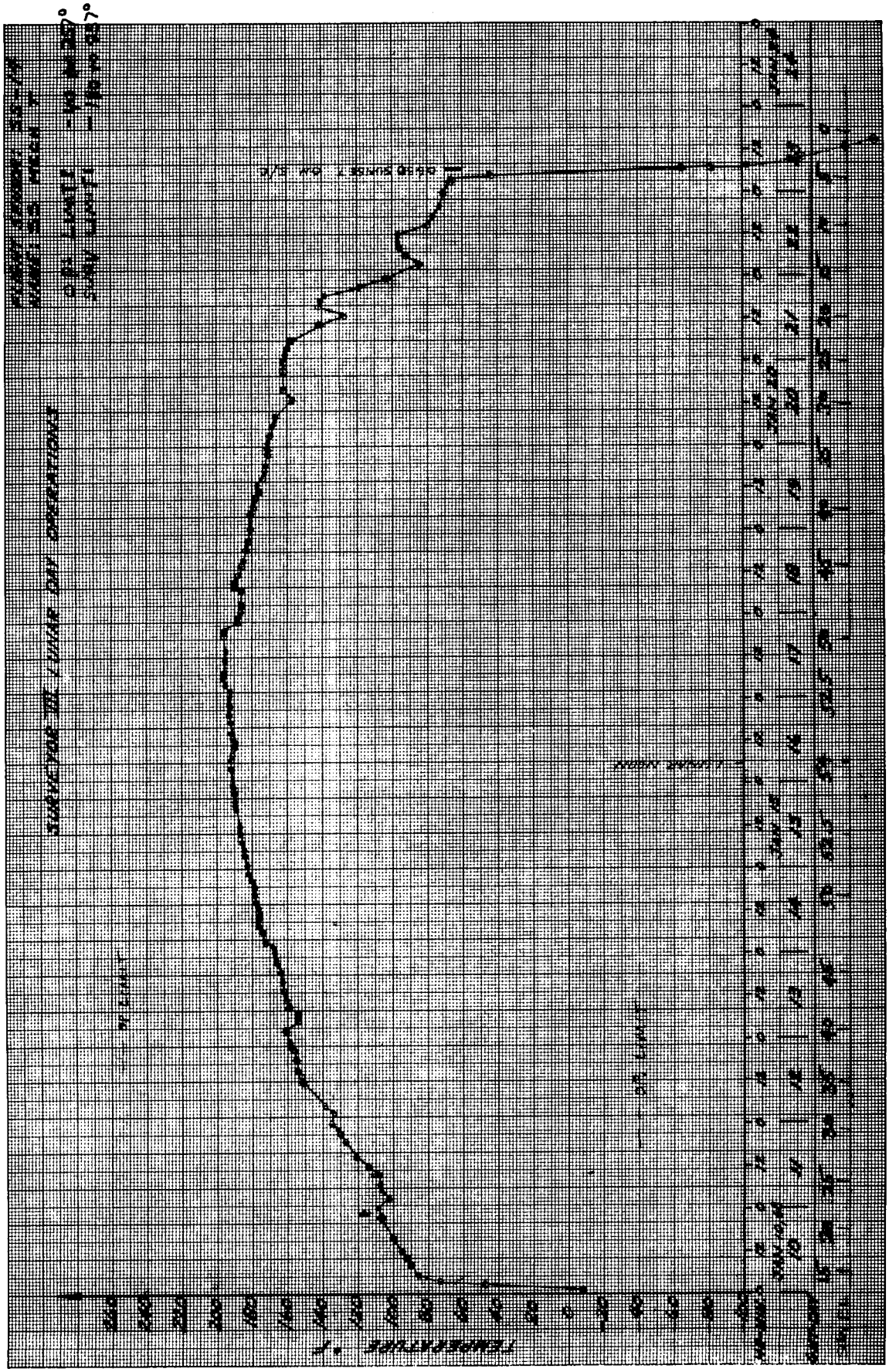

Figure 5.1-B42. Sensor SS-14: SM/SS Mechanism

88025-57(U)

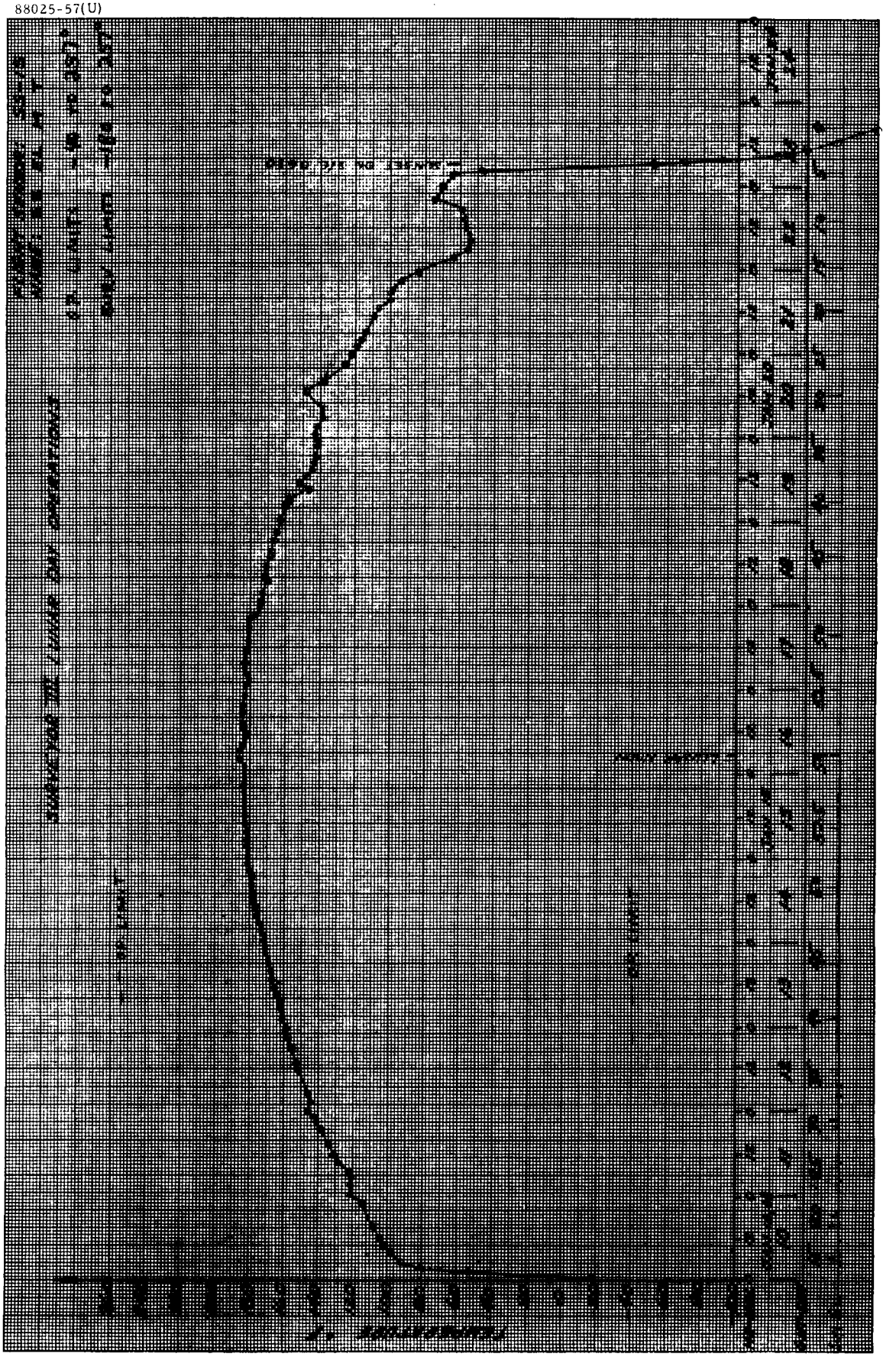

Figure 5.1-B43. Sensor SS-15: Elevation Motor

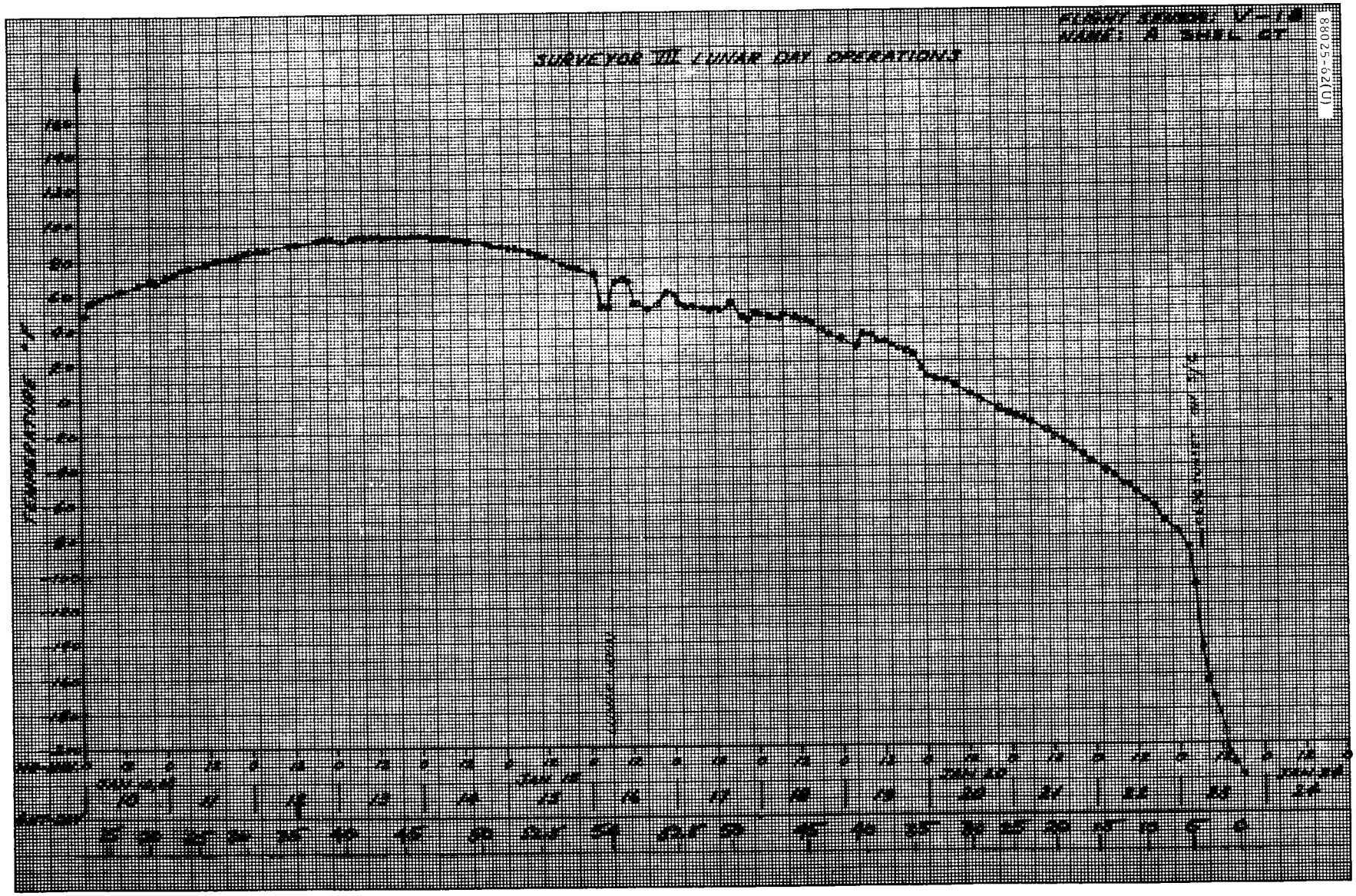

Figure 5.1-B48. Sensor V-18: Compartment A Canister

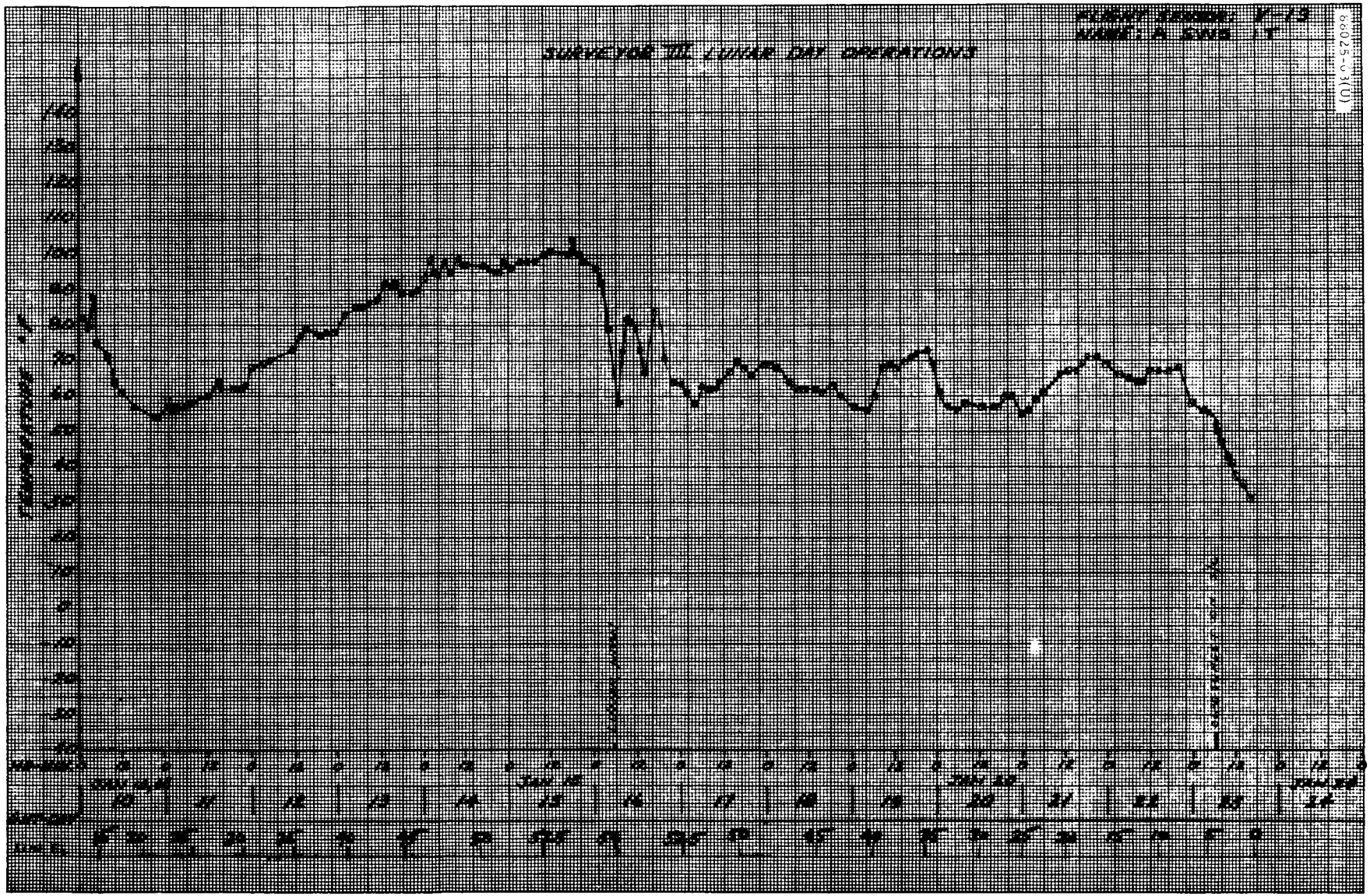

Figure 5. 1-B49. Sensor V-19: Compartment A Switch 5 Base

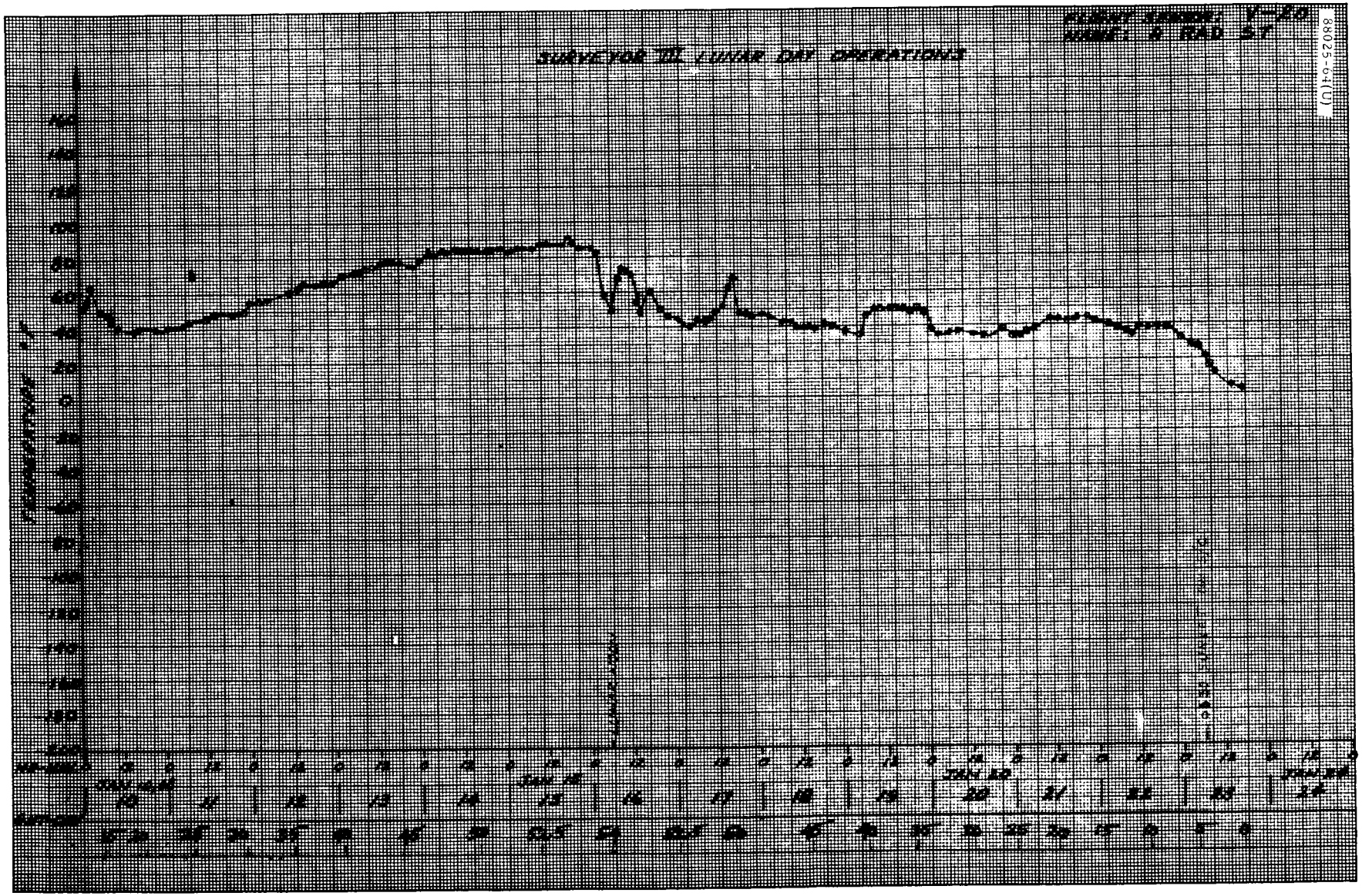

Figure 5. 1-B50. Sensor V-20: Compartment A 5 Switch 5 in Face Radiator

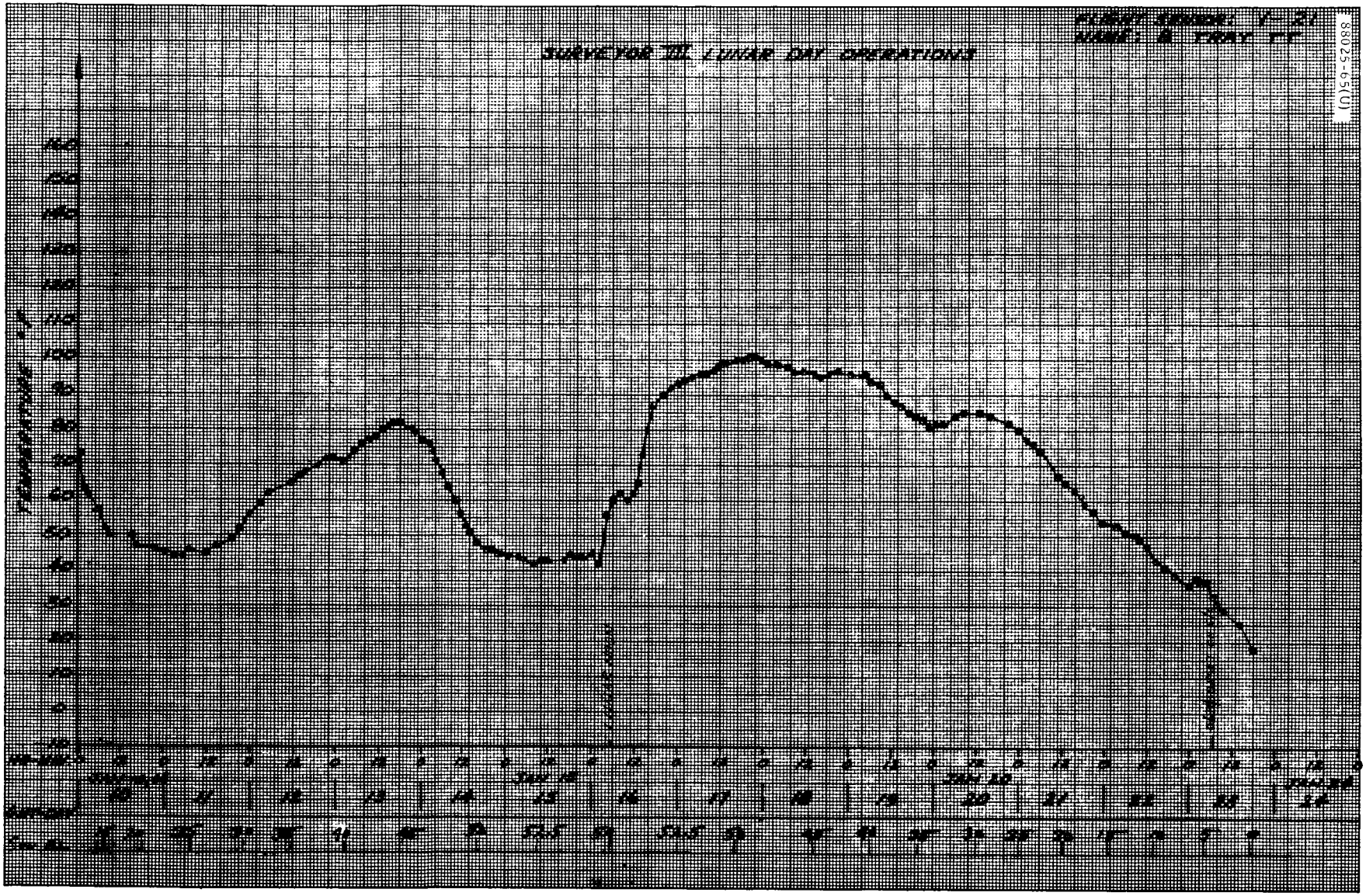

Figure 5.1-B51. Sensor V-21: Compartment B Tray Top Center

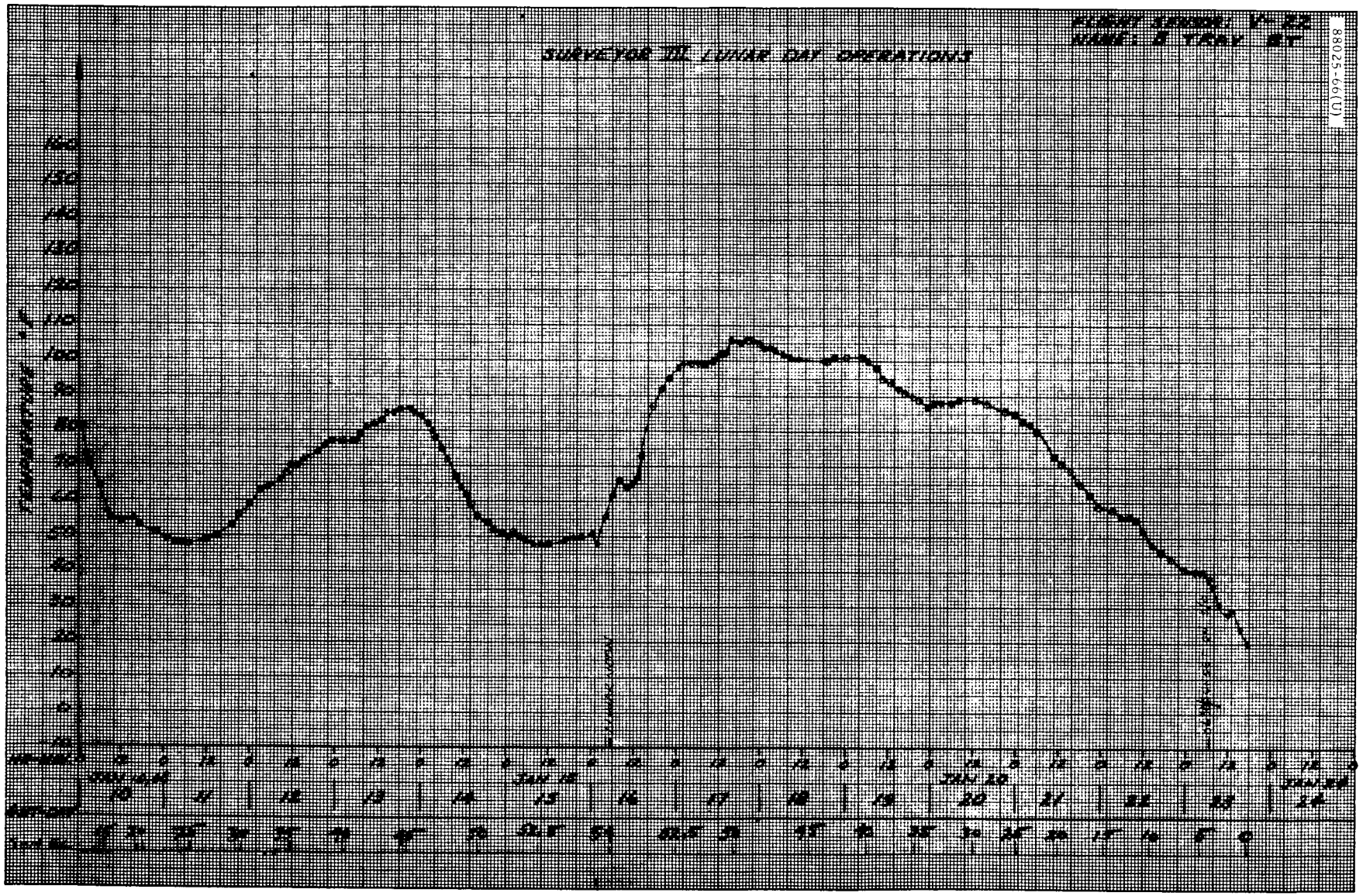

Figure 5.1-B52. Sensor V-22: Compartment B Lower Support

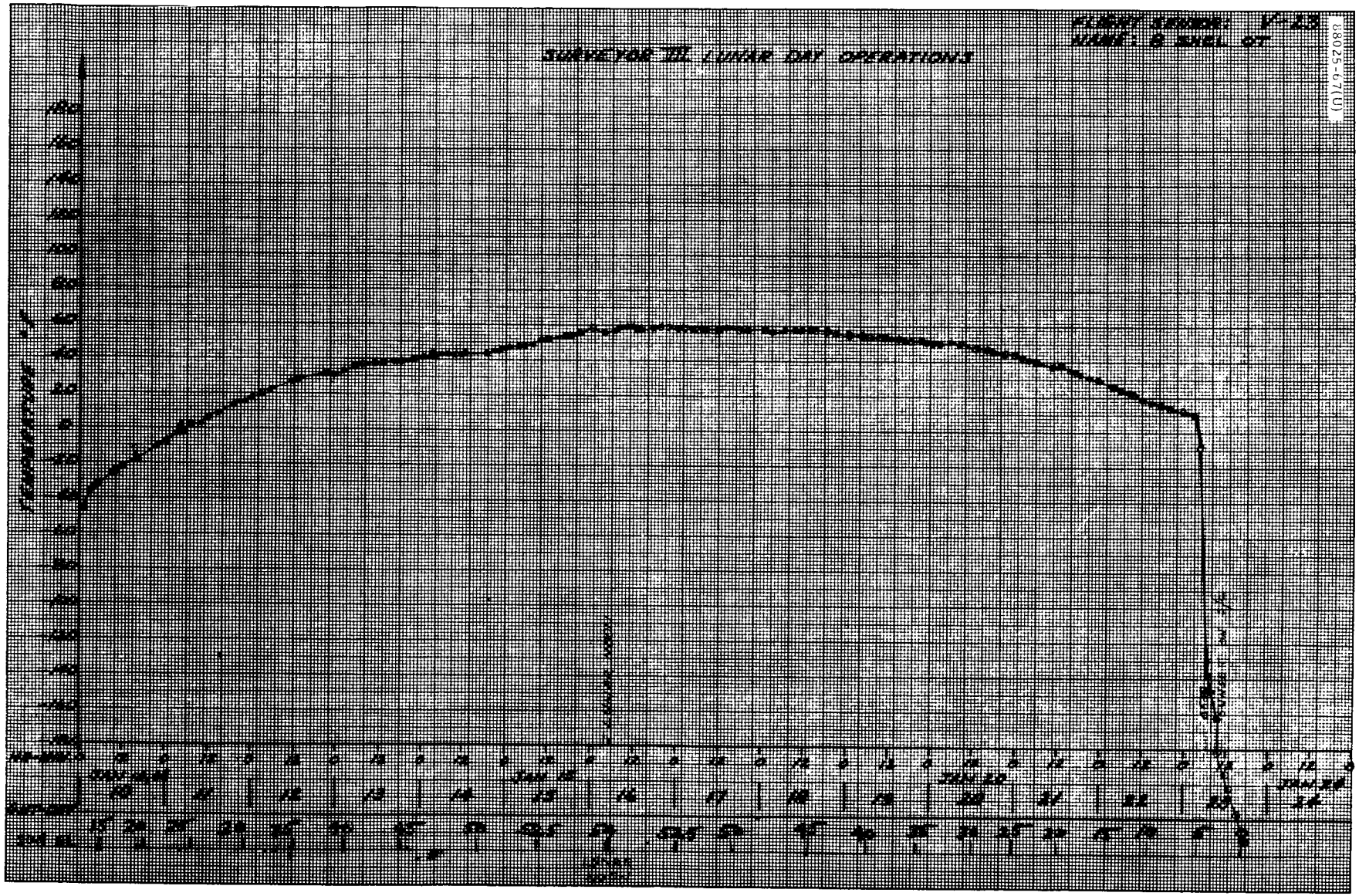

Figure 5. 1-B53. Sensor V-23: Compartment B Canister

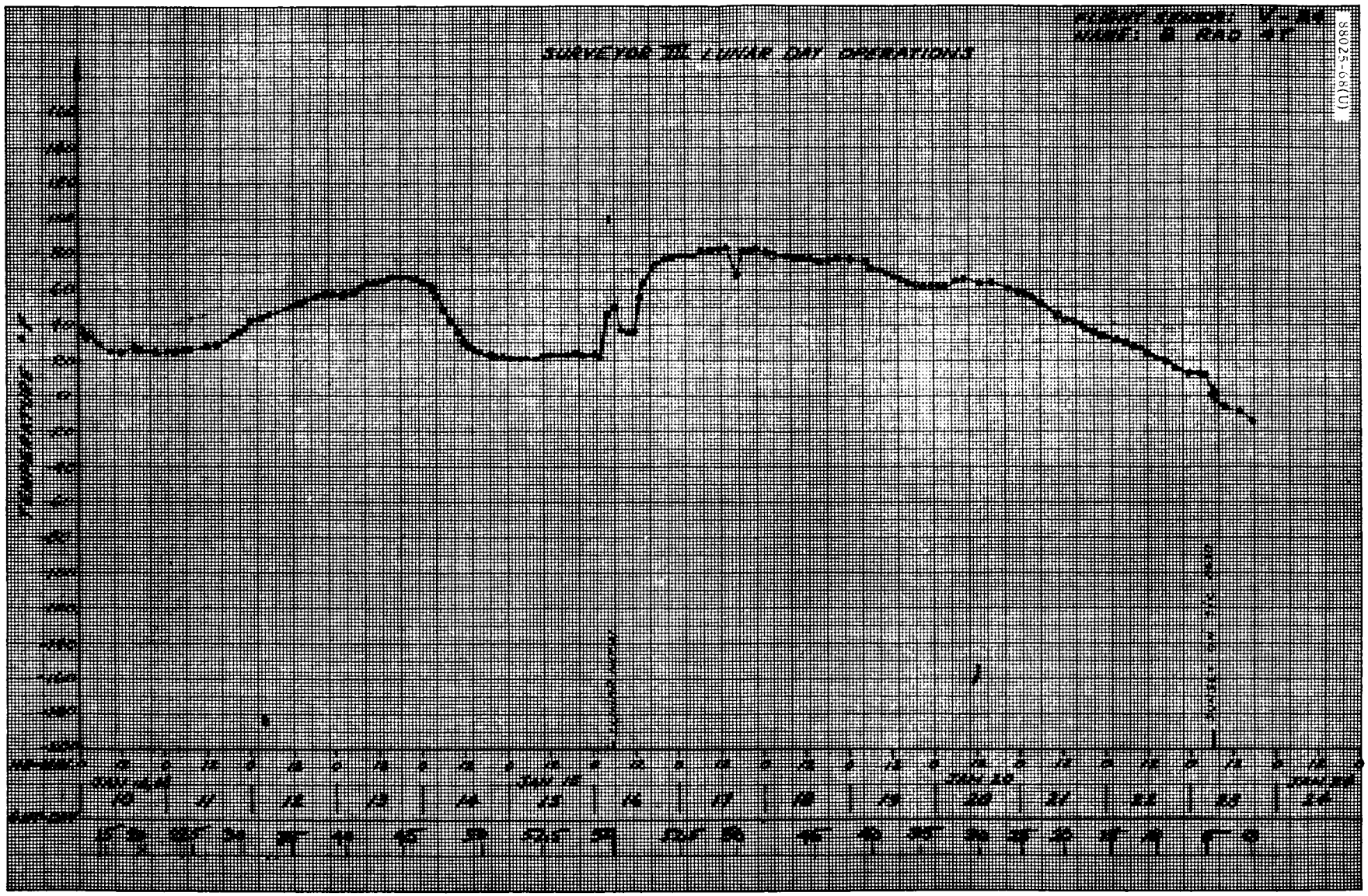

Figure 5. 1-B54. Sensor V-24: Compartment B Switch 4 in Face Radiator

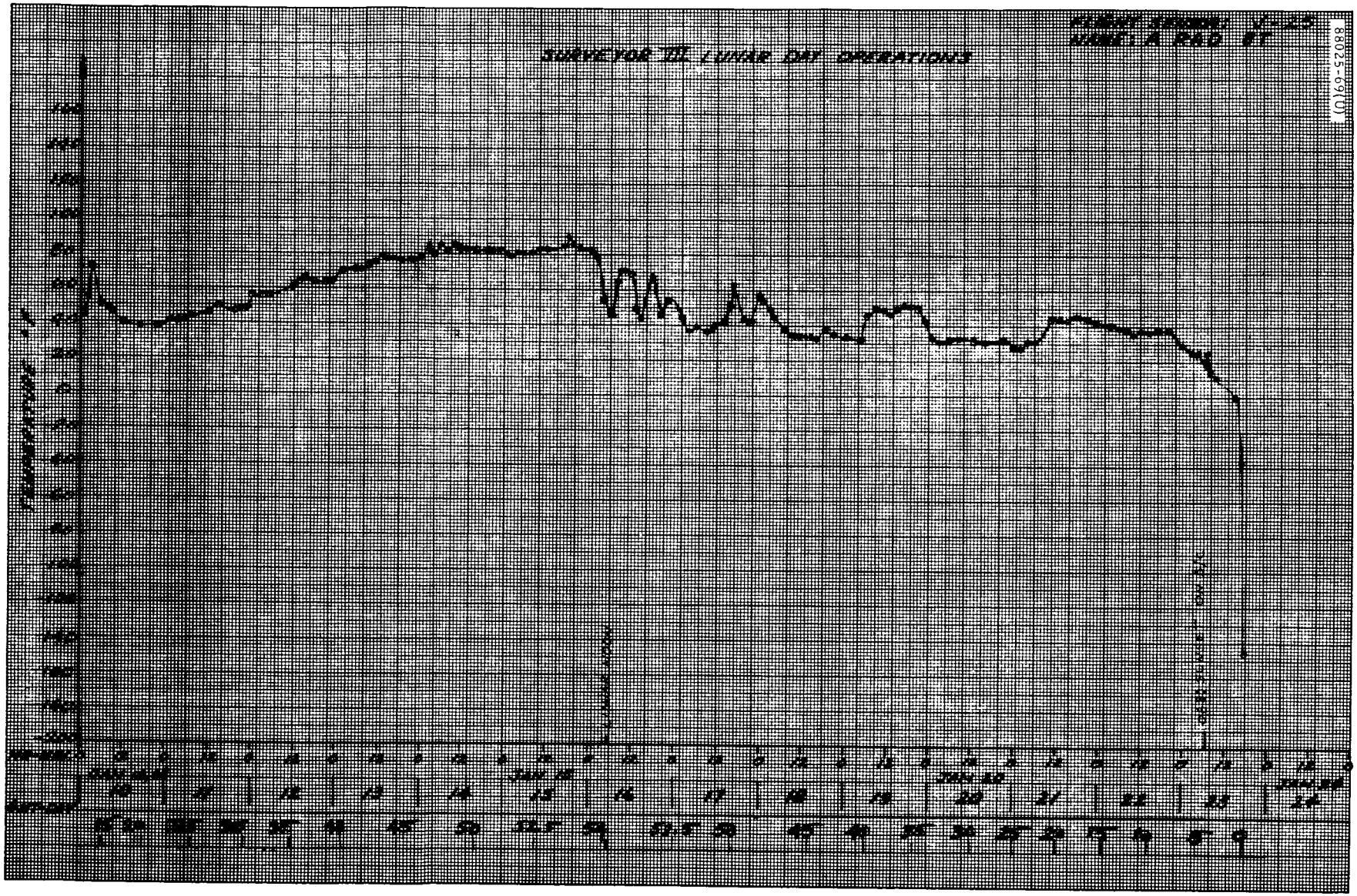

Figure 5. 1-B55. Sensor V-25: Compartment A Switch 8 in Face Radiator

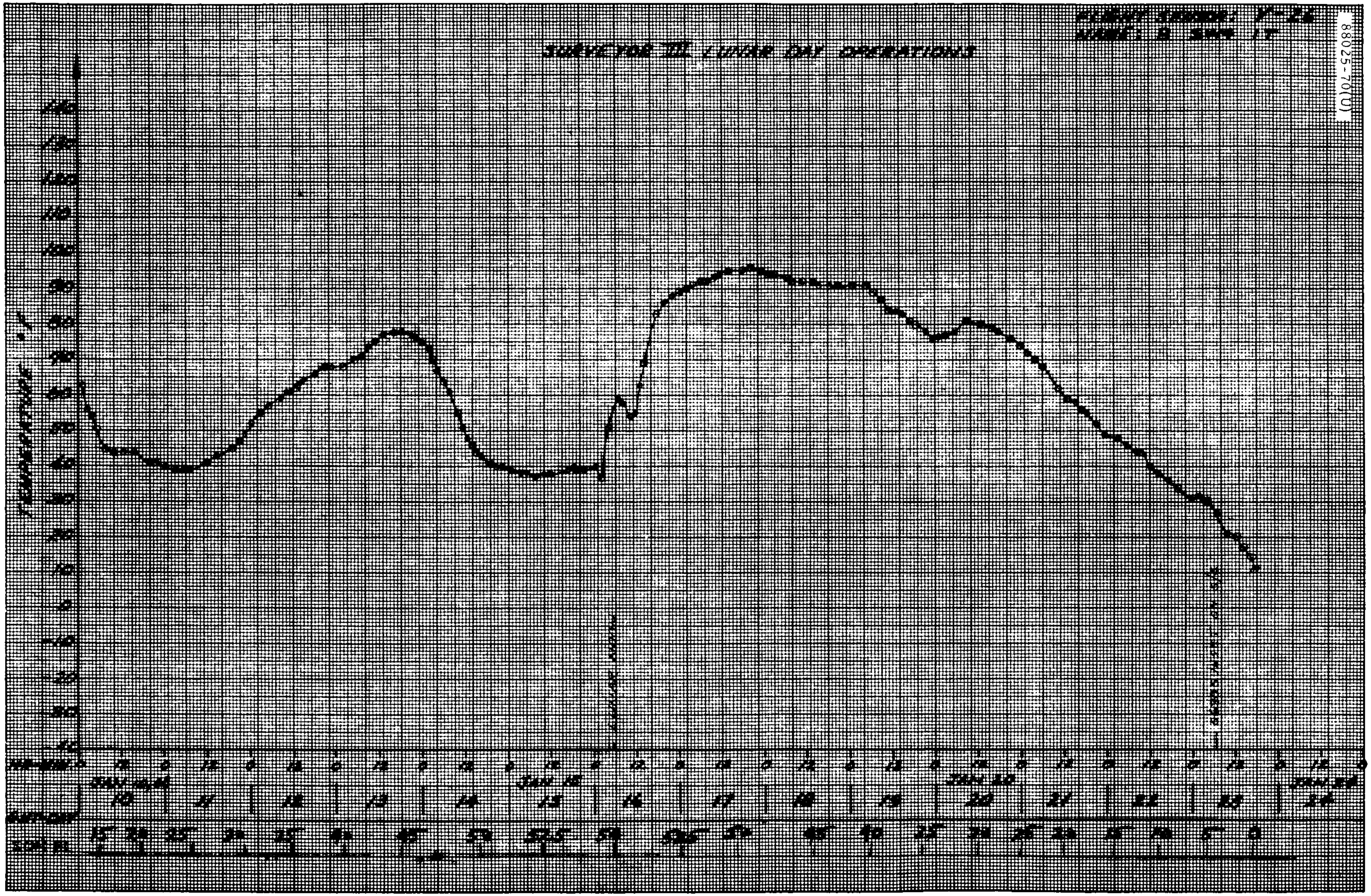

Figure 5. 1-B56. Sensor V-26: Compartment B Switch 4 Base

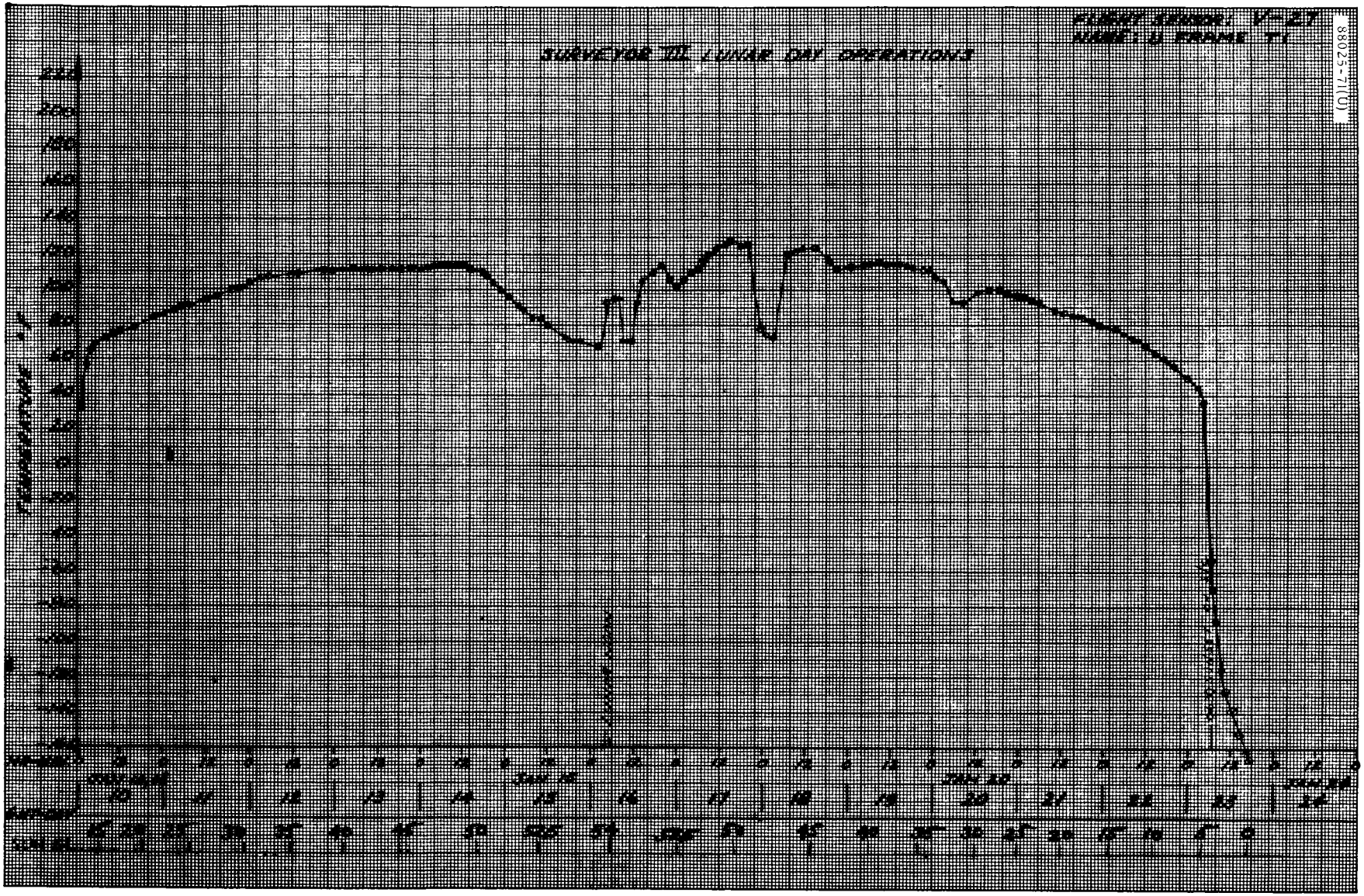

Figure 5.1-B57. Sensor V-27: Upper Spaceframe 1

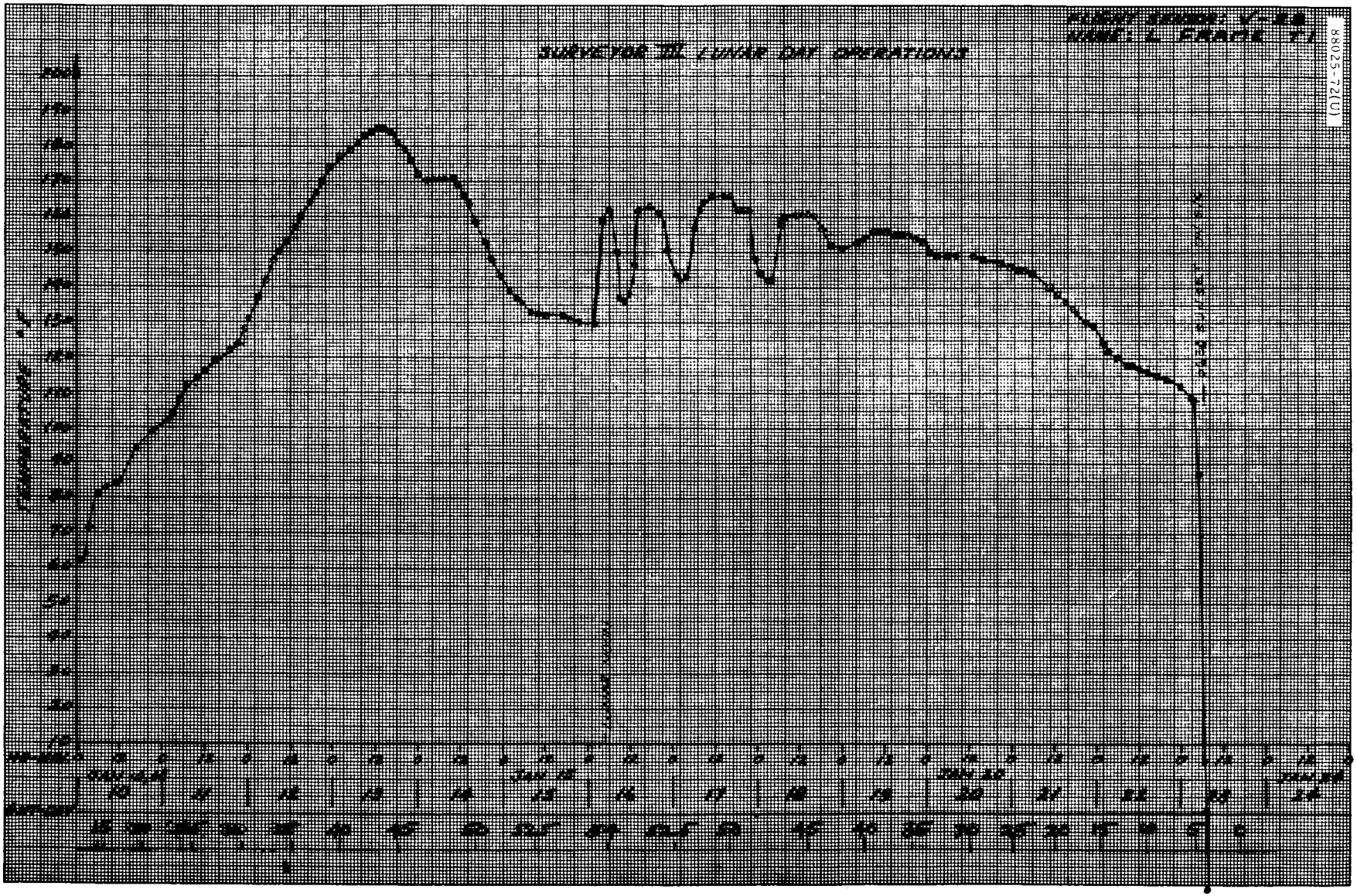

Figure 5. 1-B58. Sensor V-28: Spaceframe Temperature Under Compartment A

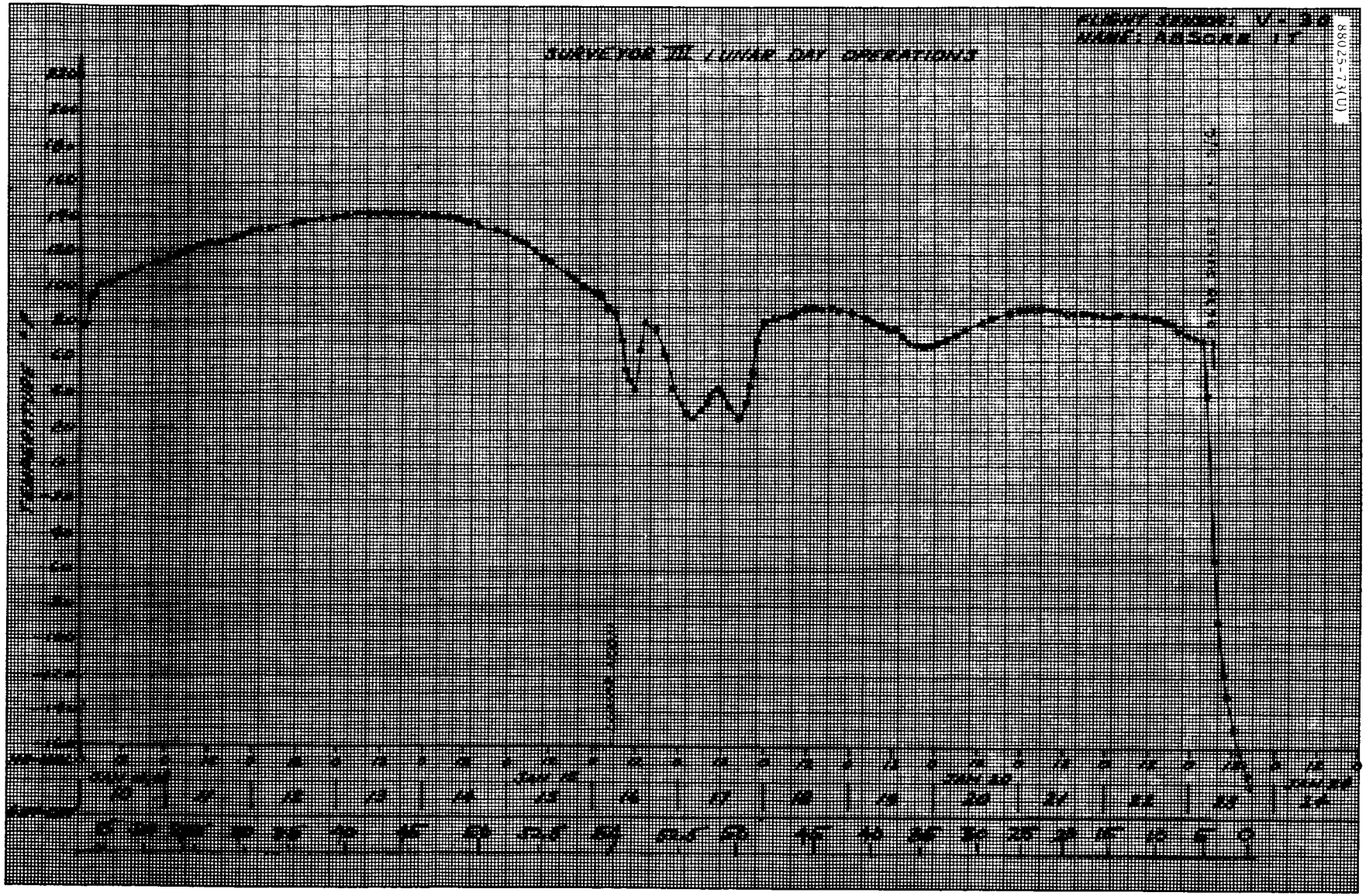

Figure 5.1-B59. Sensor V-30: Shock Absorber 1

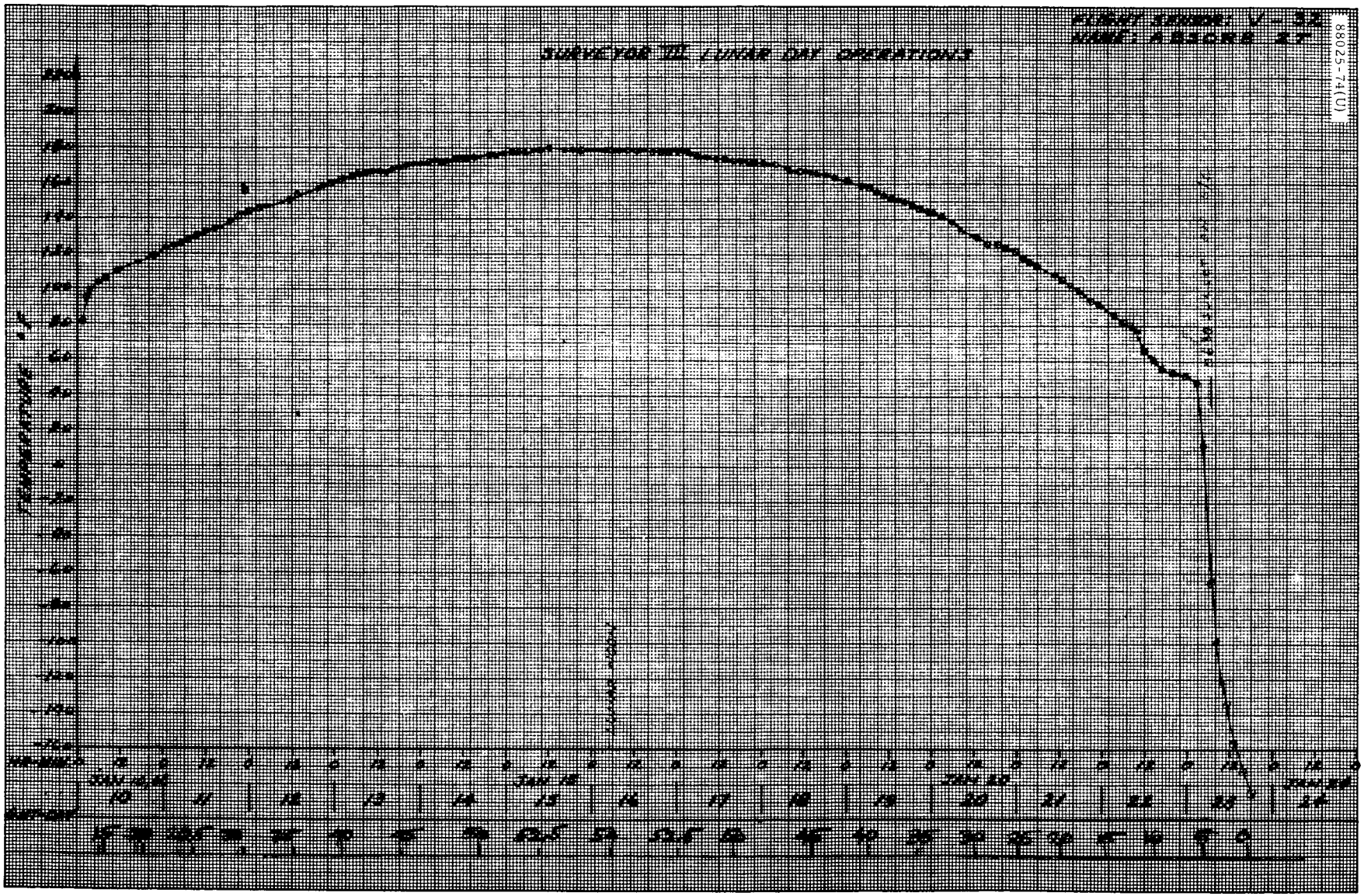

Figure 5.1-B60. Sensor V-32: Shock Absorber 2

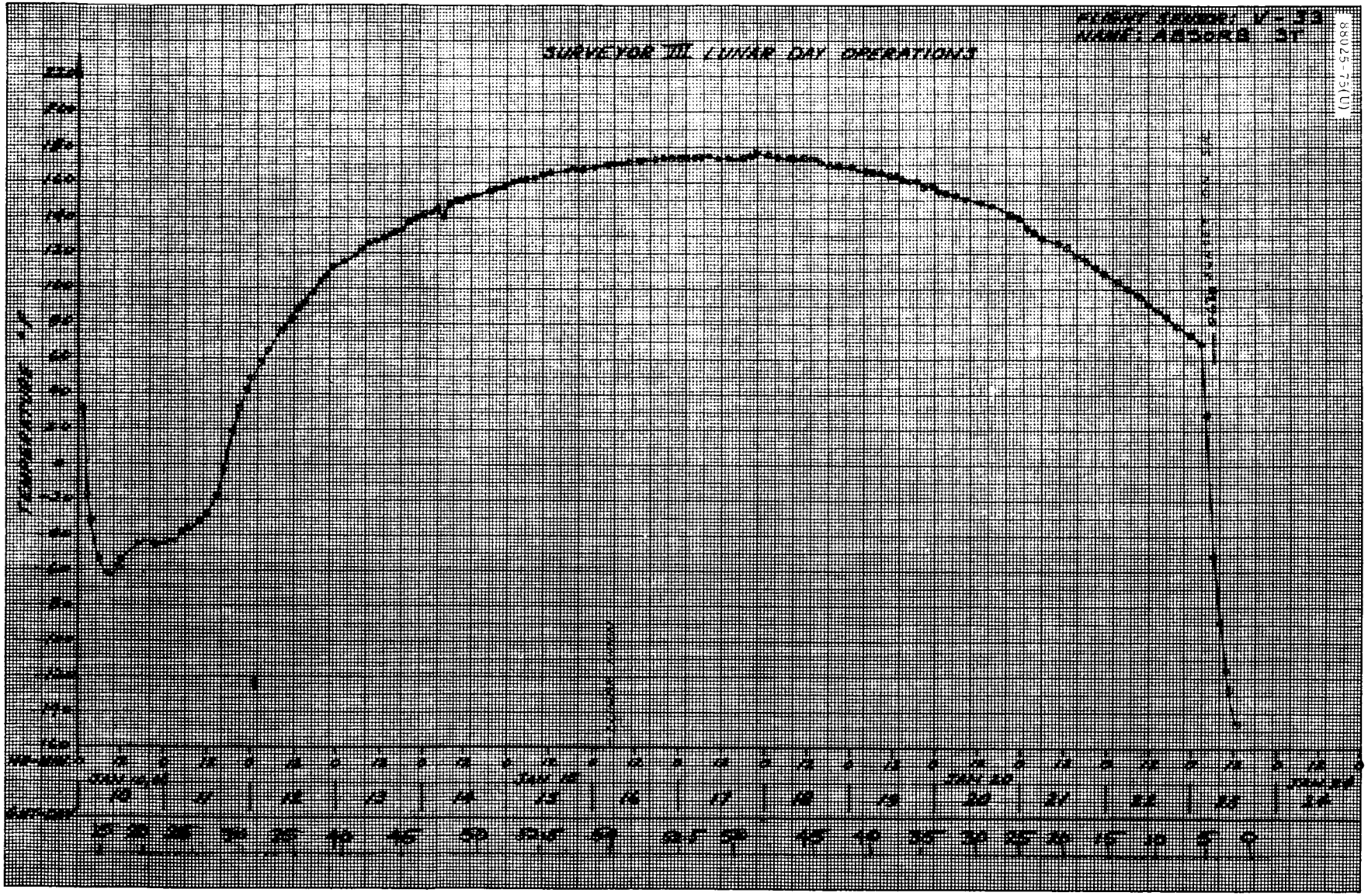

Figure 5. 1-B61. Sensor V-33: Shock Absorber 3

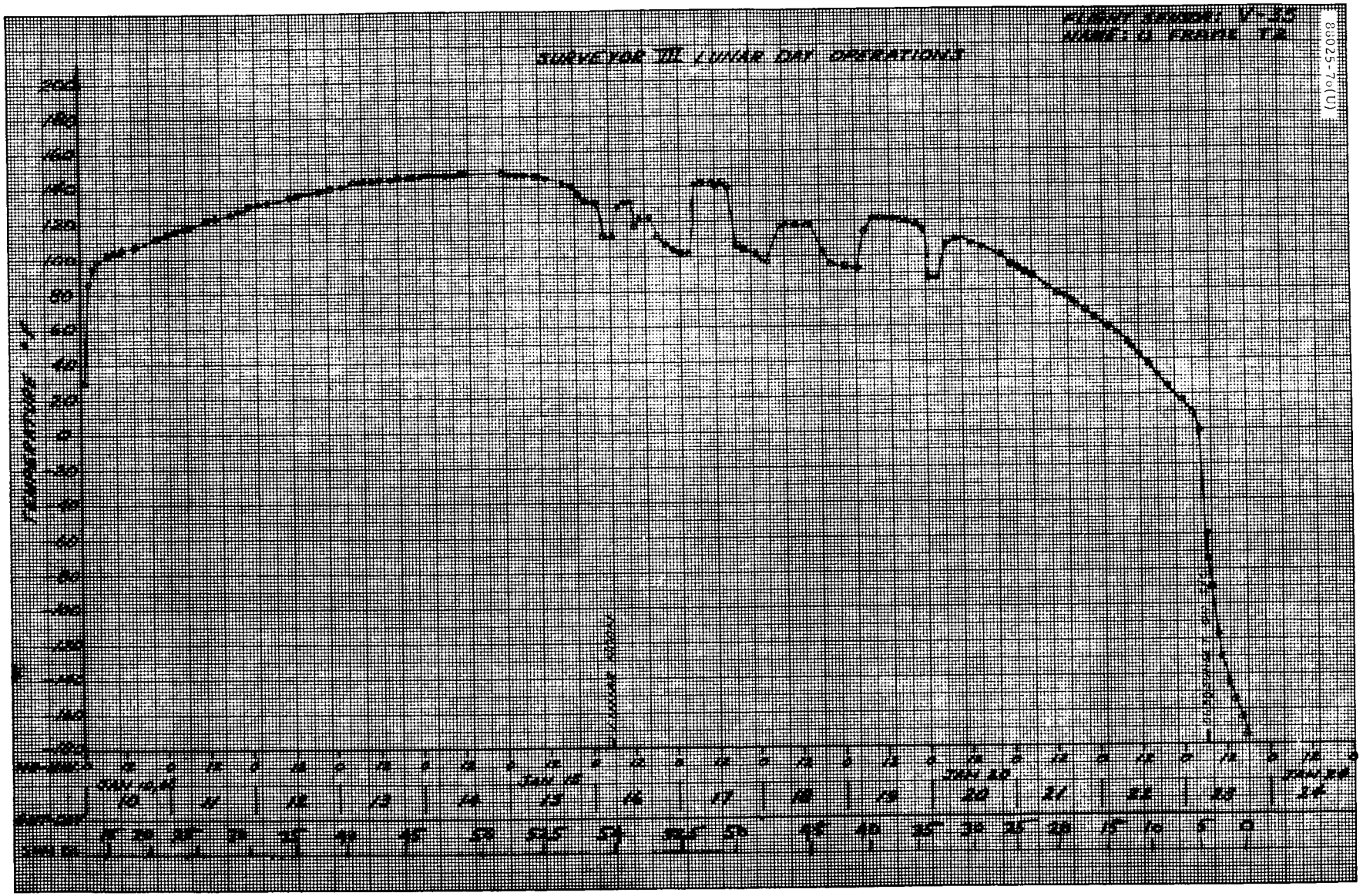

Figure 5.1-B62. Sensor V-35: Upper Spaceframe 2

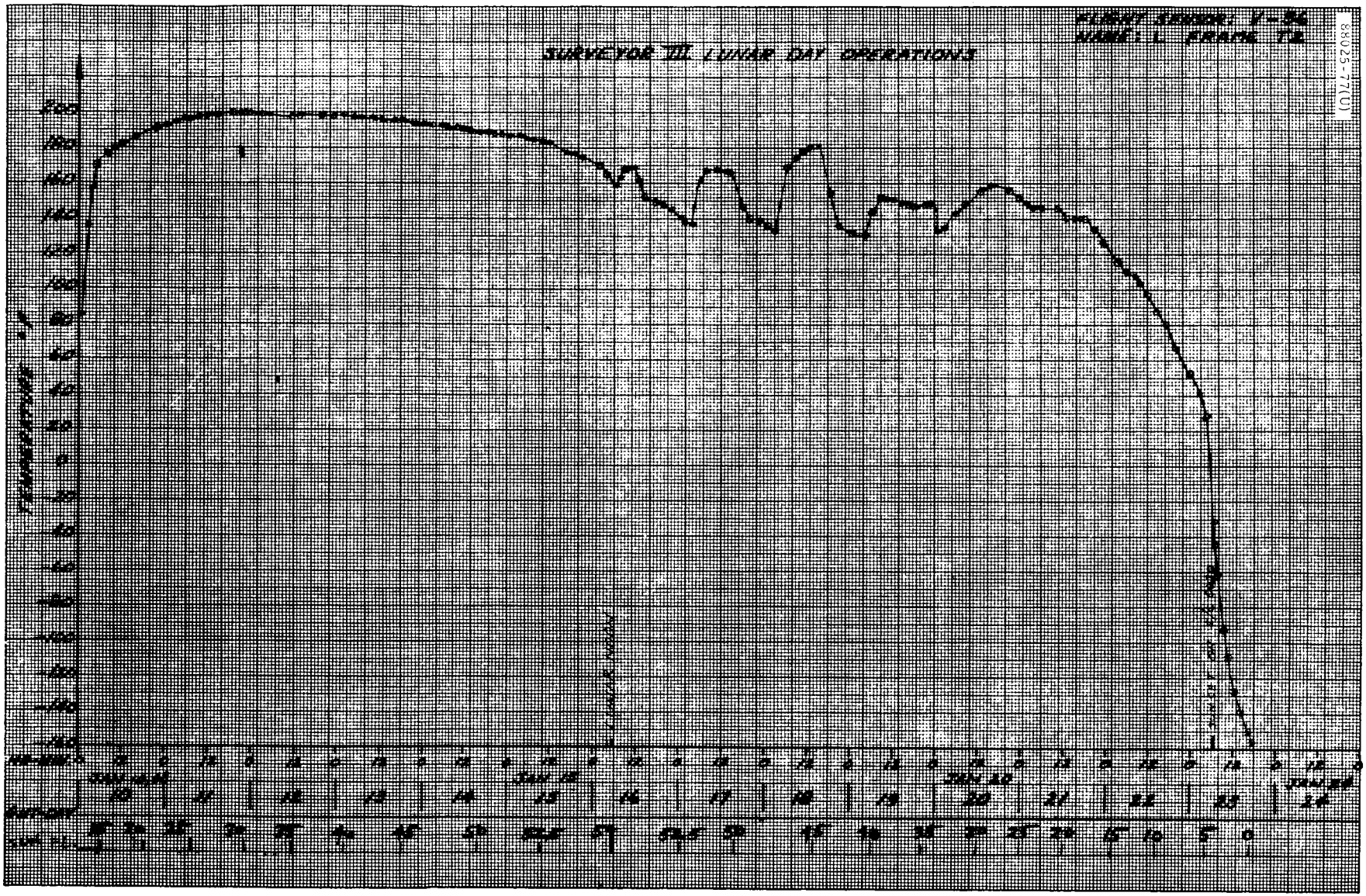

Figure 5.1-B63. Sensor V-36: Spaceframe Temperature Under Compartment 3

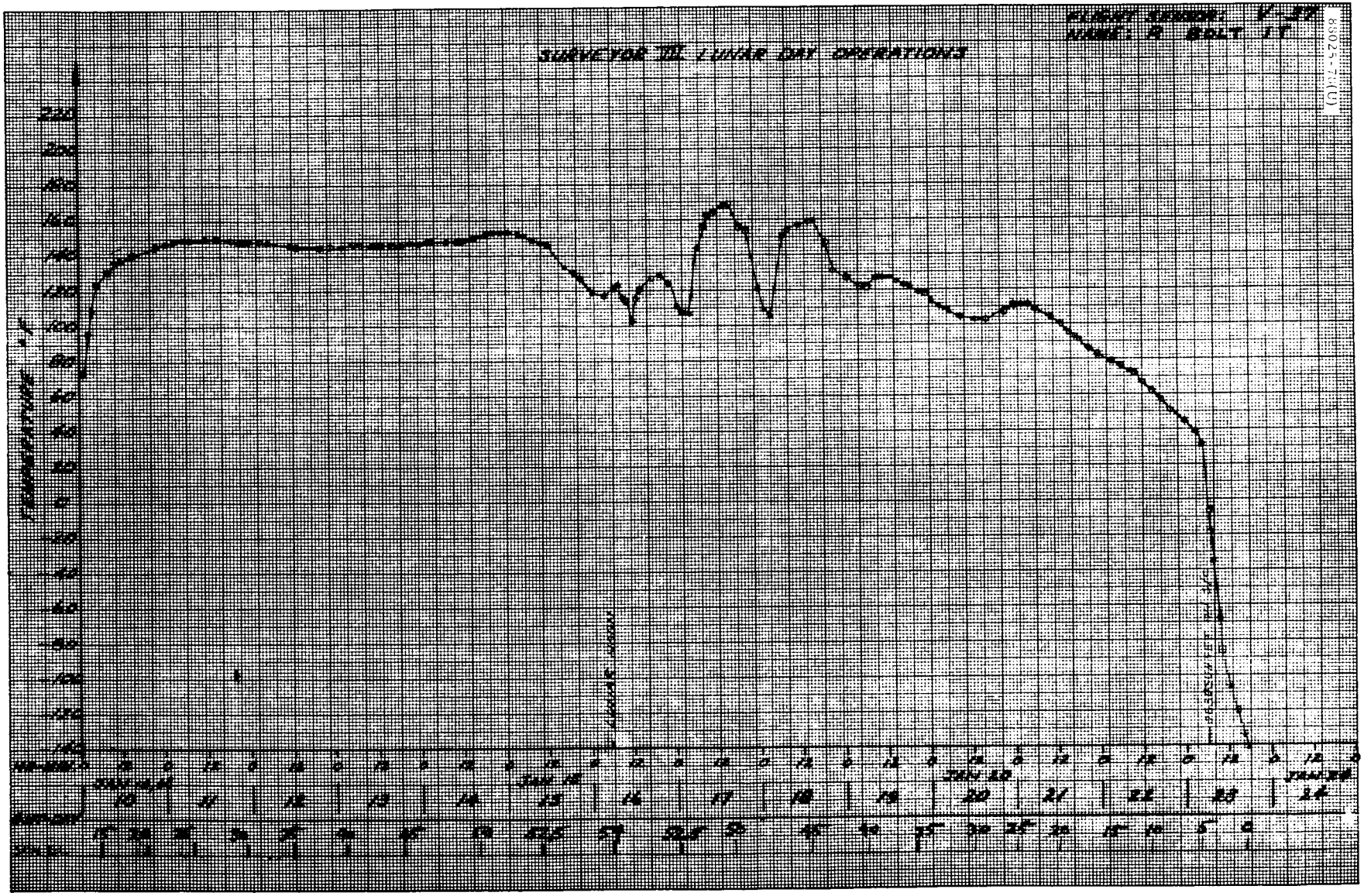

Figure 5. 1-B64. Sensor V-37: Retro Attach Point 1

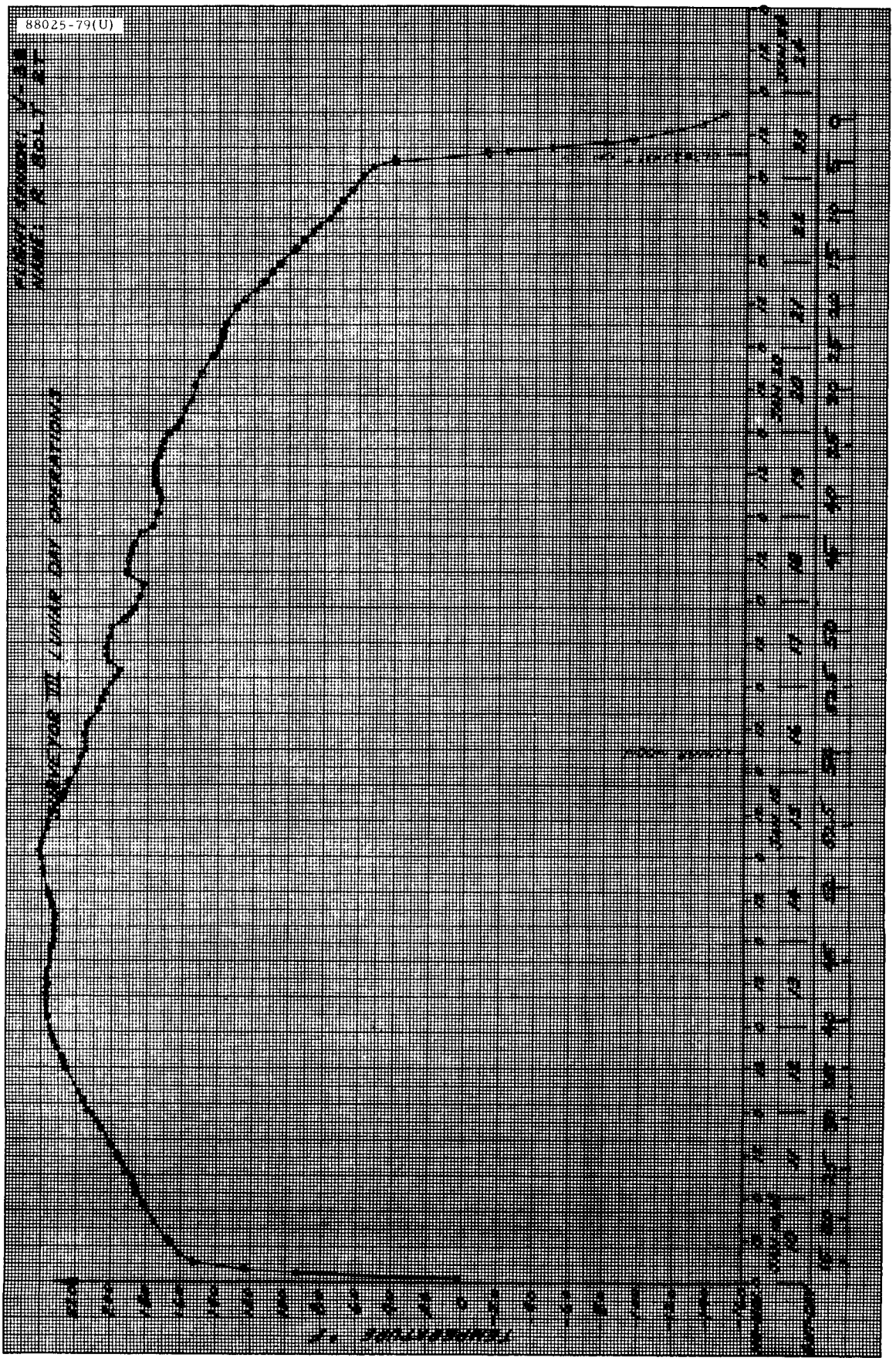

Figure 5.1-B65. Sensor V-38: Retro Attach Point 2

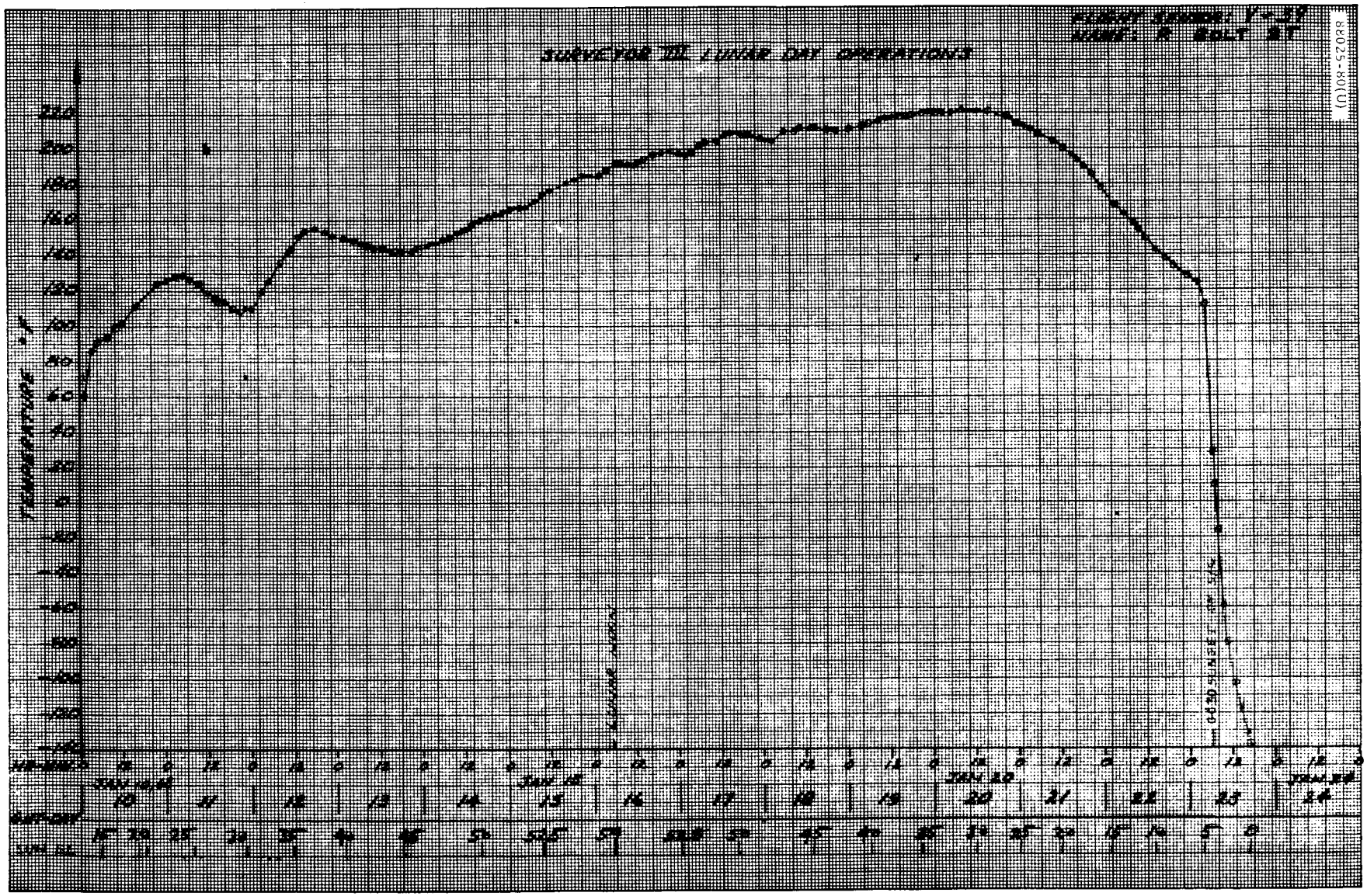

Figure 5. 1-B66. Sensor V-39: Retro Attach Point 3

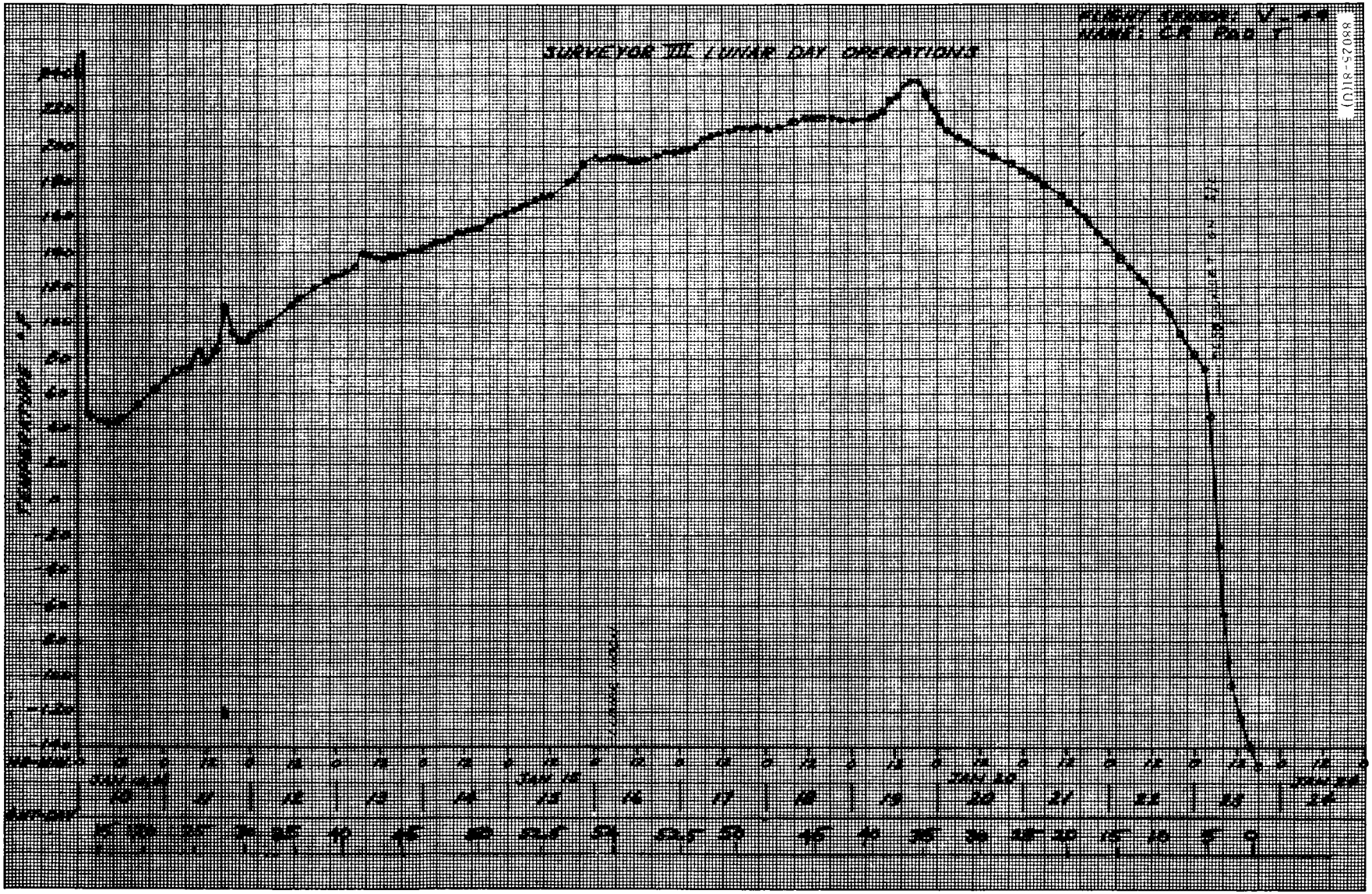

Figure 5.1-B67. Sensor V-44: Crushable Block

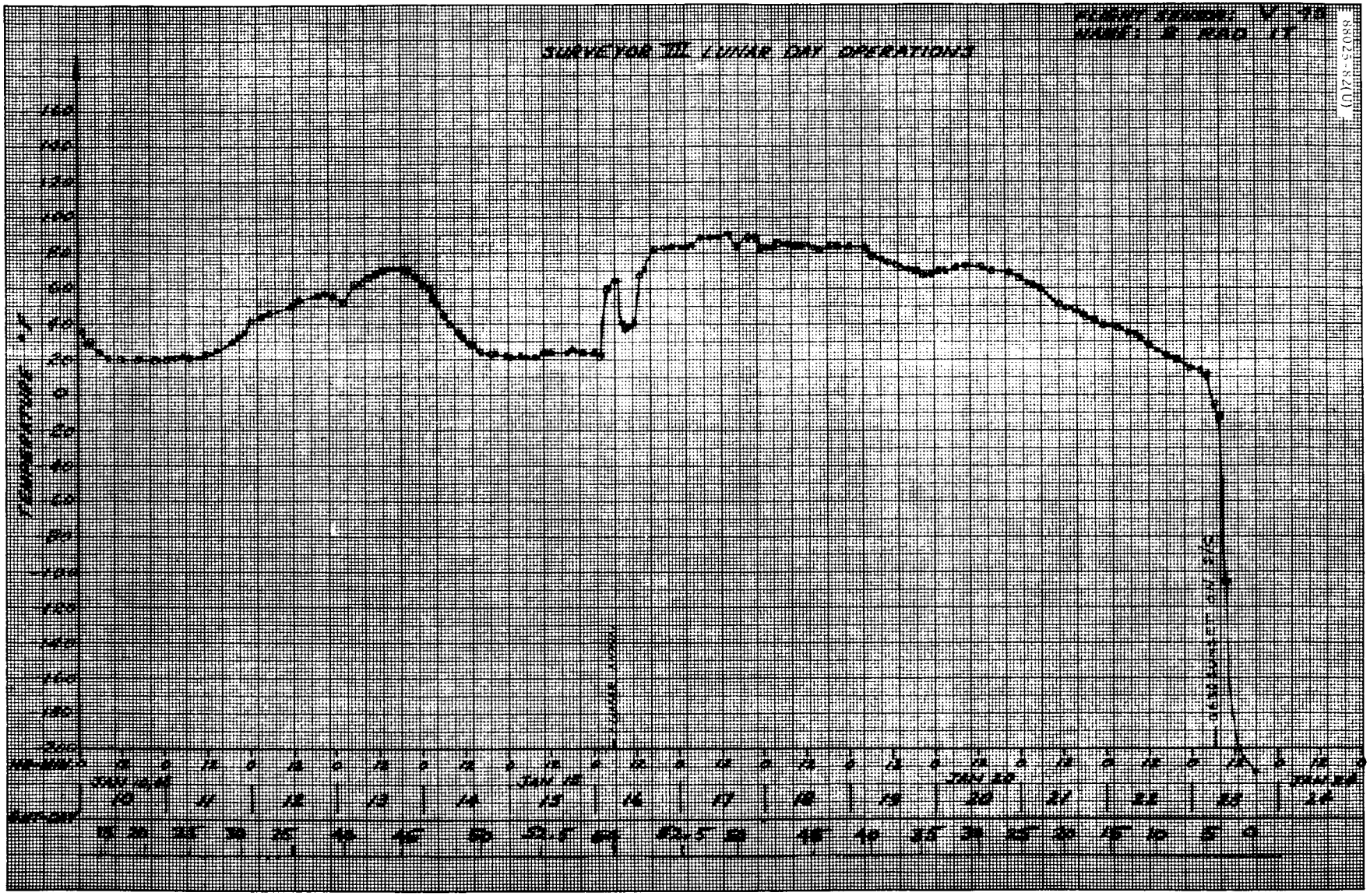

Figure 5.1-B68. Sensor V-45: Compartment B Switch 1 in Face Radiator

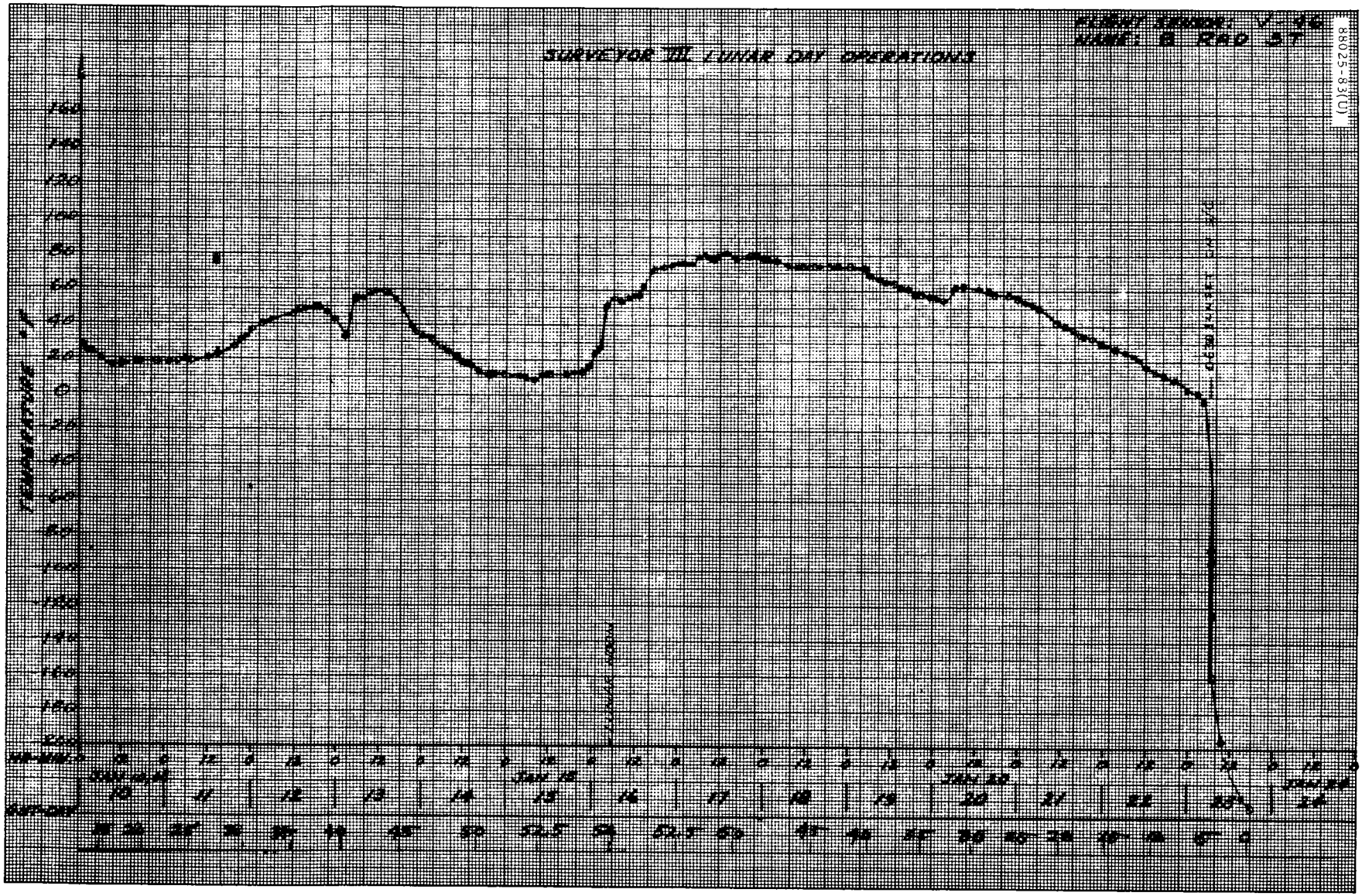

Figure 5.1-B69. Sensor V-46: Compartment B Switch 5 in Face Radiator

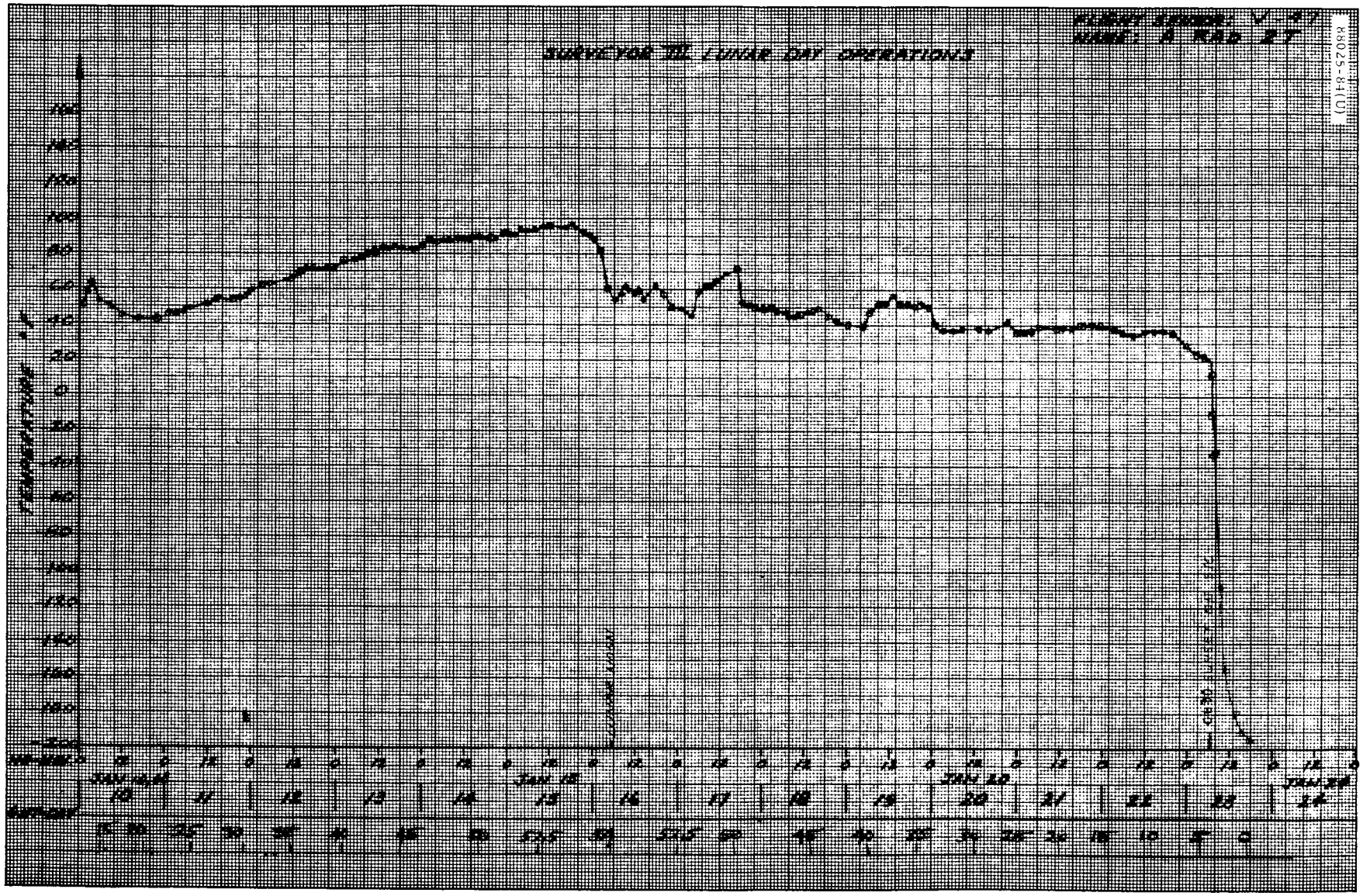

Figure 5.1-B70. Sensor V-47: Compartment A Switch 2 in Face Radiator

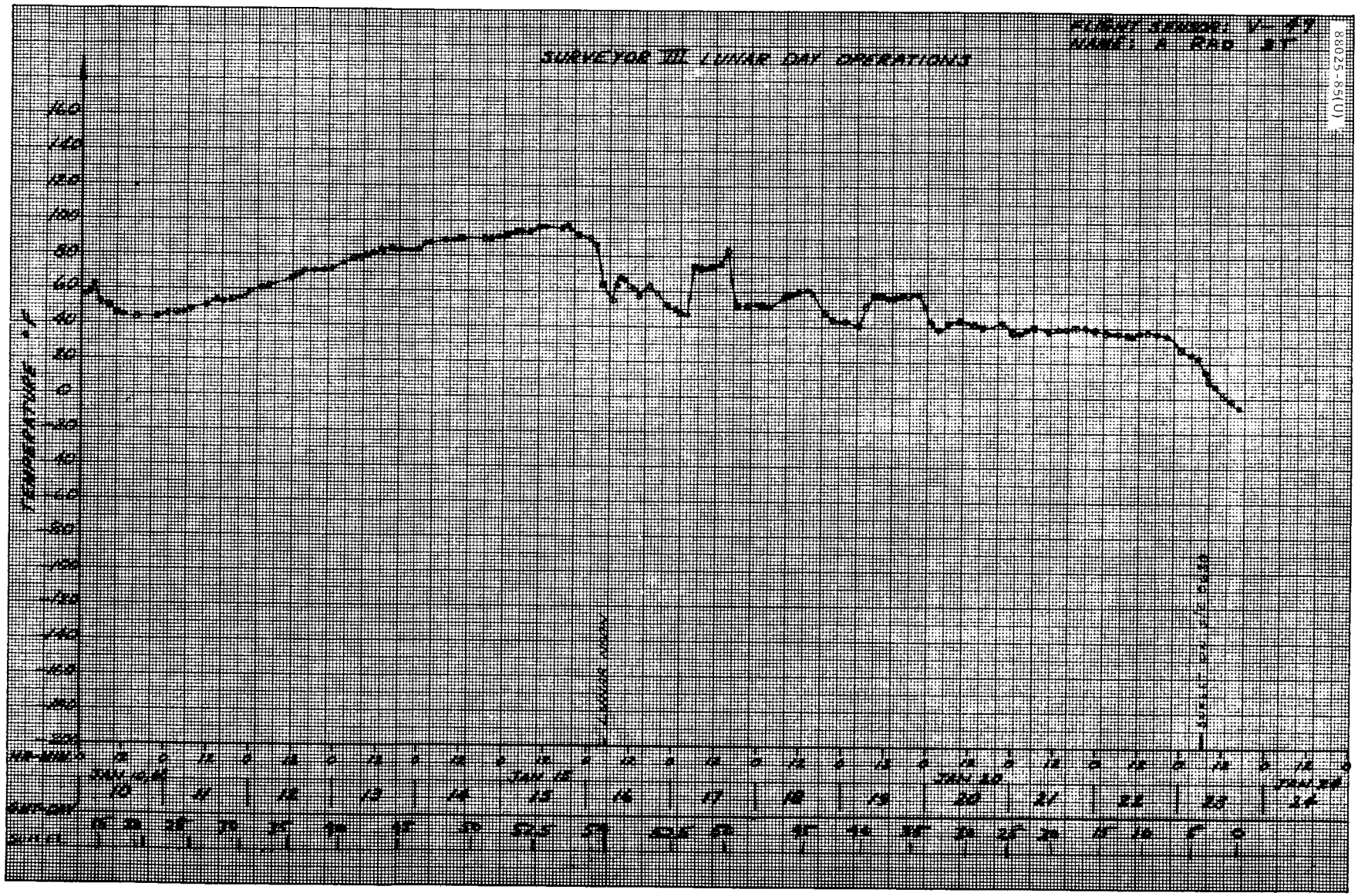

Figure 5.1-B71. Sensor V-49: Compartment A Switch 3 in Face Radiator

APPENDIX C TO SECTION 5.1

FIRST LUNAR NIGHT TEMPERATURE PLOTS

Appendix C contains Figures 5.1-C1 through 5.1-C71, first lunar night temperature plots. These plots were recorded in real time by Spacecraft Performance Analysis and Command.

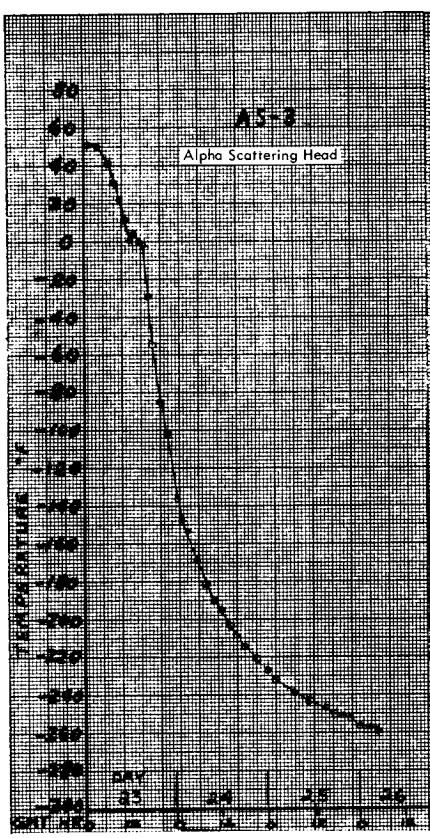

Figure 5.1-C1

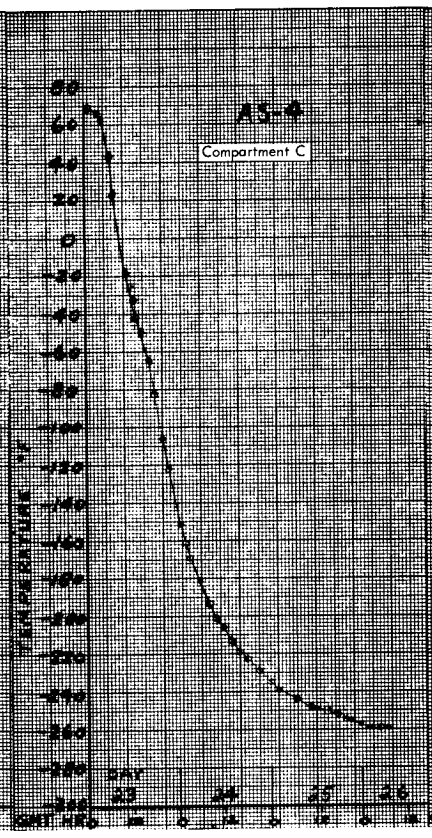

Figure 5.1-C2

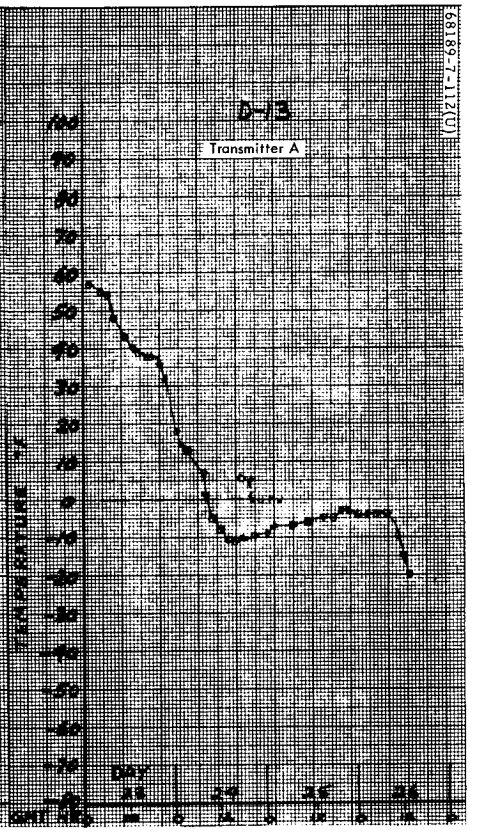

Figure 5.1-C3

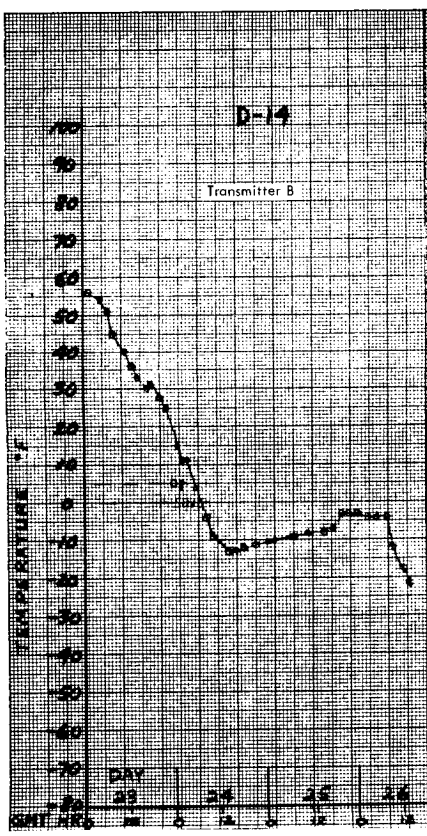

Figure 5.1-C4

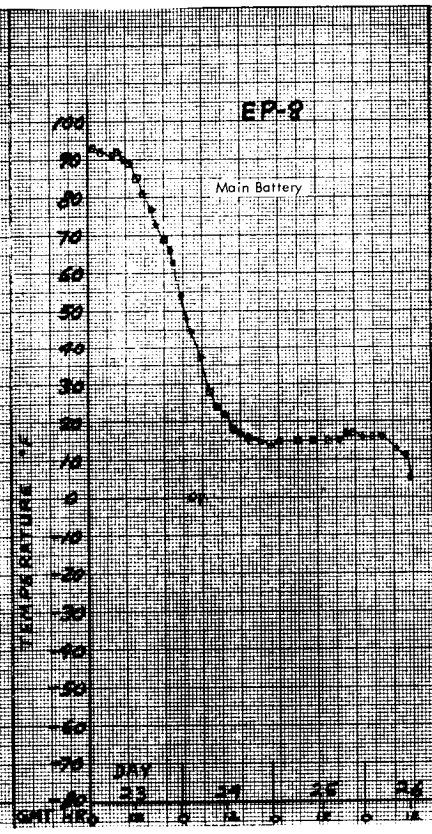

Figure 5.1-C5

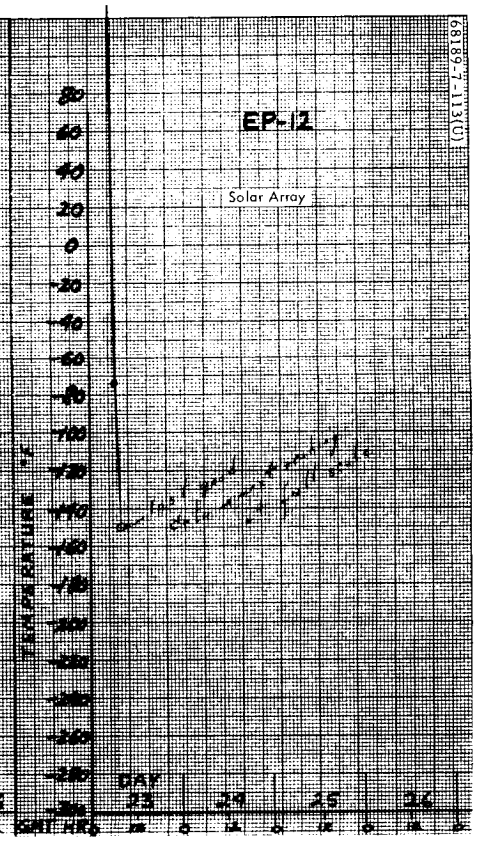

Figure 5.1-C6

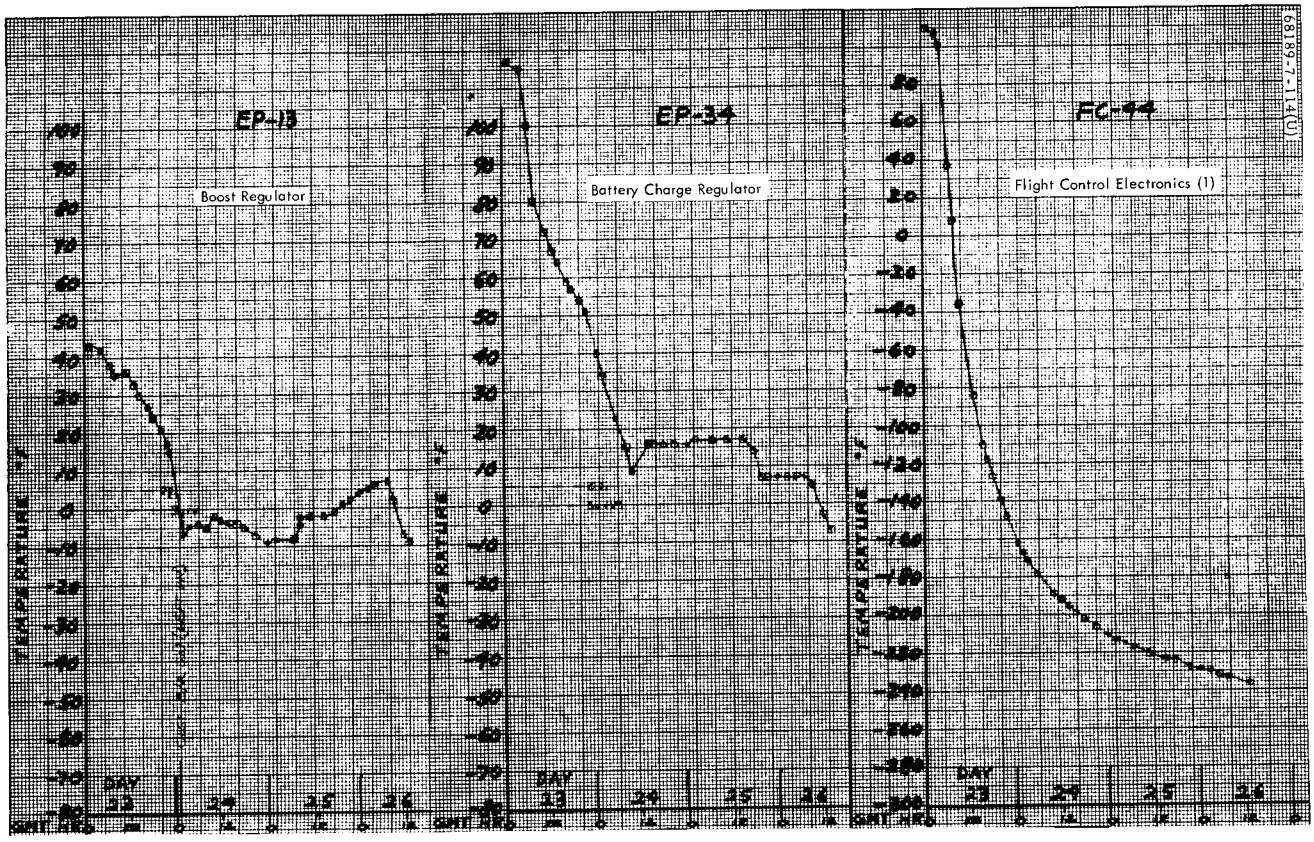

Figure 5.1-C7

Figure 5.1-C8

Figure 5.1-C9

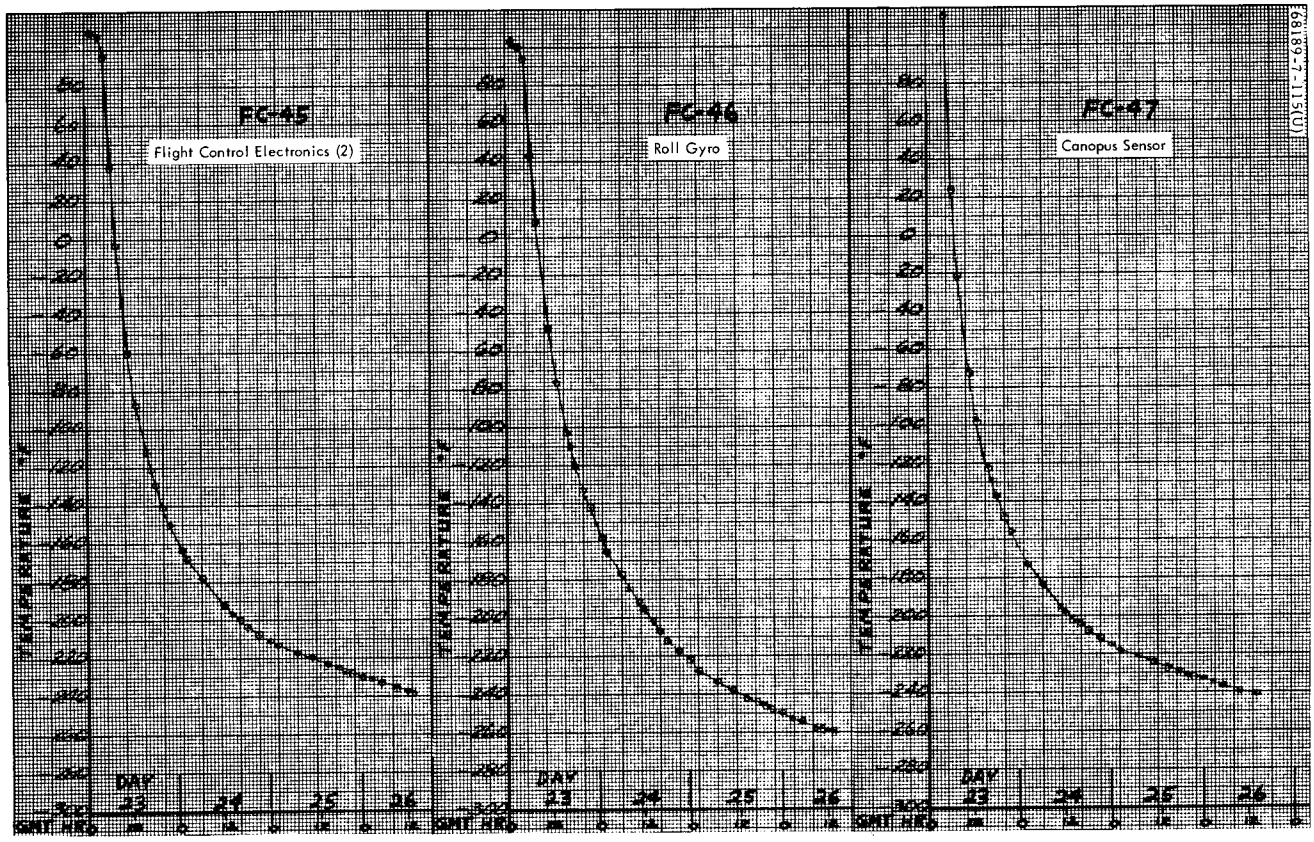

Figure 5.1-C10

Figure 5.1-C11

Figure 5.1-C12

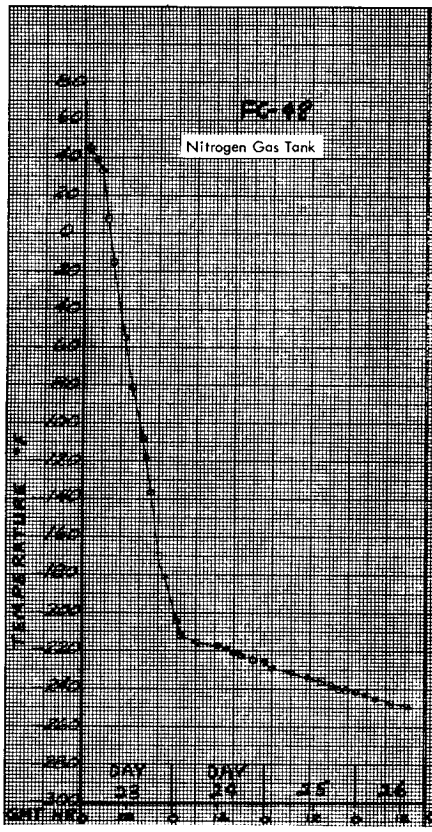

Figure 5.1-C13

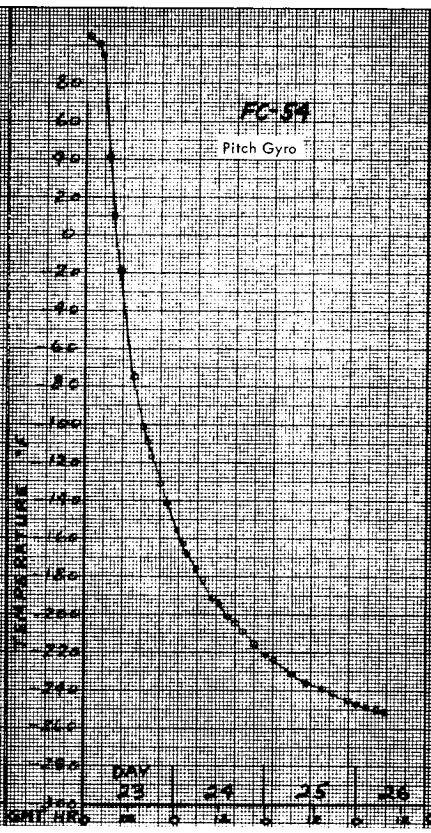

Figure 5.1-C14

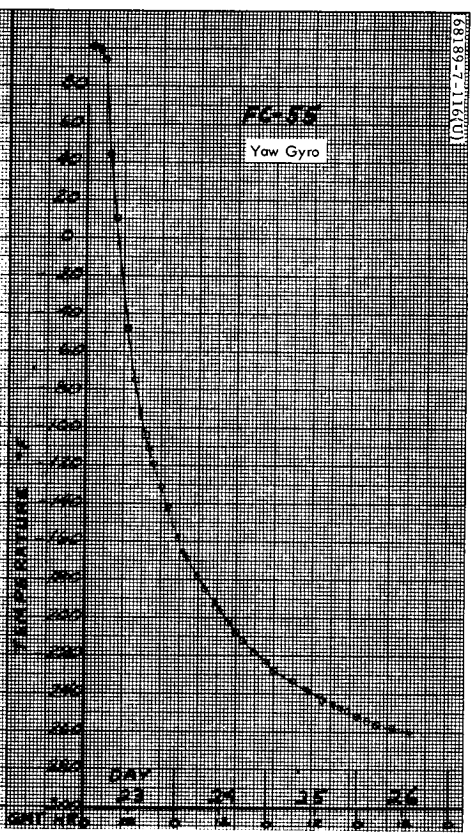

Figure 5.1-C15

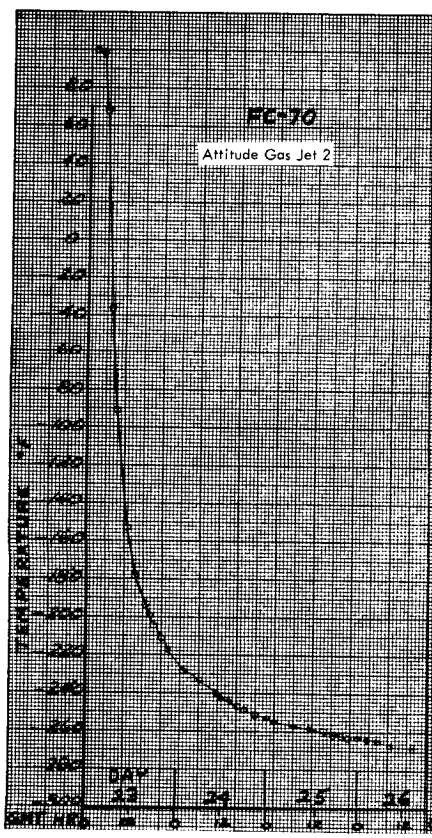

Figure 5.1-C16

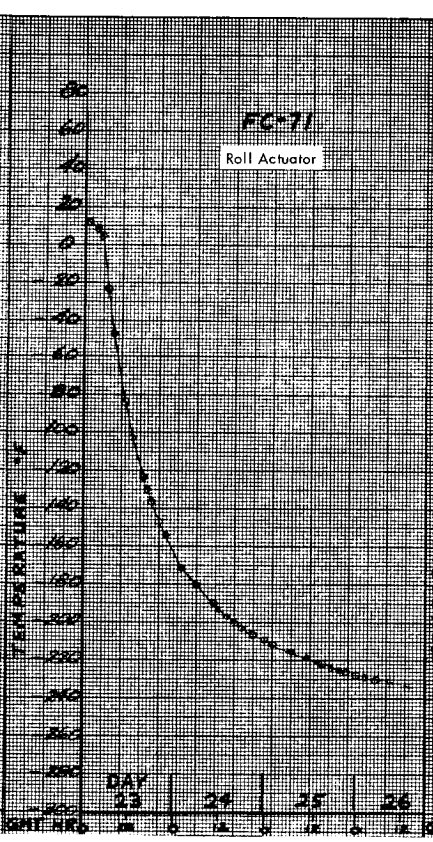

Figure 5.1-C17

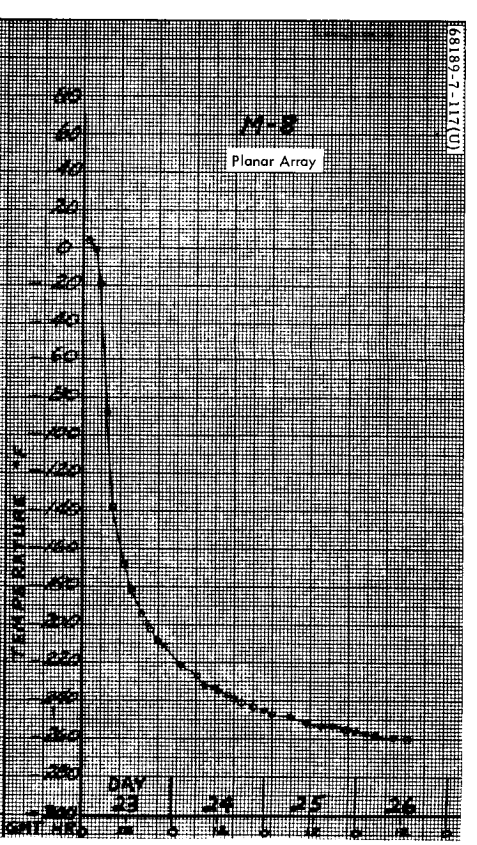

Figure 5.1-C18

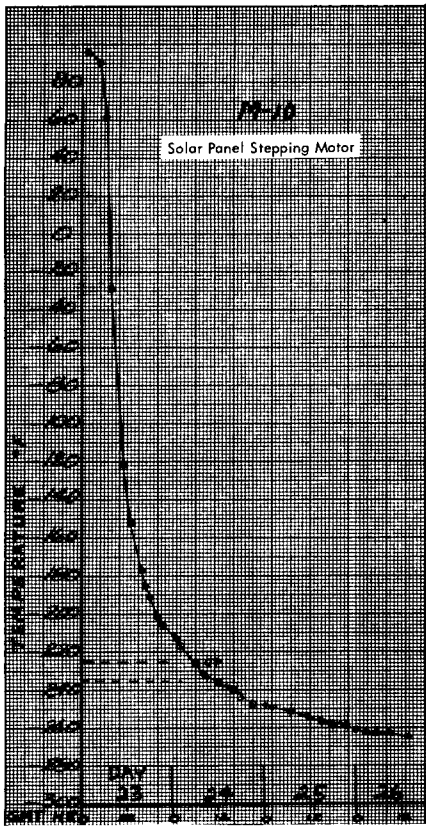

Figure 5.1-C19

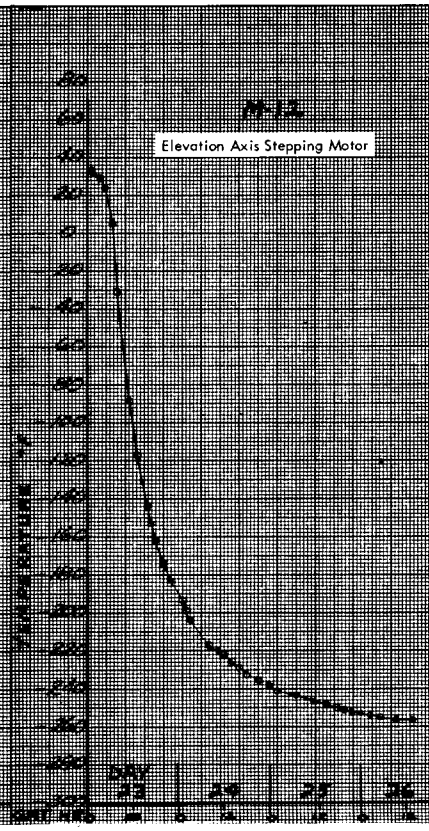

Figure 5.1-C20

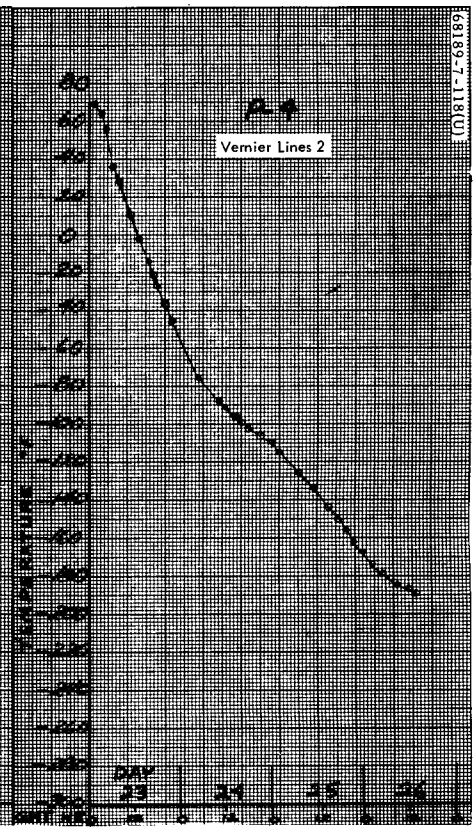

Figure 5.1-C21

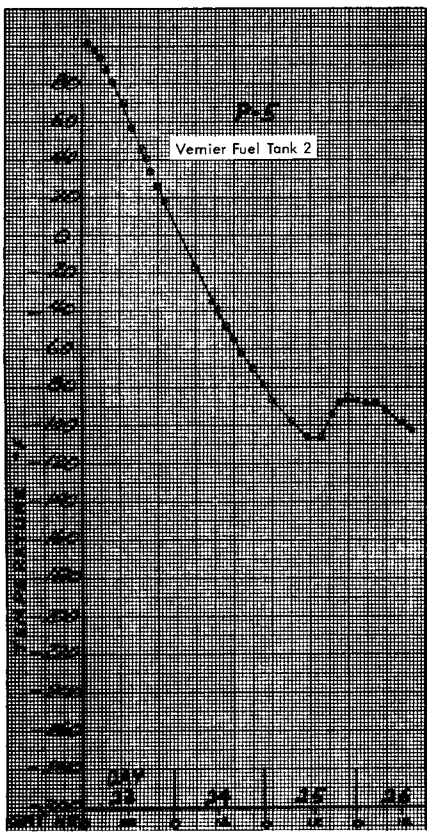

Figure 5.1-C22

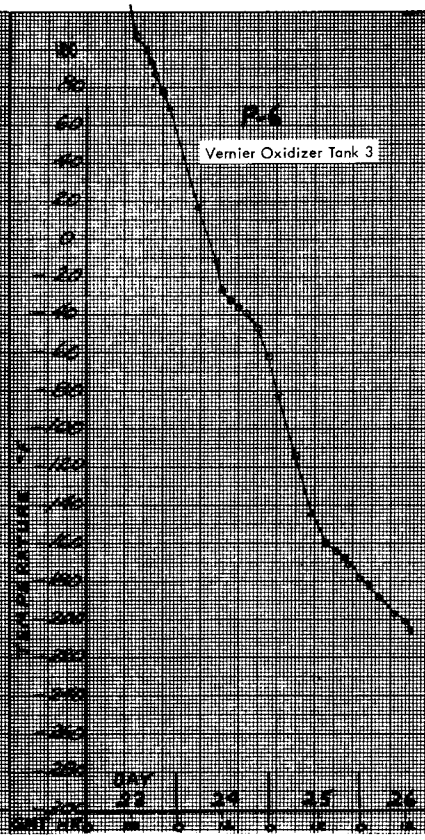

Figure 5.1-C23

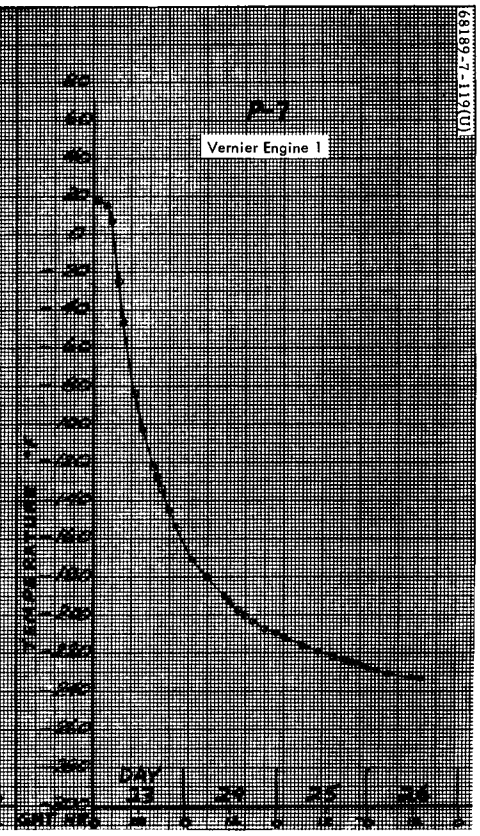

Figure 5.1-C24

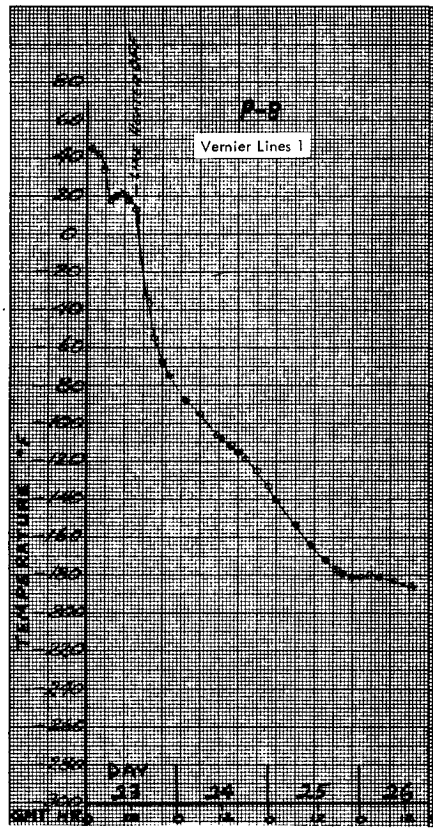

Figure 5.1-C25

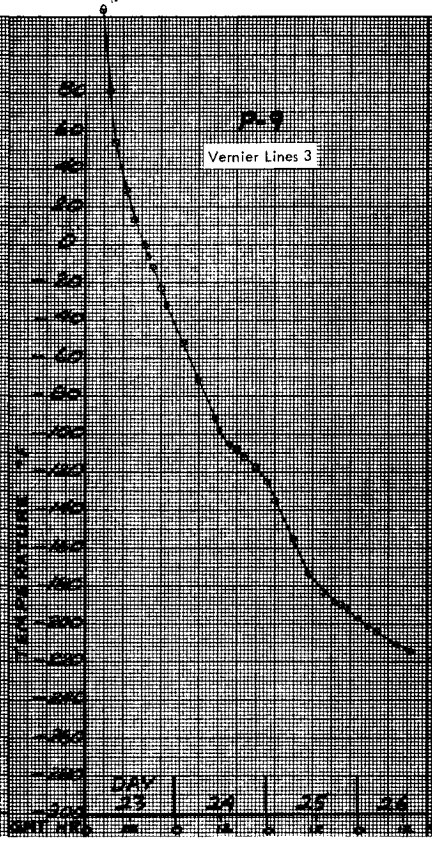

Figure 5.1-C26

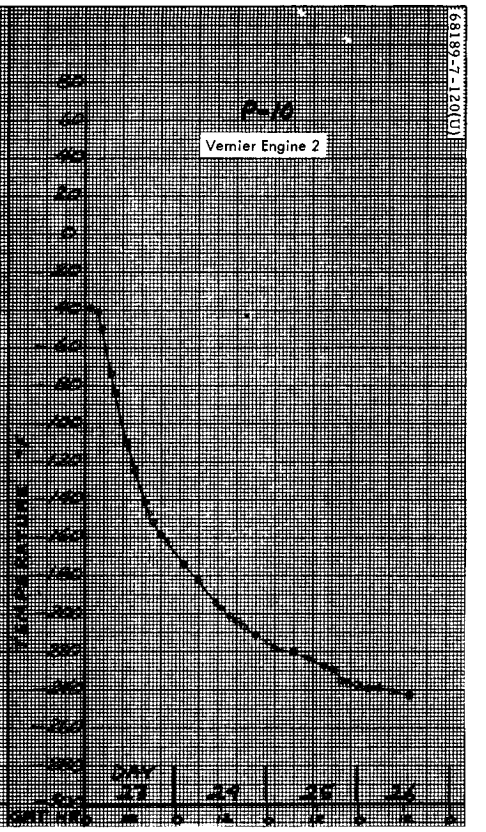

Figure 5.1-C27

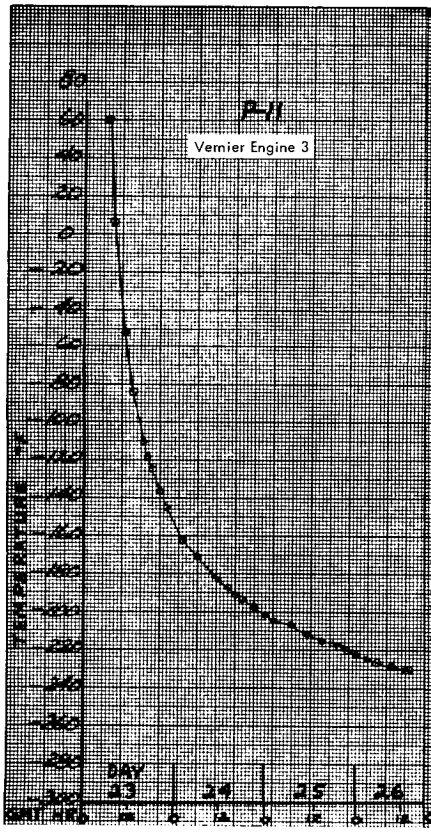

Figure 5.1-C28

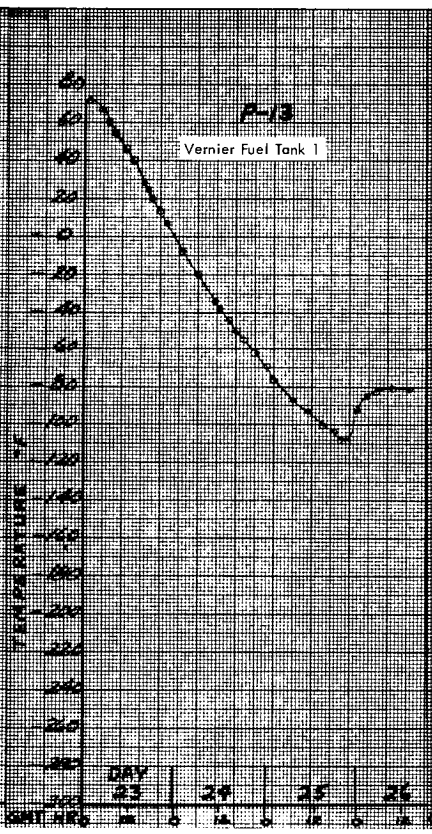

Figure 5.1-C29

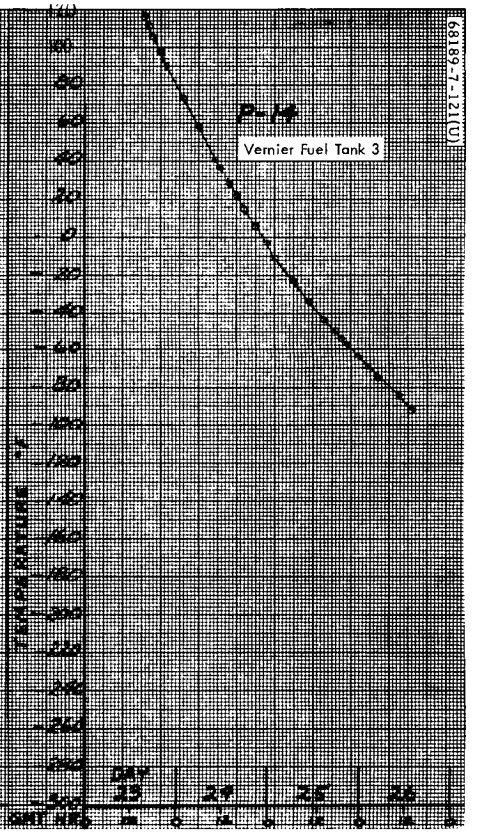

Figure 5.1-C30

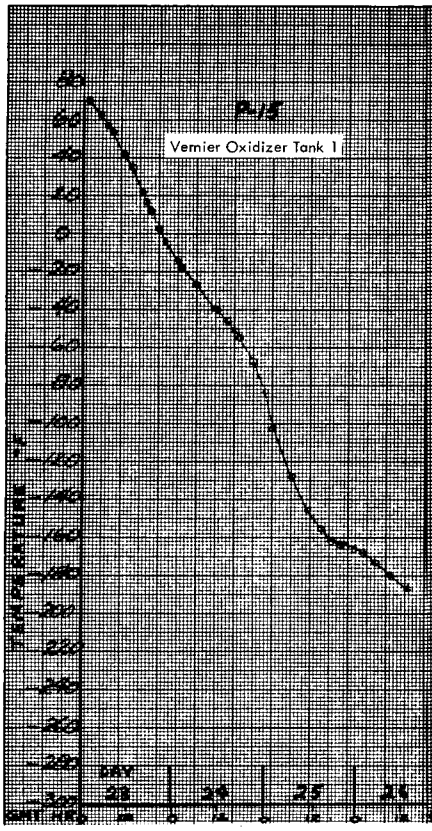

Figure 5.1-C31

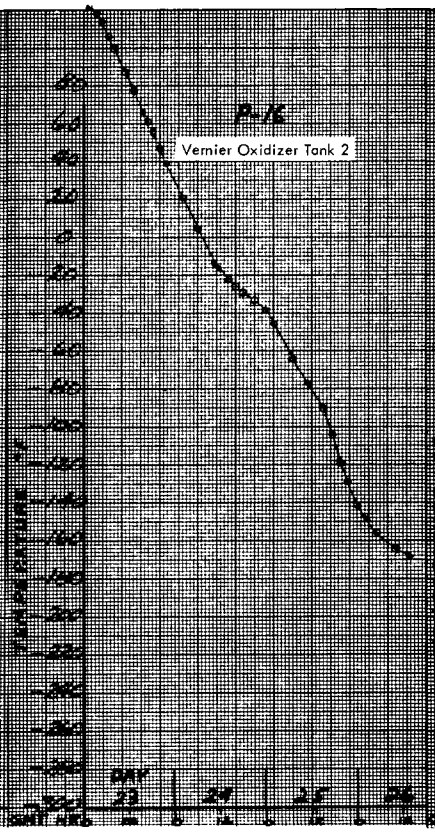

Figure 5.1-C32

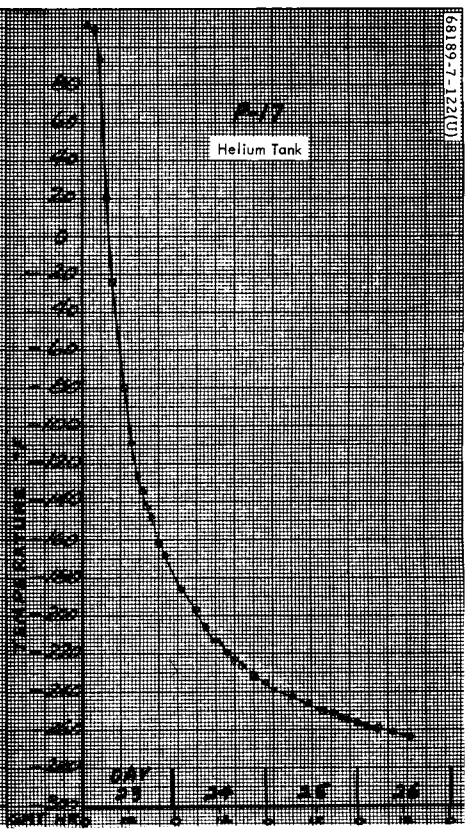

Figure 5.1-C33

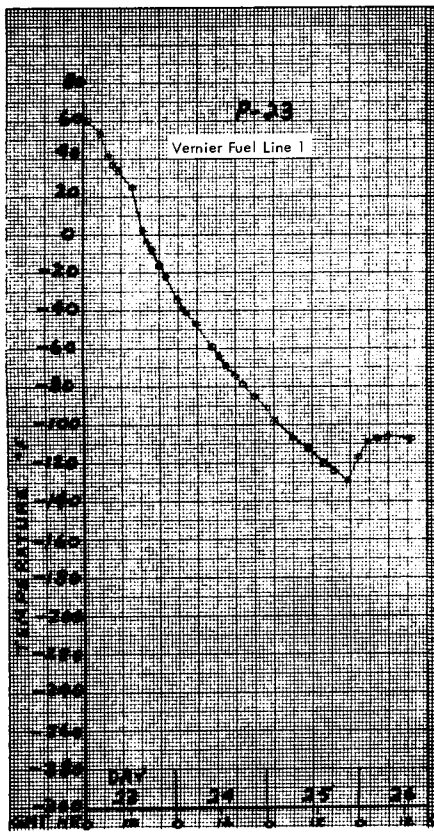

Figure 5.1-C34

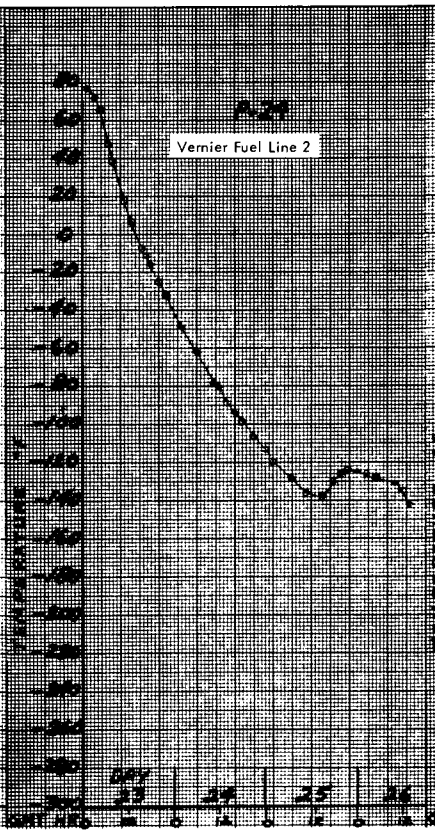

Figure 5.1-C35

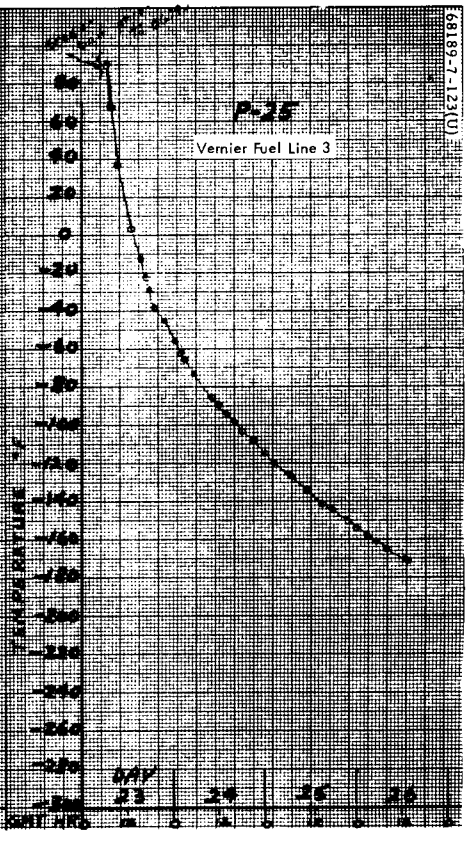

Figure 5.1-C36

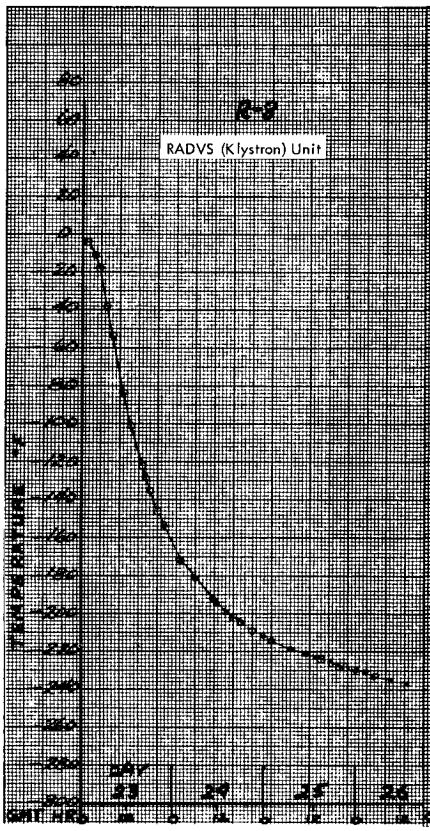

Figure 5.1-C37

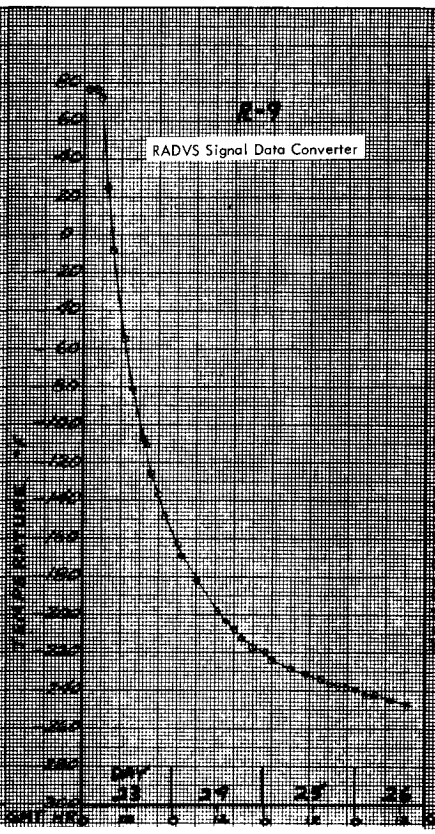

Figure 5.1-C38

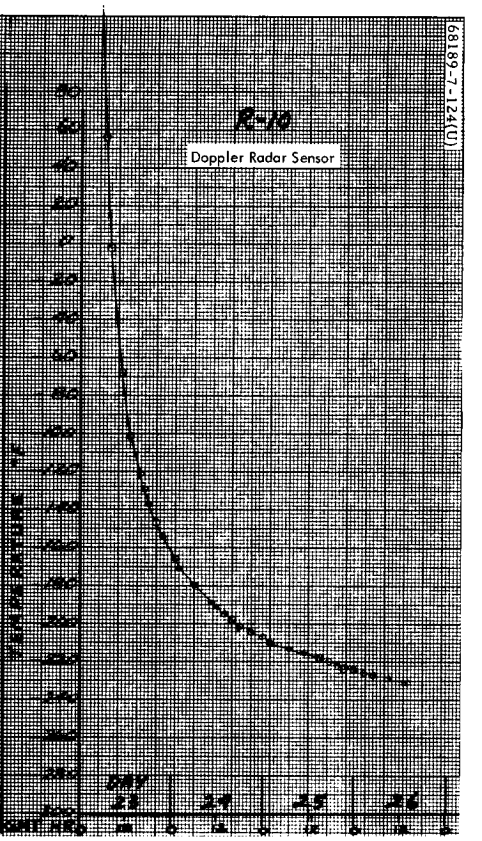

Figure 5.1-C39

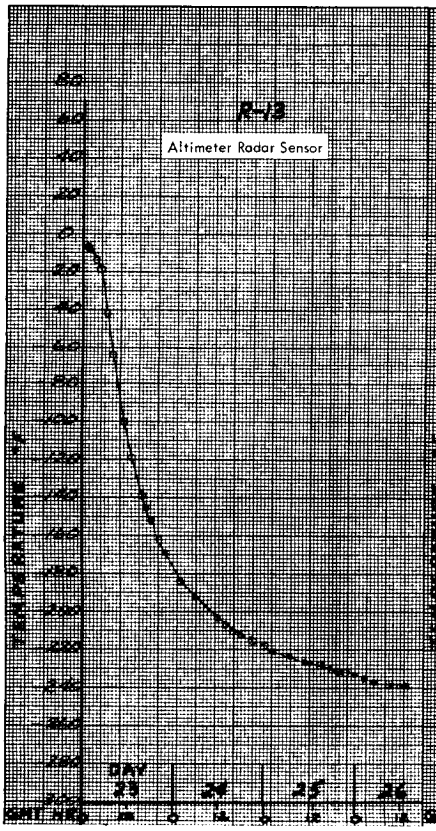

Figure 5.1-C40

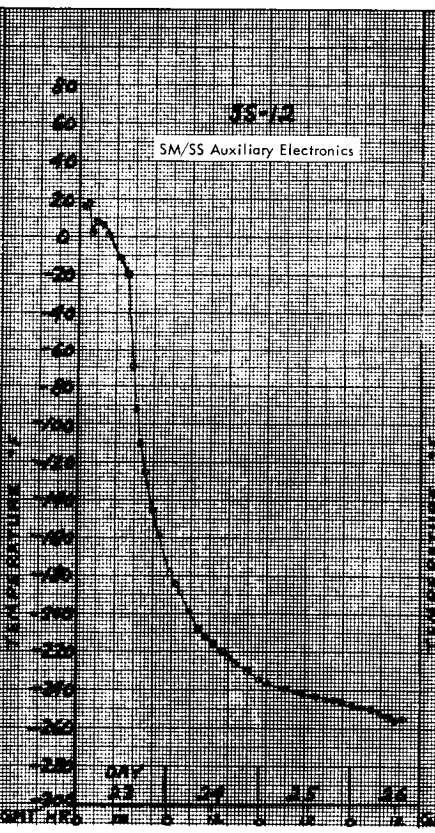

Figure 5.1-C41

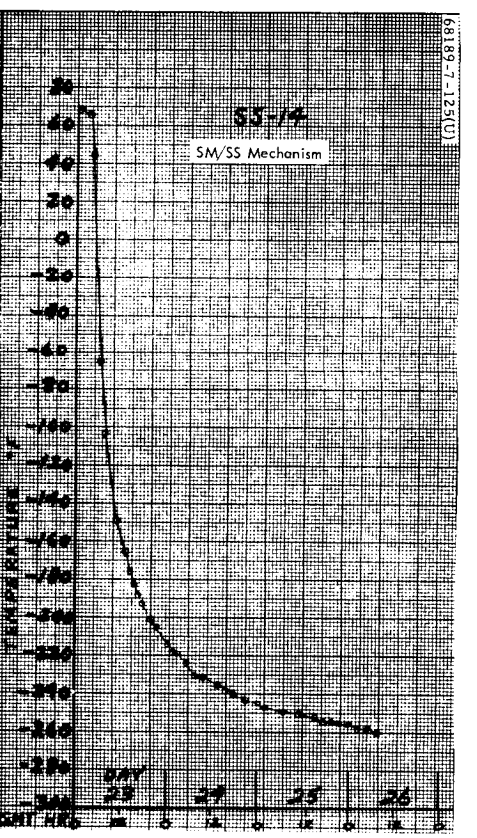

Figure 5.1-C42

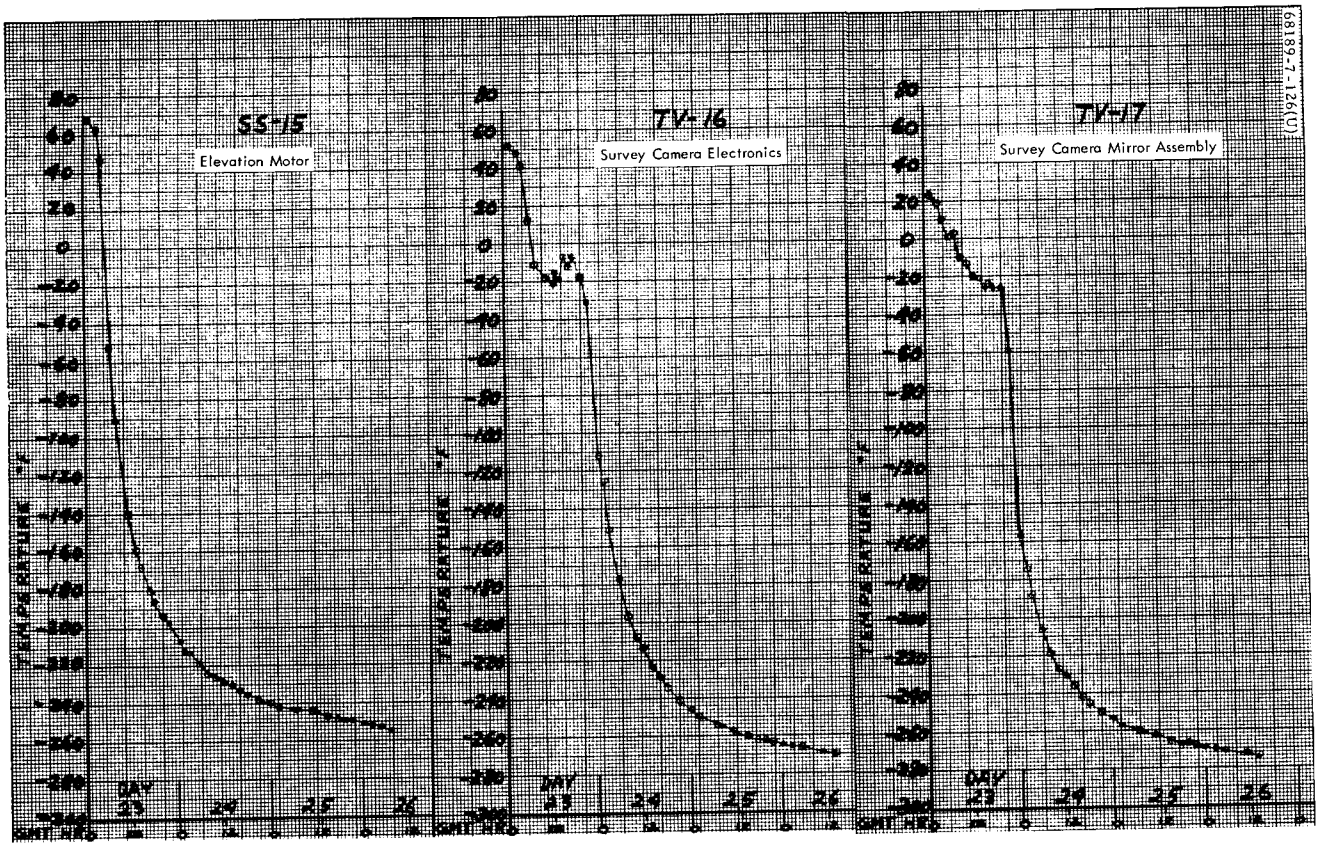

Figure 5.1-C43

Figure 5.1-C44

Figure 5.1-C45

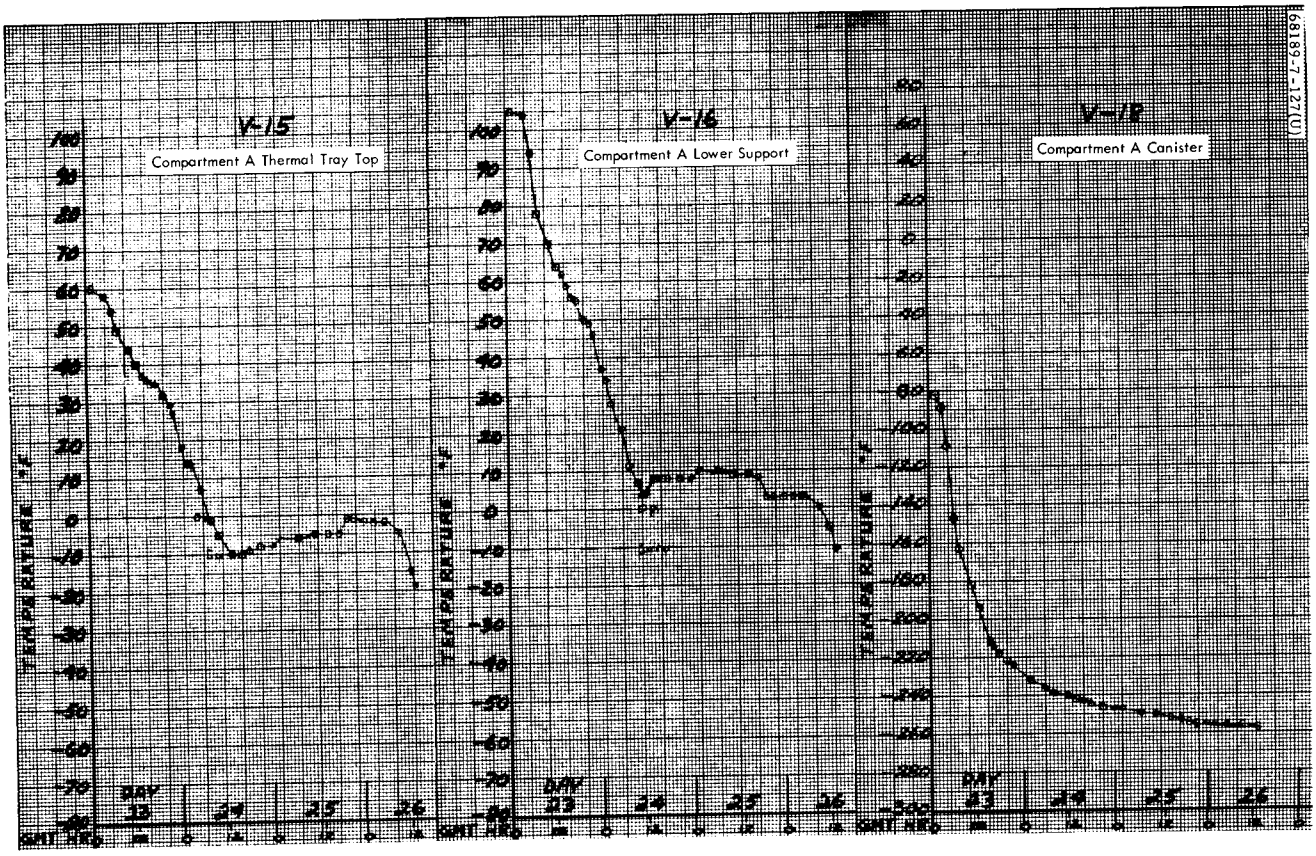

Figure 5.1-C46

Figure 5.1-C47

Figure 5.1-C48

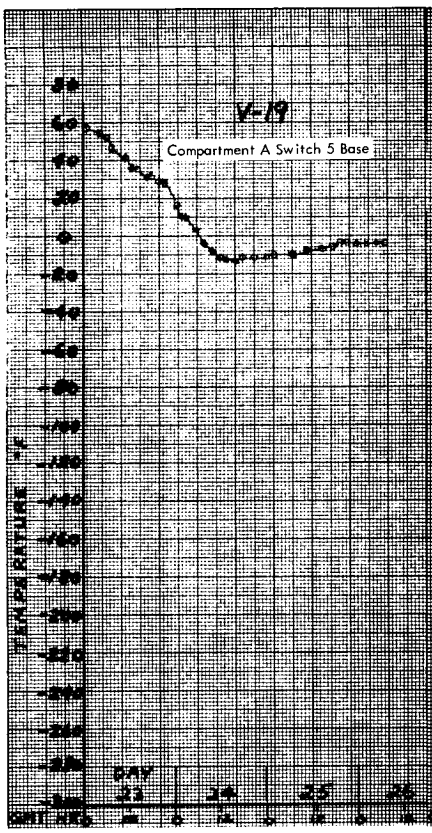

Figure 5.1-C49

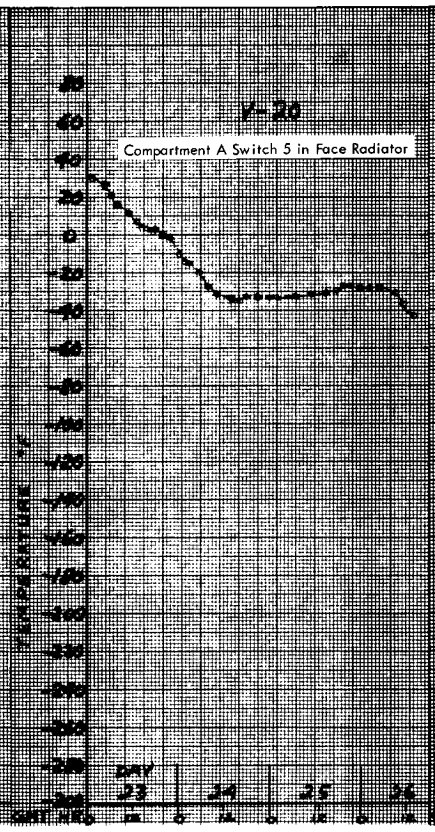

Figure 5.1-C50

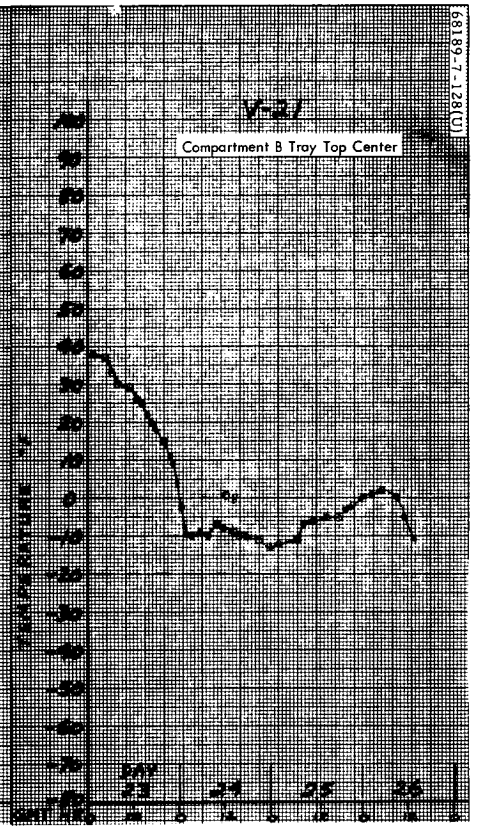

Figure 5.1-C51

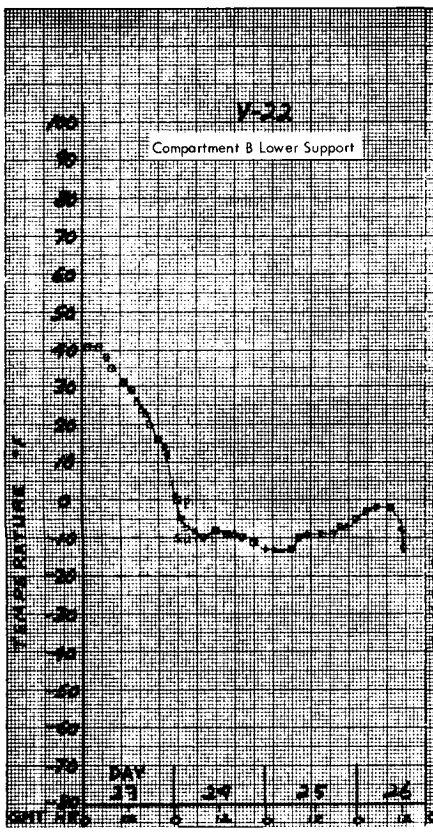

Figure 5.1-C52

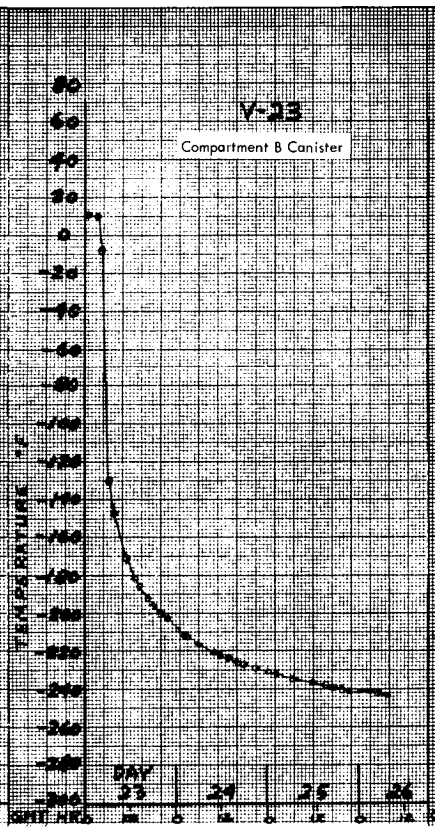

Figure 5.1-C53

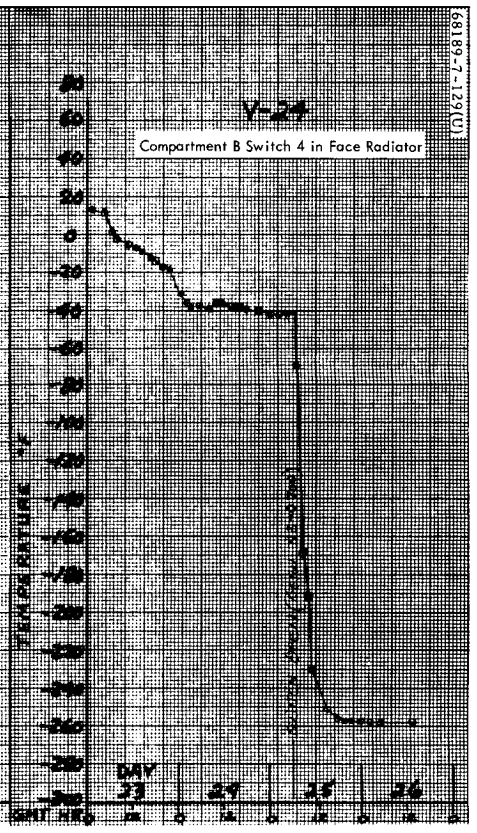

Figure 5.1-C54

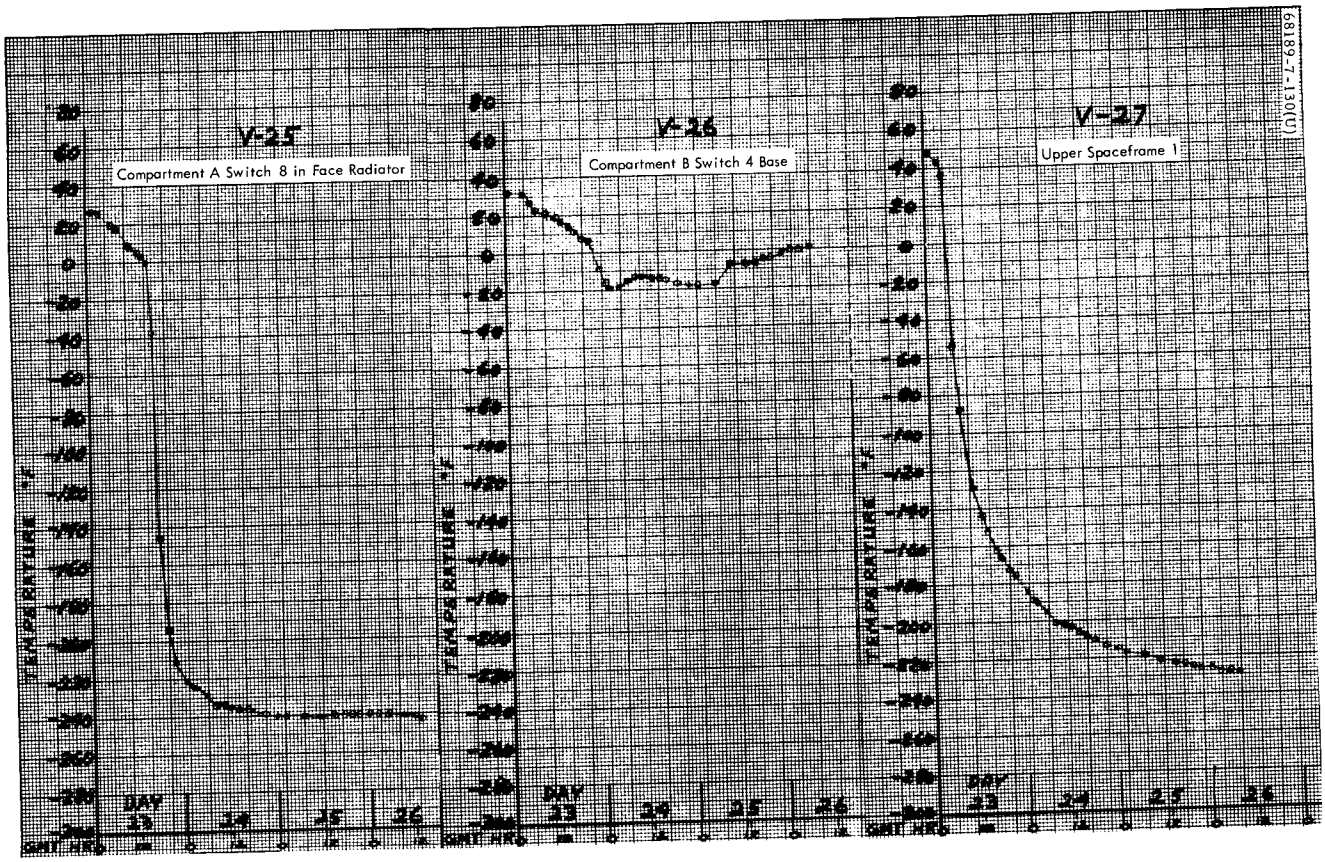

Figure 5.1-C55

Figure 5.1-C56

Figure 5.1-C57

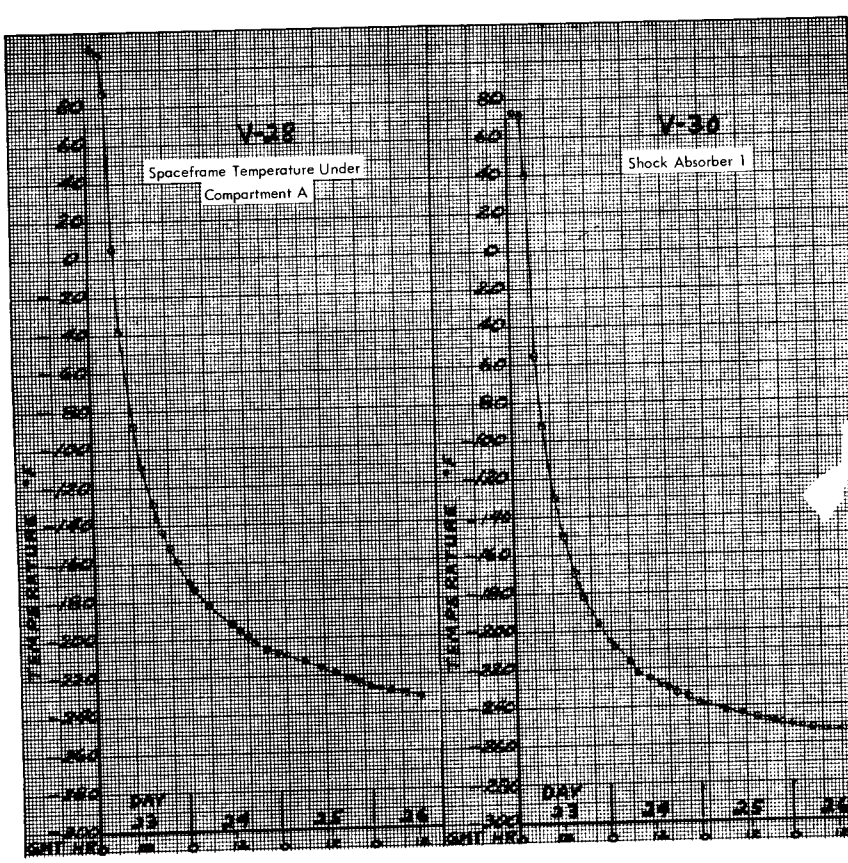

Figure 5.1-C58

Figure 5.1-C59

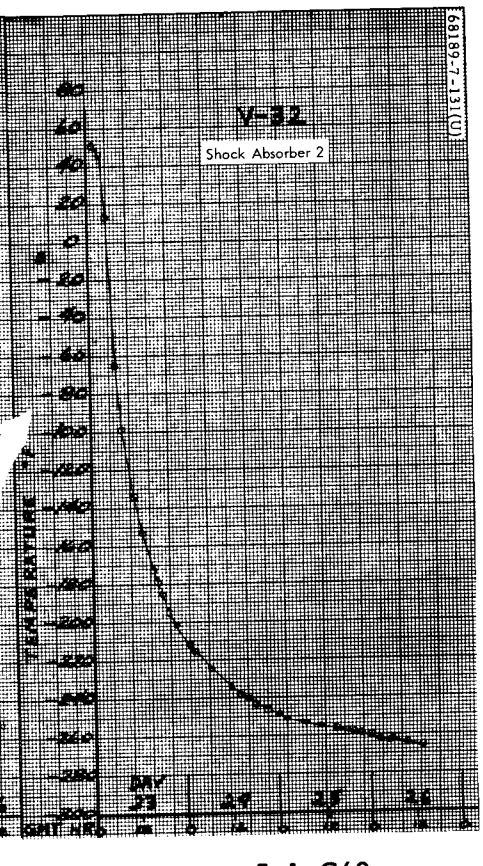

Figure 5.1-C60

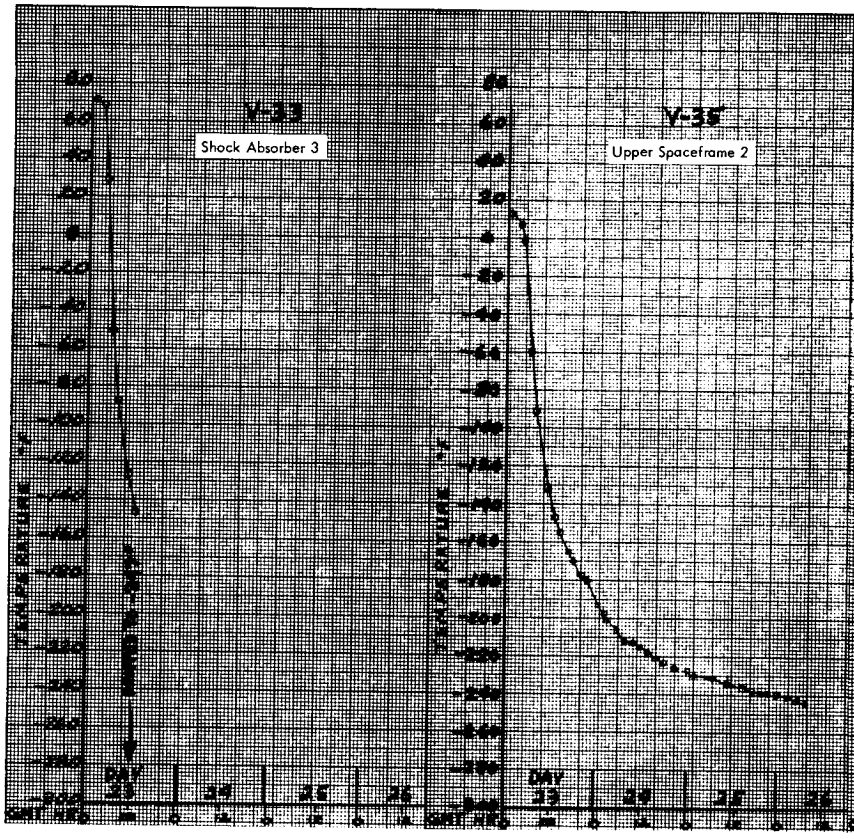

Figure 5.1-C61

Figure 5.1-C62

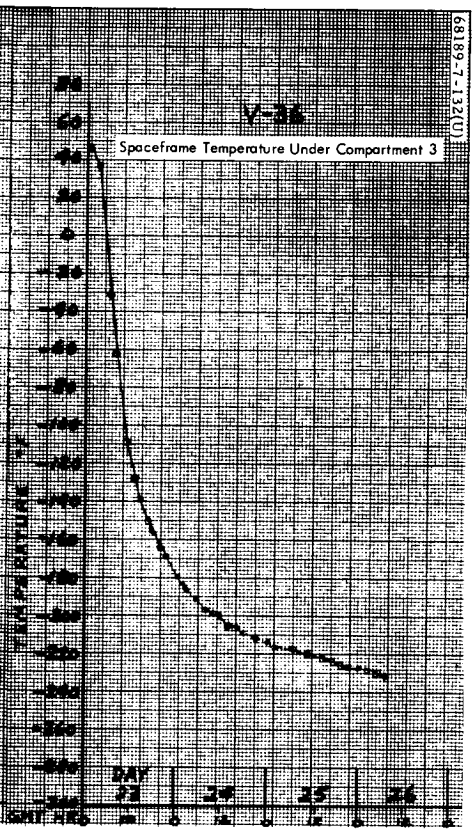

Figure 5.1-C63

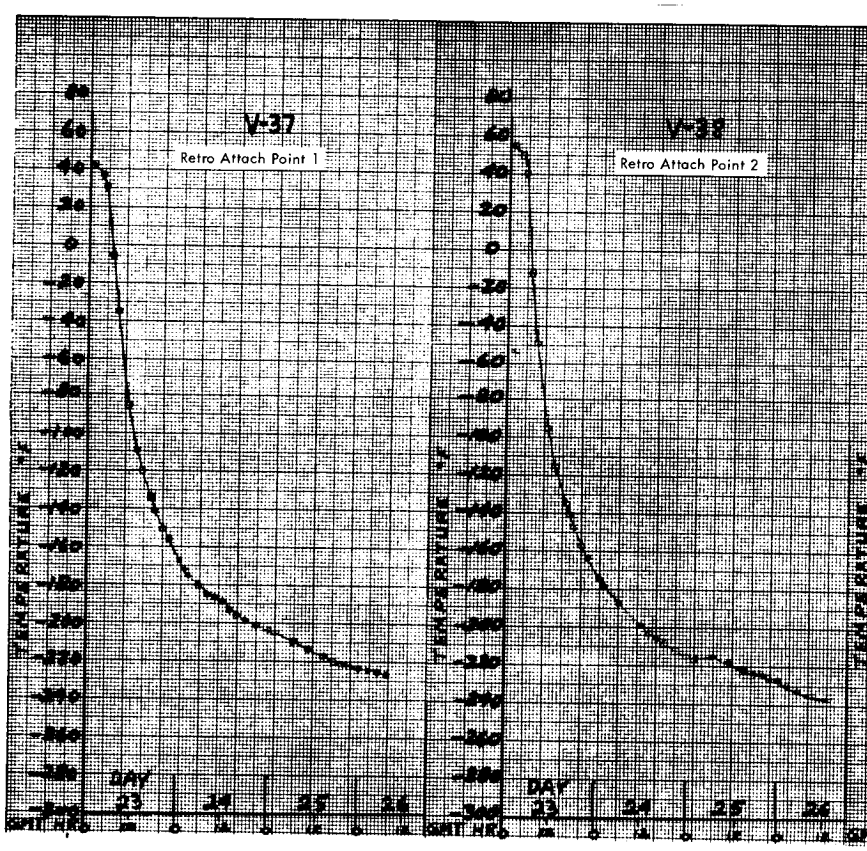

Figure 5.1-C64

Figure 5.1-C65

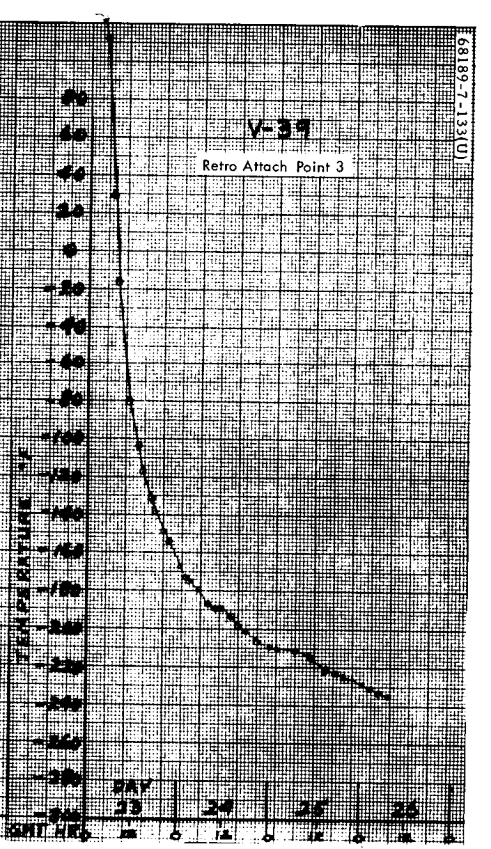

Figure 5.1-C66

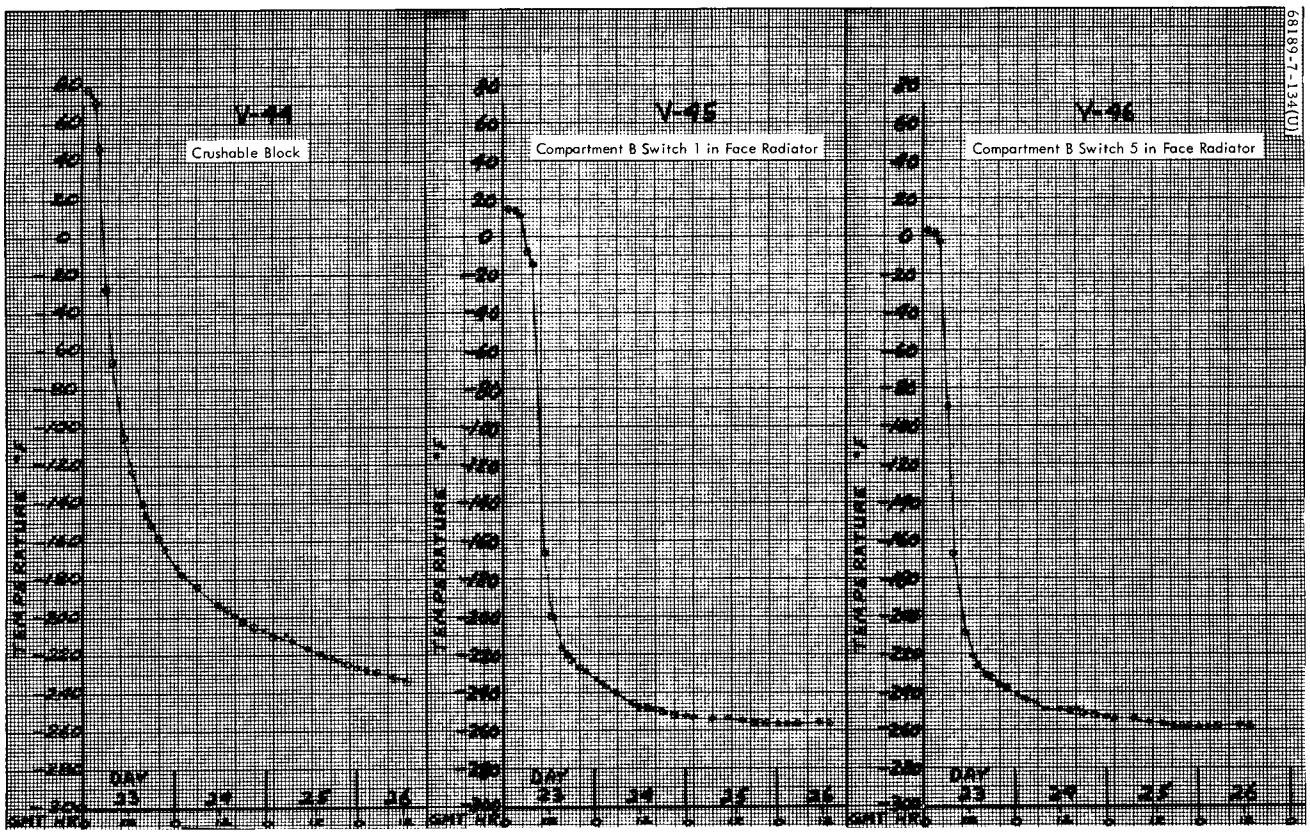

Figure 5.1-C67 Figure 5.1-C68 Figure 5.1-C69

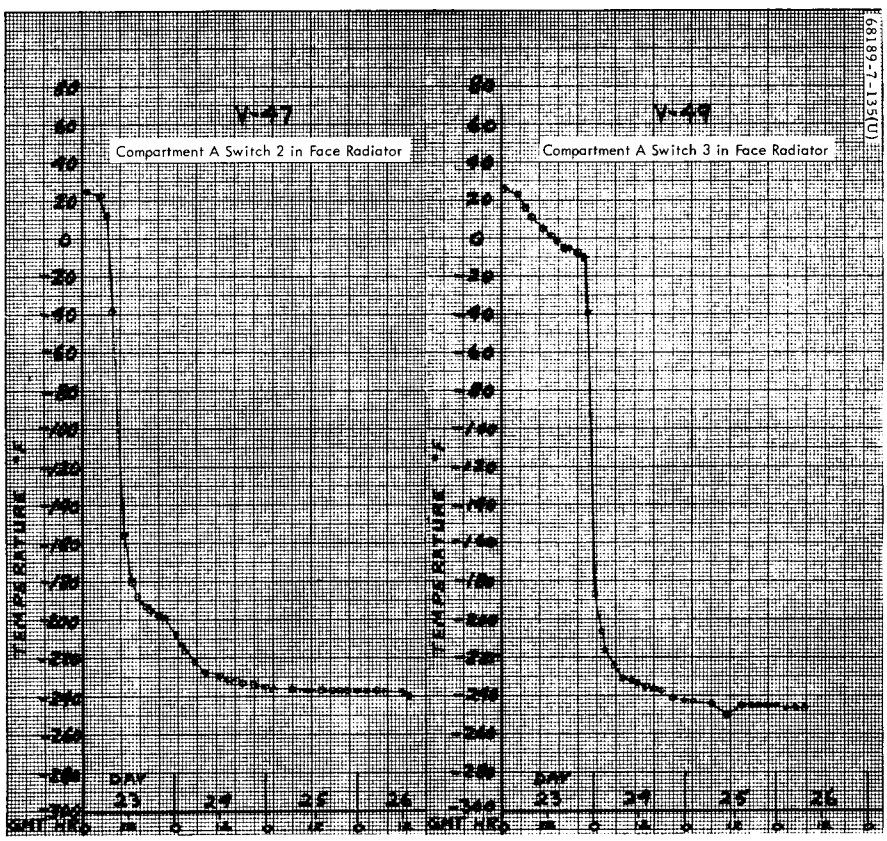

Figure 5.1-C70 Figure 5.1-C71

5.2 ELECTRICAL POWER SUBSYSTEM

5.2.1 INTRODUCTION

The electrical power (EP) subsystem generates, stores, and controls electrical energy for distribution to other spacecraft subsystems. There are two sources for this energy: a storage battery, and radiant energy converted directly to electrical energy for system loads or battery charging. During transit, the primary source of power is radiant energy via the solar panels. Figure 5.2-1 shows associated equipment groupings.

Performance of the EP subsystem during the Surveyor VII flight and first lunar day operation was entirely nominal as compared to test data and simulation analysis predictions. Solar panel output power was approximately 5.6 percent above nominal, and can be in part attributed to the greater than nominal solar intensity which occurs during a January launch window.

With this increased solar panel output, battery power utilized for the mission was slightly below the prediction of 83 amp-hr (based on the Surveyor VI mission consumption). In all, 72 amp-hr were required from the battery for the transit portion of the mission.

The power subsystem responded properly to all earth commands and performed as anticipated.

Flight data were used to calculate solar panel power and regulator efficiencies. Analysis of specific loads, comparison to prediction, and an explanation of discrepancies will be made.

In Table 5.2-1, major events are presented in GMT. In general, the division of this table corresponds to flight phases of importance to the EP subsystem and may not correspond to flight phases in other subsections. The flight is divided into times corresponding to significant changes in electrical loads. Load changes corresponding to these flight phases are partially illustrated by the regulated current (EP-14) and more completely by the battery discharge current (EP-9).

5.2.2 ANOMALY DESCRIPTION

No anomalies were detected in the electrical power subsystem during the transit or the first lunar day.

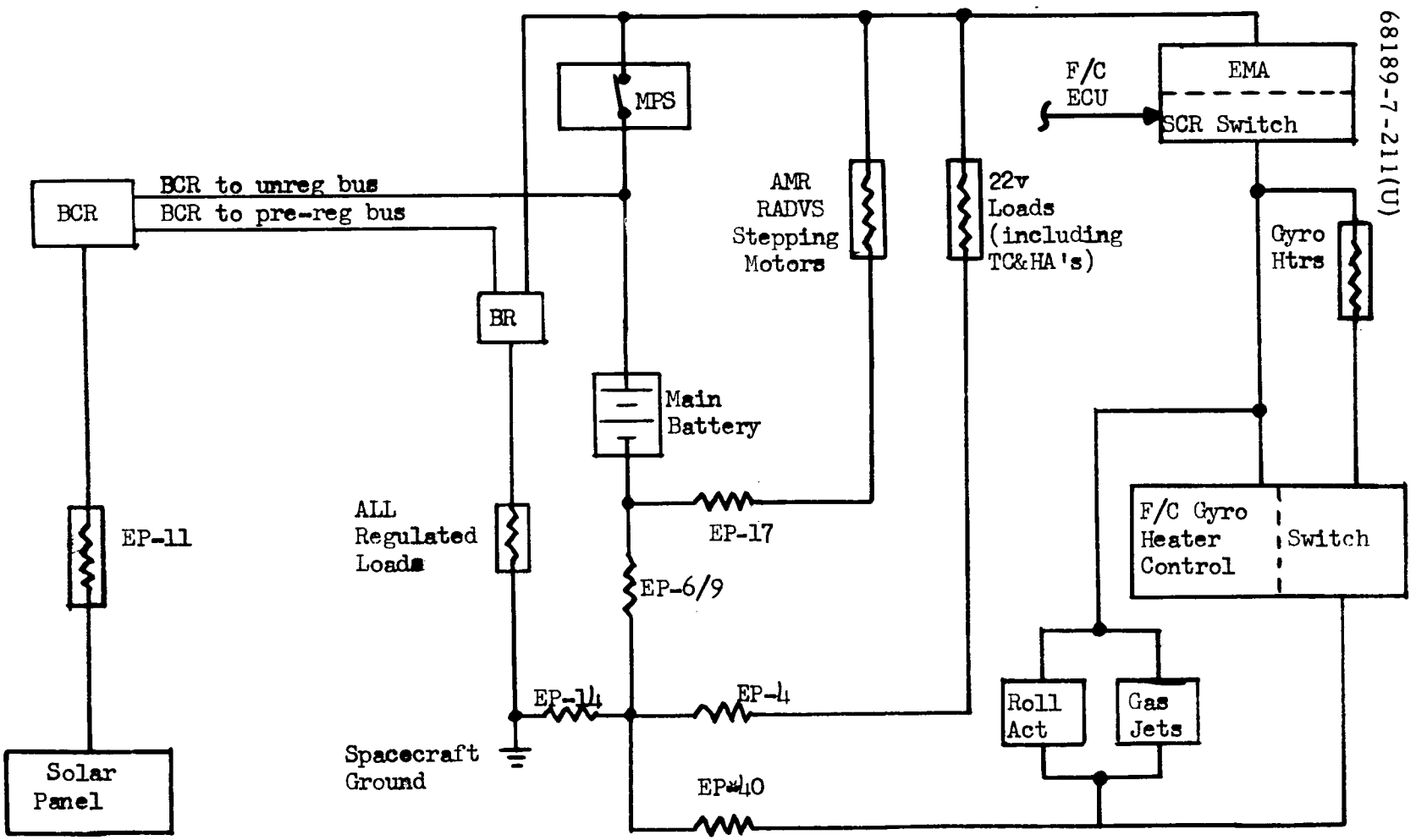

Figure 5.2-1. Power Subsystem Block Diagram, Flight Configuration

TABLE 5.2-1. ELECTRICAL POWER EVENTS AND TIMES

GMT day:hr:min:sec		Comments
From	To	
007:06:30:01	007:07:05:43	Launch and separation
007:07:05:43	007:07:32:45	Transmitter high power
007:07:32:45	007:14:18:36	Coast
007:14:18:36	007:14:58:28	Coast, transmitter high power
007:14:58:28	008:23:02:05	Coast
008:23:02:05	008:23:28:40	Transmitter high power
008:23:28:40	008:23:30:01	Midcourse maneuver, transmitter high power, and flight control thrust phase power on
008:23:30:01	008:23:30:12	Vernier engine burn period, transmitter in high power
008:23:30:12	009:14:00:19	Coast
009:14:00:19	009:22:44:03	Coast, compartment A heater on
009:22:44:03	010:00:07:28	Compartment A heater off, coast
010:00:07:28	010:00:57:41	Transmitter high power, preretro maneuvers
010:00:57:41	010:01:05:38	Transmitter high power, AMR on, thrust phase power on, RADVS on, terminal descent, and touchdown

TABLE 5.2-2. ELECTRICAL POWER SUMMARY

Item	Flight Data	Predicted or Specification
Boost regulator efficiency, transmitter low power, percent	81.0	77 (minimum)
Boost regulator efficiency, transmitter high power, percent	85.4	82 (minimum
Battery charge regulator efficiency	95.6	93.3 (minimum)
Battery charge regulator output energy, w-hr	5556	5504
Solar panel output power, watts	87.8	81 (minimum)
Battery energy used, w-hr	1584	1848
Total energy used, w-hr	7140	7352
Selected loads:		
Transmitter B high power, watts	56.35	58.0
Transmitter B filament power, watts	2.9	2.9
Flight control thrust phase power on		
Regulated, watts	35.14	35.09
Unregulated, watts	10.10	10.56
AMR on, watts	39.01	41.53
AMR enable, watts	34.98	31.60
RADVS power on, watts	520	551
Vernier ignition		
Midcourse, watts	35.11	39.6
Terminal descent, watts	32.87	39.6
Vernier line 2 heater, watts (33 percent duty cycle)	2.18	6.6 (maximum)
Altitude marking radar heater, watts (54 percent duty cycle)	2.73	5.04 (maximum)
Gyro heater, watts (30 percent duty cycle)	10.45	33.0 (maximum)
Surface sampler heater, watts (100 percent duty cycle)	8.47	8.69 (maximum)

5.2.3 SUMMARY

5.2.3.1 Transit

The transit portion of the mission was entirely nominal. The solar panel switch tripped three times on Surveyor VII as opposed to six times on Surveyor VI. The reduced occurrences of switch tripping were due to the increased load of the soil mechanics heater carried by Surveyor VII.

Minimum bus voltage during the mission was 19.33 volts, with spacecraft loads at 38.89 amperes. This bus voltage is above the minimum requirement of 17.75 volts. Table 5.2-2 presents a summary of flight data for Surveyor VII compared to test data for the electrical power subsystem. Table 5.2-3 represents typical transit data.

5.2.3.2 Lunar

Lunar operation of the power subsystem was nominal and followed the pattern of previously landed spacecraft. With approximately 56 percent charge remaining in the battery at touchdown, the solar panel was positioned to provide a charge of approximately 1 ampere. By lunar noon, battery charge had been increased to approximately 172 amp-hr and was maintained at essentially this level until lunar sunset. Table 5.2-4 represents typical lunar data.

5.2.4 ANALYSIS

The analysis considers four areas: mission telemetry plots, power loads and sources budget, comparison of flight loads and flight acceptance test loads, and cyclic loads.

5.2.4.1 Mission Telemetry Plots

Figures 5.2-2 through 5.2-7 are plots pertinent to the EP subsystem for approximately the last 72 minutes of the transit phase. They represent line plots of all telemetry points monitored during this period. With the scales used, these plots provide a good indication of spacecraft trends and allow identification of pertinent spacecraft functions. Many annotations have been made on these plots identifying spacecraft responses to ground and on-board commands. Figure 5.2-8 gives radar loads during the terminal phase. Identified on the plot is AMR power on and AMR enabled, RADVS turn-on, RADVS time in, and RADVS off.

5.2.4.2 Power Loads and Sources Budget

Energy Used

Table 5.2-2 contains a summary of energy expended as calculated from flight telemetry data. Solar panel output power was approximately 1.6 percent greater than for Surveyor VI due to an increase in solar intensity (144.5 instead of 142 mv/cm^2) Energy supplied by the battery was therefore below the 83 amp-hr predicted.

TABLE 5.2-3. TYPICAL COAST PHASE II DATA

Day 008, GMT, hr:min:sec	Regulated Bus, volts (EP-1)	Unregulated Bus, volts (EP-2)	Battery Pressure, psi (EP-3)	Unregulated Current, amperes (EP-4)	Discharge Current, amperes (EP-6/9)	Difference Current, amperes (EP-7)	Solar Voltage, volts (EP-10)	Solar Current, amperes (EP-11)	Solar Temperature, °F (EP-12)	Regulated Current, amperes (EP-14)	Preregulated Bus, volts (EP-30)	FC Unregulated Current, amperes (EP-40)
00:17:33	28.99	22.30	14.4	0.466	0.452	0.185	30.35	2.926	125.7	1.788	30.01	0.760
02:00:08	28.99	22.06	14.4	0.700	0.623	0.185	30.35	2.926	125.7	1.788	30.01	0.806
03:00:10	28.99	22.06	14.4	0.700	0.476	0.185	30.35	2.926	125.7	1.822	30.01	0.606
04:00:11	28.99	22.01	14.4	0.771	0.793	0.185	30.35	2.926	125.7	1.822	30.01	0.812
05:00:13	28.99	22.24	14.3	0.466	0.476	0.185	30.35	2.926	125.7	1.813	30.01	0.706
06:00:14	28.94	22.04	14.3	0.700	0.745	0.185	30.35	2.926	125.7	1.822	30.01	0.911
06:30:00	28.99	21.95	13.8	0.770	1.150	0.185	30.35	2.926	125.7	1.788	30.01	1.215
06:59:00	28.99	22.09	13.8	0.700	1.110	0.185	30.35	2.926	125.7	1.788	30.01	1.215
07:30:30	28.99	22.01	13.8	0.700	0.08	0.185	30.35	2.926	125.7	1.788	30.01	0.184
08:06:00	28.99	21.98	13.8	0.700	1.11	0.185	30.35	2.926	125.7	1.788	30.01	0.711
08:35:00	28.99	21.83	13.8	1.000	1.47	0.185	30.35	2.926	125.7	1.788	30.01	1.215
09:06:00	28.94	22.09	13.8	0.460	0.32	0.185	30.35	2.926	125.7	1.830	30.01	0.711

TABLE 5.2-4. TYPICAL FIRST LUNAR DAY DATA

Day 013, GMT, hr:min:sec	Regulated Bus, volts (EP-1)	Unregulated Bus, volts (EP-2)	Battery Pressure, psi (EP-3)	Unregulated Current, amperes (EP-4)	Discharge Current, amperes (EP-6/9)	Difference Current, amperes (EP-7)	Solar Voltage, volts (EP-10)	Solar Current, amperes (EP-11)	Solar Temperature, °F (EP-12)	Regulated Current, amperes (EP-14)	Preregulated Bus, volts (EP-30)	FC Unregulated Current, amperes (EP-40)
04:49:37	28.90	26.88	16.0	–	-1.18	0.336	26.8	2.340	197.1	0.776	29.96	–
06:46:30	28.90	26.91	16.0	–	-1.18	0.348	26.8	2.334	198.0	0.825	29.96	–
08:29:01	28.99	27.03	15.9	–	-1.18	0.325	27.0	2.317	199.8	0.759	30.01	–
09:42:28	28.99	27.06	16.0	–	-1.15	0.336	27.0	2.317	200.7	0.776	30.01	–
10:35:54	28.94	26.94	16.0	–	-1.11	0.348	26.9	2.311	201.6	0.825	30.01	–
11:12:25	28.94	26.97	16.0	–	-1.13	0.348	26.9	2.305	201.6	0.825	29.91	–
12:54:36	28.94	26.94	16.0	–	-1.11	0.354	26.9	2.305	202.5	0.825	29.91	–
13:09:56	28.90	27.00	16.0	–	-1.08	0.348	26.9	2.273	203.4	0.825	29.91	–
14:17:13	28.90	27.00	16.0	–	-1.11	0.355	27.0	2.294	203.4	0.859	29.91	–
16:04:27	28.99	27.06	16.5	–	-1.135	0.349	27.14	2.294	205.2	0.859	30.01	–
17:26:40	28.90	27.06	16.3	–	-1.135	0.372	27.0	2.294	206.2	0.876	29.91	–
19:00:14	28.90	27.06	16.5	–	-1.135	0.366	27.07	2.276	207.1	0.876	29.91	–

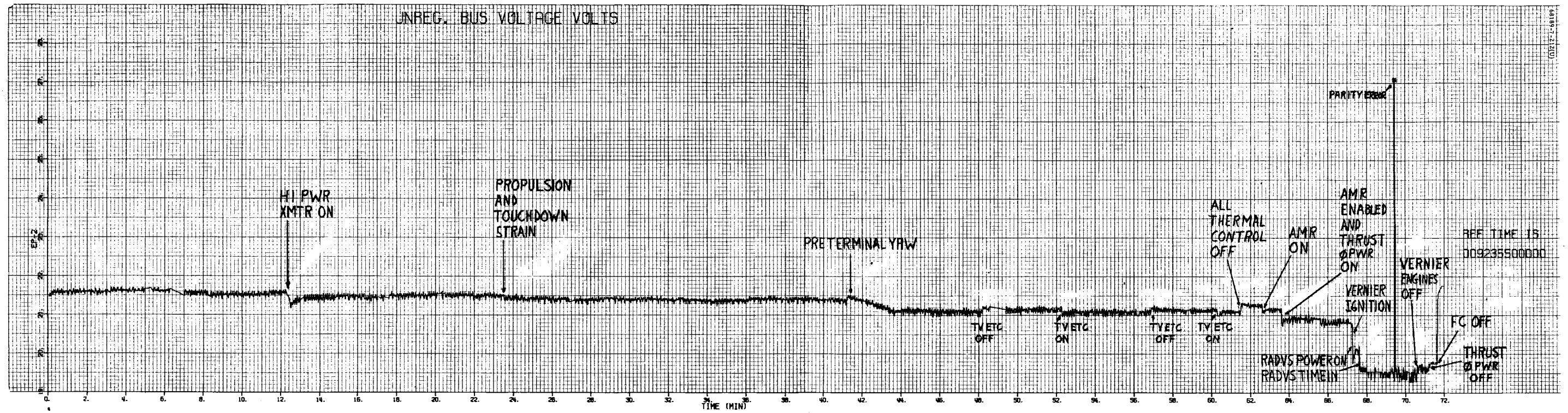

Figure 5.2-2. Unregulated Bus Voltage

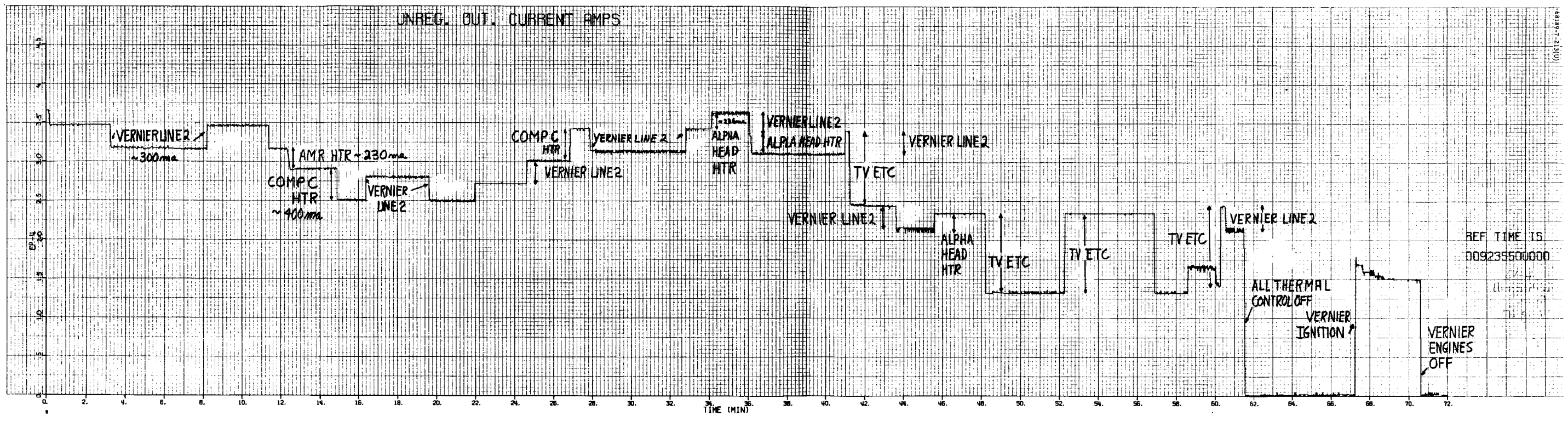

Figure 5.2-3. Unregulated Output Current

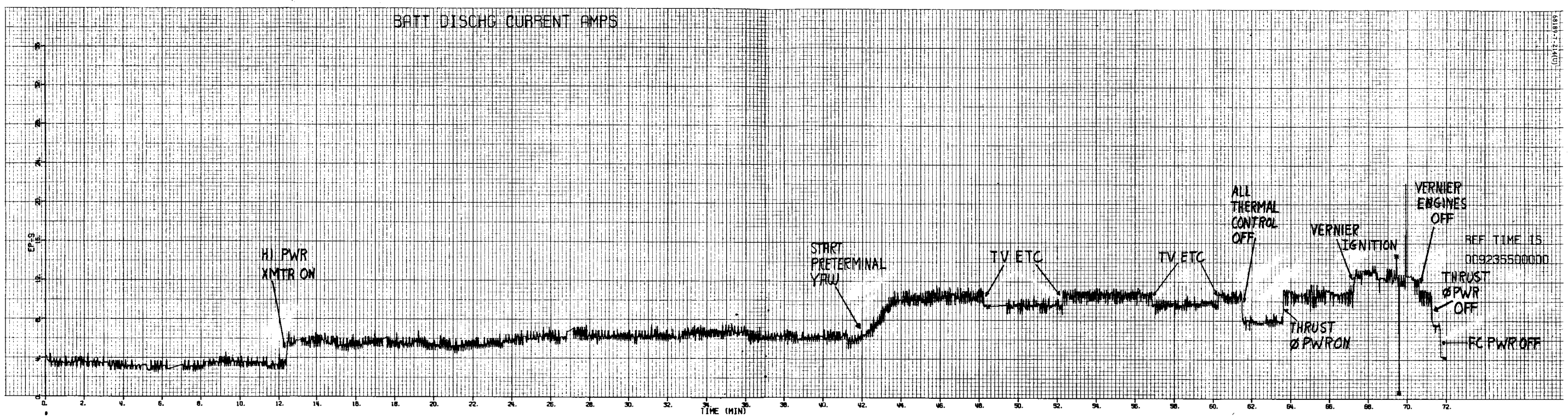

Figure 5.2-4. Battery Discharge Current

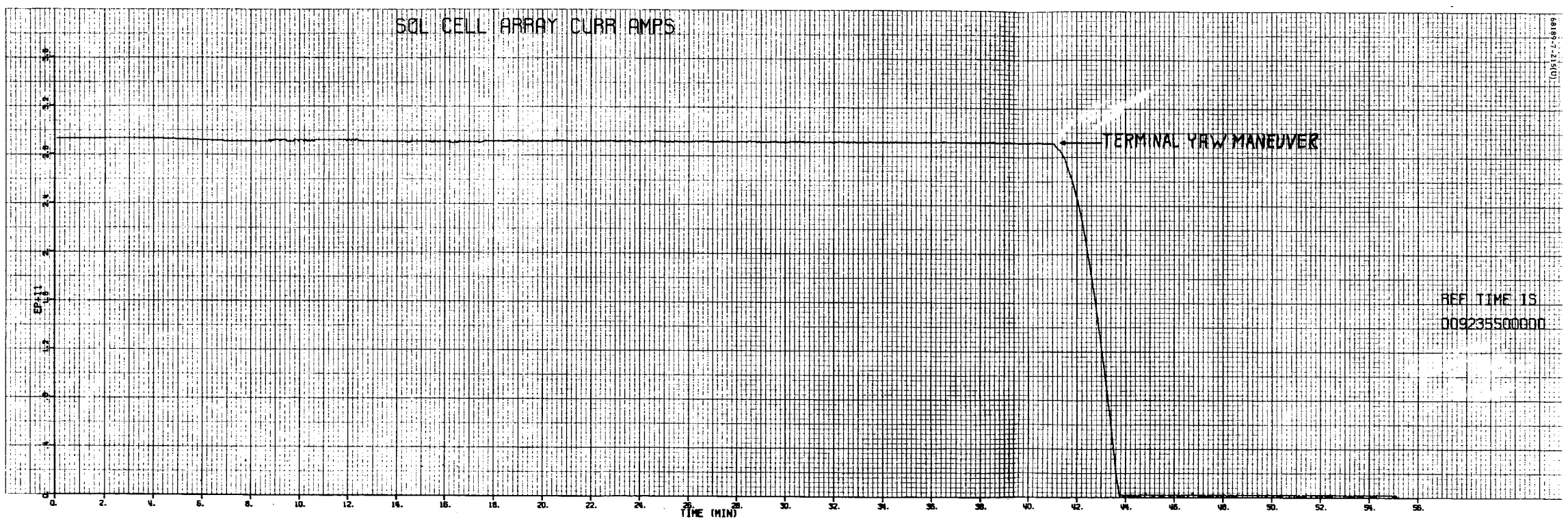

Figure 5.2-5. Solar Cell Array Current

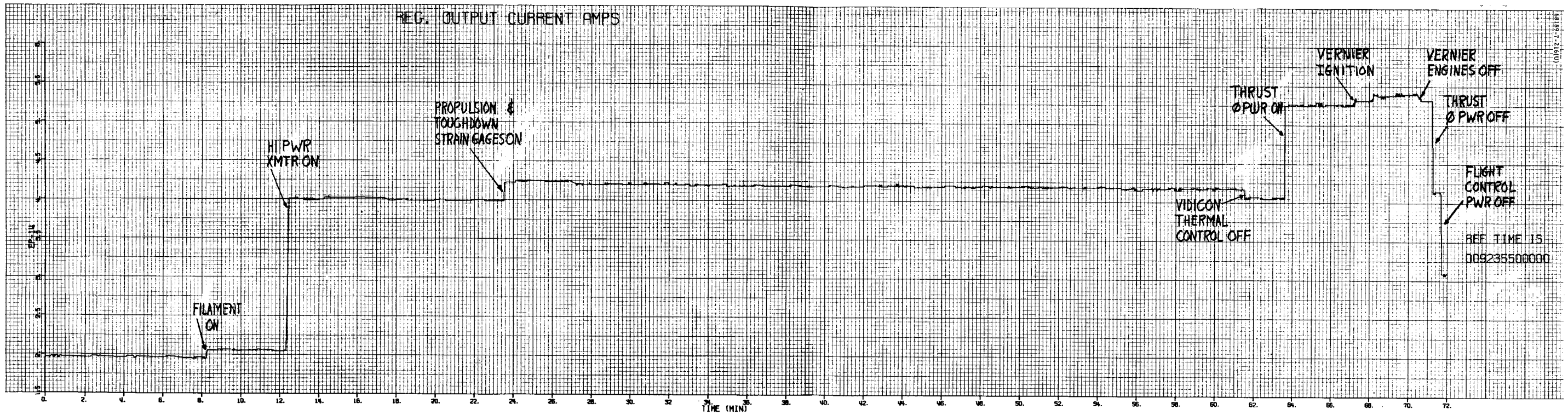

Figure 5.2-6. Regulated Output Current

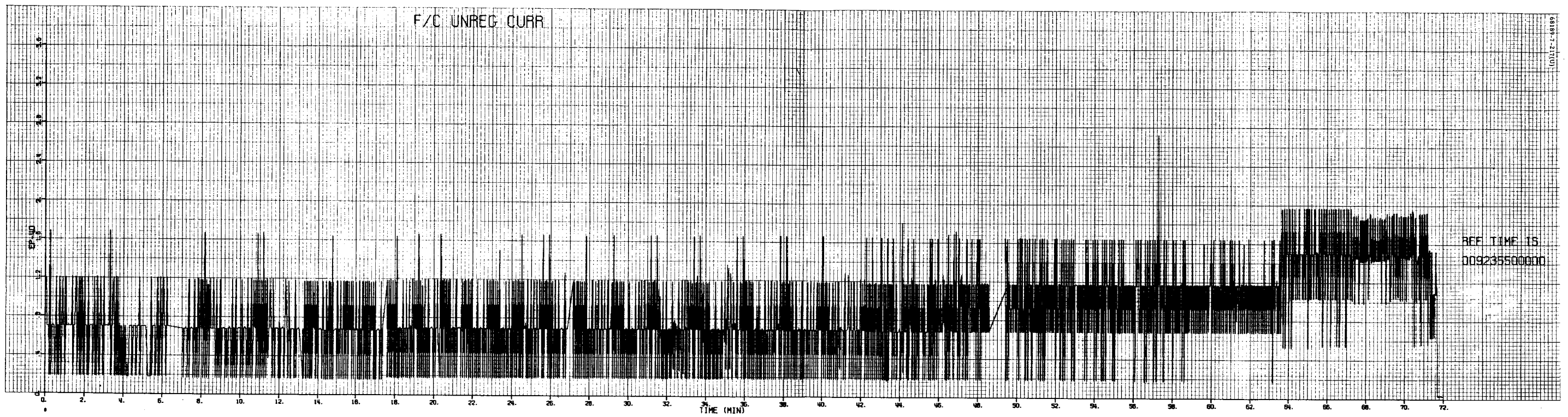

Figure 5.2-7. Flight Control Unregulated Current

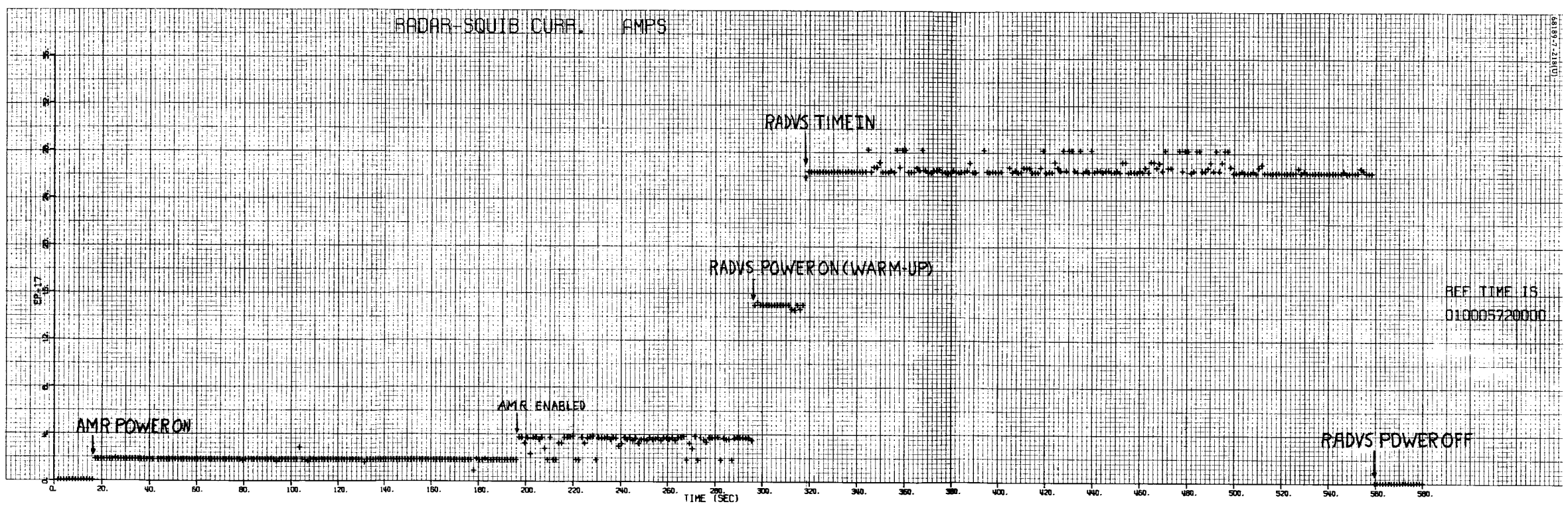

Figure 5.2-8. Radar Squib Current

TABLE 5.2-5. SELECTED EQUIPMENT LOADS

Spacecraft Load Change*	Command Time, GMT, day:hr:min:sec	Current, milliamperes		Power, watts	
		Flight	Specification (Reference 1)	Flight	Specification (Reference 1)
Flight control thrust phase power on					
R	Midcourse	1212	1210	35.14	35.09
U	007:23:28:40	481	480	10.10	10.56
R	Terminal	1212	1210	35.14	35.09
U	010:00:58:38	475	480	9.91	10.56
Transmitter B high voltage on	007:14:18:36				
R		1943	2000	56.35	58.0
Filament B power on	007:14:16:25				
R		100	100	2.9	2.9
Vernier ignition					
U	Midcourse 007:23:30:14	1680	1800	35.11	39.6
U	Terminal 010:01:02:18	1660	1800	32.87	39.6
AMR on	010:00:57:41				
U		1840	1886	39.01	41.53
AMR enable	010:01:01:03				
U		1690	1439	34.98	31.60
RADVS power on	010:01:02:18				
U		26800	29000	520	551

*R = regulated; U = unregulated.

AMR, Vernier Lines, Television, and Compartment C Heaters

Figure 5.2-3 is a plot of unregulated current. The cyclic load effects of the vernier line 2 heater are apparent. Also cycling are the alpha scattering head heater, AMR heater, television mirror assembly heater, and compartment C heater. Approximate current levels for each heater are noted on the plot.

5.2.5 REFERENCES

1) J. E. Mundy, "System Specification Power Management Data Summary SC-6 Spacecraft," Hughes Aircraft Company No. 302393, Revision A, 25 August 1967.

2) J. E. Mundy, "SC-7 Power Management Data Summary," Hughes Aircraft Company, IDC 2294.2/173, 11 September 1967.

5.2.6 ACKNOWLEDGMENT

N. J. Kaman, technical coordinator and author.

5.3 RF DATA LINK SUBSYSTEM

5.3.1 INTRODUCTION

This section contains a summary and analysis of the performance of the data link subsystem during Surveyor Mission G.

The data link subsystem consists of the transmitters, transponders, receivers, command decoders, and antennas. It is the function of this subsystem to: 1) provide engineering data transmission from the spacecraft at bit rates compatible with specific mission phases, 2) provide analog data, such as that from television and strain gages, at signal levels high enough for proper discrimination, 3) provide phase coherent two-way doppler for tracking and orbit determination, and 4) provide command reception capability throughout the mission to allow for complete control of the spacecraft from the ground. A simplified block diagram of the communications subsystem is shown in Figure 5.3-1.

The pertinent subsystem units on the spacecraft during the mission are as follows:

Unit	Part Number	Serial Number
Receiver A	231900-3	21
Receiver B	231900-3	24
Transmitter A	3024400-1	11
Transmitter B	3024400-1	15
Command decoder unit	232000-5	9

Unlike most subsystems, individual data link subsystem parameters, such as losses, threshold sensitivity, modulation index, etc., are not measured or individually determined from mission data. The composite effect of these parameters on the performance is measured as received signal power at the spacecraft and the tracking station (DSS) and as telemetry and command error rates. Consequently, it is impossible to compare individual link parameters to specified performance criteria. The best that can be done is to compare measured signal levels to predicted levels, and telemetry quality and command capability to predicted capabilities. To further cloud the analysis, omnidirectional antenna gain is a major contributor to the uncertainty in received signal levels. Accurate omnidirectional antenna gain measurements are difficult to achieve and, in most cases, deviations

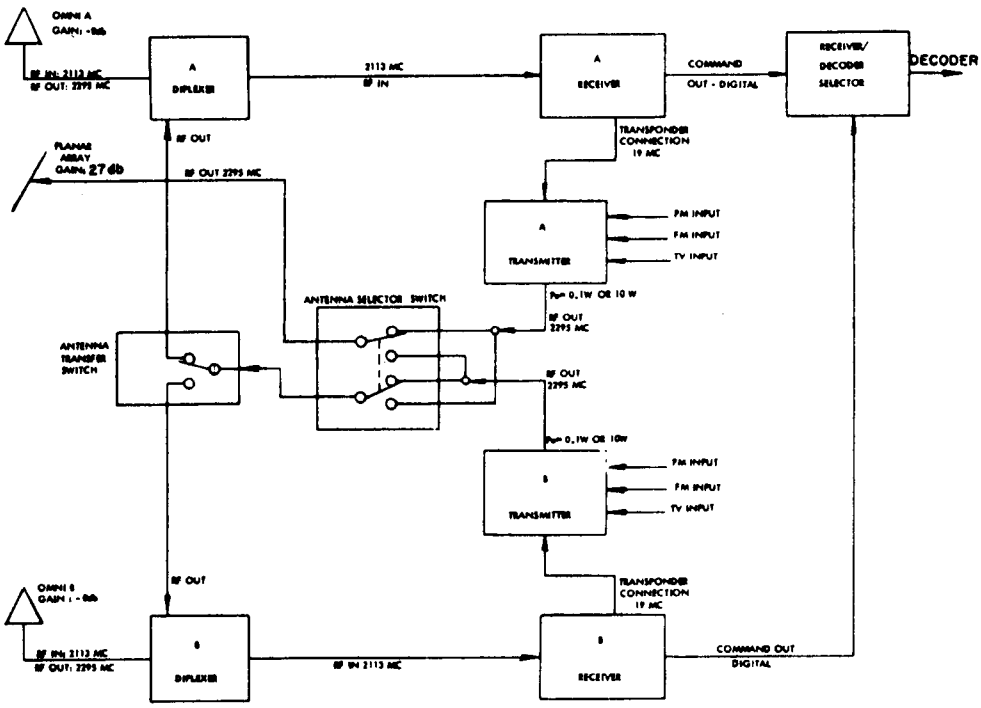

Figure 5.3-1. Communications Subsystem Block Diagram

68189-2-134

from predictions can most likely be attributed to antenna gain uncertainty. Because of the problems outlined above, analysis of the data link subsystem performance will, in general, be a qualitative analysis of the performance of the entire subsystem rather than a quantitative assessment of the performance of the individual subsystem parameters. Equally as important as subsystem performance evaluation is the qualitative assessment of the premission and real-time prediction techniques used during the mission.

In general, the RF data link subsystem performed as expected with three exceptions. Receiver/decoder indexing was experienced during the postmidcourse transit phase, up link and down link signal level variations occurred during lunar operation, and the frequency of the transmitter A wide-band voltage-controlled crystal oscillator drifted outside the ground station receiver tuning range capability. With the exception of the wide-band voltage-controlled crystal oscillator frequency drift, all subsystem units performed close to nominal predictions.

The data contained in this report consist of spacecraft telemetered, DSS, and mission event time data. Where meaningful, the data are correlated to and compared with equipment specifications, previous test data, preflight predictions, and in-flight analysis predictions. Specifically, this section contains the following discussions which are shown with the appropriate subsection notation:

Anomaly Discussion (subsection 5.3.2) – This subsection contains a discussion of three topics:

1) Receiver/decoder indexing during transit

2) Signal level variations during lunar operations

3) Transmitter A wide-band voltage-controlled crystal oscillator frequency drift

Summary and Conclusions (subsection 5.3.3) – This subsection contains a summary of subsystem performance with conclusions relative to performance and postflight analysis.

Subsystem Performance Analysis (subsection 5.3.4) – This subsection contains the following items:

1) General discussion of data, equations used, and path of the earth vector relative to omnidirectional antenna gain contours

2) Discussion of subsystem performance during specific mission phases

The major mission event times relative to the RF data link sybsystem are tabulated in Tables 5.3-1 and 5.3-2. Table 5.3-1 contains telemetry mode and bit rate, primary tracking station number, and station automatic gain control values as a function of time. Table 5.3-2 contains a tabulation of the subsystem configuration as a function of time. Both tables cover the mission from launch to touchdown. In some cases, the times in these tables are accurate only to the nearest minute.

TABLE 5.3-1. TELEMETRY MODE SUMMARY

GMT, hr:min:sec	Mode	Rate	DSIF Station	DSIF Automatic Gain Control, dbm	Telemetry Margin, db	Comments
				DAY 7		
06:30:00.545	5	550				Launch; azimuth = 102.914 degrees
07:04:49			51			Signal heard
07:04:53			51	-109		Receiver 2 in lock SAA, parametric amplifier, aided
07:04:53			51			Demodulator in lock
07:05:05			51	- 94		Servo to auto SAA
07:05:25			51			Servo to auto SCM
07:06:47			51	-105		
07:07:12			51	-108		
07:07:20			51			Antenna at pre-limits
07:08:00			51	-105		
07:08:10			51			Demodulator out of lock
07:08:38			51			Receiver 2 out of lock
07:09:30			51			Receiver 1 out of lock
07:20:00			42			Receiver in lock; SAA parametric amplifier
07:20:49			42	-128.0		
07:23:00			42	- 90.6		One-way SCM maser
07:26:00			42			Ground transmitter on
07:27:12			42			Spacecraft receiver B phase lock
07:28:00			42	- 88.9		
07:31:57						Spacecraft transmitter B low power
07:38:53	1					
07:40:06		1100				
07:42:27	4					
07:45:13	2		42	-111.6		
07:47:55	6					
07:49:56	5			-112.5		
08:00:00				-115.6		
08:20:00				-117.1		
09:00:00				-121.3		
09:30:00				-121.6	+ 17.0	
10:00:00				-123.2	+ 15.4	
10:30:00				-123.9	+ 14.7	
10:36:22	1					
10:38:20	2					
10:40:12	4					
10:42:05	5					
11:00:00			42	-124.8	+ 13.8	
11:30:00			42	-126.0	+ 12.6	
11:54:00			42			Command modulator off for transfer to DSS 51
12:00:00			51	-123.8	+ 14.8	Ground transmitter on
12:01:20			51			Command modulator on
12:30:00			42	-128.1		
12:30:00			51	-124.2		
13:00:00			51	-124.1		
13:30:00			51	-124.8		
13:54:00			51			Command modulator off for transfer to DSS 61
14:00:00			61			Ground transmitter on
14:02:20			61			Command modulator on
14:06:37	4					
14:10:31	2					
14:12:04	1					
14:15:22						Modulation interrupt
14:16:17						Transmitter B filament power on
14:17:15			61	-127.6		
14:18:28						Transmitter B high voltage on
14:18:50			61	-112.0		Δ = 15.6 db
14:19:10		4400				
14:21:20						Transponder power off
14:24:06						Start positive roll – star verification

Table 5.3-1 (continued)

GMT, hr:min:sec	Mode	Bit Rate	DSIF Station	DSIF Automatic Gain Control, dbm	Telemetry Margin, db	Comments
14:46:00						Sun mode on
14:47:32						Manual lockon (sun and star)
14:52:01	5					
14:51:04						Transponder B power on
14:52:17			61			Two-way
14:56:05			61	-115.7		Command modulator on
14:56:46		1100	61	-111.1		
14:58:14						Transmitter B low power
14:59:10				-127.3		Δ = 16.2 db
15:00:00			51	-128.0		
15:30:00			51	-127.8		
15:30:00			61	-127.2		
15:36:02						Inertial mode on
16:00:00			51	-128.3		
16:01:00			61	-127.3		
16:30:00			51	-128.4		
16:30:36	4					
16:35:43	2					
16:39:05	1					
16:43:02	5					
17:00:00			51	-128.5		
17:00:00			61	-127.1		
17:30:00			51	-128.3		
17:31:28						Cruise mode on
17:31:34						Manual lockon (sun and star)
17:32:00			61	-128.2		
17:36:33						Inertial mode on
17:54:00			61			Command modulator off for transfer to DSS 51
18:00:00			51			Ground transmitter on
18:02:10			51			Command modulator on
18:12:00			51	-129.2		
18:23:20	4					
18:30:00			51	-129.3		
18:31:27	2					
18:35:55	1					
18:38:47	5					
19:00:00			51	-129.4		
19:09:43						Cruise mode on
19:09:53						Manual lockon
19:30:00			51	-129.8		
20:00:00			51	-130.2		
20:30:00			51	-130.3		
21:00:00			51	-130.7		
21:14:00			51			Command modulator off - transfer to DSS 11
21:20:00			11			Ground transmitter on
21:22:20			11			Command modulator on
21:26:45			11	-131.5		
21:27:26	4					
21:35:51	2					
21:39:38	1					
21:43:14	5					
21:45:07		None				Gyro speed subcarrier oscillator on
21:49:13		1100				
22:02:00			11	-131.4		
22:46:46	4					
22:48:57	2					
22:51:08	1					
22:57:34						Transmitter B filament on
22:58:50			11	-131.6		
23:00:00			14	-127.2		
23:02:03			11	-115.5		Transmitter B high power; Δ = 16.1 db
23:02:41		4400				
23:03:25			11	-120.4		
23:04:00			14	-112.0		
23:05:35			11	-120.5		
23:11:38			11	-120.9		
23:18:28						Start premidcourse negative roll (3.1 deg/6.2 sec)

Table 5.3-1 (continued)

GMT, hr:min:sec	Mode	Bit Rate	DSIF Station	DSIF Automatic Gain Control, dbm	Telemetry Margin, db	Comments
23:18:35						End of roll
23:21:14						Start positive yaw (117.1 deg/234.2 sec)
23:25:09						End of yaw
23:26:47			11	-121.2		
23:30:10						Start midcourse thrust (11.35 seconds)
23:30:22						End thrust
23:31:40	5		11	-121.9		
23:34:11						Start postmidcourse negative yaw (117 degrees)
23:38:06						End postmidcourse yaw
23:38:35			11	-122.7		
23:43:38	2					
23:45:41	4					
23:48:09	5					
23:48:45			11	-120.5		
23:49:00		1100				
23:49:25			11	-115.7		
23:51:26						Transmitter B low power
23:51:30			11	-132.0		Δ = 16.3 db
START DAY 8						
00:04:12			11	-132.2		Inertial mode on
01:00:00			11	-132.2		
01:32:01	4					
01:35:25	2					
01:37:27	1					
01:41:06	5					
02:00:00			11	-132.8		
02:42:58						Cruise mode on
02:43:09						Manual lockon
02:48:55						Sun mode on
03:00:00			11	-132.8		
03:30:00			11	-133.0	+ 5.6	
04:00:00			11	-133.3		
04:30:00			11	-133.8	+ 4.8	
05:00:00			11	-133.9		
05:24:05			11			Command modulator off - transfer to DSS 42
05:30:00			42			Ground transmitter on
05:31:35			42	-136.1		Command modulator on
05:32:00			11	-134.2		
06:00:00			42	-135.0		
06:02:43						Manual lockon (terminate gyro drift check in roll only)
06:06:24						Inertial mode on
06:30:00			11	-134.2		
06:30:00			42	-135.8	+ 2.8	
06:49:00	4					
06:51:03	2					
06:54:26	1					
06:56:16	5					
07:00:00			42	-135.0		
07:30:00			42	-135.0		
08:00:00			42	-135.1		
08:30:00			42	-135.0		
08:36:50						Cruise mode on
08:37:05						Manual lockon
09:00:00			42	-135.3		
09:30:00			42	-135.2		
10:30:00			42	-135.5		
11:00:00			42	-135.7		
11:30:00			42	-135.7		
11:52:12	4					
11:55:49	2					
12:00:24	1					
12:03:51	5					
12:05:00			42	-135.8		
12:30:00			42	-136.0	+ 0.8	
12:35:00			51	-135.4		

Table 5.3-1 (continued)

GMT, hr:min:sec	Mode	Bit Rate	DSIF Station	DSIF Automatic Gain Control, dbm	Telemetry Margin, db	Comments
12:39:00			42			Command modulator off - transfer to DSS 51
12:45:00			51			Ground transmitter on 10 kw
12:45:13			51			Two-way confirmed
12:47:23			51	-133.5		Exciter at syn frequency
12:49:00			51			Command modulator on
13:00:00			51	-133.4		
13:30:00			51	-133.2		
14:00:00			51	-133.3		
14:02:22						Inertial mode on
14:30:00			51	-133.5		
15:00:00			51	-133.8		
15:30:00			51	-134.7		
16:00:00			51	-135.6		
16:00:45	4					
16:05:59	2					
16:09:09	1					
16:13:25	5					
16:24:00			51			Command modulator off - transfer to DSS 61
16:30:00			61			Ground transmitter on
16:31:35			61			Command modulator on
16:32:00			61	-134.9		
16:35:00			51	-135.8		
17:00:00			51	-135.4		
17:00:00			61	-135.7		
17:14:33						Cruise mode on
17:14:41						Manual lockon
17:30:00			51	-134.6		
17:50:00			61	-151.2		
17:51:56			61			Receiver out of lock*
17:53:27			61			Receiver in lock - servo to aided
17:54:03			61			Decommutator in lock
18:00:00			51	-134.6		
18:01:00			61	-135.6		
18:24:00			61			Command modulator off - transfer to DSS 51
18:30:00			51			Ground transmitter on
18:30:13			51			Two-way confirmed
18:32:45			51			Exciter on syn frequency
18:35:00			51	-135.1		Command modulator on
19:00:00			51	-134.9		
19:00:00			61	-134.7		
19:09:50	4					
19:13:25	2					
19:17:48	1					
19:23:59	5					
19:30:00			51	-135.1		
20:00:00			51	-135.0		
20:24:00			51			Command modulator off - transfer to DSS 61
20:30:00			61			Ground transmitter on
20:31:50			61			Command modulator on
20:35:00			51	-135.0		
21:00:00			51	-135.2		
21:00:00			61	-134.9		
21:30:00			51	-135.6		
21:30:00			61	-135.1		
21:55:35	4					
21:58:03	2					
21:59:56	1					
22:00:00			51	-135.6		
22:00:00			11	-136.9		
22:01:45	5					
22:24:00			61			Command modulator off - transfer to DSS 11
22:30:00			11			Ground transmitter on
22:30:00			51	-136.4		
22:31:40			11			Command modulator on
23:00:00			11	-136.8		

Table 5.3-1 (continued)

GMT, hr:min:sec	Mode	Bit Rate	DSIF Station	DSIF Automatic Gain Control, dbm	Telemetry Margin, db	Comments
				START DAY 9		
00:00:00			11	-136.7		
01:00:00			11	-136.7		
01:19:36	4					
01:21:51	2					
01:24:01	1					
01:26:19	5					
02:00:00			11	-136.8		
03:00:00			11	-136.9		
03:05:45						Inertial mode on
04:30:00			11	-137.1		
05:00:00			11	-137.8	+0.8	
05:30:00			11	-137.2	+1.4	
05:34:24						Cruise mode on
05:34:34						Manual lockon
05:54:00			11			Command modulator off - transfer to DSS 42
06:00:00			42			Ground transmitter on
06:02:05			42			Command modulator on
06:11:45	4					
06:14:11	2					
06:16:46	1					
06:19:16	5					
06:30:00			42	-137.0		
07:00:00			42	-137.1		
07:16:25						Inertial mode on
07:30:00			42	-137.0		
08:00:00			42	-137.0		
08:30:00			42	-137.2		
09:00:00			42	-137.2		
09:30:00			42	-137.7		
09:48:33						Cruise mode on
09:48:39						Manual lockon
10:00:00			42	-137.2		
10:30:00			42	-137.2		
10:59:49	4					
11:06:18	2					
11:09:15	1					
11:12:31	5		42	-137.2		
11:30:00			42	-137.1		
12:00:00			42	-137.5		
13:00:00			42	-137.5		
13:24:00			42			Command modulator off - transfer to DSS 51
13:30:00			51			Ground transmitter on
13:32:25			51	-136.2		Command modulator on
13:49:43						Modulation interrupt
13:59:49						Modulation interrupt
14:00:06			51	-136.2		Inertial mode on
14:02:50						Command modulator off - ground transmitter swept from track syn frequency ±20 kHz to track syn frequency to ensure automatic frequency control capture on spacecraft receiver A. Receiver A automatic gain control below indexing threshold several times since 13:33 GMT shortly after transfer to DSS 51 from DSS 42
14:11:14			51			Command modulator on
14:14:11	4					
14:18:24	2					
14:21:56	1					
14:24:50	5					
15:00:00			51	-136.3		
15:24:00			51			Command modulator off - transfer to DSS 61
15:30:00			61	-136.9		Ground transmitter on
15:31:40			61			Command modulator on
17:00:00			51	-137.4		
17:00:00			61	-137.5		

Table 5.3-1 (continued)

GMT, hr:min:sec	Mode	Bit Rate	DSIF Station	DSIF Automatic Gain Control, dbm	Frequency Margin, db	Comments
17:04:13						Cruise mode on
17:04:25						Manual lock mode on
17:04:50						Decoder indexing - receiver A automatic gain control dropping below indexing threshold
17:30:00			61	-137.3		Decoders still indexing
17:54:00			61			Command modulator off - transfer to DSS 51
18:00:00			51	-136.6		Ground transmitter on
18:01:30			51			Command modulator on - receiver A automatic gain control near command threshold, but above indexing threshold
18:07:00	4					
18:09:00			51			BER = 0.36×10^{-3}
18:11:11	2					
18:13:00			51	-136.8		
18:14:38	1					
18:19:21	5					
18:21:00			51	-136.7		
19:00:00			51	-136.8	+1.8	
19:30:00			51	-137.0	+1.6	BER = 0.63×10^{-3}
19:55:50		550				
20:00:00			51	-138.2	+5.5	
20:30:00			51	-138.3		
20:58:18	4					
21:03:39	2					
21:05:23	1					
21:07:54	5					
21:30:00			51	-138.6		
21:54:00			51			Command modulator off - transfer to DSS 11
22:00:00			11			Ground transmitter on
22:02:00			11			Command modulator on
22:05:00			11	-140.4		
22:07:00			14	-131.3		
22:30:00			11	-140.5		
22:44:00			11	-141.0		
22:47:58	4					
22:49:00			14	-131.0		
22:49:48	2					
22:53:04	1					
22:58:08	5					
22:59:17	None	None				
22:59:22						Gyro speed subcarrier oscillator on
23:02:01	5	550				
23:04:26						Transponder power off
23:06:08						Transponder B power on
23:07:55						Command modulator off
23:09:40						Command modulator on - transponder B phase lock
23:47:35			11	-140.4		Command modulator off for touchdown frequency offset
23:52:45						Command modulator on
23:57:20						Two modulator interrupts - receiver B, decoder A
23:59:11	6					
START DAY 10						
00:01:27	4		11	-140.3		
00:03:13						Transmitter B filament power on - confirmed
00:05:55						Transfer switch B high power commanded
00:05:56						Transmitter high voltage on commanded No response - decoder indexing occurred just prior to these commands
00:06:38						Two modulator interrupts - receiver B/decoder B
00:07:23						Transmitter high voltage on - confirmed
00:08:03		1100	11	-124.4		
00:08:42						Presumming amplifier off
00:09:13	2					
00:09:30			14	-113.4		
00:12:35	5					
00:19:04						TD strain gage subcarrier oscillators on (presumming amplifier off)

Table 5.3-1 (continued)

GMT, hr:min:sec	Mode	Bit Rate	DSIF Station	DSIF Automatic Gain Control, dbm	Frequency Margin, db	Comments
00:21:15						Transponder power off command - no response
00:21:45						Modulation interrupt
00:21:52						Transponder power off - confirmed
00:27:14						Start roll +80.5 degrees (161.0 seconds)
00:29:58						End roll
00:30:00			11	-124.2		
00:35:50						Start yaw +96.1 degrees (192.2 seconds)
00:39:05						End yaw
00:39:10			11	-125.9		
00:41:07						Start roll -16.5 degrees (33.0 seconds)
00:41:43						End roll
00:41:50			11	-127.0		
00:42:33						Presumming amplifier on (touchdown strain gage on)
00:43:00			11	-129.0		
00:50:10	6					
01:02:11.93						AMR mark
01:02:14.73						Vernier ignition
01:02:15.83						Retro ignition
01:02:16.34						RADVS on
01:02:18.24						Inertia switch off
01:02:49.44						RODVS on
01:02:59.028						Retro burnout
01:02:59.038						Inertia switch on
01:03:11.038						High thrust on
01:03:18.138						RADVS reliable on
01:05:13.323						1000-foot mark on
01:05:30.223						10 ft/sec
01:05:36.322						13-foot mark
01:05:37.620						Touchdown
01:05:40			11	-127.9		
01:07:14	5					
01:09:04	2					
01:11:00						Touchdown strain gage subcarrier oscillators off
01:12:46	5					
01:18:26						Analog-to-digital converter power off
01:18:36		550				Analog-to-digital converter 2 power on
01:18:37		1100				
01:19:50	4					
01:21:44		137.5				
01:22:00			11	-128.0		Transmitter B high power - omnidirectional antenna B
01:22:58						Transmitter B low power
01:23:00			11	-145.6		Transmitter B low power omnidirectional antenna B
01:24:58						Transmitter A low power on
01:26:00			11	-142.9		Transmitter A low power omnidirectional antenna B
01:28:41						Transmitter A high power
01:29:24		1100				
01:30:41						Select omnidirectional antenna A
01:31:24						Select omnidirectional antenna B
01:33:39	7					Start preparation for 200-line TV
01:41:46						To SSAC for TV
01:46:50						Start frame - first 200-line TV
02:17:08						Transmitter A high power
02:17:51	4					
02:18:58						Transponder A power on
02:29:07	5					
02:37:59						Start A/SPP stepping
03:16:26						Transmitter A low power
03:17:17						Transmitter A to planar array
03:20:58						End stepping A/SPP
03:23:22	4					
03:33:38						Transmitter A filament power on
03:34:29						Transponder power off
03:35:19			11	-115.5		
03:35:34						Transmitter A high power
03:35:50			11	- 98.1		
03:36:08		4400				
03:36:43			11	-101.6		
03:37:06						Start preparations for 600-line TV
03:41:44						Start frame - first 600-line TV

*DSS antenna slewed off spacecraft to aided track, maintaining receiver lock.

TABLE 5.3-2. SPACECRAFT CONFIGURATION SHEET

GMT, hr:min:sec	Major Sequence Title	Transmitter		Omni-directional Antenna A/B	Analog-to-Digital Converter 1/2	Receiver A		Receiver B		Command Decoder A/B	Comments
		A/B	Power, High/Low			φL/AFC*	Transponder A	φL/AFC*	Transponder B		
DAY 7											
06:30:00.545	Launch	B	Low	B	1		Off		On	B	
07:05:00			High								Confirmed by telemetry at 07:05:43
07:27:33						AFC		φL			
07:31:57			Low								Confirmed by telemetry at 07:32:45
07:51:45										A	Command modulation off for tuning – DSS 42
11:54:00											Command modulator off – transfer from DSS 42 to 51
12:01:20											Command modulator on – DSS 51
13:54:00										B	Command modulator off for transfer to DSS 61
14:02:20											Command modulator on – DSS 61
14:15:22											Modulation interrupt
14:18:28	Star acquisition		High								
14:21:20								AFC	Off		
14:51:04									On		
14:51:17										A	Command modulator off to reacquire phase lock receiver B
14:51:46										B	
14:53:03								φL			
14:56:05											Command modulator on
14:58:14	Coast phase		Low								
17:54:00											Command modulator off – transfer to DSS 51
18:02:10											DSS 51 command modulator on
21:14:00										A	Command modulator off – transfer to DSS 11
21:22:20											DSS 11 command modulator on
23:02:03	Midcourse correction		High								

Table 5.3-2 (continued)

GMT, hr:min:sec	Major Sequence Title	Transmitter		Omni-directional Antenna A/B	Analog-to-Digital Converter 1/2	Receiver A		Receiver B		Command Decoder A/B	Comments
		A/B	Power, High/Low			φL/AFC*	Transponder A	φL/AFC*	Transponder B		
DAY 7 (continued)											
23:23:51										B	Caused by receiver A during premidcourse yaw
23:35:25										A	Caused by receiver A during postmidcourse
23:51:26	Coast phase II		Low								
DAY 8											
05:24:05										B	Command modulator off – transfer to DSS 42
05:31:35											DSS 42 command modulator on
12:39:00											Command modulator off – transfer to DSS 51
12:49:00											DSS 51 command modulator on
16:24:00										A	Command modulator off – transfer to DSS 61
16:31:35											DSS 61 command modulator on
17:52:32										B	DSS 61 antenna slewed off spacecraft approximately 0.5 degree
18:24:00											Command modulator off – transfer to DSS 51
18:35:00											DSS 51 command modulator on
20:24:00										A	Command modulator off – transfer to DSS 61
20:31:50											DSS 61 command modulator on
22:24:00											Command modulator off – transfer to DSS 11
22:31:40											DSS 11 command modulator on
22:39:34										B	Receiver A automatic gain control dropped below index threshold
22:59:30										A	Receiver A automatic gain control dropped below index threshold

Table 5.3-2 (continued)

GMT, hr:min:sec	Major Sequence Title	Transmitter		Omni-directional Antenna A/B	Analog-to-Digital Converter 1/2	Receiver A		Receiver B		Command Decoder A/B	Comments
		A/B	Power, High/Low			φL/AFC*	Transponder A	φL/AFC*	Transponder B		
DAY 8 (continued)											
23:20:45										B	Decoders indexed at least seven times between 23:16:30 and 23:20:45
23:31:59										B	Decoders indexed several times between 23:30:38 and 23:31:59
DAY 9											
02:55:36										B	Intermittent indexing since 23:50 caused by low signal into receiver A
05:54:00										A	Command modulator off – transfer to DSS 42
06:02:05											DSS 42 command modulator on
13:24:00										B	Command modulator off – transfer to DSS 51
13:32:25											DSS 51 – command modulator on
13:33:14										A	Low signal into receiver A
13:37:08										B	
13:47:01										A	
13:47:09										B	
13:49:43											Modulation interrupt
13:51:08										A	
13:54:55										B	
13:55:09										A	
13:55:19										B	
13:57:36										A	
13:59:49											Modulation interrupt
14:02:50											Command modulator off – ground transmitter swept ±20 kHz to track syn frequency to ensure automatic frequency control capture on receiver A. No change
14:11:14											Command modulator on
14:13:09										B	
15:24:00										A	Command modulator off – transfer to DSS 61

Table 5.3-2 (continued)

GMT, hr:min:sec	Major Sequence Title	Transmitter		Omni-directional Antenna A/B	Analog-to-Digital Converter 1/2	Receiver A		Receiver B		Command Decoder A/B	Comments
		A/B	Power, High/Low			φL/AFC*	Transponder A	φL/AFC*	Transponder B		
DAY 9 (continued)											
15:31:40											DSS 61 command modulator on
17:04:51											Signal in receiver A approximately -128 dbm. Decoders indexing rapidly
17:51:05										B	Intermittent rapid decoder indexing since last entry
17:54:00											Command modulator off – transfer to DSS 51
18:01:30											DSS 51 command modulator on receiver A automatic gain control approximately 6 to 7 db above index threshold
21:02:08										B	One modulator interrupt
21:05:38										B	Modulator interrupt on receiver B
21:54:00										A	Command modulator off – transfer to DSS 11
22:02:00											DSS 11 command modulator on
22:04:51										B	
22:05:27											Receiver A automatic gain control at no signal value
22:46:16										A	Modulator interrupt
22:46:46											Modulator interrupt (receiver B)
23:04:26								AFC	Off		
23:06:08								Not φL	On		
23:06:58										B	
23:09:58								φL			
23:47:35											Command modulator off for touchdown frequency offset tuning
23:52:45											Command modulator on
23:53:37										A	
23:53:49										B	
23:55:39										A	
23:55:42										B	Modulator interrupt
23:57:02										A	Modulator interrupt
23:57:20											Modulator interrupt (on receiver B)

Table 5.3-2 (continued)

GMT, hr:min:sec	Major Sequence Title	Transmitter		Omni-directional Antenna A/B	Analog-to-Digital Converter 1/2	Receiver A		Receiver B		Command Decoder A/B	Comments
		A/B	Power, High/Low			φL/AFC*	Transponder A	φL/AFC*	Transponder B		
DAY 10											
00:05:46										B	
00:06:06										A	
00:06:38										B	Modulator interrupt
00:07:04											Modulator interrupt (receiver B, decoder B)
00:07:23			High								
00:12:14											Modulator interrupt
00:12:39										A	
00:21:46											Modulator interrupt (receiver B, decoder A)
00:21:54								AFC			
01:18:36					2						
01:22:58		B	Low								
01:24:58		A	Low								
01:28:41			High								
01:30:41				A							
01:31:24				B							
01:41:46											To SSAC for 200-line TV
02:11:08			High								
02:18:58							On				
02:19:15										B	Command modulator off to acquire receiver A
02:24:49						φL					
03:16:26			Low								
03:17:17											Transmitter A to planar array

*Phase lock/automatic frequency control.

5.3.2 ANOMALY DISCUSSION

Three events are discussed in this subsection. Two of these are not considered to be spacecraft data subsystem anomalies, but rather are deviations from expected or predicted performance. The other event, drift of the wide-band voltage-controlled crystal oscillator frequency outside of the ground station receiver tuning range capability, cannot be considered truly an anomaly since the magnitude of the drift was predicted prior to the mission. However, the effect of the drift did result in a deviation from the desired spacecraft RF configuration sometime during the first lunar day.

5.3.2.1 Receiver/Decoder Indexing During Transit

During the coast phases of the mission, the spacecraft attitude was such that the earth vector to omnidirectional antenna A was confined to the deep null region of the gain coverage pattern. The resulting low signal level in receiver A caused indexing of receiver/decoder combinations during the postmidcourse coast period and during preparation for the terminal maneuvers. Although operational difficulties were experienced, no spacecraft anomaly existed. A more detailed discussion is found in the subsections dealing with each mission phase (subsection 5.3.4).

5.3.2.2 Signal Level Variations During Lunar Operation

Starting at touchdown, periodic fluctuations (Reference 1) were observed in the spacecraft receiver signal levels and in the ground station signal level when the spacecraft was transmitting on either omnidirectional antenna. After positioning of the A/SPP, no fluctuations were observed when transmitting on the planar array; however, up link fluctuations still existed. During some television surveys when spacecraft receiver automatic gain control was not available, commands were missed due to one of the receiver signal levels drifting below the command threshold. Low receiver signal levels were also noted during engineering interrogations, but missed commands could be avoided by indexing to a receiver with an adequate signal level.

The following observations were made in regard to this situation:

1) Periodic variations occurred in the spacecraft receiver and Deep Space Station automatic gain control.

2) Occasionally at station transfer the period of variation abruptly changed.

3) Spacecraft receiver signal levels at times dropped not only below command threshold but also below phase lock threshold.

4) No down link signal variations were noted when transmitting on the planar array.

5) Down link fluctuations were observed simultaneously at two tracking stations.

Figure 5.3-2 is an example of the variations in both spacecraft receivers at the time of a station transfer. At this particular time, the signal in receiver A was more dynamic than that in receiver B; however, the reverse situation was also observed at other times.

The above observations suggest multipath reflections since path length is the only common parameter for all these cases. In order to have multipath interference such as this, the path length of the direct wave must be changing with respect to the path length of the reflected wave. A discussion of the multipath situation can be found in Reference 1. It was found, by considering the relative motion of the earth, spacecraft, and a reflecting surface 14 km from the spacecraft, that, in several cases, the calculated period of signal level variations taken at various times agreed with the period seen in the data. A series of ridges is located 14 km north of the spacecraft. A sample model was used in the calculations and, in some instances, the period of variation seen in the data did not check with the calculated value. However, a model can be postulated that will explain these cases.

Figure 5.3-2 shows that omnidirectional antenna A is quite sensitive to look angle variations since, at the station transfer, the receiver A signal level increased approximately 15 db. At a station transfer, the spacecraft-to-earth vector changes on the order of 1.5 degrees. Also, it is observed that the amplitude of the variations in the signal are much greater at the lower average signal levels. This indicates that the reflected wave energy is not as sensitive as the direct wave to look angle variations and therefore has a greater influence at the lower signal levels.

The observed condition is not considered to be the result of a spacecraft hardware anomaly. The less rugged terrain around previous spacecraft probably accounts for not having observed a fluctuating signal before.

5.3.2.3 Transmitter A Wide-Band Voltage-Controlled Crystal Oscillator Frequency Drift

On GMT day 14, the transmitter A wide-band voltage-controlled crystal oscillator frequency drifted outside the DSS 11 receiver tuning range. The highest tuning frequency at DSS 11 was 2295.234560 MHz and, at 22:00 GMT on day 14, the spacecraft frequency had drifted to 2295.236480 MHz. It was necessary to use transmitter B for television operation during part of the remainder of the first lunar day.

On 2 October 1967 TFR 87206 was written against this wide-band voltage-controlled crystal oscillator module when the frequency was observed to drift +254 kHz above 2295 MHz. An upward frequency drift as a function of time in a vacuum has been a characteristic of the wide-band voltage-controlled crystal oscillators. On previous spacecraft transmitters, the wide-band voltage-controlled crystal oscillators were tuned to some frequency below 2295 MHz so that the normal drift would be toward 2295 MHz. However, on Surveyor VII, the frequency was tuned to +38 kHz above 2295 MHz and the normal drift produced frequencies as high as +254 kHz above 2295 MHz. The Trouble and Failure Report was closed with no attempted realignment under

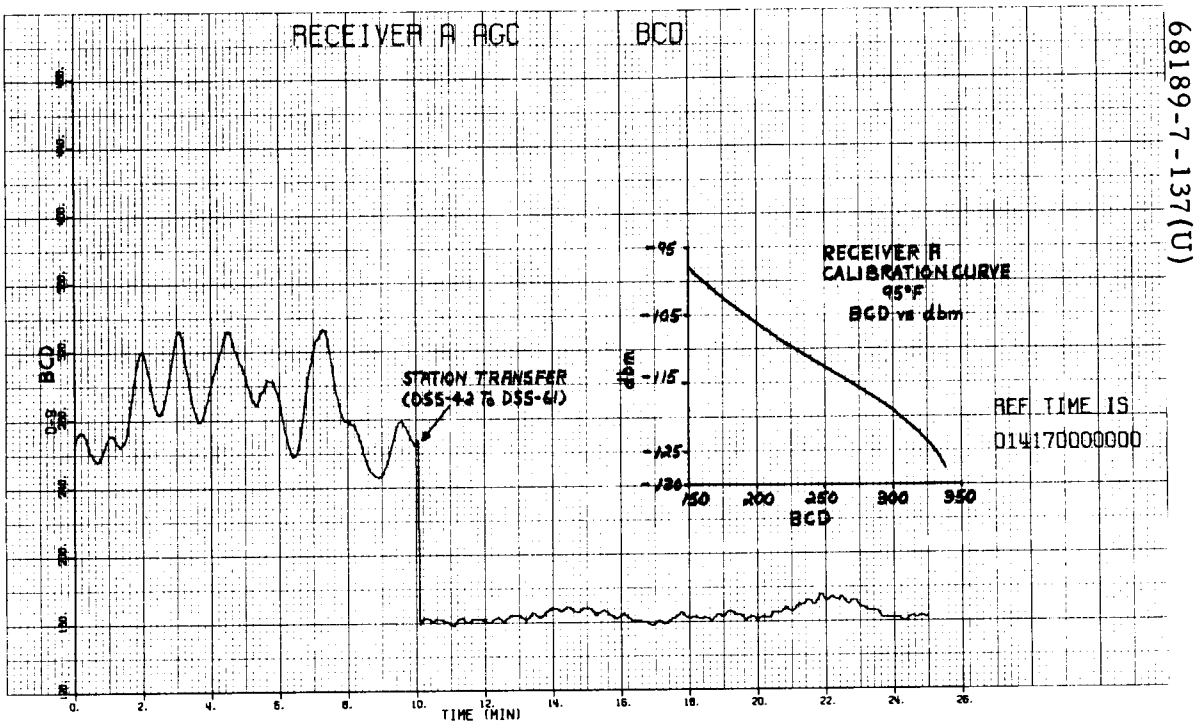

a. Receiver A AGC

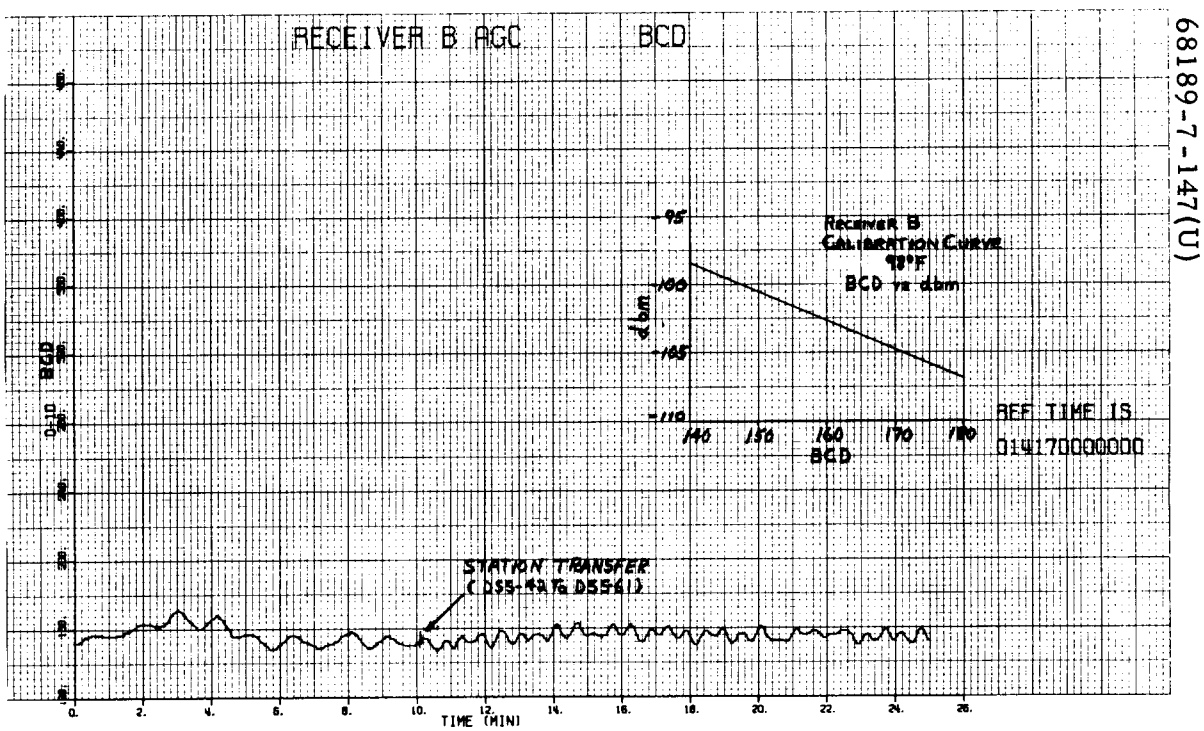

b. Receiver B AGC

Figure 5.3-2. Signal Level at Station Transfer on GMT Day 014

the assumption that the Deep Space Network could handle frequency changes of this magnitude and, therefore, the misalignment posed no mission problems. Even though the observed drift during the mission was less than that indicated in the Trouble and Failure Report, the ground station (DSS 11) was unable to tune its receiver to the transmitted frequency.

5.3.3 SUMMARY AND CONCLUSIONS

Table 5.3-3 contains a summary of the measurable performance parameters compared with applicable requirements and premission predictions. Most subsystem parameters are not directly measurable, and those that are measurable are difficult to summarize due to time variability.

Received signal level, for example, is a function of time and spacecraft attitude. The summary for these parameters reflects wide tolerances, with corresponding wide variations in actual performance in cases when the earth vector was in the omnidirectional antenna null. Performance and predictions outside the null are much more closely bounded. More detailed information is found in the subsections dealing with each mission phase.

The following conclusions can be drawn as a result of the foregoing analysis:

1) The RF subsystem performed within the predicted tolerance region for both the up and down links.

2) RF subsystem premission and real-time analysis techniques used during Mission G were relatively accurate.

3) Mission G data again verified the bias in the omnidirectional antenna B up link antenna gain pattern. This measured gain pattern had been adjusted by 2 db for all predictions and analysis as a result of postmission analysis on Mission E.

4) Receiver/decoder indices during transit and negative response to some commands during first lunar day operations were not a result of spacecraft hardware anomalies.

TABLE 5.3-3. RF PERFORMANCE PARAMETER SUMMARY

Parameter	Predicted Value	Requirement	Actual Performance
Transmitter frequency at acquisition	2294.992791 MHz	2295 MHz ± 23 kHz	2294.991200 MHz
Receiver B frequency at acquisition	2113.323442 MHz	2113.31 MHz ±21 kHz	2113.326528 MHz
Receiver A signal levels during coast phases*	Time variable predictions. Predictions are some nominal value ±10 db.	>-114 dbm**	Level between +8 and <-20 db of nominal and as low as at least -130 dbm
Receiver B signal levels during coast phases*	Time variable predictions. Predictions are some nominal value ±5 db.	>-114 dbm**	Level between +1.0 and -4 db nominal and ≥ -98.0 dbm
Receiver A signal levels during star maneuver	Time variable predictions. Predictions are some nominal value of ±10 db.	>-114 dbm**	Level between +5 and -10.5 db of expected and ≥ -111.0 dbm
Receiver B signal levels during star maneuver	Time variable predictions. Predictions are some nominal value ±8 db.	>-114 dbm**	Level between +5 and -8 db of expected a and ≥106.7 dbm
Receiver A signal levels during mid-course maneuvers	Time variable predictions. Predictions are some nominal value ±10 db with variations of 6.8 db for duration of maneuver.	>-114 dbm**	Level variations of 30.4 db and ≥ -126.3 dbm

Table 5.3-3 (continued)

Parameter	Predicted Value	Requirement	Actual Performance
Receiver B signal levels during mid-course maneuvers	Time variable predictions. Predictions are some nominal value ±5.7 db with variations of 1.8 db for duration of maneuver.	>-114 dbm**	Level variations of 6.1 db and ≥-90.3 dbm
Receiver A signal levels during terminal maneuver	Time variable predictions. Predictions are some nominal value ±10 db with variations of 23.0 db for duration of maneuver.	>-114 dbm**	Level variations of >30.0 db and as low as at least -130.0 dbm
Receiver B signal levels during terminal maneuver	Time variable predictions. Predictions are some nominal value ±6.0 with variations of 11.0 db for duration of maneuver.	>-114 dbm**	Level variations of 10.7 db and >-107.0 dbm
DSS signal levels during coast phases*	Time variable predictions. Predictions are some nominal value ±5 db.	>-157.4 dbm (carrier power) (17.2 bits/sec threshold)	Level between +3.0 and 0.0 db of nominal and >-141 dbm at 550 bits/sec
DSS signal levels during star maneuver	Time variable predictions. Predictions are some nominal value ±10 db.	None	Level between +6.0 and -6.0 db of expected and ≥-144.4 dbm (carrier power at 4400 bits/sec)
DSS signal levels during midcourse maneuvers	Time variable predictions. Predictions are some nominal value ±2.9 db with variations of 2.4 db for duration of maneuver.	>-136.1 dbm (carrier power at 4400 bits/sec/ high power)	Level variations of 3.5 db and ≥-123.8 dbm carrier power at 4400 bits/sec

Table 5.3-3 (continued)

Parameter	Predicted Value	Requirement	Actual Performance
DSS signal levels during terminal maneuver	Time variable predictions. Predictions are some nominal value ±2.9 db with variations of 5.0 db for duration of maneuver.	>-130.4 dbm (carrier power at 1100 bits/sec/ high power)	Level variations of 7.0 db and ≥-129.7 dbm carrier power at 1100 bits/sec
DSS signal levels during descent and touchdown	Time variable predictions. Predictions are some nominal value ±3.0 db with variations of 2.1 db for duration of descent.	>-131.7 dbm (carrier power at 1100 bits/sec and strain gages)	Level variations of 3.8 db and ≥ -129.1 dbm carrier power at 1100 bits/sec and strain gages on 85-foot antenna
Transmitter A high power output	40.6 dbm $^{+0.2}_{-0.0}$ db	>39.6 dbm	Output between 40.8 and 41.0 dbm
Transmitter A low power output	23.7 dbm $^{+1.6}_{-0.6}$ db	>20.0 dbm	Output between 24.5 and 25.0 dbm
Transmitter B high power output	40.6 dbm $^{+0.0}_{-0.3}$ db	>39.6 dbm	Output between 40.5 and 40.7 dbm
Transmitter B low power output	23.6 dbm $^{+2.0}_{-1.0}$ db	>20.0 dbm	Output between 23.0 and 24.5 dbm

Table 5.3-3 (continued)

Parameter	Predicted Value	Requirement	Actual Performance
Command reject rate	<1/2000	≤1/2000 at signal level >-144 dbm	Necessary to repeat three commands during transit as a result of receiver indexing. Some commands not processed during TV operation. No known rejected commands on selected receivers having signal levels >-114 dbm.
Telemetry bit error rate	<3/1000	≤3/1000 at input SNR ≥ 10 db	Calculated BER = 3×10^{-3} at input signal-to-noise ratio ≃ 10.5 ± 1.5 db. (Maximum error rate during transit = 0.63×10^{-3} at input signal-to-noise ratio ≃ 11.8 ± 1.5 db.)

*Gyro drift checks during coast phases caused antenna gain variations not taken into account in the predicted signal levels.

**Threshold value applies to command threshold and, as such, only requires one of the two receivers to be above -114 dbm at any one time.

5.3.4 SUBSYSTEM PERFORMANCE ANALYSIS

5.3.4.1 General Discussion

Before specific phases are discussed, a general treatment of the mission will be undertaken. Information applicable to all mission phases is included in this subsection.

Subsystem Parameters

Most quantitative estimates of performance are based on received signal levels which, in turn, are determined from individual link parameters. Those parameters used in the performance predictions and the subsystem analyses are tabulated in Tables 5.3-4 and 5.3-5. Equations using these data are derived here; parameters discussed in later portions can be evaluated from these data. Tables 5.3-4 and 5.3-5 consist of measured data taken from flight acceptance (FAT), solar thermal vacuum (STV), and command and data handling console (CDC) tests or specification values where measurements were not available.

Computations Used

In this subsection, reference is made to received signal levels and quantities computed from these levels. The equations used are listed below and will not be derived again:

1) Spacecraft transmitter high power output is

$$P_{xmtr}(\text{dbm}) = 10 \log (P_{tm} \times 10^3) + L$$

where

P_{xmtr} = transmitter power (dbm) = P_{high}

P_{tm} = telemetered power output (watts)

L = loss from transmitter to power monitor. (Values are determined from STV calibration data.)

2) Spacecraft transmitter low power output is

$$P_{low} = P_{high} - P_{DSS_H} + P_{DSS_L} \text{ (dbm)}$$

where

P_{low} = transmitter low power output

P_{high} = telemetered transmitter high power output

P_{DSS_H} = DSS received signal level at high power

P_{DSS_L} = DSS received signal level at low power

3) Spacecraft omnidirectional antenna gain (up-link) is

$$G_R = \frac{P_R}{P_T G_T \left(\frac{\lambda}{4\pi R}\right)^2 L}$$

where

G_R = received omnidirectional antenna gain (up-link gain)

P_R = received signal level (determined from spacecraft AGC)

P_T = DSS nominal transmitter power

G_T = DSS nominal antenna gain

λ = wavelength of up link signal

R = slant range at time of computation

L = nominal spacecraft and DSS losses

(Note: For down link gain, appropriate down link parameters are inserted in a similar equation.)

4) Signal-to-noise ratio (SNR) for any subcarrier is

$$SNR = \frac{P_S}{P_N} = \frac{MP_R}{KT_{eff}BW_{sc}}$$

where

P_S = signal power in predetection noise bandwidth

P_N = total noise power in predetection noise bandwidth

M = carrier to subcarrier modulation loss adjustment constant based on subcarrier oscillator modulation index on the carrier

P_R = received carrier power reported by the DSS

K = Boltzmann's constant

T_{eff} = DSS system temperature reported by the DSS

BW_{sc} = subcarrier equivalent predetection noise bandwidth

When using these equations, attention must be given to the desired accuracy of the answer. Since several parameters not measurable in flight, spacecraft telemetry, and DSS station reports are used, and thus computed parameters have potentially large errors. Their validity is thus weighed against similar test data and/or is judged quite subjectively based on past experience. These equations are not used so much for their numerical results as for the total picture of subsystem performance generated. Any gross subsystem problems or computation errors will tend to be uncovered in this analysis, but subtle errors will not.

Bit Error Rate Calculations

One subsystem parameter of interest is the telemetry bit error rate (BER). This parameter serves as an example of the problems encountered when attempting to evaluate postmission data. BER is required to be less than 3×10^{-3} at input SNR ratios of 9 ± 1 db. BER cannot be measured in flight, but word error rate can. On day 9 at approximately 19 hours GMT, DSS 51 began counting parity errors. Based on the assumption that a bad parity word represented a single bit error, a BER of 0.63×10^{-3} was observed at a reported -137.0 dbm ground station received carrier power (19 hours 30 minutes).

TABLE 5.3-4. UP LINK PARAMETERS FROM FAT, STV, AND CDC TESTS

Description	Value
Transmitting system (DDS)	
RF power	$70.0^{+0.5}_{-0.0}$ dbm
Antenna gain	
SAA	20.0 ± 2.0 db
SCM	51.0 (+1.0, -0.5) db
Circuit loss	
SAA	-0.5 ± 0.0 db
SCM	-0.4 ± 0.1 db
Receiving system (Surveyor VII)	
Circuit loss	
Receiver A	-4.0 ± 0.5 db
Receiver B	-3.5 ± 0.5 db
Up link carrier tracking loop	
Equivalent noise	
Bandwidth	240 ± 24 Hz
Threshold SNR	12 db
Up link channel	
Threshold SNR	9 db
System noise	
Temperature	2700° K
Equivalent noise	
Bandwidth (predetection)	13430 Hz
Data/subcarrier modulation index	7.2
Subcarrier/carrier modulation index	1.6 ± 0.16

TABLE 5.3-5. DOWN LINK PARAMETERS FROM FAT, STV, AND CDC TESTS

Description	Value
Transmitting system (Surveyor VII)	
RF power	
Transmitter A (low power)	23.7 (+1.6, -0.6) dbm
Transmitter B (low power)	23.6 (+2.0, -1.0) dbm
Transmitter A (high power)	40.6 (+0.2, -0.0) dbm
Transmitter B (high power)	40.6 (+0.0, -0.3) dbm
Planar array gain	27.0 ± 0.5 db
Circuit loss	
Transmitter A Omnidirectional antenna A	-2.77 (±0.5) db
Transmitter B Omnidirectional antenna A	-2.95 (±0.5) db
Transmitter A Omnidirectional antenna B	-2.62 (±0.5) db
Transmitter B Omnidirectional antenna B	-3.25 (±0.5) db
Planar array	-2.3 (+0.0, -0.22) db
Carrier frequency	2295 MHz
Receiving system (DSS)	
Antenna gain	
SAA (acquisition aid antenna)	21.0 ± 1.0 db
SCM (85-foot antenna)	53.0 (+1.0, -0.5) db

Table 5.3-5 (continued)

Description	Value
Circuit loss	
SAA	-0.5 ± 0.0 db
SCM	-0.18 ± 0.05 db
Effective noise temperature	
Maser	55 ± 10° K
Parametric amplifier (SAA antenna)	
All DSS except Johannesburg	270 ± 50°K
Johannesburg	320 ± 50°K
Lunar temperature	110 ± 25° K
Carrier channel	
Equivalent noise bandwidth for maneuvers (at threshold)	152 Hz
Equivalent noise bandwidth for coast mode (at threshold)	12 Hz
Threshold SNR	
Acquisition	9.0 db
Maneuvers	14.0 ± 1.0 db
Coast mode	11.4 db
Subcarrier oscillator	
Equivalent predetection noise bandwidth, Hz ± 10 percent	
4400 bits/sec	5160
1100 bits/sec	1290
550 bits/sec	685
137.5 bits/sec	169
17.2 bits/sec	26.7
Strain gauge 1	169
Strain gauge 2	169
Strain gauge 3	169
Reject/enable	405
Gyro speed	948
Alpha counts	11400
Proton counts	948

Table 5.3-5 (continued)

Description	Value
Subcarrier oscillator center frequencies, kHz	
4400 bits/sec	33.0
1100 bits/sec	7.35
550 bits/sec	3.90
137.5 bits/sec	0.96
17.2 bits/sec	0.56
Strain gauge 1	0.96
Strain gauge 2	1.30
Strain gauge 3	1.70
Reject/enable	2.3
Gyro speed	5.4
Alpha counts	70.0
Proton counts	5.4
Threshold signal-to-noise ratio for telemetry data, ±1.0 db	
4400 bits/sec	9.0
1100 bits/sec	9.0
550 bits/sec	9.0
137.5 bits/sec	9.0
17.2 bits/sec	9.0
Strain gauge 1	7.0
Strain gauge 2	7.0
Strain gauge 3	7.0
Reject/enable	10.0
Gyro speed	10.0
Alpha counts	11.0
Proton counts	10.0
Subcarrier oscillator modulation indices, ±10 percent	
4400 bits/sec	1.6
1100 bits/sec	0.935
550 bits/sec (acquisition)	0.3
550 bits/sec	1.15
137.5 bits/sec	1.45
17.2 bits/sec	1.45
Strain gauge 1	0.65
Strain gauge 2	0.65
Strain gauge 3	0.65
Reject/enable	0.655
Gyro speed	1.600
Alpha counts	1.40
Proton counts	0.60

The SNR at this time of the observed 0.63×10^{-3} BER was computed as shown below:

DSS automatic gain control /1100 bits/sec = -137.0 dbm

System noise temperature = 41.5°K = 16.18 db
(DSS 51 post-track)

Boltzmann's constant = -198.6 dbm/deg/Hz

Bandwidth = 1290 Hz ± 10 percent = 31.1 (+0.41, -0.46) db

Noise power = -151.32 (+0.41, -0.46) dbm

Modulation loss

Carrier -2.01 (+0.40, -0.46) db
Subcarrier -4.56 (+0.62, -0.73) db

Δ modulation loss = -2.55 (+1.08, -1.13) db

Subcarrier power = -139.55 (+1.08, -1.13) dbm

SNR = subcarrier power – noise power = 11.77 (+1.54, -1.54)

The tolerance in this computation is only approximate and is probably greater. Also, the computation is based on a BER of 0.63×10^{-3}, and the parameter to be compared is specified at a BER of 3×10^{-3}. Measured BER versus SNR test data indicate that a deviation of +1.25 db from the predicted SNR at a BER = 3×10^{-3} will produce a BER = 0.63×10^{-3}. Applying this to the results computed above predicts that a BER = 3×10^{-3} would occur at a SNR = 10.52 (±1.54) db, thus meeting the minimum specification of the required SNR of 9 ± 1.0 db if the associated tolerances on the two values are applied.

Omnidirectional Antenna Gain Maps

In order to better visualize and interpret the significance of the signal level data, traces of the earth vector on the omnidirectional antenna gain contour maps are presented. Figures 5.3-3 and 5.3-4 show the antenna up and down links. Since signal level variations are, for the most part, the result of increasing range (i.e., more space loss) and changing omnidirectional gain, these plots allow visualization of the expected signal level changes for comparison with plots of up and down link signal levels versus time.

5.3.4.2 Mission Phase 1: Prelaunch to Spacecraft Acquisition

Subsystem performance is assessed during the launch pad systems readiness test and prelaunch countdown test. Next to assuring normal system performance prior to launch, the most important subsystem data taken during this phase are transmitter and receiver frequency data. Frequency data are used to predict the frequencies at initial acquisition and are

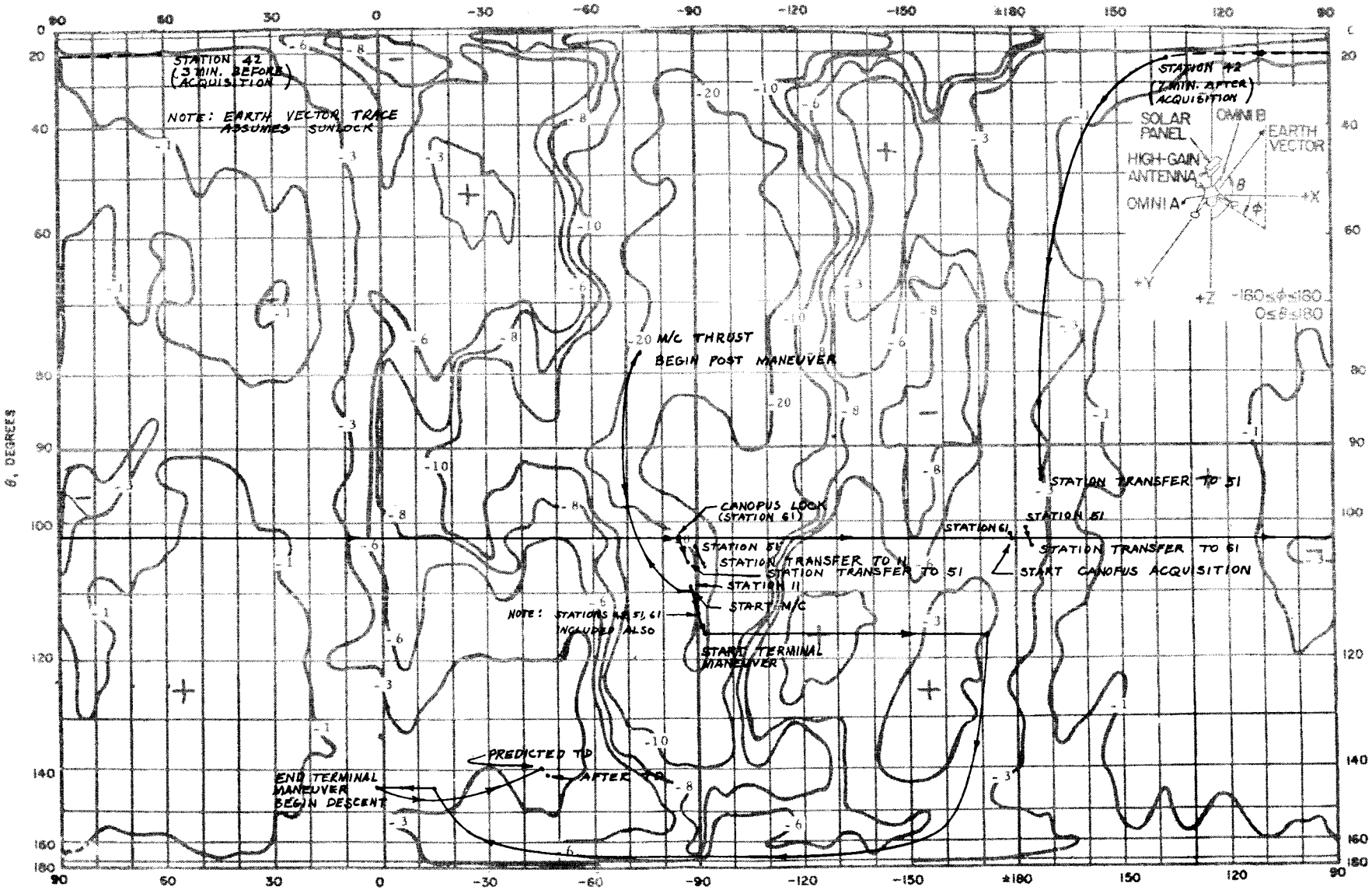

a) Antenna A

Figure 5.3-3. Omnidirectional Antenna Gain Contours (2113 MHz)

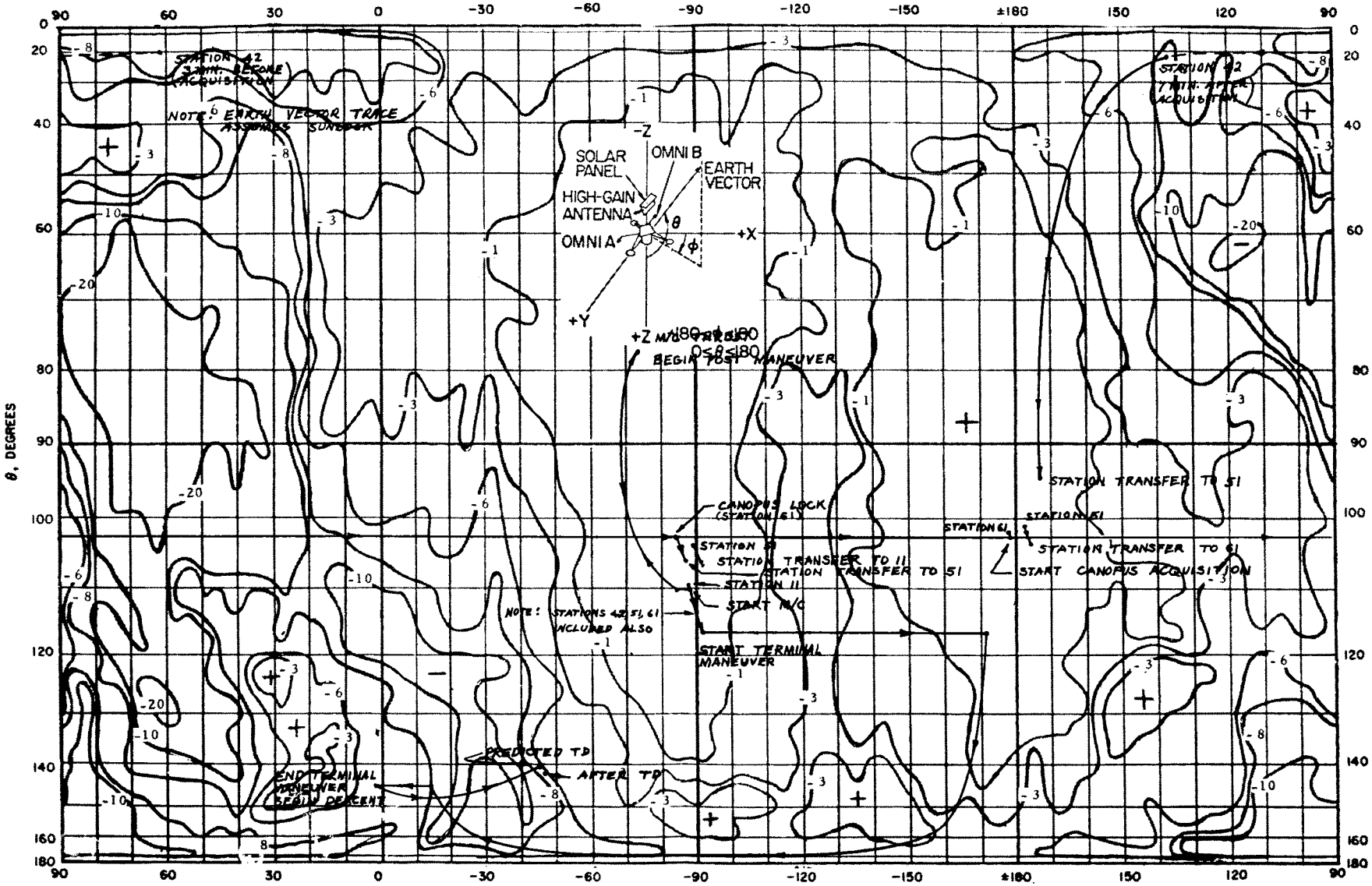

b) Antenna B

Figure 5.3-3 (continued). Omnidirectional Antenna Gain Contours (2113 MHz)

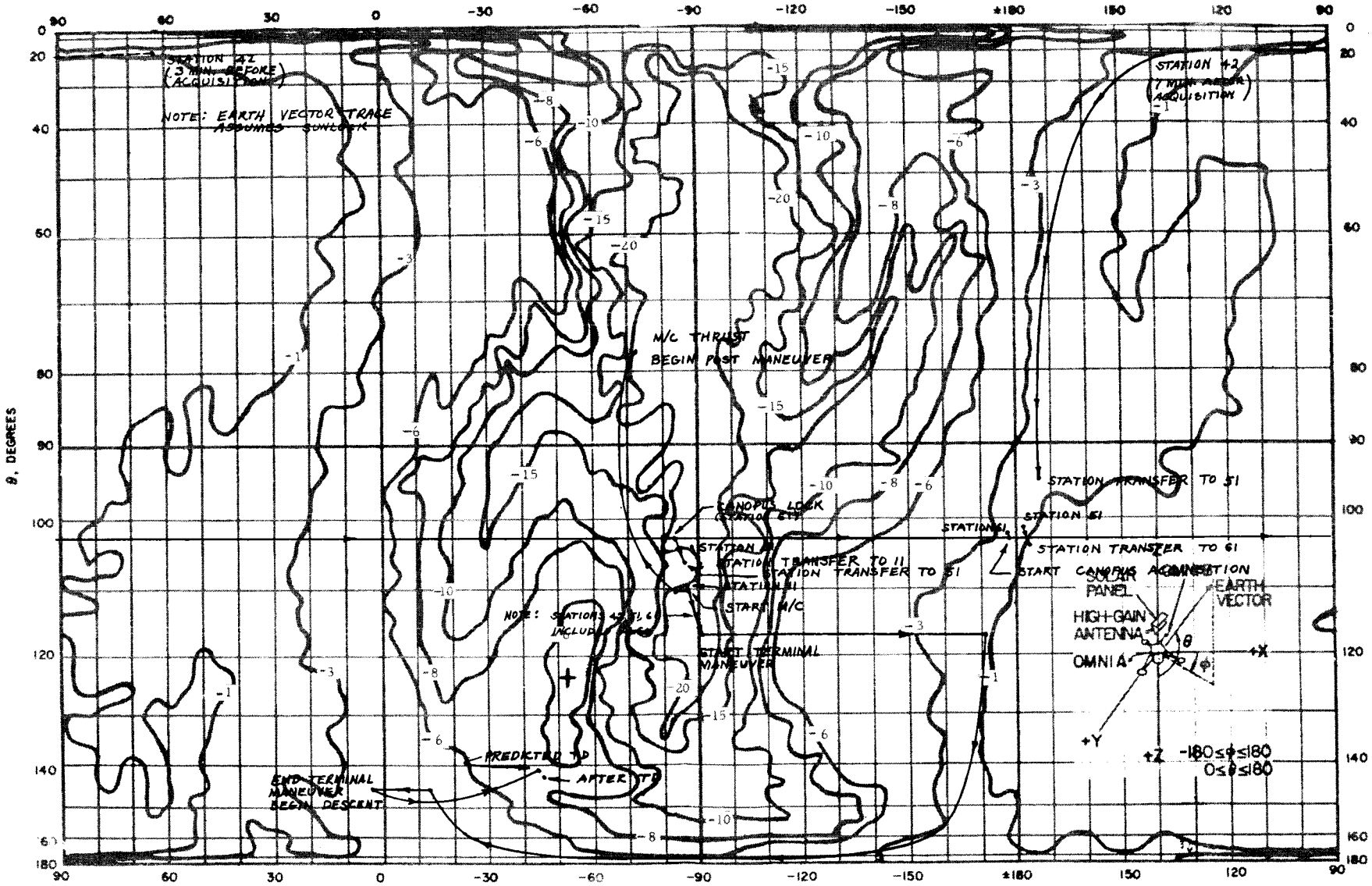

a) Antenna A

Figure 5.3-4. Omnidirectional Antenna Gain Contours (2295 MHz)

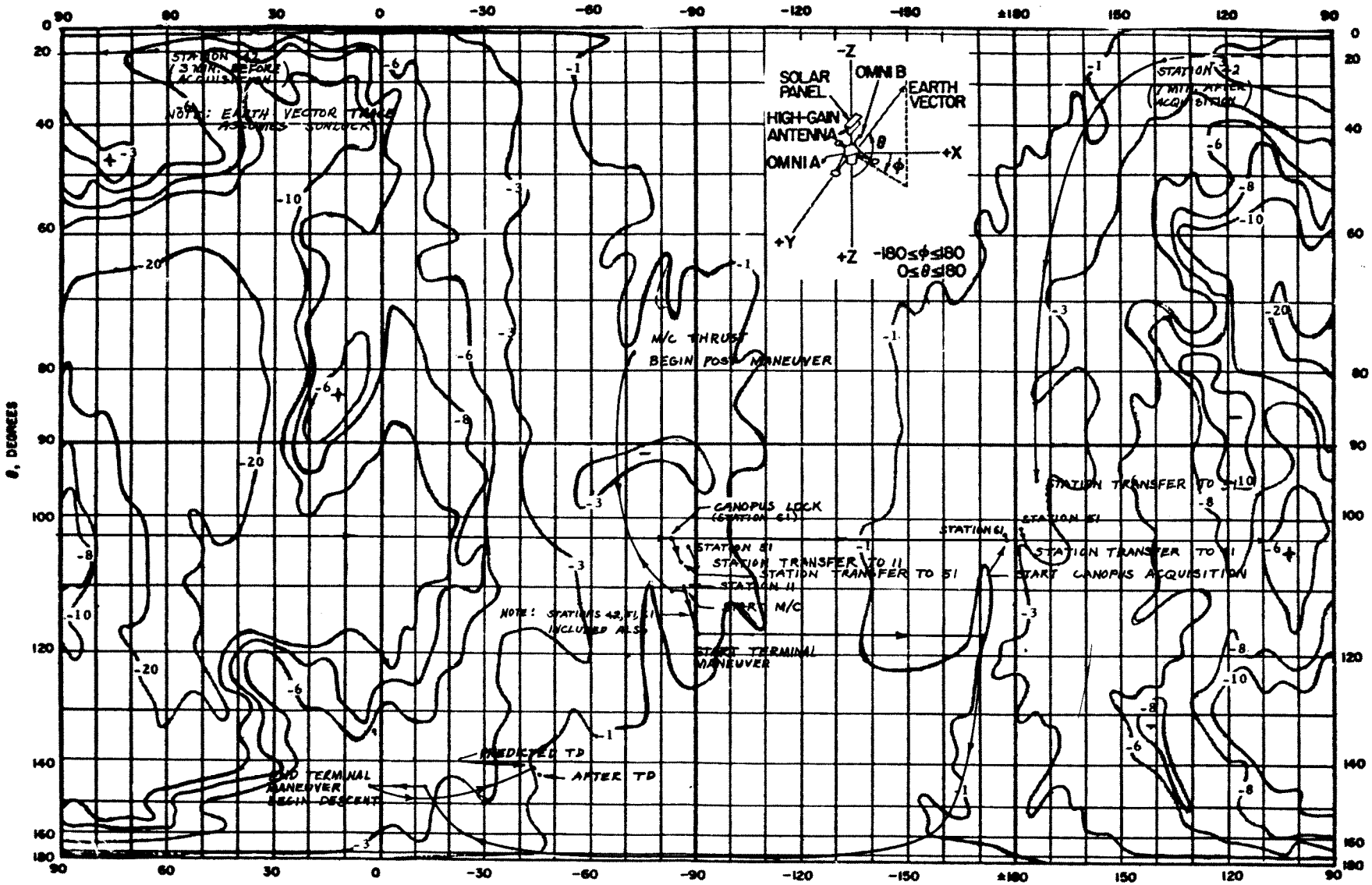

b) Antenna B

Figure 5.3-4 (continued). Omnidirectional Antenna Gain Contours (2295 MHz)

TABLE 5-3.6. PRELAUNCH FREQUENCY SUMMARY*

Frequency Message Time, minutes	Measured Frequencies, MHz		Predicted Acquisition Frequencies, MHz		Lower Tray Temperature, °F
	One-Way Narrow-band Voltage Controlled Crystal Oscillator	Best Lock	One-Way Narrow-band Voltage Controlled Crystal Oscillator	Best Lock	
T-669 (transmitter A)	2295.003688	2113.308304	2295.002188	2113.306804	75
T-565 (transmitter B)	2295.000264	2113.326904	2294.998764	2113.325404	75
T-326 (transmitter A)	2294.998776	2113.305288	2294.997276	2113.303788	78
T-50 (transmitter B)	2295.000712	2113.327416	2294.998962	2113.325666	75
T-30a (transmitter B)	2294.995928	2113.326352	2294.994178	2113.324602	78
T-30b (transmitter B)	2294.994541	2113.325192	2294.992791	2113.323442	85

*Frequencies used by FPAC for initial DSS 42 acquisition were those contained in the T-30a Report.

transmitted from the Cape prior to launch. The Deep Space Station, in turn, uses these data to tune the DSS receiver for one-way lock and the DSS transmitter for eventual two-way lock.

The measured transmitter and receiver frequency data are tabulated in Table 5.3-6. The compartment temperature during the prelaunch period was increasing, thus causing a frequency decrease as expected. The temperature directly affecting the frequency is not actually measured since the telemetered sensor is in the thermal tray and not at the voltage-controlled crystal oscillator. Relative temperature versus frequency information is thus considered to be most reliable. Based on this judgment, the measured frequency data were consistent with previous Surveyor VII test data.

Acquisition frequencies are determined by extrapolating the measured values by essentially predicting the compartment temperature increase due to the high power operation from just prior to Centaur/Surveyor separation to the time of initial spacecraft acquisition. The measured frequencies were biased by -1.75 kHz as determined from data obtained from Reference 2 and assuming 14 minutes of high power operation from injection to initial DSS 42 acquisition.

The actual frequencies at initial DSS 42 acquisition were:

Transmitter (one-way) = 2294.991200 MHz

Receiver (two-way) = 2113.326528 MHz

The difference between final predicted (T-30b report) and actual frequencies were:

Transmitter = 1591 Hz

Receiver = 3068 Hz

Table 5.3-7 is a summary of the significant events during initial RF acquisition at DSS 42 (Canberra). One-way acquisition was accomplished 21 seconds after the predicted first visibility, and good two-way lock was accomplished 7 minutes and 37 seconds later. The spacecraft received signal levels during the initial acquisition phase were -85 dbm for receiver A and -69 dbm for receiver B. Telemetry data also indicated a signal in the passband of both spacecraft receivers at DSS transmitter turn on.

No problems were encountered during initial spacecraft acquisition. The spacecraft high power transmitter was turned off 26 minutes and 47 seconds after being commanded to high power by the Centaur. The maximum allowable time to accomplish turn-off is 1 hour.

TABLE 5.3-7. ACQUISITION EVENTS

Events	GMT (Day 7), hr:min:sec	Comments
Transmitter B high power on	07:05:00	Spacecraft commanded to high power by Centaur
DSS 42 acquires spacecraft one-way on SAA (acquisition aid antenna)	07:20:25	Predicted rise was at 07:20:04
DSS 42 auto tracking on SAA parametric amplifier	07:22:50	
DSS 42 switch from SAA to SCM/maser (85-foot antenna)	07:22:57	
DSS 42 transmitter turn on	07:26:00	
Signal in passband of spacecraft receivers	07:26:07	(From telemetry.) Receiver A in automatic frequency control capture. Receiver B pulling in, not phase locked
Phase lock receiver B	07:27:26	DSS receiver dropped phase lock, indicating phase lock on receiver B
DSS 42 reports good two-way data	07:28:02	Good two-way acquisition 58 minutes and 2 seconds after launch
DSS 42 command modulation on	07:28:40	
Transmitter B high power off	07:31:47	Spacecraft was in high power for 26 minutes and 47 seconds for initial acquisition phase (a maximum time of 1 hour is allowed)

5.3.4.3 Mission Phase 2: Coast

The coast phases consist of the following:

1) Pre-Canopus acquisition – Period from initial spacecraft acquisition until Canopus acquisition. During this time, the spacecraft attitude is uncertain in roll, and the spacecraft -Z axis is pointed toward the sun.

2) Premidcourse – Period from Canopus acquisition until midcourse maneuvers.

3) Postmidcourse – Period from completion of midcourse maneuvers until terminal maneuvers.

Figures 5.3-5 and 5.3-6 are plots of DSS, receiver A, and receiver B signal levels from launch to touchdown. The premission predicted signal level after Canopus acquisition is shown in each figure. Since the spacecraft attitude in roll is uncertain to ±60 degrees about an estimated reference point prior to Canopus acquisition, no premission predictions are made for this period.

Referring to Figures 5.3-3 and 5.3-4, which show traces of the earth vector relative to omnidirectional antenna B down link and omnidirectional antennas A and B up link gain contours, it can be noted that changes in signal levels during the pre-Canopus acquisition phase and right at Canopus acquisition are in complete agreement with the antenna gain contour maps. The approximate antenna gains during the pre-Canopus phase are noted in Table 5.3-8.

Figures 5.3-5 and 5.3-6 indicate that during the premidcourse and postmidcourse coast periods, received signal levels deviated from the predicted values in both the up and down links. Gyro drift checks performed during these two periods account for earth vector variations not taken into consideration when generating the predictions. As pointed out in Reference 3, these minor look angle variations can cause the observed signal level variations. However, the data indicate that the tolerances on the nominal predicted signal level, which also includes antenna gain variations, bound those values seen in the mission data.

At approximately L+61-1/2 hours, the spacecraft data rate was reduced to 550 bits/sec. At 1100 bits/sec data, the received carrier power at DSS 51 had been running approximately -137.0 dbm with a nominal telemetry margin of +1.6 db. Excessive errors in the data were not noted. An error rate count at the station indicated a bit error rate of approximately 0.63×10^{-3} at this time. The 550 bits/sec data rate continued to be the data mode for the remainder of the coast phase.

During the coast phases of the mission, the spacecraft attitude was such that the earth vector to omnidirectional antenna A was in the deep null region of the gain coverage pattern. As a consequence, during the postmidcourse coast period, the signal level in receiver A was not only below

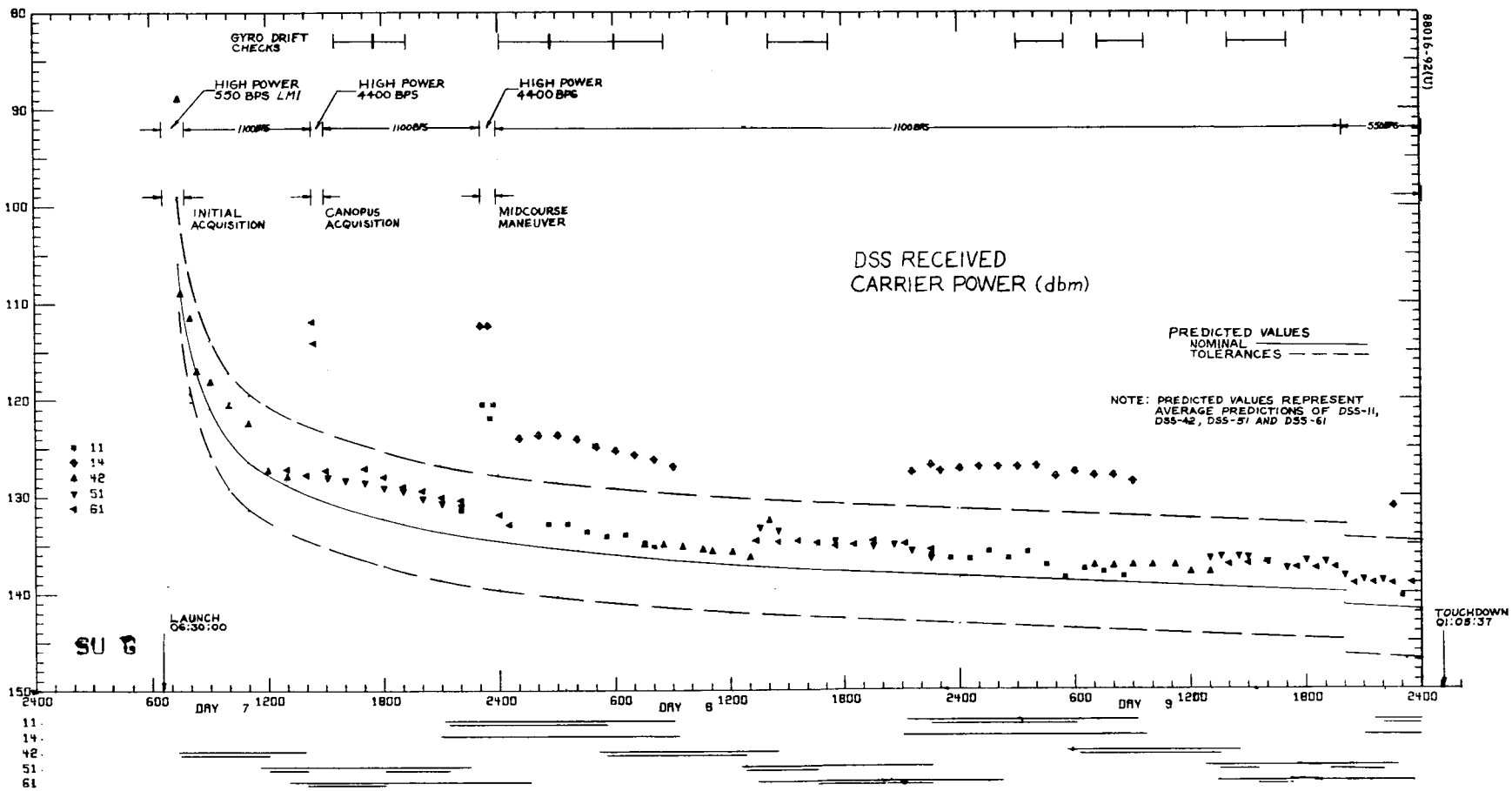

Figure 5.3-5. DSS Received Carrier Power

TABLE 5.3-8. PRE-CANOPUS ANTENNA GAIN VARIATIONS (db)

Omnidirectional Antennas	Gain Variations (Coast)		Pre-Canopus Gain		Gain at Canopus	
	Predicted	Actual	Predicted	Actual	Predicted	Actual
B down link	-1.0 to -3.0	+1.4 to -4.3	-2.9	-0.7	-1.0	+0.3
A up link	-1.0 to -5.0	-3.0 to -7.5	-3.8	-7.2	-10.3	-10.0
B up link	+0.0 to -10.0	+3.0 to -9.1	+1.0	+1.1	+0.5	-0.5

command threshold but also varied around the receiver indexing threshold. Receiver/decoder indices occurred as a result of gyro drift checks and spacecraft limit cycling; however, command activity during this phase is low and no commanding problems occurred. Intentional receiver indexing was performed to assure that receiver B was selected for command processing before commands were transmitted to the spacecraft.

5.3.4.4 Mission Phase 3: Canopus Acquisition Maneuver

At approximately L+8 hours, the star acquisition maneuver was initiated. A total roll of 626 degrees about the Z axis was required to make a star map, to adequately identify Canopus, and to finally acquire the star.

Real-time analysis indicated that the roll maneuver would take the earth vector through the deep null region of both the up and down links of omnidirectional antenna A and the down link of omnidirectional antenna B. The earth vector would not enter the deep null region of the omnidirectional antenna B up link. The two-way transponder B mode was therefore recommended for the acquisition sequence. However, the sequence was performed in the one-way mode since two-way doppler data were not desired for the roll maneuver. The analysis also indicated that no significant stars existed in the vicinity of possible data outages with the spacecraft transmitting via omnidirectional antenna B at a data rate of 4400 bits/sec. One star, Caph, was located in the null region of the transmitting antenna gain pattern, but, due to the star intensity, it was unlikely that it could be identified even with good data.

At 14:18:28 GMT, transmitter B was commanded to high power with the ground received signal indicating an increase of 16.2 db. Star mapping was initiated at 14:24:05 GMT from DSS 61 with the spacecraft operating in the one-way mode and transmitting data at 4400 bits/sec in mode 1. The 360-degree roll produced down link signal variations of approximately 31 db, which agreed with the premaneuver predictions. Data outages

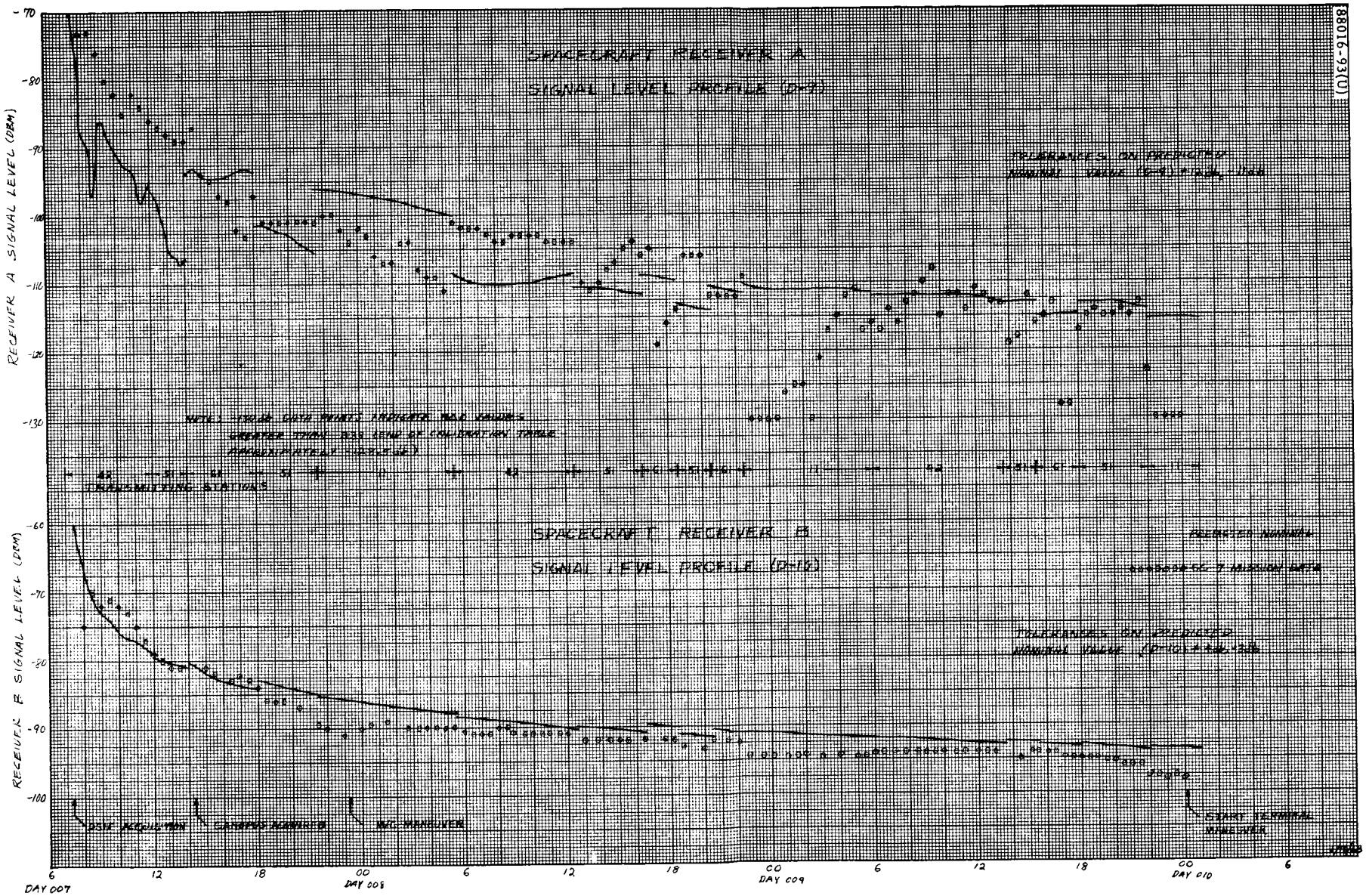

Figure 5.3-6. Spacecraft Receivers A and B Signal Level Profiles

occurred within the predicted region; however, down link carrier lock was maintained throughout the mapping maneuver. Spacecraft received signal levels during the roll maneuver indicated deviations of approximately 31 db on receiver A and 27 db on receiver B. This again agreed with premaneuver predictions. Manual Canopus lockon was successfully commanded at 14:47:32 GMT.

Transmitter B high power was commanded off at 14:56:48 GMT, which resulted in 38 minutes and 20 seconds of high power operation for star acquisition. DSS 61 received signal level for low power operation was -127.3 dbm, with a resulting +11.3 db nominal telemetry margin for 1100 bits/sec data.

Variations in antenna gain seen in the data are compared to predicted variations for both the down and up links and are illustrated in Figure 5.3-7. The correlation between the two sets of data is typical of that observed on previous spacecraft for both the up and down links of omnidirectional antenna B. Lower gain values than predicted are indicated between the -Y axis and -X axis on the omnidirectional antenna A up link. This has been observed on previous spacecraft; however, a null was also observed in the predicted high gain region which starts at the +Y axis and extends for 40 degrees in the direction of the +X axis.

5.3.4.5 Mission Phase 4: Midcourse Maneuvers

The L+16 hours standard roll-yaw was selected from 8 possibilities as the midcourse maneuver. Real-time analysis predicted the following variations in nominal omnidirectional antenna gain during the maneuver:

1) Omnidirectional antenna B down link: $-2.7 < G < -0.3$ db

2) Omnidirectional antenna A up link: $-14.7 < G < -7.9$ db

3) Omnidirectional antenna B up link: $-0.4 < G < +1.4$ db

Predicted minimum margins were 15.7 db for 4400 bits/sec telemetry, 12.2 db on receiver A, and 26.5 db on receiver B command links. Two-way (transponder B) mode was recommended.

At 007:23:02:03 GMT, the spacecraft was commanded to high power and, at 007:23:20:41 GMT, the 4400 bits/sec data rate was selected. The ground received signal increased by 15.6 db when the spacecraft was commanded from low to high power, with DSS 11 reporting a received carrier power of -120.3 dbm prior to maneuvering. Maneuver initiation times were 007:23:18:28 GMT for the roll and 007:23:21:13 GMT for the yaw. The DSS 11 received carrier power at the end of the premidcourse maneuver was reading -121.0 dbm. Signal level variations during the maneuvers are shown in Table 5.3-9.

At 007:23:30:09 GMT, midcourse thrust was executed. DSS 11 received carrier power was steady with reported 0.1-db variations during the thrusting period.

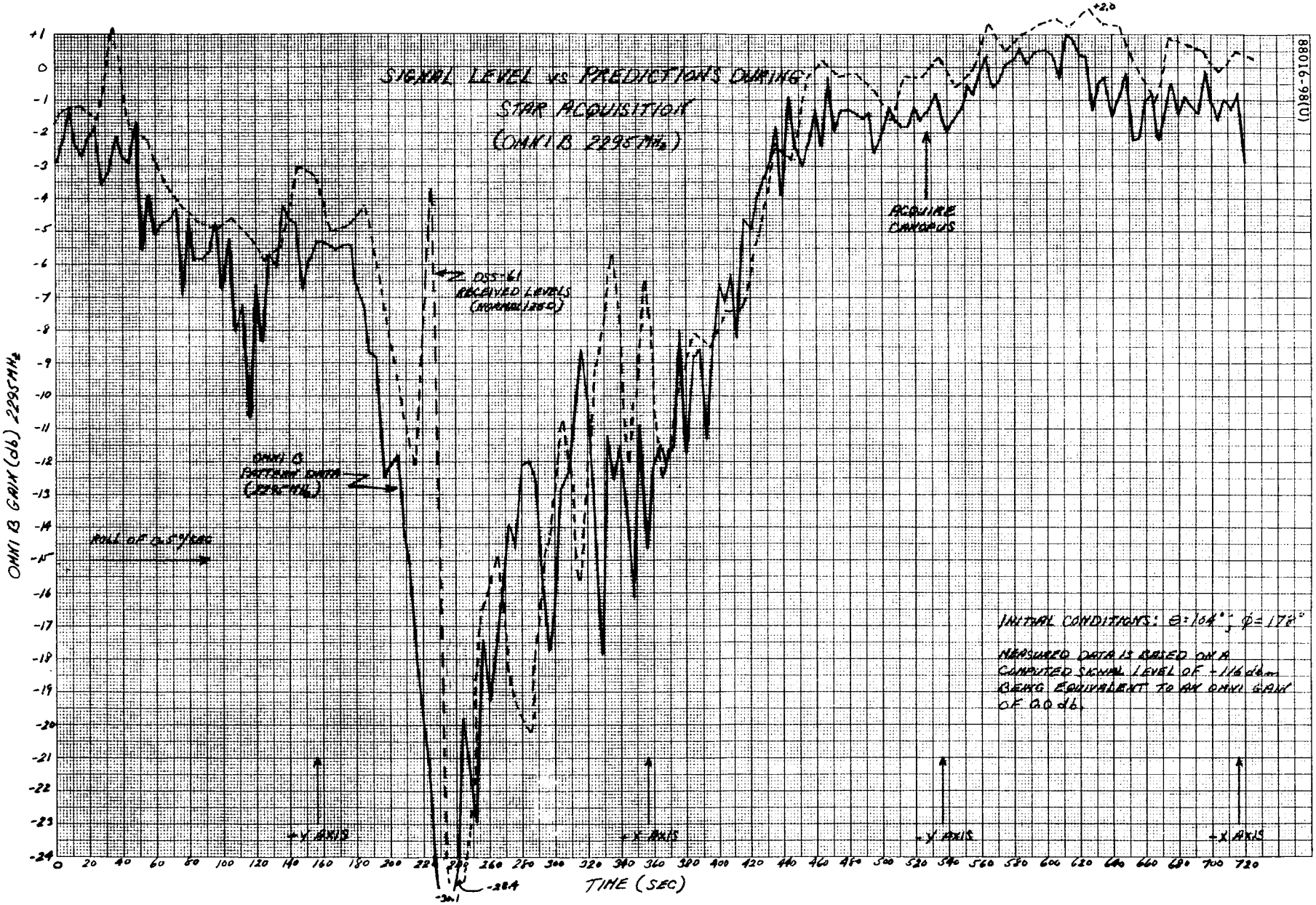

a) Omnidirectional Antenna B (2295 MHz)

Figure 5.3-7. Signal Level Versus Prediction During Star Acquisition

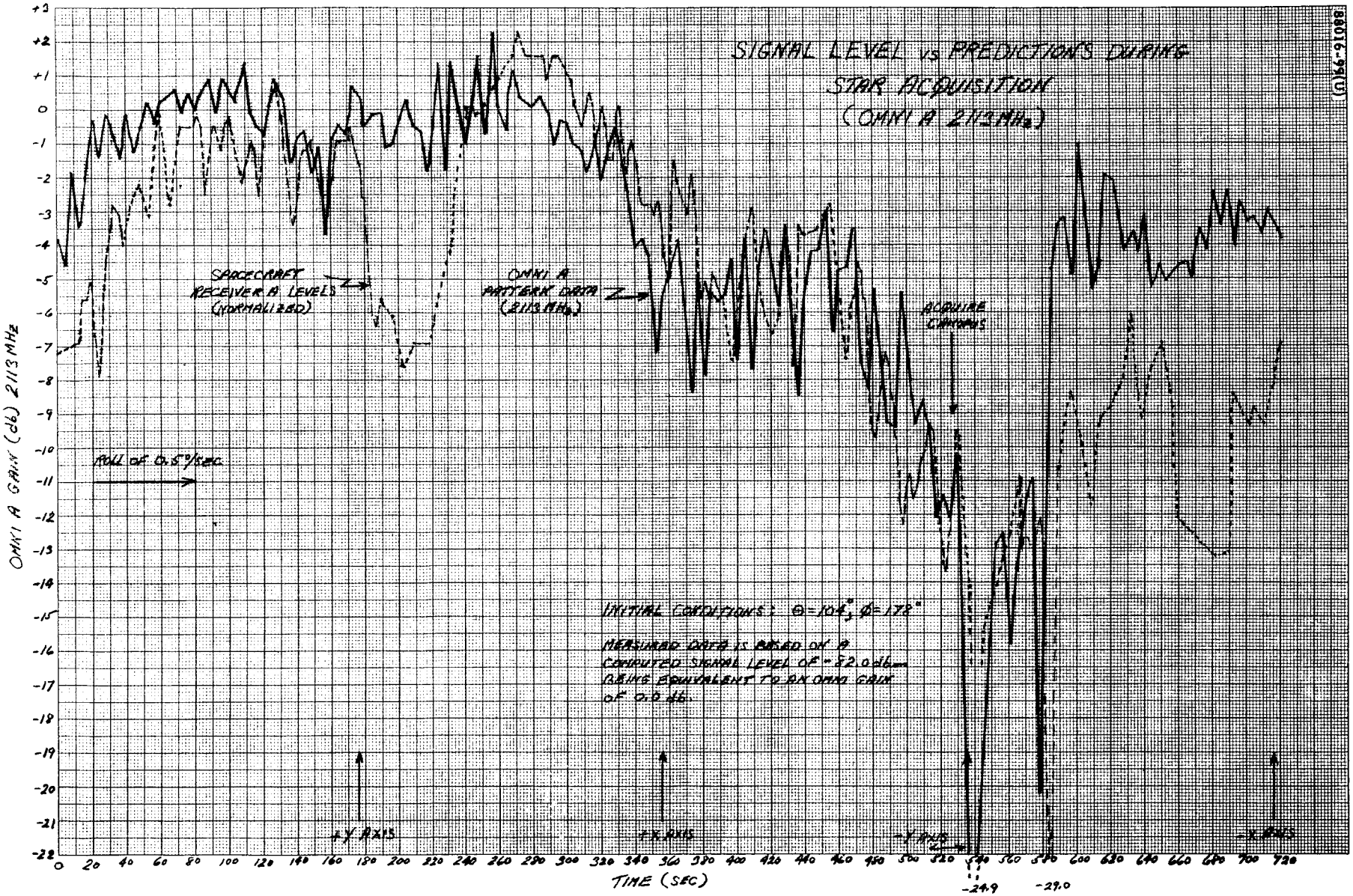

b) Omnidirectional Antenna A (2113 MHz)

Figure 5.3-7 (continued). Signal Level Versus Prediction During Star Acquisition

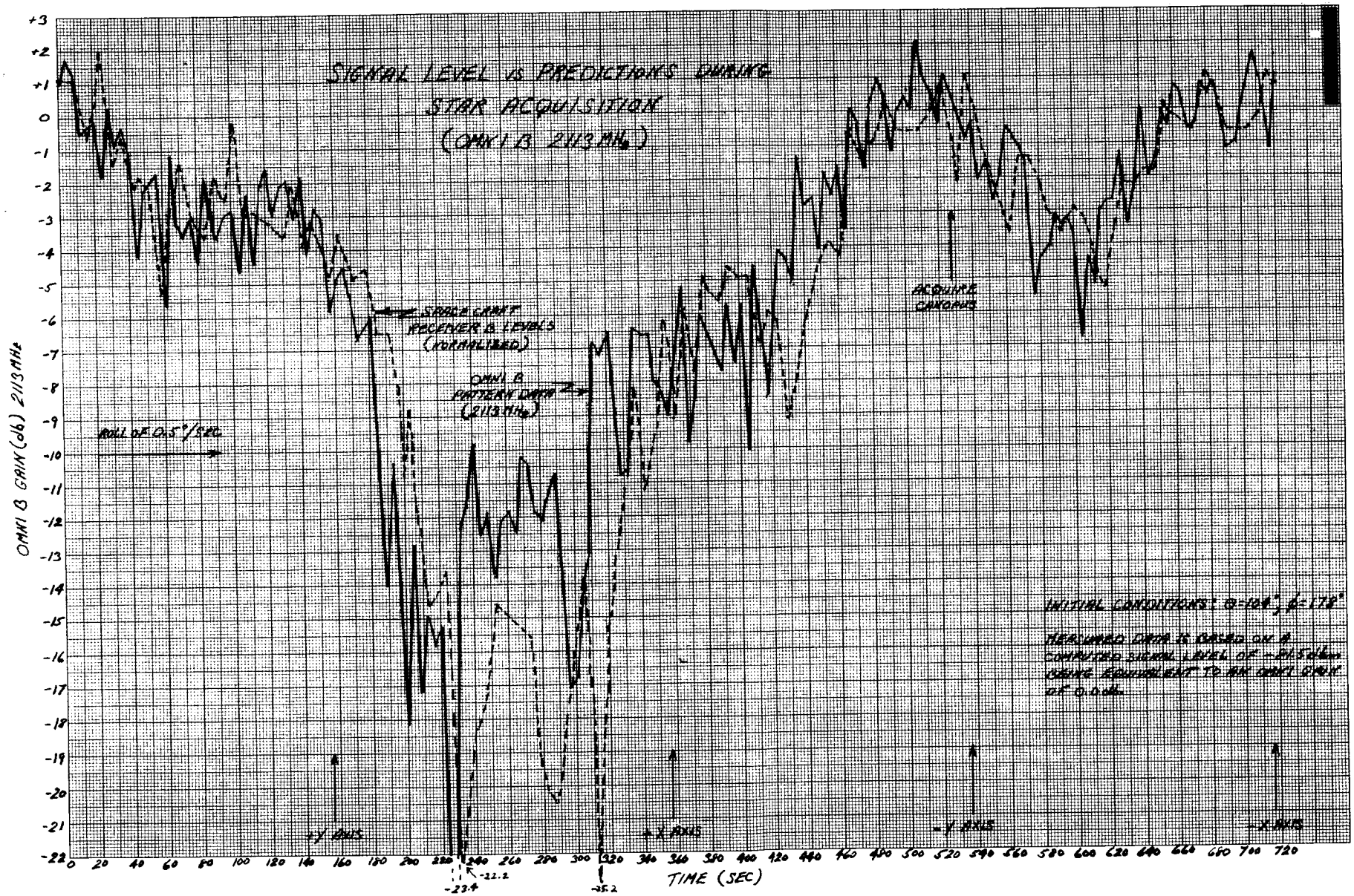

c) Omnidirectional Antenna B (2113 MHz)

Figure 5.3-7 (continued). Signal Level Versus Prediction During Star Acquisition

TABLE 5.3-9. SIGNAL LEVEL VARIATIONS (IN DECIBELS) DURING MIDCOURSE MANEUVERS

Attitude Rotation, degrees	Spacecraft to Earth (Omnidirectional Antenna B)		Earth to Spacecraft			
			Receiver A		Receiver B	
	Predicted	Observed	Predicted	Observed	Predicted	Observed
Roll -3.2	1.1	0.1	6.8	4.2	0.5	6.1
Yaw +117.0	2.4	2.4	5.6	30.4	1.8	2.3
Thrust	—	0.1	—	1.7	—	0.6

At 007:23:31:39 GMT, mode 5 data were selected in preparation for the postmidcourse maneuver. The reverse yaw maneuver was initiated at 007:23:34:11 GMT. Since Canopus was in the sensor field of view at the end of the reverse yaw, it was not necessary to execute the reverse roll maneuver. The up and down link signal levels during the postmidcourse maneuver essentially retraced those seen during the premidcourse maneuver.

Manual Canopus lockon was commanded at 007:23:41:08 GMT, and preparations were made to return the spacecraft to its cruise configuration. At the end of the midcourse sequence, the DSS 11 received carrier power (-120.3 dbm) indicated that a nominal positive telemetry margin should exist with the spacecraft at 1100 bits/sec in low power. At 007:23:49:00 GMT, the 1100 bits/sec data rate was selected and, at 007:23:51:19 GMT, transmitter B high voltage was commanded off. The spacecraft operated in high power for 49 minutes and 16 seconds during the midcourse maneuver sequence. Approximately a 16.3-db decrease from high to low power was noted. The resulting -132.0 dbm received carrier level produced a 6.6-db telemetry margin for 1100 bits/sec data.

5.3.4.6 Mission Phase 5: Terminal Maneuver

The roll-yaw-roll standard maneuver was selected from eight possibilities as the terminal maneuver and was optimum for the communications link. Real-time analysis predicted the following variations in nominal omnidirectional antenna gains during the maneuver:

1) Omnidirectional antenna B down link: $-3.9 < G < +1.0$ db

2) Omnidirectional antenna A up link: $-25.0 < G < -2.0$ db

3) Omnidirectional antenna B up link: $-11.0 < G < 0.0$ db

Predicted minimum margins were 4.7 db for 1100 bits/sec telemetry, -5.9 db on receiver A, and 8.1 db on receiver B command links. One-way mode was recommended even though adequate margins were available for the transponder operation. This recommendation was made since one-way configuration was desired for the terminal descent sequence and, operationally, it was safer to establish before the terminal maneuver.

For the greater part of the coast phase, the earth vector to omnidirectional antenna A was in the deep null region of the antenna gain pattern. At the time of preparation for the terminal sequence, spacecraft limit cycling caused the signal level in receiver A to vary through its indexing signal level value. At all times the signal was well below command threshold for this receiver. During commanding it was necessary to assure that receiver B was selected for command processing; however, receiver indexing at times occurred so frequently that it was necessary to repeat some commands. Commands to select the coast phase commutator, to turn on high power, and to turn off transponder B had to be repeated. The indexing was not a problem during descent since the earth vector to omnidirectional antenna A left the null region after the spacecraft rolled approximately 5 degrees.

The spacecraft was successfully commanded to high power on the second attempt at 00:07:23 GMT of day 10, and 1100 bits/sec data was selected at 00:12:32 GMT. The resulting -123.2 dbm carrier level indicated an increase of 15.9 db over low power operation. Transponder B was turned off at 00:21:51 GMT, establishing the spacecraft configuration for the terminal sequence. Maneuver initiation times were 00:27:14 for the first roll, 00:35:50 for the yaw, and 00:41:07 GMT for the second roll. The received carrier power at DSS 11 of -125.9 dbm at the end of the terminal maneuvers was in agreement with the predicted nominal expected value. Signal level variations during the maneuvers are shown in Table 5.3-10.

TABLE 5.3-10. SIGNAL LEVEL VARIATIONS (IN DECIBELS) DURING TERMINAL MANEUVERS

Attitude Rotation, degrees	Spacecraft to Earth (Omnidirectional Antenna B)		Earth to Spacecraft			
			Receiver A		Receiver B	
	Predicted	Observed	Predicted	Observed	Predicted	Observed
Roll +80.5	1.3	2.2	23.0	>26.6	5.0	3.7
Yaw +96.1	4.3	7.0	2.0	7.0	11.0	10.9
Roll -16.5	1.1	1.9	1.0	0.7	2.0	5.5

5.3.4.7 Mission Phase 6: Descent and Touchdown

A preterminal maneuver analysis was performed to evaluate the expected data link performance during the descent and touchdown phase with the touchdown strain gages on prior to retro ignition. Best estimates of spacecraft worst-case performance during this phase indicated that, with strain gages on, 1100 bits/sec data would be obtained at a bit error rate less than 3×10^{-3} at both DSS 14 (210-foot antenna) and DSS 11 (85-foot antenna) with the spacecraft transmitting on omnidirectional antenna B.

The touchdown strain gages were turned on at 010:00:42:33 GMT. The DSS 11 received carrier power was -125.9 dbm prior to retro ignition, which was in agreement with the predicted nominal value used for the preterminal strain gage feasibility analysis.

Retro burn was initiated at approximately 010:01:02:16 GMT, and the signal level at DSS 11 remained steady with approximately a 0.2-db variation during the burn period. Signal level variations of 3.8 db were noted during descent, with the minimum signal level being -129.1 dbm, which agreed with nominal predictions.

Touchdown occurred at 010:01:05:37.6 GMT with the carrier power at DSS 11 reported as -128.5 dbm. Good engineering data and touchdown strain gage data were obtained, and ground receiver lock was retained through touchdown.

5.3.4.8 Mission Phase 7: Lunar

The data relative to the lunar phase consist of several disjointed topics. The topics applying to the RF subsystem are summarized in the following text.

Post-Touchdown Spacecraft Assessment (Day 010)

Transmitter B high voltage was commanded off at 01:22:50 GMT after having been in high power for 1 hour 15 minutes and 27 seconds during the terminal phase of the mission. A 17.6-db decrease from high to low power was observed. Transmitter A was turned on for the first time since the prelaunch countdown approximately 20 minutes after touchdown. DSS 11 received carrier power was reported to be -125.4 dbm with the spacecraft at 1100 bits/sec data and transmitter A in high power on omnidirectional antenna B. Omnidirectional antenna A was selected with a resulting 2.1-db decrease in the ground received signal. Omnidirectional antenna B was then reselected since it was obviously the favorable transmitting omnidirectional antenna.

Starting at touchdown, fluctuations were noted in the received signal levels of both the up and down links. This condition suggested the presence of the RF multipath situation which is discussed in subsection 5.3.2 (anomaly discussion).

TV Performance

The first 200-line television picture was transmitted approximately 40 minutes after touchdown. Based on reported DSS 11 signal levels, the computed nominal SNR for the first picture was 14.8 ± 1.0 db.

The first 600-line television picture was transmitted approximately 2-1/2 hours after touchdown, shortly after the planar array was roughly aligned with the earth. Based on reported DSS signal levels, the computed nominal SNR for the first picture was 16.3 db.

In both cases, the SNR was high enough to provide good quality detected video data which is apparent in the quality and resolution of the pictures.

Transmitter A was used for 600-line television operation until day 14 when the wide-band voltage-controlled crystal oscillator frequency drifted outside the DSS 11 receiver tuning range. This condition is discussed in subsection 5.3.2 (anomaly discussion). Transmitter B was thus used for television operation until day 21. Transmitter A was reselected for use during the remainder of the first lunar day after a wide-band voltage-controlled crystal oscillator frequency measurement indicated that the frequency had returned to within the necessary range.

Alpha Scattering Performance

The alpha scattering experiment was performed during much of the first lunar day. The total power at the ground station, with the planar array pointed toward the earth, was reported to be, in general, approximately -110 dbm. This signal level for the 1100 bits/sec/alpha scattering multiplex mode resulted in nominal SNRs of 25.0 db for the 1100 bits/sec data, and 21.9 and 20.7 db for the two alpha scattering channels. Good quality data, therefore, were expected and received for this experiment.

RF Assessment

One spacecraft RF performance assessment was made on day 15 with DSS 42 providing ground support. This assessment essentially exercises the subsystem in all possible transmitting and command receiving configurations. During this assessment, all aspects of the subsystem performed in a nominal manner.

5.3.5 REFERENCES AND DOCUMENTATION

1) W.G. Moore, "Periodic AGC Fluctuations During SC-7 Lunar Operation," Hughes Aircraft Company, IDC 2292/454, 23 February 1968.

2) "Final Report, Surveyor Spacecraft 7 Mission Operations System Compatibility Test (Conducted at AFETR)," Jet Propulsion Laboratory, November 1967.

3) "Surveyor III Flight Performance Final Report," Hughes Aircraft Company, SSD 68189-3, July 1967.

4) "Surveyor Mission G Space Flight Operations Report," Hughes Aircraft Company, SSD 88016, February 1968.

5) "Surveyor Mission G Telecommunication Subsystem Prediction and Performance Summary Document," Hughes Aircraft Company, SSD 74154, 1 December 1967.

6) J.J. Dragovan, "Telemetry Calibration Data for SC-7 Rev. (B)," Hughes Aircraft Company, IDC 2294.2/174, 27 November 1967.

7) J.J. Dragovan, "Command Receiver (A) S/N 21 and Receiver (B) S/N 24 AGC Calibration in a Space Environment," Hughes Aircraft Company, IDC 2294.2/182, 17 October 1967.

8) "Surveyor V Flight Performance Final Report," Hughes Aircraft Company, SSD 68189-5, November 1967.

5.3.6 ACKNOWLEDGMENTS

1) J.O. Votaw was the coordinator and author of this section.

2) Q.D. Howard and W. Mitchell for their assistance in reducing, formatting, and analyzing much of the data contained in this section.

3) The Deep Space Station tracking advisors at JPL for supplying ground station data.

4) The Spacecraft Performance/Analysis/Command Telecommunications Team, consisting of V.S. Amstadter, W. Mitchell, W.G. Moore, Q.D. Howard, and M.R. Weiner, for maintaining accurate mission records and logs.

5.4 SIGNAL PROCESSING

5.4.1 INTRODUCTION

The signal processing subsystem is composed of the following units:

1) Engineering signal processor (ESP)

2) Auxiliary engineering signal processor (AESP)

3) Central signal processor (CSP)

4) Signal processing auxiliary (SPA)

5) Low data rate auxiliary (LDRA)

These units, containing two electronic commutators with 6 operational modes, 2 analog-to-digital converters that have available 5 digital bit rates, 17 subcarrier oscillators for transmission of pulse coded modulation data and continuous real-time data, 9 summing amplifiers, and a signal conditioning subsystem, performed normally throughout the mission.

A summary of test and flight values for signal processing telemetry can be found in Table 5.4-1. Values for the Surveyor I, 2, III, 4, V, and VI flights have been included for comparison.

5.4.2 ANOMALIES

There were no anomalies in the signal processing subsystem throughout the transit flight.

5.4.3 SUMMARY

The signal processing subsystem performed properly throughout the transit flight. A thorough analysis of the touchdown strain gages was performed in which computerized signal processing techniques were used, such as diversity combining and digital filtering. An alpha scattering bit error rate of 10^{-6} was determined from the received data.

TABLE 5.4-1. COMPARISON OF SIGNAL PROCESSING VALUES FROM TEST AND FLIGHT

Telemetry Signal	Surveyor VII STV-A1 Retest Values	Surveyor VII Flight Values	Surveyor VI STV-A1 Retest Values	Surveyor VI Flight Values	Surveyor V Flight Values, Day 251	Surveyor 4 STV Retest Values	Surveyor 4 Flight Values, Day 197	Surveyor III STV-C4 Retest Values	Surveyor III Flight Values, Day 107	Surveyor 2 Flight Values	Surveyor 1 Flight Values
S-1 reference voltage, volts*	4.89	4.885	4.895	4.89	4.90	4.88	4.875	4.86 to -4.9	4.86	4.9	4.88
S-2 reference return, volts*	0.00244	0.00244	0.00244	0.0024	0.0024	0	0	0	0	0.003	0.0024 to 0.0072
S-5 ESP commutator unbalance current, microamperes*	-0.06701	-0.06701	0.32	0.32	-0.7649	-1.7	-1.714	-2.2 to -2.6	-2.1	-1.4	-3.1
S-7 AESP commutator unbalance current, microamperes**	-2.403	-2.198	-0.9669	-0.7618	-2.062	-3.0	-2.813	-1.0 to -1.2	-1.3	-1.7	-2.8
S-8 AESP reference voltage, volts***	4.943	4.934	4.958	4.948	4.95		4.938		4.94	4.94	4.938

*Mode 4.

**Mode 5.

***Mode 5; values before Surveyor V are computed.

5.4.4 SIGNAL PROCESSING ANALYSIS

5.4.4.1 Unbalance Current Corrections

In each telemetry commutator, transistor switches connect each analog output voltage (representing a spacecraft voltage, current, or temperature) with a common commutator line connected to the input of one of two analog-to-digital converters. A bootstrap unloader circuit is connected to this common line to reduce the stray capacitance, equalize the load impedance, and provide bias currents for the commutator and master switches. Since these bias currents are not exactly equal, a difference or unbalance current exists. The telemetry circuit being sampled supplies this unbalance current, causing an error in the measured voltage proportional to the output impedance of the circuit.

The unbalance current for a specific telemetry channel in each commutator (S-5 for ESP and S-7 for AESP) is measured in telemetry modes 4 and 5, with typical values given in Table 5.4-1.

5.4.4.2 Potentiometer Reference Voltage Corrections

The nominally 4.85 reference voltage is supplied by either the ESP or AESP units to the landing gear and solar panel position potentiometers, to the propulsion pressure transducers, and to the secondary sun sensors. This reference voltage, derived from the 29-volt nonessential bus, varies due to load and input supply voltage changes. The ESP voltage is telemetered in modes 2 and 4, and can be used to correct the affected signals, whose calibrations are based on a reference voltage of exactly 4.85 volts. The AESP voltage was not telemetered prior to the Surveyor V spacecraft; therefore, the values given in Table 5.4-1 for earlier spacecraft were obtained by computation.

5.4.4.3 Current Calibration Signals

Current measurements are accomplished by measuring the voltage drop across a low resistance shunt which is in series with the power line being monitored. This measurement is in the range of 0 to 100 millivolts. Since this voltage is not referenced to ground and is not scaled to the 0- to 5-volt telemetry input level range, amplification and ground reference are provided by a differential amplifier. The nominal gain of this amplifier is 50, but its actual gain linearity and stability are not specified to a tight tolerance. To determine the current amplifier parameters and thereby increase the accuracy of current measurements, three calibration signals (with 0.2-percent stability) are introduced into the differential amplifier and telemetered in each commutator. These signals can thus be used by post-mission processing for a continual in-flight calibration of the current measurement amplifier.

The majority of Surveyor VII transit flight data was in modes 5 and 6. The AESP current calibration signals were analyzed for stability of the current measurement amplifier. Table 5.4-2 indicates that the amplifier has changed by no more than 0.5 percent (since initial setting at flight acceptance test).

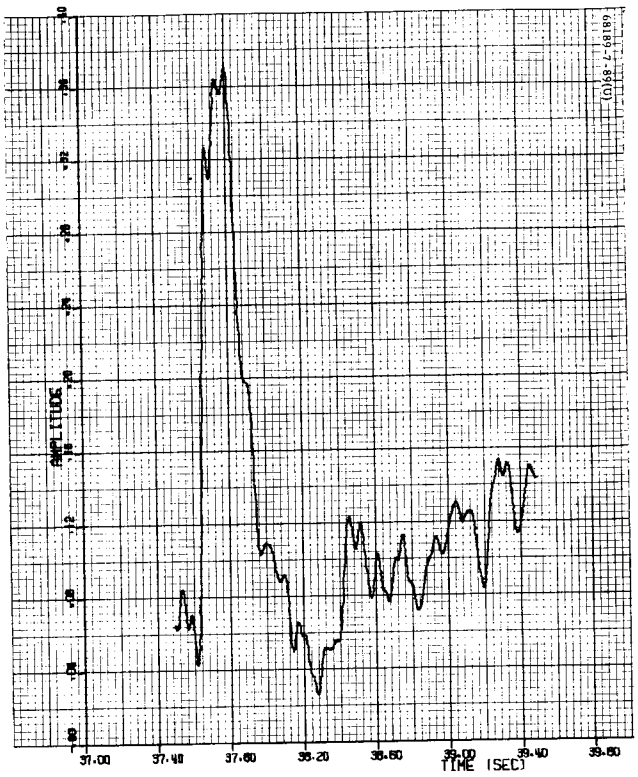

a) Strain Gauge 1

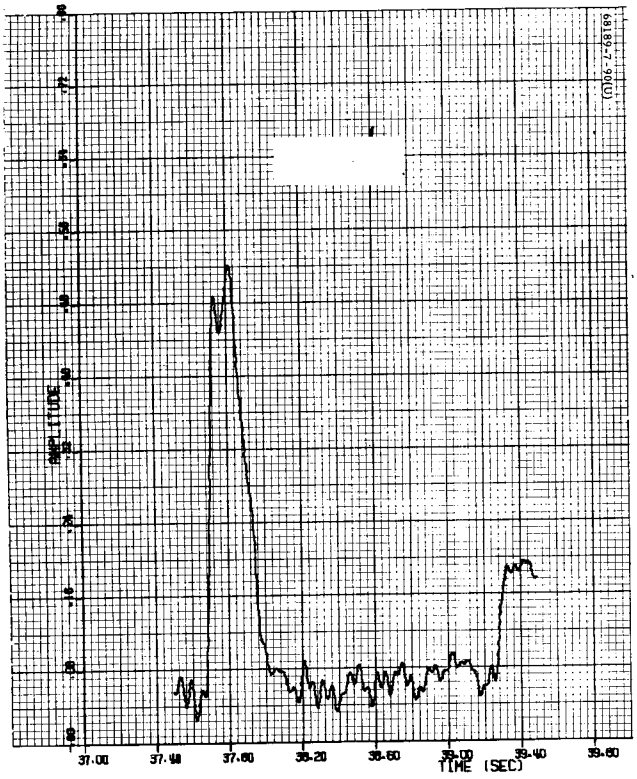

b) Strain Gauge 2

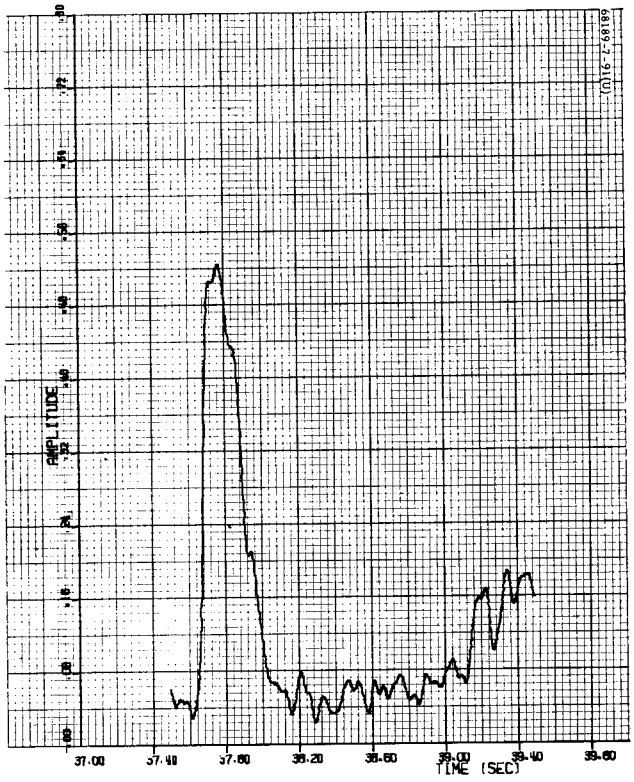

c) Strain Gauge 3

Figure 5.4-1. Diversity Combined 50-Hz Bandwidth

TABLE 5.4-2. SUMMARY OF CURRENT CALIBRATION SIGNAL DATA IN AESP

Signal	Nominal Percent of Full Scale	Flight Data, percent change	Remarks
EP-27	90	0.2164	Before midcourse
		0.2164	After midcourse
EP-28	50	0.4342	Before midcourse
		0.2389	After midcourse
EP-29	10	0.3469	Before midcourse
		0.2493	After midcourse

5.4.4.4 Touchdown Strain Gage Data

Magnetic tape data were obtained from two DSIF stations via the 85-foot diameter antenna at the Pioneer site and the 210-foot diameter antenna at the Mars site. These two independent signal paths allow the technique of space diversity combining (References 1 and 2) to be used on the two sets of touchdown strain gauge data, resulting in a signal trace with improved signal-to-noise ratio.

Footpad impact times were as follows:

Leg 1: 010:01:05:37.620 ± 0.02

Leg 2: 010:01:05:37.670

Leg 3: 010:01:05:37.650

The original data were recorded with a cutoff frequency of 100 Hz. They were then low-pass filtered (by means of digital filtering on a computer) at 100-, 50-, 30-, and 15-Hz (-3db) bandwidths before being diversity combined. This method provided better signal-to-noise ratios on the waveforms that were filtered by the 30- and 15-Hz bandwidths, because of intermodulation distortion components at approximately 45 to 50 Hz. This can be seen by comparing Figure 5.4-1 (50-Hz bandwidth) with Figure 5.4-2 (30-Hz bandwidth).

Figure 5.4-3 shows strain gages 1, 2, and 3 filtered by a sixth order Butterworth filter with a 15-Hz bandwidth. Figures 5.4-1, 5.4-2, and 5.4-4 are similar with filter bandwidths of 50, 30, and 100 Hz, respectively.

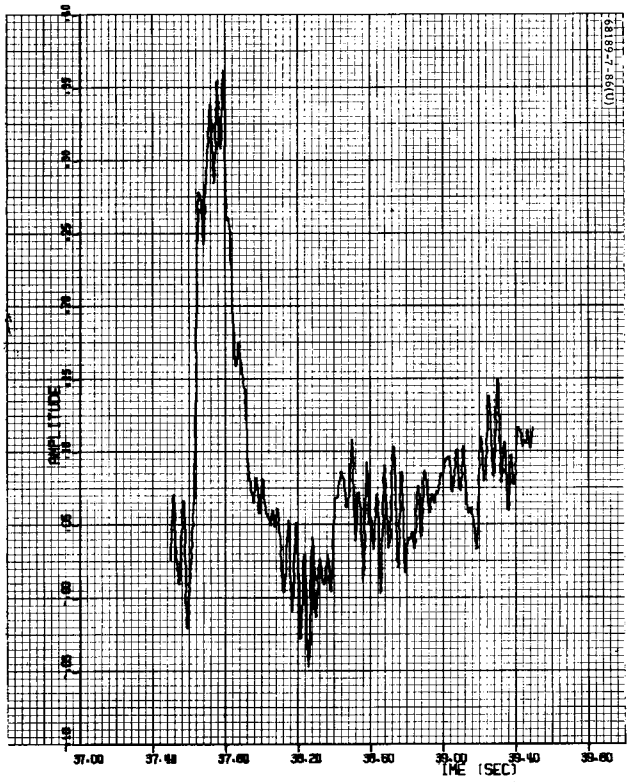

a) Strain Gauge 1

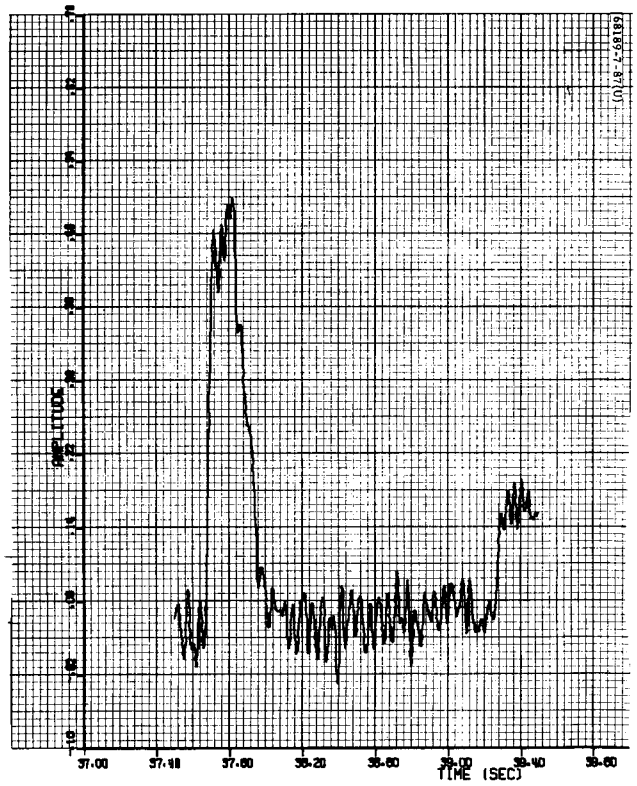

b) Strain Gauge 2

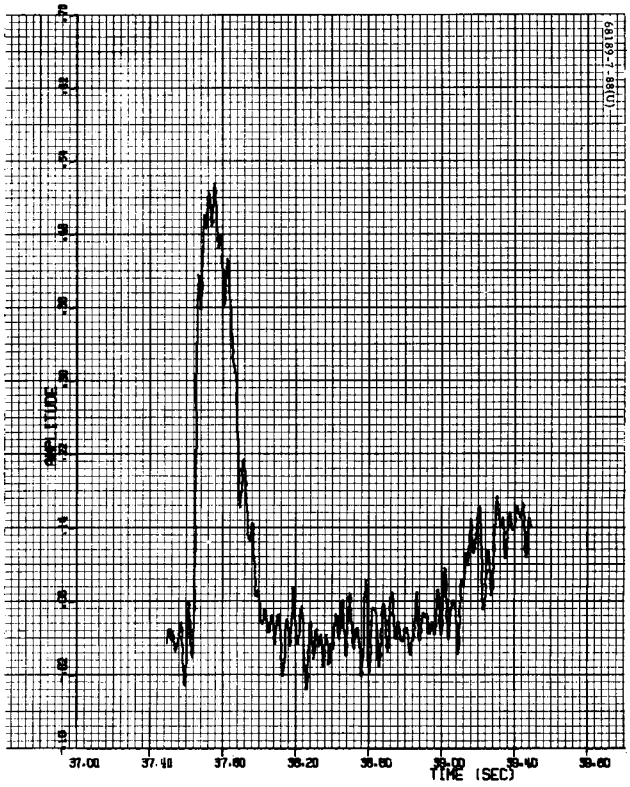

c) Strain Gauge 3

Figure 5.4-2. Diversity Combined 30-Hz Bandwidth

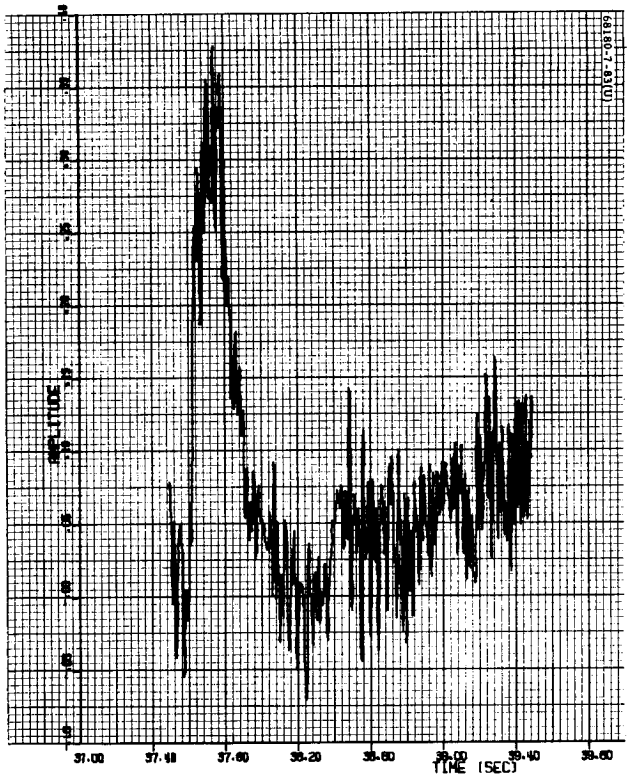

a) Strain Gauge 1

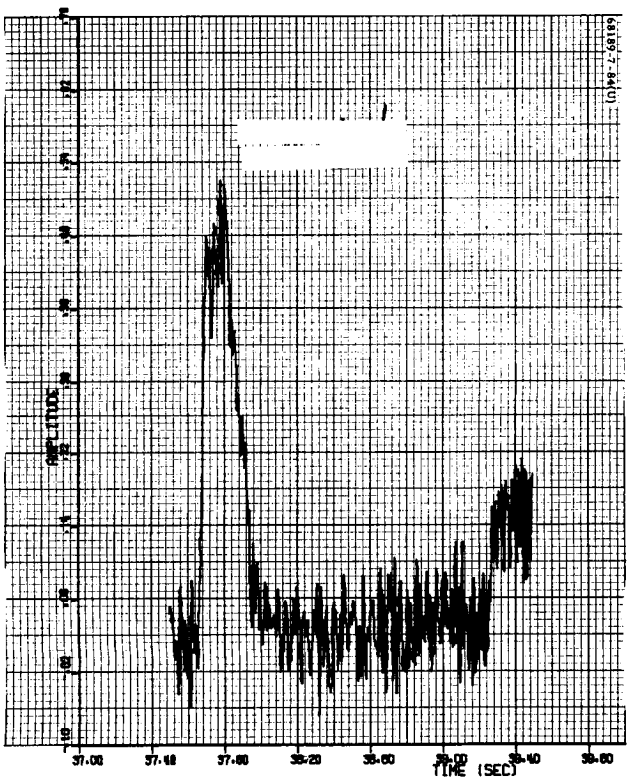

b) Strain Gauge 2

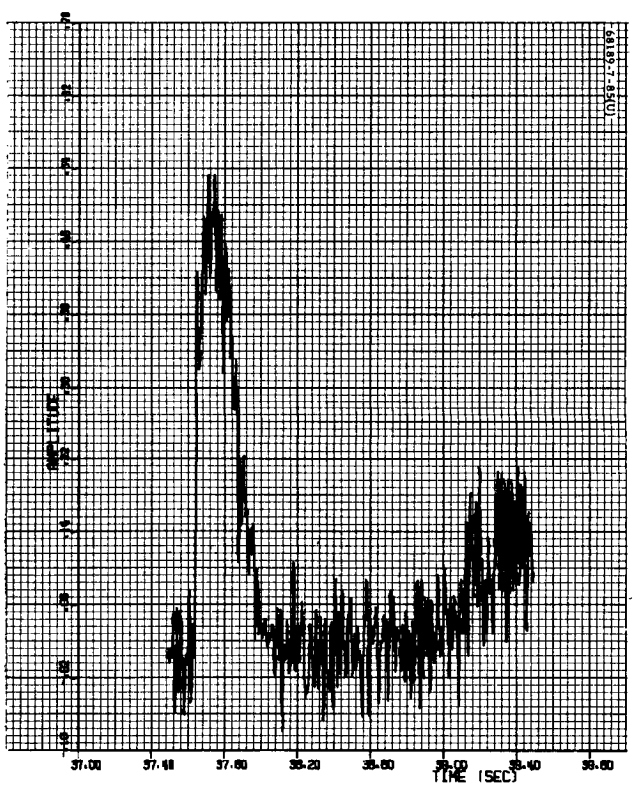

c) Strain Gauge 3

Figure 5.4-3. Diversity Combined 15-Hz Bandwidth

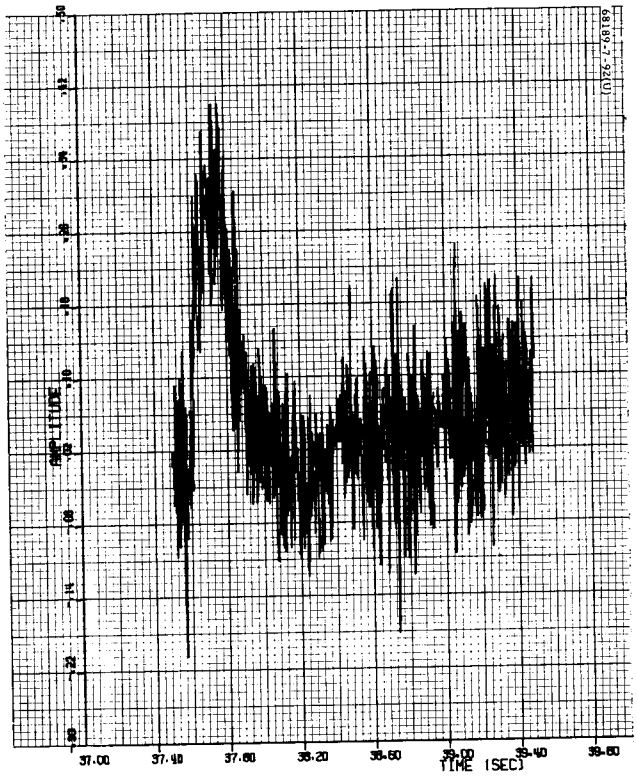

a) Strain Gauge 1

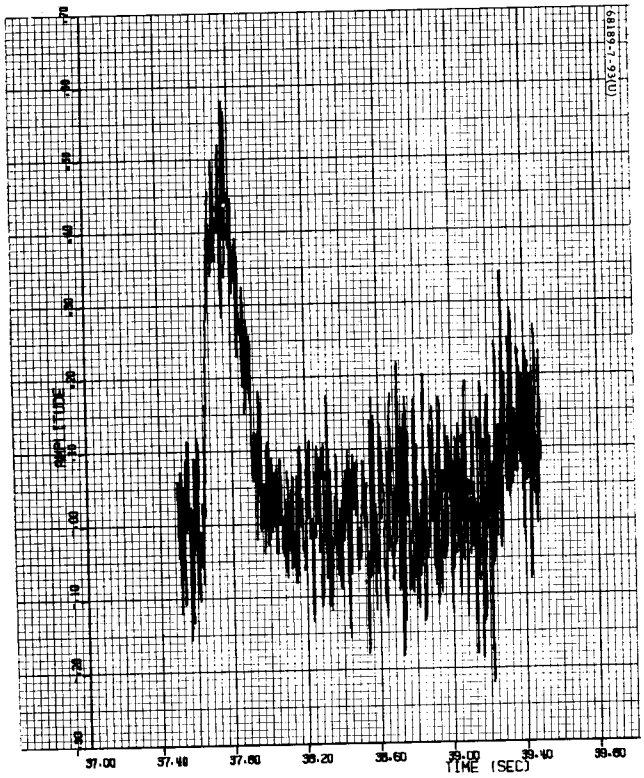

b) Strain Gauge 2

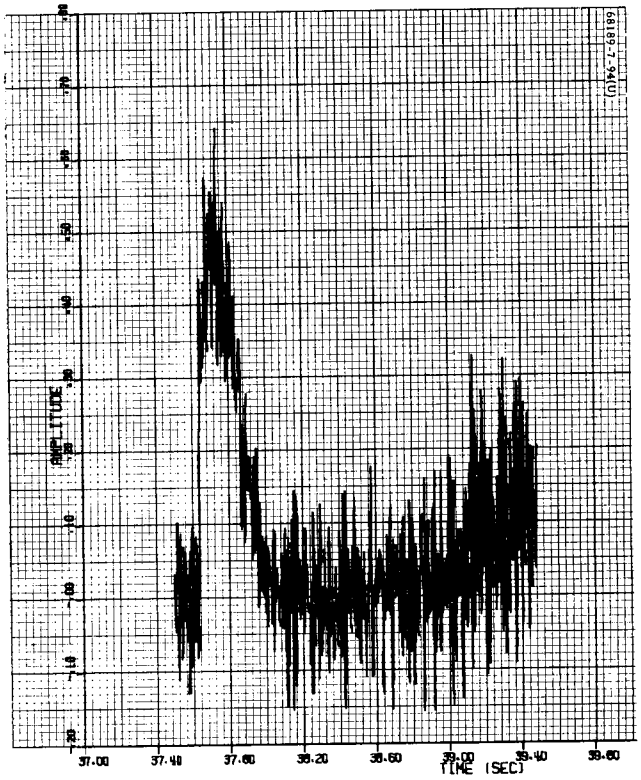

c) Strain Gauge 3

Figure 5.4-4. Diversity Combined 100-Hz Bandwidth

5.4.5 DOCUMENTATION

1. A. W. Dittmer, "The Use of Diversity Receiving Techniques to Enhance Surveyor SC-1 Strain Gage Signals," Hughes IDC 2292/188, 10 January 1967.

2. A. W. Dittmer, "Computer Analysis and Prediction of Surveyor Spacecraft (SC-1) Strain Gage Signals," Hughes IDC 2292/85, 1966.

3. R. J. Rechter, "Computer Analysis of SC-3 through SC-7 TSG Multiplex Intermodulation Distortion and Other Factors," Hughes IDC 2292/223, Revision 1, March 1967.

4. M. Fashano and R. J. Rechter, "DTRB-21 Test Procedures, Results and Summary (TSG Multiplex)," Hughes IDC 2292/267, 5 May 1967.

5.4.6 ACKNOWLEDGMENTS

This section was coordinated by A. W. Dittmer. The touchdown strain gage diversity combining and filtering was done by W. W. Mayfield.

5.5 FLIGHT CONTROL

5.5.1 INTRODUCTION

The principal requirements of the Surveyor flight control system are attitude control, accurate angular maneuvers, precision velocity corrections, and a soft lunar landing. In order to accomplish these functions, the control system utilizes such hardware as gyros, gas jets, a solid fuel engine, liquid fuel engines, optical sensors, timing devices, radars, and acceleration sensing mechanisms.

5.5.1.1 Attitude Control

Attitude control is accomplished by two basic types of active control systems. During coast phase, a bang-bang type of attitude gas jet system is employed which utilizes artificial rate feedback for loop stabilization. During periods of potentially large moment disturbances, such as the main retro phase, the throttle-controlled vernier engine system is used. The error signals required for controlling the propulsion systems are derived from optical sensors or rate integrating gyros which are mounted on the spacecraft in such a way as to provide a three-axis control system. During coast phase, when the gas jet system is used, two modes of operation are available. One is the celestial referenced mode using the sun and Canopus, and the second is self-contained inertial referencing (gyros). The first mode is used to establish accurate spatial attitude, and the second mode is generally used when an inertial reference is desired, such as during an attitude maneuver.

5.5.1.2 Angular Maneuvers

The rate integrating gyros are also used for accurate angular maneuvers, accomplished by precessing the gyros at precise rates for given time intervals and slaving the spacecraft to the gyros through the gas jet system.

5.5.1.3 Velocity Correction

A midcourse velocity correction capability is provided by a system consisting of three vernier engines, a precision timer, and an accurate accelerometer. The difference between the commanded acceleration level and the output from an accelerometer provides the error signal that commands the vernier engines to the required thrust levels. The constant

acceleration and variable time concept used by the Surveyor flight control system provides the flexibility of choosing velocity corrections from 2.0 to 100 m/sec.

5.5.1.4 Soft Landing

Surveyor's soft landing capability is provided by a sophisticated technique utilizing radars to compute velocities and range. The range information is then used by an on-board computer to provide vertical velocity commands to the vernier engine system according to an approximate, constant acceleration, V^2/R function. The velocity information is used by the vernier engine attitude control loop to produce a near-gravity turn descent by aligning the spacecraft thrust axis to the true velocity vector. The velocity information is also used, along with velocity commands, to generate error signals for the velocity control loop.

To provide the required condition of low velocity for the soft landing phase, a large amount of approach velocity is removed by a solid fuel rocket engine during the initial portion of the terminal descent phase. Spacecraft attitude during this phase is inertially stabilized by the gyro/vernier engine control system.

5.5.1.5 Mission Performance

During the Surveyor VII mission, each of the above mentioned tasks was performed satisfactorily.

5.5.1.6 Analysis

Subsection 5.5.4 contains the analysis effort. The analysis items are categorized under major mission phases for easier identification and performance evaluation. A log of time and events is presented in Table 5.5-1, and a table of results (Table 5.5-2) is given in subsection 5.5.3.

5.5.2 ANOMALY DESCRIPTION

The only flight control anomaly that occurred during the mission was the absence of a star lockon signal when the star Canopus was in the Canopus sensor field of view, thereby making it necessary to acquire Canopus manually as was done in Missions A and B. The anomaly is believed to be due to either the uncertainties associated with calibration of the sensor or presence of contamination in the sensor sun channel which partially blocked it and made the sun appear dimmer.

5.5.3 SUMMARY

A summary of flight control performance is presented in Table 5.5-2.

TABLE 5.5-1. SURVEYOR VII TIME AND EVENTS LOG

Event	Date, GMT	Mission Time	
		GMT, hr:min:sec	From Launch
Launch	7 January 1968	06:30:00	0
Injection		07:05:16	35M16S
Separation			
Electrical		07:05:10	35M10S
Mechanical		07:05:16	35M16S
Automatic sun acquisition			
Start		07:06:01	36M01S
Completed		07:14:44	44M44S
Canopus verification, started		14:18:28	7H48M28S
Canopus acquisition, completed		14:47:32	8H17M32S
Gyro drift check No. 1			
Start		15:36:00	9H06M00S
Stop		17:31:27	11H01M27S
Gyro drift check No. 2			
Start		17:36:32	11H06M32S
Stop		19:09:44	12H39M44S
Premidcourse roll, 3.1 degrees			
Start		23:18:29	16H48M29S
Stop		23:18:35	16H48M35S

Table 5.5-1 (continued)

Event	Date, GMT	Mission Time	
		GMT, hr:min:sec	From Launch
Premidcourse (+) yaw, 117.1 degrees			
Start		23:21:14	16H51M14S
Stop		23:25:08	16H55M08S
Midcourse thrust executed		23:30:10	17H00M10S
Sun reacquired		23:37:43	17H07M43S
Canopus reacquired		23:41:08	17H11M08
Gyro drift check No. 3	8 January 1968		
Start		00:04:10	17H34M10S
Stop		02:43:58	20H13M58S
Gyro drift check No. 4 (roll only)			
Start		02:48:54	20H18M54S
Stop		06:02:40	23H32M40S
Gyro drift check No. 5			
Start		06:06:21	23H36M21S
Stop		08:36:47	26H06M47S
Gyro drift check No. 6			
Start		04:02:21	31H32M21S
Stop		17:14:32	34H44M32S
Gyro drift check No. 7	9 January 1968		
Start		03:05:43	44H35M43S
Stop		05:34:23	47H04M23S

Table 5.5-1 (continued)

Event	Date, GMT	Mission Time	
		GMT, hr:min:sec	From Launch
Gyro drift check No. 8			
Start		07:16:22	48H46M22S
Stop		09:48:31	51H18M31S
Gyro drift check No. 9			
Start		14:00:04	55H30M04S
Stop		17:04:16	58H34M16S
Preretro (+) roll, 80.5 degrees	10 January 1968		
Start		00:27:17	65H57M17S
Stop		00:29:58	65H59M58S
Preretro (+) yaw, 96.1 degrees			
Start		00:35:52	66H05M52S
Stop		00:39:04	66H09M04S
Preretro (-) roll, 16.5 degrees			
Start		00:41:10	66H11M10S
Stop		00:41:43	66H11M43S
AMR mark		01:02:12	66H32M12S
Vernier ignition		01:02:15	66H32M15S
Retro eject		01:03:11	66H33M11S
1000-foot mark		01:05:13	66H35M13S
14-foot mark		01:05:36	66H35M36S
Touchdown		01:05:38	66H35M38S

TABLE 5.5-2. FLIGHT CONTROL RESULTS

	Controlling Specification	Specification Value	Results	Comments
Prelaunch				
Proper gyro temperature control			Roll 166°F Pitch 168°F Yaw 169.5°F	Time was 57:06:16 GMT
Verification of N_2 loading	224832A	4.64 pounds (loaded)	4.6 pounds	(FC-4) = 4726 psi (FC-48) = 78.1°F
Centaur separation	(3.5.2.1)			
Time required to null rates to less than 0.1 deg/sec		<0.1 deg/sec within 50 seconds	< 26 seconds	
Magnitude of angular rate at separation		≤3.0 deg/sec	No data	
Sun acquisition				
Proper sun acquisition	(7.3.3.3.4)	Minus roll maneuver until activation of acquisition sun sensor and then a plus yaw maneuver until primary sun sensor illumination		
Roll			224 degrees of roll	
Yaw			37 degrees of yaw	
Total time			523 seconds	
N_2 gas used	Design	0.054 pound (average)	<0.1 pound	
Star acquisition	(7.3.3.3.5)	Positive roll maneuver sufficient to produce an adequate star map for Canopus verification. Provide a lockon signal when Canopus appears in the sensor field of view		
Proper acquisition and verification of Canopus			Manual lockon	
Roll angle from beginning of maneuver to Canopus			269 degrees	
Objects identified			Canopus, earth, moon, Alpha C. Venaticoru, Mizar, Gamma U. Minoris/Kochab, and Caph/Shedar/Zeta Cassiopeiae	
Mean roll rate during star map phase		0.5 deg/sec	0.5018 deg/sec	
Effective gain (relative to nominal Canopus) of Canopus sensor			>1.5 xCanopus	
N_2 gas used	Design	0.048 pound (average)	<0.1 pound	
Coast mode	(7.3.3.3.6)	Roll axis shall be held to within 0.20 degree of sun-spacecraft line, plus a ±0.30 degree limit cycle Same magnitude as above for Canopus-spacecraft line		Sun and star error signal noise level were low enough to have no effect on the limit cycle performance
Limit cycle (gas jet system)	(7.3.3.3.3)			
Optical mode/inertial mode	(7.3.3.3.5)	±0.30 degree		Values are that of the total deadband. Predicted values were:
Average amplitude—roll			0.43/0.49 degree	0.44/0.44 degree
Average amplitude—pitch			0.44/0.39 degree	0.44/0.44 degree
Average amplitude—yaw			0.38/0.59 degree	0.44/0.44 degree
Gyro drift	(7.3.3.3.3C)	<1 deg/hr		
Roll			Roll +0.65 deg/hr	
Pitch			Pitch +0.2 deg/hr	
Yaw			Yaw ≈0 deg/hr	
Gas jet thrust level		>0.052 pound	0.064 pound (roll)	Design value is 0.057 pound

Table 5.5-2 (continued)

	Controlling Specification	Specification Value	Results	Comments
Premidcourse maneuvers				
Maneuver angles	(7.3.3.3.7)	Rates shall be controlled to be 0.5 ±0.0011 deg/sec		Assuming a precession level of 0.5000 deg/sec
Roll -3.1 degrees			-3.15 degrees	
Yaw +117.1 degrees			+117.008 degrees	
Precession command times		0.2 second plus 0.02 percent of command interval magnitude		These times were obtained from the gyro error signal response profile
Roll 6.2 seconds			6.3 seconds	
Yaw 234.2 seconds			234.016 seconds	
Attitude maneuver accuracy (includes drift, initial attitude errors, and limit cycle)			0.1 degree with 0.2 degree 3σ uncertainty	Calculated using actual data of drift, attitude errors, and execution errors
Maximum midcourse acceleration error	224832A	ΔV error <±1.3 ft/sec	-0.052 fps	
Expected ΔV/tracking ΔV			11.081 m/sec 11.082 m/sec	
Shutdown impulse (No. 1 burn)	(8.3.1.3.2.4.1)	<5 lb-sec/engine Δ impulse <0.66 lb/sec		
Engine 1			-0.144 lb-sec	
Engine 2			+0.259 lb-sec	
Engine 3			-0.115 lb-sec	
Preretro maneuvers				
Manuever angles	(7.3.3.3.7)	Rates shall be controlled to be 0.5±0.0011 deg/sec		Values only include execution error.
Roll +80.5 degrees			+80.498 degrees	
Yaw +96.1 degrees			+96.047 degrees	
Roll -16.5 degrees			-16.694 degrees	
Precession command times		0.2 second plus 0.02 percent of the command interval magnitude		
Roll 161 seconds			160.995 seconds	
Yaw 192.2 seconds			192.093 seconds	
Roll 33 seconds			33.389 seconds	
Pointing accuracy (includes drift, initial attitude errors, and limit cycle)		Within ±1 degree	0.23 degree with 0.20 3σ uncertainty	
Gyro drift values				
Roll			+0.65 deg/hr	
Pitch			+0.2 deg/hr	
Yaw			0 deg/hr	
Terminal descent				
Main retro				
Burn time (from ignition to 3.5 g switch)	(7.3.3.3.9)	Approximately 42.8 seconds	43.2 seconds	
Maximum retro thrust		<10,000 pounds	9200 pounds	Computed using retro accelerometer data
Peak attitude transient at vernier ignite – retro ignite	(7.3.3.3.10)			
Roll			-0.23 degree	
Pitch			-0.08 degree	
Yaw			-0.44 degree	

Table 5.5-2 (continued)

	Controlling Specification	Specification Value	Results	Comments
Main retro thrust vector to spacecraft center of gravity	(8.3.5.3.2.8)	<0.18 inch	0.04 inch	
Thrust vector pointing accuracy during retro burn	(8.3.5.3.2.9)	Within ±1 degree	0.27 degree	Based on estimated versus actual burn-out conditions
Mean attitude error during burn				
Roll			+0.1 degree	
Pitch			+0.03 degree	
Yaw			-0.28 degree	
Roll actuator position				
Peak at retro ignition			+0.43 degree	
Mean value during burn			-0.12 degree	
Time between major events	(7.3.3.3.9)			
AMR mark and vernier ignition		2.775 seconds expected	2.735 seconds	
Vernier and retro ignition		1.1 ± 0.1 seconds	1.116 seconds	
Retro ignition and RADVS on		0.55 ± 0.1 second	0.542 second	
Retro ignition and retro burnout (inertia switch closes)		42.8 seconds expected	43.2 seconds	
Retro burnout and high thrust		10.0 seconds expected	10.809 seconds	
High thrust and retro eject		2.0 seconds expected	1.825 seconds	
Retro eject and start of RADVS-controlled descent		2.15 seconds expected	2.151 seconds	
Retro burnout conditions				
Attitude			>40,000 feet	
Total velocity			448 fps	Actual
Angle between thrust vector and velocity vector			19 degrees	$V_x \approx -58$ fps $V_y = -135$ fps at start of RADVS-controlled descent
Time to align Z-axis to velocity vector		9 seconds maximum	<4 seconds	Expected
Descent segment intercept conditions			21,700 feet 457 fps	$V_x = -42$ fps $V_y = -171$ fps at start of RADVS-controlled descent
Touchdown conditions				
Vertical velocity		<15 fps	≈8 fps	
Lateral velocity		<5.0 fps	≈0 fps	
Additional information				
Total nitrogen gas used	Design	0.58 ± 0.22 pound	0.40 pound	See coast mode gas consumption
Gyro speeds	235159	Telemetry value = 50 cps for all three gyros		
Roll gyro			Roll = 50 Hz (average)	
Pitch gyro			Pitch = 50 Hz(average)	
Yaw gyro			Yaw = 50 Hz (average)	
Gyro heater duty cycle				
Roll			Roll = 16 percent (on)	
Pitch			Pitch = 40 percent (on)	
Yaw			Yaw = 28 percent (on)	

*Seen as composite signal.

5.5.4 SUBSYSTEM PERFORMANCE ANALYSIS

5.5.4.1 Prelaunch

Gyro Temperatures

The gyro temperatures at 007:06:16 GMT just prior to launch were as follows:

Roll = 166° F

Pitch = 168° F

Yaw = 169.5° F

Nitrogen Weight

The estimated on-board nitrogen weight at launch was 4.6 pounds based on a telemetered tank pressure of 4726 psi at a tank temperature of 78.1° F. This agreed closely with the best estimate of 4.64 pounds of nitrogen loaded.

5.5.4.2 Launch Through Separation From Centaur

After extending its landing legs, Surveyor is separated from the Centaur booster. When the three legs-down signals and the separation signal have been generated, the programmer removes the logic signal which has been inhibiting operation of the gas jet amplifiers. At this same instant, the magnitude register begins to count down 1024 counts for a 51-second interval; the start of sun acquisition is inhibited for this interval to give the cold gas attitude control system opportunity to rate stabilize the spacecraft. Table 5.5-1 presents these events in time reference.

Rate stabilization is accomplished by using the three-axis attitude control system to torque the spacecraft and drive the caged integrating rate gyros error signals to within the deadband of each gas jet amplifier. Thus, at the end of a nominal rate stabilization maneuver, the spacecraft has achieved a low angular velocity at a random orientation in inertial space. The system response is dependent upon the magnitude and direction of the initial velocity vector and the gas jet thrust levels, and is essentially deadbeat in nature.

Flight control system performance just after Centaur separation was evaluated for proper nulling of the separation rates and the time required to null rates to less than 0.1 deg/sec. The total angular excursion and magnitude of angular rates due to separation could not be determined because of the loss of data at the time of mechanical separation. However, when data returned approximately 26 seconds after the estimated time of mechanical separation (007:05:16:00 GMT), the indicated angular rates about all three axes were less than 0.1 deg/sec.

Figure 5.5-1 depicts the significant events from launch through separation and sun acquisition.

The expected nitrogen usage for rate dissipation is small. A typical rate dissipation transient will require the use of 0.040 pound of nitrogen. Because the measurement uncertainties are large compared to the usage, no quantitative measurement of nitrogen gas consumption during rate dissipation was attempted.

5.5.4.3 Sun Acquisition

Fifty-one seconds after electrical separation, sun acquisition is initiated by a command from the flight control programmer which causes a vehicle roll maneuver of -0.5 deg/sec and continues until the sun comes into the acquisition sun sensor field of view which is aligned approximately to the spacecraft roll-pitch plane. When this occurs, the roll command is removed and a plus yaw maneuver is initiated to point the primary sun sensor line of sight toward the sun. When the sun falls into the primary sun sensor field of view, a lockon signal is generated. This signal switches vehicle attitude control to the primary sun sensor and also serves to indicate (via telemetry) the completion of sun acquisition.

The automatic sun acquisition mode was initiated at 007:06:01.105 GMT as indicated by the countdown of the programmer clock. The estimated magnitude of the roll maneuver based on a constant gyro precession rate of 0.5 deg/sec was 224 degrees, while the yaw maneuver was estimated to be 37.0 degrees based on real time flight data. The sun acquisition phase is depicted in Figure 5.5-1.

Nitrogen Utilization

Following sun acquisition, it was estimated that <0.1 pound was consumed during the separation rate dissipation and sun acquisition maneuvers. The expected nominal value is 0.094 pound.

5.5.4.4 Canopus (Star Acquisition)

As defined in Reference 1 (Model A-21 Equipment Specification 244832), paragraphs 7.1.2.7 and 7.1.2.7.1:

> "... a star map shall ... be obtained by rotating the spacecraft about the Z-axis [Ed. note: initiated by receipt of a sun and roll command 0714] and recording the Canopus sensor output intensity signal as a function of time. Canopus shall be identified by position and magnitude relative to other stars [Ed. note: and celestial objects] passing in the field of view of the sensor .... The star acquisition mode shall be initiated when the flight control subsystem receives the Sun and Star ... command 0703 .... The spacecraft shall rotate about the Z-axis in the positive direction until the star Canopus appears within the ... sensor field-of-view. Illumination of the ...

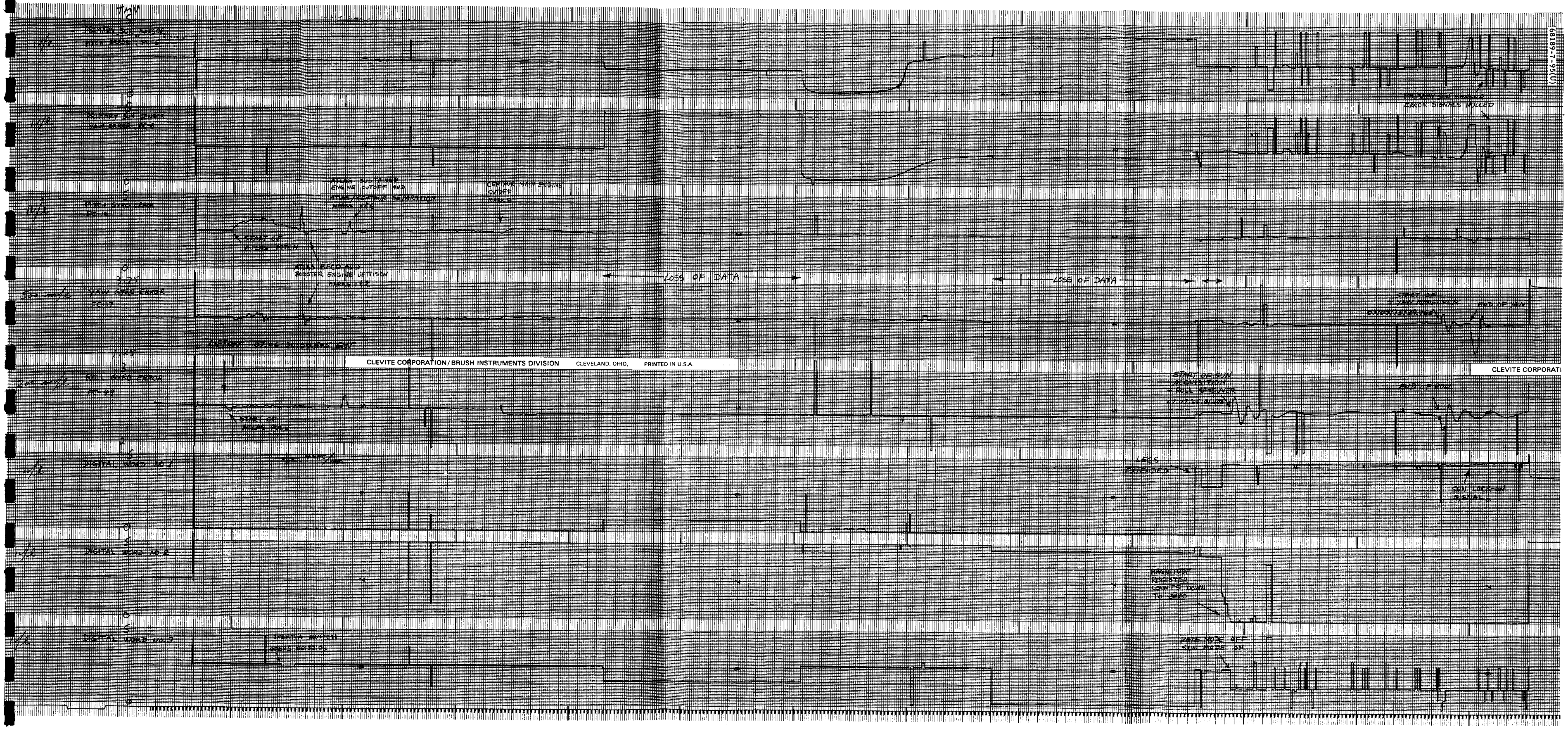

Figure 5.5-1. Launch to Sun Acquisition Phase

sensor [Ed. note: by the star Canopus] shall effect star acquisition, star lock and star track about the spacecraft Z-axis."

During Mission G, telemetered confirmation of the start of the star verification roll maneuver occurred at the received time of 07:14:24:06.125 GMT, corresponding to L+07H54M05.58S. During the ensuing roll, a star map was generated by recording the telemetered analog signals star intensity (FC-14) (i.e., output intensity signal) and star angle or roll error (FC-12) on a strip chart recorder. From this map, Canopus was positively identified during the first 360 degrees of roll by comparing the angular spacing and star intensity signal magnitudes of seven celestial objects passing through the field of view. Since the Canopus lockon signal did not occur when Canopus was in the field of view during the first roll revolution, it was decided to stop the roll maneuver by commanding cruise mode on (command 0704) when Canopus was in the field of view the second time and acquire Canopus by commanding manual lockon (command 0716). Telemetered confirmation of cruise mode on (at the end of the roll) occurred at the received time of 07:14:44:59.735. Manual lockon was confirmed at 07:14:47:32.527, after which approximately 50 seconds were required for the roll error signal to stabilize within the deadband limit.

Star Map

The spacecraft, moon, sun, and earth relationships in the ecliptic plane were as shown in Figure 5.5-2a. The center of the moon would pass approximately 17.5 degrees outside the field of view in a plus yaw direction, and the center of the earth would pass approximately 22.5 degrees outside the field of view in a minus yaw direction. As shown in Figure 5.5-2a, the spacecraft is behind the moon and would therefore "see" less than a half moon. The earth would also appear outside of the field of view in the minus yaw direction. Figure 5.5-2b depicts the relationship of the sensor field of view and the earth as the spacecraft's -X axis pointed toward the earth during spacecraft roll.

Since large area bright objects within approximately 35 degrees of the sensor's line of sight will reflect light into the sensor from baffles in the sensor's light shield, it was expected that a star intensity signal would result when the sensor was rolling past the earth, and very little, if any, signal would result when rolling past the moon. In addition, 19 stars with intensities greater than 0.42×10^{-14} w/cm^2 come within the field of view during a complete roll revolution. Based on laboratory measurements of star intensity telemetry signals versus star intensity on this particular sensor (S/N 6) it was predicted that four stars, including Canopus, might be observed. In addition, there existed the possibility that two pairs of close proximity stars might be observed as single stars. Figure 5.5-2c depicts the preflight calculated angular (roll angle) spacing of the moon, earth, Canopus, and other expected stars.

The telecommunications subsystem was in mode 1 at 4400 bits/sec, resulting in transmission of a 100-word commutator word frame each 0.25

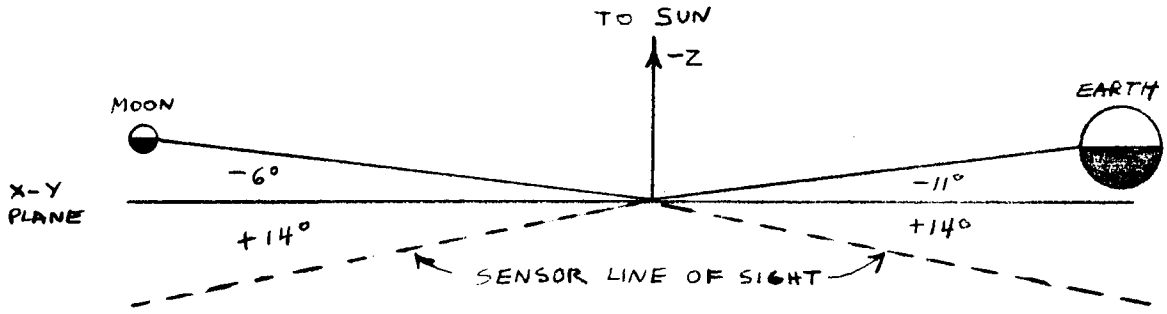

a) Ecliptic Plane Relationships

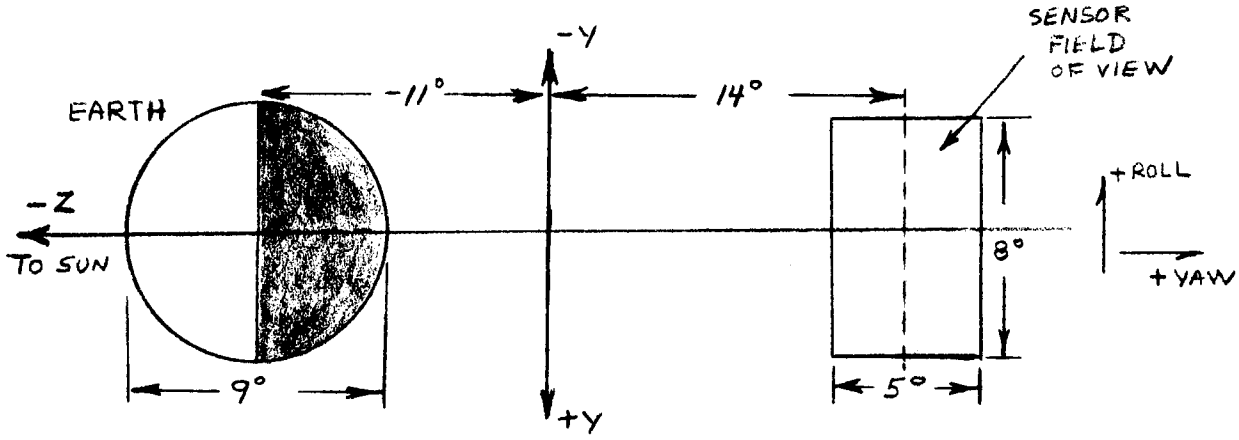

b) Sensor Field of View With Respect to Earth

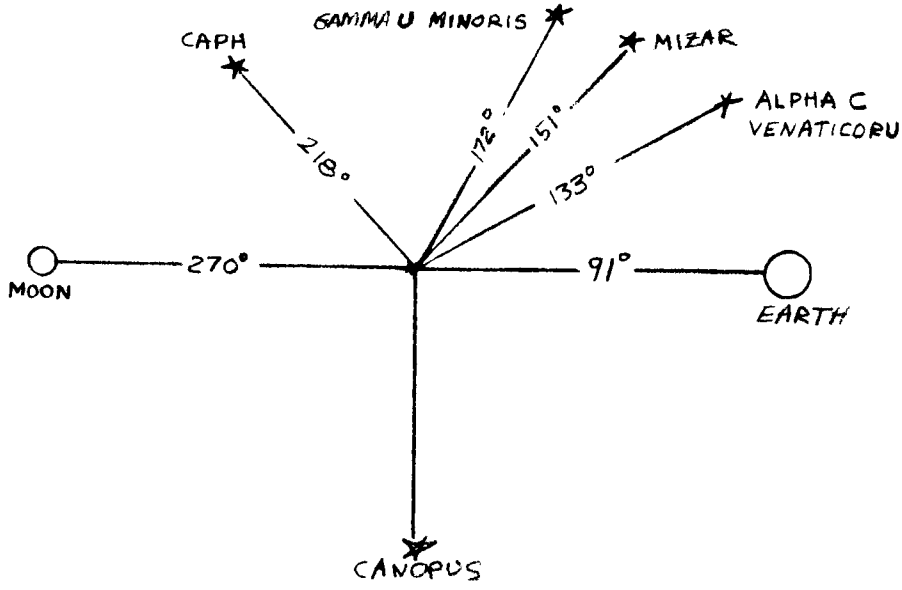

c) Angular Spacing (in Roll) of Observed Objects

Figure 5.5-2. Canopus Sensor Relationships to Observed Objects

second. Star angle and star intensity signals, plus digital word 3, are read out each 0.05 second during each frame (equivalent to each 0.025 degree of spacecraft roll at the commanded roll rate of 0.5 deg/sec) and digital words 1 and 9 are read out once per frame (equivalent to each 0.125 degree of spacecraft roll).

During the mission, spacecraft telemetry was transmitted to the Space Flight Operations Facility from Madrid (DSS 61) at 1100 bits/sec, resulting in the transmission of a 100-word commutator word frame each second. Thus, during the star mapping portion of the mission in real time at the Space Flight Operations Facility, only one-fourth of the total data was available for star identification. From the real-time Space Flight Operations Facility analog recorder traces of star angle and star intensity, it was possible to distinguish four stars plus a 45-degree-wide high star intensity signal, and two wide low-intensity signals. The angular spacing and magnitude of these signals was compared with preflight calculated star, earth, and moon angles and intensities, thus permitting positive identification of Canopus, Alpha C. Venaticoru, Mizar, the star groupings of Gamma U. Minorus/Kochab and Caph/Shedar/Zeta Cassiopeiae, plus the earth and moon. Postmission analysis of the total data, containing all commutator frames versus every fourth frame received in real time, revealed no other celestial bodies.

Figure 5.5-3 depicts analog traces of primary sun sensor pitch angular error (FC-5), primary sun sensor yaw angular error (FC-6), roll gyro error (FC-49), star angle, star intensity, digital word 1, and digital word 9 from the start of roll through Canopus acquisition.

Table 5.5-3 indicates the responses received versus predicted responses. The roll angles listed are calculated from the times when the star intensity signals reach their peak values. Although star intensity readings are commutated every 0.025 degree, the ability of the analyst to actually determine where the peak value of intensity occurs is limited to approximately ±0.3 degree due to the unknown effect of circuit time constants on the leg at peak intensities and the lack of any well defined peak on stars of low intensity.

Two objects which did not exhibit the same type of responses as celestial bodies appeared in the field of view during the first revolution (at 29.0 and 58.7 degrees) and were not seen during the second revolution.

The mean roll rate, as determined from the incremental time between the first and second Canopus peak intensity signals, was 360/717.377 = 0.5018 deg/sec. The error due to sampling timing is ±0.25 second or ±0.00003 deg/sec, and the error due to roll gyro limit cycling is ±0.2 degree or ±0.0003 deg/sec.

Star Sensor Performance

The star sensor provides three telemetry outputs: star angle or roll error, Canopus lockon, and star intensity. A comparison of in-flight and

TABLE 5.5-3. SURVEYOR VII STAR MAP – MEASURED VERSUS PREDICTED RESPONSES

GMT, hr:min:sec	Postflight Calculated Roll Angle, degree = Δt x 0.5018 deg/sec	Object or Event	Postflight Calculated Angle from Canopus, degrees	Preflight Calculated Angle from Canopus, degrees	Measured Peak Intensity During Roll, telemetry volts	Measured Peak No Roll Intensity, telemetry volts	Predicted Peak No Roll Intensity, telemetry volts
14:24:06.125	0	Start of roll	-268.7				
14:25:03.883	29.0	Particle No. 1	-239.8				
14:25:28.632	41.4	Alpha C. Venaticoru	-227.3	-227.3	0.674		
14:26:03.131	58.7	Mizar and Particle 2	-210.0	-209.3			
14:26:48.929	81.7	Gamma U. Minoris and Kochab	-187.0	-188.2/ -187.4	0.640		
14:28:28.176	131.5	Caph, Shedar, and Zeta Cassiopeiae	-137.2	-142.3, -138.2, and -135.8	0.723		
14:30:01.873	178.5	Moon	- 90.2	- 90	0.743		
14:38:01.667	268.7	Canopus	0	0	4.570		
14:36:02.212	359.3	Earth	90.6	91	2.754		
14:37:26.409	401.6	Alpha C. Venaticoru	132.8	132.7	0.665		
14:38:01.158	419.0	Mizar	150.3	150.7	0.772		
14:38:46.107	441.6	Gamma U. Minoris and Kochab	172.8	171.8 and 172.6	0.655		
14:40:22.954	490.2	Caph, Shedar, and Zeta Cassiopeiae	221.4	217.7, 221.8, and 224.2	0.719		
14:41:57.151	537.4	Moon	268.7	270	0.709		
14:44:59.045	628.7	Canopus	0	0	4.585		
14:44:59.735	629.1	End of roll	0.35				
14:47:32.527		Manual lockon					
		Canopus after acquisition				4.946	3.9 → 4.8
		No star			0.59		0.417

Figure 5.5-3. Analog Plot of Canopus Acquisition

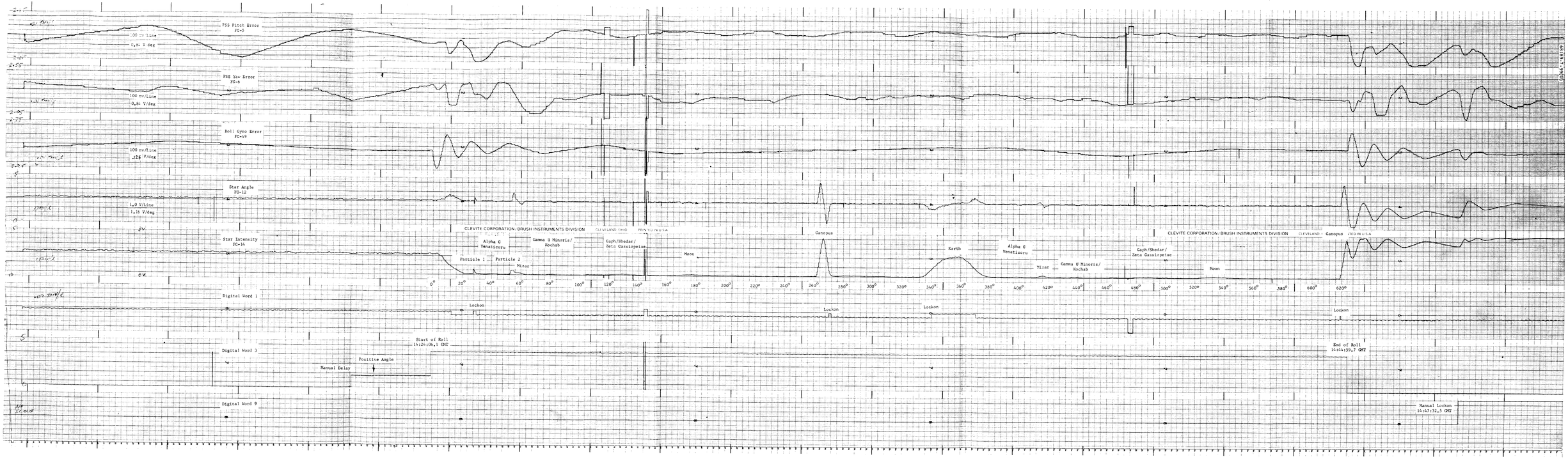

Figure 5.5-3. Analog Plot of Canopus Acquisition

preflight measurements is used to determine how well the sensor performed in flight.

The star angle telemetry signal is designed to increase from a quiescent level of close to 512 BCD when no star is in the field of view to a maximum of close to 1023 BCD when Canopus is approximately +2 degrees from the X-Z plane. It returns to its quiescent level when Canopus is in the X-Z plane, then to a minimum of close to 0 BCD when Canopus is approximately -2 degrees from the X-Z plane, and finally increases to its quiescent level as Canopus leaves the field of view.

The star intensity telemetry signal is designed to increase from a quiescent level when no star is in the field of view to a maximum when Canopus is in the X-Z plane. It then decreases to its quiescent level as Canopus leaves the field of view. No star and maximum intensity telemetry values are listed in Table 5.5-3.

Figure 5.5-3 depicts the star angle and star intensity signals for all objects observed during the star map. From this figure, it can be seen that the star angle and star intensity telemetry signals perform as designed.

In-flight star intensity telemetry values are compared with preflight star intensity values to calculate the effective gain of the sensor. The gain of a sensor is a function of the photomultiplier tube scale factor which is controlled by the intensity of the sunlight actually reaching the tube through a sun filter in the sun channel optics. All preflight star sensor measurements are made with a "unit" sun intensity illuminating the sun channel. For flight, a flight filter can be installed with a transmission factor that will admit more, equal, or less than a unit sun into the sensor.

Following are the sun filter transmission factors and calculated effective gains for Missions A through F:

	A	B	C	D	E	F
Filter factor	1.5	1.17	0.80	0.80	0.80	0.80
Effective gain	1.5+	1.5+	1.17	1.24	1.32	1.10

It was decided to install an 0.8 x Canopus sun filter for Mission G which was expected to result in an effective gain in the range of 1.10 to 1.32.

All star intensity values were greater than expected, leading to the conjecture that any or all of the following conditions prevailed:

1) Earth-based intensity measurements were too low due to incorrect simulation of sun and/or star intensities.

2) The 0.8 x Canopus sun filter installed was greater than 0.8.

3) The sun channel was partially blocked by a small particle which resulted in an apparent increase in the value of the sun filter.

4) Sun intensity was lower than predicted, or star intensities were all higher than predicted.

Based on the experience of previous flights wherein a fairly wide range of effective gains was observed, it is judged that several of the foregoing conditions probably combined to yield a sufficiently high effective gain so that the star signal was higher than the upper gate of the Canopus lockon circuit. Effective gain is determined by comparing the steady-state value of the in-flight measurement of Canopus intensity to the earth-based laboratory measurements of a simulated 1.0 X Canopus. For simulated star intensity versus telemetered star intensity in the linear region of sensor response, use of a single ratio of in-flight telemetry volts to laboratory telemetry volts yielded a reasonably accurate effective gain value. Where in-flight measurements indicate the intensity versus telemetry volts ratio is outside the linear region (which ends at approximately 1.2 X Canopus) use of a sensor response curve relating star intensity to intensity telemetry volts is required. For Surveyor VII, the steady-state value of Canopus intensity was 4.95 telemetry volts, which is near the maximum output of the sensor and very high in the nonlinear region where a large change in star intensity results in a very small change in telemetry volts. The value of 4.95 telemetry volts is slightly larger than any laboratory response to a 1.5 X Canopus intensity star, thus leading to the conclusion that the effective gain of the Surveyor VII sensor was equal to or greater than 1.5 X Canopus.

The third sensor output, Canopus lockon, is shown in Figure 5.5-3 as part of digital word 1 and did not appear as desired when Canopus was in the field of view, but did appear at the time reflected light from the earth was entering the sensor. Since a Canopus lockon signal did not appear properly, it was decided to send the cruise mode command to stop the roll maneuver, followed by the manual lockon command to acquire Canopus.

Canopus Acquisition

Figure 5.5-3 depicts the response of the star intensity signal after the roll maneuver was stopped by the cruise mode command, and receipt of the manual lockon signal put the spacecraft in a closed-loop roll error controlled mode. When manual lockon occurred, the spacecraft had a roll error of approximately +0.35 degree which caused the spacecraft to roll negatively to obtain a nulled roll error signal. After the roll error signal was nulled, the spacecraft settled down to a slow roll oscillation which caused the star intensity signal to oscillate on either side of its peak amplitude while the roll error signal oscillated above and below its null position. This oscillation is bounded, and the bounds are referred to as the roll optical limit cycle. As noted in Figure 5.5-3, the star intensity peak amplitudes increase as the limit cycle is approached since there is less attenuation due to filtering as the roll rate decreases to almost zero.

Conclusions

The Canopus sensor performed as designed in response to decreased sunlight. The star intensity signal, with Canopus in the field of view, was higher than predicted because the sensor was operating in the nonlinear region of its calibration curve. This caused the star signal to exceed the upper gate of the Canopus lockon circuit and required that the manual lockon command be utilized to acquire Canopus, thereby again proving the soundness of incorporating this optional mode of acquisition.

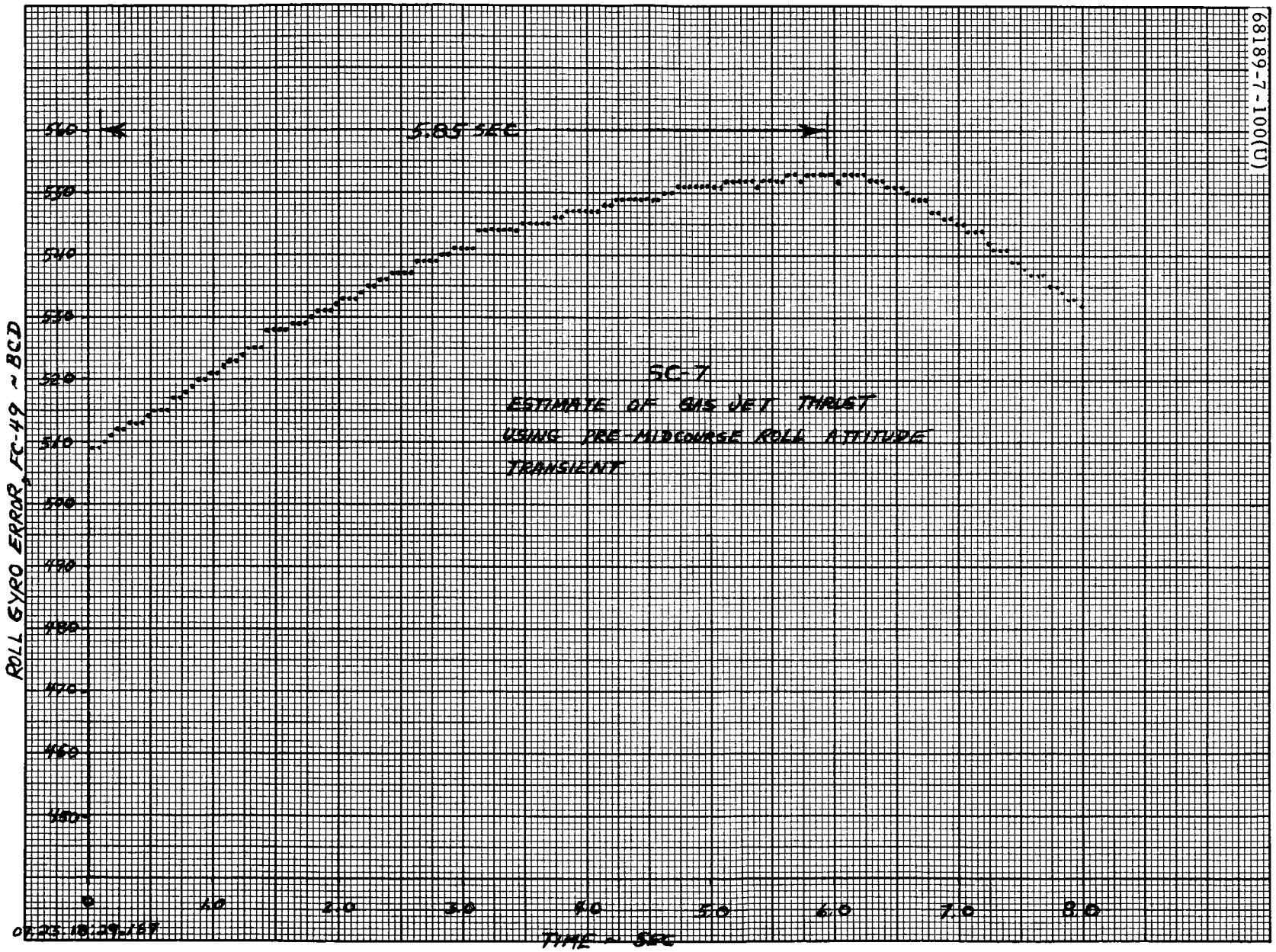

Figure 5.5-4. Gas Jet Thrust Level Determination of Firing

5.5.4.5 Coast Phase Attitude Control

Gas Jet Thrust Level

Reference 2 developed the following expression for the gas jet thrust level:

$$\text{thrust} = T = \frac{I_z \dot{\varphi}_c}{R t_p}$$

where

I_z = roll inertia = 216 slug-ft^2

$\dot{\varphi}_c$ = commanded precession rate = 0.5 deg/sec

R = gas jet movement arm = 6.47 feet

t_p = thrusting time of the gas jet

This equation was used to determine the thrust level.

Using the premidcourse roll attitude maneuver data (Figure 5.5-4), the time from command initiation until $\dot{\varphi}_{gyro} = 0$ was 5.85 seconds. Since the No. 1 gas jet amplifier is off 1.32 seconds of this time (Reference 3), t_p =(5.85 seconds -1.32 seconds)= 4.53 seconds.

$$\text{thrust} = \frac{I_z \dot{\varphi}_c}{R t_p} = \frac{(216 \text{ slug-ft}^2)(0.5 \text{ deg/sec})}{(6.47 \text{ feet})(4.53 \text{ seconds})(57.3 \text{ deg/rad})} = 0.064 \text{ pound}$$

Nitrogen Consumption

Nitrogen consumption for the period from launch to preretro maneuvers was 0.40 pound. This number compares favorably with predicted usage when measurement uncertainties and postgyro drift lockon transients are taken into account. Mission nitrogen usage was obtained from pressure and temperature information telemetered on flight control signals FC-4 and FC-48.

The predicted nitrogen usage for each manuever was determined from the simulation defined in Reference 4; a detailed breakdown of the predicted impulse and weight expenditures is documented in Reference 5.

For the number and sequence of Mission G maneuvers, Attachment 1 of Reference 5 yields the following nominal impulse consumption budget:

	lb-sec
Vernier phase of midcourse maneuver	2.00
Limit cycle operation	4.50
Sun acquisition	3.25
Inertial roll maneuvers (3)	4.50
Star verification	1.50
Star acquisition	1.40
Inertial yaw maneuvers (2)	2.50
Rate dissipation	2.75
Postmidcourse rate dissipation	1.00
Total	26.80

Assuming an average I_{sp} of 60 seconds yields a nominal nitrogen usage prior to the preretro maneuvers of approximately 0.45 pound. Reference 5 also predicts a 3σ usage uncertainty of 0.22 pound for this particular mission profile.

The fuel consumption due to postgyro drift check lockon transients was determined using the final angular attitude positions of each drift check as initial conditions to the simulation documented in Reference 4 with the following results:

1) The average impulse expenditure for one of the post-three-axis drift transients was 0.70 lb-sec.

2) The average impulse expenditure for one of the post-roll-axis-only drift transients was 0.55 lb-sec.

So there is an increase in the nitrogen consumption prediction of

$$\frac{1(0.55)\text{ lb-sec} + 8(0.90)\text{ lb-sec}}{60\text{ seconds}} = 0.13\text{ pound}$$

The net prediction would be

$$(0.45 + 0.13) \pm 0.22 = 0.58\text{ pound} \pm 0.22\text{ pound}$$

It was concluded that the measured nitrogen usage of 0.40 pound was within anticipated limits.

5.5.4.6 Premidcourse Attitude Maneuvers

In order to orient the spacecraft thrust axis properly prior to vernier engine ignition, a negative roll maneuver of 3.1 degrees and a positive yaw maneuver of 117.1 degrees were commanded. Although these were the values entered into the magnitude register, the desired maneuvers per the midcourse and terminal guidance system calculations were -3.097 degrees of roll and 117.3134 degrees of yaw.

Several variables affect the accuracy of an angular maneuver; precession rate accuracy, precession command time, gyro drift, and initial attitude errors due to biases and limit cycle. When several manuevers are performed with large time intervals between them, attitude errors due to gyro drift must be included. A list of all parameters affecting the midcourse attitude maneuver accuracy is presented in Table 5.5-4 along with their allowable 3σ values and actual performance values wherever possible.

As in Missions D, E, and F, an attempt was made to initiate the maneuvers at the optical mode limit cycle null point. The roll maneuver was started within -0.055 degree of null, while the pitch and yaw optical errors at the start of the yaw maneuver were +0.11 and -0.135 degree, respectively.

Determination of Precession Times

The register was loaded with 16 bits for roll and 586 bits for yaw. For a clock rate of 2.5 cps, the respective times are 6.2 and 234.2 seconds with a maximum error of 0.20 second ± 0.02 percent.

The telemetered gyro error signal data were used in determining the actual precession time. The sampling rate during the maneuvers was 20 times/sec, giving a resolution of 0.05 second. The results are as follows (Figure 5.5-5):

T = 6.301 seconds, or 3.15 degrees of roll

T = 234.016 seconds, or 117.008 degrees of yaw

Precession Rates. The precession rate obtained during the star mapping phase indicated that the positive precession rate was 0.5018 deg/sec.

Attitude Maneuver Error

Reference 6 develops two orthogonal equations that specify the spacecraft thrust axis pointing error during midcourse thrusting. The equations were derived for the roll-yaw rotation sequence which applies here.

Neglecting error sources that are present only after engine ignition results in the following equations:

$$\text{Error about yaw axis} = -\psi_{R_E} - \psi_{A_E} \cos\varphi - \theta_{A_E} \sin\varphi$$

$$\text{Error about pitch axis} = \left(\varphi_{A_E} + \varphi_{R_E}\right) \sin\varphi + \theta_{A_E} \cos\psi \cos\varphi$$

$$-\psi_{A_E} \sin\varphi \cos\psi$$

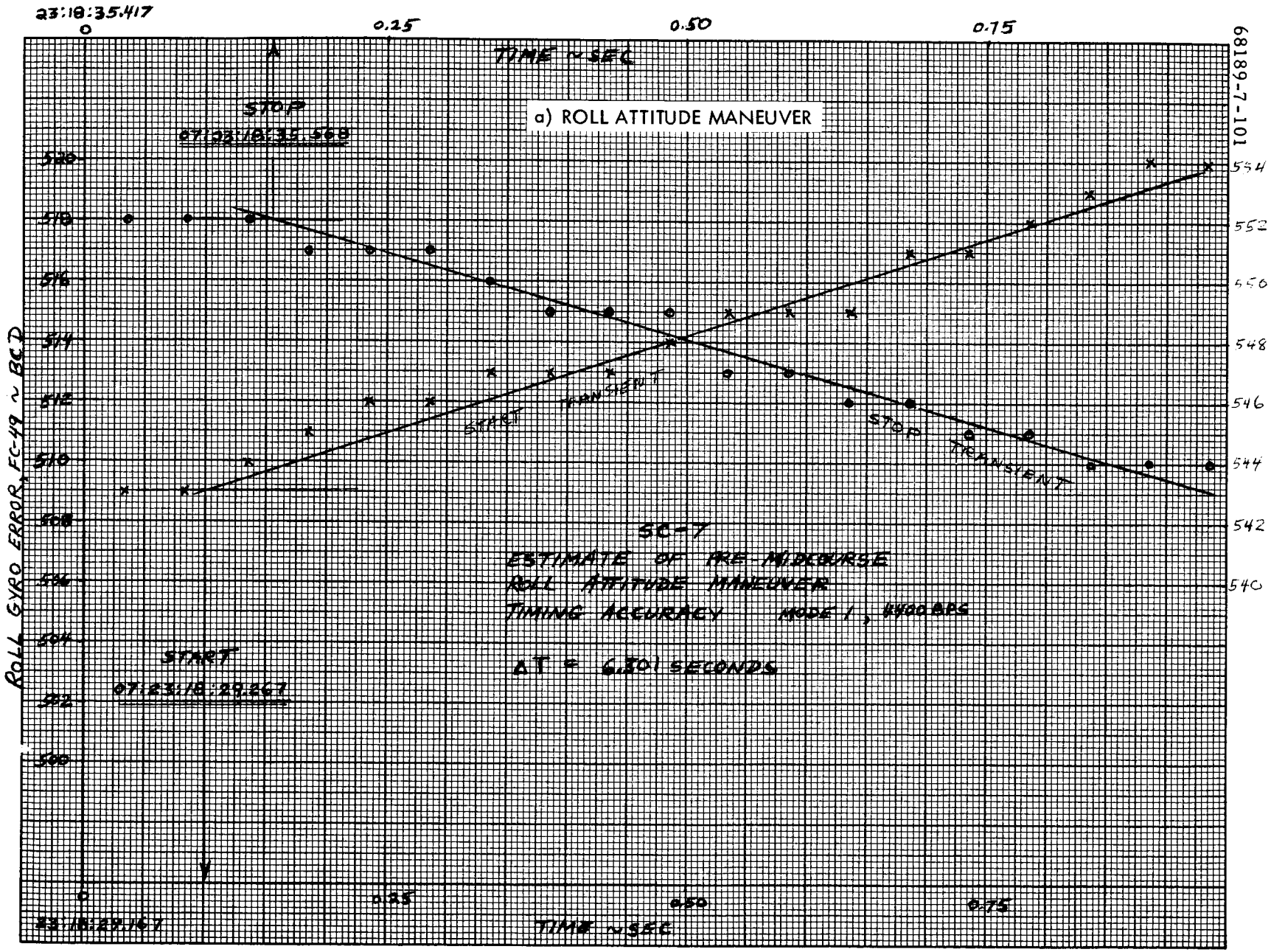

Figure 5.5-5. Premidcourse Maneuver Timing Accuracy

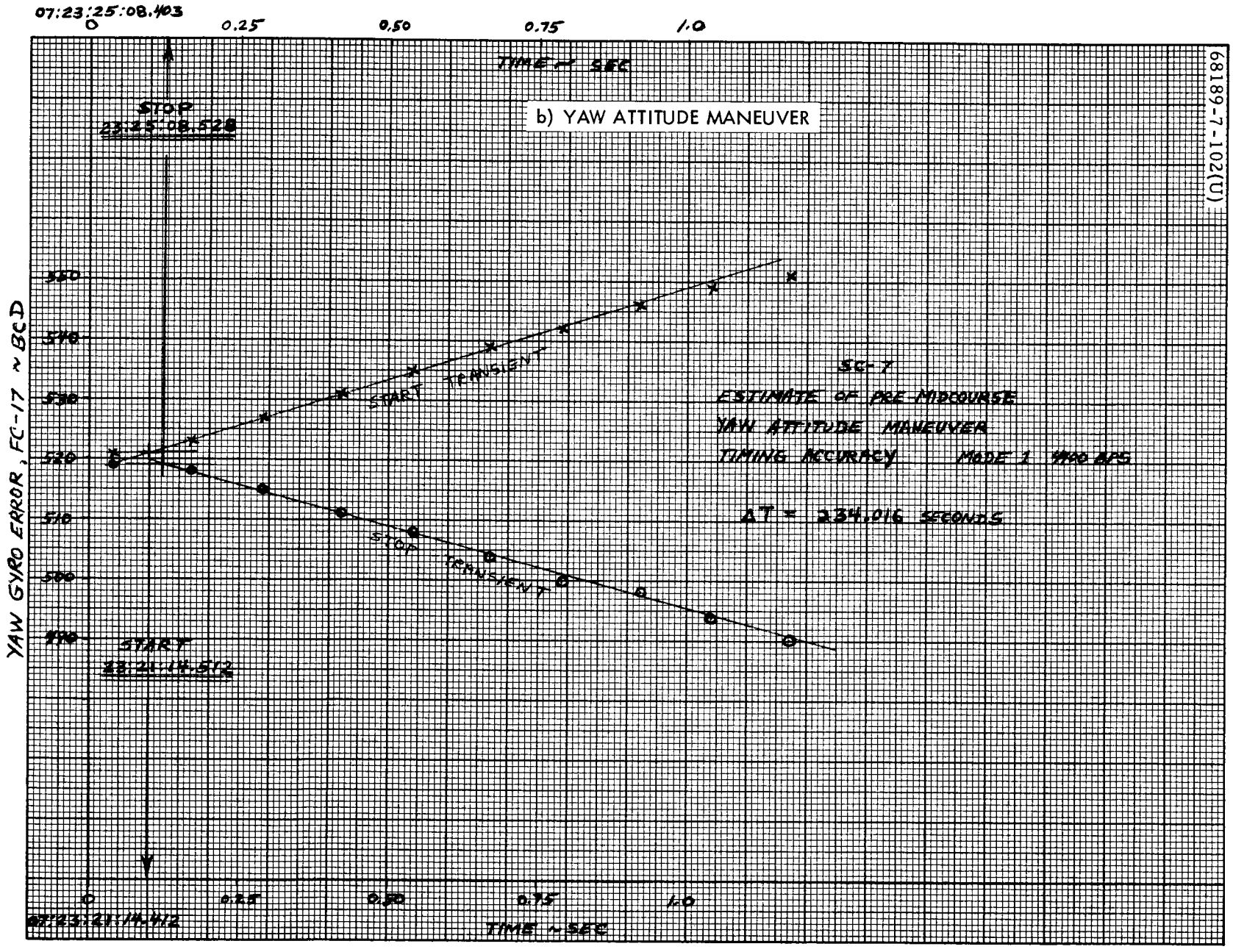

Figure 5.5-5 (continued). Premidcourse Maneuver Timing Accuracy

TABLE 5.5-4. PREMIDCOURSE ATTITUDE ERROR SUMMARY

Parameter	3σ Requirement	Reference Number	Measured Value	Comments
Primary sun sensor null with respect to FCSG roll axis	0.2 degree	2 (paragraph 4.3.1.1)	Pitch = -0.048 degree Yaw = +0.027 degree	
Canopus sensor null with respect to FCSC roll/pitch plane	0.2 degree	2 (paragraph 4.3.1.2)	+0.099 degree	
Pitch/yaw limit cycle	0.3 degree	2 (paragraph 4.3.1.1)	+0.11/-0.135 degree	Based on sun sensor error signals at start of yaw
Roll limit cycle	0.3 degree	2 (paragraph 4.3.1.2)	-0.055 degree	Based on Canopus error signal at start of roll
Gyro torquer scale factor	0.15 percent	12 (paragraph 3.2.5.1.3)	0.2 percent	
Precession current source accuracy	0.13 percent			
Precession current source drift	0.1 percent			
Timing source accuracy	0.2 second ±0.02 percent		Roll = -0.05 degree Yaw = +0.008 degree	Based on timing errors determined in subsection 5.5.4.6
Gyro alignment to FCSC roll axis	0.14 degree	12 (paragraph 3.2.5.1.4)	Pitch = +0.08 degree Yaw = +0.07 degree	
FCSG/spacecraft roll axis alignment	0.1 degree	2 (paragraph 4.1.3.7.1)		
Gyro non-g sensitive drift	1.0 deg/hr	2 (paragraph 4.3.1.5)	Roll = +0.05 degree Yaw = 0 degree Pitch = +0.03 degree	Based on measured +0.65 deg/hr in roll for 0.08 hour, +10 deg/hr in yaw, and +0.2 deg/hr in pitch for 0.15 hour
Total attitude error prior to ignition			0.1 degree with 0.2-degree 3σ uncertainty	

where

$(\varphi, \theta, \psi)_{A_E}$ = spacecraft inertial reference alignment errors

$(\psi, \varphi)_{R_E}$ = rotation errors

Use of φ = -3.1 degrees, ψ = 117.1 degrees, and the errors listed in the summary chart results in an 0.1-degree attitude error. The resultant pointing error has a 99-percent circular probable uncertainty of 0.2 degree.

5.5.4.7 Postmidcourse Attitude Maneuvers

The postmidcourse attitude maneuvers are used to realign the spacecraft to the celestial reference after performing a midcourse velocity correction. To accomplish this, two reacquisition schemes are available. One method is to perform the premidcourse attitude maneuvers in reverse, and the other is to perform another automatic sun acquisition and Canopus acquisition sequence. The first method is more desirable since real-time monitoring of optical sensor signals provides a good indication of premidcourse maneuver accuracy and attitude control during the thrust period. If reacquisition of the sun and Canopus is not achieved to within a fair degree of accuracy, one or more of the following conditions must have existed:

1) Precession commands were nonsymmetrical.

2) Spacecraft attitude change occurred between maneuver periods.

3) Premidcourse maneuvers were not accurate.

4) Postmidcourse maneuvers were not accurate.

5) Vernier engine shutoff transients were excessive.

The first method was chosen for the Surveyor VII postmidcourse yaw maneuver, and the sun was successfully reacquired. Canopus was reacquired by placing the spacecraft in the cruise mode with manual lockon since Canopus was in the sensor field of view at completion of the yaw maneuver.

Determination of Precession Times

For the postmidcourse attitude maneuver, the magnitude register was loaded with 586 bits for yaw. This corresponds to 234.2 seconds. The yaw precession time, using gyro error signal data (Figure 5.5-6), was found to be 234.217 seconds.

Since Canopus was in the sensor field of view following the postmidcourse yaw maneuver, nulling of the star error signal was achieved by commanding cruise mode on and manual lockon as shown in Figure 5.5-7.

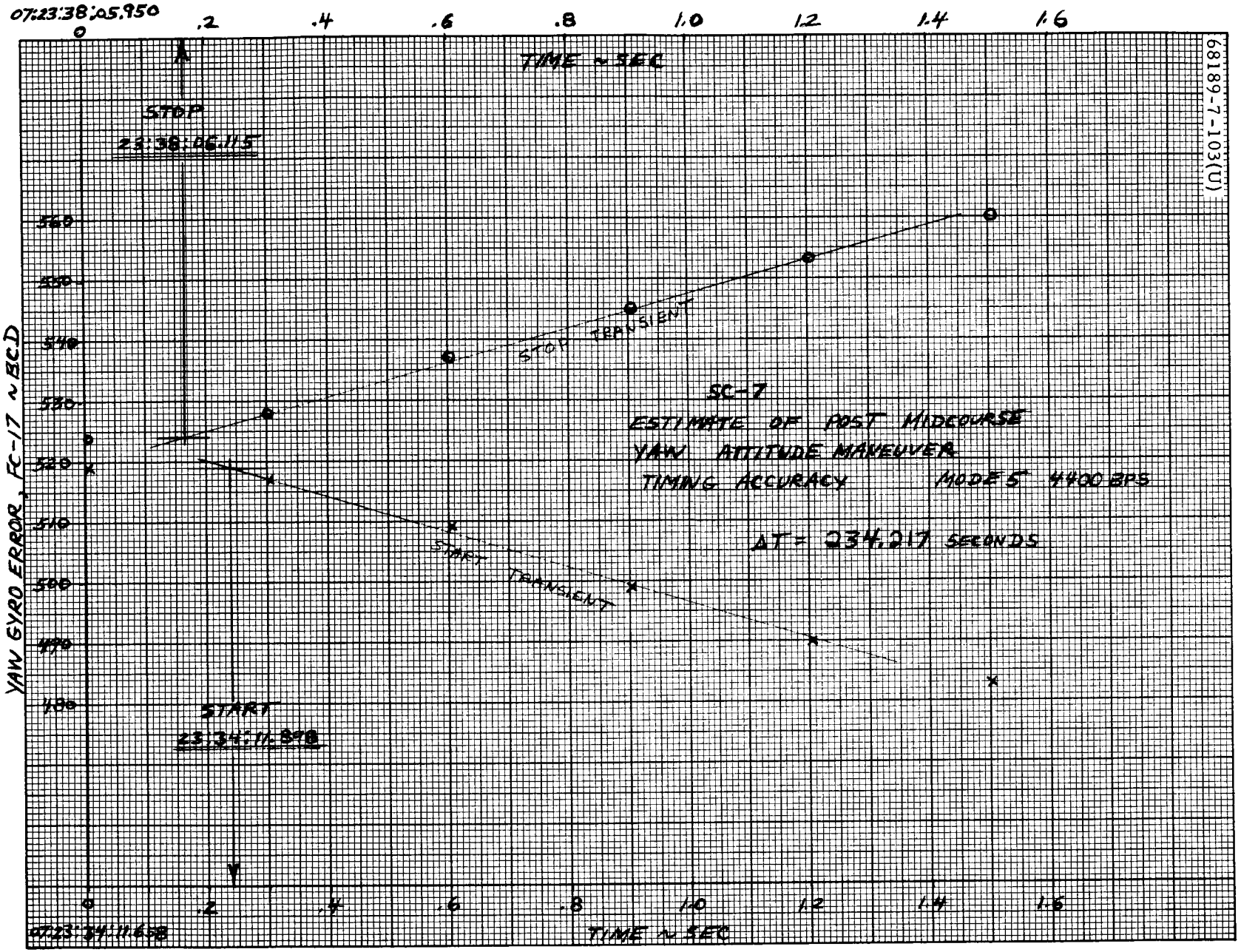

Figure 5.5-6. Postmidcourse Maneuver Timing Accuracy

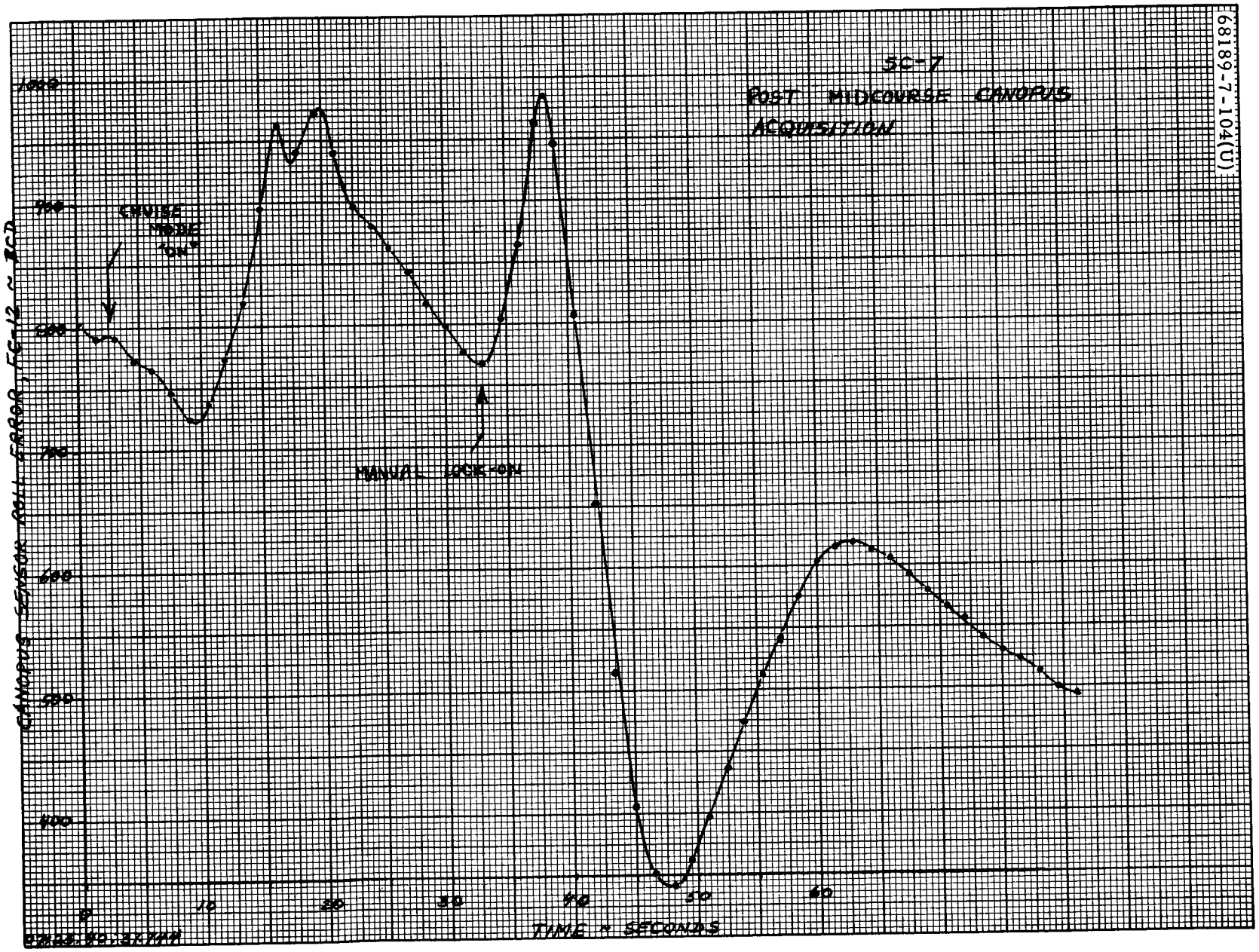

Figure 5.5-7. Postmidcourse Canopus Acquisition

The postmidcourse maneuvers were performed using the coast mode commutator at 4400 bits/sec, thereby increasing the data granularity to 0.3 second from the 0.05 second obtained for the premidcourse attitude maneuvers which were performed using the mode 1 commutator at 4400 bit/sec.

5.5.4.8 Midcourse Velocity Correction

The midcourse velocity correction was successfully executed starting at 23:30:10.410 GMT on 7 January. From orbit determination, the actual magnitude of the velocity change was estimated to be 11.082 m/sec compared to the commanded value of 11.081 m/sec (36.357 fps). This constitutes a ΔV execution error of 0.001 m/sec. Using prelaunch alignment information and in-flight data, the preignition pointing error was calculated in subsection 5.5.4.6 to be 0.10 degree.

Midcourse Engine Ignition Characteristics

The midcourse velocity correction was characterized by a smooth vernier ignition followed by a nominal, uneventful thrusting phase (Figure 5.5-8). Changes in pitch and yaw gyro errors were less than 0.2 degree during the ignition transient and less than 0.06 degree thereafter until engine cutoff.

Prior to vernier ignition, pitch and yaw gyro errors were maintained within the inertial deadband of ±0.22 degree by the gas jet system. The transient at ignition was reduced to zero in approximately 2 seconds. The yaw error transient peak was -0.20 degree, while the pitch error was -0.08 degree. The transient behavior was dominated by the 1.0-second time constant of the attitude control loops.

Based on the acceleration error telemetry signal (FC-15) (Figure 5.5-9), it was concluded that all three engines were producing controlled thrust within about 0.150 second of the ignition command signal. Therefore, acceleration signal amplifier saturation, which requires a startup delay of 0.26 second, did not occur, and no ΔV error information was lost.

Midcourse Engine Shutdown Dispersions

A summary of the peak spacecraft angles and angular rates and computed vernier engine shutdown impulse dispersions are given in Table 5.5-5.

It should be noted that peak gyro angles were less than 1.5 degrees and well within the required travel range of ±10 degrees. Inertial reference was therefore retained, and reacquisition of the sun and Canopus was possible via the reverse maneuver sequence.

Vernier engine shutdown impulse dispersions (relative to mean impulse of the three engines), calculated from pitch and yaw angular rate data as per the procedure outlined in Reference 9, were well within the specification limit of ±0.63 lb-sec (Reference 7).

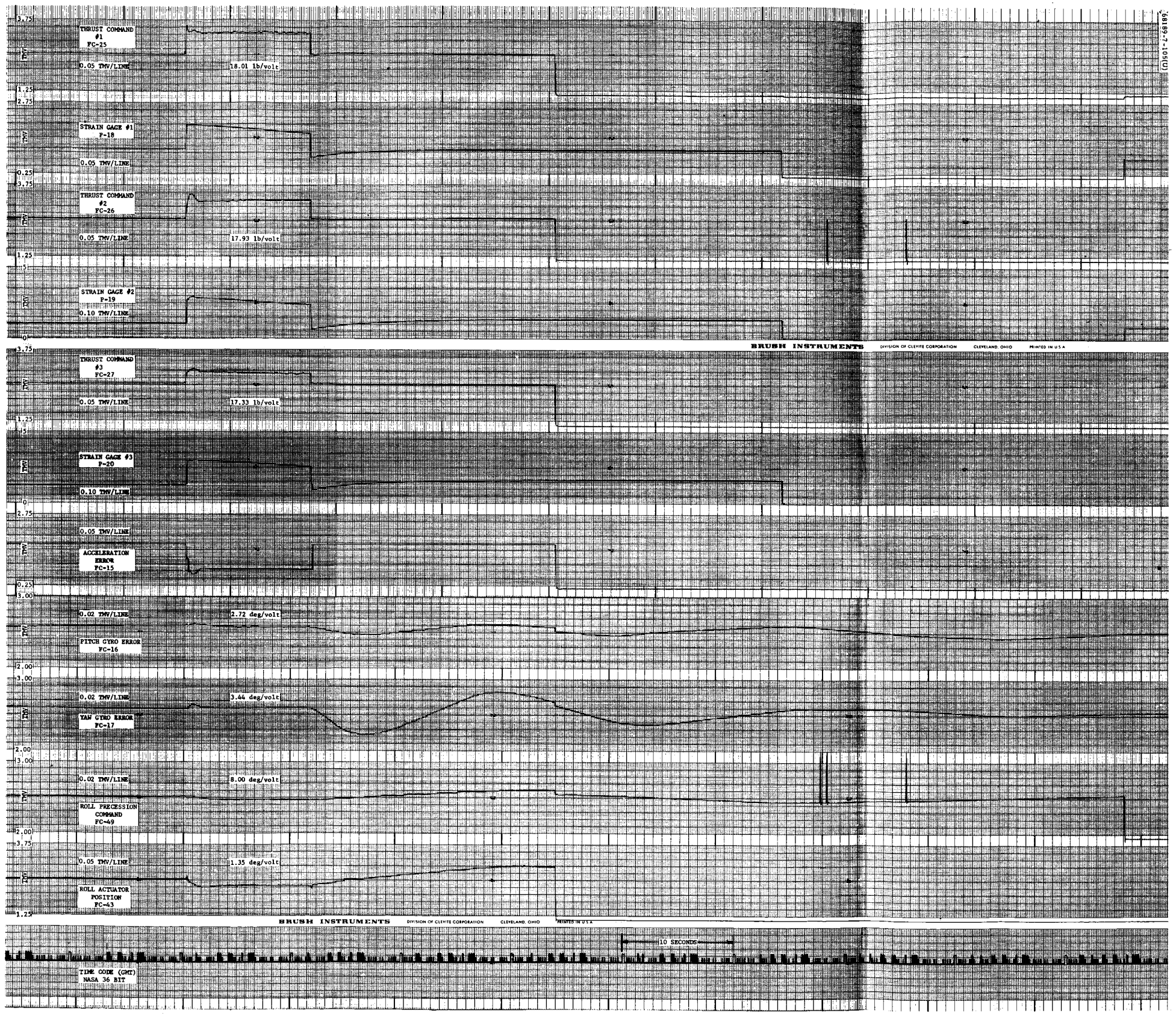

Figure 5.5-8. Midcourse Velocity Correction

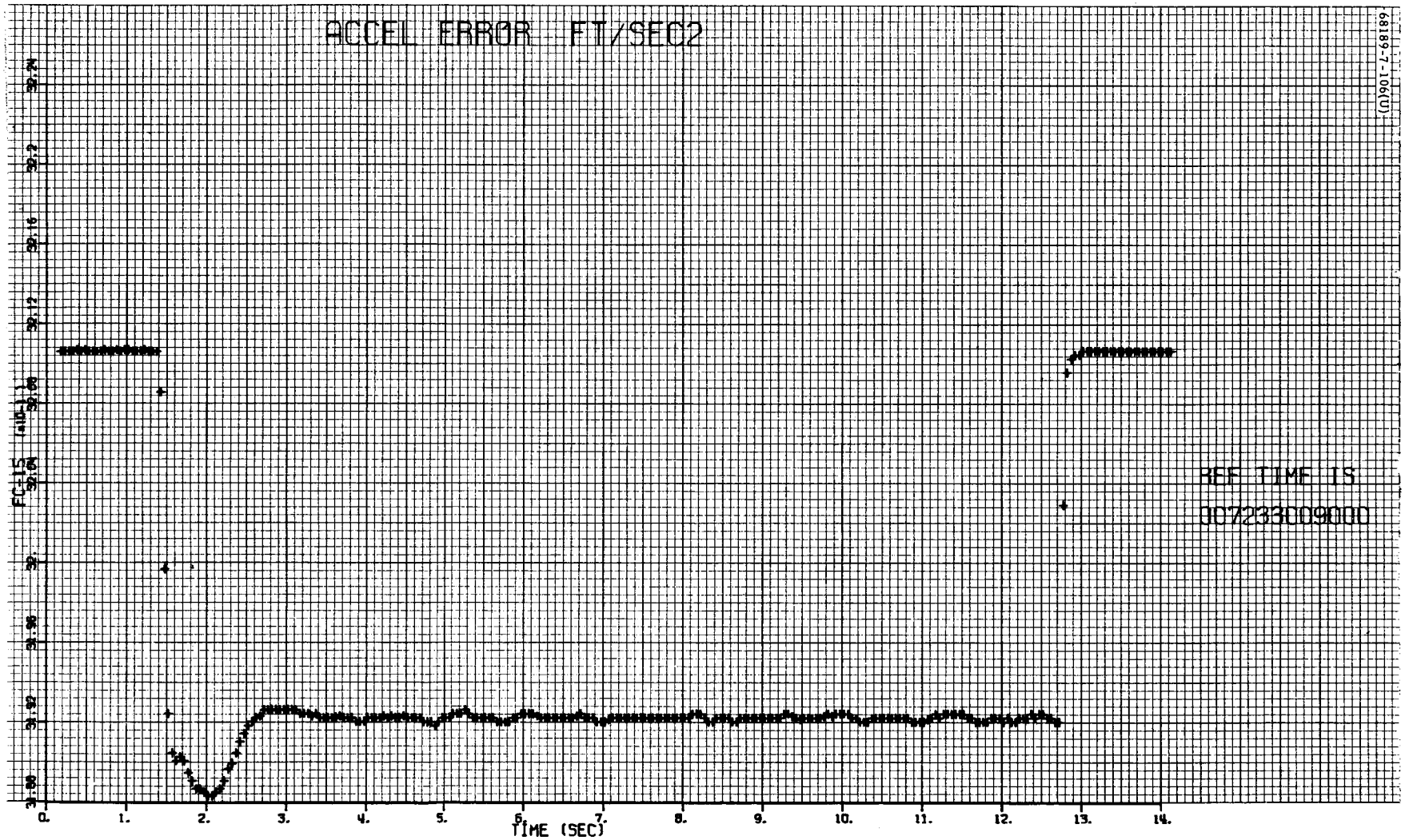

Figure 5.5-9. Acceleration Error

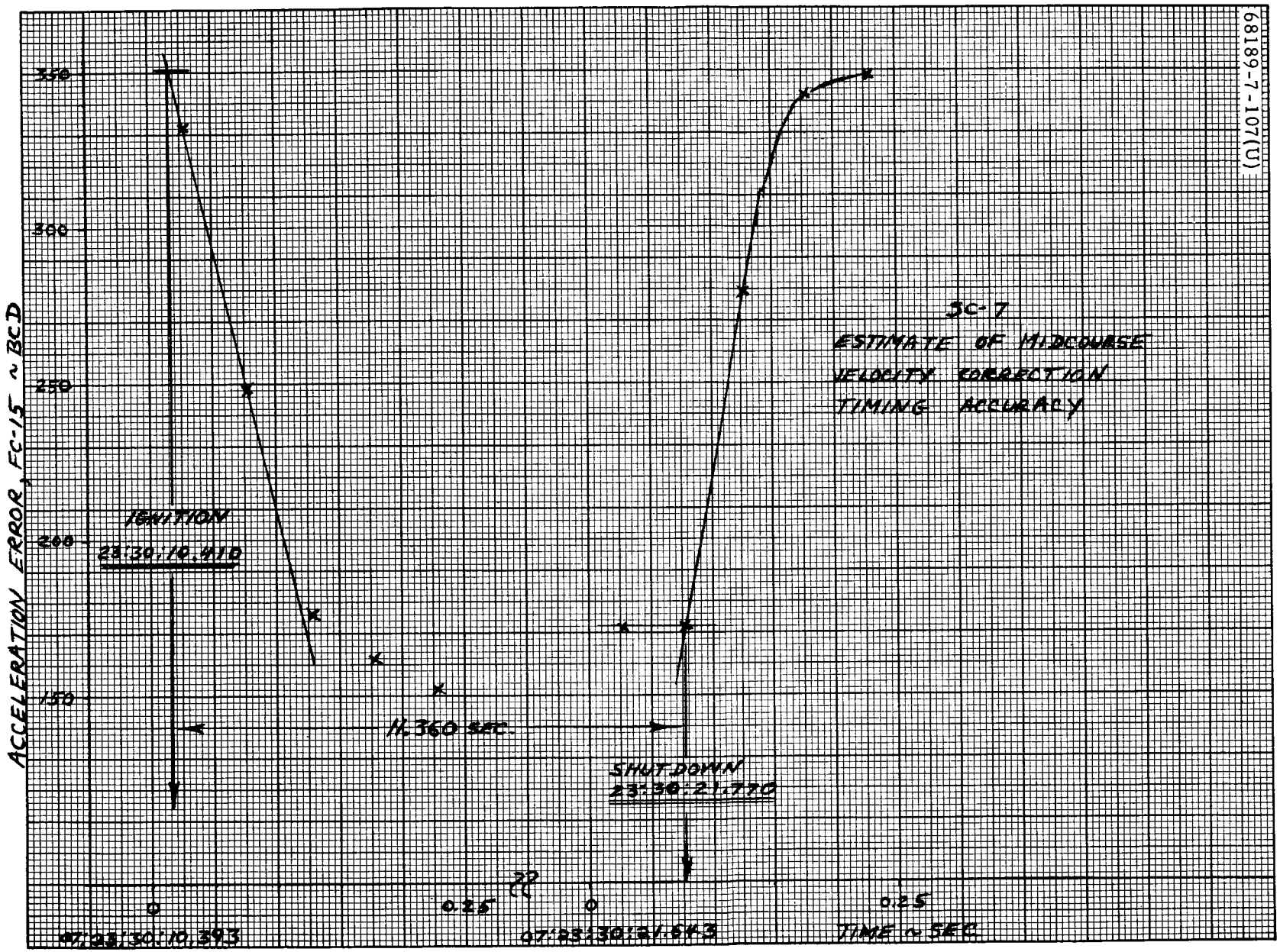

Figure 5.5-10. Estimate of Midcourse Velocity Correction Timing Accuracy

Midcourse Velocity Determination

The general concept of midcourse correction capability employed by Surveyor is to apply a constant acceleration for a finite period of time. Thus, in theory, once the magnitude of the velocity correction is known, the exact duration of the constant acceleration phase can be determined. In practice, this approach is slightly altered to account for such error sources as engine ignition transients and shutdown impulses. Thus, the actual command time ΔT is slightly higher.

The desired values used during flight were as follows:

1) Desired ΔV = 11.078 m/sec (36.336 fps)

2) Desired ΔT = 11.347 seconds

Duration of Burn Time. The acceleration error signal data were used in an attempt to determine the actual burn time. The results (Figure 5.5-10) indicated that the burn time was 11.36 seconds for a timing error of 0.01 second (the magnitude register was loaded with 114 counts or ΔT = 11.35 seconds).

Estimate of ΔV. Assuming that acceleration command remained at the design value of 3.222 ft/sec^2 (Reference 10), the actual acceleration level was determined by subtracting the acceleration error value (ϵ_A = 0.028 ft/sec^2) from the design value. The acceleration error signal remained essentially constant during the burn period. Therefore, the actual acceleration level was 3.194 ft/sec^2, and the midcourse ΔV was 3.194 $\times$ 11.36 = 36.284 fps for an error of -0.073 fps. From orbit determination, it was concluded that the actual midcourse ΔV was 11.082 m/sec (36.36 fps).

A list of parameters affecting the accuracy of the velocity correction is presented in Table 5.5-6 along with the values of maximum allowable errors. Actual performance values were used wherever possible.

Telemetered Thrust Levels

The approximate steady-state vernier engine thrust levels during the midcourse velocity correction were as follows:

Engine	Pounds
1	80.2
2	77.7
3	73.4

TABLE 5.5-5. MIDCOURSE SHUTDOWN SUMMARY

Peak angular errors, degrees:	
Pitch	= +0.32
Yaw	= +1.24
Roll	= +0.70
Roll act	= -0.66
Peak angular rates, deg/sec:	
Pitch	= +0.08
Yaw	= +0.32
Vernier shutdown impulse dispersions, lb-sec:	
Leg	
1	-0.144
2	+0.259
3	-0.115

Based on a spacecraft weight at injection of 2289.23 pounds and an estimated constant acceleration of 3.222 ft/sec^2, the expected total thrust is 228.9 which compares favorably with the total thrust of 231.3 pounds obtained from the telemetered vernier engine thrust commands.

5.5.4.9 Preretro Maneuvers

Before retro ignition, it is required that the spacecraft thrust axis (roll axis) be aligned to the translational velocity vector of the spacecraft as part of the gravity turn terminal descent phase guidance. The alignment is performed by means of two sequential rotations about the spacecraft body (gyro) axes. A third roll rotation may be required to satisfy a RADVS sidelobe constraint (Reference 8).

These maneuvers are accomplished by using the cold gas attitude control system, with the body-fixed integrating rate gyros as inertial references. To accomplish a rotation, the appropriate gyro torquer winding is driven by a constant current source for a precise length of time; the spacecraft is slaved to this changing reference at a constant rate of 0.5 deg/sec.

TABLE 5.5-6. SC-7 MIDCOURSE VELOCITY CORRECTION ACCURACY

Item	Parameter	Requirement 3σ or Limit	Limit, fps	Specification	Performance Value, fps	Comments
1	Errors proportional to maneuvers magnitude					Much of the error was anticipated and was included in the calculation of the desired burn time
	Accelerometer accuracy	1.1 percent	0.15	234632C		
	Reference signal	0.5 percent	0.068	234600E		
	Flight control electronics null	0.15 percent	0.02	234600E		
	Thrust bias variation	0.09 percent	0.01	287105	0.17	
	Control channel gain variation	0.07 percent	0.009	234600E		
	Accelerometer misalignment	0.06 percent	0.008	234600E		
	Total proportional errors (RSS)	1.22 percent	0.17			
2	Errors independent of maneuver magnitude					
	Shutdown impulse dispersion	±0.63 lb-sec	0.016	287015	+0.006	
	Hysteresis limit cycle	3 milliamperes	0.035	287105	0	
	Ignition transient	–	0.47	–	0	
	Timing granularity	±0.1 second	0.32	224832 7.2.1.9	-0.03	
	Total independent errors (RSS)		0.568		0.033	
3	Total magnitude errors (RSS)		0.782		0.172	

The major events and times associated with the positive roll, yaw, roll preretro maneuver combinations selected for Surveyor VII are given in Table 5.5-7.

The preretro maneuvers were analyzed in terms of the following:

1) The gyro precession times were determined from gyro error signals and precession logic signals and compared to commanded times.

2) Using these attitude errors and the initial sun and Canopus error signals, the preignition terminal pointing accuracy was determined.

The first attitude maneuver (roll) was initiated 34 minutes and 58.8 seconds before retro ignition. The time constraint on break of optical lock is 33 minutes based on an allowable 1 deg/hr gyro drift contribution to the pointing error (Reference 8). An attempt was made to reduce the optical

TABLE 5.5-7. MAJOR EVENTS AND TIMES (DAY 10) FOR PRERETRO MANEUVERS

Event	Command	GMT, hr:min:sec
Begin roll	0714	00:27:16.947
End roll		00:29:57.942
Begin yaw	0713	00:35:52.379
End yaw		00:39:04.472
Begin roll	0711	00:41:09.718
End roll		00:41:43.107
Retro ignition		01:02:15.709

mode limit cycle contribution to the pointing error by initiating the roll and yaw attitude maneuvers at the limit cycle null point. The degree of success is illustrated by the following data which indicates the limit cycle errors which existed at the start of each maneuver.

Maneuver	Limit Cycle Error, degree
Roll	-0.08
Yaw	+0.03 (yaw) +0.12 (pitch)

Gyro Precession Times

The attitude maneuvers entered into the flight control programmer magnitude register are as follows:

Maneuvers	Degrees	Bits
+Roll	80.5	403
+Yaw	96.1	481
-Roll	16.5	83

Table 5.5-8 presents the estimated gyro precession times.

TABLE 5.5-8. ESTIMATED GYRO PRECESSION TIMES

Attitude Maneuver	Commanded Time, seconds	Observed Time, seconds	ΔT, seconds	Rotation Error, degrees
Roll	161	160.995	-0.005	$\Delta\varphi = -0.002$
Yaw	192.2	192.093	-0.107	$\Delta\psi = -0.053$
Roll	33	33.389	+0.389	$\Delta\varphi = +0.195$

Since the gyro error signals are only sampled once every 1.2 seconds (coast mode at 1100 bits/sec) during the preretro maneuvers, it was assumed that the shapes of roll and pitch gyro transients were the same as those observed during the premidcourse attitude maneuvers when the gyro error signals were sampled once every 0.05 second. The precession times were then estimated graphically based upon the intersection points of the start and stop transients with the steady-state gyro error values (Figure 5.5-11).

Gyro Drift Compensation

Eight three-axis gyro drift checks were made during the mission, two of them prior to the midcourse velocity correction. One roll-axis-only drift check was also made. A summary of gyro drift measurements is presented in Table 5.5-9. The technique used to measure the drift rates was based on average slopes of the optical error signals obtained from analog Brush recorder and Milgo plots.

The following gyro drift rates were considered for possible compensation of the preterminal attitude maneuver magnitudes:

Roll = +0.65 deg/hr

Pitch = +0.2 deg/hr

Yaw = 0 deg/hr

These drift values were based essentially upon an average of all measurements made during the mission. For the first time, the pitch and yaw gyro drift rates were both negligible and attitude maneuver magnitudes were not changed to compensate for drift.

It was necessary to correct the roll drift measurements to compensate for the Canopus sensor acquisition mirror setting of 76 degrees with respect to the positive Z axis. Since a positive pitch rotation of the spacecraft results in a positive Canopus sensor roll error, the true roll drift rate was calculated by subtracting the measured pitch gyro drift rate multiplied by the sin 14 degrees from the measured roll gyro drift rate.

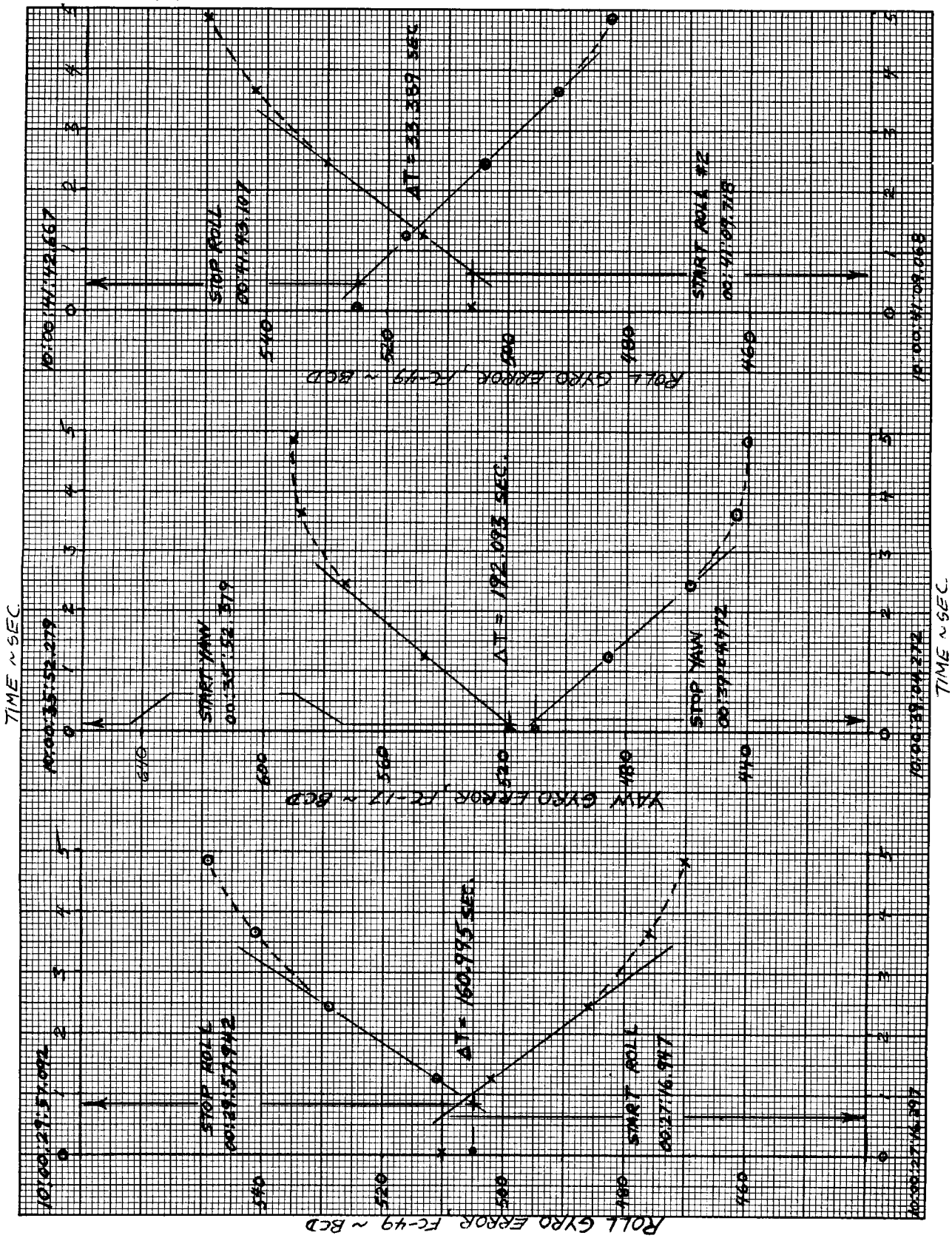

Figure 5.5-11. Estimates of Preretro Attitude Maneuver Timing Accuracies

TABLE 5.5-9. GYRO DRIFT SUMMARY

Number	Start, hr:min:sec	Stop, hr:min:sec	Drift Rate, deg/hr							
			Roll		Pitch		Yaw		Roll Corrected	
			Analog	Milgo	Analog	Milgo	Analog	Milgo	Analog	Milgo
	Day 7									
1	15:36:00	17:31:27	+0.8	+0.74	+0.355	+0.36	+0.075	+0.02	+0.714	+0.653
2	17:36:32	19:09:44	+0.8	+0.73	+0.322	+0.376	+0.109	+0.093	+0.722	+0.64
	Day 8									
3	00:04:10	02:43:58	+0.792		+0.400		+0.205		+0.696	
4	02:48:54	06:02:40	+0.700	+0.645					Roll only	Roll only
5	06:06:21	08:36:47	+0.775	+0.713	+0.21	+0.25	+0.180	+0.037	+0.724	+0.65
6	14:02:21	17:14:32	+0.754	+0.653	+0.209	+0.221	+0.03	+0.035	+0.704	+0.600
	Day 9									
7	03:05:43	05:34:23	+0.78		+0.179		0		+0.74	
8	07:16:22	09:48:31	+0.763		+0.155		0		+0.722	
9	14:00:04	17:04:16		+0.695		+0.226		+0.021		+0.641

The drift history for each gyro is depicted in Figure 5.5-12. The gyro drift rates remain within the specification limits of ±1.0 deg/hr but exhibit no apparent trends.

Preretro Pointing Error

The technique described in subsection 5.5.4.6 was used to determine the preretro attitude pointing error of 0.23 degree with a 3σ uncertainty of 0.20 degree.

5.5.4.10 Main Retro Phase

Main retro phase began at 010:01:02:11.892 GMT with the indication of altitude marking radar mark and successfully ended at 010:01:03:10.990 GMT with verification of retro eject. At the start of the RADVS-controlled descent phase, the longitudinal velocity was reduced to approximately 429 fps at an altitude of 40,000 feet. The predicted values for RADVS-controlled descent conditions were 444 fps at an altitude of 38,336 feet.

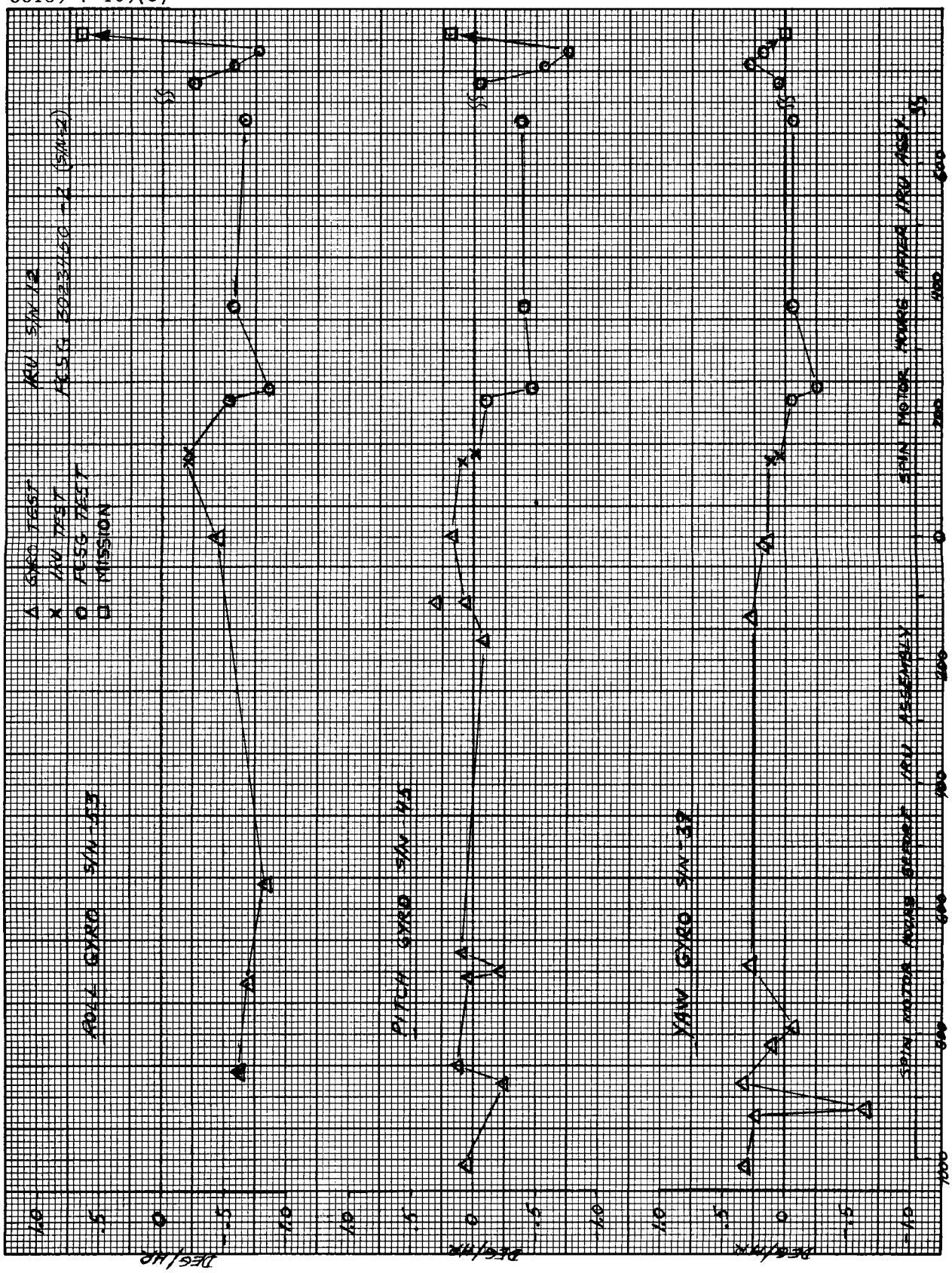

Figure 5.5-12. Gyro Drift Histories

During this phase, the function of the flight control system is to maintain the attitude of the spacecraft inertially fixed and to provide and execute a fixed sequence of commands to establish the necessary initial conditions for the vernier descent phase. The following analysis reveals that these functions were performed satisfactorily.

A list of retro phase events and their corresponding time of occurrence is given in Table 5.5-10 along with expected time intervals. These results confirm the performance of the magnitude register and programmer.

Ignition of the vernier engines during the main retro phase was executed smoothly.

Retro Phase Attitude Control

During the main retro phase, extending from vernier ignition through case separation, spacecraft attitude motion was small in all three axes (Figure 5.5-13). Peak pitch and yaw inertial attitude motion, as read directly from gyro error telemetry data (FC-16 and FC-17), occurred at vernier and retro ignition and amounted to -0.08 degree in pitch and -0.44 degree in yaw. Following ignition, static attitude error was virtually zero about the pitch axis and approximately -0.28 degree about the yaw axis. Roll inertial attitude error was less than 0.3 degree throughout the main retro phase (less than 1.0 degree is required).

Since all gyro error signals were maintained to within ±1.0 degree (during retro burn), each gyro was exercised less than 10 percent of the available travel range of more than ±10 degrees. A summary of pitch and yaw inertial attitude angles produced at various points in the retro phase is given in Table 5.5-11. No attitude disturbance was noted at retro eject, indicating a clean case separation.

Pitch and yaw control moments generated by the vernier engines were estimated by means of the following equations which are not compensated for any center of gravity offset:

$$L_x = -2.97\ T_1 + 0.574\ T_2 + 2.394\ T_3$$

$$L_y = -1.05\ T_1 + 3.095\ T_2 - 2.044\ T_3$$

where L_x and L_y are pitch and yaw control torques (ft-lb), respectively, and T_1, T_2, and T_3 are thrusts (pounds) generated by engines 1, 2, and 3, respectively. Values for T_1, T_2, and T_3 were estimated from the thrust command telemetry signals (FC-25, FC-26, and FC-27) (Figure 5.5-13). As indicated by the telemetry data, very little throttling of the engines occurred during the retro period. Approximately 0.5 second after retro ignition, differential throttling equivalent to approximately 32.0 ft-lb of control torque were produced. At all other times during the retro burn period, there was very little differential engine throttling.

TABLE 5.5-10. TIME AND EVENTS LOG, RETRO PHASE

Main Retro Phase Event	Time of Occurrence, Day 10, 1968, GMT, hr:min:sec	Time Between Events, seconds	Expected Time Intervals, seconds
Altitude marking radar signal (FC-64)	01:02:11.892 ± 0.05		
Vernier ignition (FC-28)	01:02:14.692 ± 0.05	2.80	2.775
Retro ignition	01:02:15.792 ± 0.05	1.1	1.1
RADVS on (R-28)	01:02:16.334	0.542	0.55
Retro burnout (FC-30) 3.5 g switch	01:02:58.990 ± 0.05	43.198	42.8 (retro burn)
High thrust (FC-78)	01:03:09.250 ± 0.6	10.260	10.0
Retro eject (FC-31)	01:03:10.990 ± 0.05	1.740	2.0
Start RADVS-controlled descent (FC-42)	01:03:13.090 ± 0.05	2.10	2.15

TABLE 5.5-11. RETRO PHASE ATTITUDE CONTROL SUMMARY

Peak attitude motion, degrees

Event	Pitch	Yaw
Vernier ignition Retro ignition	-0.08	-0.44
Retro burnout	0	0
Start RADVS-controlled descent	-0.4	-0.82

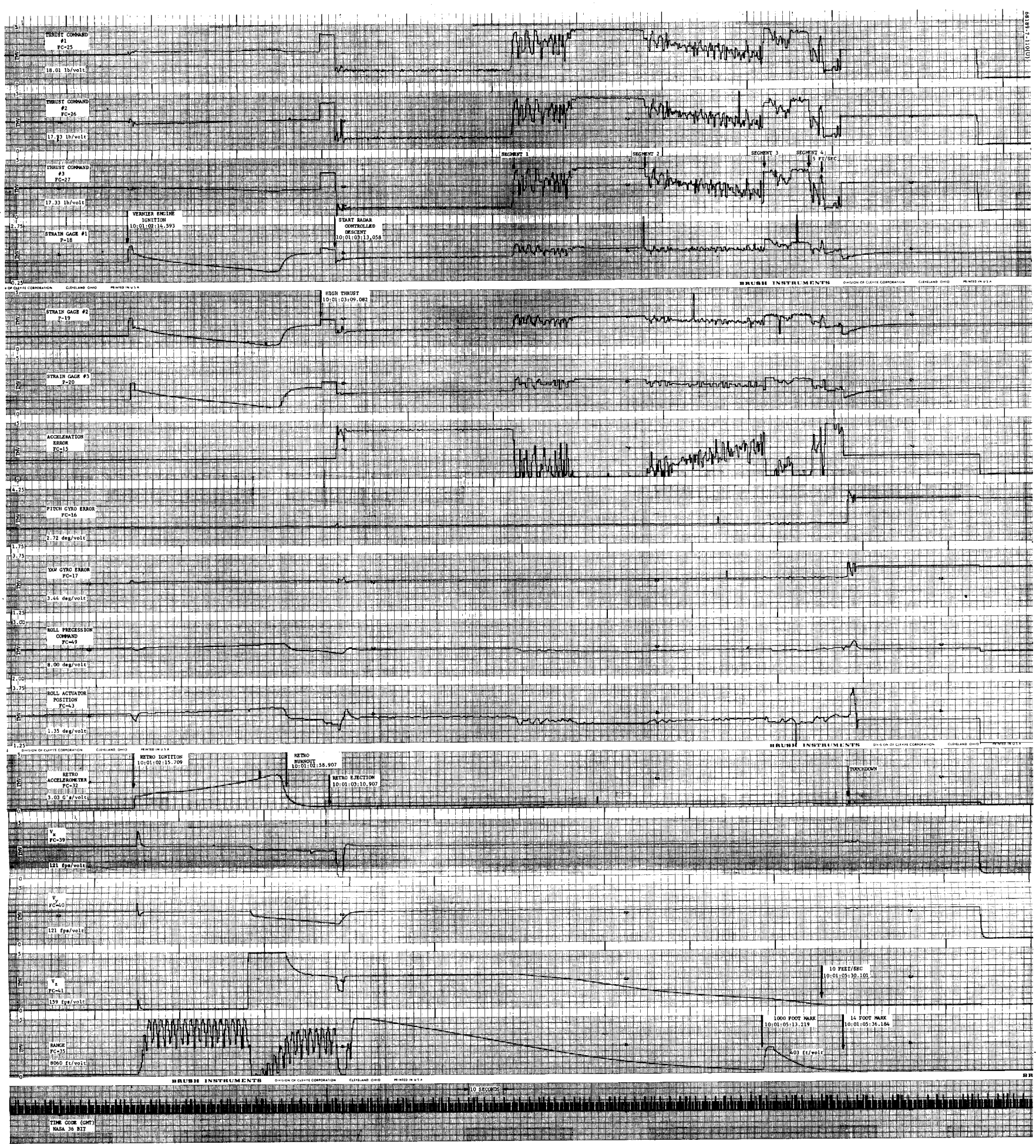

Figure 5.5-13. Terminal Descent

The maximum thrust vector to center of gravity offset can be estimated using this maximum control torque magnitude of 32 ft-lb. Assuming a 7800-pound retro thrust, the offset was estimated as

$$\text{Maximum center of gravity offset} = \frac{32.0 \text{ ft-lb}}{7800 \text{ pounds}} \times \frac{12 \text{ inch}}{\text{feet}}$$

$$= 0.05 \text{ inch}$$

This compares to the required value of 0.18 inch.

The maximum attitude error produced by the retro disturbance torques was also determined from the maximum torque magnitude of 32 ft-lb. Since the static gain (stiffness) of the pitch and yaw attitude control loops is

$$\text{static gain} = 1200 \text{ ft-lb/deg}$$

the maximum static attitude error is estimated to be

$$\text{maximum static error} = \frac{32}{1200} = 0.027 \text{ degree}$$

which is less than the allowable value of 0.12 degree.

5.5.4.11 Terminal Descent Phase

The RADVS-controlled terminal descent phase began at 010:01:03:13.090 GMT with initiation of the minimum acceleration (4.85 ft/sec^2) mode and a spacecraft attitude maneuver to null lateral velocities and align the thrust axis with the total velocity vector. The initial conditions at this time included a vertical velocity of 429 fps and an altitude of greater than 40,000 feet. The lateral velocities (V_x = -58 fps, V_y = -135 fps) were nulled within 4 seconds (9 seconds allowed) and remained essentially at zero to touchdown. It was estimated that the spacecraft roll axis was maneuvered through a total angle of 19 degrees.

Intercept of the descent line segments occurred at a vertical velocity of approximately 457 fps and a slant range of 21,700 feet. The descent segment tracking performance of the flight control system (Figure 5.5-14) was normal.

A list of pertinent terminal descent events and times of occurrence are presented in Table 5.5-12.

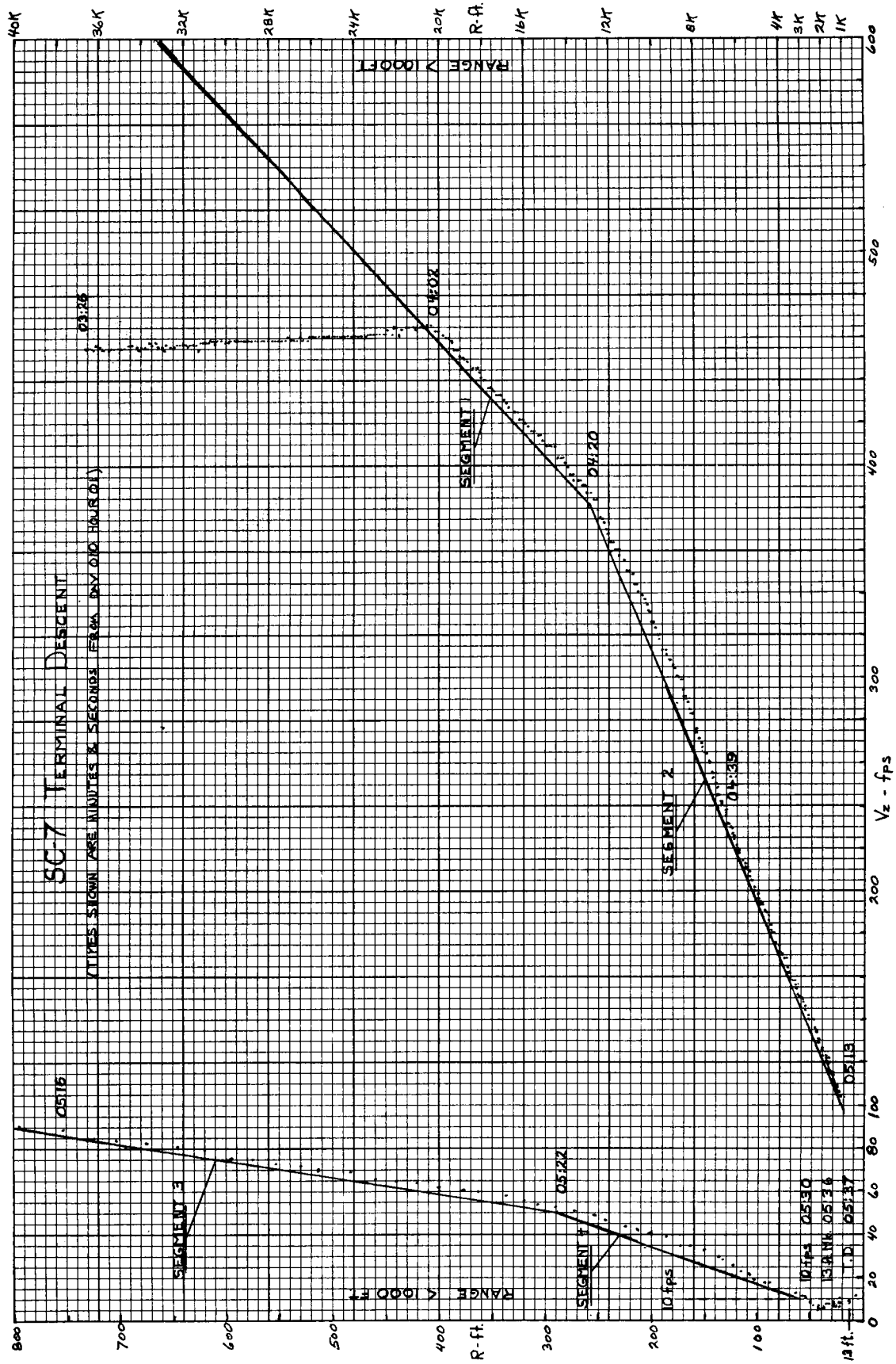

Figure 5.5-14. Range Versus V_z

TABLE 5.5-12. TERMINAL DESCENT PHASE LOG OF EVENTS, DAY 10

Event	GMT, hr:min:sec
RODVS	01:02:48.850 ± 0.6
Start of RADVS-controlled descent (minimum acceleration)	01:03:13.090 ± 0.05
RORA on	01:03:17.649 ± 0.6
Segment intercept	01:04:03.018 ± 0.15
1000-foot mark	01:05:13.285 ± 0.05
10-fps mark	01:05:30.184 ± 0.05
14-foot mark	01:05:36.284 ± 0.05
Touchdown (first "glitch" on retro accelerometer)	01:05:37.891
Thrust phase power off	01:06:14.751
RADVS off	01:06:38.751
Flight control power off	01:06:40.815

Vernier Descent Attitude Control

Spacecraft attitude motions determined from gyro error telemetry signals (FC-16, FC-17, and FC-49) were maintained to less than ±1.0 degree in each axis during the vernier descent phase.

Following generation of the RODVS signal and the start RADVS-controlled descent signal, the spacecraft initiated an attitude maneuver to align the thrust axis with the total velocity vector. Initial velocity conditions preceding the maneuver were taken from RADVS telemetry data, FC-39, FC-40, and FC-41 (see Figure 5.5-13).

Premaneuver velocity conditions were as follows:

$V_x = -58$ fps

$V_y = -135$ fps

$V_z = 429$ fps

The alignment maneuver was completed in less than 4 seconds (9 seconds allowed), after which time V_x and V_y were held essentially at zero, and V_z became equal to the total velocity of 448 fps. The attitude maneuver magnitudes were computed as follows:

$$\text{Pitch maneuver: } \Delta\theta_x = \tan^{-1} \frac{V_y}{V_z} = 17.5 \text{ degrees}$$

$$\text{Yaw maneuver: } \Delta\theta_y = \tan^{-1} \frac{V_x}{V_z} = 7.7 \text{ degrees}$$

The spacecraft Z axis was therefore maneuvered through approximately 19 degrees.

At touchdown, changes in gyro gimbal errors of -3.0 degrees in pitch, -1.68 degrees in yaw, and 0 degree in roll were observed.

5.5.5 REFERENCES

1. "Surveyor Spacecraft Equipment," Hughes Specification 224832.

2. K. Kobayashi, "A Method for Determining Gas Jet Thrust Level — Post Mission Analysis," Hughes Aircraft Company IDC 2253.4/25, 1 March 1966.

3. "Surveyor III Flight Performance Final Report," Hughes Aircraft Company, SSD 68189-3, July 1967.

4. R.H. Bernard, "Restoration and Updating of Surveyor Coast Phase Analog Computer Mechanization," Hughes Aircraft Company IDC 2223/77, 29 July 1964.

5. R.H. Bernard, "Revised Gas Jet Fuel Consumption for 66-hour Mission," Hughes Aircraft Company IDC 2223/843, 19 February 1965.

6. E.I. Axelband, "Analysis of Inertial Pointing Accuracy of Surveyor Midcourse Thrust Vector," Hughes Aircraft Company IDC 2242/2706, 17 June 1963.

7. "Interface Document, Surveyor Vernier Propulsion Thrust Chamber Assembly," Hughes Specification 287015.

8. "Standard Transit Sequence of Spacecraft Operations," Hughes Specification 224550.

9. H.D. Marbach, "Angular Rates at Midcourse Shutdown," IDC 2223/731, 3 February 1965.

10. P.L. Welton, "SC-7 F.C.S.G. Data to be Used for Predicting Acceleration Levels," Hughes IDC 2223/3229, 1 December 1967.

5.5.6 ACKNOWLEDGMENTS

J. Angerman, Technical Coordinator

B.N. Smith

L.R. Stumpf

R.H. Bernard

P.L. Welton

M.R. Buehner

5.6 VERNIER PROPULSION

5.6.1 INTRODUCTION

5.6.1.1 Description

The Surveyor vernier propulsion system (VPS) (Figure 5.6-1) is a bipropellant, variable thrust, liquid rocket system utilizing an oxidizer composed of 90 percent nitrogen tetroxide and 10 percent nitric oxide (Mon 10) and a fuel composed of 72 percent monomethyl hydrazine and 28 percent water. The VPS consists of three regeneratively cooled thrust chambers (TCAs) with radiation-cooled expansion cones. Each TCA has a variable thrust range from 30 to 104 pounds vacuum thrust.

Propellant is supplied to the TCAs from six tanks employing positive expulsion bladders. One fuel tank and one oxidizer tank supply each TCA and are located adjacent to the TCA near each of the three spacecraft landing legs.

Propellant expulsion is accomplished by pressurizing the propellant tanks on the gas side of the bladders with helium gas. The helium is stored under high pressure in a spherical pressure vessel. The helium tank, together with the pressure regulator and servicing connections, is mounted outboard of the spaceframe between landing legs 2 and 3. The dual check and relief valves are mounted on the spaceframe between landing legs 2 and 3.

Thermal control of the VPS is both active and passive. Electric heaters are installed on two oxidizer tanks, one fuel tank, and all propellant feedlines to the TCAs. Passive thermal control consists of polished aluminum or of the application of black and white paint and vapor-deposited aluminum to selected portions of the VPS, together with super insulation applied to the propellant tanks.

The feedlines are wrapped with aluminum foil to deter heat loss.

5.6.1.2 Purpose

The VPS has three main functions during the mission:

1) Midcourse velocity correction and attitude control
2) Attitude control during retro phase

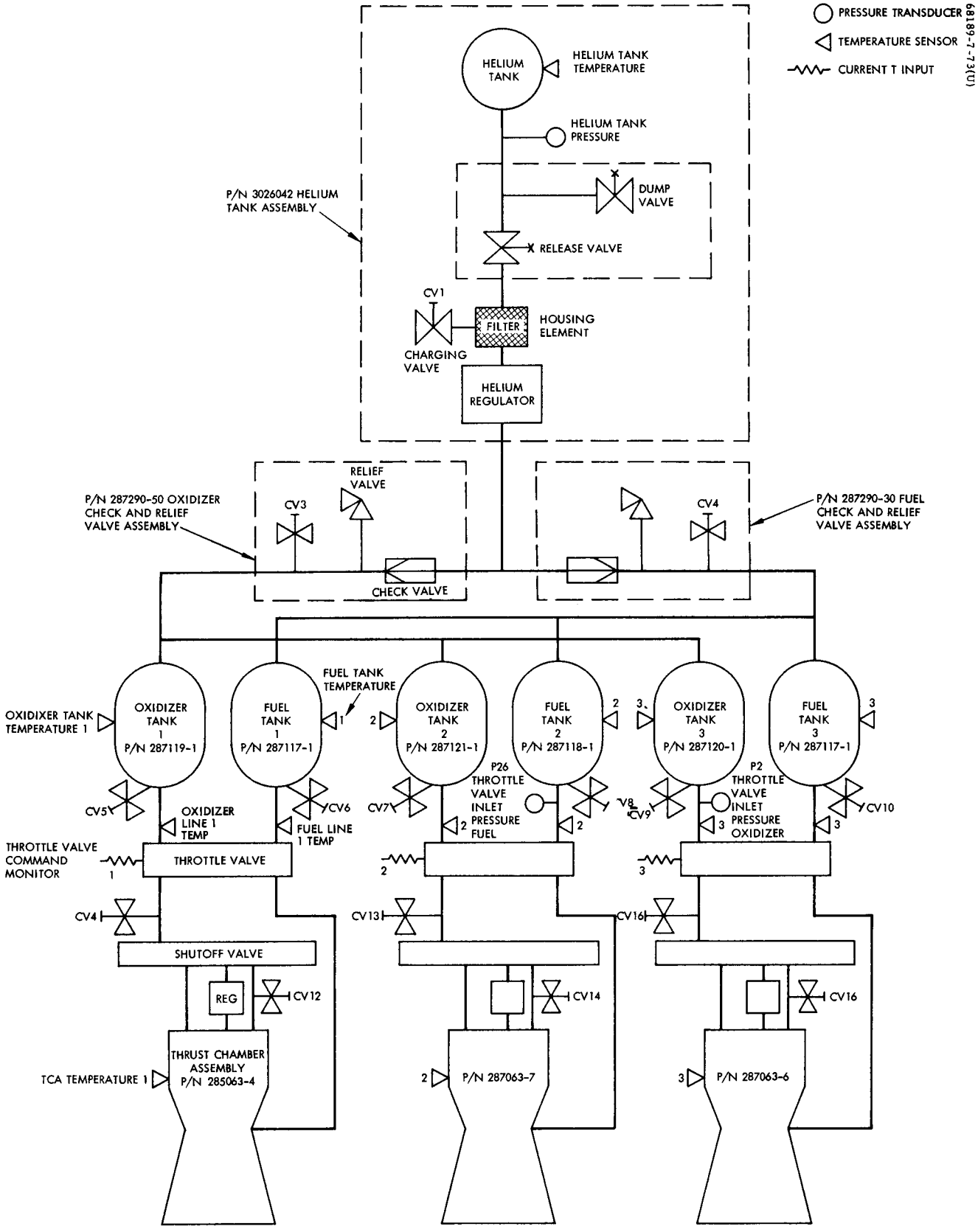

Figure 5.6-1. Vernier Propulsion System Schematic

3) Attitude control and velocity correction during the final descent maneuver

The midcourse velocity correction may be required to correct initial launching and injection errors. The VPS provides velocity corrections up to 50 m/sec with sufficient propellant remaining to successfully land the spacecraft on the moon. The required correction is transmitted to the spacecraft in the form of a desired burn time at a constant acceleration of 0.1 g, which results in a thrust level of approximately 75 pounds for each TCA. In addition to providing the required velocity change, the VPS also provides spacecraft attitude control during the maneuver.

Attitude control during firing of the spacecraft retro motor is provided by the VPS. The VPS is ignited 1.1 seconds prior to retro ignition. Attitude control by the VPS is biased around a total vernier thrust level of either 150 or 200 pounds, depending on predictions of spacecraft attitude and velocity at retro burnout. The desired vernier thrust level is transmitted to the spacecraft several minutes prior to initiation of the retro maneuver sequence. Following retro burnout, the vernier thrust level is increased to 280 pounds total thrust to further slow the spacecraft to allow the ejected retro motor case to fall clear.

Following retro motor ejection, the VPS is throttled to approximately 110 pounds total thrust under radar control. When the spacecraft intersects the first descent segment, the VPS, operating in the closed-loop mode with the radar system, provides the deceleration required to acquire the predetermined altitude-velocity profile and keep the spacecraft on the profile. Each succeeding segment of the profile is acquired in a similar manner. At an altitude of 14 feet, the VPS is shut down, and the spacecraft free falls to the lunar surface.

5.6.2 ANOMALIES

No anomalies were observed during the earth/lunar transit.

5.6.3 SUMMARY

The Surveyor VII vernier propulsion system performed in a nominal manner throughout launch, midcourse, and terminal descent.

Table 5.6-1 lists the time of occurrence of the major events concerning or influencing the vernier engine system.

TABLE 5.6-1. SURVEYOR VII PROPULSION EVENTS

Event	GMT, day:hr:min:sec	Mission Time, hr:min:sec.	Engine Burn Time, seconds
Pressurize propellant tanks	007:23:27:48	16:57:47	NA
Midcourse	007:23:30:10	17:00:09	11.3
Engine burn and terminal descent	010:01:02:15	66:32:14	201
14-foot mark (engines off)	010:01:05:36	66:35:35	NA
Touchdown	010:01:05:38	66:35:37	NA

5.6.4 SUBSYSTEM PERFORMANCE ANALYSIS

5.6.4.1 Prelaunch

Final propulsion preparations for the Surveyor VII launch were finished on 16 December when propellant loading of the vernier system was completed. The desired and actual loadings, given in Table 5.6-2, show that the spacecraft was loaded within the specified tolerance in Reference 1. The helium tank was then charged with 2.41 pounds of helium.

Prelaunch tank temperature and pressure telemetry readings were taken over a 60-hour period and indicated a helium leakage rate of 6.2 psi/day (TFR 85762) which was within the 20 psi/day of Reference 2.

5.6.4.2 Launch (L-2 Hours to L+34 Minutes)

Prelaunch monitoring of the propulsion system was initiated at 1925 hours PST on 7 January when the helium tank pressure and temperature were 5154 psia and 73°F, respectively. At launch, the pressure had increased to 5227 psia, and the temperature was 83°F. All other propulsion data were also within the range specified for launch conditions. The prelaunch conditions of the propulsion system are given in Table 5.6-3.

5.6.4.3 Coast Phase I (L+34 Minutes to L+16 Hours)

Following launch, an assessment of the propulsion functions was made and all conditions were normal. All temperatures decreased approximately as expected. The leg 2 oxidizer temperature decreased to 21°F at L+2H31M, and the heater started cycling between 21° and 25°F at that time. Nine and one-half hours after launch, the helium pressure had stabilized at 5234 psia and the tank temperature was 83°F.

TABLE 5.6-2. PROPELLANT LOADING SURVEYOR VII (POUNDS)

	Predicted at 105°F		Predicted at Ambient		Actual at Ambient	
	Oxidizer	Fuel	Oxidizer	Fuel	Oxidizer	Fuel
Total loaded gross	110.36	75.42	113.98	76.91	115.63	77.00
3 σ loading tolerance	0.75	0.75	0.75	0.75	0.75	0.75
Offload	0	0	3.62	1.49	5.61	1.69
Total loaded net	109.61	74.67	109.61	74.67	109.27	74.56
Unusable at 0°F	1.29	0.86	1.29	0.86	1.27	0.85
Total usable	108.32	73.81	108.32	73.81	108.00	73.71

During this period three three-axis gyro drift checks were performed. Although some drift was noted in all three axes, no effect on thrust chamber assembly temperatures was noted. Stabilized coast phase I thrust chamber assembly temperatures were: leg 1 thrust chamber assembly, 72°F; leg 2 thrust chamber assembly, 75°F; and leg 3 thrust chamber assembly, 80°F.

The premidcourse conditions of the propulsion system are shown in Table 5.6-4.

5.6.4.4 Midcourse (L+16 Hours to L+18 Hours)

Midcourse preparation of the propulsion system consisted of pressurizing the feed system and verification of system readiness for firing. Propellant tank pressures rose and regulator lockup was at 770 psia, well below the relief valve cracking pressures of about 825 psia. The helium tank pressure decreased 185 psi during pressurization (Figure 5.6-2a), compared to a predicted value of 180 psi (Figure 5.6-3a). During burn, the helium tank pressure decreased 248 psi (Figure 5.6-2a) as compared to a predicted value of 240 psi (Figure 5.6-3b). The commanded midcourse correction of 11.3 seconds duration was successfully completed at 07:23:30:20 GMT. The averate corrected, commanded thrust levels for thrust chamber assemblies 1, 2, and 3, as determined from telemetry, were 77.4, 77.6, and 71.5 pounds, respectively. Maximum deviation from predicted values was -3.3 pounds on engine 3, well within the telemetry calibration accuracy.

TABLE 5.6-3. CRITICAL TIME VERNIER PROPULSION SYSTEM PARAMETERS

Parameter	Prelaunch Status	Premidcourse Status	Preterminal Status
Day	007	007	010
GMT, min:sec	06:09	22:50	00:43
Launch time, min:sec	-02:04	+16:20	+66:13
Mode	5/2/1	5/2/1	5/2/1
Bit rate	550	1100	1100
P 1 Helium tank pressure, psia	5227	5154	4857
P 2 Oxidizer leg 3 pressure, psia	275	254	770
P 3 Upper retro case temperature, °F	76	73	66
P 4 Leg 2 oxidizer line temperature, °F	84	23	24
P 5 Leg 2 fuel tank temperature, °F	76	44	29
P 6 Leg 3 oxidizer tank temperature, °F	77	50	43
P 7 Leg 1 thrust chamber assembly temperature, °F	84	71	72
P 8 Leg 1 oxidizer line temperature, °F	84	42	37
P 9 Leg 3 oxidizer line temperature, °F	83	26	23
P10 Leg 2 thrust chamber assembly temperature, °F	83	74	83
P11 Leg 3 thrust chamber assembly temperature, °F	83	80	74

Table 5.6-3 (continued)

Parameter		Prelaunch Status	Premidcourse Status	Preterminal Status
P12	Lower retro case temperature, °F	77	58	42
P13	Leg 1 fuel tank temperature, °F	76	59	55
P14	Leg 3 fuel tank temperature, °F	76	59	54
P15	Leg 1 oxidizer tank temperature, °F	76	63	46
P16	Leg 2 oxidizer tank temperature, °F	75	41	15
P17	Helium tank temperature, °F	83	84	79
P23	Leg 1 fuel line temperature, °F	83	61	57
P24	Leg 2 fuel line temperature, °F	84	31	28
P25	Leg 3 fuel line temperature, °F	83	68	63
P26	Fuel leg 2 pressure, psia	269	265	770

Maximum thrust chamber assembly soak-back temperatures following midcourse were: leg 1, 367°F; leg 2, 349°F, and leg 3, 277°F. Engine start and shutdown delays are given in Table 5.6-5.

5.6.4.5 Coast Phase II (L+18 Hours to L+65 Hours 30 Minutes)

During coast phase II, the helium tank pressure and temperature remained at a constant 4900 psia and 84°F, respectively, until terminal descent maneuvers. All temperatures and pressure remained within specified limits throughout the entire phase. A final estimate for retro T_{3500} of 42.78 seconds was transmitted to FPAC at 009:21:28 GMT.

TABLE 5.6-4. MIDCOURSE DATA SUMMARY, ENGINE THRUST (POUNDS)

Day 107, 1968, GMT, hr:min:sec	Thrust Command FC-25*	Strain Gauge P-18**	Predicted	Thrust Command FC-26*	Strain Gauge P-19**	Predicted	Thrust Command FC-27*	Strain Gauge P-20**	Predicted
23:30:10.7	77.8	75.2	–	79.8	75.8	–	73.3	65.9	–
23:30:11.9	76.7	76.5	–	76.7	75.4	–	72.8	68.1	–
23:30:13.2	77.2	77.3	76.3	76.9	75.3	77.6	72.2	68.7	75.1
23:30:14.4	77.1	76.6	76.3	77.3	75.9	77.6	72.5	68.2	75.1
23:30:15.7	77.6	74.0	76.2	76.9	75.0	77.5	72.1	68.1	75.0
23:30:16.9	76.9	73.3	76.2	77.4	74.1	77.5	71.9	67.5	75.0
23:30:17.6	77.6	72.6	76.1	77.4	74.5	77.4	71.1	67.2	74.9
23:30:18.8	77.1	70.7	76.1	77.8	74.2	77.4	71.5	66.5	74.9
23:30:19.4	77.8	69.8	76.0	77.3	73.6	77.3	71.4	65.4	74.8
23:30:20.7	78.0	68.9	76.0	77.6	73.7	77.3	71.5	64.7	74.8
23:30:21.7	77.4	68.3	76.0	77.6	74.6	77.3	71.5	65.3	74.8

*Corrected for FC-77.

**Corrected for zero offset and drift.

TABLE 5.6-5. ENGINE START AND SHUTDOWN DELAYS (SECONDS)

Engine	Start Delay		Shutdown Delays	
	Midcourse	Flight Acceptance Tests	Midcourse	Flight Acceptance Tests
1	0.045 to 0.125	0.104	0 to 0.025	0.029
2	0.047 to 0.127	0.085	0 to 0.027	0.035
3	0.033 to 0.187	0.116	0 to 0.027	0.039

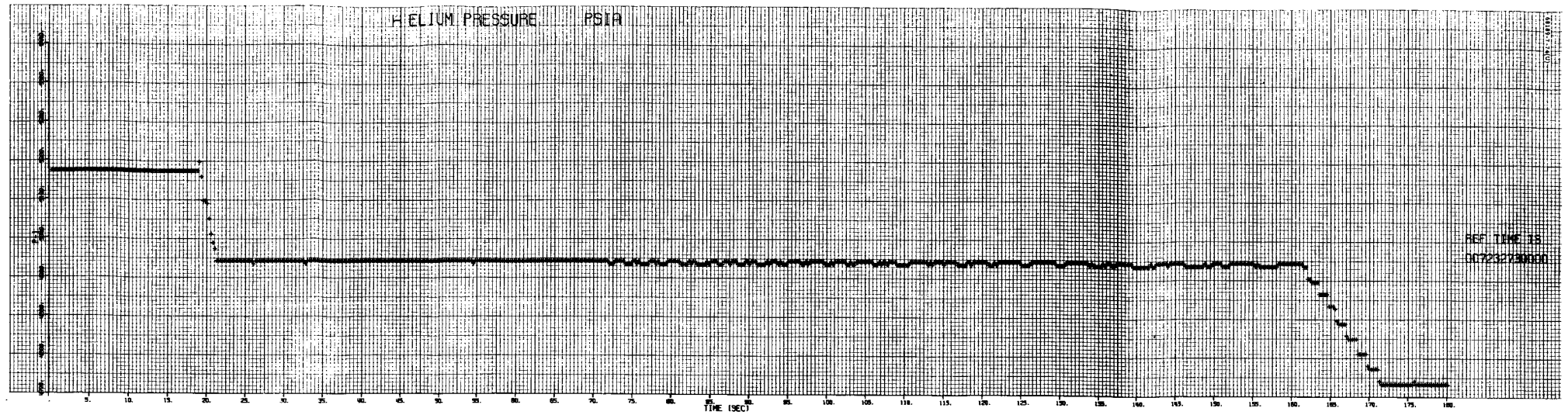

a) Helium Pressure (P-1)

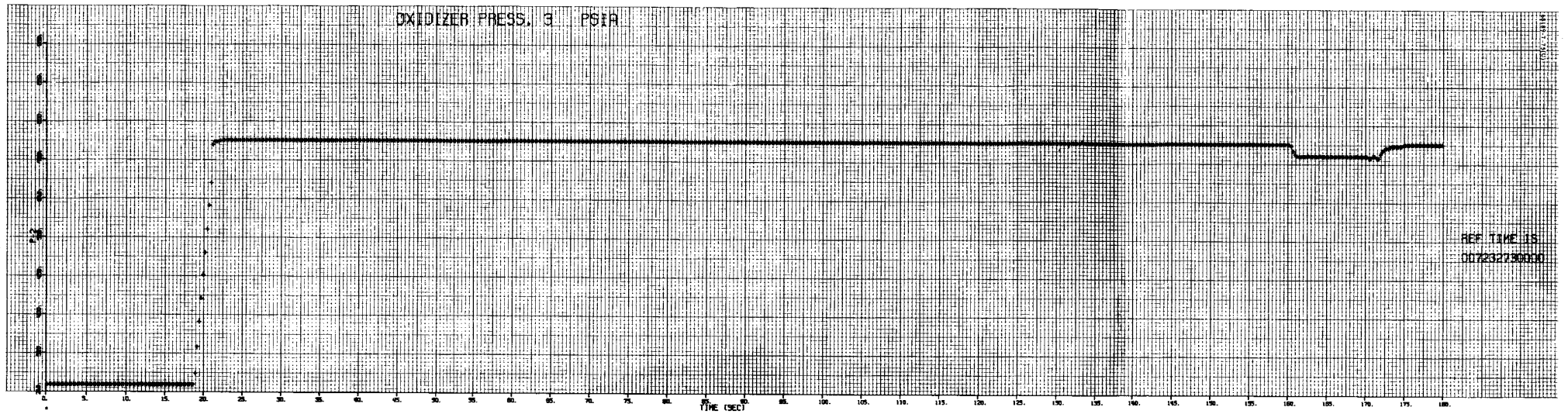

b) Oxidixer Pressure (P-2)

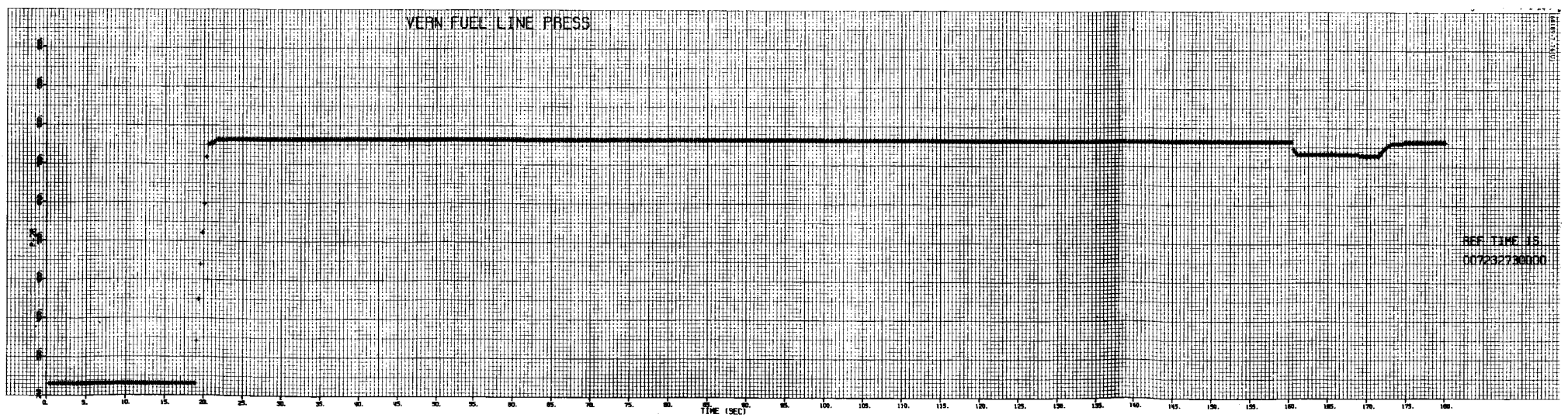

c) Vernier Fuel Line Pressure (P-26)

Figure 5.6-2. Pre- and Postmidcourse Pressure Histories

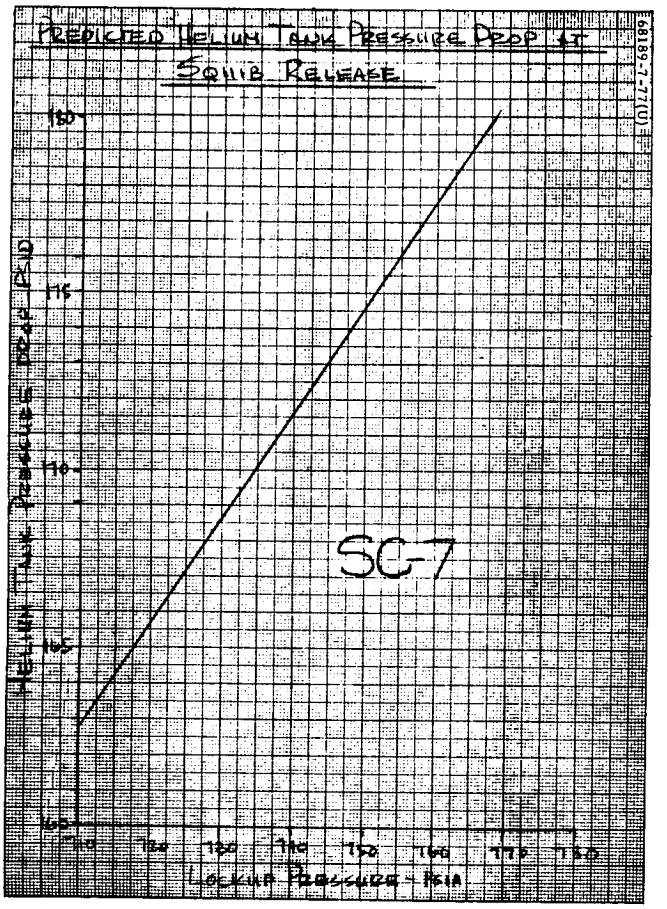

a) At Squib Release

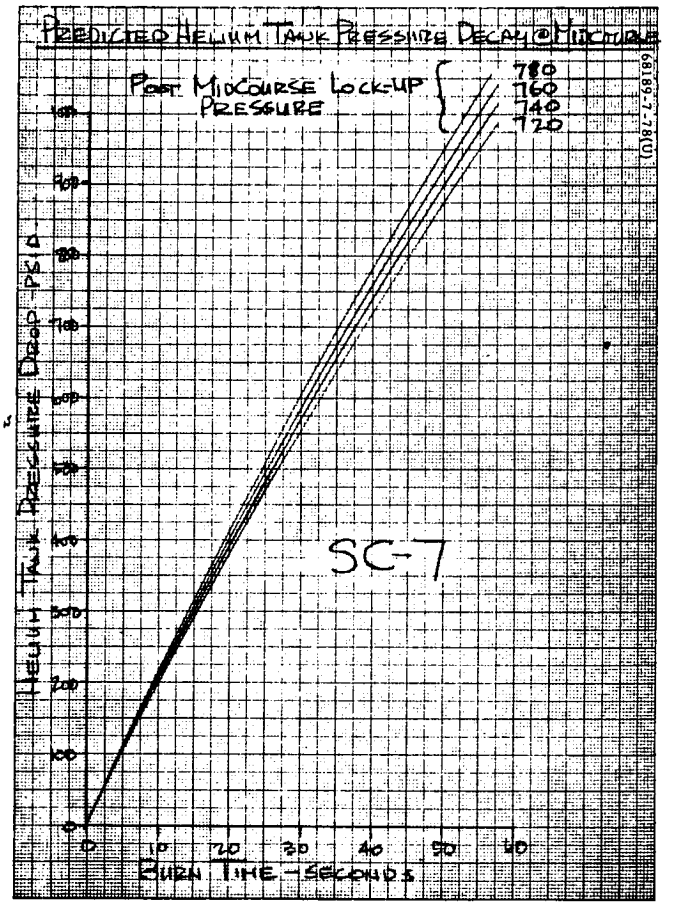

b) At Midcourse

Figure 5.6-3. Predicted Helium Tank Pressure Drop

5.6.4.6 Terminal Descent (L+65 Hours 30 Minutes to L+67 Hours)

Terminal descent operations were initiated at 010:00:03:12 GMT when the transmitter filament was turned on. At the initiation of terminal descent, all propulsion system parameters were normal. A summary of data at that time is contained in Table 5.6-3. Vernier ignition occurred at 010:01:02:15 GMT, followed by retro ignition at 010:01:02:16. Touchdown occurred at 010:01:05:38. All propulsion parameters were normal during the descent.

The observed total vernier thrust level of 193 pounds (corrected) from thrust command data agrees well with the 200-pound thrust predicted during retro burn.

Helium and oxidizer pressure histories during terminal descent are shown in Figure 5.6-4. Fuel pressure is not recorded in the descent mode.

Propellant usage is shown in Table 5.6-6.

TABLE 5.6-6. PROPELLANT USAGE (POUNDS)

Event	Propellant Used	Usable Propellant Remaining
Launch	0	183.8
Midcourse	9.4*	174.4
Terminal descent	150**	24.4

*From engine performance data.

**From helium tank pressure decay data.

5.6.4.7 First Lunar Day

At touchdown, the helium pressure was 2135 psia; the oxidizer and fuel tank pressures were 746 psia. Subsequently, it was recommended that helium not be dumped until it was decided that liftoff and translation maneuvers would not be performed.

Both the propellant tank and helium tank pressure began to increase after touchdown as a result of lunar heating. At 011:03:20 GMT, the oxidizer pressure had reached 838 psia. Shortly thereafter, the oxidizer relief valve actuated, reseating at a pressure of 830 psia. The oxidizer relief subsequently cycled ten times at 6- to 8-hour intervals. Crack and reseat pressures were about 840 and 830 psia, respectively, for each cycle. The fuel relief valve relieved initially at 012:05 GMT and cycled three more

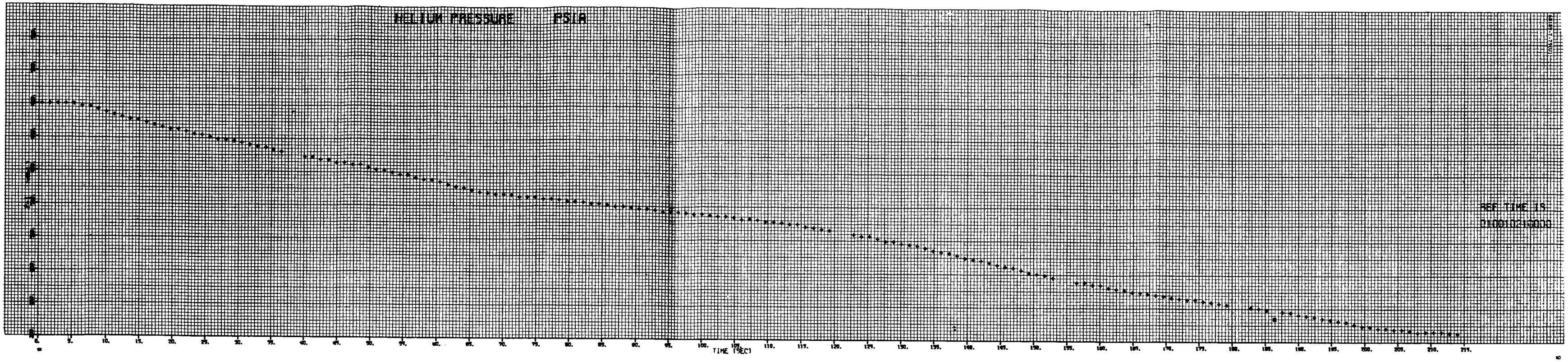

a) Helium Pressure (P-1)

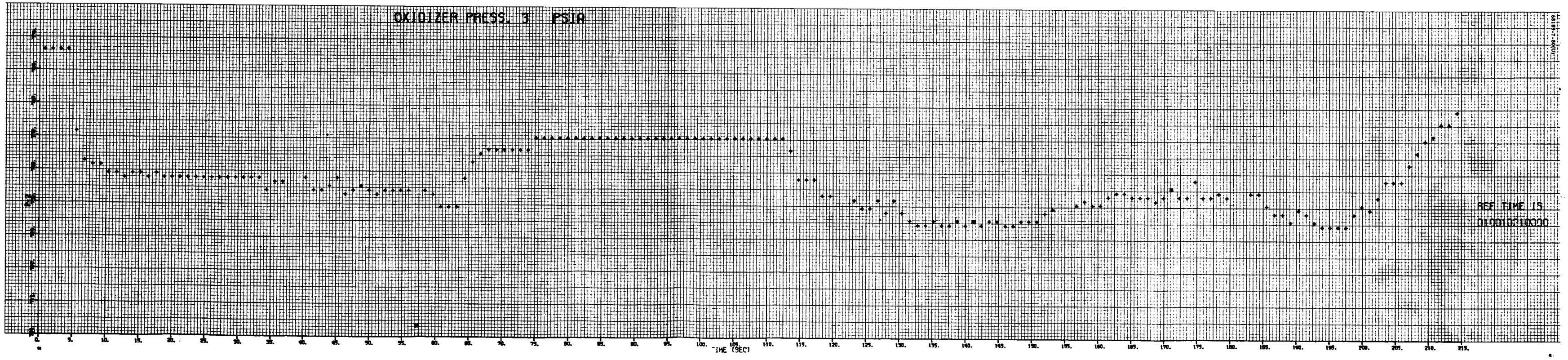

b) Oxidizer Pressure (P-2)

Figure 5.6-4. Terminal Descent Pressure Histories

times in the next 51 hours. Crack and reseat pressures for each cycle were about 810 and 795 psia, respectively.

At 013:20 GMT, the oxidizer relief valve vented and reseated at a pressure of 790 psia. Over the next 61 hours, the pressure built up to 869 psia before relieving and reseating at 845 psia at 016:09 GMT.

Following lunar noon (016:05 GMT) the propulsion system began to slowly cool with an accompanying decrease in helium and propellant tank pressures; correspondingly, no fuel or oxidizer relief valve cycles were noted after 016:09 GMT.

Between 020:21:08 and 020:23:55 GMT, the leg 2 thrust chamber assembly temperature dropped sharply from +88° to 0°F. During the same period, the leg 2 fuel line temperature increased from 139° to 151°F, approaching the leg 2 fuel tank temperature of 158°F. These data are all consistent with a fuel leak at the leg 2 thrust chamber assembly most probably in the shutoff valve poppet area. The leakage was at a slow rate since no significant changes in fuel pressure were noted during this period.

Between 022:01:51 and 022:03:24 GMT, the oxidizer pressure dropped from 699 to 601 psia. The pressure remained at about that level for 15 hours when the pressure rose to 650 psia and was constant until 023:06:32 GMT when it rose to 751 psia. Between 023:09:44 and 023:11:0; GMT, the oxidizer pressure started to decrease steadily until it reached 114 psia at 024:16:08 GMT when the oxidizer pressure transducer open circuited due to the low temperature (-108°F) on the leg 3 oxidizer line.

The variations in oxidizer system pressure noted between 022:01:51 and 023:06:32 GMT are discussed in Appendix A of this section.

The helium pressure transducer became inoperative at 023:21:36 GMT and remained at 549 psia when the helium pressure decreased to zero. The fuel pressure transducer also open-circuited due to the low temperature at 025:11:14 GMT.

By the end of day 025, all propulsion system pressures had decayed to zero.

A vernier propulsion system performance summary for all spacecraft is presented in Appendix B to this section.

5.6.5 REFERENCES

1) R. Laird to Distribution, "A21 and A21A/114 Vernier Propulsion Systems Propellant Inventory," Hughes IDC 2227.1/1110, 29.

2) G. F. Pasley to P. A. Donatelli, "Allowable Helium Leakage for SC-6," Hughes IDC 2227.2/1244, 3 October 1967.

3) T. B. Shoebotham to E. Pfund, "Mission G SPAC Report," Hughes IDC 2227. 1/2314, 23 January 1968.

4) T. B. Shoebotham to K. Filetti, "Surveyor VII First Lunar Day Report," Hughes IDC 2227. 1/2335, 1 February 1968.

5. 6. 6 ACKNOWLEDGMENTS

This section was coordinated by G. F. Pasley who also wrote Appendix A.

T. B. Shoebotham contributed to the transit section through References 3 and 4 and to Appendix B. J. P. Amelsberg contributed to the transit performance and Appendix B.

APPENDIX A TO SECTION 5.6

SURVEYOR VII FIRST LUNAR DAY VERNIER SYSTEM PRESSURE LOSS STUDY

INTRODUCTION

The vernier propulsion system exhibited normal thermal response to the changing lunar environment through most of the lunar day; however, toward the end of the day there were pressure and temperature fluctuations that indicated propellant and gas leakage. This study attempts to isolate the location and cause of these leaks.

DISCUSSION

From lunar landing at 010:01:05 until 020:21:08 GMT, the vernier propulsion system behaved normally (Figure 5.6-A1). However, at 020:23:55 GMT the engine 2 temperature had dropped sharply (Figure 5.6-A2) from +88° to 0°F. There was a simultaneous rise in the engine 2 fuel line temperature from 139° to 151°F, indicating flow to the engine from fuel tank 2 which was at 158°F. Engine cooling was due to propellant vaporization at the fuel shutoff valve poppet. An analysis of fuel system pressures and temperature shows no evidence of leakage prior to the engine 2 temperature fluctuations but does show a leakage rate of about 10 psi/hr afterwards. As soon as the fuel system pressure had dropped to 728 psia (022:17:21 GMT), the helium regulator opened and slowly repressurized the fuel system to 767 psia at 023:09:44 GMT. The pressure stabilized at that level until 023:13:06 when the decaying helium tank pressure was unable to maintain downstream regulator pressure. The fuel pressure then followed the helium tank pressure down to zero pressure, verifying the fuel side leak. Thermal sensor data taken during the lunar night show evidence of propellant freezing in both fuel line 2 and fuel tank 2, thus indicating that not all the fuel had leaked out through the engine.

Between 022:01:51 and 022:03:24 GMT, the oxidizer pressure dropped from 699 to 601 psia, indicating a leak on the oxidizer side of the vernier propulsion system. Postmission analysis of pressure and thermal data indicates that there was no leakage on the oxidizer side of the system prior to this fluctuation in pressure. Afterwards, however, the leakage rate was found to be 1.2×10^{-6} lb/sec, which corresponds to a very small orifice size of 5.5×10^{-4} inch diameter. Oxidizer pressure was maintained by the helium supply at about 600 psia for 15 hours; then it rose to 650 psia and

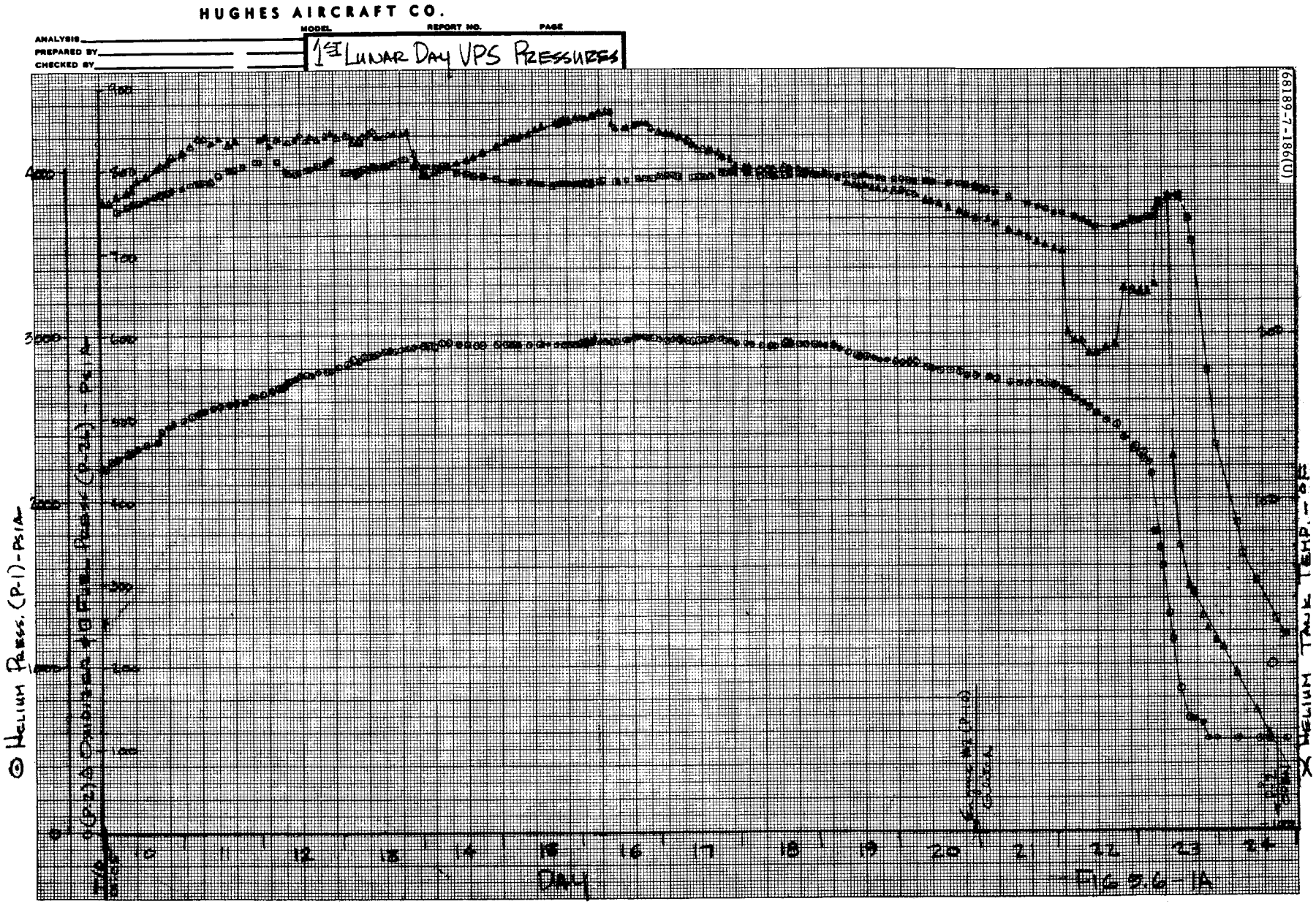

Figure 5.6-A1. First Lunar Day Vernier Propulsion System Pressures

stabilized there until 023:06:32 GMT. Postmission analysis indicates that this leakage orifice area was the same one as during the previous period; correspondingly, the change in oxidizer pressure was due to a changing flow restriction upstream of oxidizer tank 3 (the location of the oxidizer pressure sensor), rather than a decreasing leakage area. The type of restriction which could cause the observed pressure history is discussed later in this appendix. At 023:06:32 GMT, the oxidizer pressure rose again to 751 psia. Analysis of tank pressures, temperatures, and propellant vapor pressures on both fuel and oxidizer sides of the system shows that the leakage rate increased substantially during this time period. The leakage hole size increased to about 13×10^{-4} inch diameter. The data available do not indicate the location of the leak. The increase may be the result of a larger fuel leak. (A perturbation on P-8, oxidizer line 1, at 023:08 GMT was due to a line heater activation. The temperature resumed the normal profile when the heater was deactivated at 023:11.)

Since liquid leaks are usually indicated by large temperature fluctuations on the tank or engine temperature sensors, the oxidizer leakage was probably gaseous. Since the fuel pressure history verifies normal regulator operation, the variations in oxidizer tank 3 pressure must be explained by a variable flow restriction between the regulator and oxidizer tank 3 (the pressure sensor location). Either a "sticking" oxidizer check valve or a deformed teflon cap at the junction of the standpipe and propellant tank could have caused the observed behavior.

Assuming the check valve was the failure cause, the check valves normally open at a 4-psi differential; however, the data indicate the check valve did not open fully at 100 psia. These facts make this failure mode very unlikely. The observed pressure history could also have resulted from deformation of the teflon cap at the junction of the standpipe and tank. Increasing pressure during the lunar morning could have forced the cap into the tank pressurization ports and restricted gas flow. This failure mode could also account for the increasing oxidizer relief pressures seen prior to lunar noon (Figure 5.6-A1). No evidence of this type of failure has been seen on previous spacecraft and so is not considered to be any more or less likely than a check valve failure.

Since the selection of either of these problems as the explanation of the pressure history does not provide an external leak path, two simultaneous failures must be postulated. The two most likely leakage causes are relief valves and O-ring seals since they have failed on previous spacecraft. The O-ring seal in oxidizer tank 3 had experienced lower lunar day temperatures than oxidizer tank 2 (Figure 5.6-A3); however, the peak temperature was much higher (190°F) than the design limit of 100°F. The erratic behavior of the relief valve could be evidence of potential failure, but the data indicate it seated satisfactorily after the last cycle; there is no reason, therefore, to expect it to allow leakage late in the lunar day when temperatures are steadily decreasing. It is concluded, then, that both leakage sights are equally unlikely.

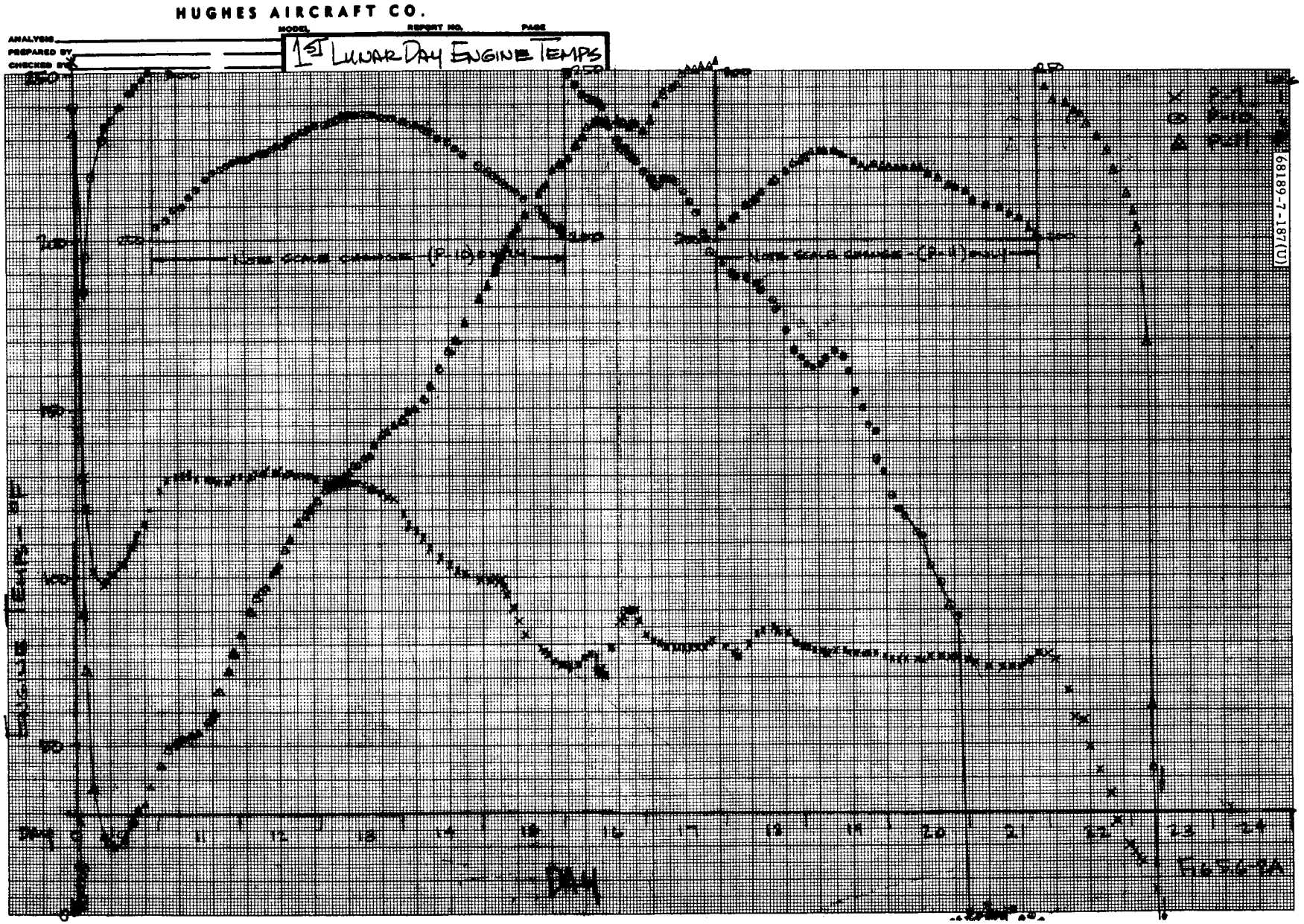

Figure 5.6-A2. First Lunar Day Engine Temperatures

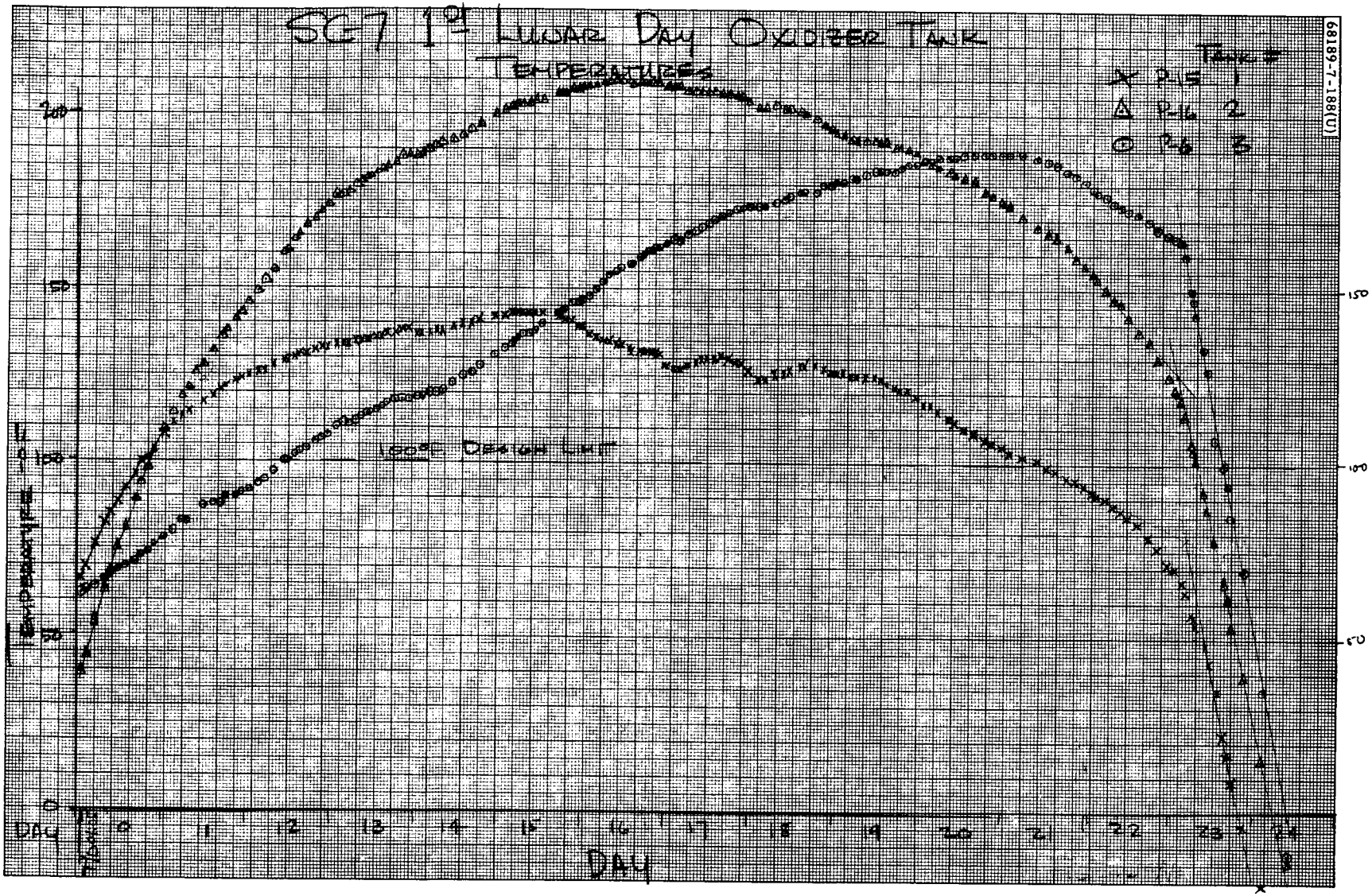

Figure 5.6-A3. First Lunar Day Oxidizer Tank Temperatures

CONCLUSIONS

A fuel and gas leak occurred through the engine 2 shutoff valve poppet. A gas leak occurred in the oxidizer system (location unknown). These leaks were the result of material degradation at the lunar temperatures.

APPENDIX B TO SECTION 5.6

SURVEYORS I THROUGH VII VERNIER PROPULSION SYSTEM PERFORMANCE SUMMARY

INTRODUCTION

To allow comparison of the major vernier propulsion system performance parameters, the parameters have been grouped into the following categories:

Engine shutdown impulse dispersons at midcourse

Propellant and helium usage

First lunar day leakage

Lunar static fire and hop performance

SUMMARY OF PERFORMANCE

Comparisons of spacecraft performance for all flights are summarized in Tables 5.6-B1 through 5.6-B3.

Thrust Chamber Assembly Shutdown Impulse Dispersions

Shutdown impulse dispersions are calculated from gyro errors observed during the engine shutdown transient and are presented in Table 5.6-A1.

Propellant Helium Usage

Table 5.6-B2 gives a summary of the propellant and helium usages for all Surveyor missions. The total usable propellant is obtained from the difference of the total loaded gross propellant and the 3σ loading tolerance, offloaded propellant, the unusable propellant due to bladder expulsion inefficiencies, and that trapped in the lines and thrust chamber assemblies. The total prelaunch helium pressure is that value read immediately prior to launch. The helium tank temperature and pressure are monitored several hours or days before launch. This value is compared to the immediate prelaunch figures from which the prelaunch helium leakage is determined. When the helium squib release valve is fired, the helium tank pressurizes the propellant to operating pressure, resulting in a decrease of helium tank

TABLE 5.6-B1. MIDCOURSE CORRECTION THRUST CHAMBER ASSEMBLY SHUTDOWN IMPULSE DISPERSIONS (LB-SEC)

Spacecraft	Leg 1	Leg 2	Leg 3
I	+0.27	-0.37	+0.10
2	—	—	—
III	-0.31	+0.42	-0.11
4	-0.18	+0.03	+0.15
V			
(1)*	-0.16	+0.05	+0.01
(2)	-0.10	+0.18	+0.08
(3)	-0.13	+0.11	+0.02
(4)	-0.17	+0.10	-0.03
(5)	-0.53	+0.65	-0.12
(6)	-0.29	+0.15	+0.14
VI	+0.085	-0.09	+0.005
VII	-0.144	+0.259	+0.115

*Parentheses denote particular vernier ignitions.

TABLE 5.6-B2. SURVEYOR MISSIONS PROPELLANT AND HELIUM USAGES

	Spacecraft						
	I	2	III	4	V	VI	VII
Total usable propellant, pounds	181.84	180.28	181.66	182.01	181.28	182.59	181.71
Total prelaunch helium, psia	5148	5168	5222	5170	5342	5219	5227
Prelaunch helium leakage, std cc/hr	346	≈0	13.5	76.6	123	167	233
Helium consumption squib release, psia	188	≈206	220	217	182	179	185
Midcourse helium usage, psi	383	*	102	208	310	208	248
Midcourse propellant usage, pounds	16.50	*	3.6	8.2	11.3	8.4	9.4
Terminal descent helium usage, psi	2122	*	2775	711**	276***	2539	2722
Terminal descent propellant usage, pounds	122.5	*	151.1	29.6**	60.1***	145	150

*Spacecraft 2 did not complete a satisfactory midcourse and the mission was aborted.

**Spacecraft 4 was lost during terminal descent, so these numbers do not represent normal usages.

***These figures represent a nonstandard descent resulting from vernier propulsion system problems.

TABLE 5.6-B3. SURVEYOR LUNAR LEAKAGE SUMMARY

Parameter	Spacecraft				
	I	III	V	VI	VII
Time from touchdown to first indication of leakage, hours	105	210	181	228	260
Propellant leakage					
Oxidizer	X	X	X	X	X
Fuel			X		X
Type of leakage					
Gas	X	*	X	*	X
Liquid		X	X	X	X
Location of leakage					
Relief valve	X				*
O-ring seal			X	X	*
Thrust chamber assembly		X			X

*Suspected, but data inadequate to determine.

pressure. The difference in the pre- and postmidcourse correction helium pressures give the midcourse correction helium usage. Midcourse correction propellant usage is determined from the thrust commands and thrust chamber assembly performance parameters. Terminal descent helium and propellant usages are calculated in the same manner as the midcourse correction values.

First Lunar Day Leakage Summary

Introduction

The vernier propulsion system was designed to function over a temperature range of 0° to 100°F and survived tests simulating this temperature range; however, prior to the first lunar landing, lunar temperatures had been predicted to vary between -250° and 250° ± 50°F, which made lunar survival of the vernier propulsion system questionable. The following discussion describes the leakage history seen on each soft landed spacecraft (I, III, V, VI, and VII).

Discussion

Surveyor I landed on the lunar surface at 153:06:17:35 GMT 1966. Helium bottle pressure was dumped, as planned, in an effort to preclude propellant expulsion in the spacecraft vicinity. It was thought the propellant vaporization might deposit film on camera mirrors and lenses and also degrade thermal finishes on critical components. The oxidizer tank relief valves cycled normally for 105 hours after touchdown and then failed to reseat, allowing the oxidizer pressure to drop to the propellant vapor pressure. The failure of the oxidizer relief valve to reseat was attributed to the valve temperatures which were far above the design limits.

Surveyor III landed at 110:00:04:51 GMT 1967. The helium tank gas was not vented immediately since a lunar translation was under consideration; however, 116 hours after landing the helium tank pressure was vented since no lunar firings were to be attempted. One hundred sixty-five hours after touchdown the oxidizer pressure began to fall, and 45 hours later the oxidizer pressure had leveled off at 712 psia. A corresponding sag in oxidizer line 1 and engine 1 temperatures indicated oxidizer liquid leakage through that engine. Pressures were not monitored beyond 215 hours after touchdown.

Surveyor V landed at 254:00:46:44 GMT 1967. Helium tank pressure was not vented since a lunar translation was under consideration. A successful static firing was accomplished 55 hours after touchdown. One hundred eighty-one hours after touchdown the oxidizer pressure began to fall. Concurrently, thermal data indicated a liquid leak through the oxidizer tank 1 O-ring seal. Two hundred seventy-five hours after touchdown the fuel pressure began to decrease steadily until zero pressure was reached 20 hours later. Since there was no indication of a liquid leak, the leakage was attributed to a gas side seal leakage.

Surveyor VI landed on 314:01:01:05 GMT 1967. Propulsion system parameters were normal for 228 hours, after which the oxidizer pressure began to fall. Thermal data indicated that oxidizer tank 1 was leaking liquid at the O-ring seal. The leakage continued and resulted in complete oxidizer pressure loss by the end of the lunar day. The fuel pressure held throughout the lunar day.

Surveyor VII landed on 010:01:05:38 GMT 1968. As before, the helium pressure was not vented since the possibility of a lunar translation existed. Propulsion parameters were normal until 260 hours after touchdown when the leg 2 thrust chamber temperature dropped sharply. Concurrently, the leg 2 line temperature rose to near propellant tank temperatures. These data indicated a liquid fuel through the engine 2 shutoff valve poppet area. Twenty-eight hours later the oxidizer pressure began to behave erractically. The thermal data indicated that a gas leak had occurred on the oxidizer side (location unknown). By the end of the lunar day all propulsion pressures had decayed to zero.

After the indication of oxidizer relief valve failure on Surveyor I, an intensive test program was run to find the offending relief valve part. Lunar temperatures and exposure times were simulated without valve malfunction or failure. Lunar vacuums and thermal gardients were not simulated.

Conclusions

The Surveyor vernier propulsion system was unable to withstand, without leakage, the extreme temperatures through a complete lunar day. Survival times ranged from 105 to 260 hours. Leakage problems are summarized in Table 5.6-B3.

Static Fire and Lunar Translation Performance Review

Surveyor V

At lunar touchdown the helium tank pressure and temperature were 574 psia and 78°F, respectively. Since the gas system was in a blowdown condition at touchdown, the oxidizer and fuel systems were also at approximately the same pressure as the helium tank. A successful static firing was accomplished approximately 55 hours after touchdown. Because of lunar heating, the helium, oxidizer, and fuel pressures gradually increased to 645, 731, and 665 psia, respectively, at the time of the static firing. The oxidizer and fuel check valves prohibited the pressures from equalizing. All thrust chamber assemblies burned for the commanded duration of 0.5 second. The indicated thrust levels were 22, 17, and 26 pounds for legs 1, 2, and 3, respectively.

Surveyor VI

At lunar touchdown the helium tank pressure and temperature were 2314 psia and approximately 42°F, respectively; the oxidizer tank pressure was 734 psia. Both the helium and propellant tank pressures began to increase after touchdown as a result of lunar heating. At 177.5 hours after touchdown, the helium pressure and temperature had increased to 3886 psia and 169°F, respectively; the oxidizer pressure had risen to 847 psia. At this time, a liftoff and translation experiment was performed. By selective positioning of the antenna/solar panel positioner, it was possible to bring all three thrust chamber assembly temperatures within the 220°F maximum lunar operating limit. The thrust chamber assembly preignition temperatures were 204°, 191°, and 189°F on legs 1, 2, and 3, respectively. The commanded thrust level and duration was 150 pounds for 2 seconds. However, post-translation data evaluation indicated an average total thrust level of 146 pounds and a duration of 2.5 seconds because the backup thrust cutoff command terminated thrust. Approximate individual thrusts were 50, 50, and 46 pounds on legs 1, 2, and 3, respectively. During the 8-foot lateral translation, the spacecraft reached an altitude of 13 feet and rotated 7 degreees counter clockwise about the roll axis. The spacecraft was aloft approximately 6.1 seconds. Maximum postshutdown thrust chamber assembly temperatures were 335°, 324°, and 232°F on legs 1, 2, and 3, respectively. Static firings or liftoffs were not attempted on the other spacecraft.

5.7 PROPULSION – MAIN RETRO

5.7.1 INTRODUCTION

The main retro-rocket, which performs the major portion of the deceleration of the spacecraft during terminal descent, is a spherical solid propellant unit with a partially submerged nozzle.

The unit is attached at three points to the spacecraft near the landing leg hinges, with explosive nut disconnects for postfiring ejection. Friction clips around the main retro-rocket engine nozzle flange provide attachment points for the altitude marking radar. The igniter gas pressure ejects the altitude marking radar when the retro firing sequence is initiated. The main retro-rocket engine ignition squibs and retro release explosive nuts operate from a pulsed, 19-ampere, constant-current source. Commands are initiated by the flight control system.

The nozzle is partially submerged to minimize overall length. The nozzle has a graphite throat insert backed up by laminates of carbon cloth phenolic with a fiberglass exit cone lined with bulk carbon phenolic. The case is of high strength steel and insulated with asbestos and inorganic fiber-filled buna-N rubber to maintain the case at a low temperature level during burning.

The main retro-rocket engine with propellant weighs approximately 1446 pounds. The engine utilizes an aluminum, ammonium perchlorate, polyhydrocarbon, case-bonded, composite-type propellant, and conventional grain geometry. The engine thrust may vary between 8000 to 10,000 pounds over the temperature range of 50° to 70°F.

Two thermal sensors are installed on the main retro-rocket engine case for telemetering engine temperature during transit. The thermal sensor for monitoring nozzle temperature during transit is no longer used.

The main retro-rocket engine employs a safe and arm device that has dual firing and single bridgewire squibs for the engine igniter. In addition, provisions for local and remote safe and actuation and remote indication of inadvertent firing of the squibs are included. Both mechanical and electrical isolation exists between squib initiator and pyrogen igniter in the safe condition.

5.7.2 ANOMALY DESCRIPTION

No anomalies were noted in the main retro subsystem.

5.7.3 SUMMARY

The Surveyor VII main retro-rocket engine operated within all required tolerances. Table 5.7-1 presents a summary of main retro performance parameters.

TABLE 5.7-1. SUMMARY OF MAIN RETRO PERFORMANCE PARAMETERS

Parameter	Predicted Main Retro Value	Required Main Retro Value or Tolerance	Actual Value	Uncertainty
Bulk temperature, °F	54	±15	54	±5
T_{3500}, seconds	42.78	±0.4	42.86	±0.1
Maximum thrust, pounds	9280	<10,000	9200	±100
Total impulse, lb-sec	376,252	±3600	376,680	±1800
Specific impulse, seconds	289.5	±0.3	289.8	±1.5
Center of gravity excursion, inch	–	<0.030		
Thrust vector excursion			0.039*	±0.020
Displacement, inch	–	<0.040		
Angular, degree	–	<0.2		
Roll torque, in-lb	–	<80	52* **	±12

*Total value from all sources.

**Maximum value occurred at ignition.

5.7.4 SUBSYSTEM PERFORMANCE ANALYSIS

Table 5.7-2 gives the major events and times associated with the firing of the retro engine. Times are referenced to ground station.

TABLE 5.7-2. MAJOR EVENTS AND TIMES FOR RETRO OPERATION

Event	Day:010:01:GMT, 1968 min:sec	Maximum Error, second
Vernier ignition	02:14.692	±0.05
Retro ignition	02:15.792	±0.05
3500-pound thrust level	02:58:652	±0.05
"Actual" 3.5 g	02:58.882	±0.05
3.5 g switch	02:58.975	±0.025
Retro eject signal	03:10.990	±0.05

Items consituting the analysis effort are as follows:

1) Reconstruction of thrust versus time curve from accelerometer and doppler data (Figure 5.7-1)

2) Calculation of engine specific impulse

3) Determination of thrust vector excursions and roll moments generated by the retro engine

4) Determination of T_{3500}

5.7.4.1 Thrust Versus Time

The technique used in reconstruction of the thrust versus time trace from both accelerometer and doppler data is discussed in subsection 5.15.6.2 of Reference 1. This reconstructed trace varies from the predicted trace as shown in Figure 5.7-1. The maximum difference is 6 percent, and it occurs 5 seconds after ignition. This, however, is in an area of higher error for the accelerometer data since the spacecraft passes through a period of rapid change in acceleration to a fairly steady acceleration.

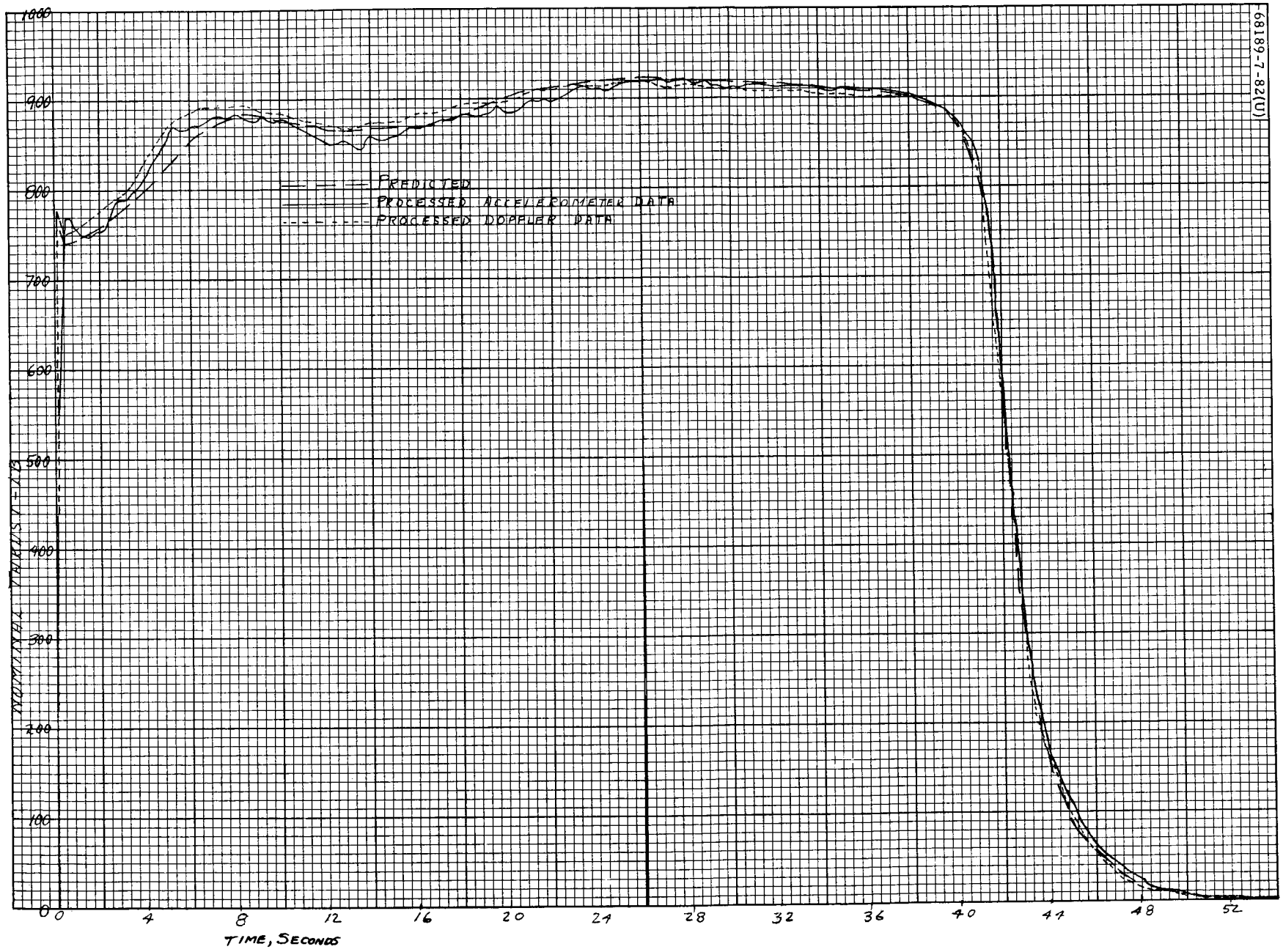

Figure 5.7-1. Main Retro Engine Thrust Versus Time

5.7.4.2 Specific Impulse

The main retro-rocket engine specific impulse was obtained by correcting the predicted nominal specific impulse used in the preflight descent trajectory computer program by the change in velocity measured during retro burning on Surveyor VII. The difference between the actual and predicted change in velocities, 8397 and 8387 fps respectively, amounts to 0.11 percent low versus the 1 percent allowed. This approach is conservative from the retro-rocket engine point of view since the velocity difference is actually due to a number of sources in addition to the main retro-rocket engine. Some of these other sources are as follows:

1) Uncertainty in vernier engine specific impulse

2) Uncertainty in vernier engine thrust level

3) Uncertainty in vernier engine weight versus time

4) Uncertainty in retro-rocket engine specific impulse versus time

5) Uncertainty in retro-rocket engine weight versus time

6) Uncertainty in doppler data

5.7.4.3 Retro Disturbance Torques

The following retro disturbances were noted:

1) Retro ignition produced a short duration disturbance torque of approximately 28 ft-lb.

2) Following retro ignition, all three vernier engines settled near their mid-thrust condition and remained steady throughout retro burning, except for one disturbance of 32 ft-lb at 39 seconds into burning. This disturbance was quickly corrected.

3) The maximum required corrective roll torque produced by the vernier engines after accounting for bracket bending was 4 ft-lb at ignition and 2 ft-lb during burning. Assuming all this torque was required due to the retro engine, the engine roll torque was still well below the 7 ft-lb maximum moment allocated to the retro engine.

4) Retro engine ejection from the spacecraft was smooth and required no apparent corrective torque.

5.7.4.4 T_{3500}

The T_{3500} (time from ignition to the time when thrust decays to 3500 pounds) prediction was acceptable. The total error of 0.2 percent is within the 1 percent tolerance for the prediction. This total error is the

result of the actual engine temperature gradient uncertainty, the error in calculating the bulk temperature corresponding to that gradient, telemetry error, and prediction error.

5.7.5 REFERENCES

1) "Surveyor Spacecraft A21 Model Description," Hughes Aircraft Company, Document No. 224847B, 1 March 1965.

2) "Surveyor Main Retro Engine A22-14 Support Documentation," Thiokol Chemical Corporation.

3) "SC-7 Event Time from Teltab," Hughes Aircraft Company.

5.7.6 ACKNOWLEDGMENTS

The following people contributed to the main retro analysis:

L. M. Spicer, Coordinator

E. W. White, Systems Analysis

L. H. Davids, Systems Analysis

5.8 ALTITUDE MARKING RADAR

5.8.1 INTRODUCTION

The Surveyor altitude marking radar (AMR) is a small, conventional, pulsed, X-band, fixed dual range gate, marking radar designed by Hughes Aircraft Company. The purpose of the AMR is to provide, with high accuracy and reliability, a signal indication that slant range from the Surveyor spacecraft to the lunar surface has decreased to a preset value, nominally 60 statute miles for the A-21 series of engineering models. This signal starts an on-board timer whose run-out time is set by ground command earlier in flight to initiate vernier and main retro engine ignition. Since the AMR is installed in the exhaust cone of the main retro engine, it is forcibly jettisoned from the spacecraft when that engine is ignited, having served its purpose in providing ignition timing.

The AMR is a conventional, noncoherent radar employing a pulsed magnetron; single antenna; duplexed mixer; crystal-controlled, solid-state local oscillator; wideband IF amplifier; noncoherent detector; and video processing circuitry. Dynamic range is extended by IF amplifier AGC; AGC voltage is telemetered, and provides an indication of received signal power. The video circuitry is of special design to mark at a preset range with high accuracy and reliability. Two fixed, adjacent range gates continuously examine the video signal; their outputs are continuously summed and differenced. When the sum exceeds a fixed threshold and the difference simultaneously crosses zero with positive slope, the mark signal is generated. Sum threshold is set for an extremely low probability of marking on noise (false mark) throughout the operating time, while video integration, plus a very substantial radar gain margin, ensures a high probability of successful marking.

Two separate ground commands, whose transmission times are controlled, are required to fully activate the AMR. The first signal, called AMR on, commands on the primary power to the AMR, which includes all internal power except high voltage to the transmitter. The video signal is inhibited from reaching the marking circuits until the second command, thus eliminating any residual probability of false marking on noise during this warm-up interval. The second signal, called AMR enable, commands on the transmitter high voltage and also removes the video inhibit. This enabling function is timed, not only for favorable thermal conditions at the expected marking time, but also for the purpose of precluding premature marking on second-round echoes at much longer ranges. In a lunar mission, FPAC supplies a

marking time prediction based upon trajectory data. The prescribed times for SPAC transmission for these two commands are: "on" at 280 ± 10 seconds, and "enable" at 100 ± 10 seconds before predicted marks.

For proper analysis, complete trajectory information is required. While either known or assumed for preflight predictions, it must be known or derived for postflight evaluation. Spacecraft attitude and velocity data are supplied by FPAC from tracking and trajectory computations. Residual range uncertainty, however, exceeds that of the AMR itself, which is assumed to have marked with mean value and dispersion predicted by radar analysis prior to each mission. In conjunction with approach velocity and attitude conditions from FPAC, the trajectory can then be extrapolated backward with high accuracy by a special two-body program. This program derives all the significant AMR parameters throughout the nominally 100-second interval from enable to mark, and calculates correction factors to be applied to observed telemetry data before comparison with predicted received signal power.

AMR telemetry includes three digital and three analog signals, plus analog temperature data. The digital signals confirm on-board discrete events: prime power application (R-1, AMR on), high voltage and video enabling (R-11, AMR enable), and slant range trigger (FC-64, AMR mark). It should be noted that FC-64 is telemetered only when the on-board mark is generated, and not in response to the backup command from earth. The three analog signals (besides temperature) are magnetron current (R-12), AGC voltage level (R-14), and late gate detected video voltage level (R-29). The AGC not only confirms receiver response to RF return, but is also useful in evaluating terrain reflectivity. The magnetron current confirms pulsing of the magnetron after enable, and is useful primarily as a transmitter failure mode indication. The late gate signal, primarily a receiver failure mode indication, normally confirms the presence of a gated video signal rising quickly to a peak at the time of mark and decaying quickly thereafter. All but a few of its values are normally at the quiescent noise level, and in no way constitute repeated events.

5.8.2 ANOMALIES

There were no anomalies in AMR operation during the Surveyor VII mission.

5.8.3 SUMMARY

The Surveyor VII AMR functioned normally. The true altitude mark was generated at the expected time and initiated the automatic terminal descent sequence as planned. The routine emergency mark backup command was received by the spacecraft after the on-board mark had been generated.

The AMR power was turned on 275.54 ± 0.24 seconds before mark, acceptable within the 280 ± 10 seconds specified. It was enabled 95.55 ± 0.24 seconds

before mark, acceptable within the 100 ± 10 seconds specified. EP-17 showed normal current drain characteristics throughout AMR operation and jettison, and AMR magnetron current (R-12) was normal before, during, and after the enable operation. The late gain signal (R-29) was normal, confirming the presence of RF return signal and detected video within the gate at the time of the mark.

The variation of the processed telemetered signal strength (AGC) is in close agreement with the variation of the nominal predicted values. However, in general, the telemetry value is 2.5 to 4.5 db higher than the predicted value. These higher received signal levels may be due to the lunar terrain having better reflectivity characteristics than expected. It should be noted that the initial telemetry data were low because of the circuit response time.

5.8.4 SUBSYSTEM PERFORMANCE ANALYSIS

5.8.4.1 Event Times

From the table of Surveyor VII events associated with radar operation (subsection 5.9.4), the following AMR events are repeated below. The times listed are GMT when recorded at DSIF 11.

Channel	Name	GMT at DSIF 11, day:hr:min:sec
R-1	AMR on	10:00:57:36.351 ± 0.19
R-11	AMR enable	10:01:00:36.345 ± 0.19
FC-64	AMR mark	10:01:02:11.892 ± 0.05
FC-28	Vernier ignition	10:01:02:14.692 ± 0.05
FC-29	Retro ignition	10:01:02:15.792 ± 0.05
FC-64	AMR mark off	10:01:02:15.792 ± 0.05

The warmup time (on to enable) was 179.99 ± 0.38 seconds, well within the nominal 180 ± 20 seconds. From readings of the magnitude register (FC-18), actual mark time can be refined to 10:01:02:11.897 ± 0.045, and actual vernier ignition time can be refined further to 10:01:02:14.657 ± 0.025. These times are referenced to GMT at DSIF 11.

5.8.4.2 Load Current Signals

Radar and squib current (EP-17) was normal. It was zero until AMR on when it rose to normal AMR warmup load, which continued until AMR enable. During the enabled interval, it properly cycled in the manner characteristic of magnetron pulsing, which is not synchronized with the telemetry data sampling. This continued until engine ignition, when the AMR load was removed (by jettison of the AMR) and replaced by the RADVS warmup load.

Magnetron current (R-12) (Figure 5.8-1) also was normal. It was zero until AMR enable, when it rose to normal high voltage load during magnetron pulsing. This continued until engine ignition, when the signal went to full scale as the AMR was forcibly jettisoned by the retro engine.

5.8.4.3 Late Gate Signal

The late gate video detected analog voltage signal (R-29) (Figure 5.8-2) was normal, confirming the presence of RF signal and detected video at the time of the mark.

From the trajectory reconstruction for AGC evaluation, the total stretched pulse length, as received, was about 24.2 microseconds and the effective closing rate was 8580.18 fps, both at time of the mark. The corresponding video pulse closing rate was therefore about 17.47 microseconds per second. The video late gate has a nominal duration of 20 microseconds (20.0 ± 1.0 required). It should therefore have produced output within 3 db peak for (24.2 + 20)/17.47 = 2.53 seconds.

With R-29 sampled at 1.2-second intervals, there should be at least one high level sample, and perhaps two, if the sampling time phase were right. In Surveyor VII it happened that there were two high level samples that occurred at the proper time relative to the mark time.

5.8.4.4 DB Budget

The Surveyor VII AMR db budget, revised for the postflight parameters in the trajectory reconstruction for AGC evaluation, shows a 30.1-db margin above that required for a 0.999 cumulative probability of successful marking, as follows:

P_t (average)	+ 33.80 dbm
G^2	+ 69.0 db
β_1	- 13.57 db
σ (0 degree) = 0.065	- 1.17 db
R^{-3}	- 53.34 db
f^{-2}	-199.36 db

f_r^{-1}	- 25.40 db
$\left(\frac{1}{2}\right) \left(\frac{c}{4\pi}\right)^3$	+122.12 db
cotan 36.43 degrees	+ 1.32 db
F (36.43 degrees)	- 11.70 db
	+226.24 dbm
	-304.54 db
P_r	- 78.30 dbm
P_{min} (10 microseconds)	- 97.3 dbm (worst case)
P_{min} (10 microseconds)	-105 dbm (measured)
P_{min} (10 microseconds-worst case)-P_{min} (10 microseconds-measured)	+ 7.7 db
P_{min} (30 microseconds)	-101.5 dbm (worst case)
P_{min} (30 microseconds)	-109 dbm (measured)
P_{min} (30 microseconds-worst case)-P_{min} (30 microseconds-measured)	+ 7.5 db
P_{min} (24.2 microseconds)	-100.8 dbm (worst case)
P_{min} (24.2 microseconds-worst case)-P_{min} (24.2 microseconds-predicted)	+ 7.6 db
P_{min} (24.2 microseconds)	-108.4 dbm (predicted)
	- 78.3 dbm
	+108.4 dbm
Total margin above threshold for 0.999 cumulative probability:	+ 30.1 db

5.8.4.5 Expected Marking Range

The expected value of the slant range along the AMR antenna electrical axis when the mark is produced will vary slightly from the nominal value of

60 statute miles. This expected value is supplied before each mission to FPAC, which inserts this value and both mechanical alignment and electrical boresight data into its trajectory programs. These determine the time delay value to be commanded into the on-board magnitude register so that automatic engine ignition will occur at the altitude desired for that mission.

Previous study and experience, confirmed by Surveyor VII itself, have demonstrated that the expected marking range is affected significantly by only two parameters, according to the well-documented equation:

$$R_m = R_o + (2.02 \times 10^{-4})\,\varphi - (1.01 \times 10^{-4})\,\varphi^2$$

The operational parameter is the angle φ, the incidence angle in degrees off the local lunar vertical of the AMR beam at its intersection with the lunar surface. The equipment parameter is the value R_o, which is the expected marking range at vertical incidence characteristic of the specific AMR hardware aboard each spacecraft. The result, R_m, is the expected marking range in statute miles.

The value R_o is determined for each AMR as the measured gate setting (leading edge of late gate) minus the nominal analytical value of range bias at vertical incidence; the latter is equal to 12.20 microseconds. The former is measured in test.

The Surveyor VII AMR (283810, S/N 11) gate setting was 657.6 microseconds. The R_o value was therefore:

Gate (measured)	657.6 microseconds
Bias (analytical)	- 12.2 microseconds
	= 645.4 microseconds
R_o	= 60.10 statute miles

(at 10.737 microseconds per round-trip statute mile)

The trajectory reconstruction for AGC evaluation (Figure 5.8-3) showed an incidence angle of 36.4 degrees at the time of the mark. The expected marking range for Surveyor VII was therefore 59.97 statute miles.

5.8.4.6 Marking Range Dispersion

The standard budget of allowances for in-flight drifts of AMR parameters that affect marking range at any incidence angle has been documented as a rss total of ±893 feet, 3σ.

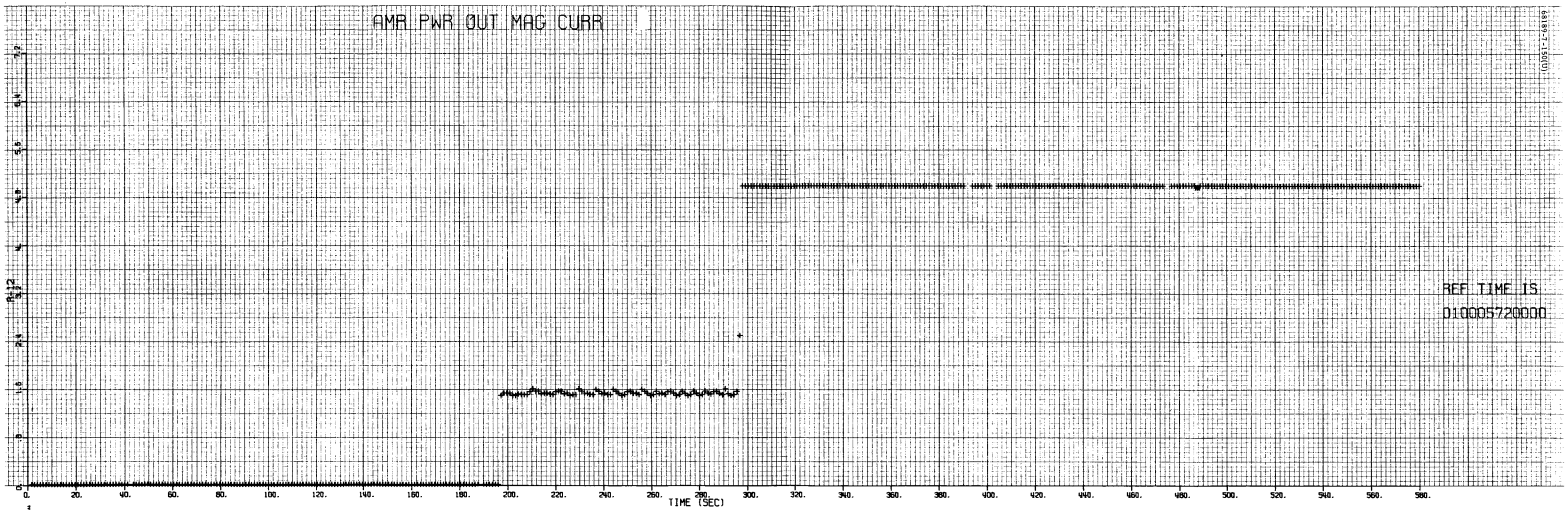

Figure 5.8-1. Magnetron Current (AMR)

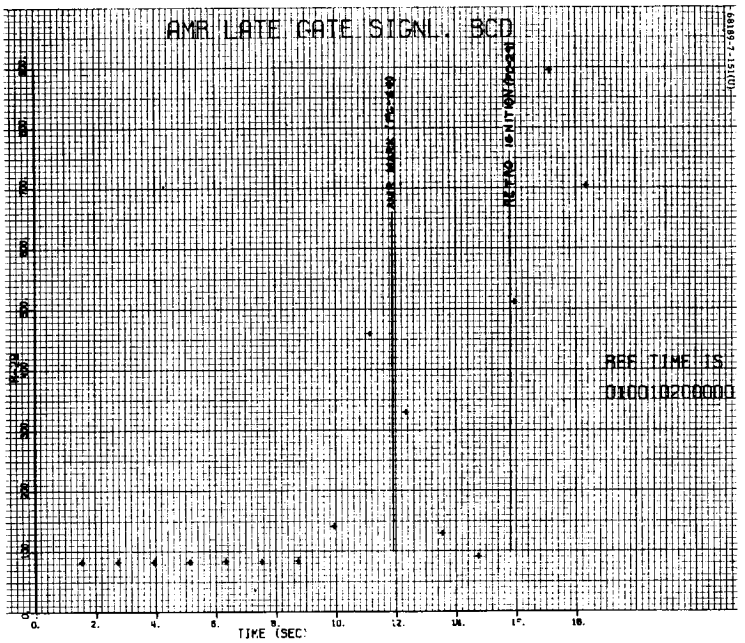

Figure 5.8-2. Late Gate Signal (AMR)

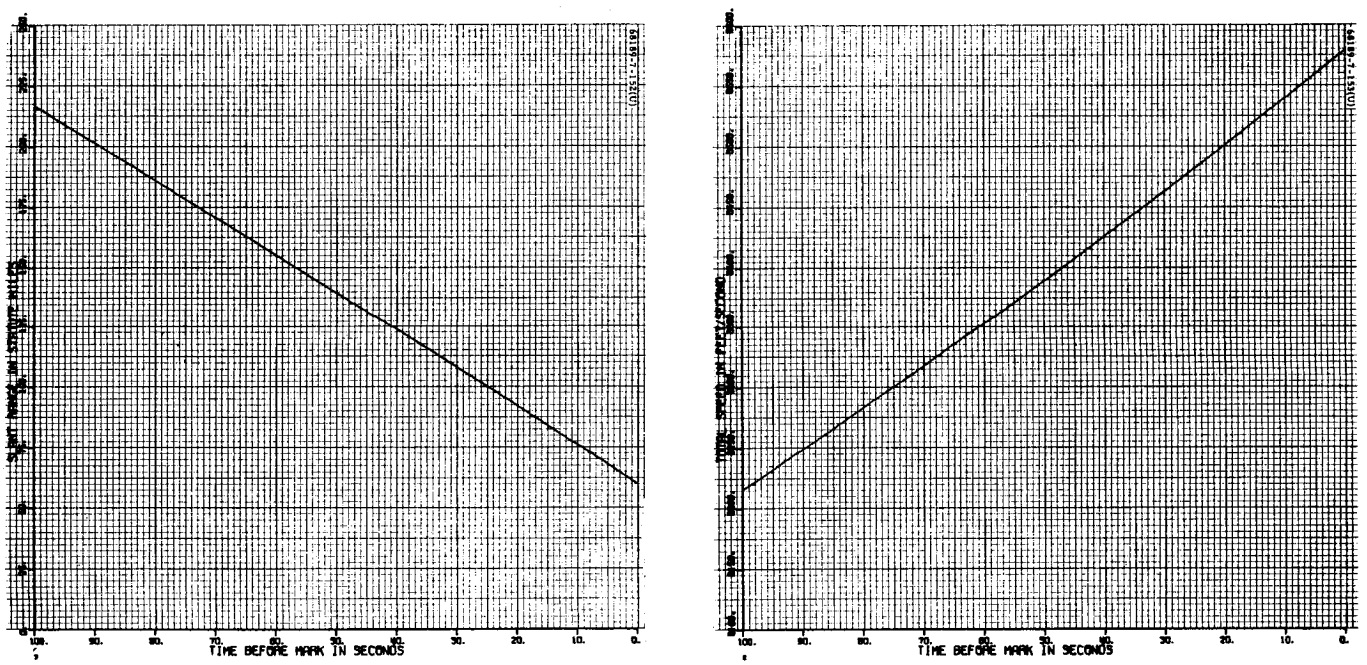

Figure 5.8-3. Trajectory Reconstruction

From the calculations of AMR cumulative probability (Reference 1) of successful marking, the spread from 0.001 to 0.999 probability is ±800 feet at 35 degrees due to scintillation. The allowable pointing error (3σ) contribution is ±2312 feet at 35 degrees.

The total (rss) marking range dispersion at 35 degrees is therefore ±2604 feet (3σ). (For perfect pointing error compensation in the guidance and trajectory programs, the actual dispersion would be only ±1200 feet (3σ) at 35 degrees, well within the specified maximum of 0.345 mile or 1820 feet (3σ).

At the Surveyor VII velocity of 8580.18 fps at the time of the mark, the total dispersion of ±2604 feet (3σ) would be a time error of ±0.304 second (3σ). By coast phase orbit determination from earth tracking, the a priori mark time uncertainty has been reported as 0.70 second (1σ), or almost seven times larger. Hence, while orbit determination provides excellent velocity data, integration into position is less accurate, and the predicted value of expected marking range remains the best available estimate of actual conditions.

5.8.4.7 AMR Parameter Reconstruction

Because of the significant distance traveled during the nominal 100 seconds of enabled operation, the AMR parameters during this interval are evaluated accurately as functions of time and of the mission variables. This is done by a separate computer program developed for this purpose.

Trajectory constants are found from conditions at mark and/or at engine ignition. Velocity, velocity angle, and attitude angle are supplied by FPAC; slant range at mark is the predicted expected marking range. All quantities are then evaluated analytically without approximation at each of a number of two-body trajectory points determined by stepping speed in arbitrary increments. Negative increments of speed produce a backward extrapolation from mark, or from ignition to enable. The only approximation used is for the time interval between trajectory points, which assumes linearized distance and velocity between points. Adequate time accuracy results with the -20 fps increments normally used.

Of particular interest are the AMR slant range, the beam incidence angle at the surface, and the accompanying received pulse stretching effect (Figure 5.8-4). The latter is seen to vary quite significantly because of slant range variation over a dynamic range of about two octaves.

The Surveyor VII trajectory conditions supplied by FPAC were as follows:

	At Mark
Velocity angle, degrees	34.84
Attitude angle, degrees	34.62
Speed, fps	8580.18

5.8.4.8 AMR AGC Evaluation

The original standard test conditions of 3, 10, and 30 microseconds for preflight AGC calibration (Figure 5.8-5) encompass approximately the region of stretched pulse lengths as received over the required range of A-21 approach angle (0 to 45 degrees) at the nominal marking range. The AGC response curves are nonlinear, however, and intermediate values are helpful for proper interpolation of a given approach angle even at the marking range. In addition, because of the appreciable variation in received pulse length during enabled operation prior to the mark, particularly at angles of more than several degrees, proper AGC interpretation at times other than the mark requires extended AGC calibration. The analysis was fully documented for Surveyor III (Reference 2).

However, reliable data of the extended AGC calibration are not available. From available data (maximum pulse length = 30 microseconds), the correction relative to 10-microsecond calibration was estimated (Figure 5.8-6). This correction was applied in the interpretation of AGC telemetry data (Figure 5.8-7). It should be noted that after the AMR was enabled, the telemetry data were initially low due to the response time of the circuit. After the initial period, the AGC data were generally 2.5 to 4.5 db higher than the nominal predicted value.

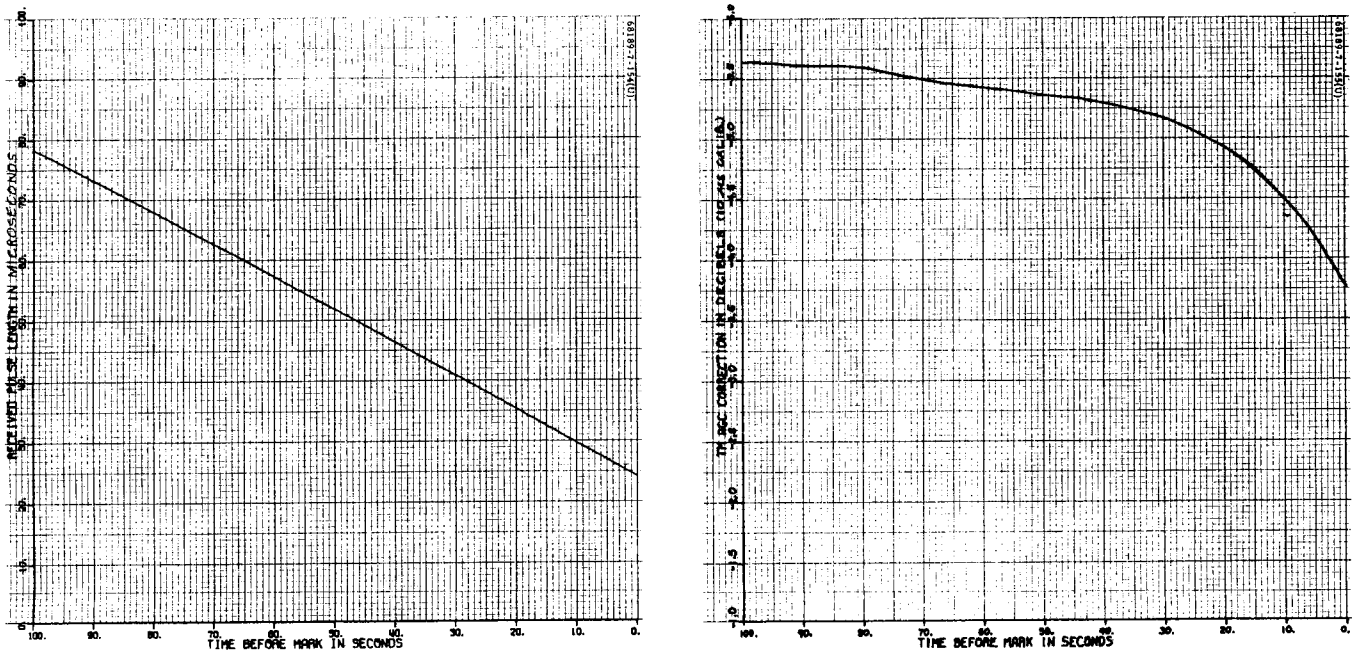

a) Received Pulse Length

b) Telemetry Correction

Figure 5.8-4. Received Pulse Length Reconstruction

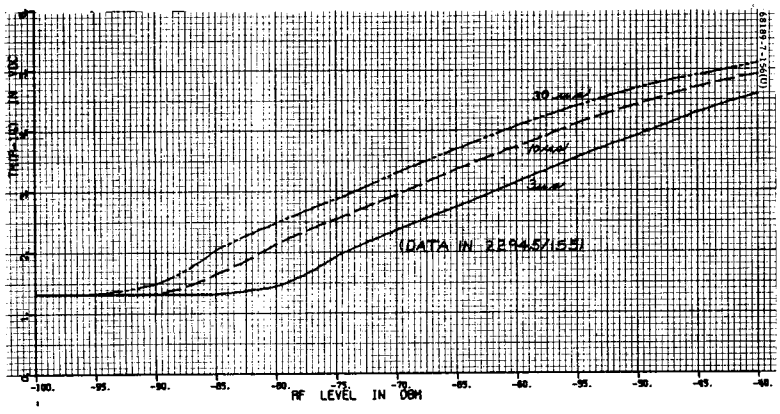

Figure 5.8-5. AGC Calibration for Constant Pulse Length

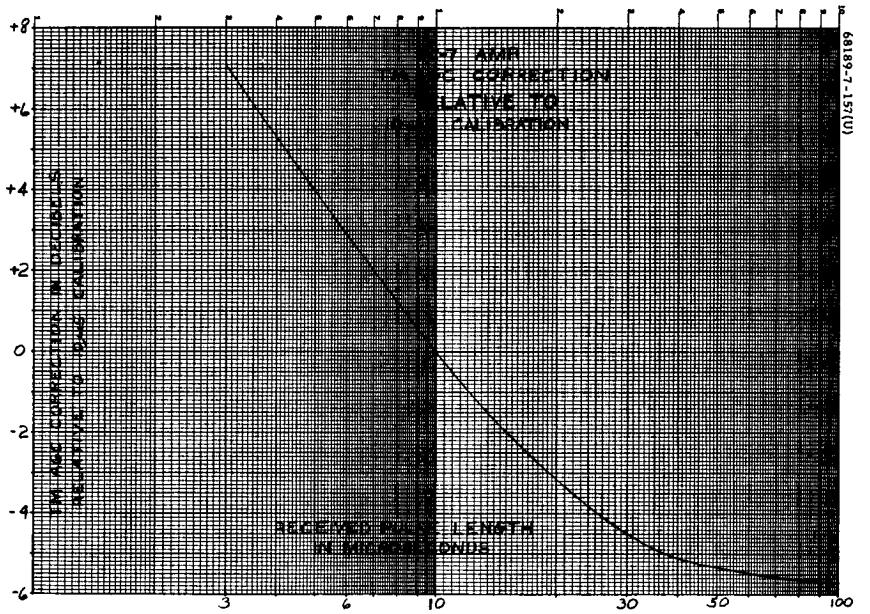

Figure 5.8-6. AGC Correction Relative to 10-Microsecond Calibration

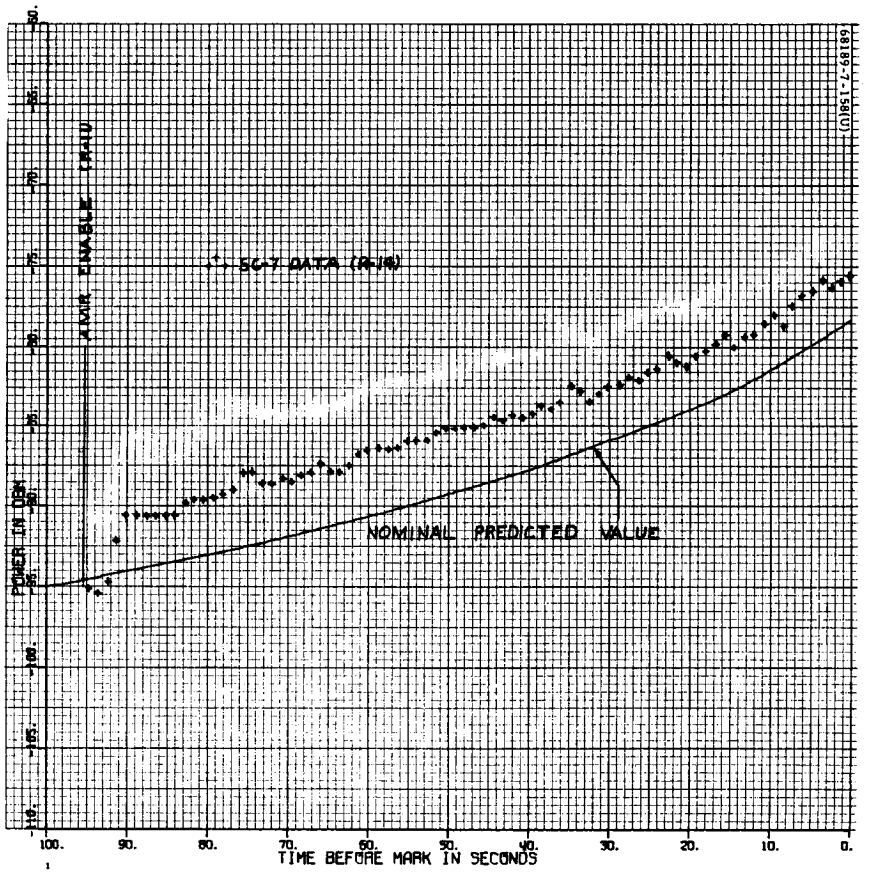

Figure 5.8-7. Altitude Marking Radar AGC (Telemetry: Sensor R-14)

5.8.5 REFERENCES AND DOCUMENTATION

1) R.A. Dibos, "Preliminary Study of AMR at Large Angles," (unpublished IDC), 4 November 1966.

2) "Surveyor III Flight Performance," Hughes Aircraft Company, SSD 68189-3, July 1967.

3) S. Thaler, "The AMR – Predicted Performance," Hughes IDC 2729.1/11, 29 March 1965.

4) I. Holtzman, "AMR Marking Range Bias as Function of Angle of Incidence," Hughes IDC 2253.3/294, 13 May 1965.

5) R.A. Dibos, "Post-Mission Analyses Involving Radar Data," (unpublished), 25 March 1966.

6) Lincoln Laboratory, "Radar Studies of the Moon," Quarterly Report No. 2, 15 May 1966, p.11.

7) R.A. Dibos, "Radar Performance Evaluation," SC-1 Symposium (NASA at JPL), September 1966.

8) "Surveyor I Flight Performance," Hughes Aircraft Company, SSD 68223R, Vol. III, October 1966.

9) "Decibel Allocation and Margin Summary," Hughes Aircraft Company, SSD 4021R-2, 28 November 1966.

10) R.A. Dibos, "AMR Test Data Required for Analyses," Hughes IDC 2253.4/71, 20 March 1967.

11) R.A. Dibos, "SC-3 AMR (S/N-15) Predictions," Hughes IDC 2253.4/79, 10 April 1967.

12) R.A. Dibos, "TM Mode 6 Data Relating to Radar Performance," Hughes IDC 2253.4/84, 15 June 1967.

13) R.A. Dibos, "AMR AGC Post-Mission Evaluation," Hughes IDC 2253.4/88, 27 June 1967.

14) "Surveyor IV Flight Performance," Hughes Aircraft Company, SSD 68189-4, September 1967.

15) "Surveyor V Flight Performance," Hughes Aircraft Company, SSD 68189-5, November 1967.

16) "Surveyor VI Flight Performance," Hughes Aircraft Company, SSD 68189-6, January 1967.

17) S. Suddick, "SC-7 AMR Marking Accuracy," Hughes IDC 2294.5/159, 22 December 1967.

18) M.R. Weiner, "SC-7 AMR Marking Range Data," Hughes IDC 2292/441, 28 December 1967.

19) S. Suddick, "SC-7 Radar Calibration Data," Hughes IDC 2294.5/155, 1 December 1967.

5.8.6 ACKNOWLEDGMENTS

Calibration data and technical assistance were provided by W.T. Black and D.W. Demaree. Telemetry data were supplied by W. McIntyre.

Guidance and trajectory data were supplied by T.L. Parker of FPAC.

This section was technically coordinated by M.R. Weiner.

5.9 RADVS PERFORMANCE

5.9.1 INTRODUCTION

The radar altimeter and doppler velocity sensor (RADVS) is a coherent CW microwave radar designed and supplied by Ryan Electronics, San Diego. Its primary function is to measure velocity and slant range relative to the lunar surface during the terminal descent of the Surveyor spacecraft. These quantities are measured directly in spacecraft coordinates, allowing direct utilization by the spacecraft flight control system for both attitude steering and deceleration thrust control.

The doppler velocity sensor (DVS) portion of the system is essentially a three-beam coherent CW autodyne doppler radar. A single klystron (two-cavity type) provides undeviated output at a nominal frequency of 13,300 MHz. Its output is divided equally among the transmitting horns for beams 1, 2, and 3. Each beam has a separate receiving horn, with adequate RF isolation against direct leakage, and a separate and independent receiver utilizing a small sample of the transmitted signal as a local oscillator (bias). Associated with each receiver is a separate and independent frequency tracker capable of acquiring and tracking the doppler signal corresponding to that component of velocity associated with the spacecraft orientation of that particular beam. The spacecraft beam orientations are such that the nominal velocity components V_i $(i = 1, 2, 3)$ along the axes of these three beams are determined by the spacecraft coordinate components of velocity according to the matrix multiplication:

$$\begin{pmatrix} V_1 \\ V_2 \\ V_3 \end{pmatrix} = \begin{pmatrix} +A & +A & +B \\ -A & +A & +B \\ -A & -A & +B \end{pmatrix} \begin{pmatrix} V_x \\ V_y \\ V_z \end{pmatrix}$$

where

$$A = \sin 45 \text{ degrees} \sin 25 \text{ degrees} = 0.29884$$

$$B = \cos 25 \text{ degrees} = 0.90631$$

and the spacecraft coordinates are a Cartesian right-handed triad with +z along the roll axis in the normally descending direction.

The frequency outputs of these three frequency trackers are properly scaled and summed in three converters whose outputs are analog voltages representing the spacecraft velocity components:

$$V_x = \frac{V_1 - V_2}{2A}; \quad V_y = \frac{V_2 - V_3}{2A}; \quad V_z = \frac{V_1 + V_3}{2B}$$

The radar altimeter (RA) portion of the system is basically a single-beam coherent FM-CW microwave radar altimeter. Beam 4, fixed along the spacecraft +Z axis, also contains separate transmit and receive horns, a fourth receiver, and a fourth frequency tracker. The same kind of transmitter-derived local oscillator (bias) signal configuration is used, but the RA uses a reflex klystron whose frequency is sawtooth deviated in standard FM-altimeter fashion. The operating portion of the sawtooth has negative slope (with time) to avoid any range-velocity ambiguities. The beam 4 receiver and frequency tracker therefore operate at a frequency which is the sum of scaled slant range and scaled doppler velocity inevitably appearing along that beam. The RA converter corrects the frequency output of the beam 4 tracker by a properly scaled term (V_z compensation), obtained from the DVS V_z converter, to provide an analog output voltage proportional to R_z, the slant range along the spacecraft +Z axis. (The nominal RA operating frequency is 12, 900 MHz. Deviation is nominally 40 MHz at 8000 MHz/sec below 1000 feet, and 4 MHz at 800 MHz/sec above 1000 feet.)

Each receiver is actually two parallel receiving channels, each with separate microwave mixers and audio preamplifiers. Microwave mixer signal and bias inputs are phased so that the parallel audio channels are essentially in phase quadrature, and with equal amplitudes, for all normal doppler signals. Each frequency tracker uses these quadrature audio signals to single-sideband modulate an internal reference signal held at 600 kHz, thus reproducing doppler frequencies unambiguously. In Surveyor, this serves primarily to reject negative velocity at tracker IF, thereby preserving the sense of the velocities. (In a more general application, this would permit measuring negative and positive beam velocities including the unwanted radar return from the main retro engine after separation from the spacecraft.) Each frequency tracking loop is closed by a voltage controlled oscillator whose frequency is controlled by a discriminator-integrator combination, whose output is a direct measure of the frequency being tracked.

To preserve the high degree of both amplitude and phase balance between the parallel quadrature channels of each receiver over the full dynamic range of signals and over the region of operating temperatures, the preamplifier gains are switched in discrete steps by wideband (at audio) gain-switching threshold circuits. Automatic gain control is <u>not</u> used. A set of discrete outputs is provided and telemetered to indicate the gain state of each receiver, as follows:

	Gain Switch 1	Gain Switch 2
High gain (DVS, 90 db; RA, 80 db)	Off	Off
Mid gain (DVS, 65 db; RA, 60 db)	Off	On
Low gain (DVS and RA, 40 db)	On	On

Other discrete outputs are also provided and telemetered. One is a confirmation of application of prime power. This initiates a warmup interval ended by an internal timer which applies high voltage to both klystrons. A set of tracker-lock signals indicates the search or track status of each of the four frequency trackers. A reliable operate doppler velocity sensor (RODVS) discrete indicates, both prior to 3.5 g + 3.7 seconds and subsequent to the 1000-foot mark, that all three DVS beams are locked; between these two times (in Surveyor IV and subsequent spacecraft), it indicates that any one or more of the DVS beams is locked. RODVS causes the flight control to switch attitude steering inputs from gyros to lateral velocities. A RORA (reliable operate radar altimeter) discrete is on when and only when beams 1, 3, and 4 are locked, thus providing reliable V_z and R_z for the flight control acceleration control loop. From the analog range output, the RADVS itself derives and supplies two discrete range mark signals, one at 1000 feet (used to change flight control loop parameters), and the other at 12 feet (used to cut off vernier engines).

The latter is termed the 14-foot mark for RADVS purposes, since it is measured from the RADVS antenna boresight reference, which is 24 inches above the legs-extended position of the landing pads on the spacecraft structure (whose position at vernier engine cut off, in turn, has been used in landing stability analyses).

The RADVS hardware is packaged in five units, each of which is a control item in Hughes Spacecraft Configuration Control. Since temperature is measured separately for most of these units, their basic composition is indicated below:

A/VS antenna	– beams 1 and 4 antenna, mixer, and pre-amplifier components
DVS antenna	– beams 2 and 3 antenna, mixer, and pre-amplifier components
Klystron power supply modulator (KPSM)	– includes all components for both DVS and RA
Signal data converter	– all frequency trackers and data converters
Waveguide assembly	

5.9.2 ANOMALIES

There were no radar anomalies in the Surveyor VII mission.

5.9.3 SUMMARY

Stations 11 and 14 provide continuous data during terminal descent. Therefore, the times for all mark events are within the accuracy determined by the bit rate. All doppler velocity sensor beams locked during retro operation. This is normal and has occurred during all previous terminal descent phases.

After retro case separation, beam 1 lost lock temporarily (RODVS was still indicated) and beam 4 was locked temporarily. About 5 seconds after the temporary acquisition, beam 4 acquired and RORA was indicated. An explanation for these events is contained in subsection 5.9.4.3. RORA was on from the initial indication until touchdown.

Good agreement exists between the processed telemetry data and the 6DOF terminal descent reconstruction for all RADVS parameters.

5.9.4 SUBSYSTEM PERFORMANCE ANALYSIS

5.9.4.1 RADVS Turn-on

RADVS power on occurred properly, within a second of retro ignition, as confirmed by EP-33, R-28, EP-17, and the altimeter search sweep pattern in FC-35. Subsequent time-in of the high voltage occurred approximately 23 seconds later, as indicated by EP-17 (Figure 5.2-8), a normal internal delay.

5.9.4.2 Velocity Acquisition Conditions

All three doppler velocity sensor beams could have acquired and commenced tracking lunar reflected signals as soon as they came within each tracker's acquisition sweep frequency limits. The acquisition conditions were determined from the 6DOF computer program reconstruction, the most probable tracker lock times, and the telemetry time accuracies (±0.6 second).

Spacecraft conditions at the time of RODVS (all doppler velocity sensor beams locked and converters reporting reliable V_x, V_y, and V_z), as extrapolated from the 6DOF program reconstruction, were as follows:

$V_x = -37.9$ fps

$V_y = -56.8$ fps

$V_z = +3250$ fps

Range = 80,639 feet

Attitude = 25.34 degrees

Altitude = 65,016 feet

again assuming conditions at the most probable time of RODVS, whose telemetry time accuracy is also ±0.6 second.

5.9.4.3 Range Acquisition Conditions

From telemetry and terminal descent 6DOF program reconstruction, conditions at the time of range tracker lockon and RORA were:

V_x = +3.7 fps

V_y = -12.7 fps

V_z = +451.8 fps

Range = 41,673 feet

Attitude = 18.4 degrees

Altitude = 39,531 feet

Altimeter frequency = 79.7 kHz

Upper sweep limit ≈ 91 kHz

Certain tracker conditions were noted near the time of RORA: 1) RORA was not generated at first beam 4 lock, and 2) loss of beam 1 lock. From Table 5.9-1, the tracker lock events were:

1) RODVS occurred prior to retro reject, but beam 1 lost lock and beam 4 acquired temporarily (indicated by the same telemetry frame).

2) The next frame of data indicated beam 1 was locked and beam 4 unlocked. (RODVS continued to be indicated even though beam 1 was unlocked so that the interruption of beam 1 was short.)

3) About 5 seconds later, beam 4 was reacquired and RORA was indicated.

The probable explanation of these events is as follows:

1) Beam 4 first acquired temporarily a signal reflected off the retro case. The second acquisition (RORA) was a true acquisition of the lunar reflected signal.

TABLE 5.9-1. SURVEYOR VII EVENTS

Sensor	Event	GMT, Day 010, hr: min:sec
R-1	AMR on	00: 57:36.351 ± 0.19
R-11	AMR enable	01: 00:36.345 ± 0.19
FC-64	AMR mark	01: 02:11.892 ± 0.05
FC-28	Vernier ignition	01: 02:14.692 ± 0.05
FC-29	Retro ignition	01: 02:15.792 ± 0.05
EP-33	RADVS pyro switch	01: 02:16.752 ± 0.6
R-28	RADVS on	01: 02:15.752 ± 0.6
FC-34	RODVS	01: 02:48.850 ± 0.6
FC-63	Inertial switch	01: 02:58.975 ± 0.025
FC-30	Retro burnout	01: 02:58.990 ± 0.05
FC-78	Start maximum thrust	01: 03:09.250 ± 0.6
FC-31	Retro eject signal	01: 03:10.990 ± 0.05
V-4	Retro ejected	01: 03:11.550 ± 0.6
FC-42	Start RADVS descent	01: 03:13.090 ± 0.05
FC-33	RORA	01: 03:17.649 ± 0.6
	Segment acquisition	01: 04:03.018 ± 0.15
FC-37	1000-foot mark	01: 05:13.285 ± 0.05
FC-36	10 fps	01: 05:30.184 ± 0.05
FC-38	14-foot mark	01: 05:36.284 ± 0.05
(Leg 1)	Touchdown	01: 05:37.620 ± 0.02

2) Beam 1 lost lock because its transmitted signal was cut by the retro case.

5.9.4.4 Revised Nominal db Budget

The db budget for RORA conditions is shown in Table 5.9-2.

TABLE 5.9-2. RADVS INDIVIDUAL BEAM DB BUDGETS AT RORA

Using measured Pt and G values and nominal reflectivity model
For φ = 18.4 degrees; ρ = +283.8 degrees; and R_z = 41,673 feet

Values	Beam 1	Beam 2	Beam 3	Beam 4
Pt, dbm	+ 34.02	+ 34.92	+ 34.07	+ 24.31
G, db	+ 28.3	+ 27.9	+ 27.7	+ 28.4
(1/2), db	- 3.01	- 3.01	- 3.01	- 3.01
λ^2, db	- 22.64	- 22.64	- 22.64	- 22.36
$(4\pi)^{-2}$, db	- 21.98	- 21.98	- 21.98	- 21.98
$(39.53 \text{ kilofeet})^{-2}$, db	- 91.94	- 91.94	- 91.94	- 91.94
$\cos^2 \theta i$, db	- 2.41	- 2.24	- 0.34	- 0.46
$F(\theta i)$, db	- 11.58	- 11.42	- 6.68	- 7.38
$\eta(K/\alpha^3)$, db	- 1.72	- 1.72	- 1.72	- 1.72
Sum of + values	62.32	62.82	61.77	52.71
Sum of - values	- 155.28	- 154.95	- 148.31	- 148.85
P_r, dbm	- 92.96	- 92.13	- 86.54	- 96.14
θi, degrees	40.7	39.4	16.0	18.4
$\sigma(\theta)$, db	- 13.30	- 13.14	- 8.40	- 9.10
R, kilofeet	52.34	51.36	41.18	41.67

5.9.4.5 Surveyor VII Event Times

The GMT at DSS 14 at the time of data recording is shown in Table 5.9-1. This table gives a number of significant spacecraft and related radar events defining the major items in the terminal descent sequence. Table 5.9-3 shows the use of the magnitude register (FC-18) to refine the times of vernier ignition and AMR mark. In these tables, a signal is shown as going on at a time interpolated between its last absence and its first presence, plus or minus one-half the data sampling interval. Table 5.9-4 shows the RADVS gain states and tracker lock conditions.

TABLE 5.9-3. TIMING REFINEMENT

GMT, Day 010, hr:min:sec	Magnitude Register, BCD
01:02:10.752	56 (stored)
11.952	55
13.152	31
14.332	7
15.532	1007

Vernier ignition at 14.332

0.325 ± 0.025

14.657 ± 0.025

Actual delay = 56 BCD

= 2.675 ± 0.025 seconds

Clock start at 02:11.902 ± 0.050

FC-64 at 02:11.892 ± 0.050

Actual mark at 02:11.942 maximum

02:11.852 minimum

= 02:11.897 ± 0.045

TABLE 5.9-4. SURVEYOR VII RADVS GAIN STATES AND TRACKER LOCK CONDITION

Reference Station 11 Frame Time, GMT day 010:01 min:sec	Gain States				Beam Lock (Lock Is 1)				Comments
	B1	B2	B3	B4	T1	T2	T3	T4	
02:13.822	3	3	3	3	0	0	0	0	Vernier ignition – 010:01:02:14.692 ± 0.05
16.222									
43.821									
47.420			2		1	0	1		
48.620					1	1	1		RODVS – 010:01:02:48.850 ± 0.6
03:00.620	2	2							
01.820	3								
03.020	2	3							Retro ejected – 010:01:03:11.550 ± 0.6
04.220	3								
09.020		2		2					
10.220	2	3		3					
11.420					1	1	1	0	
12.620				2	0	1	1	1	RODVS indicated (FC-34)
13.820		2		3	1	1	1	0	
17.419					1	1	1	1	RORA – 010:01:03:17.649 ± 0.6
04:16.217				2					
17.417				3					
33.016									
34.216									
35.416				2					
36.616				3					
41.416				2					
43.816				3					
46.216				2					
51.016				3					
52.216		1		2					
53.416		2		3					
55.816				2					
57.015			1						
58.215				3					
58.415			2						
05:00.615	1		1	2					
01.815	2	1							
03.015				3					
05.415	1			2					
06.615	2			3					
07.815	1			2					

Table 5.9-4 (continued)

Reference Station 11 Frame Time, GMT day 010:01 min:sec	Gain States				Beam Lock (Lock Is 1)				Comments
	B1	B2	B3	B4	T1	T2	T3	T4	
13.815	1	1	1	1	1	1	1	1	
15.015									
16.215									
18.615				2					
28.214	2								
29.414	1		2	3					
30.614	3	2		2					
31.814	2		3						
33.014			2						
35.414				3					
37.814	3	3	3	3	1	1	1	1	Touchdown – 010:01:05:37.664 ± 0.02
40.214	3	3	3	3	0	0	0	0	RADVS power off – 010:01:06:40

5.9.4.6 Descent Reconstruction

The set of graphs of R, V_x, V_y, and V_z (Figures 5.9-1 and 5.9-2) compare PREPRO processed telemetry data with the 6DOF program values for the revised nominal conditions. These graphs show a good correlation between the computed values and processed telemetry values.

5.9.4.7 Radar Reflectivity Analysis

Not just for radar purposes, but for the larger analyses of the entire terminal descent of each mission, an appreciable effort is devoted to a complete and accurate nine-dimensional trajectory versus real-time reconstruction. While this process is hampered by lack of direct data on spacecraft attitude once steering has started, it is possible to converge on an accurate and unique solution in which attitude is implicit by iteration of a precise spacecraft simulation against every significant telemetry channel, as described in the terminal descent discussion. Radar data aid in this reconstruction and, in return, the simulation provides expected or predicted reflectivity signal strengths throughout the descent. This process was almost trivial in the almost exactly nominal Surveyor I, but has proved its utility in matching Surveyors III, V, VI, and VII.

The results were presented in subsection 5.9.4.6, and the received signal strength versus time plots are represented here (Figure 5.9.3) along with the processed telemetered received signal strength data for comparison. Figure 5.9-4 shows beam incidence angles and reflectivity factors from 6DOF versus time.

It should be noted that the reflectivity signal voltage is not always a true indicator of received signal strength when the preamplifier is switching between two gain states. The rapid sawtooth motion of the processed telemetry data during RADVS control is due to gain switching.

5.9.4.8 Reflectivity Model

The lunar radar reflectivity model used by Hughes and approved by JPL for design and evaluation of both Surveyor radars was developed by D.O. Muhleman. This model has been completely described in previous documentation. (See, for example, the "Surveyor III Flight Performance Final Report," Hughes Aircraft Company, SSD 68189-3, July 1967.)

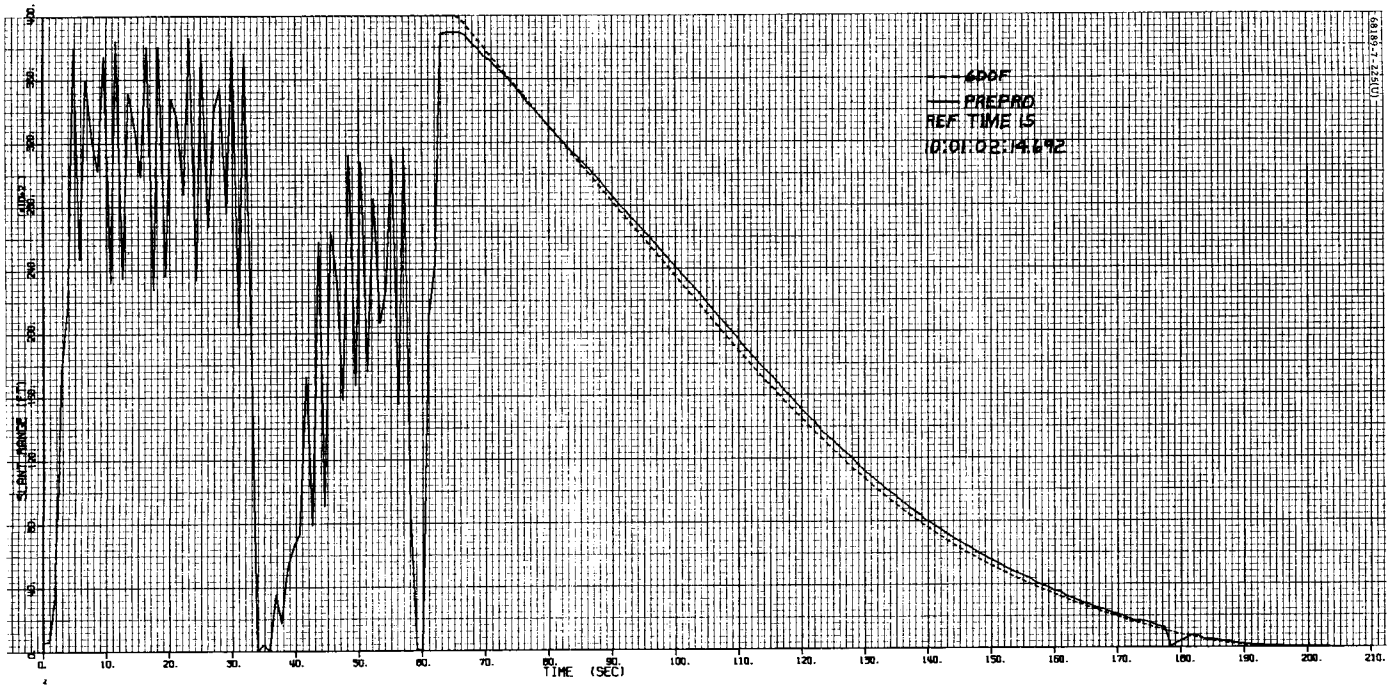

Figure 5.9-1. Slant Range Reconstructed

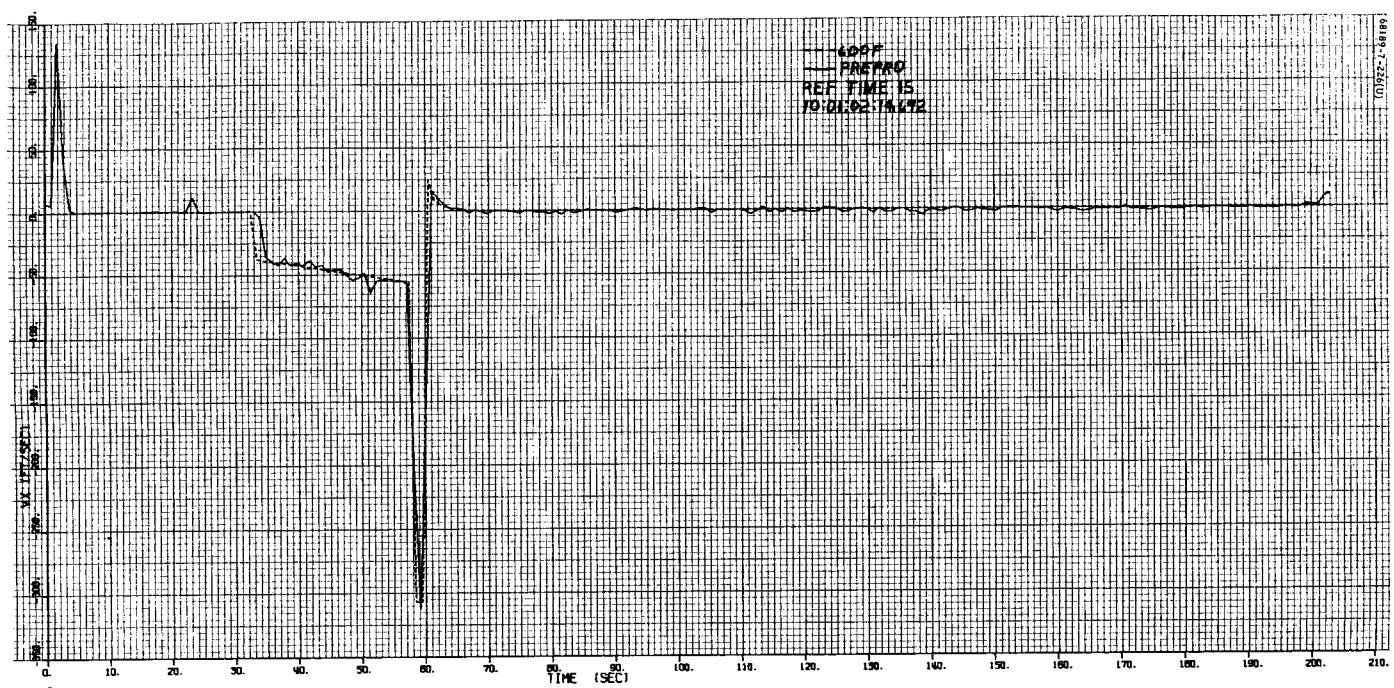

a) V_x

Figure 5.9-2. Spacecraft Velocities Reconstructed

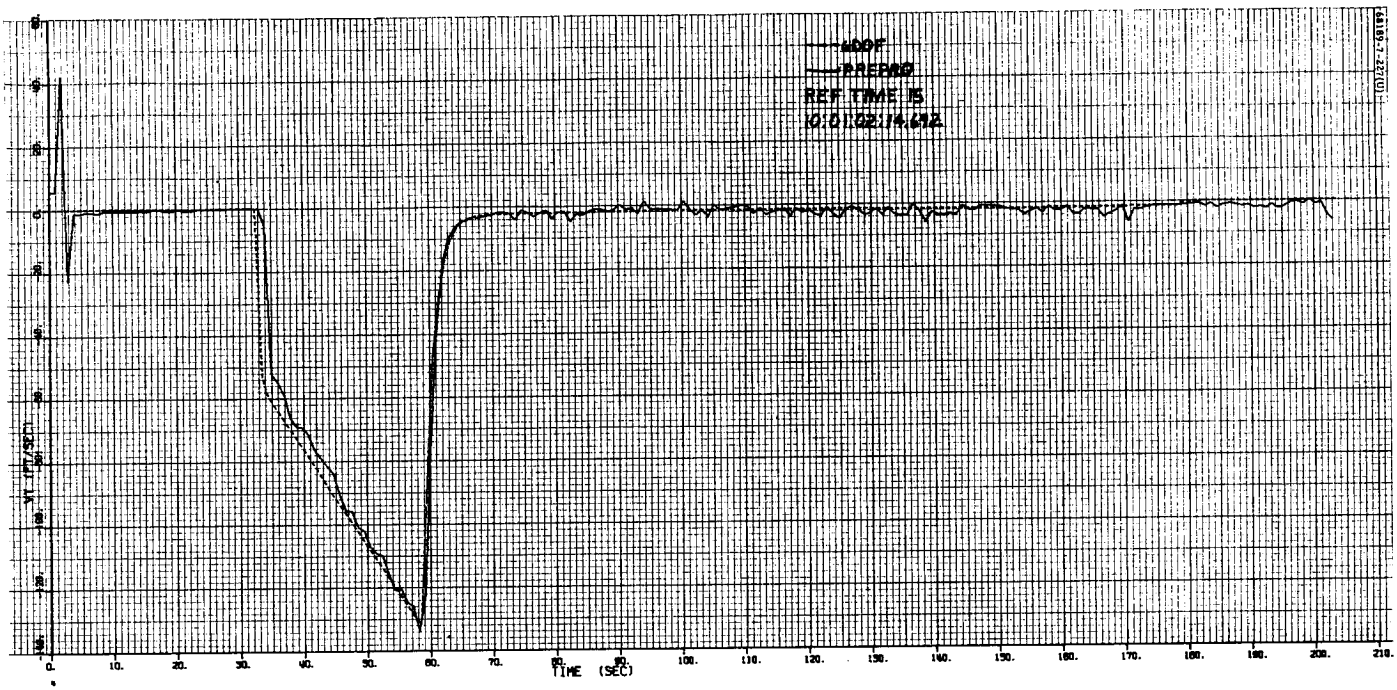

b) V_y

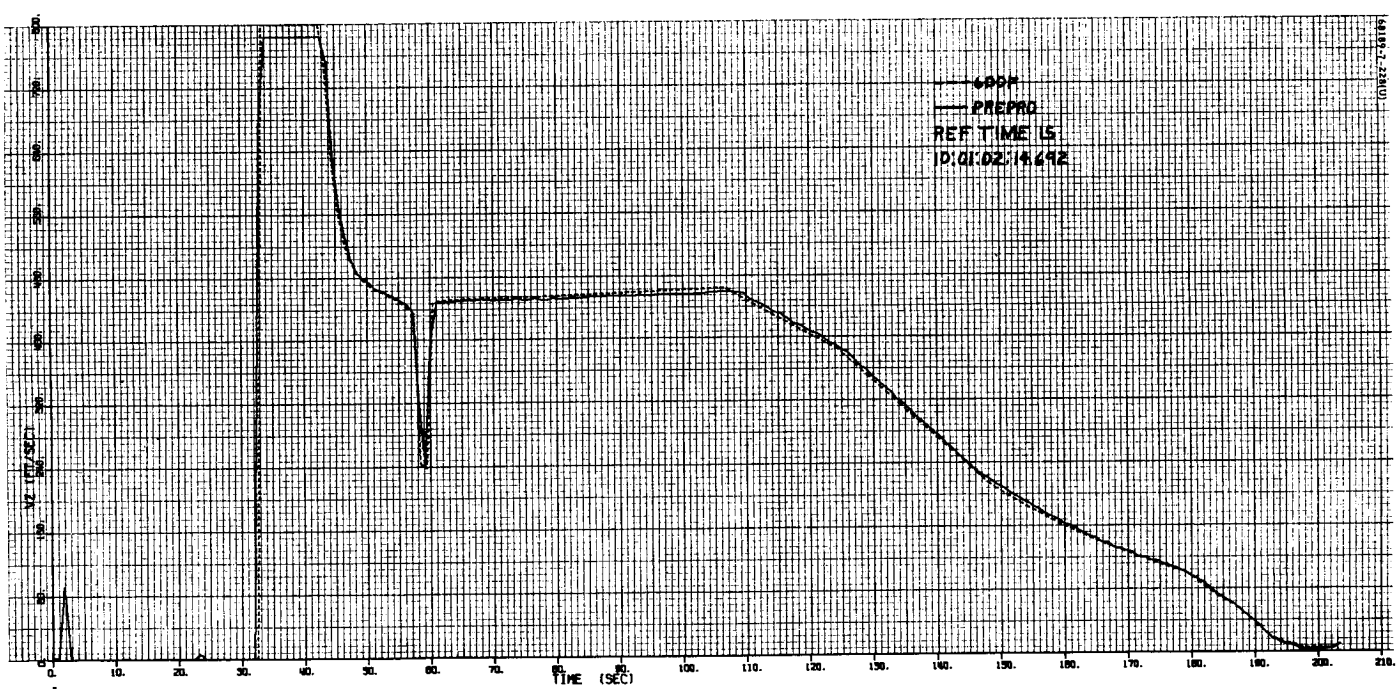

c) V_z

Figure 5.9-2 (continued). Spacecraft Velocities Reconstructed

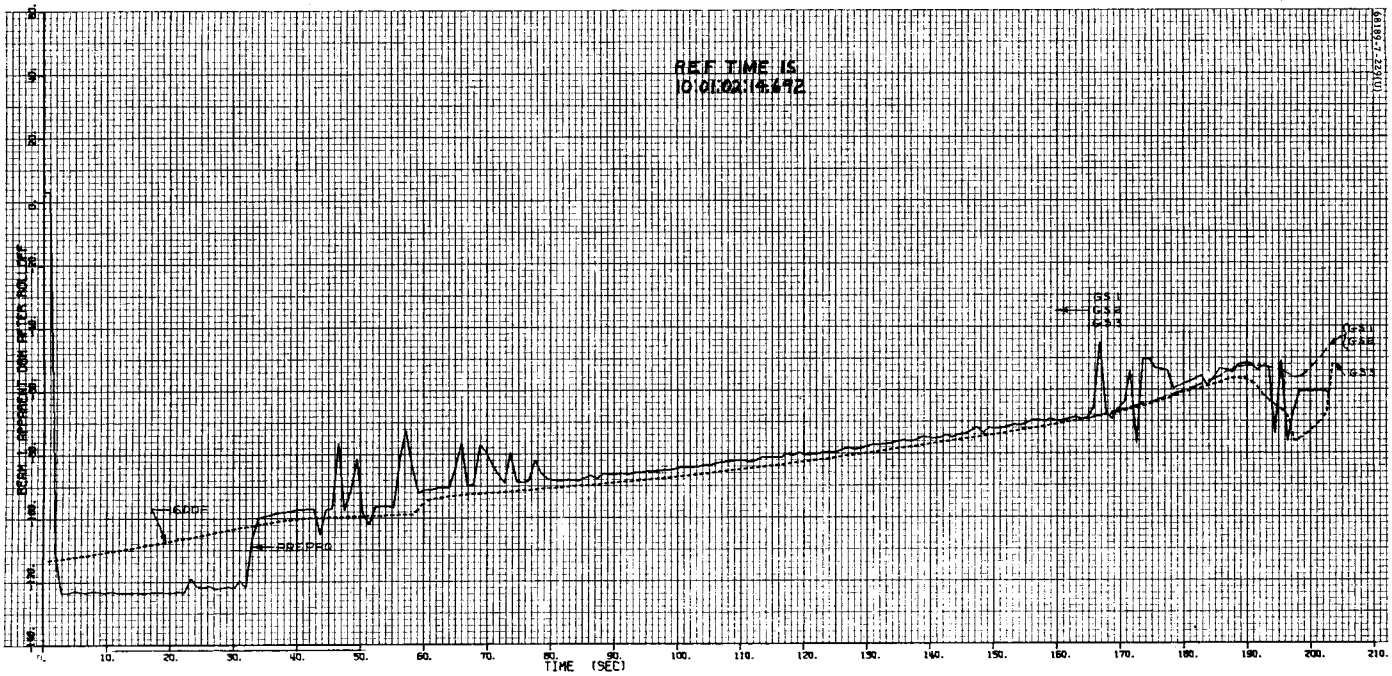

a) Beam 1

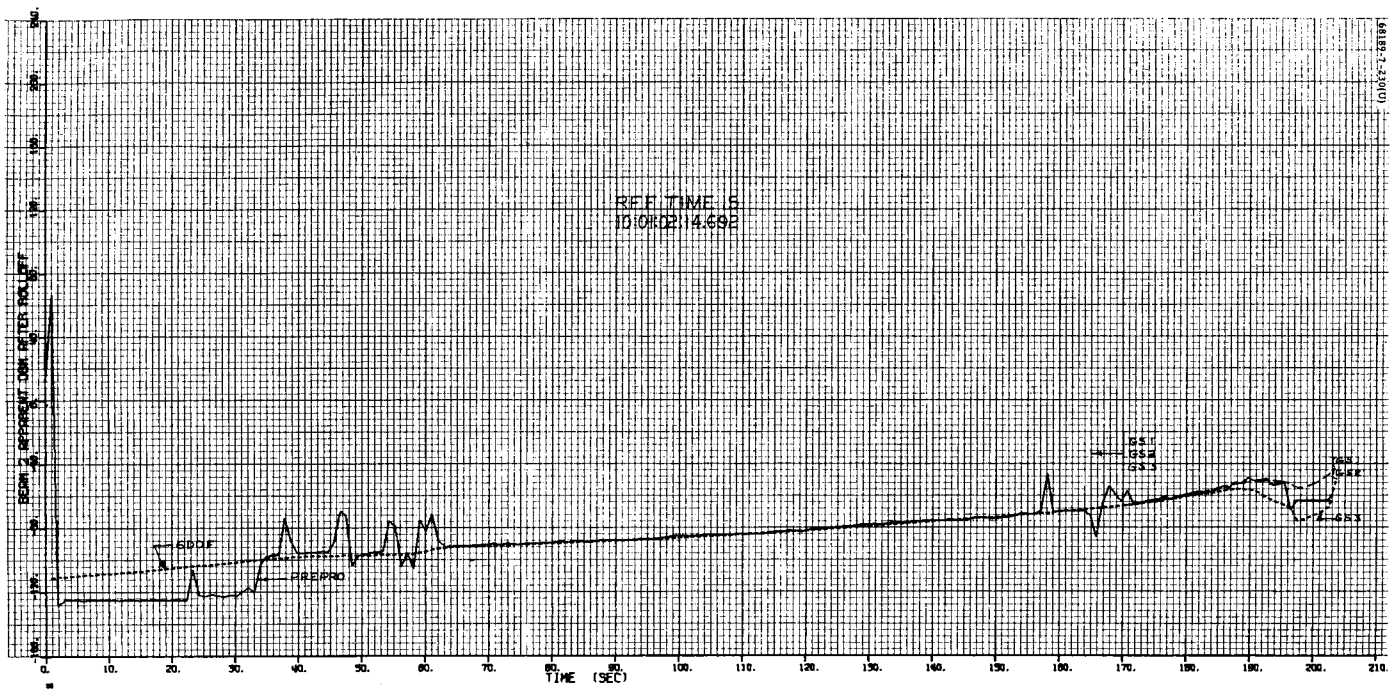

b) Beam 2

Figure 5.9-3. RADVS Reflectivity

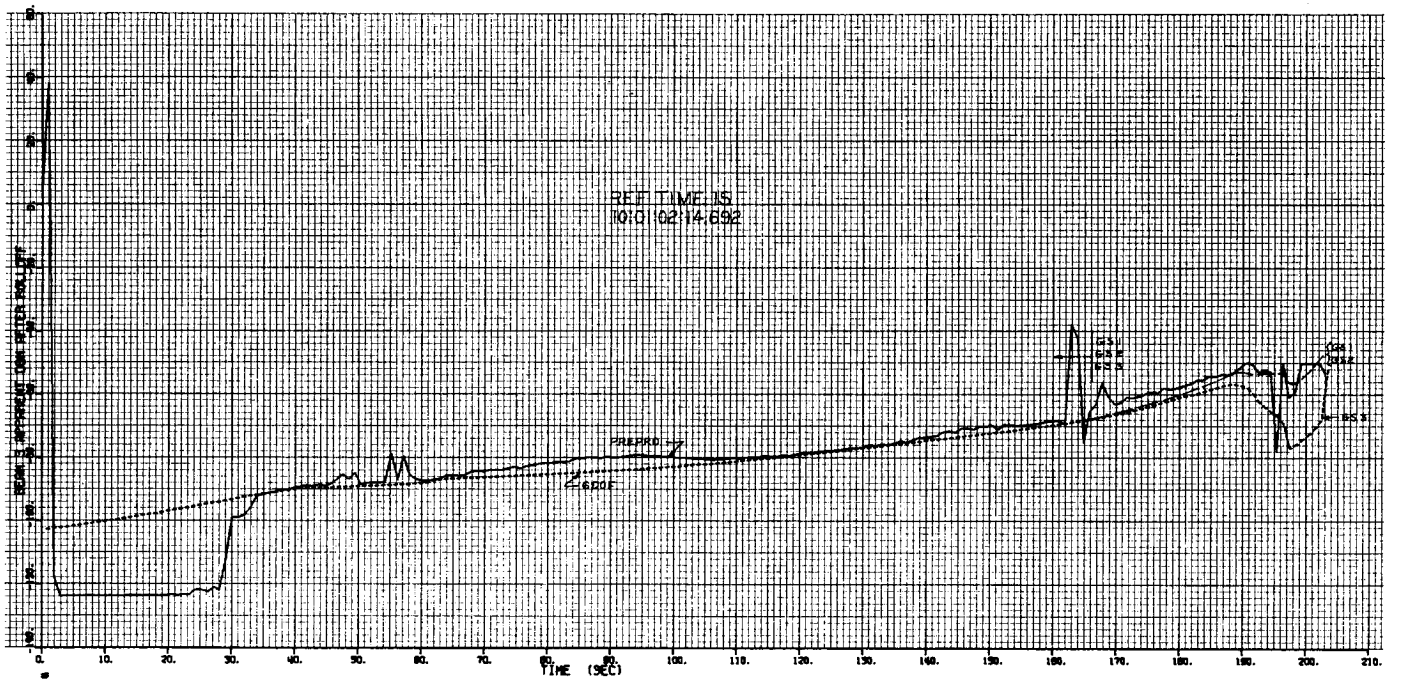

c) Beam 3

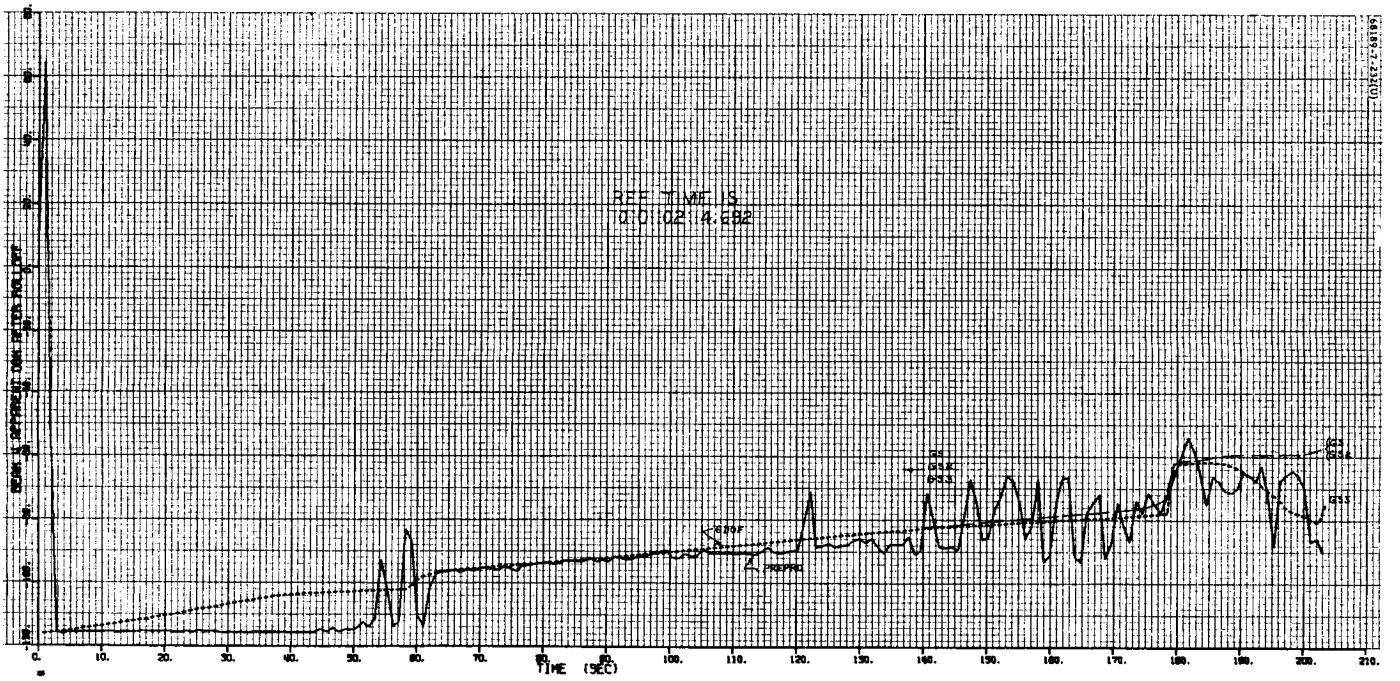

d) Beam 4

Figure 5.9-3 (continued). RADVS Reflectivity

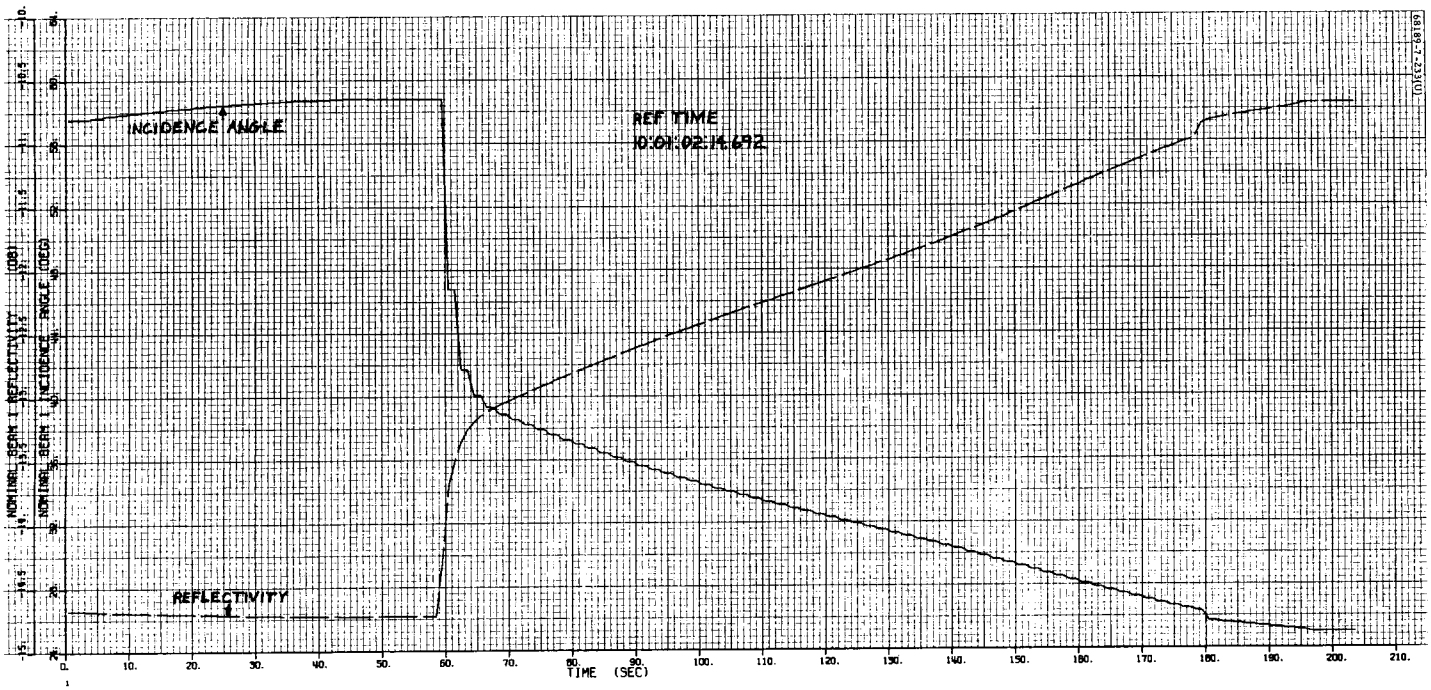

a) Beam 1

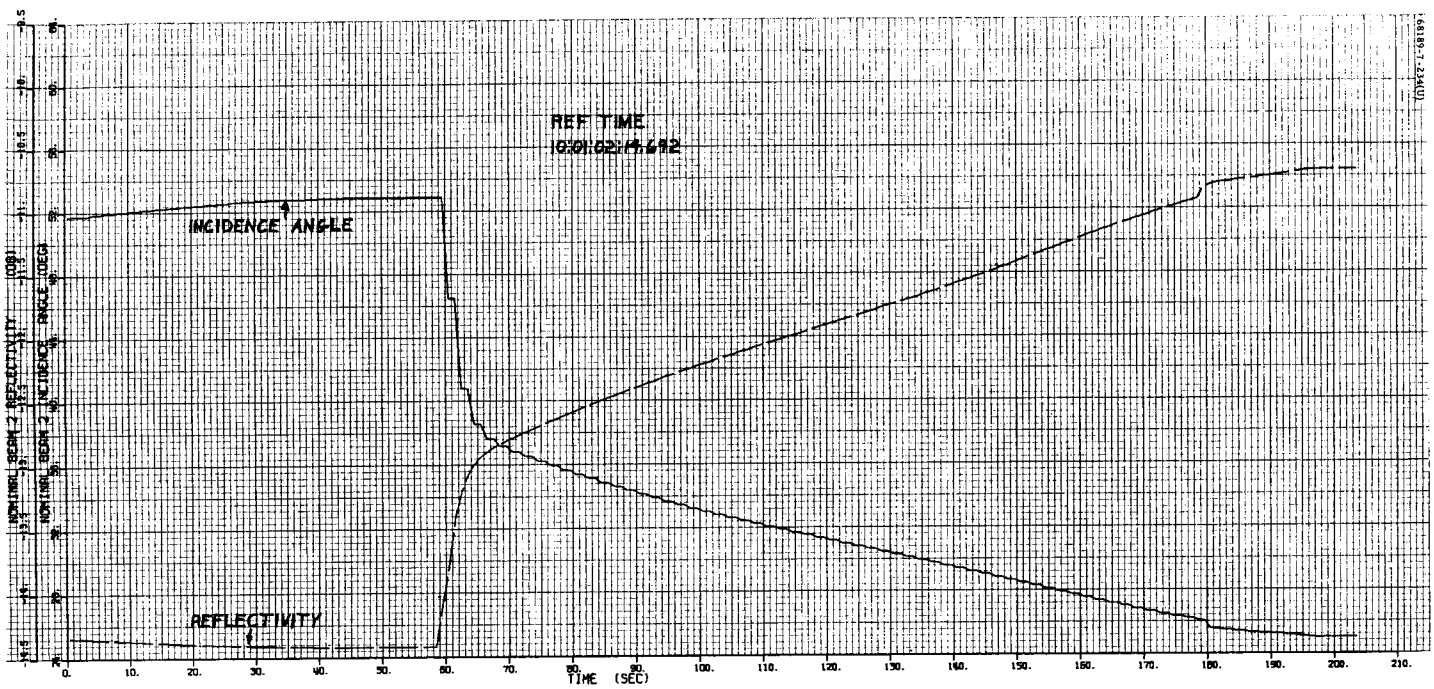

b) Beam 2

Figure 5.9-4. Beam Incidence Angles (θ) and Reflectivity Factors (σ) From 6DOF Program

5.9.5 RADVS DOCUMENTATION

R. A. Dibos, RADVS Design Review Material, 22 July 1965.

R. A. Dibos, "Behavior of Telemetered Range Near 1000-ft Scale Factor Charge," Hughes Aircraft Company, IDC 2253. 1/523, 27 December 1965.

R. A. Dibos, "Post-Mission Analyses Involving Radar Data," 25 March 1966.

R. A. Dibos, "A-21 RADVS-Predicted Minimum Margin Performance," 30 May 1966.

"Surveyor III Flight Performance Final Report," Hughes Aircraft Company, SSD 68189-3, July 1967.

M. R. Weiner, "Least Square Polynominal Fit of the DVS Tracker Non-Linearity for SC-7," Hughes Aircraft Company, IDC 2292/399, 26 September 1967.

"Surveyor IV Flight Performance Final Report," Hughes Aircraft Company, SSD 68189-4, September 1967.

R. A. Dibos, "Radar Performance Evaluation," SC-1 Symposium (NASA at JPL), September 1966.

"Surveyor I Flight Performance Final Report," Hughes Aircraft Company, SSD 68223R, October 1966.

"Decibel Allocation and Margin Summary," Hughes Aircraft Company, SSD 4021R-2, 28 November 1966.

R. A. Dibos, "RADVS Lateral Velocity Saturation," Hughes Aircraft Company, IDC 2253. 4/67, 9 March 1967.

R. A. Dibos, "Extended RADVS Equations for Six-Degree Digital Program," Hughes Aircraft Company, IDC 2253. 4/69, 15 March 1967.

E. White, "Timetic Method for Determining Surveyor System Errors," Hughes Aircraft Company, IDC 2293/105, 14 April 1967.

R. A. Dibos, "TM Mode 6 Data Relating to Radar Performance," Hughes Aircraft Company, IDC 2253. 4/84, 15 June 1967.

S. Suddick, "SC-7 Radar Calibration Data," Hughes Aircraft Company, IDC 2294. 5/155, 1 December 1967.

"Surveyor V Flight Performance Final Report," Hughes Aircraft Company, SSD 68189-5, November 1967.

5.9.6 ACKNOWLEDGMENTS

Terminal descent trajectory reconstruction – V. Mareli.

Technical assistance – W. T. Black.

PREPRO processing – N. R. Krupa.

6DOF processing – E. R. Kopitzke.

Technical coordination – M. R. Weiner.

5.10 STRUCTURES PERFORMANCE

5.10.1 INTRODUCTION

Structures postmission analysis is normally confined to launch and touchdown phases of the mission and the resulting structural loads, landing gear performance, and landing dynamics. Structures support is also required if vernier engine static firing or a hopping maneuver is performed.

During the launch phase, vehicle separation and extension of the landing gear were verified. During touchdown, shock absorber strain gages indicated the landing gear load time histories and enabled a prompt, but approximate, assessment of landing conditions, such as impact velocity and vehicle incidence relative to the lunar surface. Before and after a landing, leg deflections were monitored to establish whether or not the operating characteristics of the shock absorbers had been impaired during the mission.

Postmission analysis consists of analyzing 1) leg deflection potentiometer data, and 2) shock absorber strain gage data during landing. A mathematical model was used to simulate Surveyor VII landing conditions. The analytical results obtained from the mathematical model, combined with other data, can facilitate evaluation of lunar surface mechanical properties.

5.10.2 ANOMALY DESCRIPTION

On GMT day 21, 1968, the command to lock the landing gear was transmitted. On day 23, as the vehicle entered lunar night, a deflection of 1.43 degrees was observed on leg 2, indicating this leg had failed to lock. When the spacecraft was revived on day 43, leg 1 had deflected to 23.50 degrees, indicating that leg 1 also had failed to lock.

5.10.3 SUMMARY

Surveyor VII landing legs deployed in a normal fashion during the launch phase and operated normally during the landing and through the lunar day. With the onset of lunar night, leg 2 deflected 1.43 degrees, indicating that leg assembly 2 had failed to lock. Data received after the vehicle was revived on the second lunar day showed that leg 1 had deflected 23.0 degrees, indicating that leg assembly 1 was not locked.

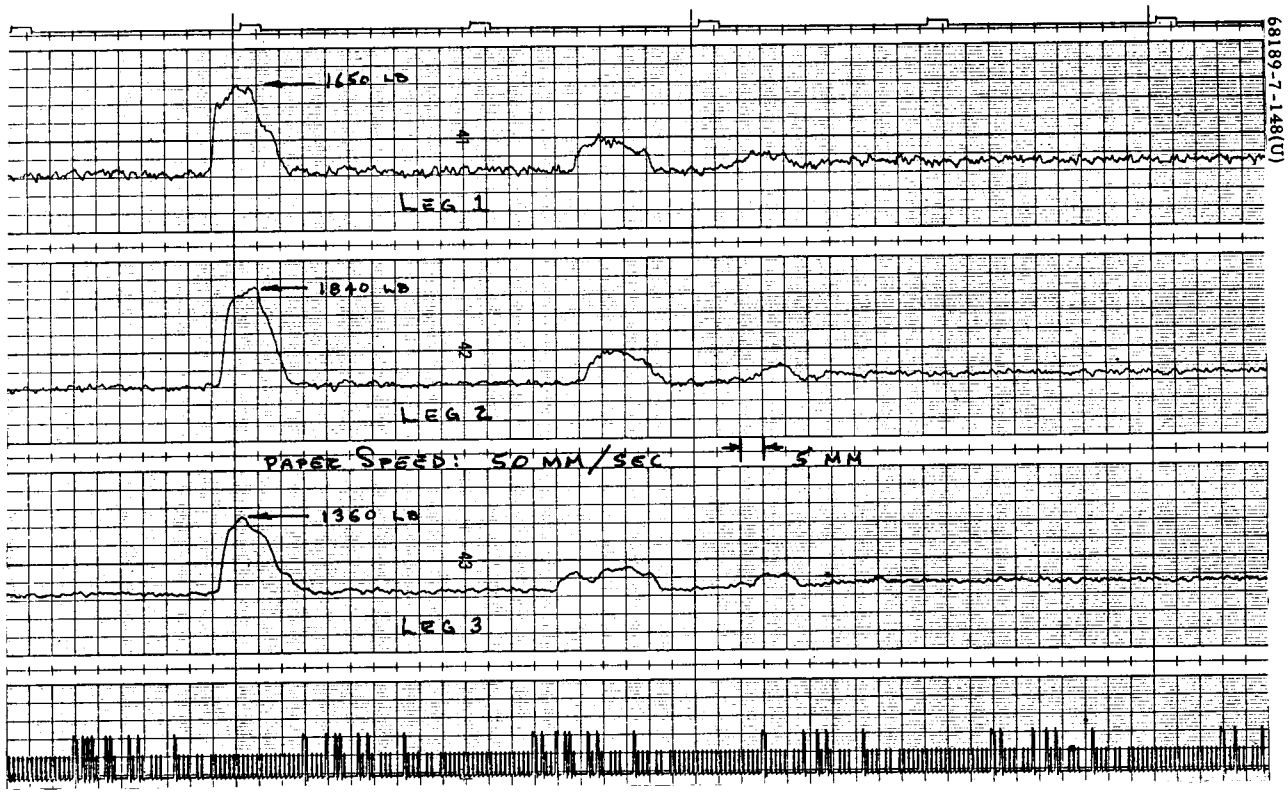

Figure 5.10-1. Initial Landing Strain Gage Histories

Analysis indicates that the spacecraft initially landed with an incidence relative to the surface of approximately 3 degrees at impact velocities of approximately 12 fps vertical and 1 fps lateral. In the analysis, these conditions resulted in footpad penetrations of between 1.7 and 2.7 inches on a surface of 5-psi static bearing strength.

The structural loads experienced by Surveyor VII during the initial landing were low relative to design levels.

5.10.4 PERFORMANCE ANALYSIS

5.10.4.1 Launch Phase

Leg Extension and Vehicle Separation

Due to a data outage, landing gear extension and vehicle separation were not confirmed in real time. Landing gear extension was first confirmed by Structures at 07:04:45 GMT and vehicle separation was confirmed at 07:05:43 GMT of day 7.

Leg Deflections

The landing gear position potentiometers were first monitored at 07:46:49 GMT of day 7 and were as follows:

Leg 1: V-5 = 0.1 degree

Leg 2: V-6 = 0.2 degree

Leg 3: V-7 = -0.2 degree

With the landing gear extended, the nominal value for these signals is 0.0 degree with an allowable variation of ±5 percent, or ±1.2 degrees.

5.10.4.2 Touchdown

Landing Conditions

Figure 5.10-1 shows the time histories of the axial forces in the landing gear shock absorbers from prior to initial surface contact until after the spacecraft came to rest. Footpad 1 contacted first, followed by pad 3 at 25 milliseconds and pad 2 at 50 milliseconds after pad 1 impact. Initially, each shock absorber experienced a force for approximately 0.4 second and then zero force for approximately 1.1 seconds as the spacecraft bounced clear of the surface. This was followed by a second touchdown during which the shock absorbers experienced forces of equal duration but smaller magnitude than those experienced on the initial landing. Again the spacecraft rebounded and the shock absorbers experienced zero force for approximately 0.3 second before the final touchdown. The shock absorber forces on the third touchdown decayed immediately to the levels required to support the

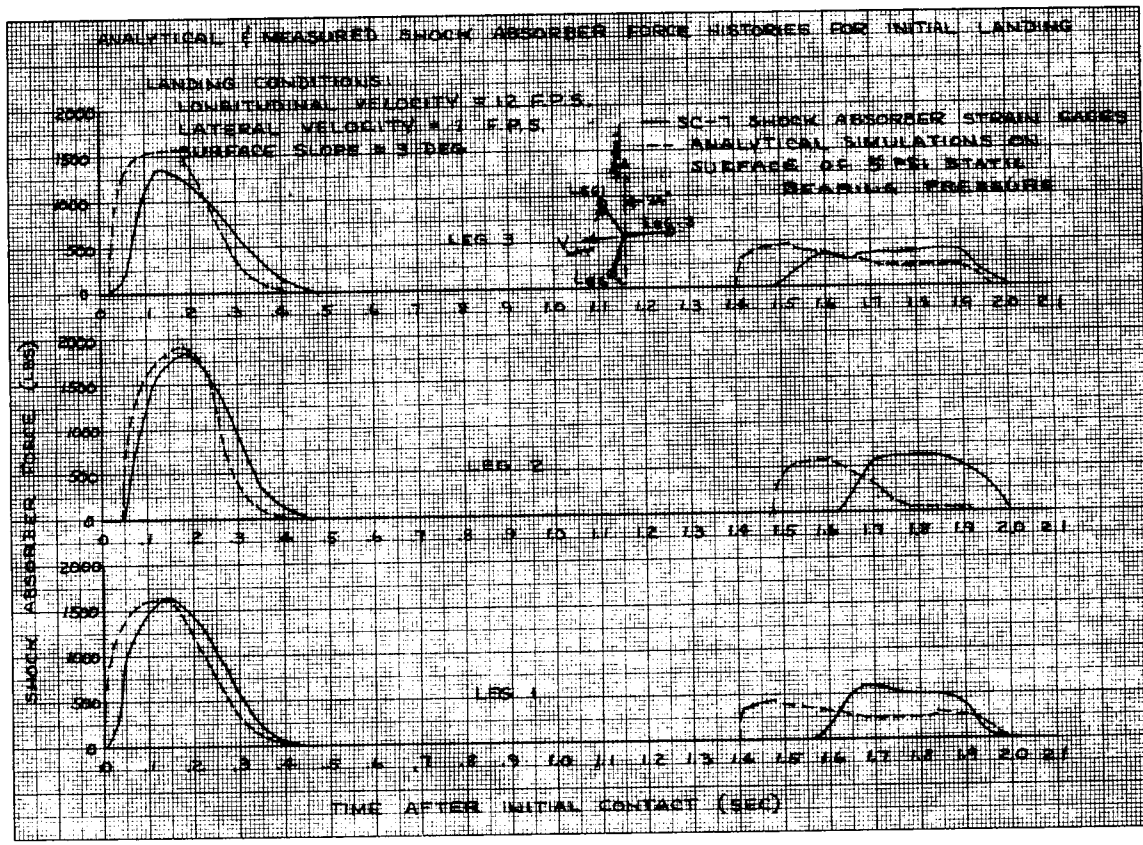

Figure 5.10-2. Analytical and Measured Shock Absorber Force Histories for Initial Landing

static weight of the vehicle, with apparently no oscillation related to the elasticity of the spacecraft and the lunar surface as was observed on previous Surveyor landings.

Table 5.10-1 gives the maximum force levels experienced by each shock absorber and the footpad impact times for the initial touchdown.

TABLE 5.10-1. MAXIMUM SHOCK ABSORBER FORCES AND FOOTPAD IMPACT TIMES

Leg Assembly Number	Maximum Shock Absorber Force, pounds	Footpad Impact Time, seconds after 010:01:05:00 GMT
1	1650 ± 80	37.620 ± 0.003
2	1840 ± 80	37.645 ± 0.003
3	1360 ± 80	37.670 ± 0.003

Dynamic Simulation

Computer simulation studies of landings were performed to estimate the landing conditions and surface properties that will yield penetration and shock absorber axial loads similar to those obtained during the Surveyor VII landing. Detailed analyses have shown that shock absorber force histories are fairly insensitive to the surface model and parameters. The closest comparison with the shock absorber forces (Figure 5.10-2) was obtained considering a vehicle landing with 12-fps vertical velocity, 1-fps horizontal velocity, a surface slope of 3 degrees, and a spacecraft incidence relative to the lunar horizontal of 0 degree. The surface on which this comparison was obtained had a 5-psi static bearing pressure — the same bearing pressure that gave the best correlation with flight data from Surveyors I, III, and VI. Analysis indicated a relatively softer landing surface for Surveyor V (Reference 1). The Surveyor VII footpad penetrations on the 5-psi surface model were 1.7, 2.7, and 1.7 inches for footpads 1, 2, and 3, respectively. For blocks 1, 2, and 3, the respective penetrations were 1.7, 2.8, and 1.6 inches.

Leg Deflections

Shortly after touchdown (01:09:07 GMT of day 10) the landing gear leg deflections were monitored and found to be as follows:

Leg 1: V-5 = 0.6 degree

Leg 2: V-6 = 0.9 degree

Leg 3: V-7 = 0.5 degree

Since these angles were not excessive, there was no necessity to lock the landing gear at that time. The decision not to lock the gear is made to facilitate gear actuation during any executed lunar hopping maneuver or during inadvertent hopping which could occur during a static firing experiment.

Structural Loads

The impact velocities, spacecraft attitude, and surface conditions for Surveyor VII were very similar to those for Surveyor I. It is therefore considered that, as on Surveyor I, the structural loads experienced by Surveyor VII at initial touchdown were less than 20 percent of the design load levels.

5.10.4.3 First Lunar Day

The shock absorbers remained unlocked during most of the lunar day, and the leg deflection signals, which were monitored at intervals, underwent small fluctuations of less than half a degree. Late in the lunar day it was decided to lock the gear to preclude the possibility of leg deflections resulting from shock absorber pressure leakage caused by the low temperatures of lunar night. The command to lock the landing gear was transmitted at approximately 15:32 GMT on day 21. The shock absorber temperatures at this time were 86°, 102° and 120° F for legs 1, 2, and 3, respectively. A check of the current level through the squib return circuit made after the landing gear lock command had been sent indicated that the squib circuits were open (i.e., all squibs had fired).

Between 07:42 and 09:31 GMT day 23, V-6 (leg 2 deflection) increased from 0.96° to 2.39° F, indicating that leg 2 had failed to lock. The shock absorber on leg 2 was cooling off rapidly during this period and the temperature (-94° F at 07:50 GMT to -121° F at 09:44 GMT on day 23) was in the range where deflections occurred on the Surveyor V landing gear. No further leg deflections occurred as Surveyor VII entered the lunar night. The final readings for the first lunar day showed the following leg angles:

Leg 1: V-5 = 0.60 degree

Leg 2: V-6 = 2.39 degrees

Leg 3: V-7 = 0.50 degree

5.10.4.4 Second Lunar Day

Readings obtained during the first engineering interrogation after the vehicle was revived on the second lunar day (approximately 19:00 on day 43) revealed the following leg deflections:

Leg 1: V-5 = 23.50 degrees

Leg 2: V-6 = 1.16 degrees

Leg 3: V-7 = 0.73 degree

The total collapse of leg 1 indicates that it also had failed to lock. This collapse is probably due to high pressure gas in the shock absorber escaping past the seals as a result of the extreme cold of lunar night. After sufficient pressure loss, this shock absorber would not be expected to reextend upon warming up on the second lunar day.

With the heat of the second lunar day, leg 2 returned from a 2.39-degree deflection to 1.16 degrees. This return was expected because the partially deflected legs of Surveyor V behaved in a similar manner. This partial deflection is probably due to a fluid contraction rather than a pressure loss as was suggested for leg 1. The change in the deflection of leg 2 was confirmation that the leg was not locked.

5.10.5 REFERENCES

1. "Surveyor V Flight Performance Final Report," Hughes Aircraft Company, SSD 68189-5, November 1967.

5.10.6 ACKNOWLEDGMENT

This section coordinated and written by C.D. Conaway.

5.11 MECHANISMS SUBSYSTEM

5.11.1 INTRODUCTION

This section deals with the mechanical performance of the spacecraft landing legs, omnidirectional antennas, and antenna/solar panel positioner (A/SPP). For purposes of this report, these mechanisms are collectively defined as the mechanisms subsystem.

1) Landing gear deployment – When each landing gear is fully deployed, it opens an electrical switch on the telescoping strut. The actuation of these switches indicates that the landing gear is deployed, and is required for initiation of automatic sun acquisition at separation from Centaur. The telemetry designations for these functions are V-1, V-2, and V-3 for each landing leg, respectively.

2) Omnidirectional antenna deployment – When each omnidirectional antenna is fully deployed, it opens an electrical switch to produce a change of state for telemetry purposes only. The telemetry designation for omnidirectional antenna A is M-1; for omnidirectional antenna B, M-2.

3) A/SPP automatic solar panel deployment – The A/SPP function after separation is to deploy the solar panel surface perpendicular to the roll axis to achieve maximum receipt of solar energy during transit.

The A/SPP has four rotation axes which are moved in steps upon command from earth. The axes are polar, solar, elevation, and roll. The polar axis rotates 1/16 degree per command; the other axes rotate 1/8 degree per command. Figure 5.11-1 illustrates the A/SPP with the polarity of rotation for each axis. The telemetry designation for the A/SPP axis positions are as follows:

Solar panel	M-3
Polar axis	M-4
Elevation axis	M-6
Roll axis	M-7

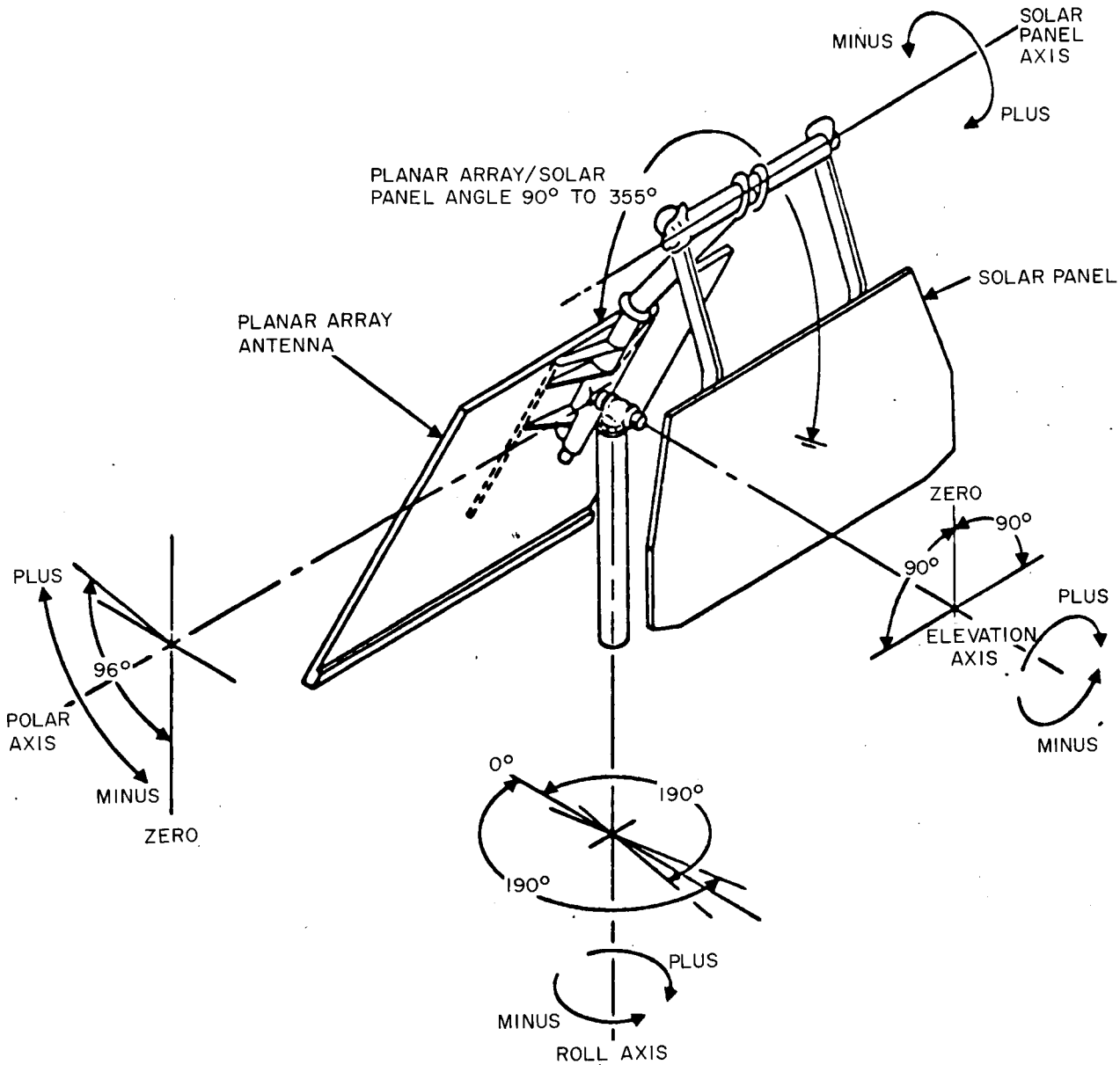

Figure 5.11-1. Antenna and Solar Panel Positioner

5.11.2 ANOMALY DESCRIPTION

No anomalies were detected in the mechanisms subsystem during separation. Telemetry data during transit indicated no anomalous conditions.

5.11.3 SUMMARY

All mechanism functions performed properly and at the correct times.

5.11.4 SUBSYSTEM PERFORMANCE ANALYSIS

Table 5.11-1 shows the occurrence of major events for the mechanisms subsystem. Table 5.11-2 presents a summary of the subsystem parameters reduced from telemetry data. The expected values were obtained from flight acceptance, type approval, and solar thermal vacuum testing, and from specified design performance values.

5.11.4.1 Landing Gear Deployment

Table 5.11-2 shows the nominal expected deployment time for the landing gear to be about 2.3 seconds. Flight data show the deployment time to be less than 0.726 second, which is somewhat smaller than nominal deployment time. The leg deflection signals (V5-7) indicated normal and complete extension of the landing gear.

5.11.4.2 Omnidirectional Antenna Deployment

The nominal expected omnidirectional antenna deployment time is 2.4 seconds. The mission deployment time was 2.616 ± 1.2 seconds, which indicates nominal deployment time. Data show that both omnidirectional antennas were deployed at the same time.

5.11.4.3 A/SPP Performance

Automatic Solar Panel Deployment

Automatic solar panel deployment begins upon closure of the 22-volt switch in the separation sensing and arming device at vehicle separation. The solar panel launch lock is unlocked and the solar panel is stepped from 355 to 270 degrees where it is relocked. At this point, the roll axis is stepped from -60 to 0 degrees and relocked. Both positions are locked until after touchdown.

The Surveyor VII mission solar panel deployment time was 553 seconds. Comparing this mission deployment time to that in solar thermal vacuum phase 1A (569 seconds), there is less than a 3 percent difference between the two times.

Table 5.11-3 shows the positions of the A/SPP axis before and after the automatic solar panel deployment. These all fall within the required limits when corrections are applied to the telemetry data.

TABLE 5.11-3. A/SPP AXIS POSITIONS FOR PRELAUNCH AND POST-AUTODEPLOYMENT CONDITIONS

	Prelaunch*				Post-autodeployment, Transit**			
	Raw Data		Corrected Data		Raw Data		Corrected Data	
	BCD	Indicated Angle, degrees	BCD	Angle, degrees	BCD	Indicated Angle, degrees	BCD	Angle, degrees
M-3 solar axis	921	353.6	921.5	353.6	710	270.96	708.4	270.4
M-4 polar axis	258	0.00	258.5	0.10	260	0.38	259.7	0.33
M-6 elevation axis	482	-0.60	482.5	-0.41	482	-0.60	481.1	-0.99
M-7 roll axis	346	-61.37	346.5	-61.17	496	-1.21	495.0	-1.61
S-1 reference voltage	1000	–	–	–	1003	–	–	–
S-2 reference return	0	–	–	–	0	–	–	–
S-5 commutator unbalance current	103	–	–	–	103	–	–	–

Note: Nominal reference voltage, 1000 (BCD)

*Prelaunch data time 007:05:07:13.257

**Post-autodeployment data time 010:00:07:30.711

Postlanding Performance

Table 5.11-4 presents the complete record of stepping commands during lunar operations. It also includes a statement of the functions being performed during stepping. Table 5.11-5 tabulates the solar panel and roll axis angles versus time.

Table 5.11-6 provides the number and direction of step commands sent for each A/SPP gimbal axis.

Drive Stepping Response

An evaluation of stepping count tallies for the first lunar day, as compared with telemetry readings, indicates that, as far as can be determined, the gimbal drives responded successfully to all commands.

TABLE 5.11-4. A/SPP STEPPING COMMAND LOG

Execution Time, GMT, day:hr:min	Command	Quantity	Function
010:01:05			Touchdown
02:38	0402	650	Begin sun and earth acquisition
02:44	0403	650	
02:50	0406	400	
02:55	0406	795	
03:02	0402	237	
03:06	0405	74	
03:07	0403	594	
03:12	0402	197	
03:18	0410	276	
10:12	0401	36	Fine sun and earth positioning
10:14	0402	72	
10:19	0401	13	
10:26	0402	5	
10:39	0405	11	
10:48	0406	4	
11:24	0407	9	
11:45	0405	4	
11:48	0406	11	
11:51	0401	11	
11:54	0402	1	
12:06	0407	26	
12:23	0410	5	
12:25	0404	4	
12:25	0403	44	
12:36	0404	8	

Table 5.11-4 (continued)

Execution Time, GMT, day:hr:min	Command	Quantity	Function
011:00:05	0403	10	Stepping blocks of 10 commands, each executed in an effort to release alpha scattering instrument
00:07	0404	10	
00:08	0403	10	
00:10	0404	10	
00:11	0403	10	
00:12	0404	10	
00:13	0407	10	
00:14	0410	10	
00:16	0407	10	
00:16	0410	10	
00:17	0407	10	
00:18	0410	10	
00:19	0405	10	
00:20	0406	10	
00:21	0405	10	
00:22	0406	10	
00:23	0405	10	
00:24	0406	10	
00:25	0401	10	
00:25	0402	10	
18:39	0401	160	
22:46	0401	240	
012:			No stepping on day 012
013:02:59	0405	1452	
03:12	0407	484	
03:18	0405	72	
03:19	0404	59	
03:20	0405	72	

Table 5.11-4 (continued)

Execution Time, GMT, day:hr:min	Command	Quantity	Function
013:03:21	0404	88	
03:22	0405	58	
03:23	0410	43	
03:23	0405	51	
03:24	0404	100	
03:25	0405	72	
03:26	0410	58	
03:27	0405	71	
03:28	0404	102	
03:29	0410	29	
03:30	0405	108	
03:31	0410	29	
014:00:36	0403	7	
00:38	0404	21	
00:40	0405	7	
00:41	0406	35	
015:07:52	0401	300	Reduce battery charge current
08:45	0401	100	
22:39	0403	20	
22:40	0410	33	
23:13	0402	180	
016:00:33	0402	36	
00:37	0402	36	
02:30	0406	1050	Shade television and part of compartment A
02:39	0410	44	
02:41	0401	224	
02:44	0403	365	

Table 5.11-4 (continued)

Execution Time, GMT, day:hr:min	Command	Quantity	Function
016:07:17	0404	365	
07:20	0402	224	
07:22	0407	44	
07:23	0405	1050	
09:25	0401	144	
10:24	0401	72	
12:05	0406	1095	
12:14	0410	44	
12:15	0403	364	
12:21	0401	39	
21:31	0402	36	
21:32	0406	217	
017:04:31	0405	867	
04:39	0402	109	
04:40	0404	263	
04:43	0410	184	
04:45	0405	831	
16:32	0406	800	
16:39	0407	189	
16:47	0406	891	
16:55	0403	311	
16:59	0401	114	
22:00	0406	260	
22:03	0401	56	
22:04	0404	47	
22:05	0407	26	

Table 5.11-4 (continued)

Execution Time, GMT, day:hr:min	Command	Quantity	Function
018:04:29	0402	165	
04:31	0404	277	
04:34	0407	145	
04:36	0405	1415	
04:50	0407	6	
04:52	0410	30	
04:56	0402	144	
07:13	0402	20	
16:48	0401	302	
16:55	0403	292	
16:58	0401	60	
16:59	0410	136	
17:01	0406	1000	
17:57	0406	394	
019:05:36	0402	446	
05:40	0403	86	
05:41	0407	259	
05:44	0405	987	
05:55	0405	12	
05:57	0406	18	
05:58	0407	6	
05:59	0410	24	
06:03	0402	82	
06:13	0401	46	
06:23	0402	29	
22:53	0406	578	
22:58	0404	71	
22:59	0410	200	
23:02	0401	572	

Table 5.11-4 (continued)

Execution Time, GMT, day:hr:min	Command	Quantity	Function
019:23:07	0406	554	
020:05:05	0402	124	
05:06	0404	10	
05:07	0410	288	
05:09	0406	230	
05:14	0403	42	
05:17	0404	28	
05:18	0406	21	
05:20	0405	42	
05:22	0410	28	
021:07:57	0402	230	
	0401	60	
10:43	0401	70	
18:44	0401	70	
022:00:57	0401	180	
07:18	0410	40	
	0404	12	
	0407	12	
	0403	6	
09:37	0405	16	
	0401	72	
023:03:40	0403	15	
03:41	0405	15	
03:41	0410	8	
06:27	0402	370	
11:17	0402	203	
21:20	0401	203	
22:14	0401	176	Reposition solar panel to second lunar day optimum position

TABLE 5.11-5. A/SPP GIMBAL ANGLES VERSUS TIME DURING FIRST LUNAR DAY

TIME DDDHHMM	ROLL AXIS	ELEVATION AXIS	POLAR AXIS	SOLAR AXIS
0100318	-155.15	-38.20	85.20	119.97
0101048	-154.18	-38.20	85.20	116.10
0101236	-155.15	-34.05	87.39	117.48
0101800	-155.15	-34.05	87.39	117.48
0110000	-155.15	-34.05	87.39	117.48
0110600	-155.15	-34.05	87.39	117.48
0111200	-155.15	-34.05	87.39	117.48
0111839	-155.15	-34.05	87.39	139.63
0112246	-155.15	-34.05	87.39	172.85
0120600	-155.15	-34.05	87.39	172.85
0121200	-155.15	-34.05	87.39	172.85
0121800	-155.15	-34.05	87.39	172.85
0130331	115.56	10.93	63.49	172.85
0131200	115.56	10.93	63.49	172.85
0131800	115.56	10.93	63.49	172.85
0140041	111.69	10.93	62.53	172.85
0140600	111.69	10.93	62.53	172.85
0141200	111.69	10.93	62.53	172.85
0141800	111.69	10.93	62.53	172.85
0150000	111.69	10.93	62.53	172.85
0150845	111.69	10.93	62.53	228.20
0151200	111.69	10.93	62.53	228.20
0151800	111.69	10.93	62.53	228.20
0152313	111.69	6.37	63.90	203.29
0160037	111.69	6.37	63.90	193.33
0160244	-33.63	.27	88.90	224.33
0160723	111.69	6.37	63.90	193.33
0161024	111.69	6.37	63.90	223.22
0161221	-39.86	.27	88.83	228.62
0162132	-69.89	.27	88.83	223.64
0170445	165.11	-25.19	70.82	208.55
0171000	165.11	-25.19	70.82	208.E5
0171659	-68.92	.97	92.12	224.33
0172205	-104.91	4.57	88.90	232.08
0180456	90.93	21.31	69.92	189.31
0180713	90.93	21.31	69.92	186.54
0181757	-102.00	2.49	89.93	236.65
0190000	-102.00	2.49	89.93	236.65
0190623	33.77	35.85	95.82	265.92
0191400	33.77	35.85	95.82	265.92
0192307	-122.90	8.17	90.95	245.09
0200522	-151.82	-35.57	91.23	227.93
0201200	-151.82	-35.57	91.23	227.93
0201800	-151.82	-35.57	91.23	227.93
0210000	-151.82	-35.57	91.23	227.93
0210757	-151.82	-35.57	91.23	204.40
0211043	-151.82	-35.57	91.23	214.09
0211844	-151.82	-35.57	91.23	223.77
0220057	-151.82	-35.57	91.23	248.69
0220937	-149.61	-39.44	90.82	258.65
0221500	-149.61	-39.44	90.82	258.65
0222100	-149.61	-39.44	90.82	258.65
0230341	-147.53	-40.55	91.85	258.65

TABLE 5.11-6. POSTLANDING A/SPP STEPPING COMMANDS SUMMARY

Axis	Solar		Polar		Elevation		Roll	
Direction	Plus	Minus	Plus	Minus	Plus	Minus	Plus	Minus
Command	0401	0402	0403	0404	0407	0410	0405	0406
Total	3330	3603	2826	1485	1236	1529	7317	8383
Total plus and minus	6933		4311		2765		15,700	
Grand total	29,709							

5.11.5 REFERENCES

1) "Surveyor VII Flight Path Analysis and Command Operations Report," Hughes Aircraft Company, SSD 88014, 25 January 1968.

2) R. L. Lackman and W. R. Heathcote, "Error Analysis of the SC-3 Spacecraft Attitude on the Lunar Surface," Hughes Aircraft Company, IDC 2292/246, 4 April 1967.

5.11.6 ACKNOWLEDGMENTS

J. M. Berger, technical coordinator and author

L. L. Gamer, lunar performance analysis

5.12 TERMINAL DESCENT TRAJECTORY PERFORMANCE

5.12.1 INTRODUCTION

The terminal descent and landing phase begins with the transition from coast mode II to the terminal descent phase. Terminal descent itself starts with the preretro attitude maneuvers which reposition the attitude of the spacecraft from the sun-star reference so that the expected direction of the retro thrust vector will be aligned with respect to the velocity vector. This alignment achieves the desired retro burnout conditions. Following completion of the attitude maneuvers, the altitude marking radar (AMR) is activated. The AMR is preset to generate a mark signal when the range to the lunar surface is 60 miles. A backup mark signal is transmitted to the spacecraft to arrive after the time the AMR mark should occur in order to initiate the automatic sequence in the event the AMR mark is not generated. The desired delay between the altitude mark and vernier ignition is stored in the flight control programmer by ground command. Retro engine ignition is automatically initiated 1.1 seconds after vernier ignition.

During the retro phase, spacecraft attitude is maintained in the inertial direction established at the end of the preretro maneuvers by the vernier attitude control system, and the total vernier thrust is maintained at mid-thrust. As the mass of the vehicle decreases due to expenditure of retro and vernier propellant, the spacecraft thrust to mass ratio (T/M) increases from approximately 4 g_e (g_e = 32.2 ft/sec^2) at ignition to 10 g_e preceding burnout. Prior to burnout, the inhibit is removed from the acceleration switch output, and the doppler radar and altimeter (RADVS) is activated.

As the thrust decays during retro burnout, the acceleration switch signals when the T/M level has dropped to 3.5 g_e. At this time, a counter in the flight control programmer is initiated and, after 10 seconds from this point, the vernier engines are commanded to high thrust. The explosive bolts attaching the retro to the spacecraft are activated 2 seconds following the high thrust command, allowing the retro case to separate from the spacecraft. Following a programmed delay of 2.15 seconds after separation begins, the vernier thrust command is changed from the open-loop mode to a closed-loop acceleration control mode. Nominal acceleration commanded at this point is 4.77 ft/sec^2.

Surveyor VII performance was near perfect; all events occurred according to specification. The preretro maneuvers properly oriented the

TABLE 5.12-1. BEST ESTIMATE TIMES FOR SURVEYOR VII TERMINAL DESCENT

Event	GMT, Day 10, Hour 01, min:sec	
	At DSS 14	At Spacecraft
AMR mark	02:11.892 ± 0.05	02:10.565 ± 0.05
AMR backup command	02:13.2	02:14.527
Vernier engine ignition	02:14.692 ± 0.05	02:13.365 ± 0.05
RADVS on	02:15.752 ± 0.6	02:14.425 ± 0.6
Retro ignition	02:15.792 ± 0.05	02:14.465 ± 0.05
RODVS on	02:48.850 ± 0.6	02:47.523 ± 0.6
3.5 g mark	02:58.975 ± 0.025	02:57.648 ± 0.025
Start maximum thrust	03:09.250 ± 0.6	03:07.923 ± 0.6
Retro eject	03:10.990 ± 0.05	03:09.663 ± 0.05
Retro ejected	03:11.550 ± 0.6	03:10.223 ± 0.6
Beam 4 lock	03:12.750 ± 0.6	03:11.423 ± 0.6
Beam 1 unlock	03:13.050 ± 0.6	03:11.723 ± 0.6
Start RADVS-controlled descent	03:13.090 ± 0.05	03:11.763 ± 0.05
Beam 4 unlock	03:13.950 ± 0.6	03:12.623 ± 0.6
Beam 1 lock	03:14.250 ± 0.6	03:12.923 ± 0.6
Beam 4 lock	03:17.549 ± 0.6	03:16.222 ± 0.6
RORA on	03:17.649 ± 0.6	03:16.322 ± 0.6
Segment intercept	04:03.018 ± 0.15	04:01.691 ± 0.15
1000-foot mark	05:13.285 ± 0.05	05:11.958 ± 0.05
10-fps mark	05:30.184 ± 0.05	05:28.857 ± 0.05
14-foot mark	05:36.284 ± 0.05	05:34.957 ± 0.05
Touchdown	05:37.744 ± 0.15	05:36.417 ± 0.15

spacecraft for the start of the retro phase sequence. The AMR mark occurred and the vernier engines ignited at the desired time delay of 2.76 seconds from AMR mark, indicating that the start of the terminal descent was generated by the true mark and not by the backup command (see Table 5.12-1). In the following, all times are from vernier ignition (VI). RODVS (all three doppler velocity sensors locked) and retro eject occurred at VI+34 and VI+56.3 seconds, respectively. Beam 4 locked temporarily at VI+58 seconds and beam 1 unlocked at VI+58.3 seconds. RODVS was still indicted (FC-34) during the beam 1 unlock, so that beam 1 unlock was brief with respect to telemetry sampling time (probably due to the receding retro case passing through the beam 1 direction). During this brief period, erroneous steering occurred (1.7 seconds after the start of RADVS-controlled descent phase – VI+58.4 seconds). The loss of lock was insignificant to the terminal descent performance because of its short duration and because the erroneous steering during this short period was in a favorable direction. The reliable operation of the radar altimeter (RORA) occurred at VI+63 seconds and remained reliable throughout the descent.

Other than the beam 1 drop lock the Surveyor VII terminal descent performance was extremely nominal as determined by postflight analysis.

5.12.2 ANOMALY DESCRIPTION

There were no anomalies during this phase of the mission.

5.12.3 SUMMARY

Table 5.12-1 lists the significant terminal descent events and time of occurrence. The DSS time is either plus or minus the one-way transit time delay (approximately 1.327 seconds), depending on whether the event is a command or a telemetered spacecraft action.

The significant terminal descent performance parameters are summarized in Table 5.12-2, along with the predicted values. From this table, it can be seen that Surveyor VII performed extremely well with respect to the predicted performance.

5.12.4 PERFORMANCE ANALYSIS

5.12.4.1 Introduction

The Surveyor VII terminal phase performance has been analyzed by comparing processed telemetry data by the PREPRO program (described in paragraph 5.12.4.2 along with other postflight analysis computer programs) with a precision six degree of freedom (6DOF) digital program simulation. Various nominal predicted preflight and preterminal in-flight parameters within the 6DOF were adjusted so as to coincide discrete time events with discrete telemetry time events. These events provide the 6DOF

TABLE 5.12-2. SUMMARY OF TERMINAL DESCENT PERFORMANCE PARAMETERS

Parameter	Predicted Value	Best Estimated Value
Vernier ignition conditions		
Time, hr:min:sec	01:02:15.367	01:02:14.692
Altitude, feet	237,933	237,933
Velocity, fps	8,588.2	8,588.1
Attitude, degrees	34.92	34.84
Misalignment angle during retro		
In-plane, degree	0	-0.213
Out-of-plane, degree	0	-0.160
Start RADVS-controlled descent		
Altitude, feet	38,736	41,510
Total velocity, fps	477	452
V_x	-42	-56.7
V_y	-171	-131.9
V_z	444	428.2
Attitude, degrees	36.26	36.17
Flight path angle, degrees	14.62	18.1
Retro burn time, seconds	42.97	42.98
Segment intercept conditions		
Slant range, feet	22,000	20,246
Velocity (V_z), fps	490	464
1000-foot mark conditions		
Slant range, feet	1,000	970
Total velocity, fps	106	102.5
V_z	—	102.3
Attitude, degrees	1.5	1.62
10-fps mark conditions		
Slant range, feet	46.0	46.0
Velocity (V_z), fps	8.6	9.2
Attitude, degree	0.03	0.03
Vernier engine cutoff conditions		
Slant range, feet	13.0	13.02
Velocity (V_z), fps	5.01	5.02
Attitude, degree	0.02	0.03
Touchdown conditions		
Longitudinal velocity, fps	12.5	12.5
Lateral velocity, fps	0.0	0.0
Total vernier propellant used, pounds	149.41	152.89

program with significant data points for constructing a best-fit trajectory. Table 5.12-3 shows the discrete time events determined from telemetry data and compared with the best match reconstruction by the 6DOF program.

The one-way doppler data, due to the velocity between the spacecraft and earth, provides information for reconstructing a highly accurate retro thrust-time curve. These data, utilized by the DOPP program, also allow determination of the retro specific impulse, retro performance, and characteristic velocity (total ΔV removed) during the retro and vernier phases. From the retro accelerometer telemetry data, a thrust-time curve is also reconstructed by the TTC program, and comparison is made with the DOPP program reconstruction.

The doppler data are also utilized to determine the radial velocity (the velocity in the direction of the earth tracking station-spacecraft line of sight). The same parameter is computed within the 6DOF program. The two methods of reconstructing the radial velocity are then compared, thus providing an additional confidence measurement in the 6DOF reconstruction.

The total vernier propellant consumption is determined by utilizing vernier engine flight acceptance test data of mixture ratio and specific impulse as a function of vernier engine thrust for the midcourse, retro, and vernier phases. The spacecraft landing location is determined from postflight orbit determination data.

The best-estimate terminal descent trajectory reconstruction scheme employed for Surveyor VII was similar to that of previous successful flights. Again, the scheme depends on establishing a good reference point near the end of the retro phase in which the spacecraft V_x, V_y, and V_z telemetry data are reliable. The point selected was at retro case eject in which all three doppler velocity sensor beams were reliable. Based on postmission assessment of the RADVS and telemetry system, the calibrated V_x, V_y, and V_z velocities at retro case eject were determined to be:

$$V_x = -54.9 \text{ fps}$$

$$V_y = -125.0 \text{ fps}$$

$$V_z = 446.3 \text{ fps}$$

These values have been corrected for biases determined in the telemetry data as indicated in subsection 5.12.4.8.

With the DOPP program retro thrust-time curve as input into the 6DOF program, the initial conditions at vernier ignition of velocity and altitude, as determined from orbit determination postflight data and retro thrust vector alignment, were perturbed within the 6DOF program until the above components of spacecraft velocity at retro case eject and the elapsed time from start of RADVS-controlled steering to the command descent contour intercept (as indicated by telemetry) were matched.

TABLE 5. 12-3. 6DOF DISCRETE TIME EVENTS VERSUS TELEMETERED

Event	6DOF Time (Figures 5. 12-7 to 5. 12-14), seconds	GMT, day 10, Hour 01, min:sec	
		Converted Figure Time to GMT	Actual GMT at DSS 14
Vernier engine ignition	0. 0	02:14. 692	02:14. 692±0. 05
Retro ignition	1. 1	02:15. 792	02:15. 792±0. 05
RODVS on	33. 50	02:48. 192	02:48. 850±0. 6
3. 5 g mark	44. 26	02:58. 952	02:58. 975±0. 025
Start maximum thrust	54. 26	03:08. 952	03:09. 250±0. 6
Retro eject	56. 26	03:10. 952	03:10. 990±0. 05
Beam 1 unlock	58. 00	03:12. 692	03:13. 050±0. 6
Start RADVS-controlled descent	58. 41	03:13. 102	03:13. 090±0. 05
Beam 1 lock	60. 10	03:14. 792	03:14. 250±0. 6
RORA	62. 90	03:17. 592	03:17. 649±0. 6
Segment intercept	108. 00	04:02. 692	04:03. 018±0. 15
1000-foot mark	178. 70	05:13. 392	05:13. 285±0. 05
10-fps mark	196. 31	05:31. 002	05:30. 184±0. 05
14-foot mark	202. 60	05:37. 292	05:36. 284±0. 05
Touchdown	203. 80	05:38. 492	05:37. 744±0. 15

With the velocities at retro case eject and the discrete time events matched, the 6DOF reconstruction provided a fairly close comparison to the telemetry data. Therefore, the 6DOF reconstruction was considered a good estimate of the actual Surveyor VII performance. This reconstruction is discussed further in paragraph 5. 12. 4. 8.

5. 12. 4. 2 Postflight Analysis Computer Programs

PREPRO

The PREPRO program converts an input tape of processed telemetry data into appropriate engineering units. The tape is preprocessed by Hughes into raw BCD counts and appears in commutator sequence. The spacecraft preflight telemetry calibration coefficients are utilized within the program for the conversion into engineering units. Prior to the conversion, the flight control reference return (FC-77 telemetry signal) correction is made to the appropriate signals. The program interpolates engineering data significant to terminal descent reconstruction into preselected equal time intervals. PREPRO then writes two output tapes: tape No. 1 of the interpolated engineering data, and tape No. 2 of all the input signals in proper engineering units as they appear in commutator sequence.

POSTPR

POSTPR provides machines plots (CALCOMP) of any combination of variables from the following input data tapes: PREPRO tape No. 1, 6DOF data tape, and both PREPRO tape No. 1 and the 6DOF tape, thus providing a superimposed plot of the best estimated 6DOF reconstruction and the telemetered data.

6DOF

6DOF is a precision six degree of freedom digital program simulating the Surveyor terminal phase from vernier ignition to touchdown. The program assumes rigid body dynamics, including spacecraft weight and moment of inertia changes. The program also models the spacecraft flight control and radar subsystems. The radar model implemented in the 6DOF program is described in Section 5. 9. The flexibility of the data input is such that preflight and postflight reconstructions of the terminal phase can be made. By matching significant time events with telemetry discrete times, a fairly accurate reconstruction of the terminal phase trajectory can be established by the 6DOF program in the absence of gross system errors or telemetry errors in spacecraft V_x, V_y, and V_z velocities. The program outputs are velocity, position, acceleration, attitude, moments, weight, inertia, angular velocity, control loop states, engine commands and thrusts, and radar system states. The program also writes a tape that can be used for machine plots (CALCOMP) of any combination of variables. The tape can also be set up for input into the POSTPR program.

TD1

TD1 is a two-dimensional, three degree of freedom simulation of the terminal phase of the Surveyor mission. The main use of TD1 is to determine the vernier propellant consumption. The program can also be used to a limited extent for terminal descent trajectory reconstruction since it is restricted to a planar case. However, the program models the spacecraft to the extent necessary for accurate propellant consumption determination, that is, if no apparent degradation appears in the vernier engine performance.

TTC

TTC reconstructs the retro thrust-time curve from raw accelerometer telemetry data. Corrections are made to the telemetry data by removing bias, scale factor, and hysteresis errors. This reconstruction is used for comparison with the DOPP program reconstruction.

DOPP

DOPP reconstructs the main retro thrust-time curve from the spacecraft transmitter's one-way doppler data. This reconstruction technique is especially accurate since the frequency of the spacecraft transmitter is very stable. The program accounts for errors introduced by the transmitter's temperature sensitive drift, variation in retro thrust vector direction during retro burn, and flight control sensor deflection. The program is also utilized for determining the main retro specific impulse and the characteristic velocity (total ΔV removed) during the retro and vernier phases.

5.12.4.3 Velocity Change Due to Thrusting During Retro Phase

Determination of Ignition Conditions

Ignition velocity V_o, flight path angle γ, and roll angle φ serve as initialization parameters and are determined from tracking data. The 3σ uncertainty in free flight velocities is <0.5 fps. Since ignition altitude has a calculated 3σ inaccuracy of 2140 feet due to marking range errors (with a V_o = 8500 fps and an incidence angle with respect to local vertical of 35 degrees), the equivalent ignition velocity uncertainty due to this error source is (g = lunar gravity):

$$\Delta V = g \cos \gamma \, t = 5 \times \frac{2140}{8500} = 1.3 \text{ fps}$$

Hence, the total uncertainty in ignition velocity is 1.4 fps when these two independent error sources are combined. The direction of $\underline{V}_o$ at ignition has an uncertainty of <0.07 degree. Therefore, the best estimate ignition conditions are

$$V_o = 8588.2 \pm 1.4 \text{ fps}$$

$$\gamma_o = -55.1 \pm 0.07 \text{ degrees}$$

Gravity-Induced Component of Velocity

During the retro phase (from vernier ignition to start of RADVS-controlled descent), gravity contributes to the spacecraft velocity by an amount $\int \underline{g}\, dt$. Lunar gravity varies in magnitude from 4.92 ft/sec^2 (at vernier ignition) to 5.26 ft/sec^2 (at start of RADVS). In addition, $\underline{g}$ varies in direction since the spacecraft has horizontal motion. The change in direction of $\underline{g}$ over the retro phase (to RADVS control) is about

$$\int_0^t \sin^{-1}\left[\frac{V \sin \psi \, dt}{R_\ell}\right] = 1.34 \text{ degrees}$$

where bar under symbol is vector quantity and

t = retro time

V = velocity vector

ψ = spacecraft velocity incidence angle

R_ℓ = moon centered radial distance

The time duration of the retro phase is 58.4 seconds (see Table 5.12-1). Actual numerical integration of $\int g\, dt$ gives $gt = 301.4 \pm 1$ fps.

Thrust-Induced Velocity Change

The two methods used to calculate velocity change during the retro phase due to the thrusting of the engines are as follows:

1) ΔV from vector addition – The vector equation (Figure 5.12-1a) $\underline{VBO} = \underline{V_o} + \underline{gt} + \underline{\Delta V}$ can be solved to find $\underline{\Delta V}$. $\underline{V_o}$ and $\underline{gt}$ are available as discussed above; the spacecraft axis components of $\underline{VBO}$ (the velocity at retro case eject) are available from calibrated telemetry data. The axial velocity V_z is known to an estimated accuracy of better than 1 percent at a given time, based on correlation of simulated versus actual discrete time events such as the 1000-foot mark and the 10-fps mark. V_x and V_y at retro case eject have calculated uncertainties of 3.3 and 2.7 fps, respectively, based on 3σ telemetry and RADVS sensor errors. At retro case eject, the velocity components are:

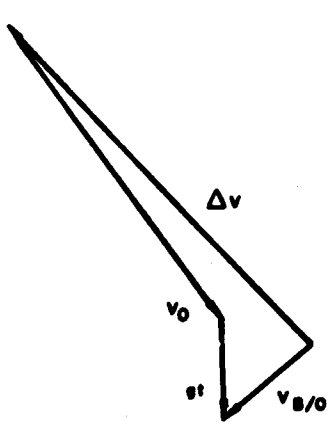

(U)06-9-68189

a) Vector Diagram

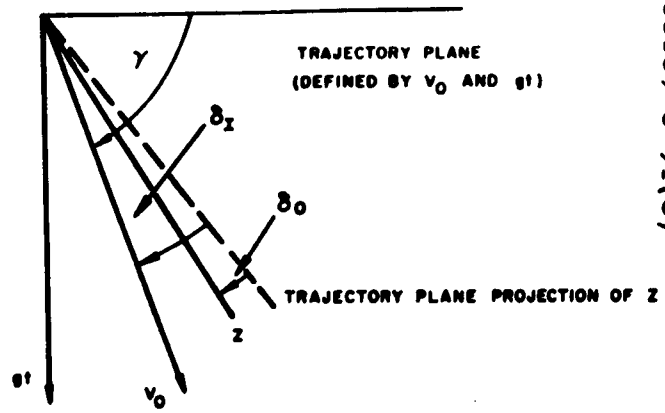

(U)16-9-68189

b) Trajectory Plane

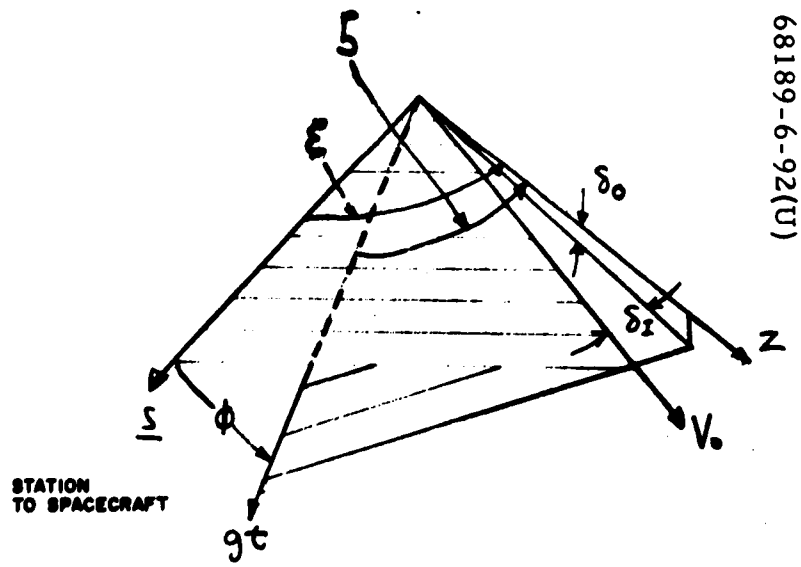

(U)26-9-68189

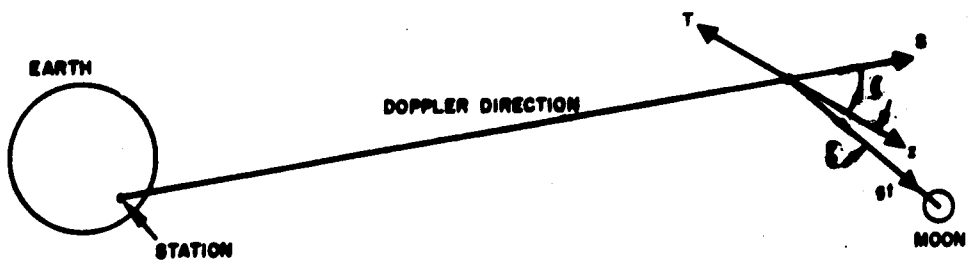

c) Doppler Geometry

Figure 5.12-1. Spacecraft Velocity During Retro Phase

$$V_{BO_x} = -54.9 \pm 3.3 \text{ fps}$$

$$V_{BO_y} = -125.0 \pm 2.7 \text{ fps}$$

$$V_{BO_z} = 446.3 \pm 4.5 \text{ fps}$$

This method will yield ΔV to an accuracy of ±5.0 fps. δi, the in-plane thrust misalignment angle (Figure 5.12-1b) between $\underline{V}_o$ and z, defined as positive when z is "above $\underline{V}_o$" as shown, is known to be within ±0.02 degree based on uncertainties in V_{BO_y}, which is primarily in-plane. δo, the out-of-plane angle between these two directions, is known to be within ±0.02 degree based on uncertainties in V_{BO_x}. δo is positive when z has a component out of the paper. This method yields ΔV at the start of RADVS-controlled descent of

$$\Delta V = 8399 \pm 5.0 \text{ fps}$$

also,

$$\delta i = -0.213 \pm 0.02 \text{ degree}$$

$$\delta o = -0.160 \pm 0.02 \text{ degree}$$

$$\text{total misalignment} = 0.266 \pm 0.03 \text{ degree}$$

Values of the other angles in degrees shown in Figure 5.12-1c are as follows:

$$\xi = 33.99$$

$$\zeta = 34.67$$

$$\varphi = 39.85$$

2) ΔV from doppler data — The thrust-induced velocity change of the spacecraft is determined from the spacecraft one-way doppler data by the DOPP program. These data are input into DOPP and are corrected for the transmitter's temperature-dependent frequency drift within the program. This correction is determined by comparing postflight doppler data prior to vernier ignition with a simulated determination of the expected doppler shift since, at this period in the flight, the actual doppler shift is well defined.

The ΔV during this phase is found by dividing the sum of the radial velocity change as determined from the doppler data and the gravity-induced velocity component in the same radial direction by the cosine of the angle between the tracking station-spacecraft line and the spacecraft thrust axis. A correction is made to the doppler data to account for the radial velocity change, ΔV_{ROT}, due to the earth's rotation. The thrust-induced velocity change, ΔV, can therefore be determined as follows:

$$\Delta V = \frac{\Delta V_{DOPP} + gt \cos \varphi + \Delta V_{ROT}}{\cos \xi}$$

where

ΔV_{DOPP} = velocity change seen by tracking station

φ = angle between tracking station-spacecraft line and lunar gravity direction

ξ = angle between tracking station-spacecraft line and thrust direction

Therefore,

$$\Delta V = \frac{6722 + 231.5 + 4.0}{\cos 33.99} = 8395 \text{ fps}$$

An uncertainty exists in the angle ξ of ±0.03 degree due to uncertainties in δi and δo, the thrust misalignment angles. An uncertainty also exists in the temperature-dependent doppler frequency drift of ±5 fps. The above uncertainties result in an uncertainty of ±8 fps in ΔV.

Comparison of ΔVs and Retro Performance Implications

It is interesting to note that not only do the absolute magnitudes of ΔV check surprisingly well, but, out of necessity, so does the inertial thrusting direction as computed from burnout conditions. The doppler data are inherently one-dimensional and, to be useful in computing the retro thrust ΔV, the angular information supplied by the vector addition method of computing ΔV must be accurate. Thus, due to the geometric relation of the earth vector and trajectory plane, an uncertainty of 0.1 degree in the in-plane angle (δi) would cause a 9.5-fps variation in the total ΔV as computed by doppler. Since the two ΔVs check to within 4 fps, this would give added confidence in the thrusting direction computed from the telemetered and corrected burnout conditions.

Assuming a nominally performing main retro and vernier system, the main retro phase ΔV should have been 8387.5 fps as compared to 8397 fps

actual (average of the two methods). Of the nominal 8387.5 fps total ΔV, a nominal performing vernier system would have contributed 290.9 fps. Based on a retro phase trajectory reconstruction by DOPP, the nominal vernier system would have contributed 292.0 fps due to the slight increase in actual time from vernier ignition to the beginning of RADVS control from that predicted.

The retro performance, based upon the ΔV which it took out, was very nearly nominal. The slight increase in actual total impulse over nominal ($\delta T_{imp}/T_{imp}$) is given by

$$\frac{\delta T_{imp}}{T_{imp}} = \frac{\delta \Delta V}{\Delta V \text{ retro}} \times 100 \text{ percent}$$

$$= \left(\frac{8397 - 292.0}{8387.5 - 290.9} - 1\right) \times 100 \text{ percent} = 0.10 \text{ percent increase}$$

The above percent increase in total impulse results in a retro specific impulse of 289.65 seconds as compared to the nominal predicted value of 289.35 seconds. The predicted and calculated specific impulses are both computed from a retro propellant weight which is corrected for buoyancy.

5.12.4.4 Main Retro Thrust Versus Time Curve

Two independent methods used to calculate the retro's thrust versus time curve are as follows:

1) Thrust/time from retro accelerometer data — Before being used to calculate a thrust curve, the raw accelerometer data are given the following three corrections:

   a) Biases are removed by comparing telemetered values with known values of acceleration which occur at times such as those prior to vernier ignition (zero g), after retro separation ($\approx$0.9 g), etc.

   b) A scale factor error is removed. This is done by integrating the unbiased accelerometer data over time and comparing the resulting integral with the retro phase ΔVs found by the other two methods of computing ΔV described above. The scale factor is then the integral divided by the mean of the other two ΔVs. The unbiased acceleration divided by this scale factor is then assumed free of bias and scale factor errors.

   c) A hysteresis error is removed by actually determining two biases: one for the rising part of the acceleration curve, and the other for the falling part.

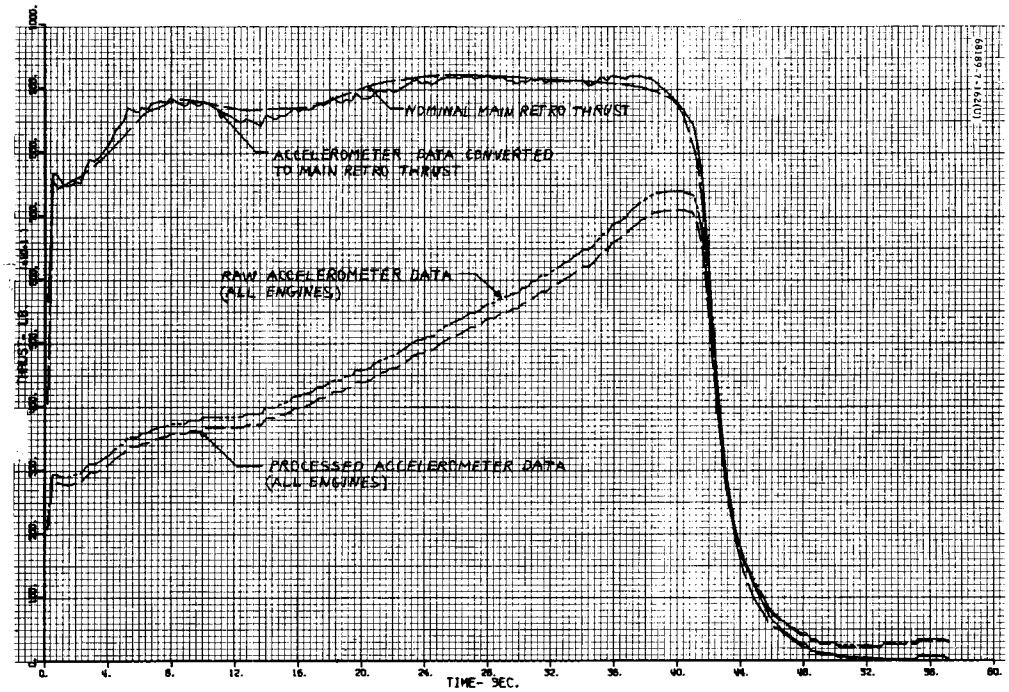

Figure 5.12-2. Retro Phase Thrust and Acceleration Versus Time (From retro phase data)

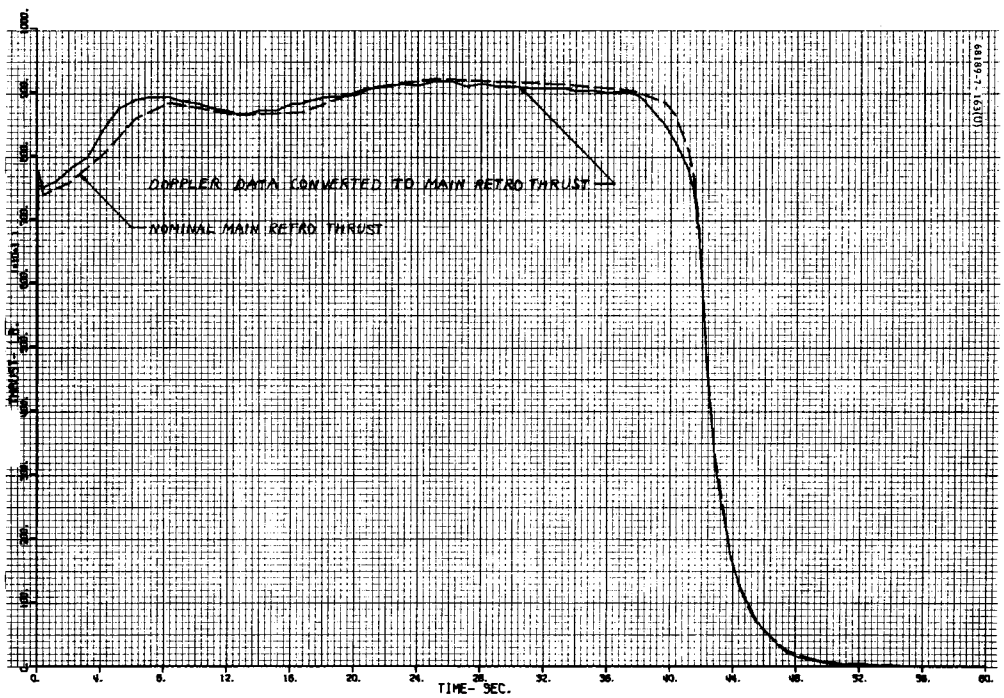

Figure 5.12-3. Main Retro Thrust Versus Time (Doppler data)

The bias on each part of the curve can be removed to an accuracy of 0.1 g_e, and the accuracy of the scale factor is 0.1 percent.

The corrected acceleration a(t) is then used in the equation

$$T(t) = \frac{a(t)}{g_e} \left[W_o - \int_o^t \frac{T(t)}{I_{sp}} \, dt \right]$$

which is integrated numerically to obtain total thrust (W_o is weight at retro ignition). Vernier thrust is then subtracted to obtain the retro thrust.

I_{sp} for this calculation is found from the following relationship where W_L is the weight lost from retro ignition to burnout.

$$I_{sp} = \frac{\Delta V}{g_e \, \ell_n \frac{W_o}{W_o - W_L}}$$

Figure 5.12-2 shows the Surveyor VII thrust-time curve as determined from accelerometer data. Also shown is the predicted thrust-time curve along with the raw accelerometer data and the corrected accelerometer data.

2) Thrust/time from doppler data – Figure 5.12-3 shows the main retro thrust curve as constructed from doppler counts received at Goldstone. Also shown is the predicted thrust-time curve.

To construct the curve, a retro phase simulation trajectory program, using a nominal thrust curve, calculates nominal radial velocities relative to the tracking station and converts these to doppler counts that the station would receive from a stable spacecraft transmitter on a nominal trajectory.

The nominal thrust curve is then perturbed until the doppler data from the perturbed curve are arbitrarily close to the doppler data actually received. For each point considered on the thrust curve, a difference between actual and perturbed counts over a 1-second interval of two counts (i.e., about 0.4 fps) is considered close enough. In addition, the sum of such differences is constrained to be within 10 counts (2.2 fps).

Radial velocity divided by the cosine of the angle between the tracking station and the thrust direction (33.99 ± 0.03 degrees) gives total velocity. When gt cos φ is added, the remaining

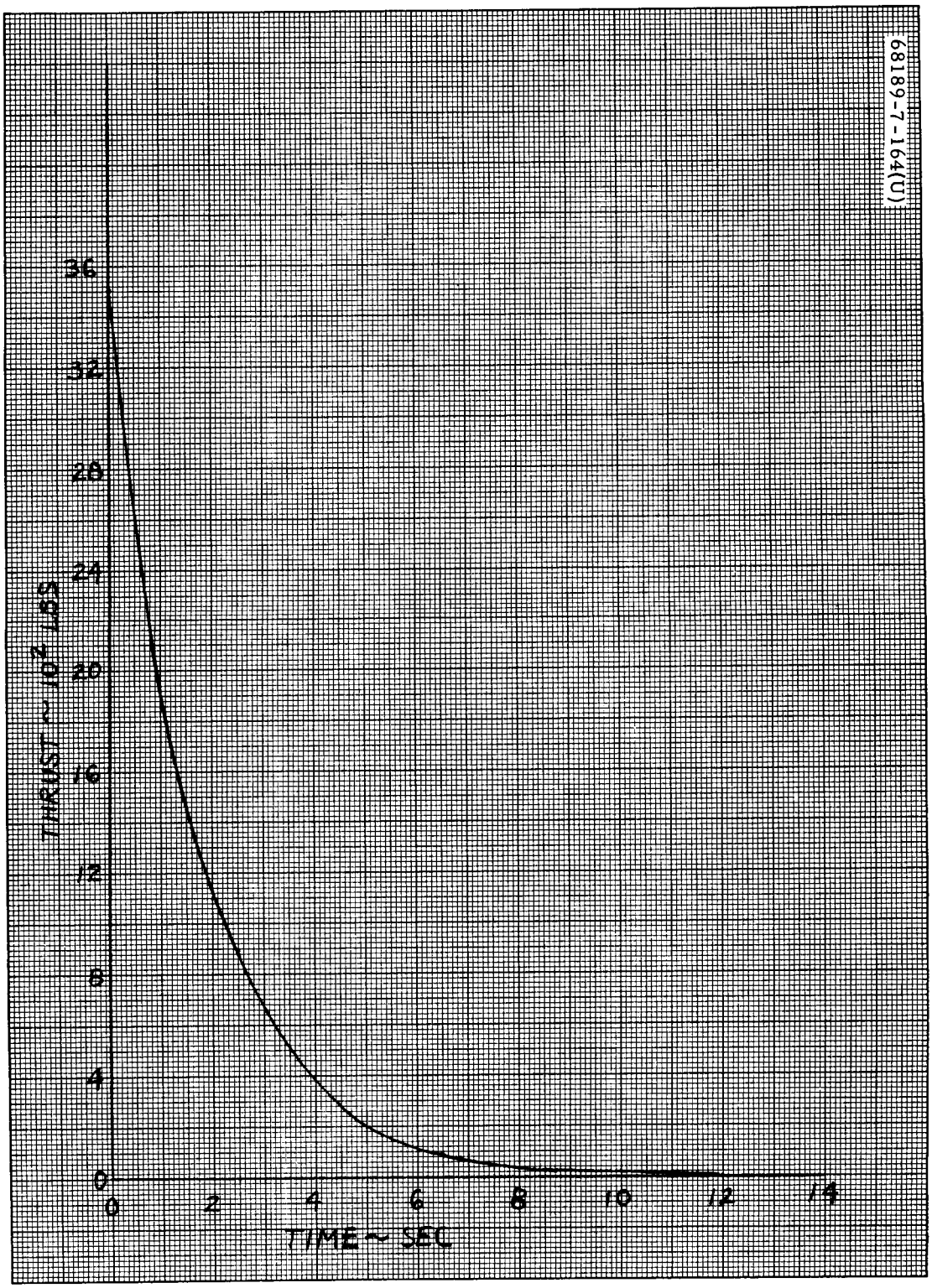

Figure 5.12-4. Main Retro Thrust Tailoff Versus Time (Doppler data)

velocity differences are entirely due to thrusting and give the thrust acceleration. Multiplication by the mass then gives the thrust level.

Comparison of Two Methods for Retro Thrust/Time Curve

Both the doppler and accelerometer reconstructed curves agree well with the predicted curve, with both deviating from the predicted by generally less than 300 pounds. The accelerometer reconstructed curve appears rough because of accelerometer stiction.

The accelerometer thrust-time curve reconstruction indicates a slightly longer burn time than does the doppler reconstruction (43.11 seconds from retro ignition to the 3.5 g_e level for the accelerometer as compared to 42.98 for the doppler). This longer burn time, as indicated by the accelerometer data, is the result of accelerometer stiction and the time lag in the telemetry system with respect to the actual 3.5 g_e point. The accelerometer stiction error is also the probable reason for the slight increase in the retro thrust level just prior to the tailoff region (Figure 5.12-2). The distinction is made here for the remainder of this section in that the 2.5 g level or point is the actual acceleration magnitude, whereas the 2.5 g mark is the telemetry discrete. The telemetry 3.5 g mark is approximately 0.2 second after the actual 3.5 g level.

Main Retro Tailoff from Doppler Data

Figure 5.12-4 shows an enlargement of the thrust tailoff region of Figure 5.12-3 (doppler reconstruction of main retro thrust). The data used in this reconstruction were first corrected for a constant temperature-dependent frequency drift which can be determined accurately by comparing preignition flight data to preignition simulated data. Since the data also contained a small random noise, it was then smoothed by fitting a second order curve through the data points since this tailoff shape has been determined from test results. If high frequency thrust oscillations were present during retro tailoff, the doppler data would not show it since these data are available only at 1-second intervals. However, the chance of such oscillations being present is small since all previous retro pressure test data have generally shown a smooth tailoff.

Assuming a normal noise distribution, the 1σ deviation (68 percent) of the data from this fitted curve was computed to be 2.3 doppler counts, which corresponds to a retro thrust deviation at any point of 17 pounds. However, the total integrated thrust after the 200-pound point has been reached is in error by 6 percent or less due to noise uncertainties which yield an average thrust error over the total length of the curve past the 200-pound point of less than 3 pounds.

5.12.4.5 6DOF Simulation of Doppler Data

The 6DOF determination of radial velocity relative to the moon (velocity component along the earth tracking to spacecraft vector), as compared to the doppler data reconstruction of this velocity, is shown in Figure 5.12-5 and 5.12-6 for the retro and vernier phases. As can be seen in the figures, excellent matches are obtained for both phases of the descent. This close correlation increases the confidence in the 6DOF reconstruction.

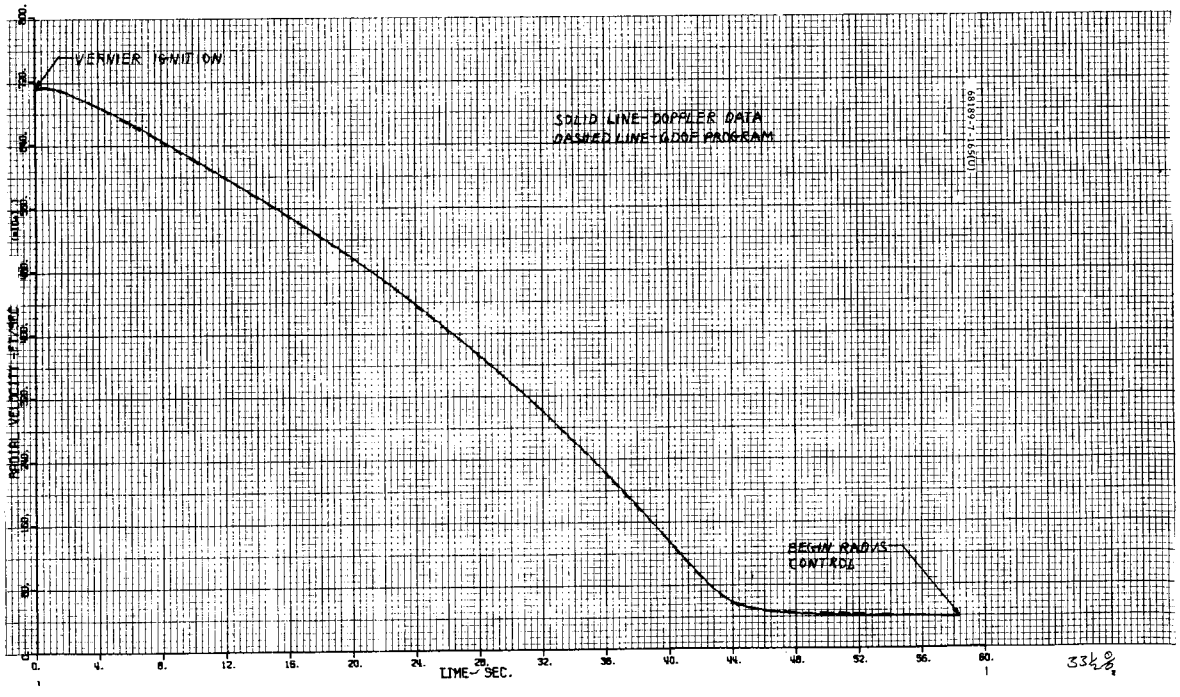

Figure 5.12-5. Radial Velocity-Retro Phase Doppler Data and 6DOF Reconstruction

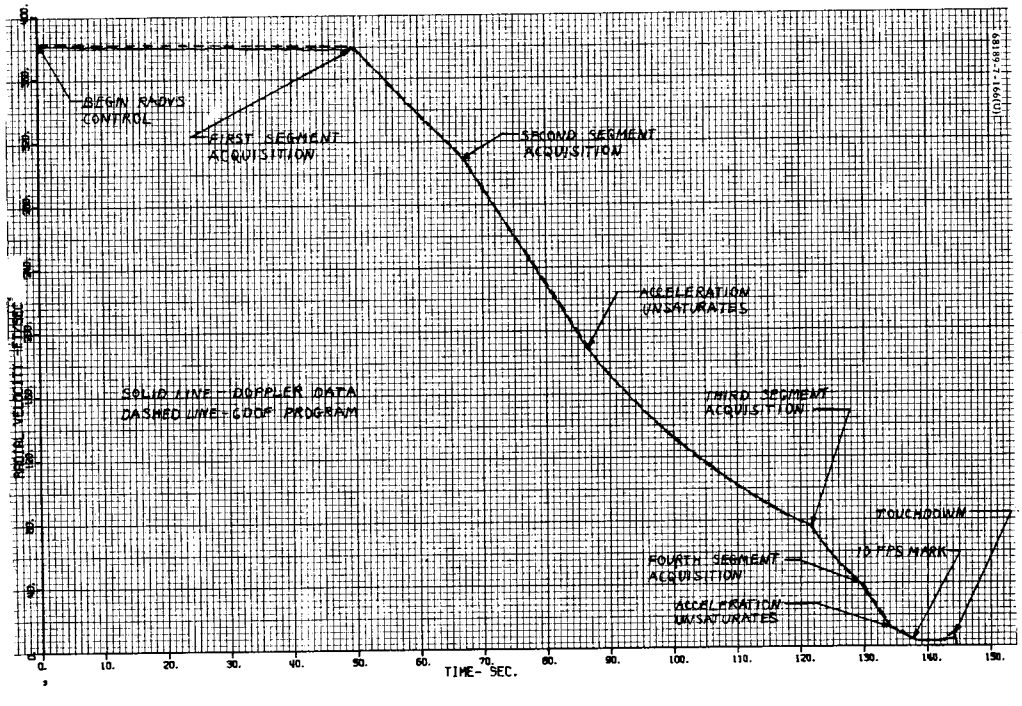

Figure 5.12-6. Radial Velocity-Vernier Phase Doppler Data and 6DOF Reconstruction

5. 12. 4. 6 Vernier Propellant Consumption

Table 5. 12-4 presents a tabulation of the propellant consumption from the individual engines based on vernier engine flight acceptance test data of both specific impulse and mixture ratio as a function of engine thrust.

For the midcourse and retro phases, the propellant consumption was obtained from the TD1 program. This program models all three engine flight acceptance performance characteristics individually. For the vernier phase portion, the propellant consumption was determined from the best-estimate 6DOF program reconstruction. However, the 6DOF program assumes that all three engines have the same specific impulse and mixture ratio performance. The input of the engine performance characteristics to the 6DOF program was the average performance of the three Surveyor VII vernier engine flight acceptance test data.

TABLE 5. 12-4. VERNIER PROPELLANT CONSUMPTION (POUNDS)

Phase	Engine 1	Engine 2	Engine 3	Total	Preterminal Mission Predictions
Midcourse	3. 19	3. 21	3. 18	9. 58	9. 58
Main retro	14. 45	14. 55	13. 71	42. 71	42. 61
Vernier phase	33. 23	33. 67	33. 70	100. 60	97. 22
Total used	50. 87	51. 43	50. 59	152. 89	149. 41
Total loaded	61. 28	61. 28	61. 28	183. 84	183. 84
Trapped (lines and expulsion efficiency)	0. 71	0. 71	0. 71	2. 13	2. 13
Usable loaded (total minus trapped)	60. 57	60. 57	60. 57	181. 71	181. 71
Remaining propellant in tanks (usable and unusable)	9. 70	9. 14	9. 98	28. 82	32. 30

The propellant consumption for the midcourse maneuver was based on postflight determination of burn time and preflight data of engine thrust for the midcourse maneuver.

The main retro phase propellant consumption computations are inherently the most inaccurate because of the open-loop nature of the thrust commands. At midcourse, the change in spacecraft velocity is a very accurate measure of engine impulse; during the retro phase, the main retro engine overshadows any expected variation in vernier performance.

In determining the vernier engine propellant consumption, preflight test computations of 192. 1 pounds of total vernier engine thrust commanded during the midthrust phase (retro burn) and 271. 2 pounds during the high thrust phase (retro separation) were assumed. Also, the preflight determination of minimum and maximum thrust acceleration commands of 4. 77 and 12. 54 ft/sec^2 were assumed. Justification for these assumptions is given in the following discussion.

The premission computations of total vernier engine thrust during retro burn is 192. 1 pounds, and for the high thrust phase, 271. 2 pounds. The 6DOF program assumed these levels as can be noted from the sum of the three engine commands (Figure 5. 12-7); however, the sum of the telemetered commands is approximately 197. 2 pounds during the low thrust phase, a 5. 1-pound difference between 6DOF and telemetry. Also, during the high thrust phase (retro separation), there is a difference between premission thrust level computations and telemetry data of 8. 1 pounds. The vernier engine midthrust level can be determined from telemetry data by observing the data prior to vernier ignition and after spacecraft touchdown. The individual engine telemetry thrust commands at these points were approximately 64. 4, 66. 8, and 66. 2 pounds for engine 1, 2, and 3, respectively. This results in a total of 197. 4 pounds, which compares with the telemetry total thrust level during the retro burn phase. However, the individual thrust levels imply a probable bias error in the telemetry data for engines 2 and 3. Accounting for these bias errors resulted in levels comparable to the premission computations.

The telemetry data indicate the same minimum acceleration as the 6DOF; however, the maximum acceleration is indicated in Figure 5. 12-7 to be higher through observation of the telemetry commands between 125 to 145 seconds. These telemetry thrust commands are equivalent to an acceleration command of 13. 08 ft/sec^2. This value is doubtful since it is considerably larger than the preflight test value of 12. 54 which is considered a reliable number.

The 6DOF reconstruction matches the telemetry data with respect to time and velocity by the following close agreements: 1) time duration during the minimum acceleration phase, 2) time duration along each command descent segment as indicated by the increase in thrust commands for both 6DOF and telemetry at 107, 124, 179, 187, and 196 seconds (Figure 5. 12-7), 3) identical matches in V_x, V_y, and V_z as shown in Figure 5. 12-9, and

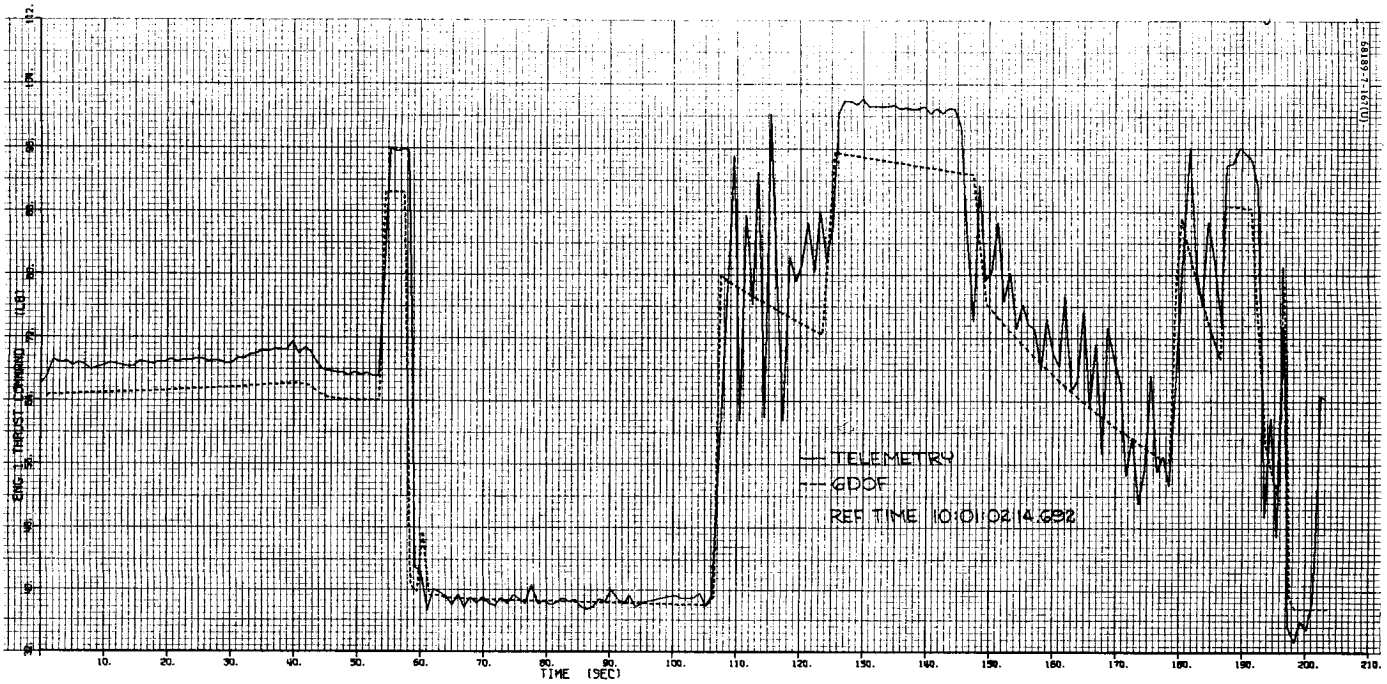

a) Engine 1

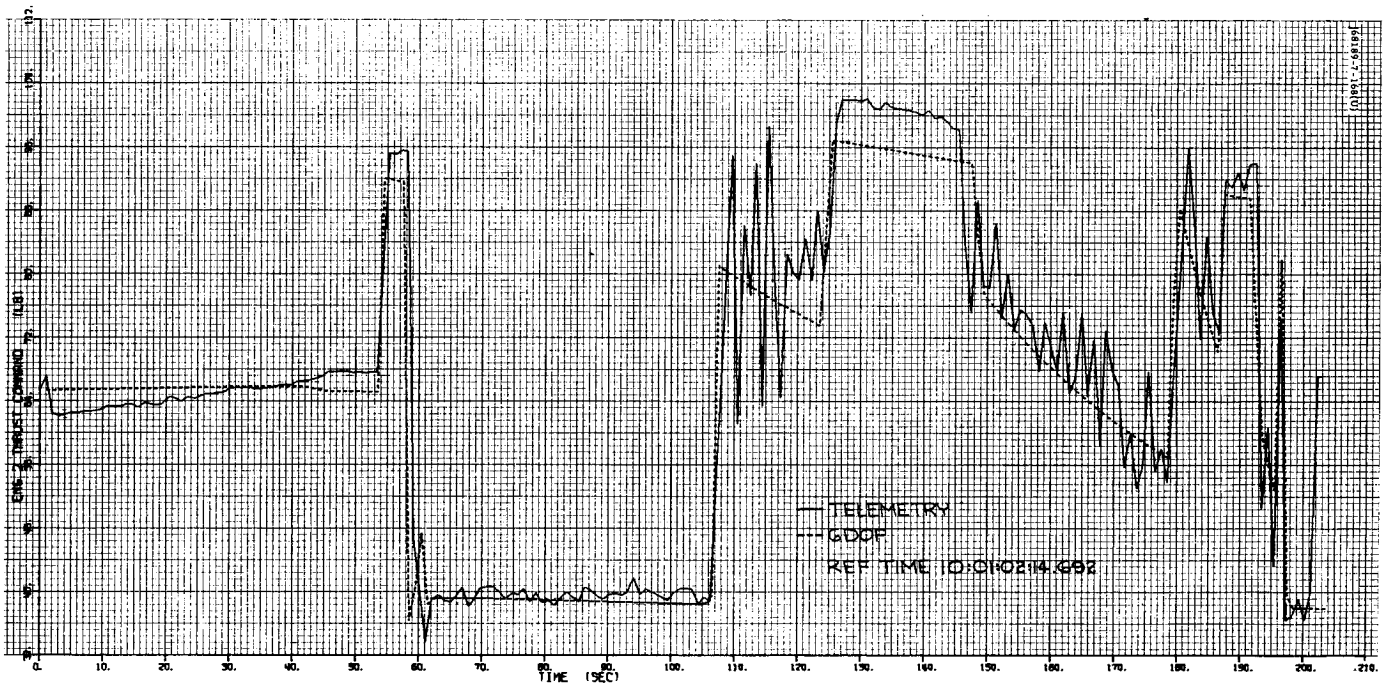

b) Engine 2

Figure 5.12-7. Vernier Engine Thrust Commands

4) an identical match in radial velocity between doppler data and 6DOF reconstructions as shown on Figure 5. 12-6. Since this is the case, the thrust commands of the 6DOF program, after the start of the RADVS-controlled descent phase, are probably more realistic than the telemetry data because the ΔV removed is a function of the total thrust over a given time.

With the above observations, the telemetry data of engine thrust commands have a probable bias and scale factor error different than that determined by preflight calibration.

5. 12. 4. 7 Spacecraft Landing Location and Touchdown Attitude

The original targeted landing site for Surveyor VII was 40. 87°S latitude and 11. 37° W longitude. The computed midcourse maneuver to enable the spacecraft to land at the desired landing site was 11. 08 m/sec. Based on orbit determination postflight analysis data, the computed landing site was determined to be 41. 059°S latitude and 11. 451° W longitude. This results in a miss of 6. 0 km from the original targeted landing site. However, a review of the Lunar Orbiter and Surveyor VII photographs of the touchdown area revealed the probable landing site to be 40. 89°S latitude and 11. 44° W longitude. From this determination, a miss of 1. 69 km is indicated.

The spacecraft roll orientation at touchdown, as determined by the best-fit 6DOF reconstruction was 20. 65 degrees from selenographic east to the spacecraft positive X axis in an east to north rotation. This orientation is within the attitude determination of 20. 23 ± 0. 62 degrees as described in subsection 4. 1. 8.

5. 12. 4. 8. Trajectory Reconstruction

This subsection discusses the reconstruction of the vernier phase of the terminal descent trajectory from the 6DOF program to provide a best estimate of the actual trajectory parameters. The DOPP program reconstruction of the retro thrust-time curve was input into the 6DOF program. The DOPP reconstructed retro burn time (from retro ignition to the 3. 5-g_e point) was 42. 98 ± 0. 08 seconds, which is in agreement with telemetry data (see Table 5. 12-1). The nominal Surveyor VII subsystem parameters from preflight assessment were input to the 6DOF program. Initial conditions at vernier ignition of velocity, altitude, and retro thrust vector misalignment, as determined from orbit determination postflight data, were perturbed until the conditions of velocity at retro case eject coincided with the calibrated telemetry data values indicated in paragraph 5. 12. 4. 1. Further perturbations had to be made to the ignition altitude to arrive at the telemetry indicated time for descent segment intercept. With these conditions matched, the 6DOF reconstruction from vernier ignition to segment acquisition agreed very well with postflight analysis of the telemetry data. Also, the telemetry discretes of the 1000-foot mark, the 10-fps mark, and the 14-foot mark resulted in perturbing the nominal values within the 6DOF program. The final reconstruction by the 6DOF program compared favorably with telemetry data, as

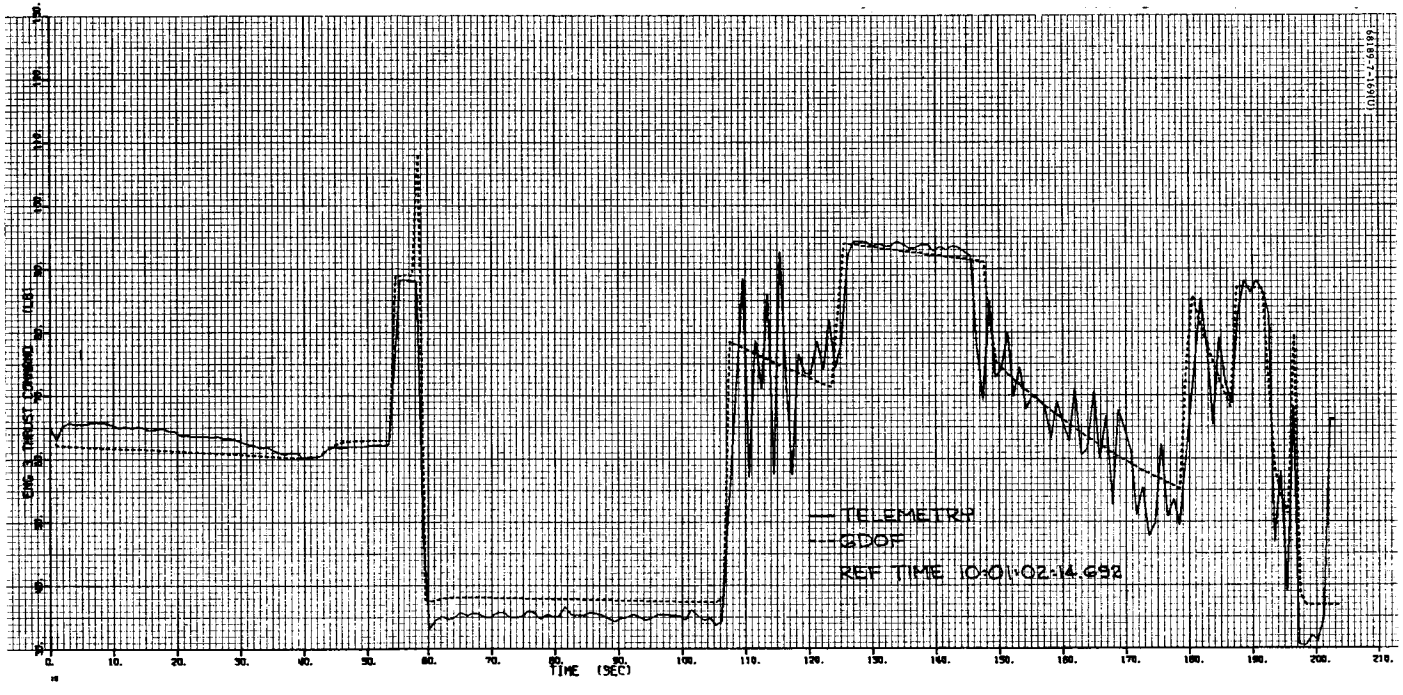

c) Engine 3

Figure 5.12-7 (continued). Vernier Engine Thrust Commands

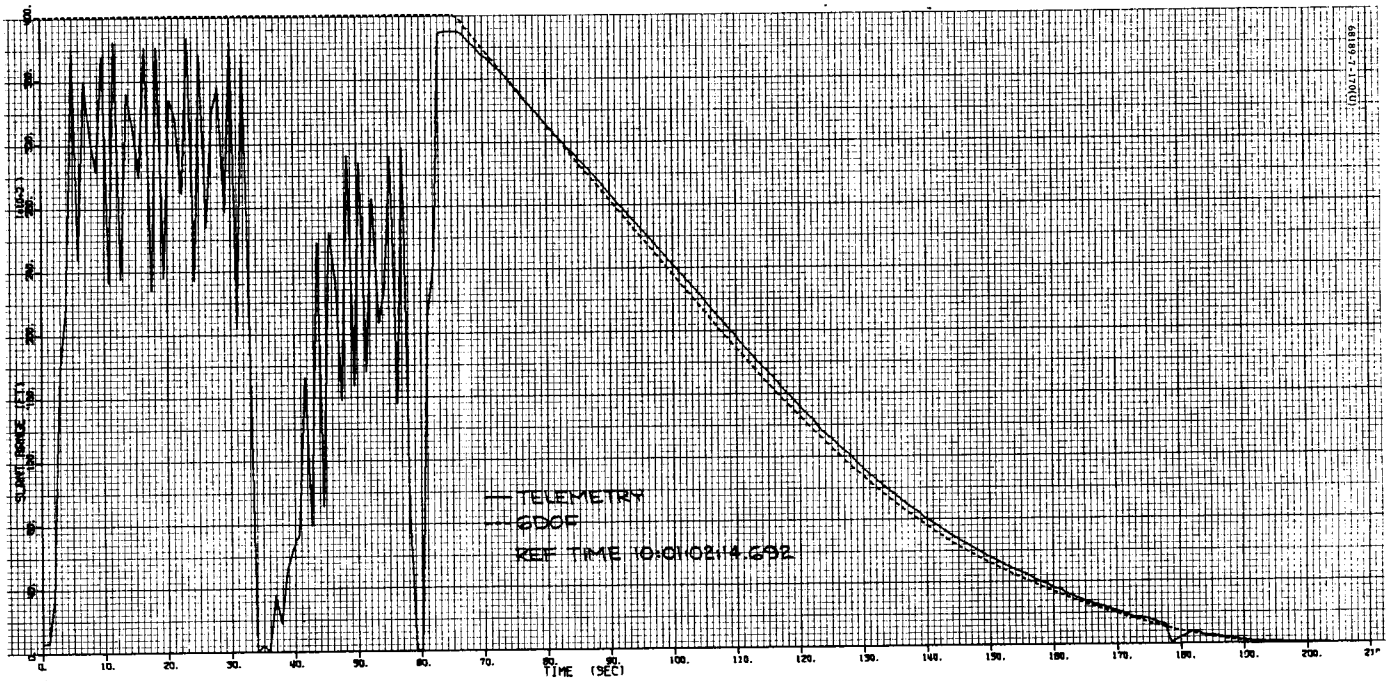

a) 6DOF Actual and Telemetry

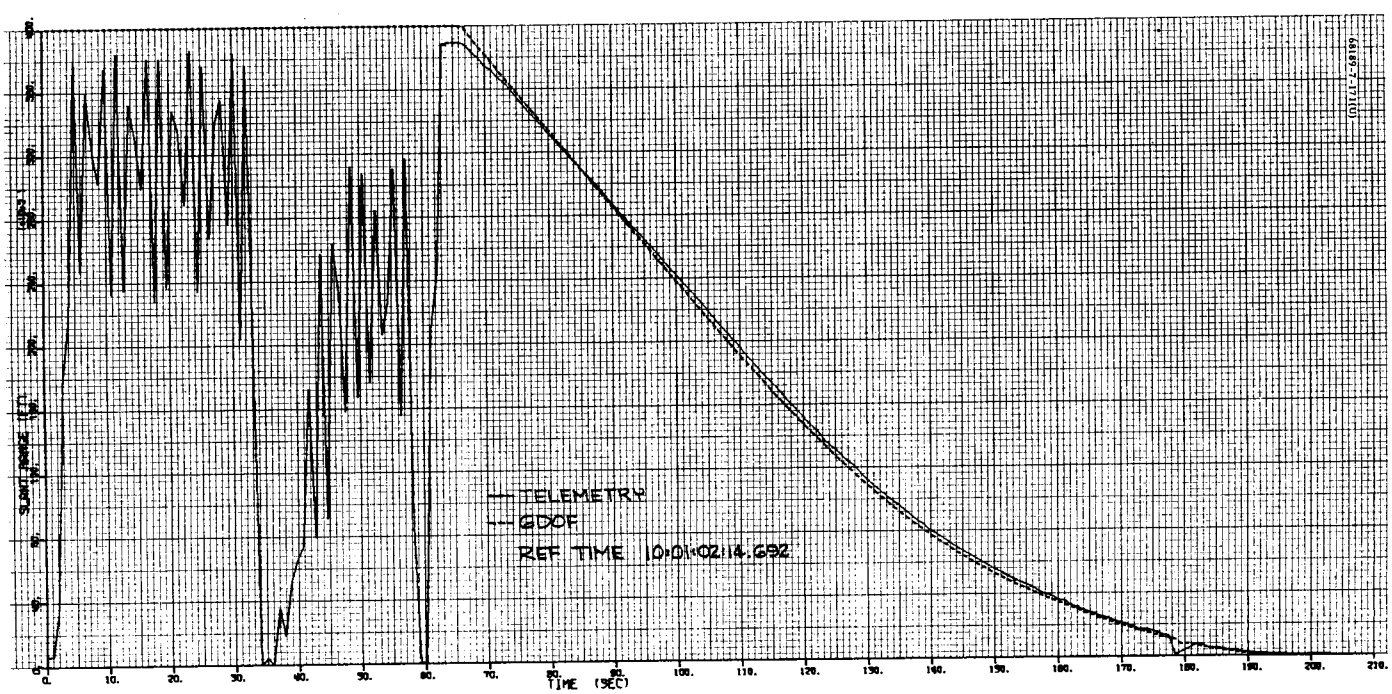

b) 6DOF Simulated Slant Range Telemetry Circuit and Telemetry

Figure 5.12-8. Slant Range

indicated by Table 5. 12-3, and the close correlation between significant subsystem parameters, as indicated by the POSTPR machine plots in Figures 5. 12-7 through 5. 12-14.

POSTPR Program Plots

Figures 5. 12-7 through 5. 12-14 are plots of important parameters for trajectory reconstruction. The processed telemetry data from PREPRO (solid lines) and the best-fit 6DOF trajectory (dashed lines) are superimposed on the plots. The time scale starts at 0. 0 second, which corresponds to vernier ignition (010:01:02:14. 692 GMT). The spacecraft touchdown at 010:01:05:37. 744 GMT corresponds to 203. 1 seconds on the time scale. After 203. 1 seconds, the magnitude changes on the PREPRO curves are the direct result of spacecraft touchdown. The PREPRO curves are plots of interpolated telemetry data in equal time intervals of 1 second designed to coincide with the 6DOF intervals. Therefore, part of the transients within the telemetry data will not be plotted on the PREPRO curves.

Table 5. 12-3 lists the time occurrences of pertinent events as reconstructed by the 6DOF program. The PREPRO curves are referenced to the actual GMT as listed in the table.

Figure 5. 12-8a shows the 6DOF true slant range and the telemetered slant range as a function of time. Figure 5. 12-8b shows the 6DOF simulated slant range as output from the telemetry conditioning circuit along with the actual telemetry data. Comparison of the two 6DOF curves shows an error between the actual slant range and the simulated telemetry circuit output of slant range within the 6DOF program. This error is due to the lag within the telemetry conditioning circuit. The oscillations in the PREPRO curves between 2 and 60 seconds are due to the radar tracker sweeping. At approximately 62. 9 seconds, RORA occurred, resulting in reliable slant range data from this point to touchdown.

Figures 5. 12-9a and 5. 12-9b show an almost identical V_x and V_y reconstruction between the 6DOF and telemetry data. As indicated in Table 5. 12-3, start of RADVS-controlled descent occurred at 58. 4 seconds. It took approximately 7 seconds to steer out the V_y component of velocity developed by the retro burn phase. The V_x component at the start of RADVS-controlled descent (58. 4 seconds on the time scale) is -300 fps (telemetry saturation limit). This situation is a result of the radar beam 1 loss of lock. The true spacecraft V_x component at this time is approximately -56. 7 fps. By the time the beam reacquired lock (at 60. 1 seconds), the true V_x component had been changed by the erroneous steering to approximately 20 fps. At this point, it took approximately 4 seconds to steer out the V_x component of velocity. Approximately 2 seconds after vernier ignition, the RADVS is turned on, resulting in the spikes in the V_x and V_y plots.

Figure 5. 12-9c is a plot of the actual V_z component of velocity as reconstructed by the 6DOF program, whereas Figure 5. 12-9d is a plot of the 6DOF simulation of the telemetry conditioning circuit for V_z. Both Figures 5. 12-9c and 5. 12-9d indicate an almost identical match with the telemetry

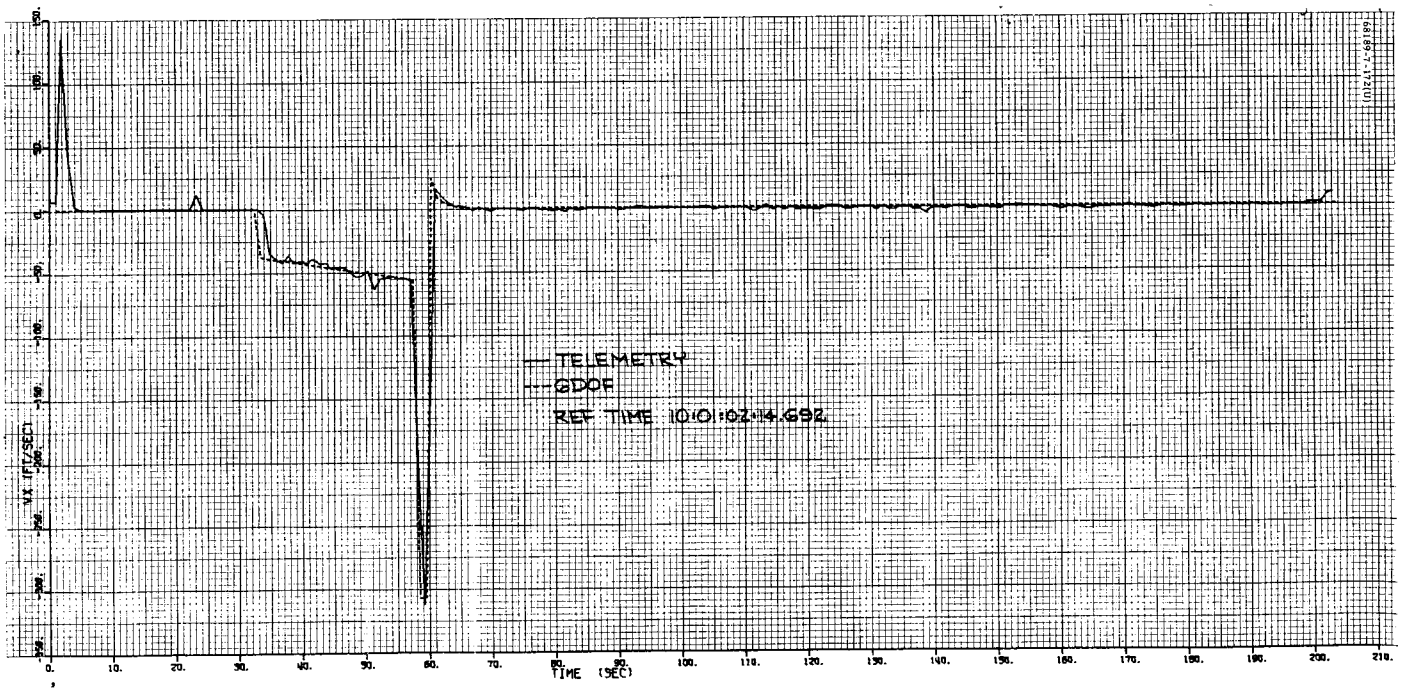

a) X Axis

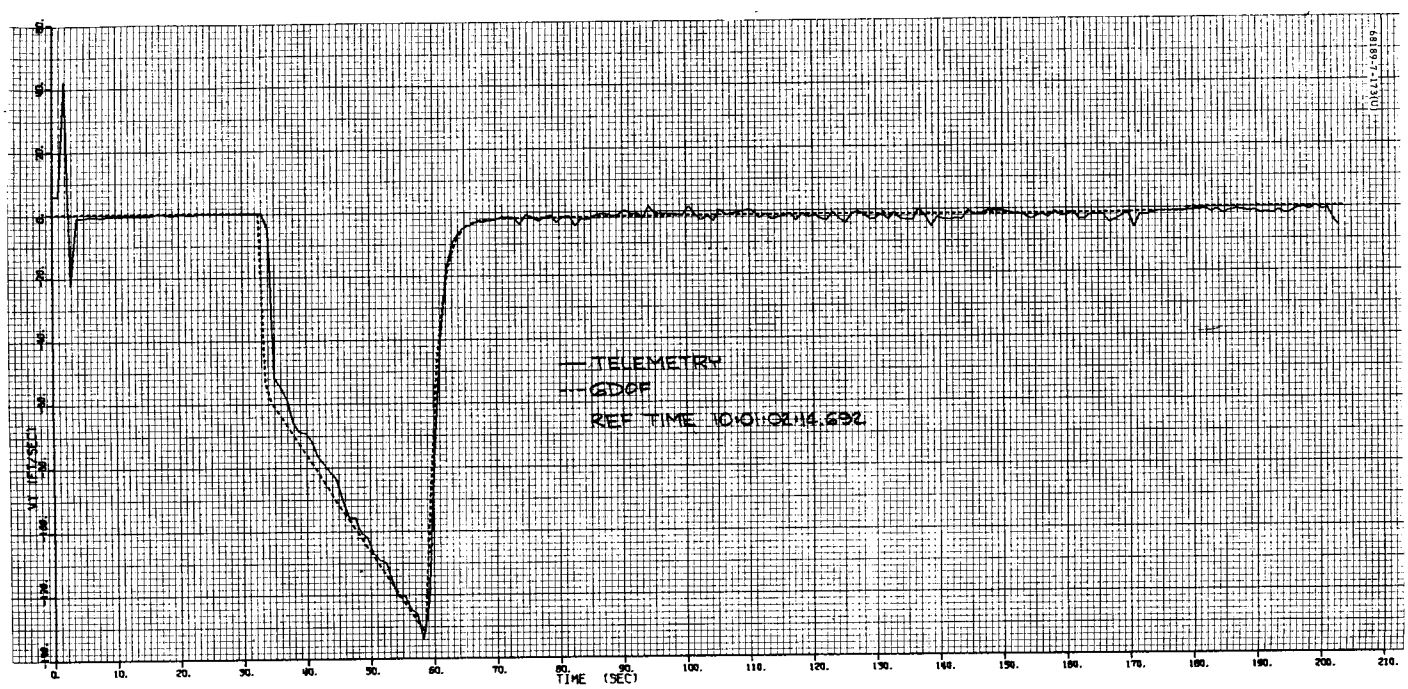

b) Y Axis

Figure 5.12-9. Spacecraft Velocity

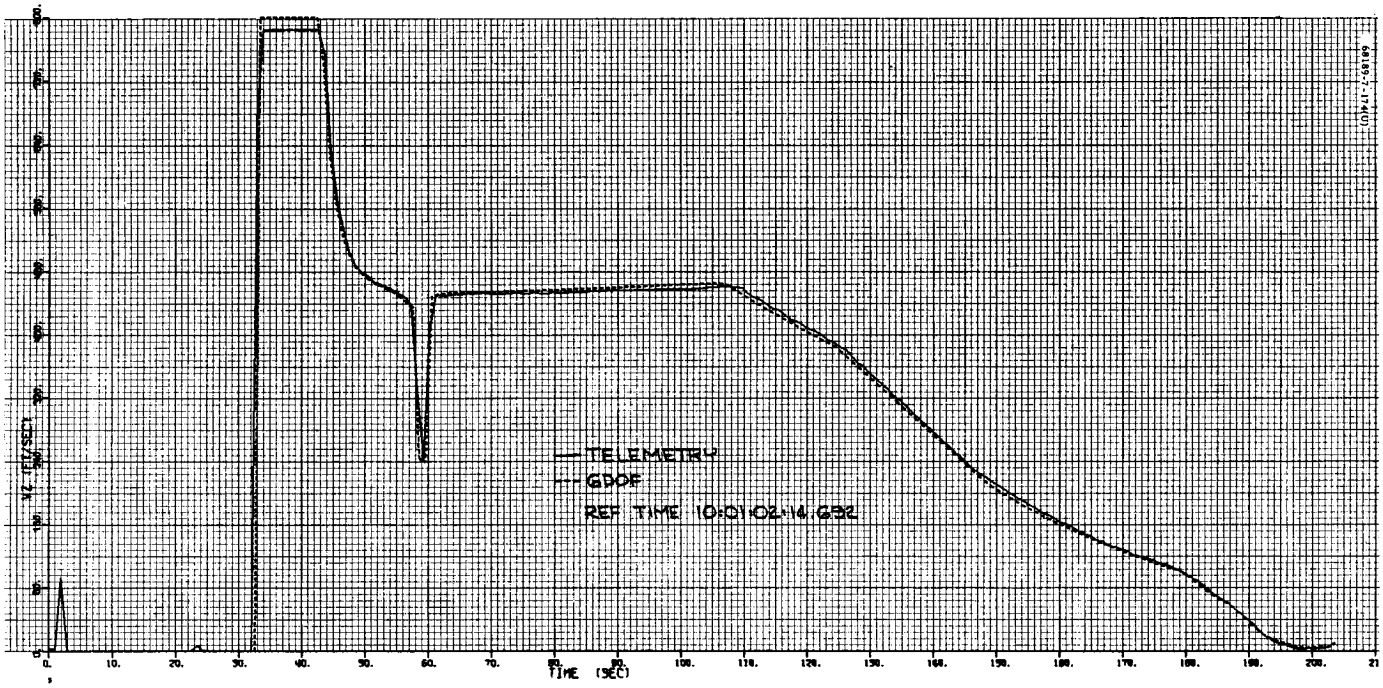

c) Z Axis (Actual 6DOF)

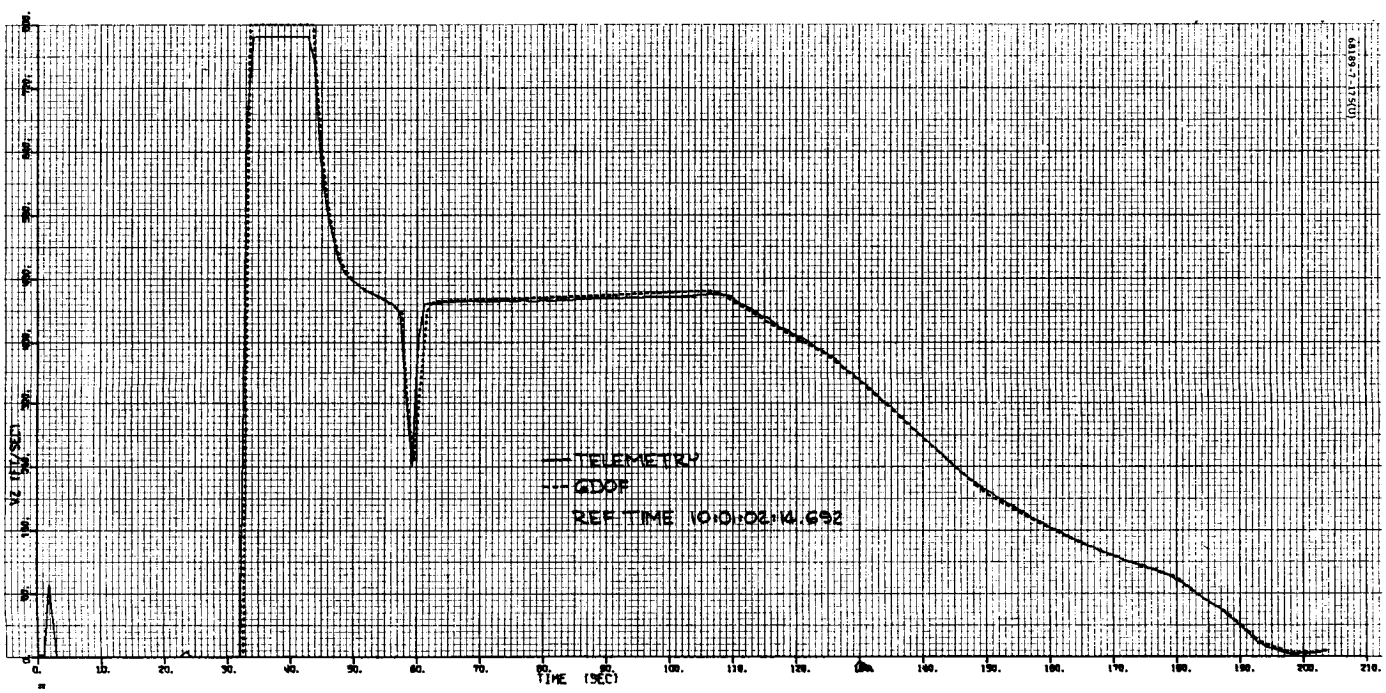

d) Z Axis (Simulated 6DOF V_z Telemetry Circuit)

Figure 5.12-9 (continued). Spacecraft Velocity

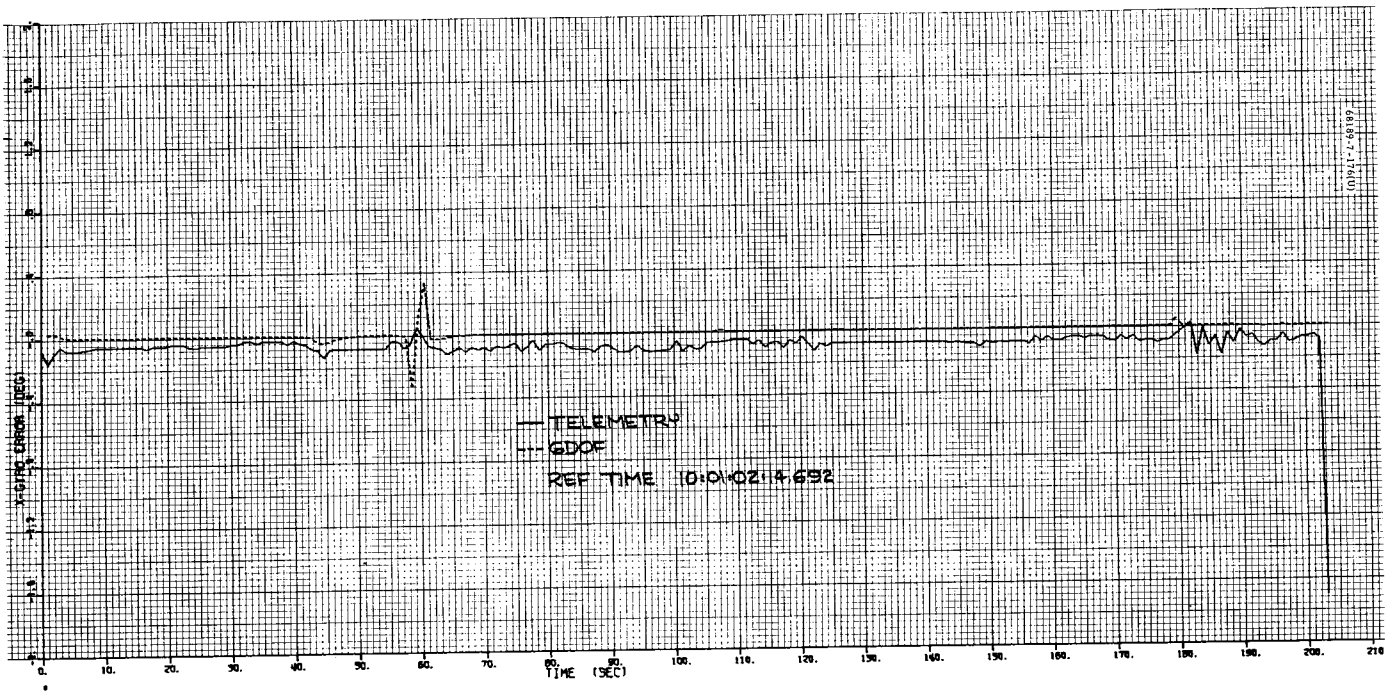

a) X Gyro

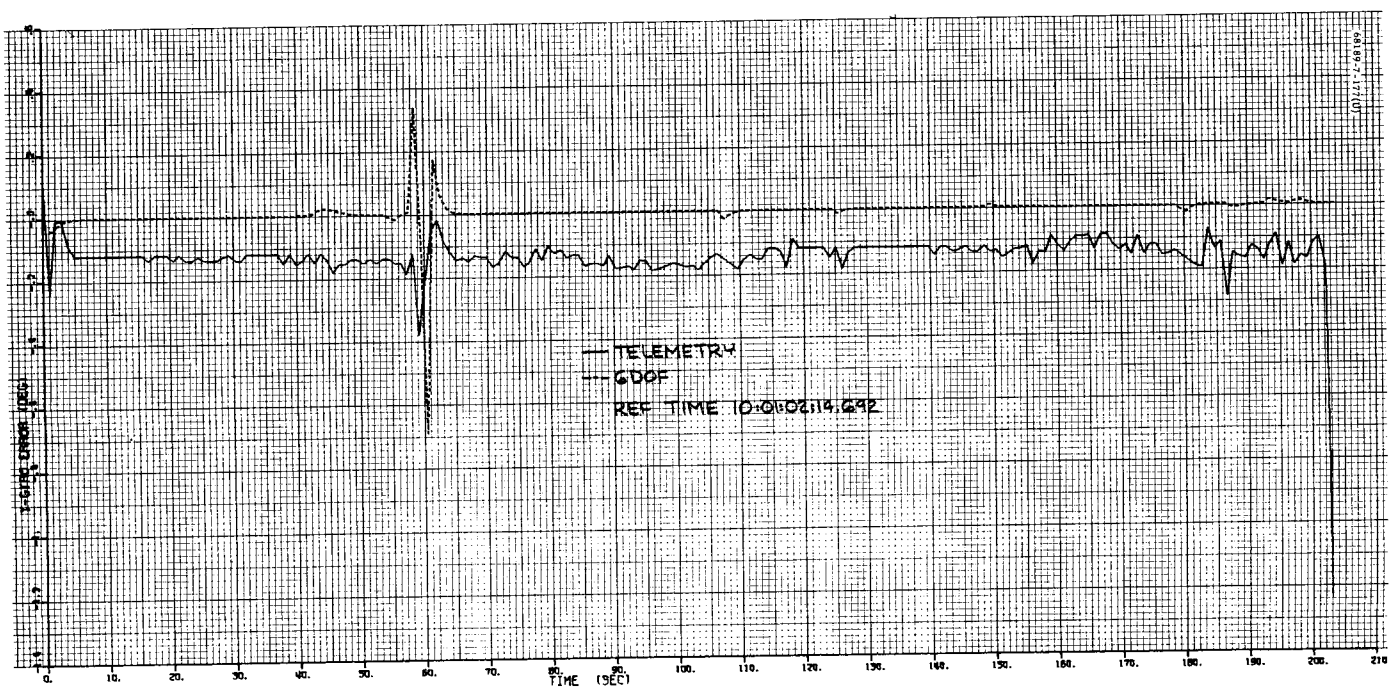

b) Y Gyro

Figure 5.12-10. Gyro Error Signal

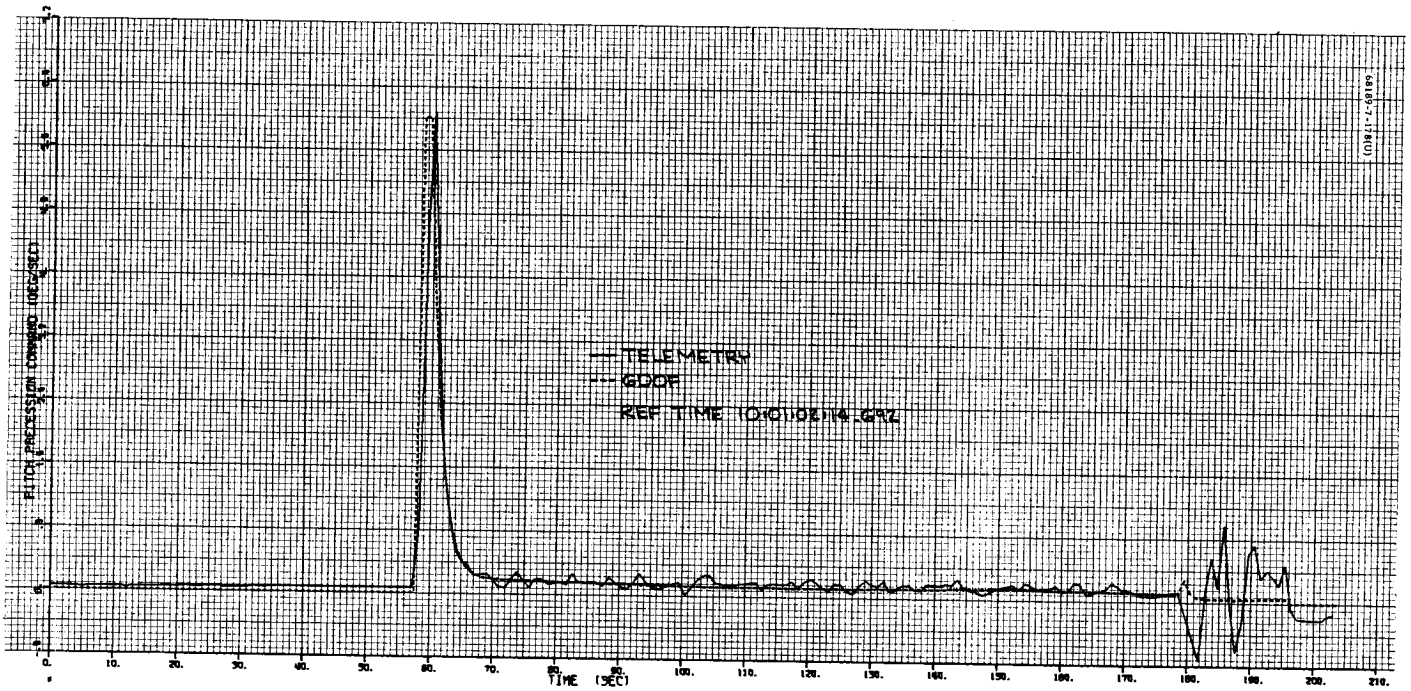

a) Pitch

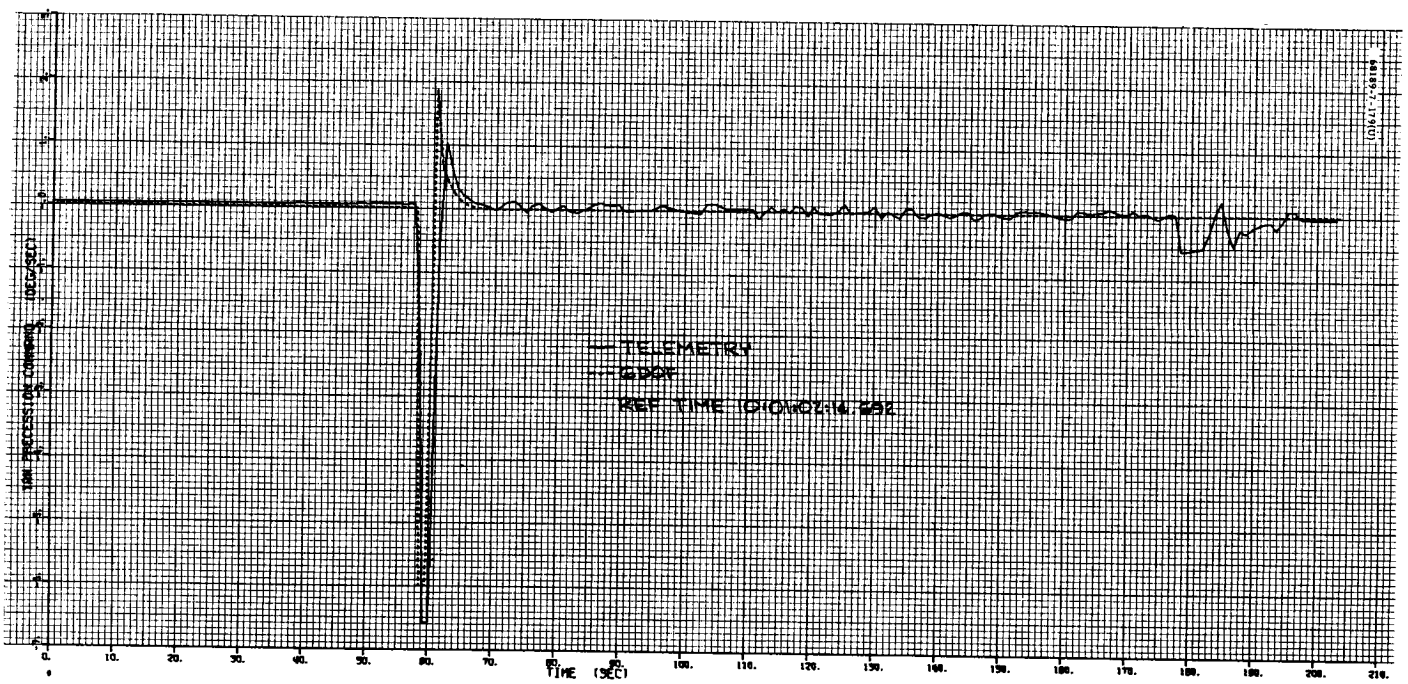

b) Yaw

Figure 5.12-11. Spacecraft Precession Commands

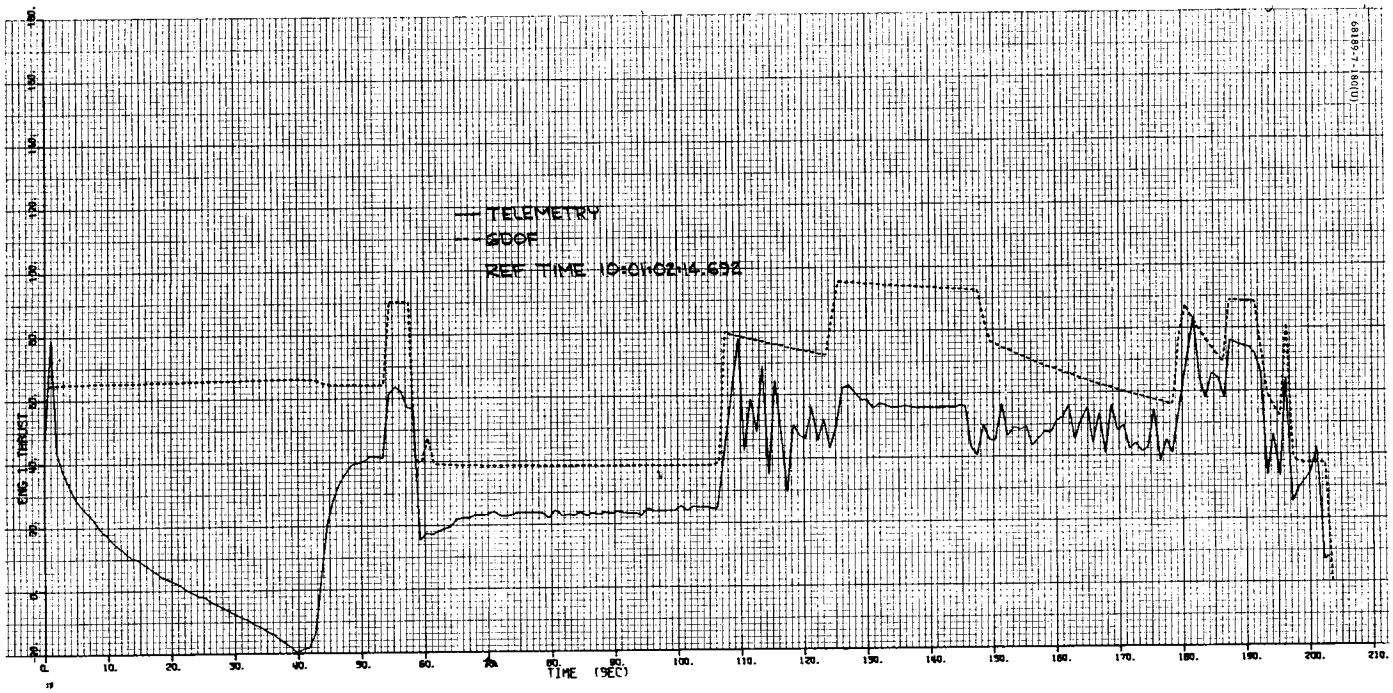

a) Engine 1

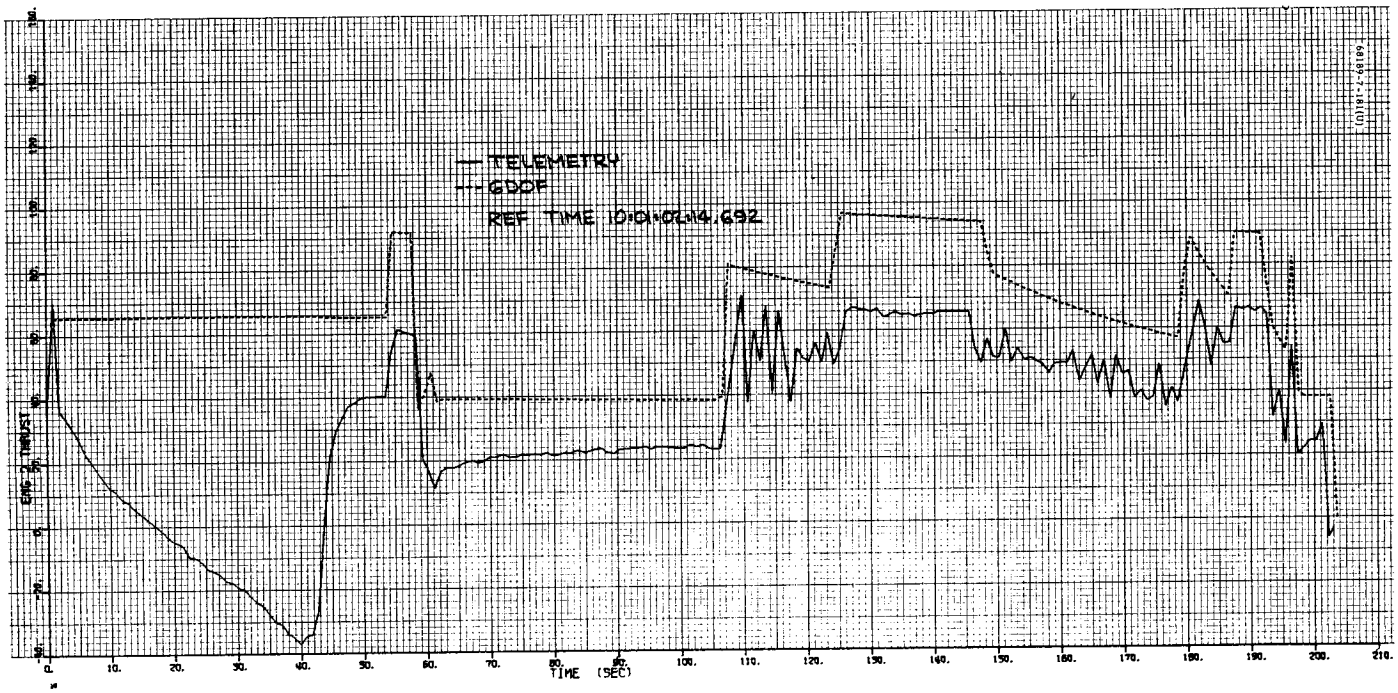

b) Engine 2

Figure 5.12-12. Telemetry Engine Strain Gage and 6DOF Engine Thrust Level Versus Time

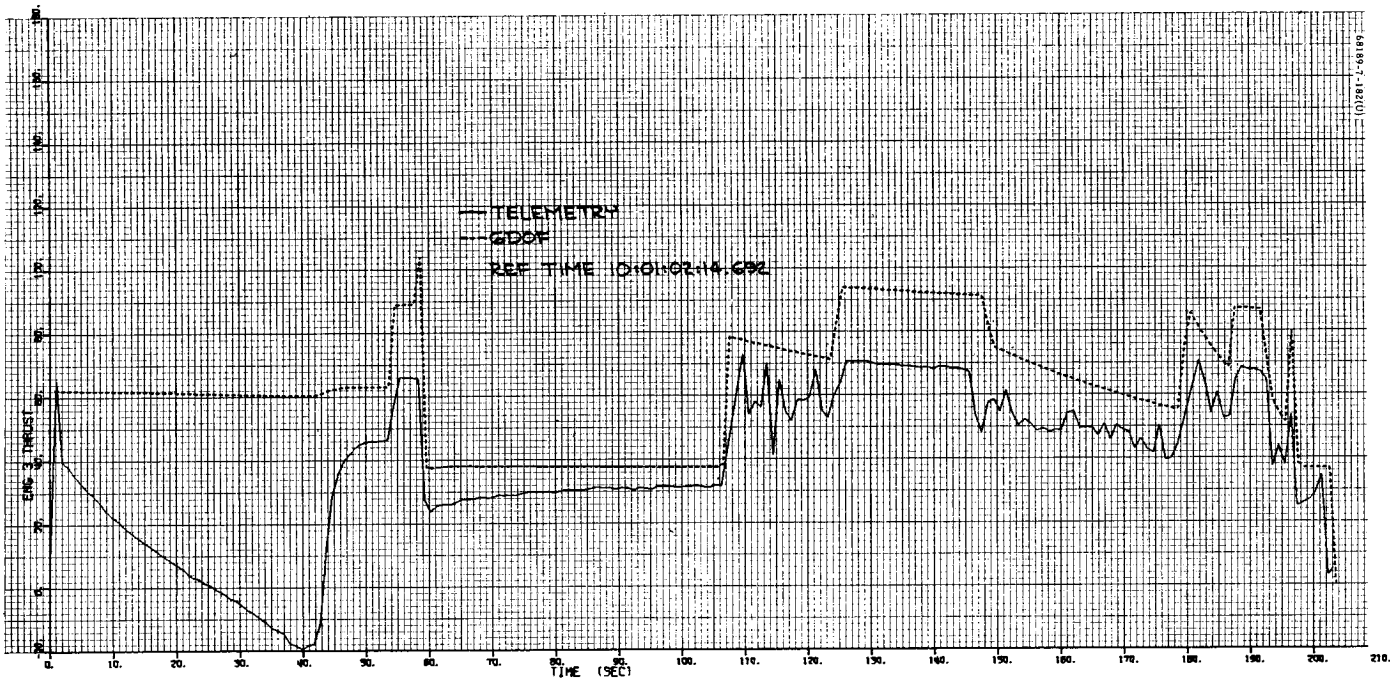

c) Engine 3

Figure 5.12-12 (continued). Telemetry Engine Strain Gage and 6DOF Engine Thrust Level Versus Time

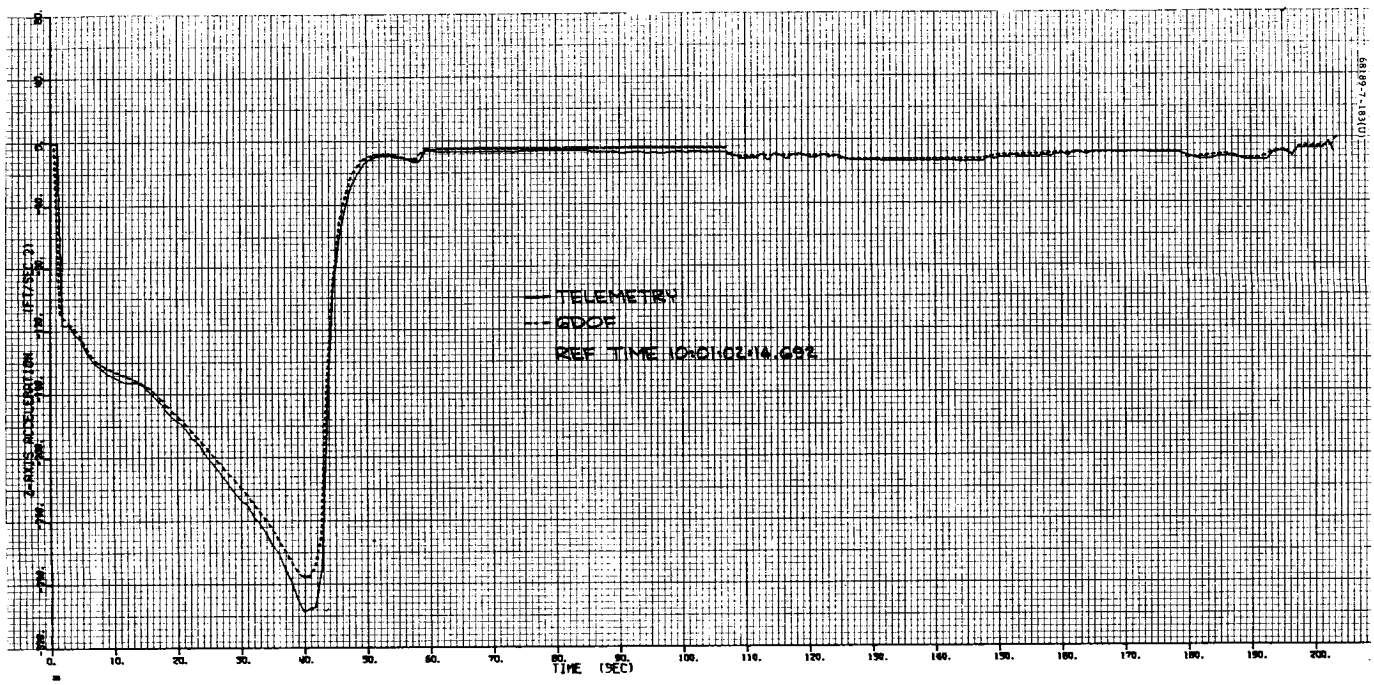

Figure 5.12-13. Telemetry Retro Accelerometer Data and 6DOF Z Axis Acceleration Versus Time

data. Slight differences can be seen between the two 6DOF curves on Figures 5. 12-9c and 5. 12-9d from 43 to 61 seconds during which V_z changes most rapidly. This is a result of the lag network in the V_z telemetry circuit. The indicated V_z of 240 fps at about 58. 4 seconds (the start of RADVS-controlled descent) is also the result of the beam 1 loss of lock. The true V_z at this time was approximately 428 fps.

The V_x, V_y, and V_z PREPRO curves in Figure 5. 12-9 were corrected for biases determined in the telemetry data. By observing the telemetry data, the following biases appeared:

$$V_x = 3.96 \text{ fps}$$

$$V_y = 3.17 \text{ fps}$$

$$V_z = 2.68 \text{ fps}$$

These bias corrections were made to the telemetry data of the velocity components at retro case eject as outlined in subsection 5. 12. 4. 1.

Figures 5. 12-10a and 5. 12-10b show both the X and Y gyro error signals to be biased about -0. 5 and -1. 2 degrees, respectively, beyond that determined by preflight calibration. The spikes in both signals at 58. 4 seconds are the result of the change from the inertial hold mode to the RADVS-controlled steering mode.

Figure 5. 12-11 shows the pitch and yaw precession commands. Both commands compare favorably with the reduction of the V_x and V_y components of velocity during the minimum acceleration phase. From Figure 5. 12-11, it can be seen that both commands saturated at the start of steering. The pitch precession command saturated due to the large V_y of -120 fps at this time. The yaw precession command saturated due to the false X-velocity measured as a result of the loss of radar beam 1 lock. The command came out of saturation after the beam reacquired lock. The 6DOF program assumed a pitch and yaw rate limit of 6. 0 deg/sec. The telemetry data indicated the same for the pitch rate limit, whereas 6. 6 deg/sec is indicated for the yaw rate limit.

Figure 5. 12-7 shows the vernier engine thrust commands. The roughness in the telemetry data is due to RADVS noise. The 6DOF curves are smooth since the RADVS noise was not simulated. The large spike in the 6DOF reconstruction of engine 3 at approximately 59 seconds is due to the large rate of steering required as a result of the loss of lock of beam 1. Due to the 1-second interval between the plotted data points, the PREPRO curve of engine 3 did not include this spike; however, closer examination of telemetry data between the plotted data points indicated a similar pattern as shown by the 6DOF construction.

The 6DOF program models the spacecraft's center of gravity change during terminal descent. The 6DOF program assumed the preflight calculations of the spacecraft center of gravity and retro nozzle center line location at retro ignition as outlined in Reference 1. However, the telemetry data indicate a slightly different spacecraft center of gravity-to-thrust vector offset than that determined by preflight computations. Further discussion of the vernier engine thrust commands is given in paragraph 5. 12. 4. 6.

Figure 5. 12-12 shows the 6DOF engine thrust levels superimposed on the processed vernier engine strain gage data. Although the strain gage data are not an accurate source for indicating the actual engine thrust magnitude, they are suitable for indicating the engine thrust variation characteristics. The telemetry data have almost the same characteristic changes in thrust as does the 6DOF program. The rapid change in slope of the telemetry data between 2 and 40 seconds is caused by the main retro thrust.

Figure 5. 12-13 compares the retro accelerometer telemetry data with the 6DOF spacecraft Z axis acceleration. The peak acceleration of approximately 10 g_e occurs at 40 seconds, which compares with the strain gage data of Figure 5. 12-12 and the retro accelerometer reconstruction on Figure 5. 12-2. The 6DOF assumed the doppler retro thrust-time curve (Figure 5. 12-3), resulting in the differences in acceleration levels near 40 seconds.

Figure 5. 12-14 is a plot of slant range versus velocity from the time of RORA to the 10-fps mark.

5. 12. 4. 9 Radar Beam Incidence Traces on Lunar Surface

The four radar beam traces along the lunar surface are shown in Figure 5. 12-15. The reference time is 50 seconds after vernier ignition (010:01:03:4. 692 GMT). The coordinate system is selenographic with the 0, 0 point being synonymous with Surveyor VII's touchdown location. The beam traces were determined from the best-fit 6DOF reconstruction by incorporating the necessary equations, as outlined in Reference 2, into the 6DOF computer program. These traces provide the data for analyzing the telemetered return radar beam signals (as described in Section 5. 9) with respect to lunar surface variations.

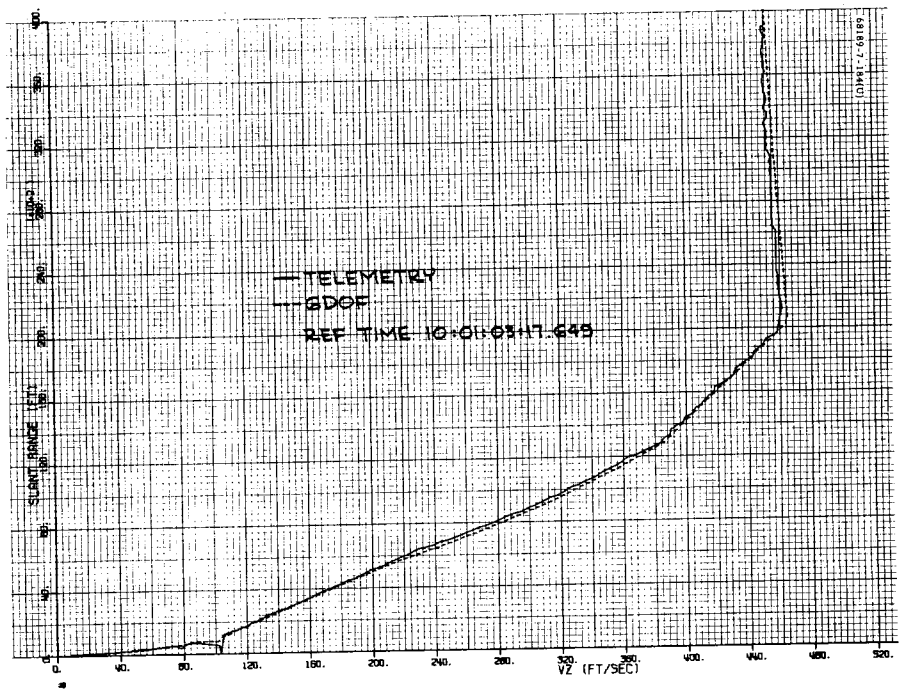

Figure 5.12-14. Slant Range Versus Z Axis Velocity

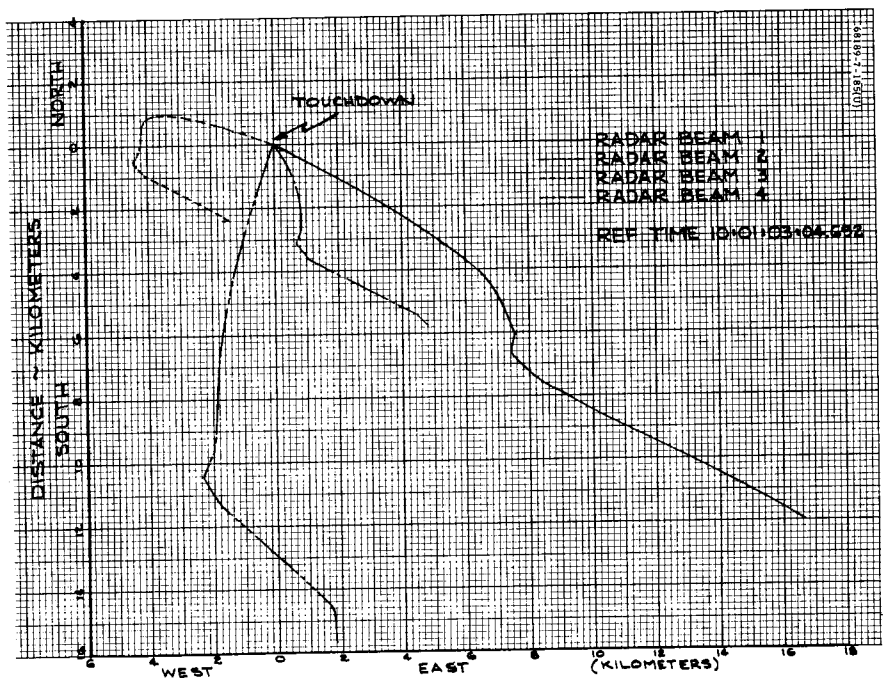

Figure 5.12-15. Radar Beam Incidence Traces

5.12.5 REFERENCES

1) C. T. Dorsett, "Mass Properties Status Report – Report Number SSD 74101 Surveyor SC-7 Final," Hughes Aircraft Company, IDC 2225.05/658, 3 January 1968.

2) E. R. Kopitzke, "RADVS Beam Incidence Traces on Lunar Surface," Hughes Aircraft Company, IDC 2293/159, 28 August 1967.

5.12.6 ACKNOWLEDGMENTS

Victor Marelia, coordinator and writer.

Eddy White, retro thrust-time curve reconstruction, main retro tailoff, retro ΔV determination, and 6DOF doppler reconstruction.

Ed Kopitzke, 6DOF reconstruction and radar beam traces.

Nancy Krupa, POSTPR machine plots.

5.13 TELEVISION

5.13.1 INTRODUCTION

Shortly after the successful soft landing of Surveyor VII in the southern hemisphere near the crater Tycho, the spacecraft was reconfigured for television camera operation, and began taking the first of 21,091 high quality pictures obtained during the 2 lunar days of the mission. Highlights of the postlanding operations were the use of the television camera to examine the deployment mechanism of the jammed alpha scattering instrument and to then visually guide the critical positioning of the surface sampler scoop in order to forcefully deploy the alpha scattering sensor head. Subsequent to the alpha scattering operation in the initial deployment area, the television camera provided many clearly detailed, narrow-angle views of the interfacing of the surface sampler scoop and the alpha scattering sensor head pickup fitting, assuring positive pickup of the sensor and its sequential redeployment to two additional analysis sites preselected from television mosaics of the landed area. Also unique to this mission were: 1) the use of the spacecraft camera narrow-angle view integrate mode to observe telescopically positioned, earth-based laser beams projected at the moon, 2) the first narrow-angle imaging of the earth and its cloud cover through polarizing filters, 3) stereo surveys of the soil mechanics/surface sampler area, 4) visual examination of particle mirrors to determine the extent of lunar material contamination of the spacecraft, 5) clearer pictures due to improved camera glare reduction techniques, and 6) positioning of the surface sampler scoop to provide shade to the alpha scatter sensor head during periods of intense solar heating.

Thermal response characteristics of the television system at its southerly lunar landing site were compromised due to the lack of shading afforded the television camera by the planar array and solar panel during the lunar noon. Consequently, it was necessary during this period to point the camera in azimuth away from the sun to minimize the solar absorption of the black interior of the television camera hood so that the vidicon faceplate temperature did not exceed acceptable limits.

5.13.2 ANOMALIES

The television system operated throughout the first lunar day with no anomalies. However, the change in the camera temperature characteristics, because of the spacecraft's southerly latitude, required certain departures

from the television operating limitations and techniques that were evolved during operation of prior spacecraft that landed in the lunar equatorial belt. High camera temperatures limited the operational periods during the 5 earth-day period near lunar noon, with severest conditions limiting operation to 5 minutes per hour.

Expected minor system performance variations not of an anomalous nature, but attributable to peculiarities of this particular hardware and its more severe solar-thermal environment, were routinely noted during the mission television operations. Specifically, these were: 1) electronic focus of the vidicon used in the Surveyor VII camera became progressively less optimum toward the bottom of all images as the temperatures increased, and 2) the camera vertical sweep period was approximately 10 percent longer when the camera was operating near its lower temperature limits (electronics chassis temperature at -20° to -30°F) during the postsunset period.

On two occasions, command sequences were transmitted to the camera with no subsequent response noted. On both occasions, the camera had been in operation for at least 30 minutes, with pretaped commands being sent when it failed to respond. From the inconclusive results of the subsequent investigation, it was thought that the most likely failure cause was a deviation in the spacecraft RF subsystem behavior.

5.13.3 SUMMARY

The television system operated for the entire first lunar day with no significant anomalous behavior. All mission objectives were accomplished despite a generally worsened television camera thermal profile and limited duty cycle due to the greater solar heat loading on the spacecraft at the southerly latitude landing site. Besides these particular achievements, the camera system accomplished the following variety of other assignments, many of which were performed on earlier Surveyor missions:

1) Numerous wide- and narrow-angle view panoramic surveys

2) Scientific instrument inspection, deployment, and observation

3) Focus ranging sequences on the surrounding terrain

4) Iris calibration tests

5) Special area surveys

6) Polarimetric surveys

7) Solar corona viewing

8) Postsunset diffraction pattern viewing

9) Integrate mode viewing of the lunar surface under earth shine illumination

10) Low light level imaging of the planet Jupiter, the constellation of Orion, and several selected stars

11) Observation of particulate matter adhering to spacecraft magnets

12) Imaging to provide photochart sun post shadows to establish solar position and resolution wedges for gross indication of camera response

13) Auxiliary viewing mirror observation of special subspacecraft structure and lunar surface

5.13.4 SUBSYSTEM PERFORMANCE ANALYSIS

5.13.4.1 Television Subsystem

The more than 21,000 pictures transmitted by Surveyor VII were some 9000 less than the over 30,000 pictures taken by Surveyor VI. However, this apparent decline in subsystem activity is reflected in the television activity being altered by the following factors peculiar to this mission:

1) The spacecraft carried three scientific experiments – soil mechanics/surface sampler, alpha scattering device, and television – each having to time share the spacecraft common transmission link to earth. As a consequence, the percentage of lunar time available for television operation decreased.

2) The nonequatorial landing site (approximately 40°S latitude) resulted in a solar angle that prohibited the solar panel or planar array from shadowing the television camera during the lunar noon period; consequently, camera temperature rise was more pronounced. Introducing further thermal complications was the low sun angle at the landing site (the sun at zenith was only about 58 degrees above the lunar horizon). As a result, solar radiation fell more nearly normal to the increased surface area offered by the camera sides as opposed to a more vertical sun on the limited top area of the camera hood for comparable times during the lunar day of earlier missions located at the Apollo "belt" landing sites.

3) Operations involving the surface sampler are, by their nature, more deliberate, with considerable time lapse normally present between television frames. Two types of sampler operation were performed, one consisting of positioning the sampler scoop to interface with the alpha sensor to deploy it, and the other using the scoop to perform soil bearing and mechanics experiments at the lunar surface. A summary of these uses is given in Table 5.13-1 which shows the approximate times they were used out of the lunar day. It should also be noted that the sampler completed 20 separate operating cycles totaling 36 hours and 21 minutes and

TABLE 5.13-1. SUMMARY OF SURVEYOR VII TELEVISION CAMERA SURVEYS

Description	Number
Wide-angle, 360-degree panorama	9
Right end stop area	5
Narrow-angle segment 1	10
Narrow-angle segment 2	12
Narrow-angle segment 3	11
Narrow-angle segment 4	9
Narrow-angle segment 5	11
Left end stop area	5
Special area coverage	10
Pad 3 to 200-line mode	1
Pad 2 magnets	7
Auxiliary viewing mirrors	8
Stereo viewing mirrors	5
Alpha scattering mirror	3
Particle mirrors	2
Omniantenna B photo chart	1
Alpha scattering deployment	4
Alpha scattering operation coverage	10
Alpha scattering repositioning	2
Surface sampler operation area	5
Surface sampler operating coverage	20
Earth pictures	7
Earth polarimetric	11
Lunar polarimetric	14
Focus ranging	5
Star survey	8
Laser experiment	6
Special rock surveys	5
Shadow progression	5
Sunset sequences	1
Solar corona sequences	6
Horizons at sunset	10

comprising 4397 mechanical motions as compared to the Surveyor III surface sampler operation where the operating time was 18 hours and 22 minutes, with only 1898 mechanical motions.

4) Certain experiments required considerable initial adjustment of the camera (azimuth and elevation positioning, focal length and focus adjustments, and filter and iris positioning) followed by relatively few pictures which were usually taken at a long exposure time. Typically, these were earth viewing, earth polarimetric studies, star surveys, laser, solar corona, and special rock analysis experiments. Surveyor VII television completed the following separate operating cycles:

   18 earth and earth polarimetric

   8 star surveys

   6 laser imaging

   5 special rock surveys

   6 solar corona

   10 horizon sunset surveys

A new performance requirement was demonstrated by the television camera: the camera was used to view the interfacing operations between the alpha scattering instrument and soil mechanics/surface sampler. These procedures commenced early during the postlanding operations when the alpha scattering sensor head failed to deploy from the background count position to the lunar surface. A counterplay between wide- and narrow-angle television views of the alpha scattering instrument structure, suspension cord, escapement, and sensor head provided inspection of the mechanism in an effort to discover the failure mode. The flexibility of operation inherent in the television camera performance permitted enhanced critical viewing of the exact region of interest via the following techniques:

1) Selection of the best of three polarizing filters for sun reflection angle to give minimum glare and highest contrast to the image

2) Stopping down of the iris in 1/2 f stop incremental settings that provided optimized lighting, shadows, and contrast balance in key areas of the pictures

3) Special sequence commanding of the iris to 1/4 f stops was used in several situations where extra critical image contrast was necessary

4) Taking frames of the various mechanisms at two adjacent azimuthal steps in order to form a three-dimensional result by creating a short baseline stereo view

5) Time exposure imaging of extremely dark areas to obtain useable images and observe shadow detail

Several days after the initial deployment of the alpha scattering sensor head, the surface sampler was manipulated to pick up and redeploy the sensor head for analysis of a second location. The television camera and the surface sampler were subsequently utilized to establish a third alpha scattering sensor analysis area and to redeploy the sensor head to this newly selected surface. This operational interaction of the soil mechanics/surface sampler and the alpha scattering device would have been extremely difficult, if not impossible, without the television camera's visual assistance. Numerous wide- and narrow-angle views of the scoop and sensor pickup fitting interface were required each time in order to successfully grasp and reposition the sensor head.

Stereo-enhanced television of the soil mechanics/surface sampler operation area was performed with the aid of a flat, optical surface mirror mounted on the antenna/solar panel positioner mast. This special mirror provided several advantages over only direct viewing, as existed on the Surveyor III surface sampler operations. First, the mirror provided long baseline stereo of a major portion of the lunar surface sampling area. Second, for certain sampling regions, the viewing perspective through the mirror was improved relative to the perspective presented by a direct view. Third, under peak thermal conditions where direct sunlight impingement on the more highly absorptive black thermal paint of the mirror hood interior caused excessive camera temperature, the camera was able to operate at lower temperatures by viewing away from the sun and through the mirror to a desired area.

Earth viewing was possible at the southerly landing site throughout the lunar day. Numerous pictures of the earth and its cloud cover were taken with better than 60 percent full earth being seen under the best viewing situation. Seven separate earth viewing cycles were accomplished, and particular cloud pattern progressions were denotable.

An earth-moon optical link was achieved in which the television camera observed laser transmission from earth observatories at Table Mountain, California, and Kitt Peak, Arizona. This, the initial attempt of its kind, provided the first known visual evidence of laser communication from the earth to another celestial body. The experiment provided valuable information in support of planned Apollo optical communication with earth. The experimental contributions were: 1) verification that laser power output as low as 1 watt would provide detectable light signals between the earth and the moon, and 2) opportunity to evaluate different laser pointing techniques and establish their workability. A 2-watt output Argon ion laser (furnished by the Hughes Malibu Research Laboratories) was used in conjunction with the JPL Coude focus reflecting telescope at Table Mountain. This produced a near collimated (2-arc-sec divergence) laser beam 24 inches in diameter which covered an area roughly 2 to 4 km in diameter on the moon's surface. Verification that the laser transmission images returned to earth by the television camera were actually received laser beams and not vidicon blemishes was accomplished by 1) noting that the geographical locations on the television earth image pin-pointed the Table Mountain and Kitt Peak

Observatory locations, 2) that turning on and turning off the laser at a specific observatory caused its beam spot to correspondingly appear and disappear, and 3) shifting the earth image on the television by stepping one azimuthal step caused the laser spot to move along with the shift of the earth image.

The particular laser used at Table Mountain was the optimum choice of a number of available lasers. It was selected because it provided the best light spectrum match to that of the television camera. Of particular interest in this laser experiment was the laser beam path on its round trip from earth to the moon (Figure 5. 13-1).

During the star surveys, difficulty was encountered with low elevation angle stars where the integrated diffuse light, reflecting from the lunar surface, onto the camera mirror was brighter than the stars being surveyed. This situation was overcome later in the lunar day when the azimuth and elevation positions of the sun were such that the diffuse light decreased significantly. It was found that the performance of the star mode was enhanced during long exposures if the camera were turned off during the exposure period. This reduced the video noise level and the black level shift in the resulting pictures. It also provided additional time for spacecraft engineering interrogation without interrupting the planned scientific operations.

Another experiment was carried out using the television camera capability. The dispersion of lunar dust on the television viewable portion of the spacecraft due to landing disturbances was assessed using six small mirrored surfaces located at various points on the space frame. In addition to the prior mentioned performance, the television camera was utilized to take numerous sunset and solar corona pictures. In obtaining these pictures, the camera was operated for more than 14 hours after lunar sunset. Many of these pictures requred 20- to 30-minute exposures to obtain adequate detail.

The television camera was turned off for the first lunar night after the 14 earth days of operation that comprised the first lunar day. A majority of the 21,046 pictures were taken using the polarizing filters, without which a high percentage of the pictures would have been badly degraded because of surface glare.

When the spacecraft was reactivated on the second lunar day, the camera did not respond properly in the 600-line mode. The camera did, however, perform properly in the 200-line mode. The problem was determined to be a failure of the 600-line horizontal sweep circuit. This failure caused the loss of scan of the vidicon faceplate and resulted in the absence of a video signal. Since the 200-line sweep circuit is separate and independent of the 600-line sweep, the camera could operate in a standard known mode. The quality of the 200-line pictures was very good. During a power system troubleshooting sequence, the television camera was in the power on state for 30 to 45 minutes. At the termination of this test, the temperature of the vidicon and electronics conversion unit had exceeded the

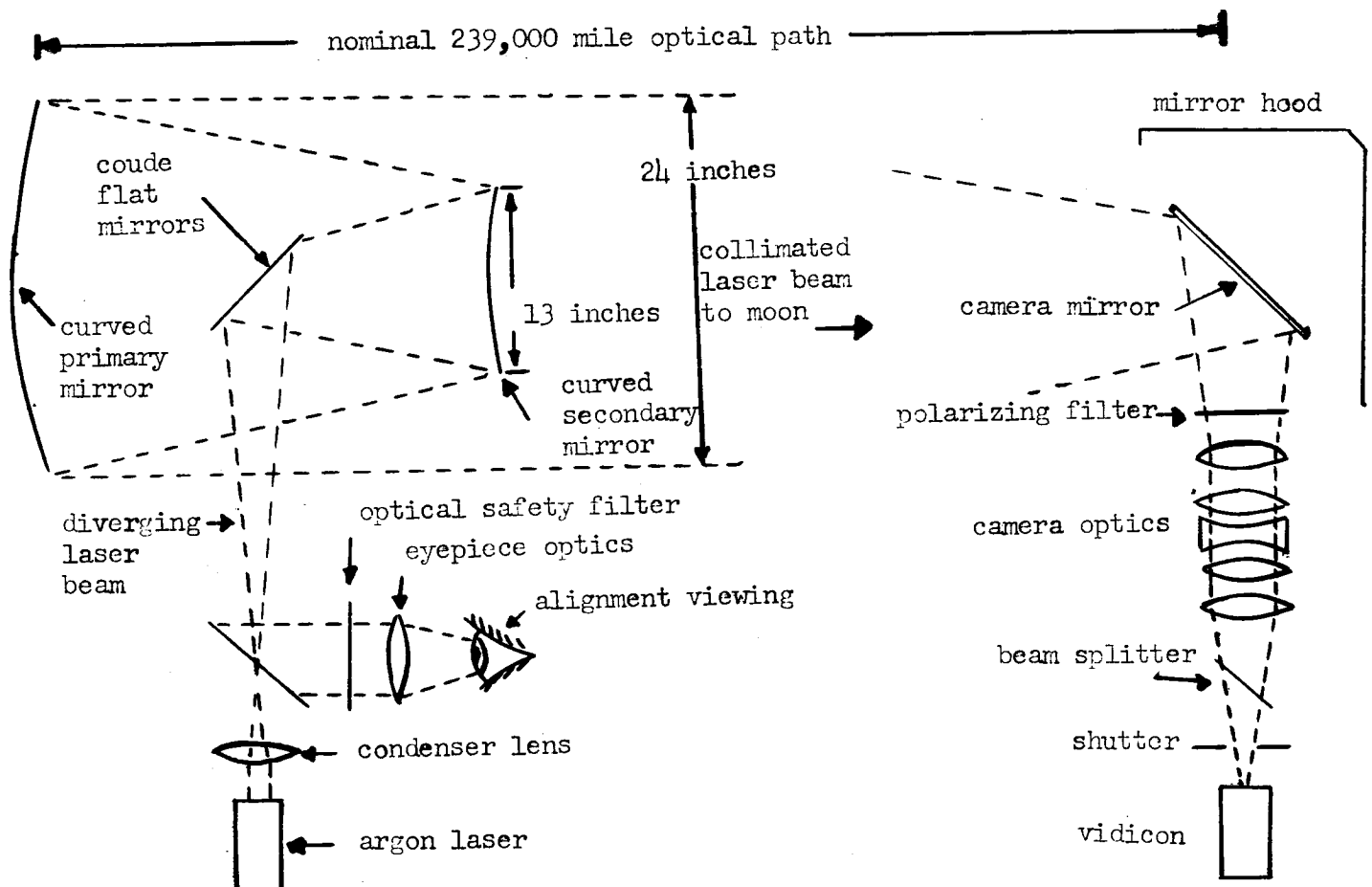

Figure 5.13-1. Laser Experiment Schematic Diagram

specified upper limit. The vidicon had reached +154°F, and the electronics conversion unit was +195°F. Both temperatures were considerably above the specified upper survival temperature of +145° and +165°F, respectively. Several pictures were taken at this temperature with no apparent degradation of visual performance. There were no white spot formations or peeling of the vidicon faceplate. In general, spacecraft operation on the second lunar day was restricted due to the low electrical storage capacity of the 22-volt battery. This power limitation degraded until only one frame could be taken every 45 to 60 minutes. Finally, the battery failed to recover and the television camera operation was terminated. Forty-five pictures were obtained during the second lunar day.

5.13.4.2 Television Camera

The success of the Surveyor VII camera, as with that of Surveyor VI, may be traced to the improvements made in the 290512 series design. The major component changes were as follows:

1) The mirror azimuth and elevation stepping motors were of improved design, using Microseal lubricant.

2) The potentiometers in the mirror and lens assemblies were modified and lubricated with Niobium Diselenide, resulting in improved reliability and life.

3) The mirror azimuth journal bearing was replaced with a ball bearing support, thereby decreasing friction and eliminating the temperature problem associated with the journal type.

4) The mirror assembly sun shade was modified to reduce the possibility of certain types of sun-caused glare.

5) The mechanical end stops on the azimuth and elevation functions were improved, eliminating end stop jamming that had occurred on the earlier cameras.

6) The iris function was changed to allow 1/2 f stop iris capability for improved control of image exposure.

7) An electronic pulse counter was added to the filter wheel circuitry to improve the positioning accuracy.

8) The vertical raster sweep direction was reversed to improve the vidicon's resolution performance.

9) The colored filters were replaced with polarizing filters to permit polarimetric studies of the lunar surface.

10) The mirror elevation positioning was changed to give 5-degree incremental steps, allowing easier elevation position computation by the Space Science Analysis and Command personnel.

5.13.5 ACKNOWLEDGMENTS

This section was compiled by W. E. Drake and R. N. Jasberg from information obtained from the following JPL personnel:

L. H. Allen
R. C. Heyser
J. N. Lindsley
W. J. Sleigh

5.14 ALPHA SCATTERING EXPERIMENT

5.14.1 INTRODUCTION

5.14.1.1 Purpose

The alpha scattering experiment was added to Surveyor VII in order to perform a compositional analysis of the lunar surface. The alpha scattering technique of surface elemental analysis takes advantage of the characteristic interactions of alpha particles with matter to provide information on the elemental composition. The energy spectrums of the large-angle, elastically scattered alpha particles are characteristic of the nuclei causing the scattering. In addition, certain elements, when bombarded with alpha particles, produce protons, again with characteristic energy spectrums. Consequently, these energy spectrums and intensities of scattered alpha particles and protons can be used to determine the elemental composition of the material being exposed to the alpha particles.

The method has good resolution for the light elements expected to be contained in rocks (unfortunately, however, it can give only indirect information about hydrogen). The resolution under this technique decreases as the atomic weight increases (Fe, Co, and Ni cannot easily be resolved), even though the sensitivity is greater for heavy elements than for most light elements. (The sensitivity for elements heavier than lithium is approximately 1 atomic percent.)

The absence of an atmosphere on the moon made practical the use, for such elemental analyses, of the relatively low-energy alpha particles from a radioactive source. Cm^{242} ($t_{1/2}$ = 163 days, T_a = 6.11 mev) is a convenient nuclide for this purpose. The use of low-energy alpha particles, however, restricts the information obtained to that pertaining to the uppermost few microns of material, i.e., the method is one of surface elemental analysis. Moreover, using practical source intensities (~100 mc), the rate of analysis is rather slow: a relatively complete analysis requires about 1 day. In spite of these disadvantages, the simplicity of the instrumentation associated with using a radioactive source made this a feasible, attractive method.

5.14.1.2 Description

The alpha scattering subsystem consisted of five principal units: sensor head, digital electronics, electronic auxiliary, thermal

compartment/heater assembly, and deployment mechanism/standard sample, having a total weight (including mechanical and electrical spacecraft interface substructure and cabling) of approximately 13. 1 kg (28. 8 pounds). Power dissipation of the subsystem was normally 2. 1 watts (approximately) which increased to 17. 1 watts, when both the thermal compartment and the sensor head heaters were active. A brief description of each principal unit follows.

Sensor Head (GFE)

The sensor head dimensions are rectangular (measuring 17.1 by 16. 5 by 13.3 cm), the bottom of which is attached to a 30.5-cm-diameter plate. The main purpose of this plate is to minimize the probability of the box appreciably sinking into a soft (lunar) surface. At the bottom of the plate is a 10.8-cm circular opening, and recessed 7.0 cm above the opening are six alpha sources, which are orientated in such a way that the alpha particles are directed only at the opening of the head. Close to the alpha sources are two silicon surface barrier-type detectors arranged to detect alpha particles scattered back from the sample at an average angle of 174 degrees from the original direction. Also contained in the head are four detectors ($\sim 1\ cm^2$ area each) designed to detect protons produced in the sample by the alpha particles. Gold foil 11 microns thick prevents scattered alpha particles from reaching these detectors. Because the proton rates were expected to be low, and because these detectors are particularly sensitive to solar protons, the proton detectors were backed by guard detectors. The electronics associated with the guard detectors were arranged so that an event registered in both detectors (and, therefore, due to space radiation) will not be counted as coming from the sample. The anticoincidence arrangement had the effect of significantly reducing the backgrounds of the instrument when operating in the proton mode.

In addition to the sources, detectors, and associated electronics, the head contained a temperature sensor, a 5-watt heater, and an electronic pulser. The electronic pulser was used to calibrate the electronics of the instrument by introducing electrical pulses of known magnitudes (two) into the detector stages of the system. The calibration mode is initiated by earth command. The sensor head has a "pickup" handle to enable the soil mechanics/surface sampler to easily relocate the heat to new positions.

The output of the head characterizes the energy of an event, in either the scattered alpha or proton mode of the instrument, by a signal in time analog (pulse) form.

Digital Electronics (GFE)

The time analog output signal of the sensor head is processed by the digital electronics units and converted into a nine-bit digital word that has seven information bits. Stated differently, the event energy spectrum is analyzed and expressed, in terms of channels, by 128-channel pulse-height analyzers having a threshold of about 600 kev and a height of about 54 kev per channel. The nine-bit digital words characterizing each event are transmitted in near-real time (essentially no spacecraft storage) to earth at a rate of 2200 bits/sec for the alpha mode and 550 bits/sec for the proton mode.

The digital electronics unit contains, in addition to the digital processing electronics, the necessary power supplies and the logical electronic interfaces between the Government-furnished and Hughes spacecraft equipment. The digital electronics units contained circuits so that the output of any one individual detector, together with its associated guard detector, could be inhibited by earth command; the temperature of the sensor head, as well as other monitoring voltages, could be transmitted to earth. Finally, a crude ratemeter provided information on the number of events occurring in the guard (anticoincidence) detectors.

Electronics Auxiliary (Hughes)

The electronics auxiliary unit provided the necessary command decoding, signal processing, and power management so that the Government-furnished equipment could interface with the basic spacecraft bus. Basic items interfacing directly with the sensor head and the digital electronics are 1) the central signal processor which provides 2200 and 550 bits/sec sync to the digital electronics clocks, and 2) the engineering signal processor which provides temperature sensor excitation current and commutation of the Government-furnished engineering data outputs.

The electronics auxiliary also provides the two data channels employed by the alpha scattering subsystem for the alpha and proton counts. The characteristics of these two subcarrier oscillator channels are as follows:

	Alpha Counts	Proton Counts
Data input to electronic auxiliary	Digital, NRZ	Digital, NRZ
Input data rate, bits/sec	2200	550
Subcarrier oscillator center frequency, Hz	70,000	5400

Thermal Compartment/Heater Assembly

The digital electronics and the electronic auxiliary units were contained in a thermal compartment attached to the spacecraft. Thermal control was obtained by compartment thermal design in conjunction with a 10-watt compartment heater assembly.

Deployment Mechanism/Standard Sample

The deployment mechanism provides for the operation of the experiment in any of the following three positions:

1) Stowed position where the standard sample was utilized for calibration of the system

2) Background position where the solar and surface natural radiation was calibrated

3) Lunar surface position where the lunar surface elemental analysis was performed

The standard sample is a sample of known chemical composition which was attached to the deployment mechanism and was used to assess subsystem performance prior to launch and after lunar landing. The standard sample covers the sensor head viewing part when in the stowed position, and is removed when the sensor head is in either the background or the lunar surface positions. Operation in this manner minimizes the entrance of both dust and light during spacecraft launch, transit, and landing and/or until the experiment is to be operated.

5.14.2 ANOMALIES

An alpha scattering subsystem anomaly occurred during the lunar phase of operation. The alpha scattering instrument deployment mechanism failed to deploy the sensor head from the background position to the lunar surface position when the deployment command was transmitted. This anomaly is documented in TFR No. 87255.

Combined operation of the television camera and the soil mechanics/surface sampler resulted in the deployment of the alpha scattering sensor head to the lunar surface. Thereafter, all alpha scattering mission objectives were achieved. Further description of these operations is contained in subsection 5.14.4.

5.14.3 SUMMARY

The alpha scattering experiment successfully accomplished all mission objectives during the first lunar day with a total operating time of 136 hours and 33 minutes during which 64 hours of science data were accumulated, including 44 hours of lunar surface analysis. On the second day, data were accumulated for approximately 34 hours with a total of 35 hours of operating time.

5.14.4 SUBSYSTEM PERFORMANCE ANALYSIS

The lunar operations plan called for five modes of operation: 1) standard sample, 2) background, 3) lunar surface positions No. 1, 4) lunar surface positions No. 2 and 5) calibration. There were, however, seven actual modes of operation provided with the moving of the sensor head to a third lunar position and operation of the experiment on the second lunar day.

Two forms of science data were recorded during the operation: the uncorrected spectra, received via teletype from the stations, which were used for near-real time analysis; and the FR-1400 prime data tapes for use during the postmission analysis. The uncorrected spectra, while not reflecting

all data transmitted from the alpha scattering subsystem, did contain the vast majority of data recorded on the FR-1400 tapes. Table 5.14-1 presents a summary of the science data accumulation time in each of the six operational configurations.

TABLE 5.14-1. SCIENCE DATA ACCUMULATION SUMMARY

Operational Configuration	Accumulation Time, minutes	
	First Lunar Day	Second Lunar Day
Standard sample	310	
Background	727	
Lunar surface positions		
No. 1 (undisturbed area)	1639	
No. 2 (over lunar rock)	600	
No. 3 (area disturbed by soil mechanics/ surface sampler – trenching	406	1974
Calibration	160	68
Total	3842 ≈ 64 hours	2042 ≈ 34 hours

Operation of the alpha scattering subsystem was initiated approximately 8 hours and 22 minutes after touchdown. Lunar operations continued during GMT days 10 through 15 and 20 through 23. During lunar operations, the majority (57.7 hours) of the science data was accumulated while the sensor head was within its operational temperature limits (-40° to 122°F); however, in order to obtain additional data, the experiment was operated for 6.5 hours when the sensor was in the range of 137° to 144°F. With the exception of 50 minutes of data, all data were accumulated while compartment C was within its operational temperature limits (-4° to 131°F). The 50 minutes of data collected while outside the operating temperature limits was recorded at the day/night terminator when the temperature of the compartment was between -30° and -56°F. Operation of the experiment while outside the specified temperature limits appeared normal.

On the first lunar day, approximately 400 commands were transmitted, received and executed with one noted error. As indicated in the anomaly section (5.14.2) the alpha scattering instrument deployment mechanism failed to deploy the sensor head from the background position to the lunar surface position. The problem was circumvented by utilizing the television for observation and the surface sampler instrument to manipulate the sensor head to the lunar surface position. The sequence of spacecraft events associated with the assisted deployment are listed in Table 5.14-2.

TABLE 5.14-2. ALPHA SCATTERING DEPLOYMENT INSTRUMENT MECHANISM ANOMALY TABLE OF EVENTS

GMT, day:hr:min:sec	Operation Description	Comment
10:22:01:44	Deploy to lunar surface command 3506 was transmitted	
22:02 to 22:08	Alpha and proton event rates were observed	Event rates did not increase as expected, indicating sensor had not deployed.
22:08:59	Deploy to lunar surface command 3506 was retransmitted	
21:10:15 to 22:20:15	A 10-minute data accumulation was accomplished	Event rates did not increase as expected, indicating sensor had not deployed.
22:41:24 to 23:44:35	Television pictures of sensor head and deployment mechanism were taken	Reference television photos (day 10) Nos. 02322, 02323 02327, 02330, 02331, 02332, 02334, 02335, 02336, 02337, 02340, 02341, 02342, 02343, 02344, 02345, 02346, 02347, 02350, 02351, 02607, 02610, 02627, and 02630. Photos showed that pin puller had operated (cable compartment door was open), but that sensor had remained in background position.
11:02:18:35 to 02:49:06	Television pictures of alpha scattering instrument deployment escapement mechanism were taken	Reference television photos (day 11) Nos. 03013, 03016, 03042, 03043, 03044, and 03051. These photos were taken to provide views of the escapement mechanism.

Table 5.14-2 (continued)

GMT, day:hr:min:sec	Operation Description	Comment
07:23:45 to 08:09:01	Soil mechanics/surface sampler scoop positioned over skirt of alpha scattering sensor and downward movement of soil mechanics/surface sampler was applied to alpha scattering	Reference television photos (day 11) Nos. 03541, 03542, 03543, 03544, 03545, 03546, 03547, 03550, 03551, 03552, 03553, 03554, 03555, 03556, 03557, 03560, 03561, 03562, 03563, 03564, 03565, 03566, 03567, 03570, 03571, 03572, 03573, and 03574. Alpha scattering sensor swung slightly. Close examination of photos 03575 and 03551 indicates that sensor possibly moved down slightly.
08:15:08 to 08:50:04	Soil mechanics/surface sampler scoop was used to make the alpha scattering sensor swing by pushing sensor sideward and downward	Reference television photos (day 11) Nos. 03576, 03577, 03600, 03601, 03602, 03603, 03604, 03605, 03606, 03607, 03610, 03611, 03612, 03613, 03614, 03615, 03616, 03617, 03621, 03620, 03622, 03623, 03624, 03625, 03626, 03630, 03631, 03632, and 03633. Sensor swung several degrees. Examination of photos 03551 and 07422 indicates sensor may have moved down slightly.
23:14:38 to 23:41:28	Television pictures of alpha scattering instrument deployment escapement mechanism were taken	Reference television photos (day 11) Nos. 13077, 13100, 04222, 13102, 13103, 13107, 04233, 13112, 04234, 04235, 13113, 13114, 04236, 04237, 04240, 04241, 04242, 04243, and 04250. These photos were taken to provide views of the escapement mechanism at a different sun angle.

Table 5.14-2 (continued)

GMT, day:hr:min:sec	Operation Description	Comment
12:05:48:29 to 07:33:49	The soil mechanics/ surface sampler scoop was positioned to turn the alpha scattering head about 45 degrees and push it against the helium tank and standard sample and then to apply a downward force with three "fine" lowering commands	Reference television photos (day 12) Nos. 05100, 05101, 05102, 05103, 05104, 05105, 05106, 05107, 05110, 05111, 05112, 05113, 05114, 05115, 05116, 05117, 05120, 05121, 05122, 05123, 05124, 05125, 05126, 05127, 05130, 05131, 05132, 05133, 05134, 05135, 05136, 05137, 05140, 05141, 05142, 05143, 05144, 05145, 05146, 05147, 05150, 05151, 05152, 05153, 05154, 05155, 05156, 05157, 05160, 05161, and 05162. Alpha scattering sensor moved down several inches.
07:36:42 to 08:01:22	Soil mechanics/surface sampler was positioned on top of alpha scattering head near eye bolt. Alpha scattering head was pushed downward.	Reference television photos (day 12) Nos. 05163, 05164, 05165, 05166, 05167, 05170, 05171, 05172, 05173, 05174, 05175, 05176, 05177, 05200, 05201, 05202, 05203, 05204, 05205, 05206, 05207, 05210, 05211, 05212, 05213, 05214, and 05215. Alpha scattering head appeared to lower to surface position.
08:28:30 to 08:40:30	A 12-minute data accumulation was accomplished	Event rates indicated that sensor was not on surface.
09:10:52 to 10:05:06	Soil mechanics/surface sampler was positioned on top of alpha scattering sensor for final movement to surface	Reference television photos (day 12) Nos. 05253, 05254, 05255, 05256, 05257, 05260, 05261, 05262, 05263, 05264, 05265, 05266, 05267, 05270, 05271, 05272, 05273, 05274, 07275, 05276, 05277, 05300, 05301, 05302, 05303, 05304, 05305, 05306, 05307, 05310, 05311, 05313, 05317, 05320, 05321, and 05322. Shadowing on lunar surface indicated sensor was fully deployed.
11:18:00 to 11:30:00	12 minutes of data were accumulated	Event rates and spectrum indicated that the sensor was on lunar surface.

The exact cause for the failure to deploy is unknown; however, it appears that the most likely causes were as follows:

1) A foreign object was lodged in the escapement mechanism.

2) The nylon cord experienced water-loss embrittlement (References 1 and 2) which occurs during vacuum conditions, causing a stiffening of cord escapement mechanism operation.

A careful review of the television pictures taken during the assisted sensor head deployment indicates that the deployment mechanism was near the threshold of movement and that only very small forces were applied by the surface sampler to move the sensor head downward.

By using the surface sampler, the alpha scattering sensor was successfully moved to two additional sample positions, permitting analysis of lunar materials in three locations.

In general, the communications link during the first lunar day from the spacecraft was excellent and the bit error rate of 10^{-6} was at least a factor of 100 better than the predicted worst-case value.

On the second lunar day, approximately 128 commands were successfully executed and 34 hours of data were accumulated; however, only 20 hours of this data were usable as a result of low communication link signal strength. Proton data could not be accumulated because the proton data logic circuits in the alpha scattering electronics unit did not survive the lunar night and were being dumped into a single channel.

For ancillary information, Table 5. 14-3 is a summary of preliminary results of the elemental analysis of the moon at the Surveyor V and VI landing sites (Reference 3). Table 5. 14-4 is a detailed account of SSAC alpha scattering operations during the first lunar day, and Table 5. 14-5 outlines the overall operation of the alpha scattering experiment.

TABLE 5. 14-3. CHEMICAL COMPOSITION OF LUNAR SURFACE AT SURVEYOR V, VI, AND VII SITES

Element	Surveyor V Atomic, percent*	Surveyor VI Atomic, percent*	Surveyor VII Atomic, percent, Position 1
Carbon	< 3	< 3	< 2
Oxygen	58 ± 5	57 ± 5	58 ± 5
Sodium	< 2	< 2	< 3
Magnesium	3 ± 3	3 ± 3	4 ± 3
Aluminum	6. 5 ± 2	6. 5 ± 2	8 ± 3
Silicon	18. 5 ± 3	22 ± 5	18. 5 ± 4
28 < A < 65**	13 ± 3		
Calcium		6 ± 2	6 ± 2
(Fe, Co, Ni)	< 3		
Iron		5 ± 2	2 ± 1'
A > 65	< 0. 5		

*Excluding hydrogen, helium, and lithium. These numbers have been normalized to approximately 100 percent.

**This group includes, for example, S, K, Ca, Fe, Co, and Ni.

TABLE 5.14-4. SURVEYOR VII ALPHA SCATTERING DETAILED DATA ACCUMULATION LOG

GMT Day	Position	Calibration Period	Accumulation Period	GMT, hr:min:sec		Comments
				Start	End	
10	Stowed		10M	09:28:00	09:38:00	
		23M		09:40:00	10:03:00	
			30M	10:04:30	10:34:31	
			30M	10:34:31	11:04:30	
			30M	11:04:30	11:34:30	
			30M	11:34:30	12:04:30	
			30M	12:04:30	12:34:30	
			30M	12:34:30	13:04:30	
			30M	13:04:30	13:34:30	
			30M	13:34:30	14:04:30	
			30M	14:04:30	14:34:30	
			10M	14:34:30	14:44:30	
			10M	14:52:10	15:02:10	
		13M20S		15:04:40	15:18:00	
			10M	15:19:00	15:29:00	
	Background		30M	16:13:00	16:43:00	
			30M	16:44:50	17:14:50	
			30M	17:16:00	17:46:00	
			8M	17:47:00	17:55:00	
			30M	18:15:30	18:45:30	
			30M	18:53:15	19:23:15	
			30M	19:24:55	19:54:55	
			30M	19:56:20	20:26:20	
		16M10S		20:30:30	20:46:40	
			30M	20:48:20	21:18:20	
			40M	21:19:10	21:59:10	
			10M	22:10:15	22:20:15	Unsuccessful attempt to deploy to lunar position.
11			21M	14:31:30	14:52:30	
			15M30S	14:37:20	14:52:50	
			15M	15:07:40	15:22:40	
			30M	15:23:30	15:53:30	
		17M40S		15:56:20	16:14:00	
			40M	16:16:00	16:56:00	
			40M	16:56:55	17:36:55	
			30M	17:37:45	18:07:45	
			60M	18:09:00	19:09:00	
			60M	19:10:05	20:10:05	
			60M	20:10:05	21:10:05	
			30M	21:10:05	21:40:05	
		15M10S		21:45:25	22:00:35	
			50M	22:03:50	22:53:50	

Table 5.14-4 (continued)

GMT Day	Position	Calibration Period	Accumulation Period	GMT, hr:min:sec Start	GMT, hr:min:sec End	Comments
12			12M	08:28:30	08:40:30	Sensor deployed part way to surface by soil mechanics/ surface sampler
	Lunar surface position No. 1		12M	11:18:00	11:30:00	
			10M	16:42:25	16:52:25	
			40M	16:52:25	17:12:25	
			40M	17:12:25	17:52:25	
		15M35S		17:54:20	18:09:55	
			40M	18:13:20	18:53:24	
			40M	18:54:05	19:34:05	
			40M	19:37:00	20:17:00	
			40M	20:17:00	20:57:00	
			40M	20:57:00	21:37:00	
			40M	21:38:30	22:18:30	
		13M35S		22:20:15	22:33:50	
			40M	22:35:05	23:15:05	
			45M	23:16:25	00:01:25	
13			20M	05:04:30	05:24:30	
			20M	06:45:20	07:05:20	
			20M	10:56:49	11:16:49	
			12M	11:20:27	11:32:27	
			40M	12:52:30	13:12:30	
			20M	14:14:10	14:34:10	
			5M	15:44:35	15:49:35	
			20M	15:53:40	16:13:40	
			20M	16:23:30	16:43:30	
			20M	16:43:30	17:03:30	
		15M5S		17:05:45	17:20:50	
			40M	17:22:25	18:02:25	
			40M	18:15:10	18:55:10	
			40M	18:55:10	19:35:10	
			40M	19:35:10	20:15:10	
			5M	20:15:10	20:20:15	
			10M	22:40:25	22:50:25	
			20M	22:51:50	23:11:50	
			20M	23:11:50	23:31:50	
14			10M	16:47:30	16:57:30	
		15M30S		17:20:40	17:36:10	
			40M	17:37:40	18:17:40	
			40M	18:17:40	18:57:40	
			40M	18:57:40	19:37:31	
			20M	19:37:31	19:57:31	
			40M	20:01:20	20:41:20	
			40M	20:46:10	21:26:10	A_1, A_2, P_1, P_2, and P_4 on
			40M	21:26:10	22:06:10	A_1, A_2, P_1, P_2, and P_4 on
			40M	22:56:20	23:36:20	A_1, A_2, P_1, P_2, and P_4 on

Table 5.14-4 (continued)

GMT Day	Position	Calibration Period	Accumulation Period	GMT, hr:min:sec Start	GMT, hr:min:sec End	Comments
		13M40S		23:37:40	23:51:20	
15			40M	00:09:45	00:49:45	A_1, A_2, P_1, P_2, and P_4 on
			10M	01:01:59	01:11:59	A_1, A_2, P_1, and P_2 on
20			10M	21:15:30	21:25:30	
			10M	21:25:30	21:35:30	
			10M	21:35:34	21:45:34	
			30M	21:45:34	22:15:34	
		12M30S		22:18:30	22:31:00	
			30M	22:32:00	23:02:00	
			40M	23:02:00	23:42:00	
21			40M	23:42:00	00:22:00	
			40M	00:29:00	01:09:00	
			40M	01:09:00	01:49:00	
			40M	01:49:00	02:29:00	
			40M	02:35:05	02:55:05	
			10M	03:21:25	03:31:25	
			20M	03:34:05	03:54:05	A_1, A_2, and P_1 on
			20M	03:55:35	04:15:35	A_1, A_2, and P_2 on
			20M	04:17:30	04:37:30	A_1 and P_3 on
			20M	04:39:10	04:59:10	A_2 and P_4 on
			40M	05:00:30	05:40:30	
		16M15S		05:42:50	05:59:05	
			40M	06:00:45	06:40:05	
			40M	06:40:50	07:20:50	
	Lunar position No. 2		10M	12:42:30	12:52:30	
			20M	12:54:30	13:14:30	
			5M	13:16:10	13:21:10	A_1, A_2, and P_1 on
			5M	13:22:30	13:27:31	A_1, A_2, and P_2 on
			5M	13:30:00	13:35:00	A_1 and P_3 on
			5M	13:36:40	13:41:40	A_2 and P_4 on
			10M	23:01:00	23:11:00	
		12M55S		23:11:40	23:24:35	
22			40M	23:26:00	00:06:00	
			40M	00:06:00	00:46:00	
			30M	00:23:45	00:53:45	
			40M	00:53:45	01:33:45	
			40M	01:38:00	02:18:00	

Table 5.14-4 (continued)

GMT Day	Position	Calibration Period	Accumulation Period	GMT, hr:min:sec		Comments
				Start	End	
23	Lunar surface position No. 3		40M	02:18:00	02:58:00	
			40M	02:58:00	03:38:00	
			40M	03:38:00	04:18:00	
			40M	04:18:00	04:58:00	
			40M	04:58:00	05:38:00	
			40M	05:38:00	06:18:00	
		14M15S		06:19:15	06:33:30	
			40M	06:35:05	07:15:05	
			13M	07:15:05	07:28:00	
			40M	07:29:30	08:09:00	
			30M	08:09:00	08:39:00	
			20M	08:39:00	08:59:00	
			50M	09:01:00	09:51:00	
			10M	12:06:30	12:16:30	
			20M	20:19:55	20:39:55	
		13M20S		20:41:20	20:54:20	
			40M	20:55:30	21:35:30	
			40M	21:36:00	21:16:00	
			40M	21:16:30	22:56:30	
			40M	23:37:30	00:17:30	
			35M	00:19:30	00:54:30	
			40M	01:12:30	01:52:30	
			30M	01:53:00	02:33:00	
			20M	02:33:00	02:53:00	
			10M	03:28:40	03:38:40	
			10M	03:39:00	03:49:00	
		12M40S		03:50:20	04:30:00	
			40M	04:04:05	04:54:05	
			15M	13:00:00	13:15:00	
			15M	13:15:00	13:30:00	
			15M	13:30:00	13:45:00	
			5M	14:35:10	14:40:10	

TABLE 5. 14-5. SURVEYOR VII ALPHA SCATTERING EXPERIMENT SEQUENCE OF OPERATION

GMT, day:hr:min:sec	Function
9:22:27:22	Compartment C heater commanded on
2:31:58	Sensor head heater commanded on
10:00:56:26	Compartment C and sensor head heaters commanded off
01:15:03	Compartment C and sensor head heaters commanded on
07:43	Compartment C and sensor head heaters commanded off
09:27:32	Alpha scattering power commanded on
15:48:52	Deploy to background command sent
22:01:44	Deploy to lunar surface command sent
22:08:59	Second deploy to lunar surface command sent
12:05:59	Alpha scattering power commanded off
08:26:57	Alpha scattering power commanded on
09:10:10	Alpha scattering power commanded off
10:35	Deployment to lunar surface by means of soil mechanics/surface sampler completed
11:16:31	Alpha scattering power commanded on
11:31:34	Alpha scattering power commanded off
16:41:31	Alpha scattering power commanded on
13:00:02:43	Alpha scattering power commanded off
05:03	Alpha scattering power commanded on
08:21:27	Alpha scattering power commanded off
10:55:17	Alpha scattering power commanded on
20:21:32	Alpha scattering power commanded off
22:36:12	Alpha scattering power commanded on
23:33:07	Alpha scattering power commanded off
14:16:46:10	Alpha scattering power commanded on
15:01:15:59	Alpha scattering power commanded off
20:21:13:09	Alpha scattering power commanded on
21:08:51	Alpha scattering power commanded off
—	Location changed to sample position No. 2
12:40:43	Alpha scattering power commanded on

Table 5.14-5 (continued)

GMT, day:hr:min:sec	Function
22:09:51:55	Alpha scattering power commanded off
—	Location changed to sample position No. 3
09:52:12	Sensor head heater commanded on
09:52:28	Compartment C heater commanded on
12:04:38	Alpha scattering power commanded on
23:15:36:07	Alpha scattering power commanded off
15:37:11	Sensor head heater commanded off
15:37:53	Compartment C heater commanded off

5.14.5 REFERENCES

1) R.G. Nagler, "Parachute Sterilization and Vacuum Compatibility," JPL Space Programs Summary No. 37-29, Vol. IV, pp. 52-57.

2) H.E. Pettus, "The Effect of Space Environment on Textile Materials," Northrop Corporation, Ventura Division, Technical Paper No. 83.

3) A.L. Turkevich, E.J. Franzgrote, and J.H. Patterson, "Chemical Analysis of the Moon at the Surveyor V Landing Site: Preliminary Results."

5.15 SOIL MECHANICS/SURFACE SAMPLER

5.15.1 INTRODUCTION

The Surveyor VII soil mechanics/surface sampler (SM/SS) subsystem (see Figure 5.15-1) was identical to that of Surveyors III and 4 with the singular exception of the cable (P/N 3025708) that connected the auxiliary to previous spacecraft was not required since the wiring had been modified. The subsystem consisted of two major units: a mechanism (P/N 3024700) and an auxiliary (P/N 3024536). In addition, there were two cables that interconnected the auxiliary to the mechanism (P/N 3025707) and the auxiliary to the squib pin puller (P/N 3025706), as well as the hardware that mechanically connected the mechanism and the auxiliary to the spaceframe.

The basic SM/SS mechanism consists of a bucket or scoop attached to the end of a lazy-tongs extension arm. The arm is attached to a base that is pivoted in elevation and azimuth with respect to the spaceframe, and is manipulated by three motors that control the azimuth, elevation, and extension motions. A fourth motor opens and closes the scoop door. The lazy-tongs extension mechanism joints include torsion springs that provide the extension force, while the retraction force is provided by a motor that winds up a steel tape attached to the scoop. The elevation drive motor includes a positive latching clutch that can be disengaged from the gear train by actuation of a solenoid and allows the elevation torsion spring to drive the mechanism downward.

The purpose of the SM/SS subsystem is to manipulate the lunar surface via the mechanism within a 112-degree sector lying between legs 2 and 3. The mechanism (upon receipt of command sequences from the auxiliary) can pick, dig, scrape, and trench the lunar surface; transport lunar surface material from one point to another within the sphere of operation; and apply downward forces to the lunar surface. Picking is accomplished by elevating the scoop to a predetermined point (storing torsional spring energy) and then releasing the elevation drive train clutch, allowing the scoop to impact the lunar surface. Digging, retaining, transporting, and dumping samples of the lunar surface are accomplished by sequentially operating the four motors (extension/retraction, azimuth, elevation, and scoop door), while scraping and trenching are accomplished by opening the scoop door, applying a downward force to the surface, and operating the extension/retraction motor. The downward force is obtained by pressing the scoop to

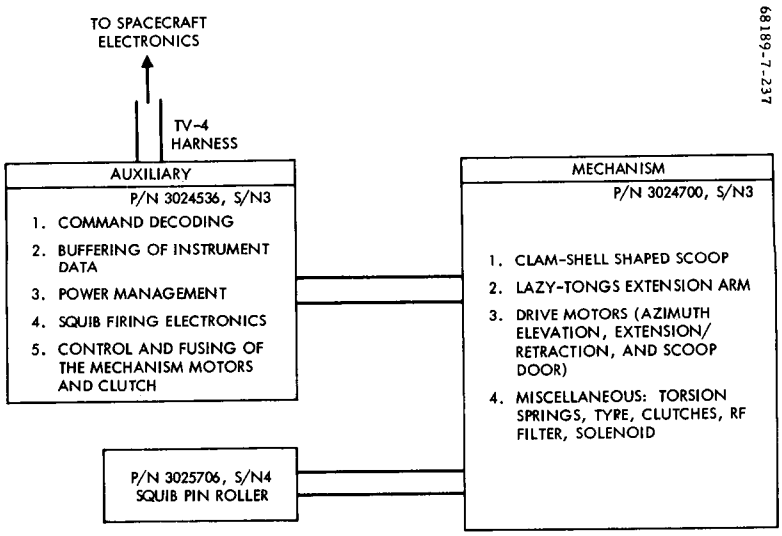

Figure 5.15-1. Soil Mechanics/Surface Sampler System

the lunar surface by selective operation of the elevation motor. The SM/SS mechanism on Surveyor VII was mounted at an angle of approximately 103 degrees (away from leg 2) so that the section of operation permitted contact with the alpha scattering instrument.

5.15.2 ANOMALIES

There were no anomalies on the SM/SS subsystem during the Surveyor VII mission. Additional heating capacity was added to the SM/SS auxiliary after the Surveyor III flight transit performance showed temperatures of -12°to -35°F instead of the predicted -4°F. The transit temperature profile was entirely within predicted levels.

5.15.3 SUMMARY

The SM/SS on Surveyor VII assisted in the deployment of the alpha scattering instrument after the sensor head failed to fully lower to the lunar surface. The SM/SS scoop was positioned over the sensor head skirt and small downward and sideways forces were applied to the sensor head. Examination of television pictures of this operation indicated the sensor head swung and may have moved down slightly. In order to obtain greater leverage, an improved technique was devised and executed (see Figure 5.15-2). The SM/SS was manipulated so as to turn the sensor head approximately 45 degrees and wedge it against the helium tank and standard sample and then to force it downward. The sensor head was thus lowered several inches. The SM/SS was then able to be positioned directly on top of the sensor head and successfully force the device to the lunar surface. During this period, the sensor head moved downward approximately 17 inches as a result of nine downward fine pushes, each exerting a maximum force of approximately 4 ounces.

When critically high temperature levels occurred during days 015 to 020 GMT, the SM/SS was positioned so as to cast its shadow upon the alpha scattering instrument in order to cool the device. On day 021, the SM/SS was used to redeploy the alpha scattering instrument sensor head over a rock at a second lunar position. Redeployment was accomplished by grasping the sensor head pickup fitting, with the scoop then lifting, translating, and lowering the sensor head to the new position. On day 022, the SM/SS redeployed the sensor head to a position that had been previously disturbed by the SM/SS during trenching operations.

During the 12 earth days of operation, the SM/SS performed 16 bearing tests, five of which were performed with the scoop door open and one of which was done near the wall of a deep trench; dug seven trenches, two of which were subjected to a multiple (more than one pass) trenching operation; and moved or manipulated four rocks, one of which was weighed (by measuring the elevation motor current required to lift it) several times and photographed in stereo. In addition one rock was broken and photographed, and two impact tests were performed. Television photos of the magnets attached to the SM/SS

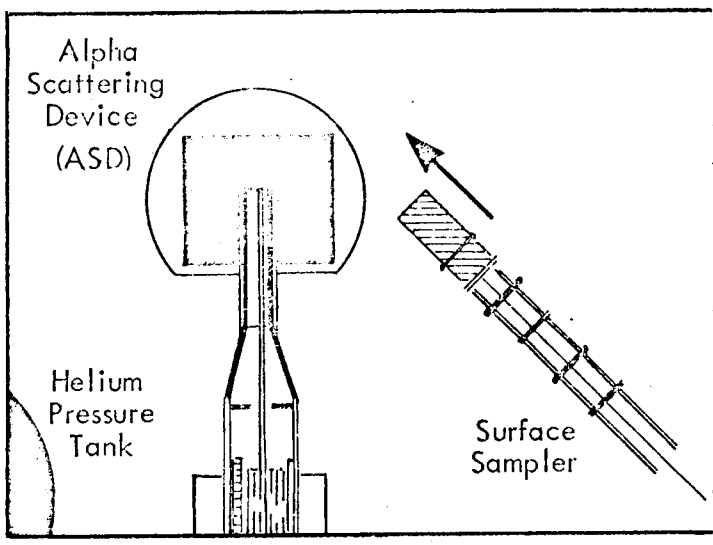

ASD lowering mechanism not functioning.

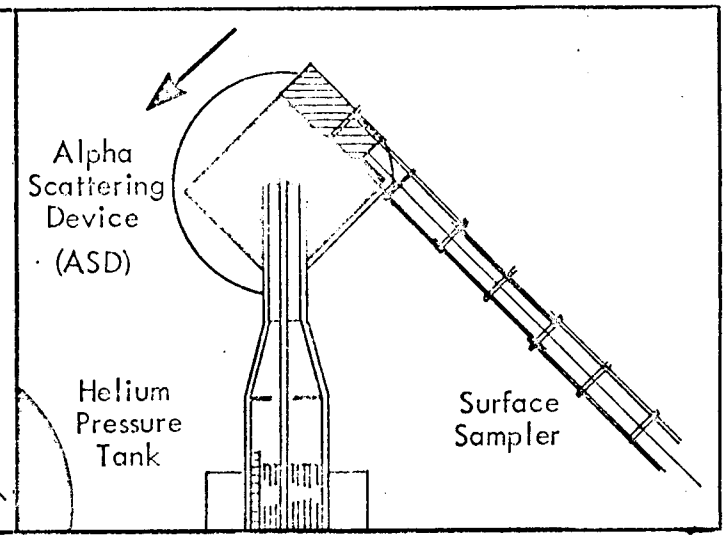

Extended surface sampler turns ASD.

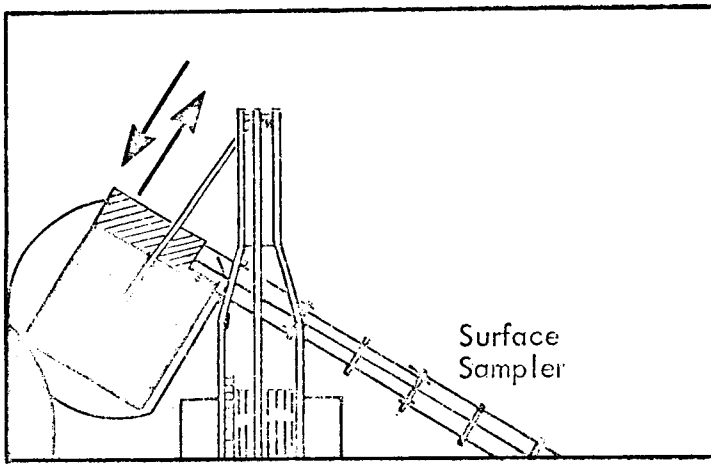

Surface sampler forces ASD down and laterally against helium tank and ASD standard sample mechanism to apply pressure to top of ASD to force it to lunar surface.

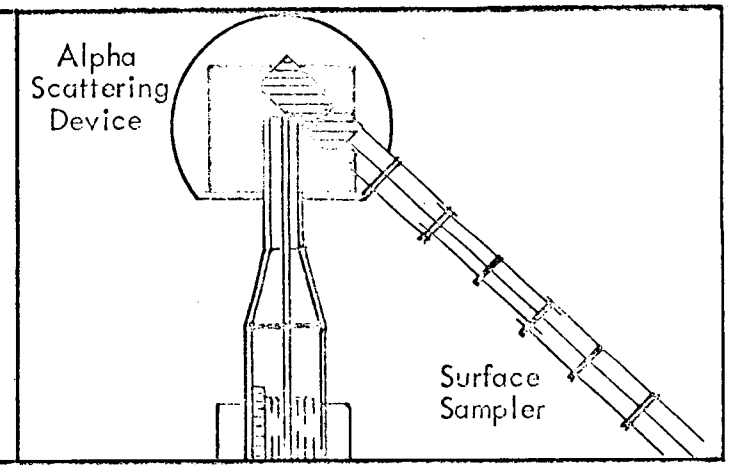

Surface sampler withdraws, leaving ASD still hanging above surface. Surface sampler returns to force ASD the remaining distance to lunar surface.

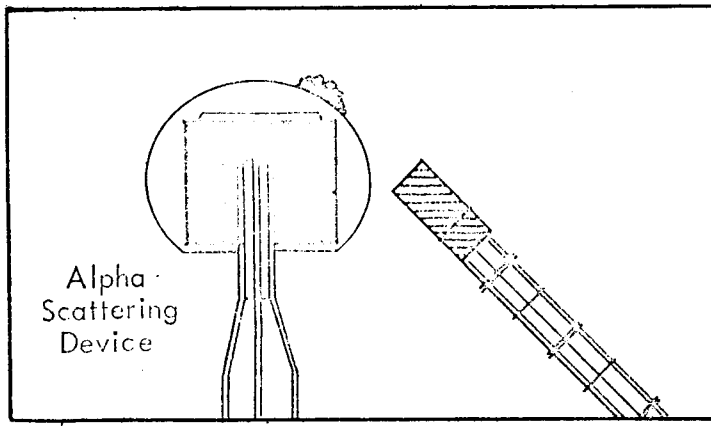

ASD rests on lunar rock; it will not function properly in this position.

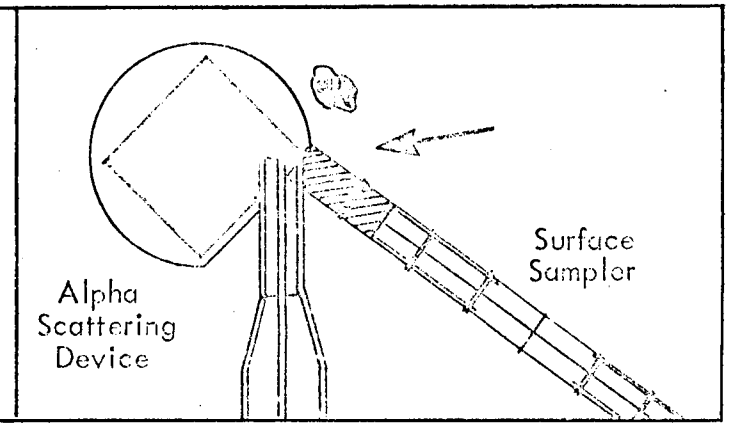

Extended surface sampler pushes ASD off rock to proper horizontal functioning position.

Figure 5.15-2. Sequence of Steps Taken to Free Jammed Alpha Scattering Device as Viewed From Above

scoop door were examined after each significant contact with the lunar surface, and one observation disclosed a magnetic fragment (approximately 3/8-inch in diameter) adhering to the magnet.

The SM/SS was operated for 36 hours and 21 minutes during the 12 earth days comprising the first lunar day. During this period, 12,639 commands were transmitted to the SM/SS system. In response to the transmitted commands, the auxiliary subsystem performed 6956 functions composed of mechanism responses, resets of the four-bit register, and timing mode changes. The mechanism subsystem responded to 4397 commands executed from the command decoding circuitry of the auxiliary subsystem. The operating times and the command breakdown for each earth day are tabulated in Table 5. 15-1.

TABLE 5.15-1. OPERATION TIMES FOR SM/SS

GMT Day, 1968	Operating Time, minutes	Command Sent to SM/SS	Auxiliary Functions Performed	Mechanism Motions Performed
11	239	806	371	184
12	390	1581	766	426
13	209	1499	853	561
14	223	2008	1190	828
15	9	73	38	22
16	0	0	0	0
17	10	42	18	6
18	3	21	9	3
19	187	1364	898	590
20	335	2006	1022	596
21	277	1289	713	463
22	241	1830	1017	685
23	58	120	61	33
Total	2181	12,639	6956	4397

5.15.4 ACKNOWLEDGMENTS

Summary flight data were obtained from Maurice Clary of JPL. This section was compiled by E. R. Zinn and J. M. Berger.